

**UNIVERSITÄT
BAYREUTH**

Development of natural product-derived anti-tumoural metal complexes

Dissertation zur Erlangung des akademischen Grades
eines Doktors der Naturwissenschaften (Dr. rer. nat) an der
Fakultät für Biologie, Chemie und Geowissenschaften der
Universität Bayreuth

vorgelegt von

Sebastian Werner Schleser

aus München

Bayreuth, 2023

Die vorliegende Arbeit wurde in der Zeit von April 2020 bis Januar 2023 in Bayreuth am Lehrstuhl für Organische Chemie I unter Betreuung von Herrn Professor Dr. Rainer Schobert angefertigt.

Vollständiger Abdruck der von der Fakultät für Biologie, Chemie und Geowissenschaften der Universität Bayreuth genehmigten Dissertation zur Erlangung des akademischen Grades eines Doktors der Naturwissenschaften (Dr. rer. nat.).

Art der Dissertation: Kumulative Dissertation

Dissertation eingereicht am: 17.01.2023

Zulassung durch die Promotionskommission: 25.01.2023

Wissenschaftliches Kolloquium: 25.04.2023

Amtierender Dekan: Prof. Dr. Benedikt Westermann

Prüfungsausschuss:

Prof. Dr. Rainer Schobert (Gutachter)

Prof. Dr. Rhet Kempe (Gutachter)

Prof. Dr. Matthias Breuning (Vorsitz)

Prof. Dr. Peter Strohriegl

Für meine Mutter und im Gedenken an meinen Vater

*“And you run, and you run to catch up with the sun, but it's sinking
Racing around to come up behind you again”*

~Pink Floyd, Time

Abstract

The world is facing the late phase of an epidemiological transition, with cancer becoming the leading cause of death in the developed world for people under 70 years of age. Yet, as variable and unique as cancer may be, so are its treatment options. While its treatment is increasingly shifting towards personalised therapy using immuno-oncology, chemotherapy is still the method of choice, especially for advanced stages of cancer. The three most common chemotherapeutic agents are cisplatin (**1**), carboplatin (**7**) or oxaliplatin (**8**), which are used in over 50% of all chemotherapies. Existing or developing resistances against these cytostatic drugs can, however, reduce their rate of successful applications. In addition, their sometimes severe side effects can significantly impact the patient's quality of life.

Consequently, a search for alternatives in cancer treatment began, quickly expanding to include other transition or noble metals for developing chemotherapeutic drugs. Compared to organic compounds, metal complexes generally have the advantage of unique geometries to fit into the targets' binding pockets. Furthermore, a charge can easily be introduced into metal complexes, significantly affecting their pharmacokinetics. Hence, mechanisms of action can be achieved other than binding to the DNA, as in the case of the mainstay platinum complexes. Among others, gold complexes such as auranofin (**29**) have proven to be particularly effective in inducing cancer cell apoptosis via mitochondrial pathways. In addition to the central atom, the ligands play the main role in unfolding anti-tumoural effects. *N*-heterocyclic carbenes (NHC) have proven to be extraordinarily versatile and potent. Thus, by appropriate design, target-specific or pleiotropic chemotherapeutics can be generated.

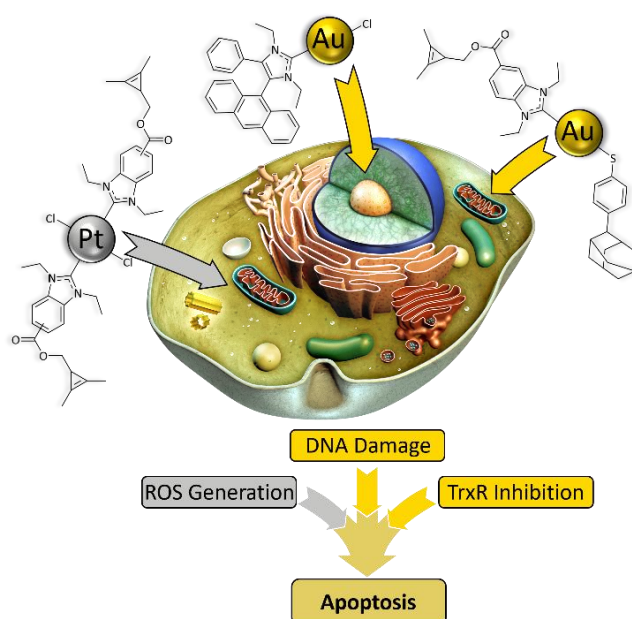
Improving the effects of an already active substance by combining it with a central metal to design compounds with specific mechanisms of action can create metal complexes with reduced adverse side effects or enhanced anti-tumoural activity. Therefore, insight into these complexes' mechanisms of action is of great interest. In addition to *in vitro* assays, subcellular localisation serves this purpose, for example, via bioorthogonal click chemistry.

This dissertation comprises three publications detailing the synthesis, characterisation, and evaluation (e.g., IC_{50} , cellular uptake, ROS generation and DNA Interaction) of metal complexes, addressing one or more Hallmarks of Cancer. The main features of the complexes developed in the course of this research are their unique anti-tumoural effects and their subcellular localisation via bioorthogonal chemistry.

The first publication examines NHC-gold(I) thiolato complexes, mimicking the HIF-1 α inhibitor AC1-004. Compared to the lead structure, improved cytotoxicity was achieved through accompanying effects, such as thioredoxin reductase (TrxR) inhibition, inhibition of tube formations or disruption of the cytoskeleton formation. Their IC_{50} values were mainly in the low micromolar range. Bioorthogonal click chemistry of their cyclopropene-bearing analogues also demonstrated the accumulation of the thiolato complexes in the cancer cells' mitochondria.

The second publication focuses on *trans*-bis platinum(II) complexes, analysing their geometry's effects to circumvent cisplatin (**1**) resistance. The cytotoxicity of some compounds reached two-digit nanomolar IC_{50} values against several human cancer cell lines. Furthermore, a structure-activity relationship (SAR) study was conducted, revealing that the cytotoxicity, stability, and mechanism of action correlated with the geometry and the *N*-substituents. The latter was proven via cyclopropene-tagged derivatives, which accumulated in the cancer cells' nuclei (*cis*) or mitochondria (*trans*).

The third publication discusses gold complexes derived from the mitotic inhibitor combretastatin-A4 (CA-4). The ligands were synthesised following VAN LEUSEN imidazole cycloaddition reaction. Different subcellular accumulations could be achieved, depending on the second ligand of the Au(I) species, which was demonstrated via fluorescence experiments with anthracene-bearing congeners. The neutral gold chlorides bound with the DNA, the cationic phosphane complexes led to TrxR inhibition and the bis-NHC complexes accumulated in the lysosomes, all of which led to apoptosis with IC_{50} values in the low three-digit to the two-digit nanomolar range.



Kurzzusammenfassung

Die Welt befindet sich inmitten eines epidemiologischen Wandels: Krebs ist in den Industrieländern mittlerweile die häufigste Todesursache bei Menschen unter 70 Jahren. So variabel und einzigartig, wie eine Krebserkrankung sein kann, so unterschiedlich sind auch die Therapiemöglichkeiten. Während sich der Trend aktuell immer mehr in Richtung personalisierte Therapie unter Einsatz von Immunonkologie entwickelt, ist die Chemotherapie vor allem in fortgeschrittenen Stadien nach wie vor das Mittel der Wahl. Die Komplexe Cisplatin (**1**), Carboplatin (**7**) oder Oxaliplatin (**8**) sind dabei in gut 50% der Therapien vertreten. Bestehende oder sich entwickelnde Resistenzen können allerdings den Therapieerfolg mindern. Die teilweise starken Nebenwirkungen der Zytostatika können zudem die Lebensqualität der Patienten massiv beeinträchtigen.

Daher begann früh nach der Entdeckung von Cisplatin (**1**) die Erforschung möglicher Alternativen und diese weitete sich schnell auf andere Übergangs- oder Edelmetalle aus. Gegenüber organisch-chemischen Verbindungen haben Metallkomplexe allgemein den Vorteil, dass sich einzigartige Geometrien erzeugen lassen, um so in die Bindungstaschen des Zielmoleküls zu passen. Außerdem kann leicht eine Ladung in den Komplex gebracht werden, was die Pharmakokinetik maßgeblich beeinflusst. Dadurch können andere Wirkmechanismen erzielt werden als die der Platinkomplexe, welche in die DNA interkalieren. Als besonders wirksam haben sich dabei unter anderem Goldkomplexe wie Auranofin (**29**) erwiesen, die über mitochondriale Wege die Apoptose einleiten. Nebst dem Zentralatom spielen die Liganden eine wichtige Rolle in der Entfaltung der antitumoralen Wirkung. Dabei bestechen NHCs durch ihre Vielseitigkeit und leichte Anpassbarkeit. Durch gezieltes Design lassen sich so target-spezifische oder pleiotropische Chemotherapeutika erzeugen.

Die Kombination einer bereits aktiven Substanz mit einem Zentralmetall kann deren Effekte verbessern und Komplexe mit besonderen Wirkmechanismen, geringeren unerwünschten Nebenwirkungen oder verstärkter antitumoraler Aktivität generieren. Deshalb ist die Aufklärung des Wirkmechanismus dieser Komplexe von großem Interesse. Dazu dient neben *in vitro* Assays vor allem die subzelluläre Lokalisation zum Beispiel durch bioorthogonale Click Chemie.

Diese Arbeit umfasst drei Publikationen, welche die Synthese, Charakterisierung und Evaluierung (unter anderem IC_{50} , zelluläre Aufnahme, ROS-Erzeugung und DNA-Interaktion) von Metallkomplexen beschreiben, welche einen oder mehrere der Hallmarks of Cancer adressieren. Das Hauptmerkmal der im Zuge dieser Arbeit entstanden Verbindungen sind deren einzigartige antitumorale Effekte sowie deren subzelluläre Lokalisation via bioorthogonaler Chemie.

Die erste Publikation beschäftigt sich mit NHC-Gold(I) Thiolkomplexen, die dem HIF-1 α Inhibitor AC1-004 nachempfunden wurden. Durch einhergehende Effekte wie die TrxR Inhibition, die Inhibition der Angiogenese oder die Störung der Ausbildung des Zytoskeletts, konnte eine verbesserte Zytotoxizität verglichen mit der Leitstruktur erzielt werden. Die IC_{50} Werte lagen dabei hauptsächlich im niedrigen mikromolaren Bereich. Bioorthogonale Click Chemie von Cyclopropen-tragenden Analoga bewies außerdem eine Akkumulation in den Mitochondrien der Krebszellen.

Die zweite Veröffentlichung behandelt vor allem *trans*-bis Platin(II) Komplexe, die durch ihre Geometrie die Resistenz gegenüber Cisplatin (**1**) umgehen sollten. Dabei wurden bis zu zweistellig nanomolaren IC_{50} Werte erreicht. Außerdem wurde eine Struktur-Aktivitäts-Beziehung beobachtet. Nicht nur die Zytotoxizität, sondern auch die Stabilität und der Wirkmechanismus hingen dabei von der Geometrie und den *N*-Substituenten ab. Der Wirkmechanismus wurde anhand von Cyclopropenen-tragenden Derivaten nachgewiesen, die sich in den Zellkernen (*cis*) oder Mitochondrien (*trans*) der Krebszellen anreicherten.

Die dritte Publikation thematisiert Gold Komplexe, deren Imidazolliganden dem Mitoseinhibitor CA-4 nachempfunden wurden. Die Liganden wurden gemäß einer VAN LEUSEN Cycloadditionsreaktion synthetisiert. Je nach Wahl des zweiten Liganden der Au(I) Spezies konnten hier verschiedene subzelluläre Akkumulationen erreicht werden, was durch Anthracen tragende Analoga bewiesen wurde. Die neutralen Goldchloride banden dabei an die DNA, die kationischen Phosphankomplexe führten zur Inhibition von TrxR und die bis-NHC Komplexe reichert sich in den Lysosomen an. Alle Komplexe führten zur Apoptose mit IC_{50} Werten im niedrig dreistellig bis zweistelligen nanomolaren Bereich.

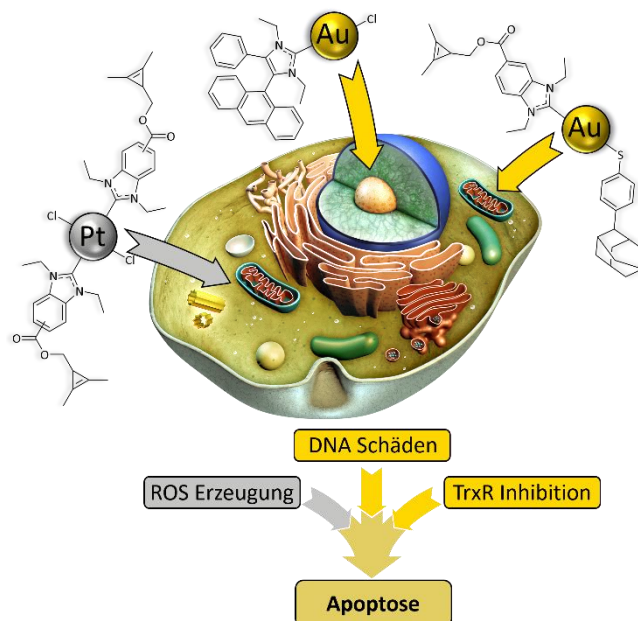


Table of Contents

Abstract	I
Kurzzusammenfassung	III
Table of Contents	V
Abbreviations	VI
1 Introduction	1
1.1 Cancer: Statistics, characteristics, and hurdles of novel therapies	1
1.2 From cisplatin to Pt ^{IV} prodrugs	5
1.2.1 (Re)discovery and synthesis of cisplatin	5
1.2.2 Cisplatin: mechanism of action, toxicity, and resistance	6
1.2.3 New generations of chemotherapeutic agents based on cisplatin	8
1.2.4 NHC platinum complexes	9
1.2.5 Alternative geometry	11
1.3 Transitioning to other transition metal complexes	14
1.3.1 Advanced and promising Ru, Cu and Fe complexes	14
1.3.2 Palladium complexes	17
1.3.3 Chrysotherapy	19
1.4 Metal Drug Synergism	24
1.4.1 Complexes with biologically active ligands	24
1.4.2 Bioorthogonal chemistry.....	28
2 Synopsis	32
2.1 Objectives and overview of the subprojects	32
2.2 NHC-Au-SR complexes derived from AC1-004 as potential HIF-Inhibitors	34
2.3 Synthesis and evaluation of new <i>cis</i> and <i>trans</i> bis NHC-Pt ^{II} complexes.....	36
2.4 Metal-Drug-Synergism: Gold complexes of CA-4.....	38
3 Bibliography	40
4 Publications	47
4.1 Presentation of the own contribution.....	47
4.2 Publication I	49
4.3 Publication II	82
4.4 Publication III	150
4.5 List of all publications and poster contributions to conferences	178
Acknowledgements (German)	VIII
Eidesstattliche Versicherung und Erklärung des Verfassers	X

Abbreviations

Ac	acetate
Alloc	allyloxycarbonyl
Aq	aqueous
Ar	aryl
ATP	adenosine triphosphate
BiP	binding immunoglobulin protein
Bn	benzyl
Boc	<i>tert</i> -butyloxycarbonyl
Bu	butyl
CA-4	combretastatin A-4
CAM	chorioallantoic membrane
cisplatin	<i>cis</i> -diamminedichloroplatinum
Cp	cyclopentadienyl
CuAAC	copper(I)-catalysed azide-alkyne cycloaddition
CVD	cardiovascular disease
Cy	cyclohexyl
DACH	1,2-diaminocyclohexane
DLC	delocalised lipophilic cations
DLT	dose-limiting toxicity
DMSO	dimethyl sulfoxide
DNA	deoxyribonucleic acid
EGFR	epidermal growth factor receptor
EMSA	electrophoretic mobility shift assay
<i>E. coli</i>	<i>Escherichia coli</i>
Eq	equivalents
Et	ethyl
FDA	Food and Drug Administration
GI_{50}	half maximal inhibitory concentration of cell proliferation
HDI	human development index
HIF	hypoxia-inducible factor
HMG	high mobility group
HOMO	highest occupied molecular orbital
HSAB	hard and soft acids and bases

<i>i</i>	<i>iso</i>
IC_{50}	half maximal inhibitory concentration
Im	imidazole
In	indazole
LUMO	lowest unoccupied molecular orbital
Me	methyl
MeCN	acetonitrile
MMP	mitochondrial membrane potential
MMR	mismatch repair
6-MP	6-mercaptopurine
NADH	dihyronicotinamide adenine dinucleotide
NER	nucleotide excision repair
NHC	<i>N</i> -heterocyclic carbene
NSCLC	non-small-cell lung cancer
PCC	pearson correlation coefficient
Ph	phenyl
Pn	pentane
Pr	propyl
PSP	purine salvage pathway
ROS	reactive oxygen species
r.t.	room temperature
SA	serum albumin
SAR	structure-activity relationship
SPh	thiophenol
StA	sterulic acid
<i>t</i>	<i>tert</i>
6-TG	6-thioguanine
TME	tumour microenvironment
TNM	tumour node metastasis
TosMIC	toluene sulfonylmethyl isocyanide
TrxR	thioredoxin reductase
UPR	unfolded proteins response
VEGF	vascular endothelial growth factor
xs	excess

1 Introduction

1.1 Cancer: Statistics, characteristics, and hurdles of novel therapies

After decades as the leading cause of premature death, cardiovascular diseases (CVD) have been surpassed by cancer in recent years, especially in countries with a high human development index (HDI).^[1-3] The International Agency for Cancer Research reported 19.3 million new cancer cases and 10.0 million cancer-related deaths in their 2020's GLOBOCAN statistics, ranking cancer among the top two most common causes of death before the age of 70 in 112 out of 183 countries (Figure 1).^[4]

Interestingly, the incidence of different cancer types varies between countries due to exposure to other risk factors. The most diagnosed cancer types in industrialised countries are breast-, prostate- and lung cancer due to more prevalent obesity, smoking or an unhealthy diet. Low HDI countries show a higher frequency of poverty-based and infection-related cancer types, e.g. abdominal-, liver- and cervical cancer.^[5] Vaccination against the latter has been promoted for decades, leading to this type of cancer being listed at the lower end of the incidence range in high HDI countries, thus emphasising the importance of prevention and access to health care.^[6] Country-specific differences can also be identified, such as the high proportion of lung cancer in China due to high air pollution.^[7]

Predictions for the cancer burden of 2040 forecast a rise of new cancer diagnoses by 47% worldwide, with low to medium HDI countries suffering the most due to the growth and ageing of the population in combination with poor access to healthcare in those transitioning countries.^[8]

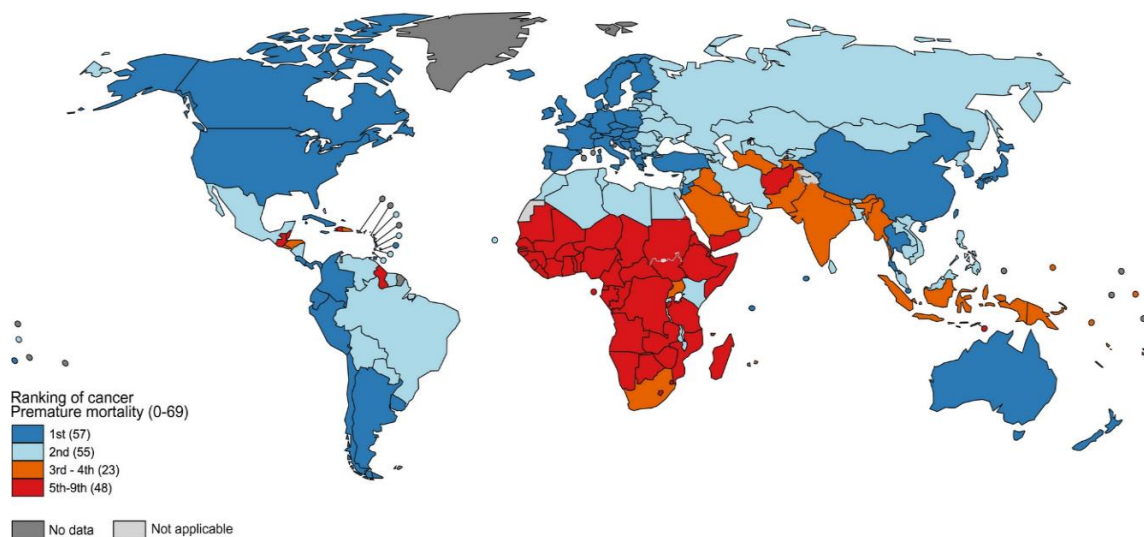


Figure 1. National ranking of cancer as a cause of death at ages <70 years in 2019. Reprinted with permission from^[8]. Copyright © American Association for Cancer Research.

However, the future increase in cancer numbers may be even more significant than predictions indicate due to the still unknown full extent of the COVID-19 pandemic.^[9-11] The resulting strain on the healthcare system likely led many people not to undergo a necessary cancer screening examination with or without suspicion. Therefore, the number of unreported cases and cancer-related deaths in the coming years could be much higher than expected. After all, a later diagnosis and, thus, a more advanced stage of cancer is the most avoidable cause of a poor prognosis for the patient.^[12-14]

Concerning cancer research, the COVID-19 pandemic has also had positive effects. The gene technologies behind the mRNA-1273 (*Moderna*) and BNT162b2 (*BioNTech, Pfizer*) vaccines are re-energising research into mRNA-based cancer treatment as the currently most promising approach to fighting cancer. Today, more than a hundred clinical trials (phase I – III) based on immunological drugs are registered for different kinds of cancer, for example, prostate cancer, melanoma, leukaemia or non-small-cell lung cancer (NSCLC).^[15, 16] However, the 2018 Nobel prize awarded discovery of using the body's immune system as a weapon against cancer is a double-edged sword, leading to some trials already having been terminated due to lack of efficiency, unwanted immunogenicity or other side effects. Normally, the immune response is downregulated to prevent autoimmunity by so-called checkpoint inhibitors, e. g., CTLA-4 or PD-1. Yet, the FDA-approved monoclonal antibodies ipilimumab and pembrolizumab, for example, release these brakes and make the cancer cell attackable by the immune system again by attracting and activating T-Cells and thus generating an immune responsive tumour microenvironment (TME), while risking aforementioned autoimmunity.^[17] Another disadvantage of immunotherapy is congenital or acquired resistance caused either by immunosuppressive diseases, tumours with small molecule cues or the possibility of cancer cells simply escaping the immune system.^[18]

While promising, this immunotherapy research is still in its infancy, mainly because there is no universally applicable scoring system like the tumour node metastasis (TNM) staging system in chemotherapy to predict whether a patient will respond to immunotherapy or what side effects there might be.^[16] Consequently, this methodology is still at the bottom of cancer treatment statistics today. The even more sophisticated approach of personalised cancer therapy based on a person's omics to not rely on any prediction method is a dream of the future.^[19]

Today, the choice of therapeutic approach mainly depends on the cancer type and its progression. While surgical resection is the most prominent choice for early cancer stages, used for up to 70% of TNM stage I tumours according to the UK Cancer Research from 2016 to 2019, the use of radio-

and chemotherapy increases with the stage of the disease.^[20] Nevertheless, not every type of cancer can be treated equally. The most common cancer types, breast-, uterine corpus- and colorectal cancer, are all treated in early stages via breast-conserving surgery (or more rarely mastectomy), hysterectomy or colectomy, respectively. However, later stages of these diseases are mainly treated with chemotherapeutic drugs, less frequently with radiotherapy, but often with a combination of these.^[21] For other types of cancer, e. g., leukaemia, HODGKIN and Non-HODGKIN lymphoma or small cell lung cancer, chemotherapy remains the first choice of treatment. Compared to radio- or immunotherapy, the advantages of chemotherapeutics are the simple and cheap production of the drugs in connection with targeted applications depending on the compound.

The drugs used in chemotherapy can be subdivided into two major groups depending on their mode of action. The most commonly used anti-tumoural agents can be categorised as cytostatic drugs, hampering the cancer cells' growth. These, in turn, can be divided into four subgroups, depending on which phase of the cell cycle they inhibit. Table 1 lists a few examples of clinically approved drugs. Today, in about 50% of chemotherapies, one of the metallodrugs mentioned in the fourth row, cisplatin (**1**), carboplatin (**7**) and oxaliplatin (**8**), are applied. They can intersect the cell cycle at S or G2/M stage and are described in more detail in the upcoming chapters.

Table 1. An excerpt of clinically used chemotherapeutic drugs and their mode of action.

Type of drug	Mode of action	FDA approved examples
Mitotic inhibitors	Inhibiting microtubule dynamics, thereby constraining cell division. ^[22, 23]	vinblastine, cabazitaxel, docetaxel, colchicine
Topoisomerase I/II inhibitors	Trapping the single- or double-strand break of the DNA caused by the enzymes. ^[24, 25]	daunorubicin, doxorubicin, irinotecan, topotecan
Antimetabolites	Erroneous incorporation into DNA results in the arrest of replication. ^[26, 27]	6-mercaptopurine (6-MP), 6-thioguanine (6-TG), fluorouracil, fludarabine
Alkylating or metalating agents	Attaching to N7 of guanine bases of the DNA inducing irreparable damages. ^[28, 29]	cisplatin (1), carboplatin (7), oxaliplatin (8), carmustine

The compounds belonging to the second main group of chemotherapeutics cannot be generalised because they vary significantly from each other in their mechanism of action, e.g. HDAC-inhibitors, asparaginase- or HIF-1 α inhibitors.^[30-33] However can also be assigned to a specific target, which corresponds to one of the hallmarks of cancer, recently updated by HANAHAN *et al.* (Figure 2). Their review underlines the complexity of the disease while also showing which targets cancer cells, as opposed to non-malignant cells, might offer chemotherapy.

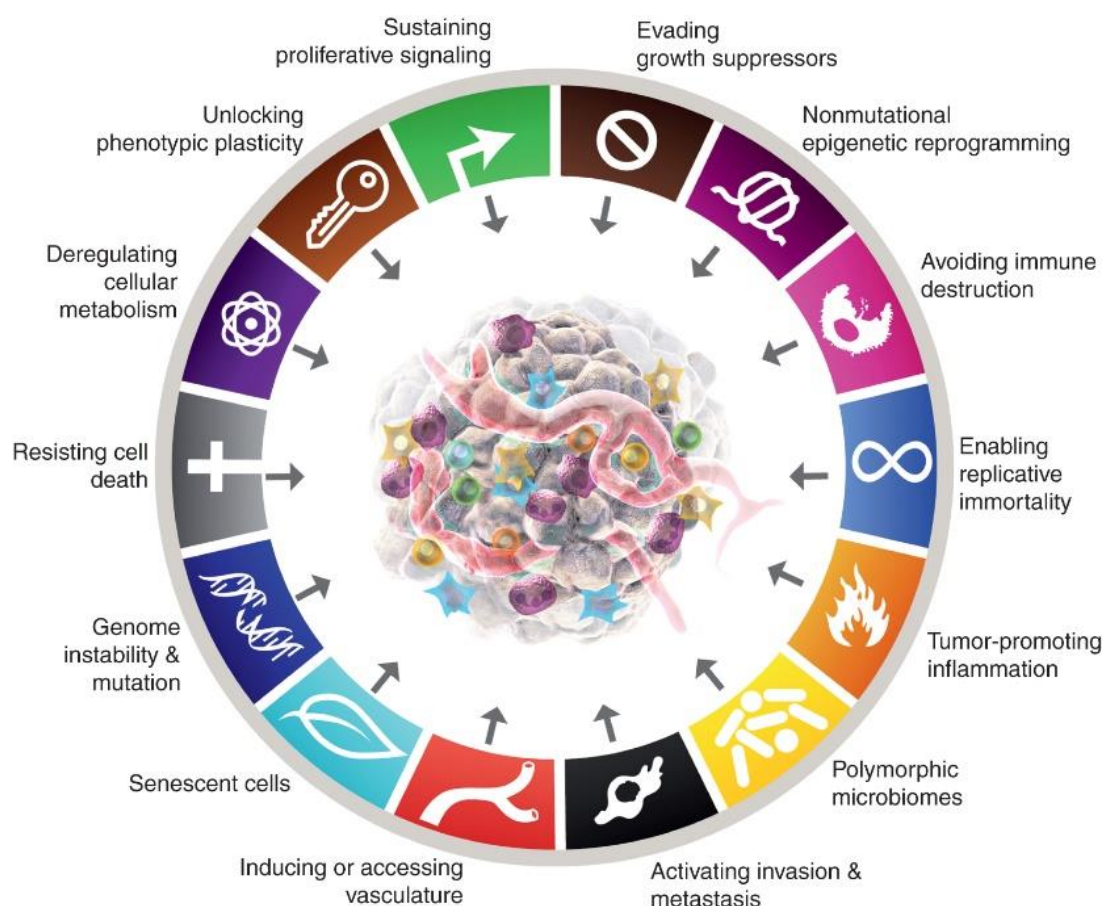


Figure 2. Hallmarks of Cancer 2022. Reprinted with permission from^[34]. Copyright © John Wiley and Sons.

Current research on chemotherapeutic agents is therefore focused on tumour-only targets. The resounding success of the aforementioned platinum drugs also paved the way for a variety of improved target-selective or pleiotropic metal-based chemotherapeutics. The following chapters will explain this development and the extent to which metal complexes are superior to organic compounds.

1.2 From cisplatin to Pt^{IV} prodrugs

1.2.1 (Re)discovery and synthesis of cisplatin

Today, approximately 50% of patients treated with chemotherapeutic agents receive infusions with cisplatin (**1**) or an analogue thereof.^[35] However, it was a long journey to reach the current chemotherapy standard. Like many pioneering breakthroughs and discoveries in medicine or chemistry, the discovery of the effect of **1** was also serendipitous. In 1965, ROSENBERG *et al.* set out to examine the effect of an electric current on the growth process of *Escherichia coli* (*E. coli*), discovering that the platinum electrodes, which they believed inert, caused the inhibition of cell division, not the electric field applied.^[36] After some experiments to exclude the factors of filament formation, such as UV light, pH value or magnesium concentration, these variables were kept constant, and various transition metals were evaluated. These tests elucidated that, in addition to rhodium and ruthenium, oxidised platinum species are the main reason for cell division inhibition.^[36] Further investigations revealed that mainly the neutral Pt^{II}, namely *cis*-diamminedichloroplatinum (cisplatin) (**1**) and the Pt^{IV}, called *cis*-diamminetetrachloroplatinum (**2**), species (Figure 3), were excessively active. Another early discovery made by Rosenberg in 1967 revealed that only the *cis* configuration of the metal complexes showed effectiveness, while the *trans*-complexes did not display cell growth inhibition.^[37, 38]

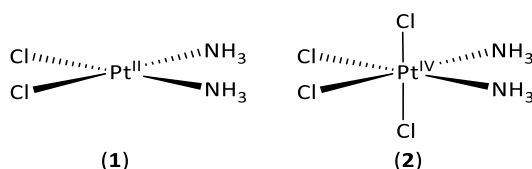
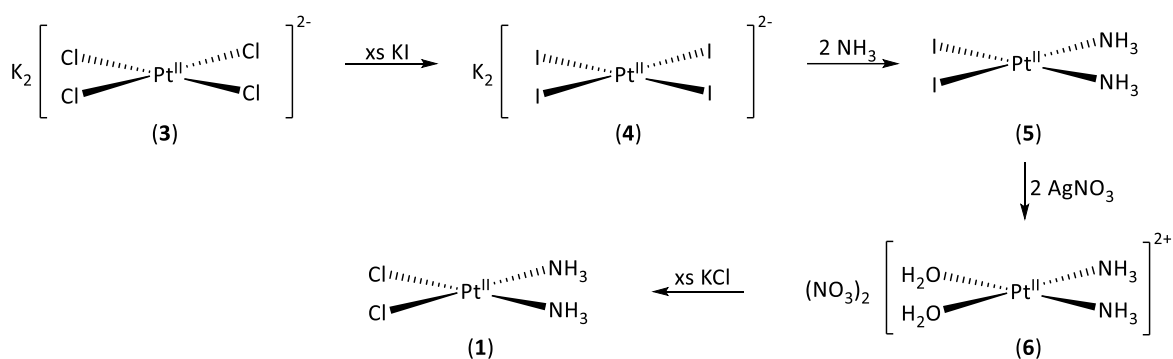


Figure 3. Structures of *cis*-diamminedichloroplatinum (**1**) and *cis*-diamminetetrachloroplatinum (**2**).

Furthermore, both **1** and **2** were evaluated in Sarcoma 180- and Leukaemia L1210-bearing mice, revealing a high potency with complete regression of the tumour in some cases. However, a high dose-response curve of side effects limited dosage.^[39, 40] Further evaluation and subsequent clinical trials led to the approval of **1** for the treatment of advanced testicular, ovarian and bladder cancer in 1978 - a breakthrough in chemotherapeutic research.

Nevertheless, early synthesis of **1** was challenging. For example, the formation of MAGNUS´S Green Salt (MGS), a complex of alternating [Pt(NH₃)₄]²⁺ and [Pt(Cl)₄]²⁻ ions which, in sum, displays the same molecular formula as **1** but lacks its chemotherapeutic efficacy.^[41] Thus, DHARA developed a

method exploiting the *trans* effect of ligands by reacting potassium tetrachloroplatinate(II) (**3**) with potassium iodide to form potassium tetraiodoplatinate(II) (**4**). The iodido ligands of the latter can be exchanged with ammonia selectively in *cis* position. Dissolving this $[\text{Pt}(\text{NH}_3)_2\text{I}_2]$ (**5**) species in an aqueous solution of AgNO_3 led to the precipitation of insoluble AgI , whereas the diaqua complex **6** in the filtrate is treated with KCl to eventually form cisplatin (**1**) in its pure form as yellow crystals (Scheme 1).^[42] Another versatile and one-pot method substitutes the chloride ligands with ammonia generated *in situ* via ammonium acetate.^[43]



Scheme 1. Synthesis of cisplatin (**1**) by Dhara.^[42]

1.2.2 Cisplatin: mechanism of action, toxicity, and resistance

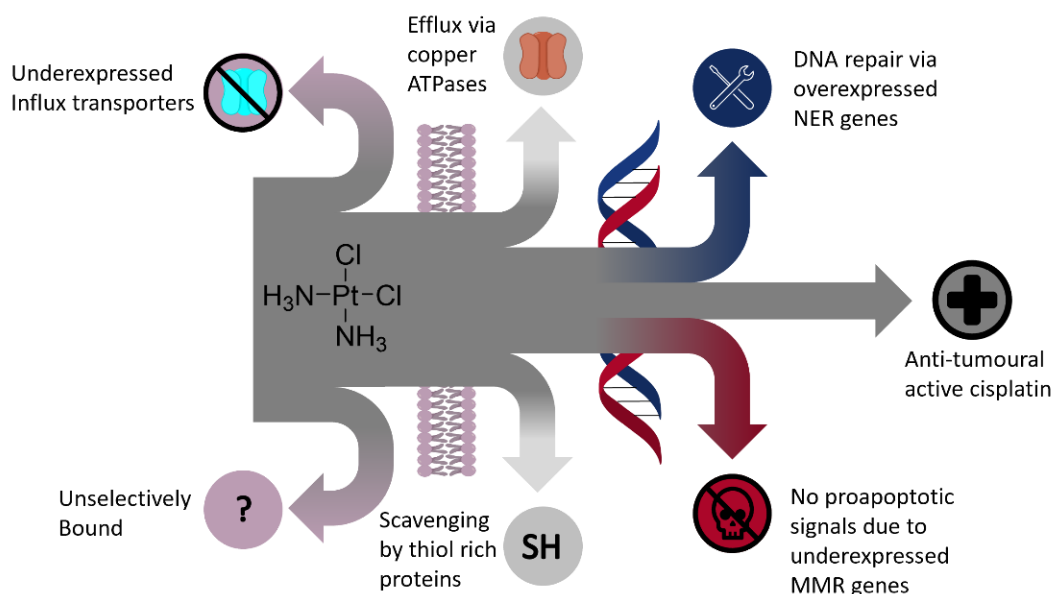
In clinical practice, **1** is applied intravenously, dissolved in physiological saline. In serum, it circulates in its relatively inactive form. However, once it enters the cell, mainly through passive diffusion or copper transporters,^[44] **1** undergoes ligand exchange with water due to the rapid fall of chloride concentration. The now present cationic diaqudiammino Pt^{II} complex can bind to the N7 of the imidazole ring of guanine and adenine bases leading to 1,2-intrastrand crosslinks of the DNA, which, in turn, inhibit the transcription and replication, arresting the cell cycle at S, or G2-M phase. Less frequently, 1,3-intrastrand, interstrand or monofunctionally bound platinum adducts are formed, showing the same effect of inducing cell apoptosis.^[45-47] While the DNA is considered the main target of **1**, other accompanying effects leading to cell death are, for example, the generation of ROS and hence the loss of mitochondrial membrane potential (MMP)^[48, 49] or the induction of endoplasmic reticulum (ER) stress.^[50]

However, various disadvantages are associated with cisplatin's (**1**) application. There are, for instance, dose-limiting toxicities (DLT) of the chemotherapeutic agent that become apparent in the toxicological effects, e. g., ototoxicity, which up to 80% of patients treated with **1** will develop

to some degree.^[51] Other unwanted side effects are nephro-^[52], hepato-^[53] and most seriously cardio-^[54] and neurotoxicity.^[55]

Besides DLTs, intrinsic or developed resistances to **1** are detrimental to its successful application in cancer therapy. The latter can be divided into two mechanisms. Off-target resistance, for example, emerges in mutated cancer cells, which show a lower expression of copper transporters responsible for the uptake of **1** in cells^[44], leading to decelerated uptake rates of the chemotherapeutic agent.^[56] Alternatively, efflux via copper ATPases is increased so that **1** is flushed out of the cell before reaching its target.^[57] Moreover, **1** can also be scavenged after entering the cell by thiol-rich proteins like metallothioneins or glutathiones.^[58, 59]

On-target resistance mechanisms describe resistances towards cisplatin's (**1**) mechanism of action, which can be hindered by under- or overexpression of specific genes capable of destroying DNA distortions induced by **1** or repairing them, respectively. For example, the heritable BRCA genes, essential parts of the homologous recombination system, can repair double-strand DNA breaks, such as those caused by interstrand adducts of **1** within the DNA.^[60] Hence, overexpression and mutations thereof lead to lower responsiveness of cancer patients to therapy with **1**.^[61] The opposite is true for proteins involved in the mismatch repair (MMR) process. In charge of sending signals to induce apoptosis, underexpression or mutation of these genes leads to resistance towards **1** (Scheme 2).^[62] Undoubtedly the most prominent gene involved in cisplatin (**1**) resistance is the TP53 tumour suppressor gene, as it is the most frequently mutated gene in human cancers.^[63, 64]



Scheme 2. Schematic representation of the resistance of a cancer cell towards cisplatin.

1.2.3 New generations of chemotherapeutic agents based on cisplatin

Due to its many disadvantages, the search for cisplatin (**1**) alternatives led to carboplatin (**7**) as a second-generation drug, which the FDA approved in 1989 (Figure 4). It differs from **1** only through the replacement of the chloride ligands with the bidentate chelating ligand 1,1-cyclobutanedicarboxylic acid, increasing stability and thus decreasing reactivity and improving water solubility.^[65] In contrast to the chloride ligands of **1**, which dissociate readily, carboplatin (**7**) is transformed into its active form via enzymatic cleavage of the ester functionality. Activated carboplatin then displays the same mechanism of action as its predecessor **1** resulting in comparable efficacies for both complexes.^[66] However, carboplatin (**7**) is characterised by its lower toxicity, allowing high dosages to treat aggressive tumours. For example, neither ototoxicity nor nephrotoxicity occurs with carboplatin (**7**), but myelosuppression is considerably higher.^[67] Sharing the same mechanism of action as **1** leads to similar resistances. Hence, cross-resistances to the two complexes were found in ovarian cancer patients regardless of the treatment order.^[68]

The third generation of platinum chemotherapeutic agents, oxaliplatin (**8**), was developed and approved by the FDA in 1996.^[69] It features a bidentate oxalate group and a chiral bidentate *trans*-1,2-diaminocyclohexane (DACH) ligand instead of the amino ligands. This ligand is considered the reason for oxaliplatin's (**8**) higher cytotoxicity and lack of resistance against its chemotherapeutic effects compared to **1** and carboplatin (**7**). While the nucleotide excision repair (NER) system, one of the main contributors to the resistance towards **1** and its analogues, has a wide range of substrates it can identify, the same does not apply to the MMR system. The DACH ligand of **8** cannot be recognised by the MMR, eventually resulting in a broader tumour range treatable with **8**.^[70, 71] **8** showed efficacy against cisplatin (**1**)-insensitive cancers such as colorectal-, advanced ovarian cancer and NSCLC.^[69] In addition to oxaliplatin's (**8**) mechanism of action involving a similar if faster formation of DNA adducts as with **1**, a mode of action leading to cell death involving the immune system was published.^[72] Nevertheless, the dose-limiting factor of oxaliplatin (**8**) is its severe neurotoxicity^[73], which is why research into alternatives is ongoing.

In general, the selectivity of the platinum drugs (**1**, **7** and **8**) is solely based on increased proliferation and nutrient requirement of cancer cells, leading to DNA damage not only in malignant tissue but to a certain extent in healthy tissue as well. To increase selectivity for malignant cells, the fourth generation of platinum drugs is comprised of a square plane spanned by platinum bound to two chlorido, one amine and one cyclohexylamine ligand. Two more ligands are bound axially to form the biologically inactive octahedral Pt^{IV} species. For example, satraplatin (**9**) consists of two additional acetato ligands in *trans* position, increasing the drug's lipophilicity

for oral administration. Once in the cancer cell, this prodrug is reduced by dihydronicotinamide adenine dinucleotide (NADH) or heme proteins to transform into its biologically active state.^[74, 75] After metabolism, satraplatin (**9**) reveals a similar mechanism of action as cisplatin (**1**). However, the bulky cyclohexyl amine ligand prevents the DNA adducts from being recognised by the MMR system, as aforementioned in the case of oxaliplatin (**8**).^[76] Even though the application of satraplatin (**9**) led to less severe side effects and better bioavailability due to its chemical inertness, it is not yet approved by the FDA. The same applies to other alternatives, e. g. nedaplatin^[77], picoplatin^[78], heptaplatin^[79] and lobaplatin.^[80] Yet, some of those compounds are regionally approved, especially in Asian countries.

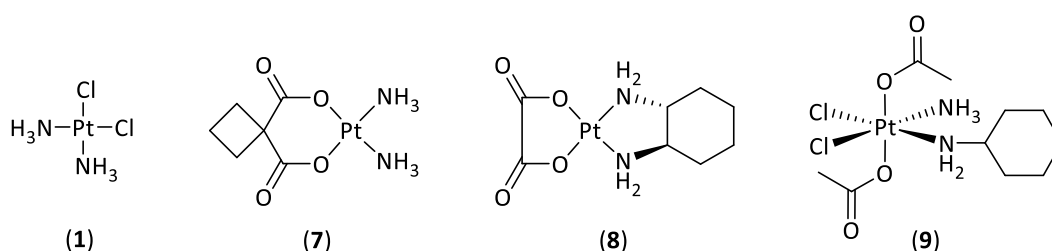


Figure 4. FDA-approved Pt^{II} drugs cisplatin, carboplatin, and oxaliplatin, as well as Pt^{IV} prodrug satraplatin.

Although the above-mentioned platinum drugs (**7**, **8** and **9**) have many advantages, such as circumventing inherited or *de novo* resistances in the case of oxaliplatin (**8**) or fewer side effects as for applications of satraplatin (**9**), they all inherit limitations in the form of low selectivity accompanied by high toxicity. Therefore, current research focuses on synthesising novel platinum complexes, which are stable under physiological conditions, allowing the compounds to reach their site of action without triggering side effects. One class of ligands meeting these criteria are NHCs.

1.2.4 NHC platinum complexes

Carbenes are conceivable in the triplet state, in which the electrons are present with parallel spin in two p-orbitals and the singlet state, in which the electron pair is antiparallel in the sp²-hybrid orbital.^[81] The so-called Push-Pull effect stabilises the latter. The adjacent nitrogen atoms +M effect, thereby donating to the lowest unoccupied molecular orbital (LUMO) of the C²-Atom. Their higher electronegativity further lower the highest occupied molecular orbital (HOMO), making the NHC ligand a strong σ -donor, stabilising the complex.^[82] With similar binding ratios as phosphanes,

NHCs are neutral ligands so that the positive charge of the central metal ion is maintained, which is essential for cellular uptake.^[83]

However, the main advantage of NHC complexes is the easy adjustment in combination with simple synthesis requiring only a few steps. The (benz)imidazole heterocycle can be formed in various synthesis routes depending on the desired substituents.^[84] According to PHILLIP'S Method, benzimidazoles are readily achieved by reacting *o*-diaminobenzenes with an acid.^[85] The widely used method to synthesise imidazoles is the DEBUS-RADZISZEWSKI reaction. It resembles a three-component imidazole synthesis reacting a 1,2-diketone, an aldehyde, and an amine to plain imidazole or up to 1,2,4,5-tetrasubstituted imidazoles depending on the starting material.^[86] Alternatively, the *Van Leusen* reaction, a three-component imidazole synthesis which reacts a TosMIC reagent with an amine and an aldehyde to 1,4,5-trisubstituted imidazoles, can be conducted.^[87]

Besides the various synthesis routes leading to different backbone structures, the choice of N-substituents plays a significant role in adjusting the pharmacokinetic properties of the final complex. Depending on the synthesis route, the final precursor of an NHC ligand in the form of an (inner) salt can be established via symmetrical N,N'-dialkylation or asymmetrical N-alkylation.^[88, 89] The free carbene can finally be obtained and trapped by the present metal either by deprotonation with a strong base^[90], elimination of a leaving group in C-2 position, e. g., CO₂^[91] or by complexation with easily accessible silver salts.^[92]

Prominent examples of anti-tumoural Pt complexes developed over the last few years bear benzimidazolium-ylidene NHCs in combination with a coordinating picoline type as ligands **10** (Figure 5) published by DINDA *et al.* However, first studies of mixed NHC-amine Pt^{II} complexes showed only modest cytotoxicity against human cancer cell lines HeLa (cervix cancer) and HepG2 (hepatocellular cancer).^[93]

In 2011, CHE *et al.* developed another series of cyclometalated Pt^{II} complexes with NHC ligands **11**, stabilised against a substitution with thiol-rich proteins *in vitro* via insertion of a strongly coordinating 6-phenyl-2,2'-bipyridine heterocycle. These complexes achieved IC₅₀ values up to double-digit nanomolar concentrations against cancer cell lines HeLa and HepG2, but also single-digit micromolar values against healthy endothelial cells, against which cisplatin (**1**) is nearly ineffective. Due to the luminescent properties of the heterocyclic structure of **11**, subcellular accumulation can be investigated, showing that this complex preferably accumulates in the cytoplasmic structures (e.g., mitochondria) of the cells rather than the DNA. Further *in vivo* tests demonstrated tumour growth inhibition by 55% in NCI-H640 (NSCLC) tumour-bearing mice.^[94]

Furthermore, a small library comprised of ten *cis*-[Pt^{II}(NHC)¹(NHC)²Cl₂] complexes with variously substituted imidazolium-ylidine NHCs **12**, resulting in a comprehensible SAR was reported by our group in 2016. With few exceptions, their *IC*₅₀ values against various human cancer cell lines were found to be in a low single-digit micromolar range and thus comparable with **1**. More interesting, however, was that the novel NHC platinum complexes revealed a modest activity against cisplatin (**1**)-resistant cell lines HT-29 (colorectal cancer) and the multidrug-resistant cell line KB-V1/Vbl (cervical cancer). This may be due to a slightly different mechanism of action, shown by an electrophoretic mobility shift assay (EMSA) where the *cis*-bis(NHC) complexes not only acted like **1** by unwinding the DNA but also resulted in the aggregation of DNA strings.^[89]

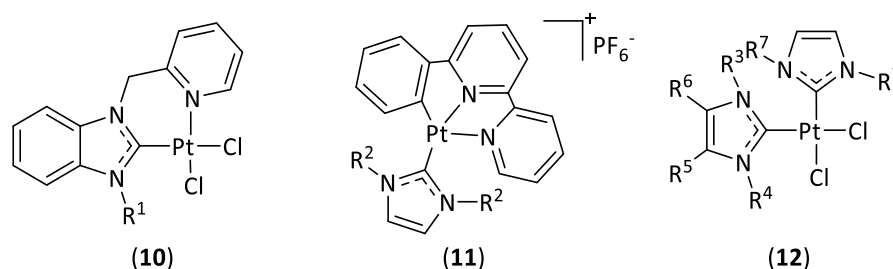


Figure 5. Chemical structures of anti-tumoural mixed NHC-amine or (NHC)₂ Pt(II) complexes. R¹ = Me, Bn; R² = Me, Et, Pr, Bu; R³ = Me, CH₂Ar; R⁴ = Me, CH₂Ar; R⁵ = H, 4-OMePh; R⁶ = H, 3,4,5-OMePh; R⁷ = CH₂Ar.

1.2.5 Alternative geometry

Another way, besides ligand exchange, to circumvent cisplatin (**1**) resistance is to choose different complex geometries. Even though research regarding transplatin (**13**) analogues was initially neglected due to the ineffectiveness of the lead compound^[38], in 1989, FARRELL *et al.* discovered that, due to ligand exchange, *trans*-Pt^{II} complexes could indeed be effective anti-tumoural agents.^[95] Their *trans*-[Cl₂(amine)₂]Pt^{II} complexes (**14**), with the amine being either pyridine or picoline, proved to be more cytotoxic against leukaemia cells than their *cis*-configured counterparts or **1**, leading to a growing interest in transplatin derivatives. NATILE *et al.*, for example, investigated three isomers of methyl acetimidates complexed in *trans*-position with Pt^{II}Cl₂ **15** and discovered that in comparison to their *cis*-configured analogues, an increased efficacy could be observed. Moreover, the *EE*-complex displayed cytotoxicity against leukaemia cells comparable with that of **1**. The *in vivo* effects observed in cisplatin (**1**)-resistant P388 (leukaemia) tumour-bearing mice were significantly higher than those of the corresponding *cis* complexes.^[96] The complexes of REEDIJK *et al.* published in 2006, bearing an isopropyl amine ligand and a variable azole **16** (Figure 6), revealed anti-tumoural effects as well, displaying low

micromolar IC_{50} values against various human cancer cell lines. In addition, increased cytotoxicity against cisplatin (**1**)-resistant cell lines was observed.^[97]

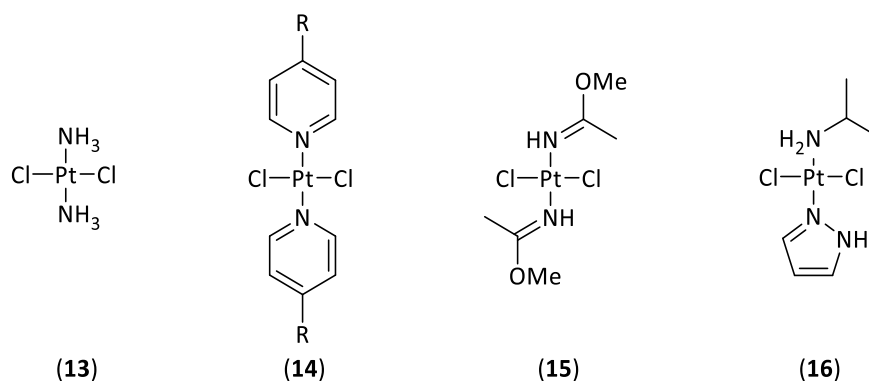


Figure 6 Chemical structures of anti-tumoural *trans* Pt(II) complexes. R = H, Me.

The mechanism of action of *trans*-Pt^{II} complexes differs from **1** because their geometry does not allow for 1,2-intrastrand crosslinks, accounting for the main cytotoxicity of platinum complexes. Transplatin mainly induces the formation of mono-adducts or interstrand crosslinks, which do not influence the DNA's structure. Furthermore, these adducts are repaired quickly and are hardly recognisable by the high mobility group (HMG) proteins that initiate apoptosis. In addition, transplatin appears more reactive than **1**, leading to increased deactivation before reaching the site of action.^[98-100]

To avoid this obstacle, transplatin complexes can be modified with NHC ligands. In 2010, MARINETTI *et al.* first presented mixed amine-NHC *trans*-Platinum complexes with varying N-substituents and different amines. The exemplary complex **17** of this library is drawn below (Figure 7). Their Pt^{II} diiodo complexes displayed IC_{50} values in the low single-digit micromolar range against cisplatin (**1**)-sensitive cell lines, e. g. CEM (leukaemia) and H460 (lung cancer) but also against cisplatin (**1**)-resistant cell lines SKOV-3 and A278 (ovarian cancer).^[101]

In 2012, BELLEMIN-LAPONNAZ *et al.* built on this idea further and developed a series of mixed *trans* NHC-amine Pt^{II} complexes, the amine being an amino acid or a small peptide. One example with proline as a ligand **18** is shown below. The ligands' hydrogen bond acceptors and -donors, forming dimers as shown in an exemplary crystal structure of the tripeptide val-phe-Gly bearing Pt^{II}₂ complex, lead to better bioavailability. The complexes evaluated proved significantly more cytotoxic against various human cancer cell lines, including the cisplatin (**1**)-resistant SKOV-3 ovarian cancer cell line. However, the IC_{50} values of the compounds evaluated were also in the

nanomolar range against the healthy cell line MRC5 (foetus lung cells), implementing a significant burden for healthy tissue *in vivo*.^[102]

Recently, our group published the synthesis and evaluation of mixed NHC-amine complexes **19** and *trans*-bis NHC complexes **20** with varying N-substituents. Two examples of this library are shown below. The bis-NHC complexes **20** showed moderate activity against several human cancer cell lines with two-digit micromolar IC_{50} values even against the cisplatin (**1**)-resistant HT-29 cells while being ineffective against the multidrug-resistant KB-V1/Vbl cells. Yet, the complexes were, albeit to a lesser extent, active against non-malignant human colon fibroblasts (CCD18Co). The picoline-bearing *trans* complex **19** was active in the single-digit μM range against the same cell lines as the former but lacked efficiency against HT-29 cells. Yet, it showed no activity against healthy cells. Neither of the *trans* complexes showed any effect on the EMSA tests, contributing to the assumption that the mechanism of action differs from its *cis* congeners.^[103] Nevertheless, some research still needs to be done to fully elucidate the potential of *trans*-Platinum complexes.

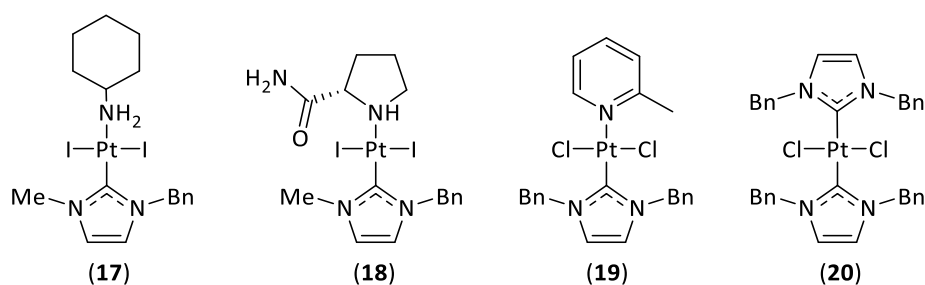


Figure 7. Chemical structures of anti-tumoural mixed NHC-amine or $(\text{NHC})_2$ *trans* Pt(II) complexes.

1.3 Transitioning to other transition metal complexes

1.3.1 Advanced and promising Ru, Cu and Fe complexes

Cisplatin's (1) resounding success, accompanied by gradually elucidating its mechanism of action, manifested rules for research about what properties a complex must have to be an effective anti-cancer agent. Many subsequent complexes, e. g. the next generation of platinum drugs, adhere to this and vary only marginally in their structure from the lead compound. This bias may be the reason why no non-platinum complex has yet made it to FDA-approved use in cancer therapy.^[104] Nevertheless, research into organometallic complexes using different transition metals (e.g. Ru, Cu, Fe, Pd) is ongoing.

These metallodrugs share the same characteristics, albeit in different forms or dimensions. Depending on the coordination number, unique geometries can be achieved, influencing the pharmacokinetics of the complexes. Furthermore, the oxidative states of the central atom can change during *in vivo* redox reactions, transforming the complexes into their biologically active forms after reaching the target, consequently increasing selectivity. Complexes can be designed to be either negatively charged, neutral or positively charged to determine their site of action.^[105-109] The LEWIS acidic character of the metal also polarises the ligands and contributes to their exchange by hydrolysis, which can be a desired effect, e. g., in biocatalytic processes.^[110]

This large variability in organometallic complexes allows fine-tuning of the compounds' final properties. ALESSIO *et al.* described five categories of medically relevant metal complexes. The first category comprises functional complexes forming covalent bonds (mostly with DNA). That includes the FDA-approved platinum complexes. Categories 2 and 3 fall into the metal-drug synergism principle, which is described in more detail in the following chapter. Here, either the structural fixation can cause or improve the biological effect, or the inertness of the central metal can serve as a delivery system of the active ligand. In category four, the redox potential of the metal can serve as a catalyst for mitochondrial processes, e.g. generating ROS. A few examples of these categories are discussed below. Lastly, the fifth category represents organometallic complexes which act as a photosensitiser.^[111]

Fast ligand exchange kinetics are widely seen as a disadvantage of organometallic complexes. Therefore, efforts are made to avoid these instabilities. As ruthenium complexes exhibit the most similar ligand exchange kinetics as Pt^{II}, several approaches were reported in the literature dealing with their optimisation. Compared to other transition metal complexes, ligand exchange kinetics

for Ru^{II} and Pt^{II} complexes are in minutes to days ratio rather than microseconds, thereby mimicking the lifespan of a cell.^[112] There may be less overall cytotoxicity towards cancer cells of ruthenium complexes compared to platinum drugs regarding *IC*₅₀ values. However, toxicity was also observed to be reduced for ruthenium compounds.^[113]

Ruthenium can mimic iron as both belong to the eighth group of the periodic table, and thus is bound and transported via albumin and transferrin proteins in the serum. At first, this mechanism of action might seem detrimental to the metaldrug's pharmacokinetics, but it is, in fact, beneficial for incorporating the metal compounds into cancer cells. Those proteins are overexpressed on a cancer cell's surface resulting in a 2- to 12-fold higher concentration of ruthenium in cancer cells depending on the cell line.^[114, 115] Ru^{III} complexes are also considered prodrugs that only transform into their active Ru^{II} form in the hypoxic and, thus, reductive TME.^[116] In contrast to cisplatin (**1**), DNA is not the primary target of Ru complexes attributing to their higher selectivity. Instead, inhibition of the binding immunoglobulin protein (BiP) displays as the mechanism of action. This protein is a chaperon of the ER overexpressed in cancer cells directly resulting from the unfolded proteins response (UPR) caused by the tumours' higher proliferation rate.^[117] Furthermore, the generation of ROS by Ru^{II} complexes was observed, leading to apoptosis via the mitochondrial dysfunction pathway.^[118]

However, of the large number of developed complexes, only four have advanced to clinical trials so far. N-heterocycle-bearing *trans* Ru^{III} tetrachlorido complexes NAMI-A (**21**) and KP1019 (**22**), shown below in Figure 8, proved especially convincing. The former complex led to slower tumour progression in 19 patients. One patient with metastatic NSCLC displayed a stable disease for 21 weeks.^[119] Even though the poor solubility of **22** led to significant limitations in infusion volumes, disease stabilisation was observed for five out of six patients at low dosages in first clinical trials. Furthermore, no observable DLTs were detected.^[120] Resulting from those promising findings, a phase II study of **22** and its sodium salt NKP1339 as new clinical candidates are currently planned.

Besides Ru^{II}, complexes with iron as the metal centre can be used as anti-cancer agents. Since iron is ubiquitous in the human body's biological processes, including electron transport, DNA synthesis and oxygen transport via heme metalloproteins, it is easily tolerated.^[121] Malignant cells, however, display a phenotype not yet fully elucidated referred to as "iron addiction", where the otherwise tightly regulated iron metabolism is distorted by overexpression of uptake genes, a lack of storage proteins, e. g. ferritin or resistance to ferroptosis.^[122] This combination eventually leads to a higher percentage of physiological, divalent iron present in its loosely bound form in the cytosol, where it catalyses FENTON-type reactions, ultimately leading to DNA mutations.^[123, 124]

The first iron complexes with anti-cancer properties reported back in 1984 were ferrocenium ions with picrate or trichloroacetate counter anions **23**. An example is shown in Figure 8. Their mode of action was attributed to the generation of ROS.^[125] Since then, a broad range of ferrocenyl derivatives with varying substituents on one or both cyclopentadienyl rings, polypyridyl iron complexes or salophen iron complexes were investigated preclinically. Nevertheless, to date, not a single iron complex has advanced into clinical trials for cancer therapy.^[126, 127] Metallocenes or half sandwich complexes became a prominent vehicle for delivering metallodrugs over time. Especially promising from this consideration arose Ru-arene complexes^[118], zirconocenes,^[128] titanocenes^[129], cobaltocenes^[130] and many more.^[131]

Another micronutrient metal whose natural abundance in cellular processes can be exploited is copper.^[121] Since copper plays an essential role in angiogenesis and proliferation, it is no surprise that cancer cells display elevated concentrations of copper.^[132] Copper-mediated cancer therapy can be divided into three distinct mechanisms. The first cannot be classified as metal-based chemotherapy because it is aimed at lowering the cellular copper level by chelating compounds to such an extent that angiogenesis and tumour growth is prevented.^[133] The second, however, is the classical approach with Cu^{I-III} complexes designed to target one or more cancer-specific sites of action. This ranges from the generation of ROS to interaction with DNA to the almost unique properties of copper complexes to act as topoisomerase inhibitors.^[134] An example of a copper complex acting as such is shown below in the form of Top I inhibitor Oxindolimine-copper(II) (**24**).^[135] Yet, only a handful progressed into clinical trials.^[136]

The focus of copper-based cancer research is currently shifting towards radiopharmaceuticals, which displays the third mechanism of action. For example, the positron-emitting ⁶⁴Cu^{II}(atsm) complex used as a hypoxia marker is presently tested in several clinical trials.^[137] Furthermore, this field of research can also be applied to almost all radioactive transition metal isotopes, which are mainly complexed by chelating agents bound to targeting moieties. Radioligand therapy, specifically addressing cancer cells, further emphasises the usefulness of transition metals.^[138]

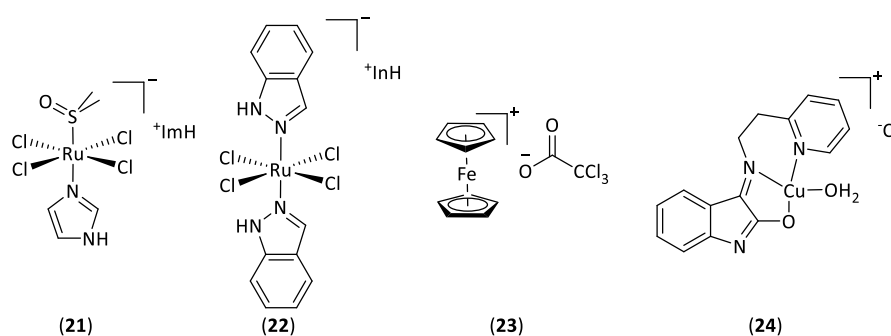


Figure 8. Chemical structures of anti-tumoural active organometallic complexes with non-Platinum transitional metals.

1.3.2 Palladium complexes

Another transition metal well-studied for its anti-cancer properties is palladium. Of all other transition metals used for chemotherapeutic research, it displays the highest similarity to platinum, such as coordination number and geometry. Palladium's cheaper production and higher water solubility are advantageous compared to platinum.^[139] The ligand exchange kinetics, however, are significantly accelerated for palladium complexes. Hence, particular ligands are required to avoid the formation of reactive species.^[140] Many such palladium compounds, mainly with NHC ligands, have been established addressing DNA or, to a lesser extent, other cellular targets.^[141]

In 2007 GOSH *et al.* pioneered synthesising the first acyclic and asymmetric *trans* bis(NHC) Pd^{II} dichlorido complex **25** shown below. The compound displayed sub-micromolar *IC*₅₀ values against several human cancer cell lines, e. g. HeLa, HCT116, and MCF-7, which were a magnitude lower compared to cisplatin's (**1**) values. Upon treatment with **25**, a cell cycle arrest in the G2-M transition phase was observed, preventing the cells from entering mitosis.^[142] Furthermore, elevated levels of p53 were detected, indicating that the cell cycle arrest activates the p53 pathway.^[143] The latter may sound counterintuitive at first since *trans* platinum complexes differ in their mode of action compared to their *cis* congeners, suggesting that palladium may indeed behave slightly differently.

Further and more recent research into palladium organometallic complexes and their mechanisms of action was conducted by VISENTIN *et al.* In 2019, they created a library of 14 tetraacetatecyclopentadienyl palladium complexes with different spectating ligands such as phosphanes, N-heterocycles bound via nitrogen or sulphur atoms, or NHCs. The most promising complexes identified within this series were the chelating imidazolium NHC-bearing complexes **26**, shown in Figure 9. Stability studies of these compounds in D₂O with an excess of glutathione revealed that the chelating NHC-bearing complexes did not undergo ligand exchange reactions under pseudo-physiological conditions. Furthermore, the palladium compounds **26** showed cytotoxicity against several human cancer cell lines, including the cisplatin (**1**)-resistant A2780cis cell line, in the two-digit nanomolar range while being inactive against healthy fibroblasts in contrast to **1**. However, no effect was observed on the cell lines A549 (lung cancer) and DLD1 (colon cancer).^[139] Biological studies further showed that the complex arrests cells in the sub-G1 phase and activates the caspase 3/7 cascade responsible for apoptosis similar to **1**.^[144]

VISENTIN's group further enhanced the potency of palladium complexes by generating another series of organometallic compounds in 2020. Within this series, an allylic chelator, a benzimidazolium NHC, and a phosphane ligand were complexed in a square planar fashion. The latter's stability was proven crucial for the complex's selectivity towards cancer cells. PPh₃ tends to dissociate and form its corresponding oxide, leading to increased cytotoxicity but a complete loss of selectivity. PTA, as the phosphane ligand shown below, on the other hand, has been proven to be stable even in the presence of glutathione.

Complex **27**, shown as an example for this library in Figure 9, displayed a cytotoxicity towards human cancer cell lines, including cisplatin-resistant ones, with up to two-digit nanomolar *IC*₅₀ values while being inactive against fibroblasts. Further *ex vivo* studies were performed, comparing the toxicity against liver organoids of **27** with that of **1**. Even though the *IC*₅₀ values of **27** were 100-fold higher, they were found to be in a considerable single-digit micromolar range. More in-depth mechanistic studies revealed that the mitochondria are the primary target of those palladium complexes, and the allyl ligands mainly influence their mode of action. The authors propose a TSUJI-TROST type allylation of the targeted biomolecule. The PTA ligand and the methyl group stabilise the allyl moiety to reach the target unaltered, while the CF₃ group favours the nucleophilic attack.^[145]

CHE *et al.* reported another approach for developing palladium-based chemotherapeutic agents via the incorporation of pincer-type cyclometalated complexes **28** into the field of palladium chemistry in 2016. Compared to their platinum analogues **11**, changing the central metal atom led to significantly altered anti-cancer properties and modes of action. Besides sub-micromolar *IC*₅₀ values towards human cancer cell lines, including cisplatin (**1**)-resistant cell lines, activity against fibroblast cells in the two-digit μM range was observed. Furthermore, stability studies revealed promising results in the presence of glutathione, ascorbic acid, and cell medium. Further experiments concerning the mechanism of action of those compounds elucidated that mitochondrial depolarisation is the main reason for the induced apoptosis. At the same time, cell growth inhibition is caused by addressing the epidermal growth factor receptor (EGFR) pathway. Further anti-angiogenic assays confirmed the latter. *In vivo* studies in NCI-H460 tumour-bearing mice revealed a dose-dependent tumour growth inhibition of up to 61% without observable toxicities or body weight loss.^[146]

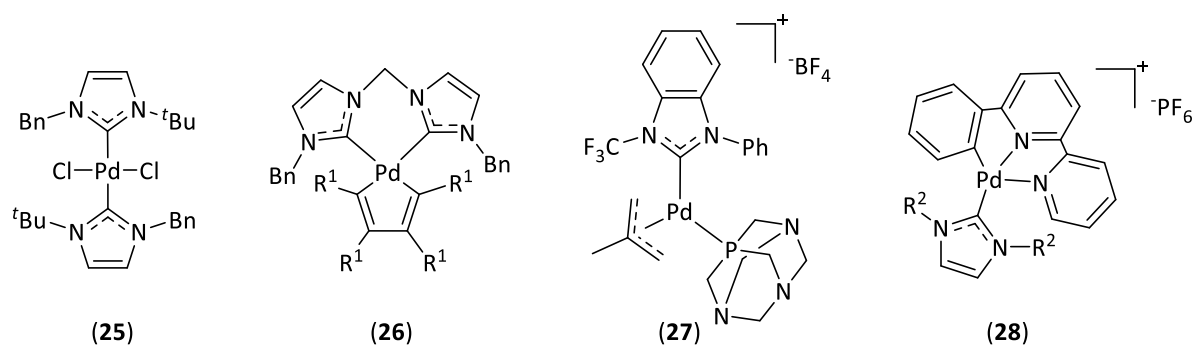


Figure 9. Chemical structures of anti-tumoural active palladium complexes. R¹ = COOMe; R² = Me, Et, Pr, Bu.

In summary, a broad range of palladium organometallic complexes has been synthesised and evaluated. Their potency, as well as their mechanisms of action, strongly depend on geometry and choice of ligands. *In vitro*, *ex-* and *in vivo* studies brought forward promising candidates with mechanisms of action differing from cisplatin (**1**). Yet, no palladium-containing compound, except ¹⁰³Pd seeds for brachytherapy, has so far advanced into clinical trials.^[147]

1.3.3 Chrysotherapy

Chrysotherapy, by definition, describes the use of gold in medicine and dates back thousands of years to the alchemists of ancient Greece, China and Arabia.^[148-150] However, a targeted approach was first documented in 1972. Auranofin (**29**) (Figure 10) is one of three FDA-approved gold complexes and the only one still in clinical use. It was initially intended as a treatment for rheumatoid arthritis^[151], though its off-label use as an anti-neoplastic agent was recognised early on and has since been researched excessively.^[152] Mainly due to the entirely different mechanism of action of gold(I) complexes compared to cisplatin (**1**) and its analogues, they seem up-and-coming candidates for metal drugs in cancer therapy. The unique mechanism of action of **29** and its congeners, addressing the mitochondrial thioredoxin system in general and TrxR in particular, has increased interest in these compounds.^[153] TrxR plays a crucial role in proliferation, reduces disulphide bridges to modify protein structures and averts DNA damage caused by oxidative stress through its reductive character in an NADPH-dependent manner.^[154] Given the higher metabolism of cancer cells, the enzyme is consequently overexpressed in many tumours, as their adaptive antioxidant nature ensures their survival, promotes proliferation and eventually leads to migration.^[155] In the course of xenograft studies with mice inoculated with Trx-deficient MCF-7 (breast cancer) cells, there was hardly any growth of the tumours and no metastases.^[156] Hence,

the overexpression of TrxR is associated with a poorer prognosis for patients with breast-, ovarian- or lung cancer, as rendered in exemplary *KAPLAN MEIER* survival plots.^[157]

Since gold(I) with its closed 5d¹⁰ shell is considered a soft cation according to the Hard and Soft Acids and Bases (HSAB) theory, it also tends to form bonds, in a linear geometry, with soft ligands such as cyanides, phosphanes but also thiols.^[158] The latter is crucial for one mechanism of action of gold-based chemotherapeutics, yet also inducing side reactions. Under physiological conditions, **29** undergoes ligand dissociation to a triethylphosphane-gold(I) cation or, in combination with subsequent hydrolysis, a thioglucose gold(I) species with a variable number of acetate groups still attached.^[159] Hence, the fragments form irreversible bonds with the cysteine or selenocysteine residues of enzymes via a three-coordinated gold(I) intermediate.^[160, 161] TrxR is a cysteine and selenocysteine-rich enzyme leading to **29** being able to bind irreversibly to its active sites, eventually inhibiting its function. As a result, the increased ROS levels in the cell lead to apoptosis.^[162]

Serum albumin (SA) is also a thiol-rich enzyme with a concentration of roughly 422 ± 52 µM in human blood. Its thiol groups are primarily present in their oxidised form as disulphide bridges.^[163] However, the one remaining reduced Cys-34 in SA is responsible for binding 80% of the gold compound in the blood.^[158] **29** forms gold(I)-SA adducts, which is why serum acts not only as a transporter but also as a scavenger for this type of drug. This is accompanied by a decreased cellular uptake resulting from the much lower rate at which the thiol proteins in the cell membrane can transfer the albumin-bound gold fragments into the cell.^[164] This is a potential explanation for **29** showing no effect in *in vivo* studies with P388-bearing mice after intravenous administration but only when administered intraperitoneally.^[165]

The *WARBURG* effect is the foundation of auranofin's (**29**) second mechanism of action. It describes the cancer cell's altered glucose metabolism. In this process, the glycolysis product pyruvate is reduced to lactate instead of being fed into the citrate cycle to generate acetyl-coenzyme A, suppressing catabolism and enhancing anabolism. However, instead of generating up to 36 molecules of adenosine triphosphate (ATP) through the complete oxidation of a glucose molecule, this anaerobic glycolysis only generates two molecules of ATP.^[166] Regardless of the oxygen concentration present, cancer cells prefer this metabolism pathway mainly because it is faster. At the same time, however, since this pathway is far less efficient, it ultimately leads to increased consumption and expression of the corresponding transporter enzymes, e. g., GLUT1, in the membrane.^[167, 168] This overexpressed enzyme on the surface of cancer cells can recognise the glucopyranose unit of **29**, acetylated fourfold or not, thus contributing to the selectivity of the

metallo-drug. Consequently, **29** and comparable gold complexes can inhibit various such glycolytic enzymes, which means that further ATP deficiency of the cancer cells leads to inhibition of their growth or apoptosis, respectively.^[169]

In vitro tests were carried out with comparable gold(I) phosphanes such as PEt_3AuCl , PEt_3AuBr or triethyl phosphane gold(I) complexes in combination with thiourea or thiocyanate thiols. These complexes exhibited similar IC_{50} values against various human cancer cell lines in the sub-micromolar range and thus revealed increased cytotoxicity compared to cisplatin (**1**). However, uptake into the cell and inhibitory activity against TrxR of the novel gold complexes differed significantly, which was explained by different characteristics, like steric and electronic properties and lipophilicity.^[170] These attributes can easily be fixed by using NHC as ligands.

The antiproliferative NHC-Au-SR complexes published by TACKE *et al.* in 2020 are examples of such compounds. 4,5-Diphenyl-1,3-dibenzyl imidazolium was chosen as NHC ligand in combination with varying sulphur-containing ligands, namely thiocyanide, dithiocarbamate or the auranofin motif tetra-O-acetyl-D-glucopyranosyl. Within this series, the gold(I) complex **30** shown in Figure 10 proved particularly potent with nanomolar GI_{50} values against OVCAR3 and NCI-H522 cell lines. The inhibition of mammalian TrxR with an IC_{50} value of $7.4 \pm 0.4 \mu\text{M}$ proved much lower than that of **29** ($IC_{50} = 0.09 \mu\text{M}$). Nevertheless, compound **30** achieved an optimal treatment-to-control coefficient of 0.44 after 16 days when administered intraperitoneally daily in PC3 tumour-bearing mice. In addition, immunohistochemistry demonstrated reduced levels of antigen Ki67, a proliferation protein. These studies also demonstrated the previously mentioned WARBURG effect by fitting the complex into the GLUT1 transporter.^[171]

In 2014, CASINI *et al.* studied Au(I) complexes bearing a coumarin substituent at one of the nitrogen atoms of the imidazolium ligand. They were able to gain insight into compounds' mechanism of action via fluorescence by confocal microscopy. However, moderate biological activity, low selectivity and a modest inhibitory effect against TrxR1 limit the clinical potential of these derivatives. Colocalisation with propidium iodide revealed that compound **31** accumulated mainly in the cell nuclei as expected for coumarin derivatives serving as a potential explanation for the relatively low anti-cancer activity.^[172]

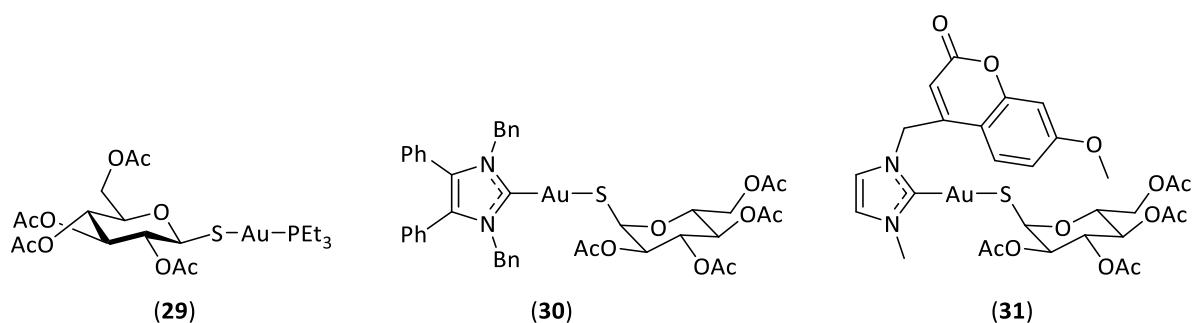


Figure 10. Chemical structures of auranofin (**29**) and NHC-bearing analogues thereof.

Even though these results were somewhat discouraging, they showed that the choice of the metal centre and ligand structure are crucial for enhancing the biological effect of chemotherapeutic agents. Studies by BAZZICALUPI *et al.* in 2020 further developed Au-NHC compounds using methylated caffeine ligands. Particularly the cationic bis-NHC Au(I) complex **32** was detected in cytoplasmic structures and the cells' nuclei.^[173]

As shown in some examples of platinum or ruthenium complexes in the previous chapters, the oxidation state of gold can also be altered to form stable Au(III) complexes. This is expected to increase the complexes' selectivity, as they are reduced in the hypoxic TME, where they locally exert their effect or that of their releasing ligands. It was assumed that, by using gold in the +III oxidation state and the resulting d_8 electron configuration of the gold atom, the complexes would display a similar mechanism of action to that of cisplatin (**1**). This was because Au(III) also forms square planar geometries and is, according to the HSAB principle, a hard cation preferably binding with hard anionic groups, for example, the nitrogen atoms of the DNA bases guanine and adenine. Indeed, those bindings have been proven for a few gold(III) complexes, but in a much weaker, and sometimes reversible, form compared with those formed with **1** which are irreversible.^[174, 175] In this oxidative state, gold displays an accelerated hydrolysis rate and redox potential compared to gold(I), calling its stability under physiological conditions into question. Consequently, strong donor ligands are needed to ensure the stability of Au(III)-compounds in serum. Upon reduction of the central metal atom, the unbound ligands can also unfold their biological effects.

In 2013, CHE *et al.*, for example, reported on cyclometallated NHC-Au(III) complexes **33** (Figure 11) with varying residues at the nitrogen atoms of the imidazolium ligand or using benzimidazoles instead of imidazoles in the chelating ligand pyridine. Within this study, all compounds evaluated proved stable in aqueous solutions. After the addition of GSH, a change in the $^1\text{H-NMR}$ spectrum was observed as an NHC-Au(I)-GSH species was formed. This observation was accompanied by a difference in the complexes' UV/VIS spectrum because the fluorescence of the chelating ligand

2,6-bis(imidazol-2-yl)pyridine in bound form is quenched by the low $5d_{x^2-y^2}$ orbital. Since this change can only be detected after ligand dissociation, it was used to demonstrate the subcellular accumulation of **33** in living HeLa cancer cells. Emission of the free ligand was detected in the mitochondria, indicating a reduction of **33** without prior side reactions. In addition, IC_{50} values against various human cancer cell lines in the low single-digit micromolar range were achieved, displaying higher biological effectiveness compared to **1** and **29**. By lengthening the alkyl chains at the nitrogen atoms, a direct correlation between cytotoxicity and lipophilicity was established as the overall cytotoxicity of the complexes increased. Further *in vivo* studies revealed that when administered intratumorally, **33** reduced the growth of HeLa tumours in mice by up to 76%.^[176]

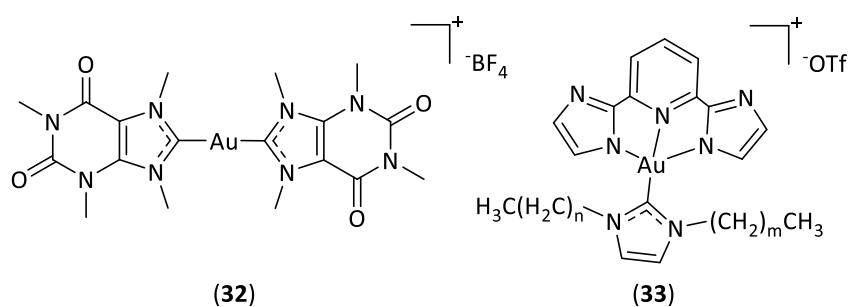


Figure 11. Chemical structures of NHC gold(I) and gold(III) complexes with ligands who displayed an intriguing mode of action $n = 0, 3, 5$; $m = 0, 3, 5, 7, 9, 15$.

The anti-tumoural gold complexes in this chapter vary significantly from one another. Not only because of the central metal being either Au(I) or Au(III) but also because of the corresponding ligands. This then results in the most diverse mechanisms of action, which lead to apoptosis of cancer cells. Consequently, the relatively young area of gold-based anti-cancer agents warrants further scientific exploration to generate a lead structure. The best-known auranofin (**29**), which continues to be used as a comparator for research, is currently part of clinical trials for the therapy of several types of cancer.

1.4 Metal Drug Synergism

1.4.1 Complexes with biologically active ligands

As ALESSIO has noted in his perspective, the synthesis of anti-tumoural metal complexes still relies on random hits as part of the "carpet-bombing" strategy. This is partly because of the challenging syntheses of metal complexes based on lead structures. In addition, minor structural changes can significantly impact the overall pharmacokinetic significantly.^[111] However, one approach to achieve targeted applications is using biologically active ligands for metal complexation.

Fixating the ligand structure via complexation with a metal atom stabilises different ligand configurations. This process changes the ligand electronically and sterically, which influences the overall lipophilicity and, thus, the pharmacokinetics of the final complex. This, in turn, alters the ligand's biological effect. Complexation also adds a third dimension to sometimes planar molecules that can facilitate binding into the corresponding pocket of the biotarget. Essential requirements for this approach are an inert metal centre and the ligand is not bound via a functional group crucial for its potency. A more reactive metal centre, e.g. Pt(IV), Au(III) or Ru(III), could also enhance the ligand's efficiency via a selective delivery, as a reduction in the hypoxic TME allows the ligands to be released directly at the site of action.^[111]

Below is a brief overview of metal complexes that combine one or more aspects of metal-drug synergism and a suggested categorisation. One example of metal-drug synergism, reported by TIEKINK *et al.* in 1996, is a series of complexes containing antimetabolites as ligands. Their mechanism of action has yet to be fully elucidated. However, their complexation to form the trialkyl thiopurine gold(I) complexes **34** and **35** most likely contributes to stability. These complexes combine the AuPR₃ motif of auranofin (**29**), which already displays anti-tumoural properties, with the thiopurines 6-MP and 6-TG, known and used clinically for their antimetabolic characteristics.^[26] These antimetabolites' mechanism of action relies on both representatives being antimetabolic prodrugs that are converted into the corresponding thioguanine nucleotides in the purine salvage pathway (PSP) and consequently being incorporated into the RNA or DNA structure to induce apoptosis through the MMR system. However, the metabolism of **34** and **35** via methylation of the thiol by S-methyltransferase renders the compounds unable to pass through the PSP, thus deactivating the prodrugs. By complexing the thiopurines, they are no longer accessible to enzymatic degradation and can undergo metabolism to yield the corresponding DNA building blocks.^[177]

The complexes showed sub-micromolar IC_{50} values against various human cancer cell lines. Most importantly, they showed cytotoxicity against cell lines such as SKOV-3, against which the free purine bases have lost their effect.^[178, 179] *In vivo*, the representative $Ph_3PAu-6MP$ of this series has also been proven to be highly effective. After intraperitoneal administration of the complex in ADJ/PC6 tumour-bearing mice, tumour size was reduced by 60%. At the same time, the compound was less toxic than cisplatin (**1**).^[178]

The previously mentioned HSAB principle, in combination with the coordination number of gold(I), is the main reason for the selective formation of S-Au- PR_3 bonds. Complexes comprising purine ligands were developed with other central metals, such as ruthenium or platinum, forming chelating ligands with nitrogen atoms.^[180] Purines and nucleoside metal complexes can also be synthesised via a novel pathway. Their C8 atom can be selectively brominated, with subsequent oxidative addition of an M^0 complex forming the $M^{II}-Br$ nucleoside complex with correspondingly *trans*-positioned ligands, e. g., PPh_3 .

An example of such nucleoside complexes **36** is shown in Figure 12, published by PETRONILHO *et al.* Several alkene platinum and palladium complexes and corresponding cationic NHC complexes were evaluated in this study, showing almost complete inactivity against a healthy cell line. However, all compounds exhibited only moderate cytotoxicity against several human cancer cell lines, with values in the double-digit micromolar range.^[181] The mediocre effect of these complexes was explained by the fact that guanosine, as such, is a physiological building block of the RNA and not, per se, an anti-cancer ligand. The protecting acetyl groups still attached to the hydroxyl groups of the D-ribose moiety could also negatively impact the pharmacokinetics of the complex, i. e., lipophilicity. Hence, hydrolysis of the acetyl groups or utilising an unnatural nucleoside, for example, an L-ribose group, to activate the MMR system after incorporating the metabolite in the cells could enhance the efficacy of such complexes.

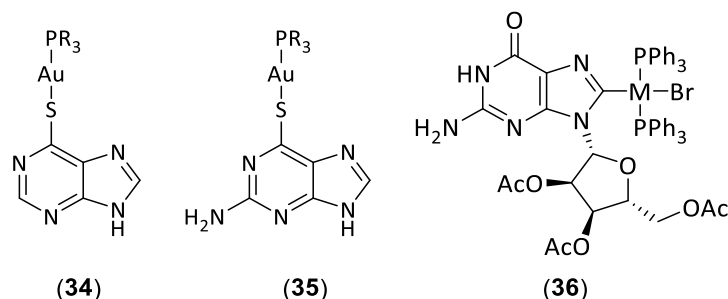


Figure 12. Metal complexes with purines and purine nucleoside ligands, respectively. R = Et, Cy, Ph; M = Pd, Pt.

Examples of both structural and delivering compounds evaluated in our group are complexes with biologically active Combretastatin A-4 (CA-4) (**37**) as ligand(s) shown in Figure 13. CA-4 belongs to a group of *cis*-stilbenes isolated from the South African bushwillow tree *Combretum Caffrum*, which revealed intriguing anti-tumour properties. The mechanism of action is based on an anti-vascular pathway activated by the inhibition of tubulin polymerisation.^[182] The 3,4,5-trimethoxyphenyl moiety of CA-4 is structurally similar to other mitotic inhibitors such as colchicine. Therefore, it fits into the colchicine binding pocket. The selectivity of these anti-cancer agents is based on differences between the neovascular system of cancer cells and that of healthy cells. For instance, the formation of the neovascular system in cancer cells is accelerated through the overexpression of corresponding signal molecules, such as the vascular endothelial growth factor receptor (VEGF).^[183] In addition, an increased sensitivity of the neovascular system is assumed, making it more vulnerable to small molecules such as CA-4.^[184]

One major disadvantage of CA-4 is its very low solubility in water. Yet, hydrophilicity was improved by phosphorylation of the free hydroxy group. The resulting prodrug fosbretabulin was found to be equally effective and is currently undergoing several phase II/III clinical trials.^[185] The second main drawback of CA-4 is the tendency to isomerise the double bond with the steric hindrance of the two aromatics favouring the thermodynamically more stable *trans* form. This stereoisomer showed no anti-tumoural effect.^[186]

Synthesising such compounds typically includes a WITTIG reaction that yields the 1,2-diarylethene in an *E/Z* mixture. The alternative PERKIN reaction requires decarboxylation under high temperatures. Both synthesis routes are unsuitable for obtaining CA-4-derived substances in good yields and high purities. The remedy is the synthesis of 4,5-diarylimidazoles which can be conducted under mild conditions as described previously.^[184] This simultaneously fixes the *Z*-configuration and increases the water solubility. In addition, imidazole heterocycles can be transformed into NHCs in a one-step reaction.

An extensive SAR study with corresponding methylated imidazole analogues **38** with varying substituents at one or both aryl rings of **37** has been reported by our group. Those compounds demonstrated similar cytotoxicity compared to the lead structure against various human cancer cell lines. In addition, activity against the CA-4-resistant HT-29 cell line was observed. The results of the *in vivo* studies conducted on 1411HP-bearing mice were what made these findings particularly interesting. When administered intratumorally, swelling and haemorrhage of the tumour due to the anti-vascular effect were observed, accompanied by a decrease in tumour size.

However, sometimes several dosages over a certain period were required to observe the impact.^[187]

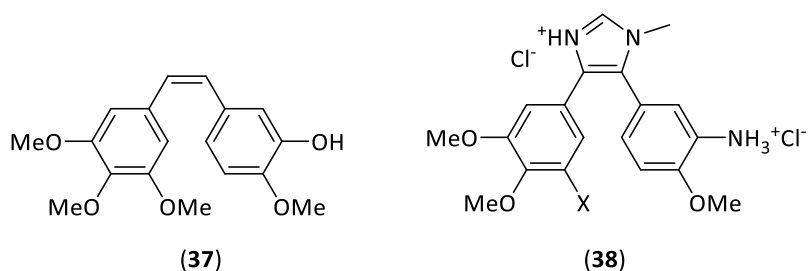


Figure 13. Chemical structures of CA-4 and an imidazolium analogue thereof. X = Cl, Br.

The usage of imidazolium analogues of CA-4 as NHC ligands led to enhanced anti-tumoural properties. As one example, the half-sandwich Ru(II) complexes **39** (Figure 14) revealed low single-digit micromolar IC_{50} values against the CA-4-resistant HT-29 cell line. As a potential mechanism of action, a strong influence on the actin and tubulin cytoskeleton and a strong anti-vascular effect was observed in chorioallantoic membrane (CAM) assays. Unlike CA-4, however, **39** was virtually inactive against the multidrug-resistant Kbv1 cells.^[188]

Within the series of NHC platinum complexes **12** mentioned in chapter 1.2.4, there was also a representative with an imidazolium NHC ligand derived from CA-4. Although the mechanism of action of this ligand was not investigated in detail at the time, it stood out in this SAR study because it exhibited exceptionally high cytotoxicities against CA-4-sensitive cell lines. Otherwise, it had a rather mediocre IC_{50} indicating a drug-related effect of this particular ligand.^[89]

In 2016, the group of WANG *et al.* evaluated various Pt(IV) prodrugs containing CA-4 ligands modified by a carboxylic acid group. They revealed cytotoxicity in the low single-digit micromolar range against different human cancer cell lines and, simultaneously, high double-digit levels against healthy lung cells. However, the inhibition of tubulin polymerisation was much weaker than the effect of CA-4, suggesting some pleiotropic mechanisms of action. The most active compound of this series, **40**, showed a substantial decrease in tumour growth in Hep-2G-bearing mice without reducing body weight.^[189]

The cationic bis-NHC Au(I) complexes **41** were the most potent complexes within the metal-complexed CA-4 analogues, displaying single-digit nanomolar IC_{50} values against all cancer cell lines tested. Yet, their mechanism of action deviated from CA-4 as the cell cycle was arrested in the G_1 instead of the G_2/M phase. In mice bearing B16-F10 tumours, after injection with **41** ($R^1 = OMe$, $R^2 = Et$), a significant decrease in tumour size was observed with slight or reversible

loss in body weight. Furthermore, the CAM assay supported the formation of new blood vessels after blood vessel destruction.^[190]

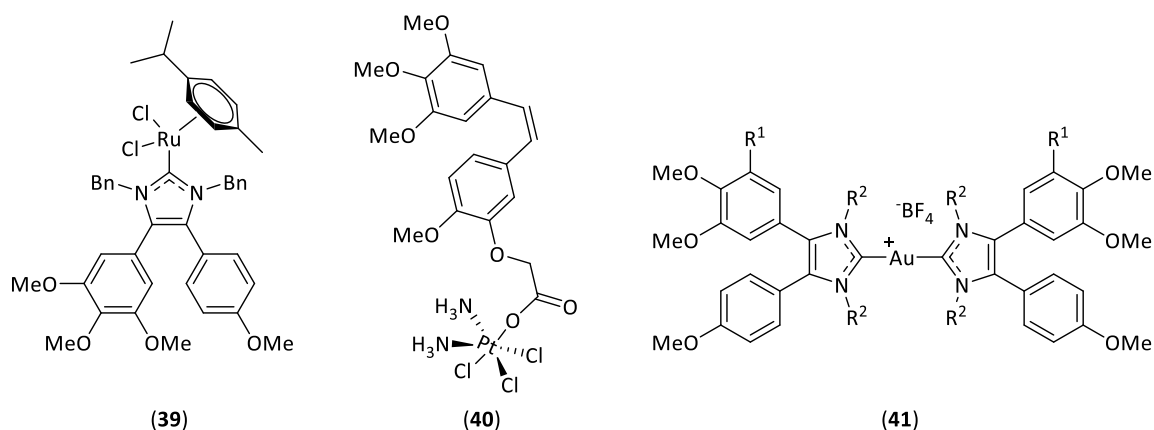


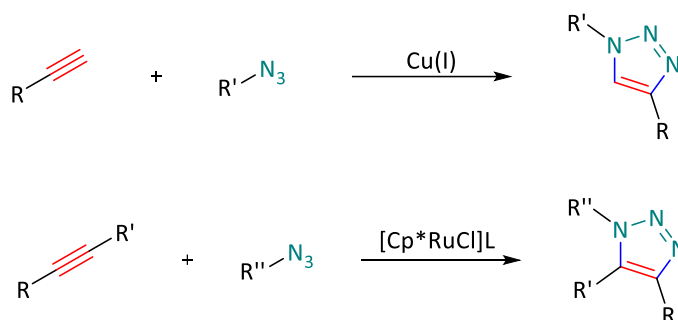
Figure 14. Chemical structures of CA-4 derived anti-tumoural Pt, Ru and Au complexes. R¹ = OMe, Cl, Br; R² = Me, Et.

1.4.2 Bioorthogonal chemistry

A rational approach to designing anti-tumoural metal complexes can be based on their underlying mechanisms of action. However, these are often only partially understood, even among the most widely researched representatives.^[111] A first clue for the mechanism of action is provided by localising the drug in the cancer cells' individual components. To date, there are three different approaches to determining the subcellular accumulation of complexes. The drug can be localised by determining the amount of metal in the individual cell components using ICP-MS. However, this method is very time-consuming.^[191] For the second approach, a fluorescing molecule is incorporated into the complex's structure, enabling the imaging of cells via confocal fluorescence microscopy. The cyclometalated complexes studied by CHE *et al.*, **11**, **28**, **33**, mentioned in the previous chapters, fall into this category.^[94] More recently, the boron dipyrromethene (BOPIDY)-bearing half-sandwich Ir, Rh and Ru complexes have been suggested by LEE *et al.* as potential counter stains for mitochondrial tracking as they, like the known Pt-BOPIDY complexes, accumulate in mitochondria.^[192] However, these molecules are usually large, aromatic substituents, e.g. anthracene, fluorescein^[193] or acridine^[194], which considerably influence the structure, lipophilicity and thus the pharmacokinetics of the drug. Therefore, comparability is debatable if such a fluorescent group is incorporated into the complex structure only to detect the active drug's subcellular accumulation.

The third and most effective approach is bioorthogonal chemistry, developed by BERTOZZI *et al.*^[195] It describes the reaction of two components under physiological conditions without disturbing

other cellular processes. The functionalities of the reactants must therefore react selectively with each other, creating a stable product without causing other effects in the cell. Ideally, the reaction is rapid and quantitative to prevent subsequent metabolism and excretion from living organisms.^[196] Reactions particularly suitable for this application fall under the terminology of click chemistry. The term was established by SHARPLESS *et al.* and describes reactions of two mostly small molecules with a large thermodynamic driving force that are insensitive to H₂O or O₂ and yield solely one product with high selectivity. The prototype of the Click reaction is the cycloaddition of an azide with a terminal alkyne under copper catalysis (CuAAC) to yield 1,4-triazole, shown in Scheme 3.^[197] It displays an improved variant of the HUISGEN version of the reaction, which does not require any catalyst present but high temperatures, restricting its applicability in cell organisms. However, SHARPLESS's version is limited to terminal alkynes and requires the cell toxin copper, preventing its usage in living organisms. In addition, orthogonality may no longer be given for some metals since especially d¹⁰ metals enter into reactions with terminal alkynes.^[198] The need for terminal alkynes could be circumvented via catalysis with half-sandwich ruthenium complexes, as they tolerate internal alkynes in [3+2] cycloaddition. Yet, the catalysts are unstable when moist, preventing their use as bioorthogonal markers.^[199]



Scheme 3. General reaction equation for Click Chemistry with internal or terminal alkynes with azides via Cu or Ru catalysis.

Nevertheless, once a terminal alkyne group is attached, the application of CuAAC reactions in *in vitro* studies with fixed cells is not hindered by those limitations. Furthermore, only minor structural changes occur via introducing an alkyne or azide into a compound structure to enable visualisation. Two examples of post-treatment functionalisation of metal complexes and their subcellular accumulation are shown in Figure 15. The top images display a platinum-acridine complex **42** that showed high cytotoxicity towards NSCLC. However, the fluorescence of the heterocycle is quenched by intercalation into the DNA, which is why an azide-bearing analogue was synthesised. Co-localisation with the nuclear stain Hoechst 33342 showed that the complex accumulates in the cells' nuclei, a result consistent with the high level of DNA adducts detected.^[200]

An example of an alkyne-bearing complex structure, described in 2020, is a *cis*-bis(NHC) complex with *p*-acetylene substituted benzyl residues at the nitrogen atoms **43**. Despite its structural similarity to cisplatin (**1**), this complex accumulated in the mitochondria as indicated by co-staining with Mitotracker™. Remarkably, this complex was much less cytotoxic against several human cancer cell lines than its analogue without the alkynes attached.^[90]

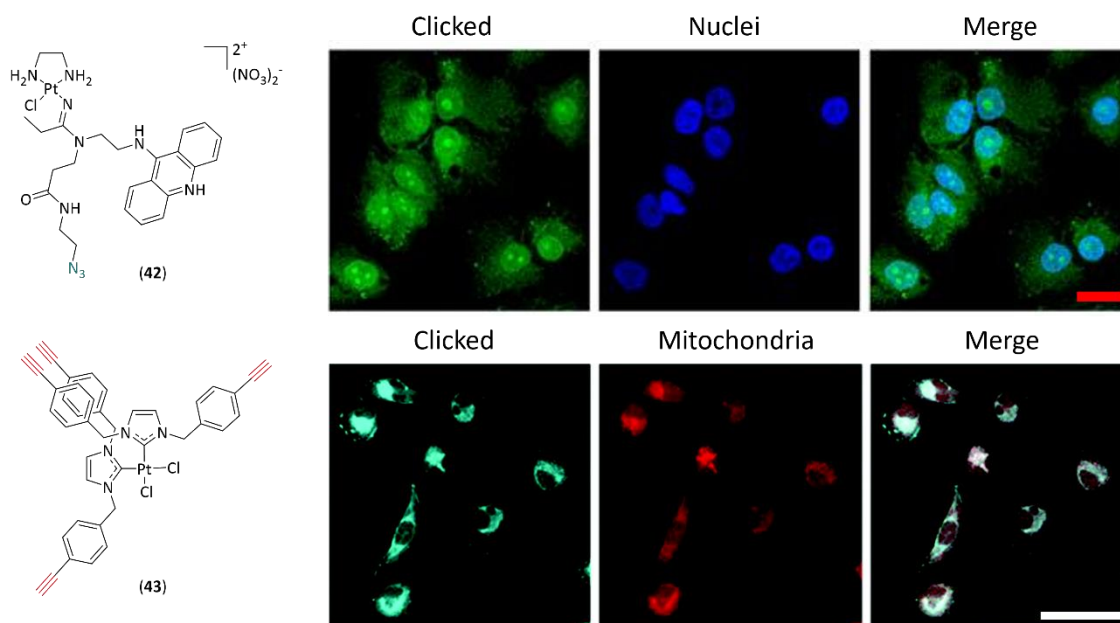
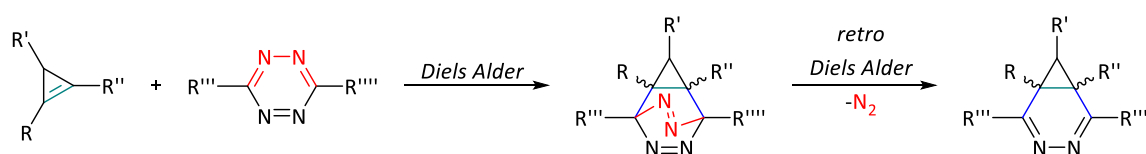


Figure 15. Examples of clickable functionalised Pt complexes and their subcellular localisation in fixed NCI-H460 lung cancer cells above or 518A2 melanoma cells below, respectively.^[90, 200] The red scale bar represents 10 μm , and the white scale bar represents 50 μm . Reprinted with permission from^[90, 200]. Copyright © John Wiley and Sons and Royal society of chemistry, respectively.

Cyclopropene is another small molecule which can facilitate click reactions, using a cascade of a DIELS ALDER reaction followed by a retro DIELS ALDER reaction (Scheme 4). Despite its tremendous amount of ring strain, metabolic stability can be expected due to the occurrence of cyclopropene units in natural products like fatty acids or sterols of marine invertebrates.^[201, 202] In this domino reaction, the ring strain relief represents the catalyst of the cascade reaction with inverse electron demand of 1,2,4,5-tetrazines. Consequently, it functions without adding the cytotoxin copper, making it applicable for localising compounds in living organisms.^[203]



Scheme 4. General equation of the reaction cascade of cyclopropene with tetrazine.

One natural substance bearing a cyclopropene unit is *cis*-configured sterculic acid (StA) (**44**). VAN KASTEREN *et al.* have recently exploited this small molecule's clickability and demonstrated the uptake of **44** in dendritic cells by visualising it through the click reaction with BODIPY-Tetrazines **45**. In this study, they compared the uptake of **44** in fixed cells with that in living cells (Figure 16). The bioorthogonality of the cyclopropene moiety was further demonstrated by localising co-incubated azides and alkynes, respectively, in subsequent CuAAC.^[204]

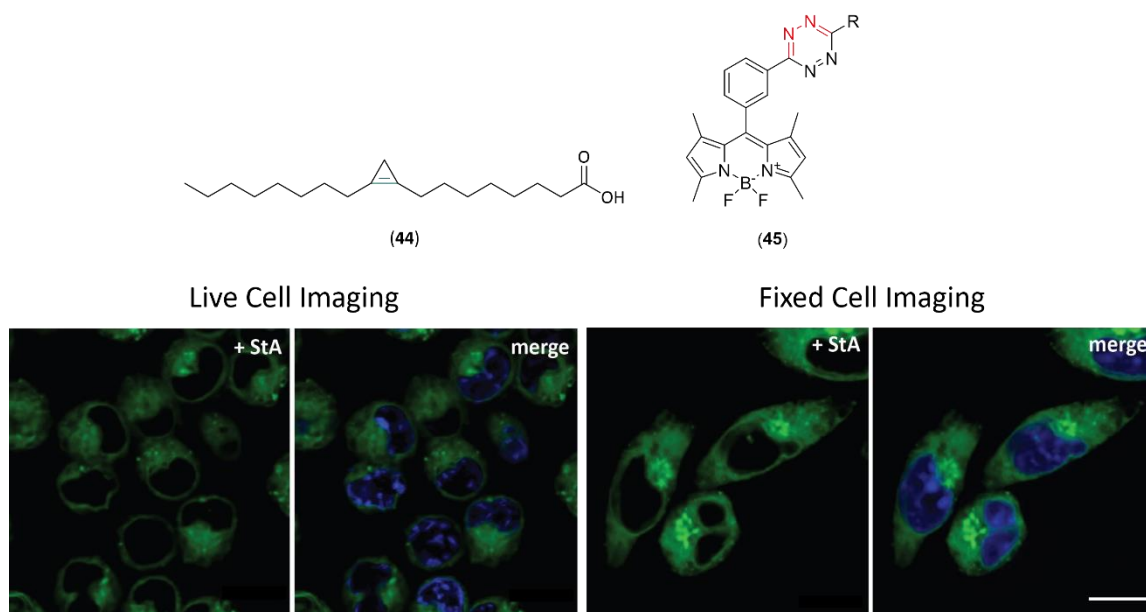


Figure 16. Sterculic acid (**44**) co-incubated with Hoechst33342 in live DC2.4 and fixed cells.^[204] The scale bar represents 10 μm . R = Me, pyridyl. Reprinted with permission from^[204]. Copyright © John Wiley and Sons

However, this strategy has not been applied to metal complexes in extant research. This thesis comprises publications exploring this promising field.

2 Synopsis

2.1 Objectives and overview of the subprojects

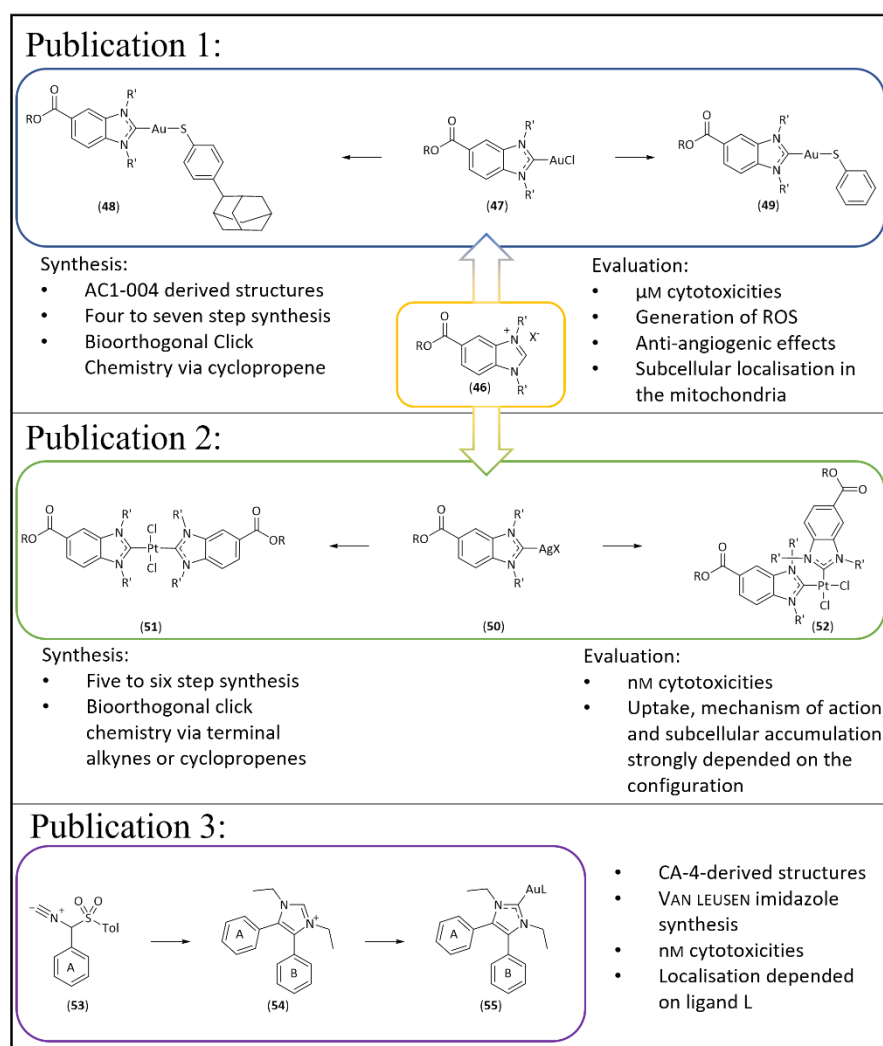
The present cumulative thesis comprises three publications listed in chapter 4. The aim of this work, in general, and of the individual papers in particular, was to synthesise pleiotropic or target-specific metal complexes that circumvent the disadvantages of the mainstay chemotherapeutic drug cisplatin (**1**) via their mechanism of action. The complexes synthesised were platinum and gold compounds containing NHC ligands derived from benzimidazole **46** with varying substituents (Scheme 5). The ligands were selected according to the principle of metal-drug synergism. Known biologically active substances were modified to bind to a central metal ion. Furthermore, these modifications were intended to improve the general cytotoxicity but also influence the pharmacokinetics of the original compound to achieve additional anti-tumoural effects. The mechanisms of action of these complexes were demonstrated by subcellular localisation of the compounds in cancer cells via bioorthogonal click chemistry. *In vitro* evaluation of the complexes synthesised was carried out in cooperation with the biochemists of the Chair of Organic Chemistry I of the University of Bayreuth.

The first project dealt with gold(I) complexes **48** and **49** carrying a benzimidazolium ligand (Scheme 5), which directly mimics one-half of the lead structure AC1-004 (Figure 17) and differs from it only in the N-substituents. The 4-adamant-1-yl phenyl methyl ether unit was replaced by 4-(adamantan-2-yl)benzenethiol, making use of the high aurophilicity of sulphur. A SAR was observed by different substituents of the nitrogen atoms of the NHC ligand and by the thiol ligand. The IC_{50} values of the complexes against eight human cancer cell lines were in the low single-digit micromolar range and were thus far better than the lead structure. Associated effects were mainly the generation of ROS but also anti-angiogenic effects. The subcellular localisation through bioorthogonal click chemistry of cyclopropene-bearing analogues also supported these findings as the complexes primarily accumulated in the cancer cells' mitochondria.

The second publication focused on synthesising and evaluating a small library of *trans*- and *cis*-[bis(5-alkoxycarbonyl-1,3-dialkyl-benzimidazol-2-ylidene)dichlorido]platinum(II) complexes **51** and **52**, respectively (Scheme 5). They were tested for their activity against eight human cancer cell lines and healthy fibroblasts to determine their selectivity. A few complexes emerged more active than **1** with low single-digit micromolar IC_{50} values. **51c**_(n=0) (Scheme 7), for example, even achieved nanomolar IC_{50} values against several cancer cell lines. The most active complexes were investigated for their mechanism of action in various biochemical assays, with DNA proving to be

the target of the *cis*-[Pt^{II}Cl₂(NHC)₂] complexes **52**, while the *trans*-[Pt^{II}Cl₂(NHC)₂] complexes induced apoptosis via a mitochondrial pathway. In addition, a synthetic route was developed for alkyne and cyclopropene-bearing ligands, whose complexes were used as probes for the subcellular accumulation of the respective series, again via biorthogonal click chemistry.

The third publication describes another example of metal-drug synergy. Here, the NHC ligands derived from CA-4 were obtained via VAN LEUSEN imidazole synthesis and, after N-alkylation, subsequently complexed to form Au(I) NHC complexes **55** with various second ligands L (Scheme 5). Namely, monomeric gold chloride complexes **59**, cationic bis-NHC complexes **60** or cationic phosphane complexes **61** (Scheme 8). The compounds reached two-digit nanomolar IC₅₀ values against various human cancer cell lines. The anthracene-bearing complexes **59-61b** addressed targets depending on the second ligand. In the case of the neutral gold chloride complex **59b**, the cells' nuclei were the target. The mitochondria were the place of action for the cationic PPh₃ bearing complex **61b**, and the dimer **60b** was found in the lysosomes.



Scheme 5. Overview of the publications discussed in this work.

2.2 NHC-Au-SR complexes derived from AC1-004 as potential HIF-Inhibitors

To selectively treat cancer, the corresponding drugs must address a tumour-only target. The Hallmarks of Cancer by HANAHAN *et al.* are an effective tool for identifying such potential targets. These hallmarks include (neo)vascularisation and altered metabolisms of cancer cells. Both directly result from the oxygen and nutrient undersupply tumours suffer from due to their excessive proliferation. The cancer cells thus switch to an anaerobic metabolism steered by the expression of transcription genes, e. g., HIF-1 α . The inhibition of which consequently represents an interesting and selective target. Adamantyl-bearing drugs, namely nicotinic or *iso*-nicotinic ester derivatives in general and AC1-004 (2-(4-adamantan-1-yl-phenoxy)methyl)-1H-benzimidazole-5-carboxylate) in particular were proven to be especially potent inhibitors of this transcription factor. The structure of AC1-004 can be easily adjusted to function as a ligand to form gold(I) complexes. Its benzimidazole moiety can be turned into an NHC ligand via N-alkylation, while its 4-adamant-1-yl phenyl methyl ether can be replaced by a 4-(adamantan-2-yl)benzenethiol ligand to exploit the high aurophilicity of the chalcogen sulphur. This NHC-Au-SR moiety should thus mimic the lead structure while enhancing its anti-tumoural activity through further accompanying effects, namely the generation of ROS, TrxR inhibition and anti-angiogenic effects.

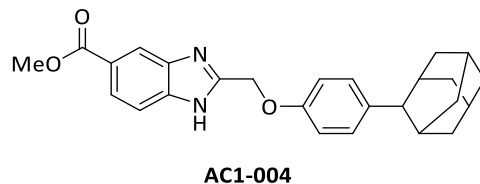
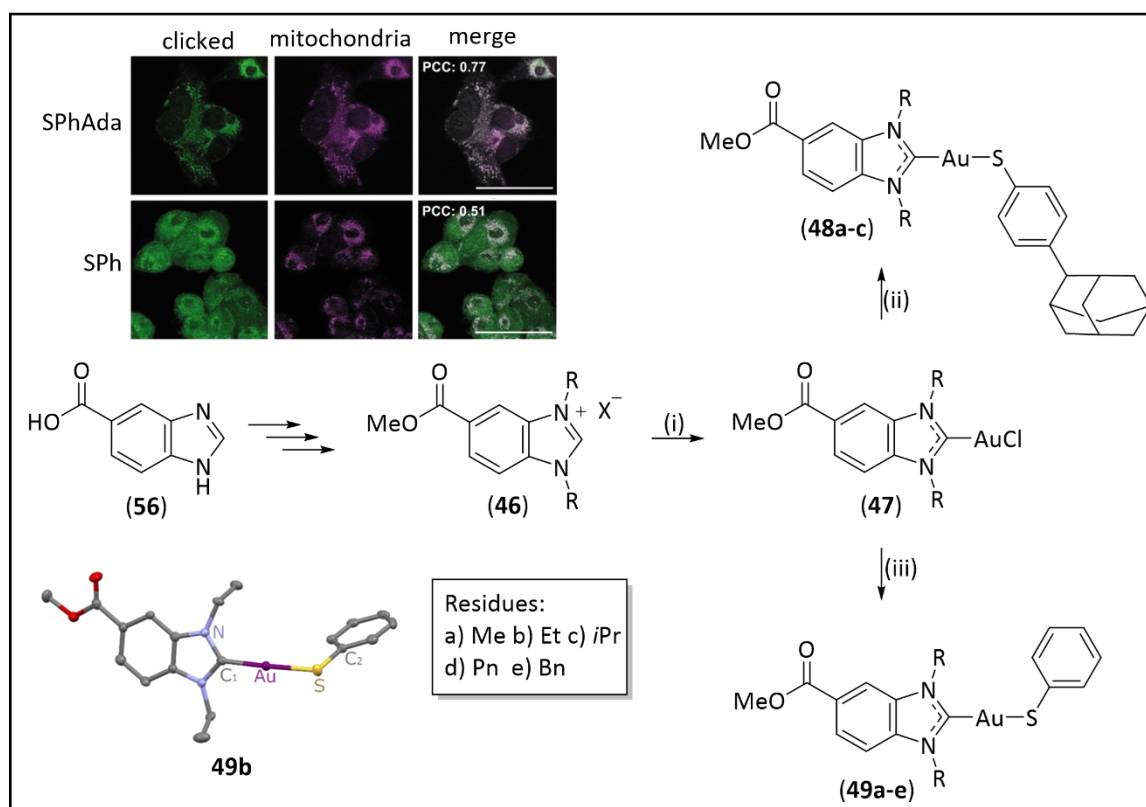


Figure 17. Chemical structure of AC1-004.

The novel 4-(adamantan-2-yl)benzenethiol ligand was synthesised starting from benzene which could be selectively monoalkylated with 2-bromoadamante in a FRIEDEL-CRAFTS reaction yielding 4-(adamantan-2-yl)benzene in 84%. A chlorosulfination in *para*-position with 98% yield followed by a reduction with zinc to the corresponding thiol in 46% yield were successfully conducted. The benzimidazolium salts were generated according to literature protocols. Complexation with Ag₂O and subsequent transmetalation with AuCl(SMe₂) to afford the corresponding gold chlorides **47** was successful regardless of the N-substituent. The exchange of the chloride anion with thiophenol or 4-(adamantan-2-yl)benzenethiol via sodium in MeOH or KO^tBu in CH₂Cl₂, respectively, was also effective. Yet, the reaction with thiophenol yielded roughly 60% of the final complexes, while 4-(adamantan-2-yl)benzenethiol could be inserted with only 45% yield (Scheme 6). Notable characteristics of this research were the preparation of cyclopropene-bearing

derivates and their biorthogonal click chemistry. After protecting the free amine of **56** with an allyloxycarbonyl (alloc) group, the clickable (2,3-dimethylcycloprop-2-en-1-yl)methanol was attached to the 5-carboxylic group via STEGLICH-HASSNER esterification. After deprotection of the alloc group under Pd(0) catalysis, the remaining synthesis to afford NHC-Au(I)-SR complexes thereof proceeded analogously.

The complexes were tested for their cytotoxicity against eight human cancer cell lines. The thiophenol derivatives were more active than AC1-004, with IC_{50} values in the low single-digit micromolar range. However, the corresponding 4-(adamantan-2-yl)benzenethiol complexes were less active than the lead structure. The main effect of the complexes leading to apoptosis was the generation of ROS together with TrxR inhibition. Anti-angiogenic effects of the complexes were also demonstrated in zebrafish larvae. This effect on the vascular system was further proven by the subcellular accumulation of the cyclopropene-bearing congeners, as the click chemistry showed that those mainly accumulate in the cells' mitochondria.



Scheme 6. Synthesis overview of the complexes of the publication: Fischer esterification and N-dialkylation followed by (i) 1. Ag₂O, CH₂Cl₂, light exclusion, r.t., 6 h; 2. AuCl(SMe₂), CH₂Cl₂, light exclusion, r.t., 24h; (ii) KO^tBu, 4-(adamantan-2-yl)benzenethiol, CH₂Cl₂, r.t., 24h; (iii) Na, SPh, MeOH, r.t., 24h. In addition, the presentation of the most interesting results, such as the crystal structure of **49b** in the bottom left corner. The subcellular localisation of the cyclopropene-bearing analogues of 4-(adamantan-2-yl)benzenethiolato complex **48b** (SPhAda) and benzenethiolato complex **49b** (SPh) are in the top left corner. The pearson correlation coefficient (PCC) is given for overlapping values. The white scale bar corresponds to 50 μ m.

2.3 Synthesis and evaluation of new *cis* and *trans* bis NHC-Pt^{II} complexes

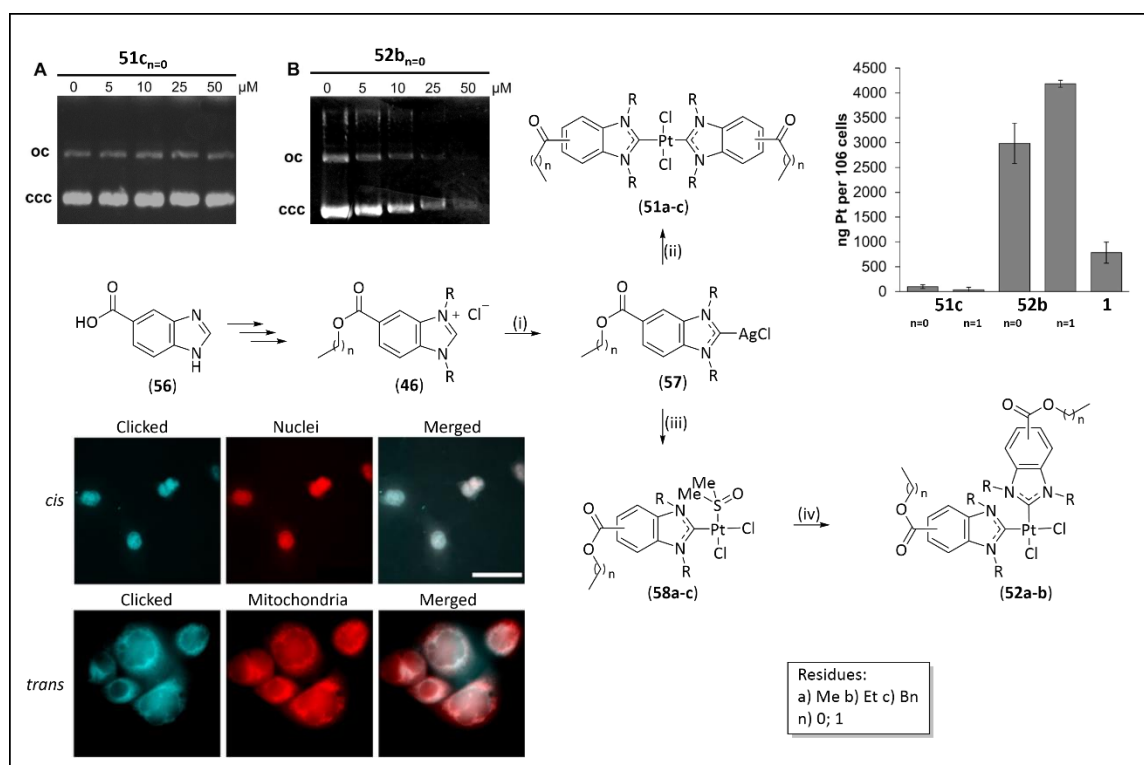
Cisplatin (**1**) and its analogues carboplatin (**7**) and oxaliplatin (**8**) are still the drugs of choice in 50% of chemotherapies. However, their sometimes severe side effects and swift indication of resistances have led to an early search for alternatives. This recently expanded to include novel NHC platinum complexes, which show improved stability and adjustability. This class of ligands can be fine-tuned by simple changes e. g. in the N-substituents. Another possibility to circumvent resistances is to generate *trans*-complexes that display a different mechanism of action due to their geometry. The second publication of this work is based on a small library of such bis-NHC platinum complexes to demonstrate not only the effect of the configuration (*cis* or *trans*) but also of the N-substituents (methyl, ethyl or benzyl).

The syntheses followed well-known routes established in our labs. Those started from the aforementioned benzimidazole-5-carboxylic acid (**56**), which underwent a FISCHER esterification with methanol or ethanol, respectively, followed by N,N'-dialkylation. A subsequent anion exchange formed the corresponding benzimidazolium chlorides **46**. Complexation with Ag₂O yielded [5-alkoxycarbonyl-1,3-dialkyl-2-ylidene] silver(I) chlorido complexes **57**, which could be transmetalated with K₂PtCl₄ yielding platinum complexes **51** and **58**, respectively. The configuration and the ligands depended on the solvent and equivalents of K₂PtCl₄. The complexations with Ag₂O and the final transmetalation with K₂PtCl₄ for yielding *trans*-[bis(5-alkoxycarbonyl-1,3-dialkyl-benzimidazol-2-ylidene)dichlorido]platinum(II) complexes **51** were successful regardless of the N-substituents. The ligand exchange of the DMSO ligand of **58** by an *in situ*-generated benzimidazolium carbene was successful for **58a-b**, but **58c** could not be converted into its corresponding *cis*-[bis(5-alkoxycarbonyl-1,3-dialkyl-benzimidazol-2-ylidene)dichlorido]platinum(II) complex (Scheme 7).

Besides, *cis*-[(5-methoxycarbonyl-1,3-dipropargylbenzimidazol-2-ylidene) (dimethylsulfoxide) dichlorido]platinum(II), a terminal alkyne-bearing *cis*-DMSO complex, was synthesised to determine the subcellular accumulation of this series of complexes via Click chemistry. HCT116 cells were treated with this clickable complex, fixed, and incubated with CuSO₄. The fluorescent stain 3-Azido-7-hydroxycoumarin was added, allowing the clicked complex to be visualised in the cellular compartments via confocal microscopy. The cyclopropene bearing complex *trans*-bis(5-(dimethylcyclopropenyl)methyl-carbonyl-1,3-diethylbenzimidazol-2-ylidene)dichlorido]platinum(II) was visualised using a click reaction with BDP-FL-tetrazine (Scheme 4).

The results of these visualisations overlapped with the localisations of compounds with known targets, i. e., propidium iodide and Mitotracker™ to visualise the nuclei or the mitochondria, respectively, can be seen in Scheme 7, top right.

The IC_{50} values of the most potent complexes of this library against eight human cancer cell lines were in the sub-micromolar range, e. g., $0.05 \pm 0.02 \mu\text{M}$ against HeLa cells in the case of **51c**_(n=0). The IC_{50} values of *cis*-[bis(5-methoxycarbonyl-1,3-diethyl-benzimidazol-2-ylidene) dichlorido] platinum(II) **52b**_(n=0) were also in the sub-micromolar range against several cell lines. Yet, no stringent SAR was observable. Due to the high activity, those two complexes were examined in more detail. Subcellular localisation of the clickable congeners in the cell and several biochemical assays have shown that the *cis*-[Pt^{II}Cl₂(NHC)(L)] complexes (L = NHC, DMSO) behaved akin to cisplatin (**1**), with the DNA as their primary target. In contrast, the *trans*-[Pt^{II}Cl₂(NHC)₂] complexes targeted mainly the mitochondria. Remarkably, the uptake of *cis*-[Pt^{II}Cl₂(NHC)₂] complexes **52b** was 40-fold higher compared to the *trans*-bis complexes **51c** and 5-fold higher compared to **1**.

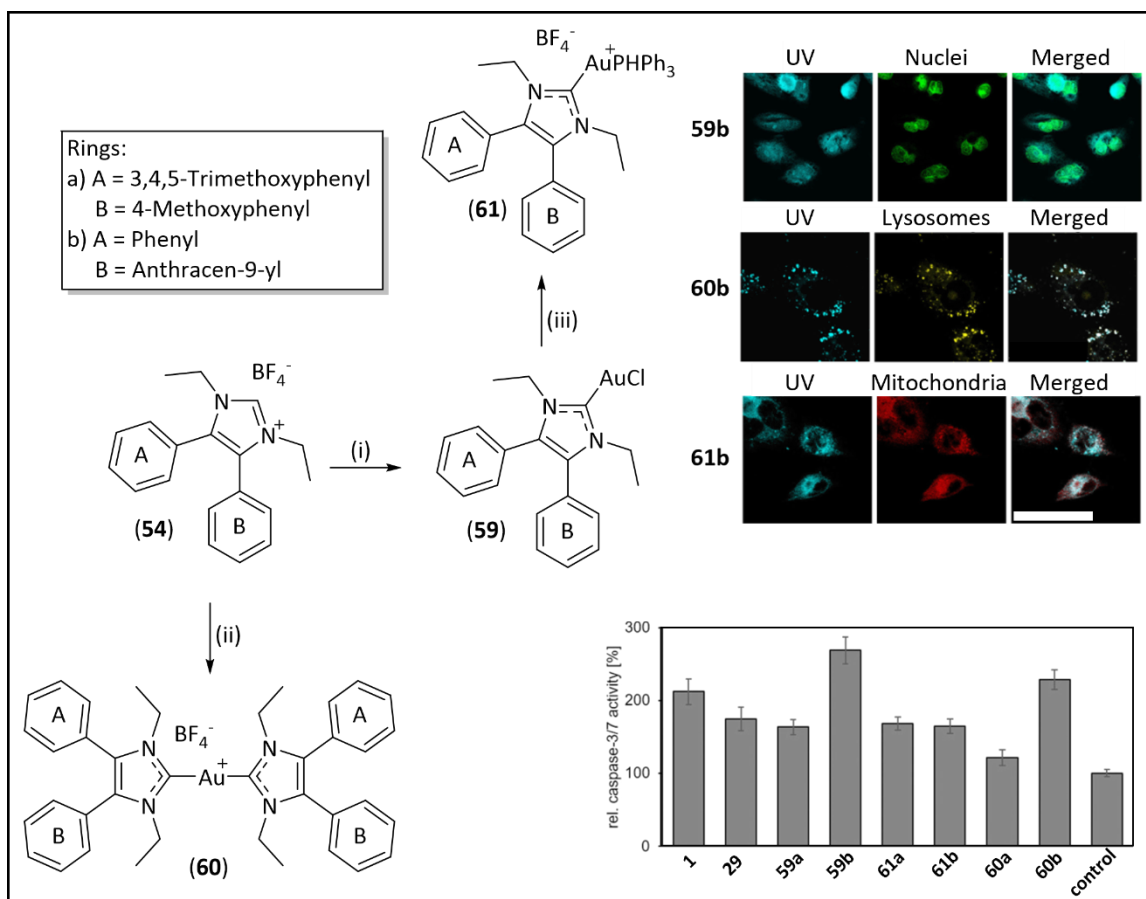


Scheme 7. Synthesis overview of the complexes of the publication: FISCHER esterification, N-dialkylation, and anion exchange followed by (i) Ag₂O, CH₂Cl₂, light exclusion, r.t., 24 h; (ii) 0.5 eq. K₂PtCl₄, CH₂Cl₂, r.t., 4 d; (iii) 1.0 eq. K₂PtCl₄, DMSO, 60 °C, 24 h; (iv) benzimidazolium salt **46**, KOtBu, CH₂Cl₂, r.t., 3d. In addition, the presentation of the most interesting results, such as cellular uptakes of **51c** and **52b** compared to **1** in the top right corner, the EMSA of **51c** and **52b** in the top left corner. The subcellular localisation of an alkyne-bearing analogue of *cis*-DMSO complexes **58**_(n=0) (*cis*) and a cyclopropene-bearing analogue of **51b**_(n=0) (*trans*) is displayed in the bottom left corner. The white scale bar corresponds to 30 μm .

2.4 Metal-Drug-Synergism: Gold complexes of CA-4

The third publication revolved around the topic of metal-drug synergism. Gold(I) complexes were synthesised with ligands that mimicked the mitotic inhibitor CA-4 (**37**). The NHC ligands were obtained from a VAN LEUSEN reaction. The synthetic route started from reacting toluenesulfonylmethyl isocyanide (TosMIC) reagent **53** with the corresponding aldehyde and EtNH₂, followed by N-ethylation to form 4,5-biaryl-1,3-diethyl-imidazolium salts **54** (Scheme 5). The phenolic rings A and B (Scheme 8) were explicitly modelled on the lead structure, i.e. 3,4,5-trimethoxyphenyl and 4-methoxyphenyl. At the same time, analogues with phenyl and anthracenyl residues were prepared to determine the subcellular accumulation via the fluorescence of the latter. Both the neutral gold chloride **59** and the cationic bis-NHC complex **60** with BF₄ counter anion were then generated from these imidazolium salt in one step, depending on the equivalents of AuCl(SMe₂). Ligand exchange of the former with PPh₃ additionally provided the cationic phosphane complex **61**.

The bis-NHC complexes **60** proved highly cytotoxic, with up to double-digit nanomolar *IC*₅₀ values against various human cancer cell lines. The phosphane complexes **61**, like the neutral chlorides **59**, were active with *IC*₅₀ concentrations in the one- to two-digit micromolar range. To determine the mechanism of action of the three different complexes, anthracene-bearing analogues, i. e., **59-61b**, were synthesised. The fluorescence of this residue allowed the subcellular visualisation of the complexes via confocal microscopy. The neutral complexes **59b** migrated into the cancer cells' nuclei, which was explained by the function of the chloride as a leaving group. This enables a reaction with the bases of the DNA. The cationic phosphane complexes **61b** accumulated mainly in the mitochondria, which has often been observed for complexes with delocalised lipophilic cations (DLC). Due to their size, the cationic bis-NHC complexes **60b** were primarily found in the lysosomes as those organelles are responsible for the degradation of macromolecules. All compounds showed high cytotoxicity, inducing apoptosis of the cancer cells, as seen in the induction of Caspase 3/7. However, they each reached this result via their own mechanisms of action.



Scheme 8. Synthesis overview of the complexes of the publication: (i) 1. Ag_2O , CH_2Cl_2 , light exclusion, r.t., 6 h; 2. $\text{AuCl}(\text{SMe}_2)$, CH_2Cl_2 , light exclusion, r.t., 24h; (ii) 0.5 eq. Ag_2O , CH_2Cl_2 , light exclusion, r.t., 6 h; 2. $\text{AuCl}(\text{SMe}_2)$, CH_2Cl_2 , light exclusion, r.t., 24h; (iii) PPh_3 , NaBF_4 , CH_2Cl_2 , r.t., 24 h. In addition, the presentation of the most interesting results, such as the subcellular localisation in the top right corner. The white scale bar corresponds to 50 μm . The cells' relative caspase-3/7 activity after treatment with the complexes compared to **1** and **29** is displayed in the bottom right corner.

3 Bibliography

- [1] F. Bray, M. Laversanne, E. Weiderpass, and I. Soerjomataram, *Cancer*, **2021**, 127, 3029-3030.
- [2] G. R. Dagenais, D. P. Leong, S. Rangarajan, F. Lanas, P. Lopez-Jaramillo, R. Gupta, R. Diaz, A. Avezum, G. B. F. Oliveira, A. Wielgosz, S. R. Parambath, P. Mony, K. F. Alhabib, A. Temizhan, N. Ismail, J. Chifamba, K. Yeates, R. Khatib, O. Rahman, K. Zatonska, K. Kazmi, L. Wei, J. Zhu, A. Rosengren, K. Vijayakumar, M. Kaur, V. Mohan, A. Yusufali, R. Kelishadi, K. K. Teo, P. Joseph, and S. Yusuf, *Lancet*, **2020**, 395, 785-794.
- [3] M. Harding, C. Sloan, R. Merrill, T. Harding, B. Thacker, and E. Thacker, *Prev. Chronic Dis.*, **2018**, 15, E158.
- [4] J. Ferlay, M. Colombet, I. Soerjomataram, D. M. Parkin, M. Piñeros, A. Znaor, and F. Bray, *Int. J. Cancer*, **2021**, 149, 778-789.
- [5] M. M. Fidler, I. Soerjomataram, and F. Bray, *Int. J. Cancer*, **2016**, 139, 2436-2446.
- [6] D. K. Gaffney, M. Hashibe, D. Kepka, K. A. Maurer, and T. L. Werner, *Gynecol. Oncol.*, **2018**, 151, 547-554.
- [7] M. C. Turner, Z. J. Andersen, A. Baccarelli, W. R. Diver, S. M. Gapstur, C. A. Pope III, D. Prada, J. Samet, G. Thurston, and A. Cohen, *CA: Cancer J. Clin.*, **2020**, 70, 460-479.
- [8] H. Sung, J. Ferlay, R. L. Siegel, M. Laversanne, I. Soerjomataram, A. Jemal, and F. Bray, *CA: Cancer J. Clin.*, **2021**, 71, 209-249.
- [9] A. Kutikov, D. S. Weinberg, M. J. Edelman, E. M. Horwitz, R. G. Uzzo, and R. I. Fisher, *Ann. Intern. Med.*, **2020**, 172, 756-758.
- [10] C. Maringe, J. Spicer, M. Morris, A. Purushotham, E. Nolte, R. Sullivan, B. Rachet, and A. Aggarwal, *Lancet Oncol.*, **2020**, 21, 1023-1034.
- [11] J. Y. Blay, S. Boucher, B. Le Vu, C. Cropet, S. Chabaud, D. Perol, E. Barranger, M. Campone, T. Conroy, C. Coutant, R. De Crevoisier, A. Debreuve-Theresette, J. P. Delord, P. Fumoleau, J. Gentil, F. Gomez, O. Guerin, A. Jaffré, E. Lartigau, C. Lemoine, M. A. Mahe, F. X. Mahon, H. Mathieu-Daude, Y. Merrouche, F. Penault-Llorca, X. Pivot, J. C. Soria, G. Thomas, P. Vera, T. Vermeulin, P. Viens, M. Ychou, and S. Beaupere, *ESMO Open*, **2021**, 6, 100134.
- [12] L. G. Qu, N. R. Brand, A. Chao, and A. M. Ilbawi, *Oncologist*, **2020**, 25, e1382-e1395.
- [13] Y. Y. Ding, S. Ramakrishna, A. H. Long, C. A. Phillips, R. Montiel-Esparza, C. J. Diorio, L. C. Bailey, S. L. Maude, R. Aplenc, V. Batra, A. F. Reilly, S. R. Rheingold, N. J. Lacayo, K. M. Sakamoto, and S. P. Hunger, *Pediatr. Blood Cancer*, **2020**, 67, e28427.
- [14] O.-P. Alho, H. Teppo, P. Mäntyselkä, and S. Kantola, *CMAJ* **2006**, 174, 779-784.
- [15] C. Chakraborty, A. R. Sharma, M. Bhattacharya, and S. S. Lee, *Front. Immunol.*, **2021**, 12, 679344.
- [16] K. Esfahani, L. Roudaia, N. Buhlaiga, S. V. Del Rincon, N. Papneja, and W. H. Miller, Jr., *Curr. Oncol.*, **2020**, 27, 87-97.
- [17] M. J. Smyth, S. F. Ngiew, A. Ribas, and M. W. L. Teng, *Nat. Rev. Clin. Oncol.*, **2016**, 13, 143-158.
- [18] J. S. O'Donnell, G. V. Long, R. A. Scolyer, M. W. Teng, and M. J. Smyth, *Cancer Treat. Rev.*, **2017**, 52, 71-81.
- [19] S. Supplitt, P. Karpinski, M. Sasiadek, and I. Laczmanska, *Int. J. Mol. Sci.*, **2021**, 22, 1422.
- [20] C. R. UK, *Chemotherapy, Radiotherapy and Surgical Tumour Resections in England. 2022*: National Disease Registration Service.
- [21] K. D. Miller, L. Nogueira, T. Devasia, A. B. Mariotto, K. R. Yabroff, A. Jemal, J. Kramer, and R. L. Siegel, *CA: A Cancer Journal for Clinicians*, **2022**, 72, 409-436.
- [22] M. A. Jordan and L. Wilson, *Nat. Rev. Cancer*, **2004**, 4, 253-265.
- [23] K. A. Lyseng-Williamson and C. Fenton, *Drugs*, **2005**, 65, 2513-2531.
- [24] Y. Pommier, *Nat. Rev. Cancer*, **2006**, 6, 789-802.
- [25] O. Tacar, P. Sriamornsak, and C. R. Dass, *J. Pharm. Pharmacol.*, **2012**, 65, 157-170.

- [26] P. N. Munshi, M. Lubin, and J. R. Bertino, *Oncologist*, **2014**, 19, 760-765.
- [27] D. B. Longley, D. P. Harkin, and P. G. Johnston, *Nat. Rev. Cancer*, **2003**, 3, 330-338.
- [28] S. Aldossary, *J. Biomed. Pharmacol.*, **2019**, 11, 7-15.
- [29] J. Reedijk and P. H. M. Lohman, *Pharma. Weekbl.*, **1985**, 7, 173-180.
- [30] T. J. Greshock, D. M. Johns, Y. Noguchi, and R. M. Williams, *Org. Lett.*, **2008**, 10, 613-616.
- [31] J. D. Broome, *Cancer Treat. Rep.*, **1981**, 65 Suppl 4, 111-114.
- [32] M. S. Won, N. Im, S. Park, S. K. Boovanahalli, Y. Jin, X. Jin, K. S. Chung, M. Kang, K. Lee, S. K. Park, H. M. Kim, B. M. Kwon, J. J. Lee, and K. Lee, *Biochem. Biophys. Res. Commun.*, **2009**, 385, 16-21.
- [33] D. H. Shin, J. H. Kim, Y. J. Jung, K. E. Kim, J. M. Jeong, Y. S. Chun, and J. W. Park, *Cancer Lett.*, **2007**, 255, 107-116.
- [34] D. Hanahan, *Cancer Discov.*, **2022**, 12, 31-46.
- [35] A. Khoury, K. M. Deo, and J. R. Aldrich-Wright, *J. Inorg. Biochem.*, **2020**, 207, 111070.
- [36] B. Rosenberg, L. VanCamp, and T. Krigas, *Nature*, **1965**, 205, 698-699.
- [37] B. Rosenberg, E. Renshaw, L. VanCamp, J. Hartwick, and J. Drobnik, *J. Bacteriol.*, **1967**, 93, 716-721.
- [38] B. Rosenberg, L. VanCamp, E. B. Grimley, and A. J. Thomson, *J. Biol. Chem.*, **1967**, 242, 1347-1352.
- [39] B. Rosenberg, L. VanCamp, J. E. Trosko, and V. H. Mansour, *Nature*, **1969**, 222, 385-386.
- [40] B. Rosenberg and L. VanCamp, *Cancer Res.*, **1970**, 30, 1799-1802.
- [41] J. J. Wilson and S. J. Lippard, *Chem. Rev.*, **2014**, 114, 4470-4495.
- [42] S. Dhara, *Indian. J. Chem.*, **1970**, 8, 193-194.
- [43] V. Y. Kukushikin, Å. Oskarsson, L. I. Elding, N. Farrell, S. Dunham, and S. J. Lippard, *Facile Synthesis of Isomerically Pure cis-Dichlorodiammineplatinum(II), Cisplatin*, in *Inorg. Synth.* 1998. p. 141-144.
- [44] M. T. Kuo, H. H. Chen, I. S. Song, N. Savaraj, and T. Ishikawa, *Cancer Metastasis Rev.*, **2007**, 26, 71-83.
- [45] A. M. Fichtinger-Schepman, J. L. van der Veer, J. H. den Hartog, P. H. Lohman, and J. Reedijk, *Biochemistry*, **1985**, 24, 707-713.
- [46] V. Cepeda, M. A. Fuertes, J. Castilla, C. Alonso, C. Quevedo, and J. M. Pérez, *Anticancer Agents Med. Chem.*, **2007**, 7, 3-18.
- [47] M. A. Fuertes, J. Castilla, C. Alonso, and J. M. Prez, *Curr. Med. Chem.*, **2003**, 10, 257-266.
- [48] M. Kleih, K. Böppe, M. Dong, A. Gaißler, S. Heine, M. A. Olayioye, W. E. Aulitzky, and F. Essmann, *Cell Death Dis.*, **2019**, 10, 851.
- [49] S. Kumar and P. B. Tchounwou, *Oncotarget*, **2015**, 6, 40734-40746.
- [50] L. Shen, N. Wen, M. Xia, Y. U. Zhang, W. Liu, Y. E. Xu, and L. Sun, *Oncol. Lett.*, **2016**, 11, 2411-2419.
- [51] L. P. Rybak, D. Mukherjea, and V. Ramkumar, *Semin. Hear.*, **2019**, 40, 197-204.
- [52] S. Manohar and N. Leung, *J. Nephrol.*, **2018**, 31, 15-25.
- [53] M. Waseem, M. Bhardwaj, H. Tabassum, S. Raisuddin, and S. Parvez, *Drug Chem. Tox.*, **2015**, 38, 452-459.
- [54] G. J. Dugbartey, L. J. Peppone, and I. A. de Graaf, *Toxicology*, **2016**, 371, 58-66.
- [55] G. Cavaletti, G. Pezzoni, C. Pisano, N. Oggioni, F. Sala, C. Zoia, C. Ferrarese, P. Marmioli, and G. Tredici, *Neurosci. Lett.*, **2002**, 322, 103-106.
- [56] S. Ishida, F. McCormick, K. Smith-McCune, and D. Hanahan, *Cancer Cell*, **2010**, 17, 574-583.
- [57] F. Tadini-Buoninsegni, G. Bartolommei, M. R. Moncelli, G. Inesi, A. Galliani, M. Sinisi, M. Losacco, G. Natile, and F. Arnesano, *Angew. Chem. Int. Ed.*, **2014**, 53, 1297-1301.
- [58] S. Vascellari, E. Valletta, D. Perra, E. Pinna, A. Serra, F. Isaia, A. Pani, and T. Pivetta, *RSC Adv.*, **2019**, 9, 5362-5376.

- [59] S. Borchert, P.-M. Suckrau, R. F. H. Walter, M. Wessolly, E. Mairinger, J. Steinborn, B. Hegedus, T. Hager, T. Herold, W. E. E. Eberhardt, J. Wohlschlaeger, C. Aigner, A. Bankfalvi, K. W. Schmid, and F. D. Mairinger, *Sci. Rep.*, **2020**, *10*, 18677.
- [60] J. Smith, L. Mun Tho, N. Xu, and D. A. Gillespie, *Chapter 3 - The ATM-Chk2 and ATR-Chk1 Pathways in DNA Damage Signaling and Cancer*, in *Adv. Cancer Res.*, G.F. Vande Woude and G. Klein, Editors. 2010, Academic Press. p. 73-112.
- [61] C. Balia, A. Galli, and M. A. Caligo, *Breast Cancer Res. Treat.*, **2011**, *129*, 1001-1009.
- [62] R. P. Topping, J. C. Wilkinson, and K. D. Scarpinato, *J. Biol. Chem.*, **2009**, *284*, 14029-14039.
- [63] E. Kotler, O. Shani, G. Goldfeld, M. Lotan-Pompan, O. Tarcic, A. Gershoni, T. A. Hopf, D. S. Marks, M. Oren, and E. Segal, *Mol. Cell*, **2018**, *71*, 178-190.
- [64] A. J. Levine, *Nat. Rev. Cancer*, **2020**, *20*, 471-480.
- [65] I. Ott and R. Gust, *Pharm. unserer Zeit*, **2006**, *35*, 124-133.
- [66] G. Y. Ho, N. Woodward, and J. I. Coward, *Crit. Rev. Oncol. Hematol.*, **2016**, *102*, 37-46.
- [67] A. J. Wagstaff, A. Ward, P. Benfield, and R. C. Heel, *Drugs*, **1989**, *37*, 162-190.
- [68] M. E. Gore, I. Fryatt, E. Wiltshaw, T. Dawson, B. A. Robinson, and A. H. Calvert, *Br. J. Cancer*, **1989**, *60*, 767-769.
- [69] C. R. Culy, D. Clemett, and L. R. Wiseman, *Drugs*, **2000**, *60*, 895-924.
- [70] S. G. Chaney, S. L. Campbell, E. Bassett, and Y. Wu, *Crit. Rev. Oncol. Hematol.*, **2005**, *53*, 3-11.
- [71] A. M. Di Francesco, A. Ruggiero, and R. Riccardi, *CMLS*, **2002**, *59*, 1914-1927.
- [72] A. Tesniere, F. Schlemmer, V. Boige, O. Kepp, I. Martins, F. Ghiringhelli, L. Aymeric, M. Michaud, L. Apetoh, L. Barault, J. Mendiboure, J. P. Pignon, V. Jooste, P. van Endert, M. Ducreux, L. Zitvogel, F. Piard, and G. Kroemer, *Oncogene*, **2010**, *29*, 482-491.
- [73] A. A. Argyriou, *Toxics*, **2015**, *3*, 187-197.
- [74] G. K. Poon, P. Mistry, F. I. Raynaud, K. R. Harrap, B. A. Murrer, and C. F. Barnard, *J. Pharm. Biomed. Anal.*, **1995**, *13*, 1493-1498.
- [75] J. L. Carr, M. D. Tingle, and M. J. McKeage, *Cancer Chemother. Pharmacol.*, **2002**, *50*, 9-15.
- [76] H. Choy, C. Park, and M. Yao, *Clin. Cancer. Res.*, **2008**, *14*, 1633-1638.
- [77] M. Shimada, H. Itamochi, and J. Kigawa, *Cancer Manag. Res.*, **2013**, *5*, 67-76.
- [78] L. Kelland, *Expert Opin. Investig. Drugs*, **2007**, *16*, 1009-1021.
- [79] C.-H. Choi, Y.-J. Cha, C.-S. An, K.-J. Kim, K.-C. Kim, S.-P. Moon, Z. H. Lee, and Y.-D. Min, *Cancer Cell Int.*, **2004**, *4*, 6.
- [80] M. J. McKeage, *Expert Opin. Investig. Drugs*, **2001**, *10*, 119-128.
- [81] F. E. Hahn and M. C. Jahnke, *Angew. Chem. Int. Ed.*, **2008**, *47*, 3122-3172.
- [82] T. Zou, C.-N. Lok, P.-K. Wan, Z.-F. Zhang, S.-K. Fung, and C.-M. Che, *Curr. Chem. Bio.*, **2018**, *43*, 30-36.
- [83] W. Liu and R. Gust, *Chem. Soc. Rev.*, **2013**, *42*, 755-773.
- [84] D. A. Shabalina and J. E. Camp, *Org. Biomol. Chem.*, **2020**, *18*, 3950-3964.
- [85] S. I. Alaqeel, *J. Saudi Chem. Soc.*, **2017**, *21*, 229-237.
- [86] S. Saxer, C. Marestin, R. Mercier, and J. Dupuy, *Polym. Chem.*, **2018**, *9*, 1927-1933.
- [87] A. M. Van Leusen, J. Wildeman, and O. H. Oldenziel, *J. Org. Chem.*, **1977**, *42*, 1153-1159.
- [88] T. Rehm, M. Rothmund, T. Dietel, R. Kempe, and R. Schobert, *Dalton Trans.*, **2019**, *48*, 16358-16365.
- [89] T. Rehm, M. Rothmund, J. K. Muenzner, A. Noor, R. Kempe, and R. Schobert, *Dalton Trans.*, **2016**, *45*, 15390-15398.
- [90] M. Rothmund, S. I. Bär, T. Rehm, H. Kostrhunova, V. Brabec, and R. Schobert, *Dalton Trans.*, **2020**, *49*, 8901-8910.
- [91] M. Fèvre, J. Pinaud, A. Leteneur, Y. Gnanou, J. Vignolle, D. Taton, K. Miqueu, and J.-M. Sotiropoulos, *J. Am. Chem. Soc.*, **2012**, *134*, 6776-6784.
- [92] H. M. J. Wang and I. J. B. Lin, *Organometallics*, **1998**, *17*, 972-975.

- [93] S. D. Adhikary, D. Bose, P. Mitra, K. D. Saha, V. Bertolasi, and J. Dinda, *New J. Chem.*, **2012**, 36, 759-767.
- [94] R. Wai-Yin Sun, A. Lok-Fung Chow, X.-H. Li, J. J. Yan, S. Sin-Yin Chui, and C.-M. Che, *Chem. Sci.*, **2011**, 2, 728-736.
- [95] N. Farrell, T. T. Ha, J. P. Souchard, F. L. Wimmer, S. Cros, and N. P. Johnson, *J. Med. Chem.*, **1989**, 32, 2240-2241.
- [96] M. Coluccia, A. Nassi, F. Loseto, A. Boccarelli, M. A. Mariggio, D. Giordano, F. P. Intini, P. Caputo, and G. Natile, *J. Med. Chem.*, **1993**, 36, 510-512.
- [97] E. Pantoja, A. Gallipoli, S. van Zutphen, S. Komeda, D. Reddy, D. Jaganyi, M. Lutz, D. M. Tooke, A. L. Spek, C. Navarro-Ranninger, and J. Reedijk, *J. Inorg. Biochem.*, **2006**, 100, 1955-1964.
- [98] T. Kishimoto, Y. Yoshikawa, K. Yoshikawa, and S. Komeda, *Int. J. Mol. Sci.*, **2019**, 21, 34.
- [99] T. Peleg-Shulman, Y. Najajreh, and D. Gibson, *J. Inorg. Biochem.*, **2002**, 91, 306-311.
- [100] V. Marchán, E. Pedroso, and A. Grandas, *Chem. Eur. J.*, **2004**, 10, 5369-5375.
- [101] M. Skander, P. Retailleau, B. Bourrié, L. Schio, P. Mailliet, and A. Marinetti, *J. Med. Chem.*, **2010**, 53, 2146-2154.
- [102] E. Chardon, G. Dahm, G. Guichard, and S. Bellemin-Laponnaz, *Organometallics*, **2012**, 31, 7618-7621.
- [103] J. K. Muenzner, T. Rehm, B. Biersack, A. Casini, I. A. M. de Graaf, P. Worawutputtpong, A. Noor, R. Kempe, V. Brabec, J. Kasparkova, and R. Schobert, *J. Med. Chem.*, **2015**, 58, 6283-6292.
- [104] I. Ott and R. Gust, *Arch Pharm (Weinheim)*, **2007**, 340, 117-126.
- [105] M. Frezza, S. Hindo, D. Chen, A. Davenport, S. Schmitt, D. Tomco, and Q. P. Dou, *Curr. Pharm. Des.*, **2010**, 16, 1813-1825.
- [106] Y. K. Yan, M. Melchart, A. Habtemariam, and P. J. Sadler, *ChemCom*, **2005**, 4764-4776.
- [107] K. L. Haas and K. J. Franz, *Chem. Rev.*, **2009**, 109, 4921-4960.
- [108] U. Jungwirth, C. R. Kowol, B. K. Keppler, C. G. Hartinger, W. Berger, and P. Heffeter, *Antioxid. Redox Signal.*, **2011**, 15, 1085-1127.
- [109] U. Ndagi, N. Mhlongo, and M. E. Soliman, *Drug. Des. Devel. Ther.*, **2017**, 11, 599-616.
- [110] M. P. Ngoepe and H. S. Clayton, *Pharma. Fronts*, **2021**, 03, 164-182.
- [111] T. Gianferrara, I. Bratsos, and E. Alessio, *Dalton Trans.*, **2009**, 7588-7598.
- [112] J. Reedijk, *Proc. Natl. Acad. Sci.*, **2003**, 100, 3611-3616.
- [113] S. Zorzet, A. Bergamo, M. Cocchietto, A. Sorc, B. Gava, E. Alessio, E. Iengo, and G. Sava, *J. Pharmacol. Exp. Ther.*, **2001**, 295, 927-933.
- [114] M. Liu, Z. J. Lim, Y. Y. Gwee, A. Levina, and P. A. Lay, *Angew. Chem. Int. Ed.*, **2010**, 49, 1661-1664.
- [115] M. M. Henke, H. Richly, A. Drescher, M. Grubert, D. Alex, D. Thyssen, U. Jaehde, M. E. Scheulen, and R. A. Hilger, *Int. J. Clin. Pharmacol. Ther.*, **2009**, 47, 58-60.
- [116] E. S. Antonarakis and A. Emadi, *Cancer Chemother. Pharmacol.*, **2010**, 66, 1-9.
- [117] S. J. Bakewell, D. F. Rangel, D. P. Ha, J. Sethuraman, R. Crouse, E. Hadley, T. L. Costich, X. Zhou, P. Nichols, and A. S. Lee, *Oncotarget*, **2018**, 9, 29698-29714.
- [118] S. Y. Lee, C. Y. Kim, and T. G. Nam, *Drug. Des. Devel. Ther.*, **2020**, 14, 5375-5392.
- [119] J. M. Rademaker-Lakhai, D. van den Bongard, D. Pluim, J. H. Beijnen, and J. H. Schellens, *Clin. Cancer. Res.*, **2004**, 10, 3717-3727.
- [120] C. G. Hartinger, M. A. Jakupec, S. Zorbas-Seifried, M. Groessl, A. Egger, W. Berger, H. Zorbas, P. J. Dyson, and B. K. Keppler, *Chem. Biodivers.*, **2008**, 5, 2140-2155.
- [121] M. Arredondo and M. T. Núñez, *Mol. Aspects Med.*, **2005**, 26, 313-327.
- [122] K. Salnikow, *Sem. Cancer Biol.*, **2021**, 76, 189-194.
- [123] O. Kakhlon and Z. I. Cabantchik, *Free Radic. Biol. Med.*, **2002**, 33, 1037-1046.
- [124] M. Patra and G. Gasser, *Nat. Rev. Cancer*, **2017**, 1, 66.
- [125] P. Köpf-Maier, H. Köpf, and E. W. Neuse, *J. Cancer. Res. Clin. Oncol.*, **1984**, 108, 336-340.

- [126] W. A. Wani, U. Baig, S. Shreaz, R. A. Shiekh, P. F. Iqbal, E. Jameel, A. Ahmad, S. H. Mohd-Setapar, M. Mushtaque, and L. Ting Hun, *New J. Chem.*, **2016**, *40*, 1063-1090.
- [127] M. Bouché, C. Hognon, S. Grandemange, A. Monari, and P. C. Gros, *Dalton Trans.*, **2020**, *49*, 11451-11466.
- [128] D. Wallis, J. Claffey, B. Gleeson, M. Hogan, H. Müller-Bunz, and M. Tacke, *J. Organomet. Chem.*, **2009**, *694*, 828-833.
- [129] R. Serrano, I. Martinez-Argudo, M. Fernandez-Sanchez, P. J. Pacheco-Liñan, I. Bravo, B. Cohen, R. Calero, and M. J. Ruiz, *J. Inorg. Biochem.*, **2021**, *223*, 111562.
- [130] M. Rothmund, A. Bär, F. Klatt, S. Weidler, L. Köhler, C. Unverzagt, C.-D. Kuhn, and R. Schobert, *Bioorg. Chem.*, **2020**, *97*, 103703.
- [131] E. Meléndez, *Inorganica Chim. Acta*, **2012**, *393*, 36-52.
- [132] F. Wang, P. Jiao, M. Qi, M. Frezza, Q. P. Dou, and B. Yan, *Curr. Med. Chem.*, **2010**, *17*, 2685-2698.
- [133] K. Camphausen, M. Sproull, S. Tantama, S. Sankineni, T. Scott, C. Ménard, C. N. Coleman, and M. W. Brechbiel, *Bioorg. Med. Chem.*, **2003**, *11*, 4287-4293.
- [134] C. Santini, M. Pellei, V. Gandin, M. Porchia, F. Tisato, and C. Marzano, *Chem. Rev.*, **2014**, *114*, 815-862.
- [135] E. E. Aranda, T. A. Matias, K. Araki, A. P. Vieira, E. A. de Mattos, P. Colepicolo, C. P. Luz, F. L. Marques, and A. M. da Costa Ferreira, *J. Inorg. Biochem.*, **2016**, *165*, 108-118.
- [136] R. Tabti, N. Tounsi, C. Gaidon, E. Bentouhami, and L. Désaubry, *Med. Chem.*, **2017**, *7*, 875-879.
- [137] M. V. Babak and D. Ahn, *Biomedicines*, **2021**, *9*, 852.
- [138] E. Boros and A. B. Packard, *Chem. Rev.*, **2019**, *119*, 870-901.
- [139] T. Scattolin, I. Caligiuri, N. Mouawad, M. El Boustani, N. Demitri, F. Rizzolio, and F. Visentin, *Eur. J. Med. Chem.*, **2019**, *179*.
- [140] A. R. Kapdi and I. J. S. Fairlamb, *Chem. Soc. Rev.*, **2014**, *43*, 4751-4777.
- [141] T. Scattolin, V. A. Voloshkin, F. Visentin, and S. P. Nolan, *Cell Rep. Phys. Sci.*, **2021**, *2*, 100446.
- [142] S. Ray, R. Mohan, J. K. Singh, M. K. Samantaray, M. M. Shaikh, D. Panda, and P. Ghosh, *J. Am. Chem. Soc.*, **2007**, *129*, 15042-15053.
- [143] P. Bragado, A. Armesilla, A. Silva, and A. Porras, *Apoptosis*, **2007**, *12*, 1733-1742.
- [144] V. Velma, S. R. Dasari, and P. B. Tchounwou, *Biomark. Insights*, **2016**, *11*, 113-121.
- [145] T. Scattolin, E. Bortolamiol, F. Visentin, S. Palazzolo, I. Caligiuri, T. Perin, V. Canzonieri, N. Demitri, F. Rizzolio, and A. Togni, *Chemistry*, **2020**, *26*, 11868-11876.
- [146] T. T. Fong, C. N. Lok, C. Y. Chung, Y. M. Fung, P. K. Chow, P. K. Wan, and C. M. Che, *Angew. Chem. Int. Ed.*, **2016**, *55*, 11935-11939.
- [147] R. Czarnomysy, D. Radomska, O. K. Szewczyk, P. Roszczenko, and K. Bielawski, *Int. J. Mol. Sci.*, **2021**, *22*.
- [148] G. B. Kauffman, *Gold Bull.*, **1985**, *18*, 31-44.
- [149] G. B. Kauffman, *Gold Bull.*, **1985**, *18*, 69-78.
- [150] G. B. Kauffman, *Gold Bull.*, **1985**, *18*, 109-119.
- [151] G. C. Bernhard, *J. Lab. Clin. Med.*, **1982**, *100*, 167-177.
- [152] Y. Lu, X. Ma, X. Chang, Z. Liang, L. Lv, M. Shan, Q. Lu, Z. Wen, R. Gust, and W. Liu, *Chem. Soc. Rev.*, **2022**, *51*, 5518-5556.
- [153] K. Becker, S. Gromer, R. H. Schirmer, and S. Müller, *Eur. J. Biochem.*, **2000**, *267*, 6118-6125.
- [154] P. Nagakannan, M. A. Iqbal, A. Yeung, J. A. Thliveris, M. Rastegar, S. Ghavami, and E. Eftekharpour, *Free Radic. Biol. Med.*, **2016**, *101*, 53-70.
- [155] C. I. Yeo, K. K. Ooi, and E. R. T. Tiekink, *Molecules*, **2018**, *23*.
- [156] A. Gallegos, J. R. Gasdaska, C. W. Taylor, G. D. Paine-Murrieta, D. Goodman, P. Y. Gasdaska, M. Berggren, M. M. Briehl, and G. Powis, *Cancer Res.*, **1996**, *56*, 5765-5770.

- [157] T. Onodera, I. Momose, and M. Kawada, *Chem. Pharm. Bull.*, **2019**, 67, 186-191.
- [158] P. J. Sadler and R. E. Sue, *Met. Based Drugs*, **1994**, 1, 107-144.
- [159] M. Kupiec, R. Ziółkowski, L. Massai, L. Messori, and K. Pawlak, *J. Inorg. Biochem.*, **2019**, 198, 110714.
- [160] C. Zoppi, L. Messori, and A. Pratesi, *Dalton Trans.*, **2020**, 49, 5906-5913.
- [161] S. Urig, K. Fritz-Wolf, R. Réau, C. Herold-Mende, K. Tóth, E. Davioud-Charvet, and K. Becker, *Angew. Chem. Int. Ed.*, **2006**, 45, 1881-1886.
- [162] I. Ott, *Coord. Chem. Rev.*, **2009**, 253, 1670-1681.
- [163] L. Turell, R. Radi, and B. Alvarez, *Free Radic. Biol. Med.*, **2013**, 65, 244-253.
- [164] T. Zou, C. T. Lum, C.-N. Lok, J.-J. Zhang, and C.-M. Che, *Chem. Soc. Rev.*, **2015**, 44, 8786-8801.
- [165] C. K. Mirabelli, R. K. Johnson, C. M. Sung, L. Faucette, K. Muirhead, and S. T. Crooke, *Cancer Res.*, **1985**, 45, 32-39.
- [166] M. G. Vander Heiden, L. C. Cantley, and C. B. Thompson, *Science*, **2009**, 324, 1029-1033.
- [167] G. Chiappetta, T. Gamberi, F. Faienza, X. Limaj, S. Rizza, L. Messori, G. Filomeni, A. Modesti, and J. Vinh, *Redox. Biol.*, **2022**, 52, 102294.
- [168] R. J. DeBerardinis and N. S. Chandel, *Nat. Metab.*, **2020**, 2, 127-129.
- [169] L. Kou, S. Wei, and P. Kou, *Front. Chem.*, **2021**, 9, 733463.
- [170] V. Gandin, A. P. Fernandes, M. P. Rigobello, B. Dani, F. Sorrentino, F. Tisato, M. Björnstedt, A. Bindoli, A. Sturaro, R. Rella, and C. Marzano, *Biochem. Pharmacol.*, **2010**, 79, 90-101.
- [171] W. Walther, D. Althagafi, D. Curran, C. O'Beirne, C. Mc Carthy, I. Ott, U. Basu, B. Büttner, A. Sterner-Kock, H. Müller-Bunz, G. Sánchez-Sanz, X. Zhu, and M. Tacke, *Anti-Cancer Drugs*, **2020**, 31, 672-683.
- [172] B. Bertrand, A. de Almeida, E. P. M. van der Burgt, M. Picquet, A. Citta, A. Folda, M. P. Rigobello, P. Le Gendre, E. Bodio, and A. Casini, *Eur. J. Inorg. Chem.*, **2014**, 2014, 4532-4536.
- [173] S. M. Meier-Menches, B. Neuditschko, K. Zappe, M. Schaier, M. C. Gerner, K. G. Schmetterer, G. Del Favero, R. Bonsignore, M. Cichna-Markl, G. Koellensperger, A. Casini, and C. Gerner, *Chemistry*, **2020**, 26, 15528-15537.
- [174] G. Marcon, L. Messori, P. Orioli, M. A. Cinellu, and G. Minghetti, *Eur. J. Biochem.*, **2003**, 270, 4655-4661.
- [175] J. Liao and L. Zhou, *Struct. Chem.*, **2016**, 27, 651-662.
- [176] T. Zou, C. T. Lum, S. S.-Y. Chui, and C.-M. Che, *Angew. Chem. Int. Ed.*, **2013**, 52, 2930-2933.
- [177] P. Karran and N. Attard, *Nat. Rev. Cancer*, **2008**, 8, 24-36.
- [178] L. K. Webster, S. Rainone, E. Horn, and E. R. Tiekink, *Met. Based Drugs*, **1996**, 3, 63-66.
- [179] D. Crump, G. Siasios, and E. R. T. Tiekink, *Met. Based Drugs*, **1999**, 6, 576438.
- [180] R. Mitra, A. K. Pramanik, and A. G. Samuelson, *Eur. J. Inorg. Chem.*, **2014**, 5733-5740.
- [181] M. Leitão, F. Herrera, and A. Petronilho, *ACS Omega*, **2018**, 3, 15653-15656.
- [182] G. R. Pettit, S. B. Singh, E. Hamel, C. M. Lin, D. S. Alberts, and D. Garcia-Kendall, *Experientia*, **1989**, 45, 209-211.
- [183] D. Neri and R. Bicknell, *Nat. Rev. Cancer*, **2005**, 5, 436-446.
- [184] G. C. Tron, T. Pirali, G. Sorba, F. Pagliai, S. Busacca, and A. A. Genazzani, *J. Med. Chem.*, **2006**, 49, 3033-3044.
- [185] R. Zhao, Y. Wu, Y. Zhang, J. Ling, X. Liu, J. Xiang, X. Zeng, and T. Chen, *Sci. China Chem.*, **2022**, 65, 694-698.
- [186] L. Wang, K. W. Woods, Q. Li, K. J. Barr, R. W. McCroskey, S. M. Hannick, L. Gherke, R. B. Credo, Y. H. Hui, K. Marsh, R. Warner, J. Y. Lee, N. Zielinski-Mozng, D. Frost, S. H. Rosenberg, and H. L. Sham, *J. Med. Chem.*, **2002**, 45, 1697-1711.
- [187] R. Schobert, B. Biersack, A. Dietrich, K. Effenberger, S. Knauer, and T. Mueller, *J. Med. Chem.*, **2010**, 53, 6595-6602.
- [188] M. M. Rothmund, Julienne; Rehm, Tobias; Schobert, Rainer, unpublished results.

- [189] X. Huang, R. Huang, S. Gou, Z. Wang, Z. Liao, and H. Wang, *Bioconjug. Chem.*, **2016**, 27, 2132-2148.
- [190] J. K. Muenzner, B. Biersack, H. Kalie, I. C. Andronache, L. Kaps, D. Schuppan, F. Sasse, and R. Schobert, *ChemMedChem*, **2014**, 9, 1195-1204.
- [191] L. Côrte-Real, F. Mendes, J. Coimbra, T. Morais, A. I. Tomaz, A. Valente, M. Garcia, I. Santos, and M. Bicho, *J. Biol. Inorg. Chem.*, **2014**, 19.
- [192] G. Gupta, P. Kumari, J. Y. Ryu, J. Lee, S. M. Mobin, and C. Y. Lee, *Inorg. Chem.*, **2019**, 58, 8587-8595.
- [193] C. Molenaar, J.-M. Teuben, R. J. Heetebrij, H. J. Tanke, and J. Reedijk, *J. Biol. Inorg. Chem.*, **2000**, 5, 655-665.
- [194] R. Visbal, V. Fernández-Moreira, I. Marzo, A. Laguna, and M. C. Gimeno, *Dalton Trans.*, **2016**, 45, 15026-15033.
- [195] H. C. Hang, C. Yu, D. L. Kato, and C. R. Bertozzi, *Proc. Natl. Acad. Sci.*, **2003**, 100, 14846-14851.
- [196] E. M. Sletten and C. R. Bertozzi, *Angew. Chem. Int. Ed.*, **2009**, 48, 6974-6998.
- [197] V. V. Rostovtsev, L. G. Green, V. V. Fokin, and K. B. Sharpless, *Angew. Chem. Int. Ed.*, **2002**, 41, 2596-2599.
- [198] S. Bellemin-Laponnaz, *Eur. J. Inorg. Chem.*, **2020**, 2020, 10-20.
- [199] B. C. Boren, S. Narayan, L. K. Rasmussen, L. Zhang, H. Zhao, Z. Lin, G. Jia, and V. V. Fokin, *J. Am. Chem. Soc.*, **2008**, 130, 8923-8930.
- [200] S. Ding, X. Qiao, J. Suryadi, G. S. Marrs, G. L. Kucera, and U. Bierbach, *Angew. Chem. Int. Ed.*, **2013**, 52, 3350-3354.
- [201] X. Bao, S. Katz, M. Pollard, and J. Ohlrogge, *Proc. Natl. Acad. Sci.*, **2002**, 99, 7172-7177.
- [202] L. N. Li, H. T. Li, R. W. Lang, T. Itoh, D. Sica, and C. Djerassi, *J. Am. Chem. Soc.*, **1982**, 104, 6726-6732.
- [203] J. M. J. M. Ravasco, C. M. Monteiro, and A. F. Trindade, *Org. Chem. Front.*, **2017**, 4, 1167-1198.
- [204] K. Bertheussen, M. van de Plassche, T. Bakkum, B. Gagestein, I. Ttofi, A. J. C. Sarris, H. S. Overkleef, M. van der Stelt, and S. I. van Kasteren, *Angew. Chem. Int. Ed.*, **2022**, 134, e202207640.

4 Publications

4.1 Presentation of the own contribution

The publications presented in this dissertation were developed in cooperation with other researchers at the chair of Organic Chemistry I, the Chair of Inorganic Chemistry II, and the Chair of Developmental Biology of the University of Bayreuth. The own contribution to the respective publications will be described in the following paragraphs.

Publication I:

This work was submitted to Dalton Transactions with the title:

Anti-tumoural NHC Au(I) thiolato complexes derived from HIF-1 α inhibitor AC1-004 target the mitochondrial redox system and show antiangiogenic effects *in vivo*

from the authors Sebastian W. Schleser, Leonhard H. F. Köhler, Florian Riethmüller, Sebastian Reich, Robin Fertig, Gerrit Begemann, Rhett Kempe and Rainer Schobert.

This work was conceived by me in collaboration with Leonhard H. F. Köhler. The synthesis and stability tests of the complexes, as well as their purification and characterisation, were carried out by me. Florian Riethmüller played a supporting role. The crystal structure was solved by Robin Fertig. Leonhard H. F. Köhler carried out all *in vitro* evaluations with the support of Sebastian Reich. Prof. Gerrit Begemann supported us with the *in vivo* experiments in zebrafish larvae. The publication was written by me, Leonhard H. F. Köhler and Prof. Schobert.

Publication II:

This work was published in the Journal of Inorganic Biochemistry with the title:

Trans-[bis(benzimidazol-2-ylidene)dichlorido]platinum(II) complexes with peculiar modes of action and activity against cisplatin-resistant cancer cells

from the authors Sofia I. Bär, Sebastian W. Schleser, Natalie Oberhuber, Alexander Herrmann, Luca Schlotte, Stefanie E. Weber and Rainer Schobert.

This work was conceived by me in collaboration with Sofia I. Bär. The synthesis and stability tests of the complexes, as well as their purification and characterisation, were carried out by me. Luca Schlotte and Stefanie E. Weber played supporting roles. Sofia I. Bär carried out all *in vitro* evaluations with the support of Natalie Oberhuber and Alexander Herrmann. The publication was written by me, Sofia I. Bär and Prof. Schobert.

Publication III:

This work was published in the European Journal of Chemistry with the title:

Guided Antitumoural Drugs: (Imidazol-2-ylidene)(L)gold(I) Complexes Seeking Cellular Targets Controlled by the Nature of Ligand L

from the authors Sofia I. Bär, Madeleine Gold, Sebastian W. Schleser, Tobias Rehm, Alexander Bär, Leonhard Köhler, Lucas R. Carnell, Bernhard Biersack, and Rainer Schobert.

The synthesis, purification, and analysis, as well as the stability studies of the complexes, were carried out by me, Dr Tobias Rehm, Dr Alexander Bär and Dr Bernhard Biersack. Sofia I. Bär and Dr Madeleine Gold conducted all *in vitro* evaluations with the support of Leonhard Köhler and Lucas R. Carnell. The publication was written by Sofia I. Bär, Dr Madeleine Gold, Dr Bernhard Biersack and Prof. Schobert.

Anti-tumoural NHC Au(I) thiolato complexes derived from HIF-1 α inhibitor AC1-004 target the mitochondrial redox system and show antiangiogenic effects in vivo

Received 00th January 20xx,
Accepted 00th January 20xx

DOI: 10.1039/x0xx00000x

Sebastian W. Schleser^a, Leonhard H. F. Köhler^a, Florian Riethmüller^a, Sebastian Reich^a, Robin Fertig^b, Gerrit Begemann^c, Rhett Kempe^b and Rainer Schobert^a

AC1-004 is a potent inhibitor of the hypoxia-inducible factor alpha (HIF-1 α) pathway which is essential for the growth, angiogenesis and metastasis of tumours. We modelled a series of gold(I) complexes on AC1-004 by retaining its 5-carboalkoxybenzimidazole as an NHC ligand while replacing its 2-aryloxymethyl residue with diversely modified thiolato gold(I) fragments. The intention was to augment a potential HIF-1 α inhibition by further conducive effects typical of NHC gold complexes, such as an inhibition of the tumoural thioredoxin reductase (TrxR), an increase in reactive oxygen species (ROS), as well as cytotoxic and antiangiogenic effects. We report on the synthesis and biological effects of twelve such N,N'-dialkylbenzimidazol-2-ylidene gold(I) complexes. They were obtained in average yields of 65% for the thiophenolato and 45% for the novel 4-(adamant-2-yl)benzenethiol complexes. The structure of one complex was validated via single-crystal X-ray diffraction. Structure activity relationships (SAR) were derived by variation of the N-substituents (Me, Et, iPr, pentyl, Bn) and of the thiolato ligand. Their cytotoxicity against various human cancer cell lines of different entities reached IC_{50} values in the single digit micromolar range. The complexes were assayed also for the induction of tumour cell apoptosis (activation of caspase-3/7), TrxR inhibition and antiangiogenic effects in zebra fish. Cyclopropene bearing congeners were employed in click reactions to examine the subcellular accumulation of the complexes.

Introduction

Earlier this year, Hanahan et al. published another update on their hallmarks of cancer, underlining the complexity of the disease.¹ This update also shows which targets cancer cells, as opposed to nonmalignant cells, might offer for chemotherapy. Approved metalodrugs such as cisplatin draw what little selectivity they have for cancer cells only from their higher proliferation rate. Alternatives that address tumour-only targets would be less likely to cause unwanted side effects and drug resistance, the main problems which hamper the efficacy of cisplatin, carboplatin and oxaliplatin^{2,3}. Two such cancer-specific hallmarks are the alteration of the cancer cells' metabolism and tumour (neo)vascularisation. The irregular microcirculation and diffusion conditions in solid tumours lead to hypoxic areas and eventually a necrotic core.⁴ The subsequent switch to an anaerobic metabolism occurs through the expression of transcription genes like HIF-1 α . Given that chronic hypoxia is a unique feature of malignant cells, the inhibition of HIF-1 α represents an interesting and selective therapeutic approach.⁵ Besides the well know HIF-1 α inhibitor YC-1 (*Lifiquat*)⁶, adamantyl-bearing drugs

namely nicotinic or isonicotinic ester derivatives as well as a morpholine substituted analogue stood out in a chemical library screening.⁷ Arising as particularly promising from this HRE-dependent, cell-based assay was methyl 2-(4-adamantan-1-yl-phenoxy)methyl-1H-benzimidazole-5-carboxylate (**AC1-004**). The compound showed low single-digit micromolar GI_{50} values against various human cancer cell lines. Mechanistically, **AC1-004** inhibits angiogenesis *in vivo* and *in vitro*. The *in vivo* studies were particularly striking, showing that tumour growth in mice could be reduced by up to 59%.⁸ The aim of our current study was to enhance the effects of the drug by making use of the so-called metal drug synergism. The coordination of an already active compound as a ligand to a metal fragment frequently leads to complexes of higher selectivity, a lower risk of unwanted side effects and a higher retention time due their greater stability.⁹⁻¹³ Via N,N'-dialkylation the 5-carboalkoxybenzimidazole moiety of **AC1-004** can be transformed into an NHC ligand. By simultaneously replacing the 4-(adamant-1-yl) phenyl ether by the corresponding thiol as the second ligand incorporating the Au-S-R motif of auranofin, which has proven to be highly effective in preclinical studies¹⁴⁻¹⁶, we expected to achieve accompanying anti-tumour effects such as inhibition of TrxR and an increase in ROS.^{17,18} We synthesised twelve new NHC gold(I) chlorido and thiolato complexes based on **AC1-004** and investigated their stability, cytotoxicity, mode of action as well as their subcellular accumulation via biorthogonal click chemistry.

^aChair of Organic Chemistry I, University of Bayreuth, Bayreuth, 95440, Germany.

^bChair of Inorganic Chemistry II, University of Bayreuth, Bayreuth, 95440, Germany.

^cDevelopmental Biology, University of Bayreuth, Bayreuth, 95440, Germany.

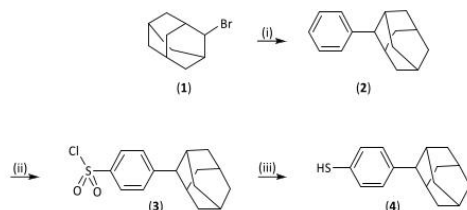
† These authors contributed equally to this work.

Electronic Supplementary Information (ESI) available: NMR spectra; stability studies; crystallographic data; cellular uptake of complexes; Caspase-3/7 activation; inhibition of thioredoxin reductase (TrxR); electrophoretic mobility shift assays etc. See DOI: 10.1039/x0xx00000x

Results and discussion

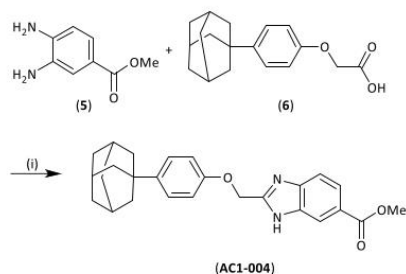
Synthesis and characterization

The novel ligand 4-(adamantan-2-yl)benzenethiol (**4**) was synthesised in three steps with an overall yield of 53% (scheme 1). Benzene, used as the solvent, was alkylated with 2-bromoadamantane (**1**) in a *Friedel-Crafts* reaction affording monosubstituted 2-phenyladamantane (**2**) with a yield of 84% which was used without further purification. Chlorosulfonation led, nearly quantitatively and exclusively, to 4-(adamantan-2-yl)benzenesulfonyl chloride (**3**) which, again without further purification, was reduced to the desired 4-(adamantan-2-yl) benzenethiol (**4**) with a yield of 64%.¹⁹



Scheme 1: Synthesis of 4-(adamantan-2-yl)benzenethiol (**4**). Reagents and conditions: (i) FeBr_3 , PhH, $0^\circ\text{C} \rightarrow 80^\circ\text{C}$, 48 h, 84%; (ii) H_2SO_4 , CH_2Cl_2 , $0^\circ\text{C} \rightarrow 45^\circ\text{C}$, 4.5 h, 98%; (iii) Me_2SiCl_2 , Zn, DMAC, DCE, 75°C , 1 h, 64%.

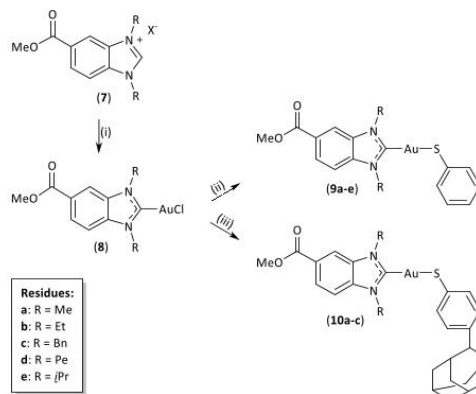
The reference, methyl 2-(4-adamantan-1-yl-phenoxy)methyl)-1H-benzimidazole-5-carboxylate (**AC1-004**), was synthesised as described in the literature by reacting methyl 3,4-diaminobenzoate (**5**) with 2-(4-(adamantan-1-yl)phenoxy)acetic acid (**6**) in a cycloaddition reaction (scheme 2).⁸ High-resolution mass spectra confirmed that only one species was present and the duplication of the signals of the aromatic protons in the ^1H NMR spectrum arose from imine-enamine tautomerism.



Scheme 2: Synthesis of **AC1-004**. Reagents and conditions: (i) PPSE, 140°C , 4 h, 89%.

The synthesis of 5-methoxycarbonyl-1,3-dialkylbenzimidazolium halides **7a-e** followed our established procedure (scheme 3).²⁰ Their subsequent complexation and transmetalation proceeded well and reproducibly for all salts with hardly any noticeable influence of the N-substituents on the yield of the complexation. The final exchange of the chlorido for a thiophenol ligand in complex **8** was carried out in methanol with *in situ* generated NaOMe to afford thiophenol complexes **9**. However, this method could not be applied to an exchange of chlorido for thiol **4** because of the insolubility of the

latter in methanol. Changing the solvent to CH_2Cl_2 and the base to KO^tBu eventually gave the desired thiol complexes **10a-c**. However, the isopropyl and pentyl analogues **10d** and **10e** could not be obtained in this way, despite variation of the reaction conditions.



Scheme 3: General synthetic route to NHC-Au(I) thiolato complexes **9a-e** and **10a-c**. Reagents and conditions: (i) 1. Ag_2O , CH_2Cl_2 , light exclusion, r.t., 6 h; 2. $\text{AuCl}(\text{SMe}_2)$, CH_2Cl_2 , light exclusion, r.t., 24h; (ii) Na, SPh, MeOH, r.t., 24h; (iii) KO^tBu , **4**, CH_2Cl_2 , r.t., 24h.

Crystals of **9b** suitable for X-ray diffraction analyses were grown by slow evaporation of a saturated solution in $\text{CH}_2\text{Cl}_2/n$ -hexane. Figure 1 shows the resulting molecular structure. The bond lengths were 1.990 Å for the C-Au bond and 2.292 Å for the Au-S bond. The latter is longer than an average Au-S bond which nicely visualises the *trans* effect of the NHC ligand.²¹ Both ligands, thiophenol and the benzimidazolium ylidene are arranged in a near-linear fashion with a C-Au-S bond angle of 177.76° . Furthermore, apart from the methyl group of the N-substituents and the phenyl ring of the thiophenolato ligand, the molecule lies in one plane.

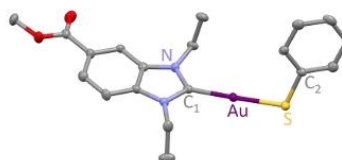
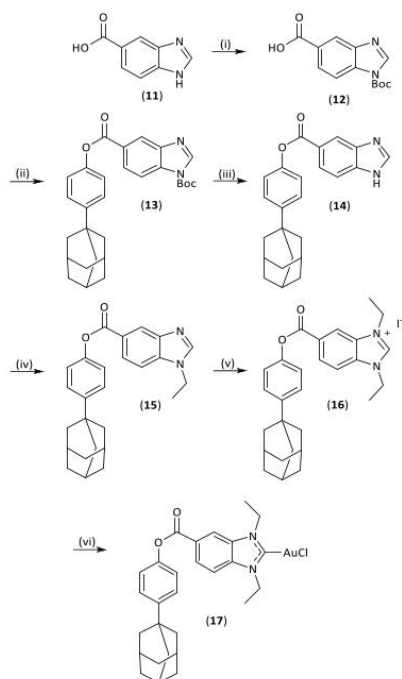


Figure 1: Molecular structure of complex **9b** as thermal ellipsoid representations at the 50% probability level (H atoms omitted). Selected bond lengths [Å] and angles [°]: C1-Au 1.990, Au-S 2.292, Au-S-C2 106.09, C1-Au-S 177.76.

To further determine the influence of the thiol ligands on the cytotoxicity of the compounds, the gold chlorido complex **17** was synthesised. This connects the 4-adamantylphenyl motif of **AC1-004** with the benzimidazolium NHC ligand via an ester bond (scheme 4). Moreover, as our group has found in previous studies that the target of certain gold(I) NHC-complexes depended on their second ligand,⁹ with chlorido ligands directing them towards cell nuclei, the evaluation of complex **17** should provide insight into the influence of the thiol ligands of complexes **9** and **10** on their overall cytotoxicity mechanism of action. Protection of the amine group was necessary

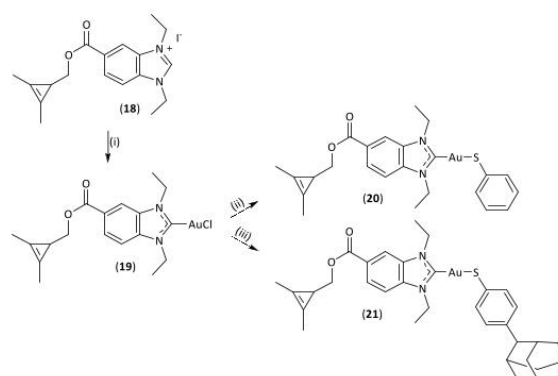
to achieve an esterification of benzimidazole carboxylic acid **11** with sterically more demanding alcohols like phenols. Boc was chosen for its acid lability, since the ester itself proved to be rather labile in upcoming steps. After a *Steglich-Hassner* esterification of protected benzimidazole **12** and a subsequent deprotection of product ester **13**, the N-alkylation of benzimidazole **14** had to be conducted in two steps. Direct N,N'-dialkylation attempts resulted in poor yields mainly because of saponification of the ester functionality. Under milder condition, compound **14** was monoalkylated by ethyl iodide / potassium carbonate to afford **15** in 80% yield and high purity. The ethylation of **15** afforded, without any base present, iodide **16** quantitatively. The latter was converted to the gold complex **17** in 66% yield via the silver complex as usual, just like the methyl esters. It is worth noting, that attempts to react iodide **16** with Ag₂O followed by half an equivalent of AuCl(SMe₂) in MeOH/CH₂Cl₂ in order to generate the cationic [(NHC)₂Au⁺]BF₄⁻ complex failed, leading instead to the bis[5-(methoxycarbonyl)-(N,N'-diethyl)benzimidazol-2-ylidene]Au⁺ complex and recovered 4-(1-adamantyl)phenol. Apparently, dry methanol and the intermediate AgOH were nucleophilic and basic enough to cleave the labile, sterically crowded phenol ester. Repeating the reaction in dry CH₂Cl₂ likewise failed to produce the desired product, but resulted in saponification.



Scheme 4: Synthesis of chlorido complex **17**. Reagents and conditions: (i) Boc₂O, 10% Na₂CO_{3(aq.)}, 1,4-dioxane, r.t., 16 h, 80%; (ii) EDC-HCl, DMAP, 4-(1-adamantyl)(C₆H₄)OH, CH₂Cl₂, r.t., 24 h, 84%; (iii) TFA, CH₂Cl₂, r.t., 4 h, quant.; (iv) EtI, K₂CO₃, DMF, 50 °C, 24 h, 80%; (v) EtI, 1,4-dioxane, reflux, 24 h, quant.; (vi) 1. Ag₂O, CH₂Cl₂, light exclusion, r.t., 6 h; 2. AuCl(SMe₂), CH₂Cl₂, light exclusion, r.t., 24 h, 66%.

The ethyl substituted complexes of the respective series **9b**, **10b** and **17** were subjected to stability studies. None of the complexes showed a change of their signals in ¹H NMR spectra over a period of at least three days when dissolved in DMSO-d₆ + 5% D₂O, i.e. under biotest-like aqueous conditions (*cf. supporting information*). Hence, they can be considered stable under conditions prevailing in the bio-evaluation assays.

In order to determine the subcellular accumulation and so obtain an indication of the mechanism of antitumoural action, cyclopropene analogues of complexes **9b** and **10b** were synthesised (scheme 5). This moiety allows a visualisation of the compound via a ring strain promoted *Diels Alder*_(inv.) cycloaddition reaction with fluorescent tetrazine dyes while retaining a high structural similarity to the corresponding methyl esters. The synthesis of the benzimidazolium precursor was recently published by us.²⁰ Its complexation to give gold complex **19** via the formation of a silver complex and its transmetalation with AuCl(SMe₂) proceeded analogously to the synthesis of complexes **8** and **17**. Likewise, the exchange of the chlorido ligand of **19** for the respective thiol which afforded the complexes **20** and **21** with 70 percent yield.



Scheme 5: Synthetic route to cyclopropene-bearing (NHC) Au(I) chlorido and thiolato complexes. Reagents and conditions: (i) 1. Ag₂O, CH₂Cl₂, light exclusion, r.t., 6 h; 2. AuCl(SMe₂), CH₂Cl₂, light exclusion, r.t., 24 h, 74%; (ii) KO^tBu, SPh, CH₂Cl₂, r.t., 24 h, 82%; (iii) KO^tBu, **4**, CH₂Cl₂, r.t., 24 h, 72%.

Biological evaluation

Inhibitory effect on cancer cell proliferation

To determine the cytotoxicity of the compounds **9a-e**, **10a-c**, **17**, **20**, **21** and of the positive controls **AC1-004**, YC-1, and auranofin, their antiproliferative activity was tested via MTT assays. Eight different cancer or hybrid cell lines of six different entities were treated for 72 h and IC₅₀ values were calculated using GraphPad Prism 9 (Table 1). The IC₅₀ values for all cell lines were averaged and compared to derive a general structure-activity relationship (Fig. 2).

Table 1: Mean IC_{50} values \pm SD [μ M] of test compounds **9a-e**, **10a-c**, **17**, **20-21**, **AC1-004**, YC-1, and auranofin against 518A2 melanoma, EA.hy926 endothelial hybrid, U-87 glioblastoma, MCF-7 breast carcinoma, HT-29 colorectal adenocarcinoma, KB-V1^{vbl} cervix carcinoma, HCT116 wildtype and p53 knockout colon carcinoma cells after 72 h.

	IC_{50} (72 h) [μ M]								mean IC_{50}
	518A2	EA.hy926	U-87	MCF-7	HT-29	KB-V1 ^{vbl}	Hct116	Hct116p53	
AC1-004	17.3 \pm 1.7	5.7 \pm 0.4	45 \pm 0.6	12.5 \pm 1.1	17.9 \pm 1.5	1.4 \pm 0.2	11.4 \pm 2.0	12.3 \pm 0.6	15.4
YC-1	0.9 \pm 0.04	>50	> 50	5.1 \pm 0.3	1.2 \pm 0.1	21.6 \pm 5.3	0.8 \pm 0.1	12.3 \pm 0.6	17.7
auranofin	1.6 \pm 0.1	5.2 \pm 0.2	4.6 \pm 0.1	4.5 \pm 0.09	5.0 \pm 0.1	3.4 \pm 0.4	2.4 \pm 0.2	2.2 \pm 0.3	3.6
9a	15.6 \pm 0.8	4.1 \pm 0.4	3.7 \pm 0.08	4.2 \pm 0.5	14.5 \pm 0.6	4.8 \pm 0.5	16.5 \pm 1.1	10.6 \pm 1.5	9.3
9b	18.8 \pm 1.3	6.8 \pm 0.7	5.7 \pm 1.0	14.0 \pm 0.5	11.8 \pm 1.3	18.8 \pm 1.2	11.6 \pm 0.8	5.9 \pm 0.1	11.7
9c	20.7 \pm 1.0	2.1 \pm 0.2	2.8 \pm 0.2	2.5 \pm 0.3	5.4 \pm 0.2	10.6 \pm 1.1	12.8 \pm 1.8	5.3 \pm 0.2	7.8
9d	7 \pm 0.2	5.5 \pm 0.3	7.2 \pm 0.2	8.1 \pm 0.1	16.6 \pm 0.6	15.7 \pm 1.2	7.2 \pm 0.5	2.3 \pm 0.3	8.7
9e	6.1 \pm 0.4	9.7 \pm 0.7	2.0 \pm 0.04	4.0 \pm 0.04	6.6 \pm 0.6	14.2 \pm 0.5	5.2 \pm 0.2	3.6 \pm 0.4	6.4
10a	17.8 \pm 1.4	15.7 \pm 1.5	20.6 \pm 2.0	14.4 \pm 1.6	19.8 \pm 1.2	27.1 \pm 1.1	17.0 \pm 0.9	13.8 \pm 0.9	18.3
10b	17.2 \pm 1.3	17.2 \pm 1.2	33.4 \pm 1.1	12.7 \pm 0.8	29.2 \pm 2.2	39.6 \pm 4.5	8.5 \pm 0.8	7.1 \pm 0.5	20.6
10c	> 50	> 50	35.1 \pm 0.8	23.8 \pm 2.0	25.3 \pm 1.8	> 50	42.0 \pm 2.2	8.7 \pm 0.6	35.6
17	>50	>50	19.2 \pm 2	8.6 \pm 1.5	7.0 \pm 0.7	32.0 \pm 2.2	> 50	42.2 \pm 0.3	32.4
20	5.2 \pm 0.04	5.5 \pm 0.2	6.7 \pm 0.3	7.8 \pm 0.4	15.6 \pm 1.2	16.4 \pm 1.7	7.0 \pm 0.4	5.9 \pm 0.1	8.8
21	9.3 \pm 0.7	11.4 \pm 1.0	36.3 \pm 0.8	22.9 \pm 4.4	43.3 \pm 6.2	20.3 \pm 2.5	17.7 \pm 3.0	11.6 \pm 1.0	33.3

By and large, the thiophenol Au(I) complexes **9** with mainly single-digit micromolar IC_{50} values were more active than the 4-(adamantan-2-yl)benzenethiolato Au(I) complexes **10**, which featured IC_{50} values predominantly in the double-digit micromolar range. The IC_{50} values of the thiophenolato Au(I) complex with a cyclopropene moiety **20** are lower on average than those of its bulkier analogue **21** and they are comparable to or lower than those of its methyl ester analogue **9b**. Within series **9** (thiophenolato), there was a slight increase in activity with increasing lipophilicity of the N-substituents. The opposite effect was found for complexes **10** whose activities declined with increasing size of the residue, possibly due to an associated decrease in solubility.

The cells were additionally treated with the lead compound **AC1-004**⁸ (15.4 μ M), the known HIF-1 α inhibitor YC-1⁶ (17.7 μ M) and the clinically approved gold(I) complex auranofin²² (3.6 μ M) for comparison. Cell line specific effects were observed for the multi-drug resistant KB-V1 cervix carcinoma cell line, which was relatively sensitive to **9a** as well as **AC1-004** and auranofin.²³ Some cell lines showed compound-specific resistance within the concentration range tested (100 μ M - 0.5 nM) with IC_{50} values above 50 μ M. These included 518A2 melanoma cells (**10c** and **17**), EA.hy926 endothelial hybrid cells (YC-1, **10c** and **17**), U87 glioblastoma cells (YC-1) or HCT116 colon carcinoma cells (**17**). HCT116 cells lacking functional p53 were more sensitive to most test substances than the wildtype with functional p53.

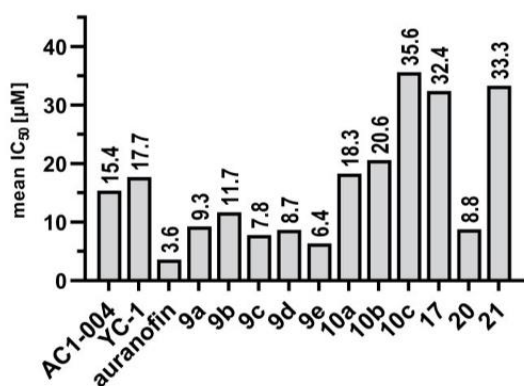


Figure 2: Mean IC_{50} values [μ M] over all tested cell lines for each of the test compounds **9a-e**, **10a-c**, **17**, **20**, **21** and positive controls **AC1-004**, YC-1, and auranofin.

Impact on the cellular redox system

Substance induced toxicity in cancer cells can originate from oxidative stress due to an elevated level of reactive oxygen species (ROS).²⁴ This often leads to cell cycle arrest, senescence or cell death and counteracts the tumor-promoting effects of ROS in many cancer types.²⁵ Intracellular formation of ROS can be quantified by 2',7'-dichlorodihydrofluorescein diacetate (DCFH-DA), which is converted to DCFH by cellular esterases and turns fluorescent when oxidized by intracellular ROS.²⁶ Gold(I) complexes like auranofin might induce ROS formation by interacting with thiol-containing enzymes like thioredoxin reductase (TrxR).²⁷ The measurement of ROS in 518A2 melanoma cells after treatment with 5 μ M of test compounds **9a-e**, **10a-c**, **17**, **20**, **21** and with the controls **AC1-004**, YC-1, and auranofin showed a distinct increase for all Au(I) complexes (Fig. 3). An exception was the Au(I)-chlorido complex **17**, which, like **AC1-004** and YC-1, induced no ROS increase. Once more, the complexes **9**

showed activities ascending when going from **9e** to **9a**. Moderate ROS inductions were observed for complexes **10** and for the cyclopropenyl derivatives **20** and **21**. The Au(I)-thiolato motif, which the lead structure **AC1-004** lacks, is apparently essential for a distinct ROS induction. Complexes **9a-c** and **10a-c** also inhibited the activity of TrxR, as was previously shown also for auranofin (Fig. S26, Supporting Information), suggesting a similar mechanism through a deficient control of oxidative stress and redox regulation.²⁸

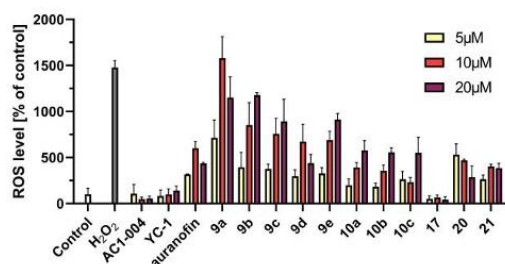


Figure 3: Fluorescence based DCFH-DA assays showed the reactive oxygen species (ROS) levels in 518A2 melanoma cells treated with 5, 10 and 20 μM of test compounds **9a-e**, **10a-c**, **17**, **20**, **21**, **AC1-004**, YC-1, auranofin and the positive control hydrogen peroxide (H_2O_2 , 1 μM) compared with solvent treated cells set to 100%. The values are means \pm SD from at least three independent experiments.

Interference with the cancer cell cycle

A common down-stream effect of increased ROS levels and TrxR inhibition is the alteration of the number of cells in the different cell cycle phases. We analysed such potential effects by the new complexes on 518A2 melanoma cells using fluorescence-assisted cell sorting (FACS) (Fig. 4)

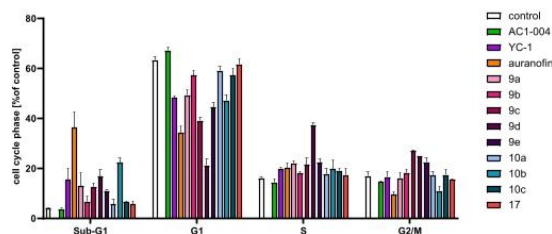


Figure 4: Effect of compounds **9a-e**, **10a-c**, **17**, **AC1-004**, YC-1, (10 μM) and auranofin (5 μM) on the cell distributions in the different cell cycle phases of 518A2 melanoma cells after 24 h of treatment. Values \pm SD of two independent experiments were derived from at least 10000 counted cells with solvent treated control set to 100%.

In contrast to compounds **AC1-004**, **9b**, **10a**, **10c**, and **17**, which showed no change in cell cycle distributions, the complexes **9a**, **9c-e**, **10b**, compound YC-1, and especially auranofin induced an increase in the sub-G1 cell population, which is indicative of apoptosis, and subsequently led to a decrease in G1-phase cells. The investigation of cell death using a caspase 3/7 assay kit revealed a significant increase in activity for **9d** and the positive control staurosporine (STA) after incubation for 6 h (Fig. S2, Supporting Information). This

suggests an apoptotic pathway for **9d**, which also caused a notable S-phase arrest in 518A2 cells. Since S-phase arrest is usually associated with disruption of DNA replication or impairment of CDK (cyclin dependent kinases)-controlled cell cycle checkpoints, a possible interaction with DNA was investigated via electrophoretic mobility shift assays (EMSA), which revealed no interaction of **9d** with ds-DNA (Fig. S3, Supporting Information).²⁹ In addition, a slight increase in G2/M-phase cells for **9c-e** was observed.

Reorganisation of the actin cytoskeleton

Cell apoptosis and oxidative stress are frequently associated with the dynamics of the actin cytoskeleton.³⁰ A considerable body of evidence suggests a close relationship between the actin cytoskeleton and the regulation of mitochondrial function as a possible point of apoptotic regulation in eukaryotic cells.³¹ Fluorescence microscopy images of 518A2 cells after treatment with Au(I)-complexes **9a-c**, **10a-c**, **17** (10 μM), **9d-e** (5 μM) and auranofin (1 μM) revealed a concentration-dependent remodelling of the actin cytoskeleton (Fig. 5).

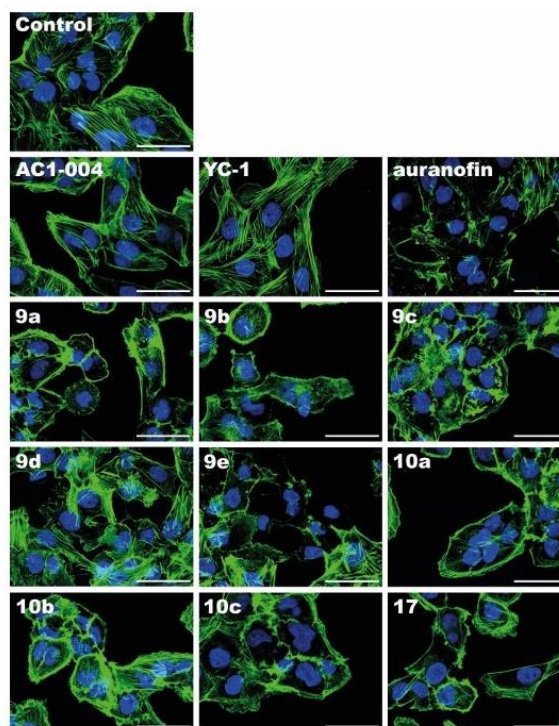


Figure 5: Immunofluorescence images of the actin cytoskeleton (green) and the nuclei (blue) of 518A2 melanoma cells after treatment with compounds **9a-c**, **10a-c**, **17**, **AC1-004**, YC-1, (10 μM), **9d-e** (5 μM) or auranofin (1 μM) for 24 h. Images are representative of at least two independent experiments. Scale bars correspond to 50 μm , magnification 640 \times .

The concentrations of auranofin and complexes **9d** and **9e** were reduced to 1 and 5 μM , respectively, due to their stronger cytotoxic effects on the cells. Reorganisation of the actin cytoskeleton resulted

in alterations such as stress fiber formation, actin degradation and clustering. The integrity of cells was also affected, resulting in detachment of focal adhesions and a rounded cell morphology.³² The degradation of the actin cytoskeleton already begins in the initiation stage of apoptosis, whereas the fragmentation of the cell nucleus only occurs at the end of the execution stage.³³ The absence of fragmented cell nuclei suggests that an early stage of apoptosis has not yet led to nuclear degradation. In contrast, **AC1-004** and the HIF-1 α -inhibitor YC-1 (10 μ M) showed no effects on the actin filaments, indicating that it might be the gold complex fragment that is responsible for the effects on the actin cytoskeleton.

Subcellular localisation

The similarity of the cyclopropene derivatives **20**, **21** and their counterparts **9b** and **10b** in terms of their effects in the MTT and DCFH-DA ROS formation assays, suggests a related mode of action, very likely also involving similar targets and sites of accumulation in the cells. This justifies the use of the compounds **20** and **21**, which can be fluorescently labelled by a *Diels-Alder* reaction,³⁴ as a probe for identifying not just their site of intracellular localisation but that of **9b** and **10b** as well. Figure 6 shows the subcellular distribution of the fluorescent click-products of the complexes **20** and **21** in 518A2 cells with counterstained nuclei and mitochondria.

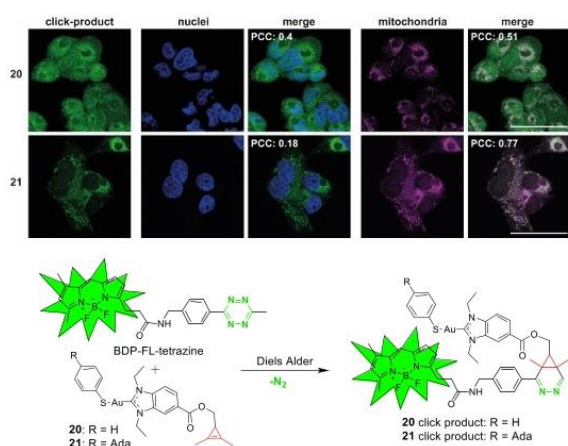


Figure 6: Confocal imaging of 518A2 melanoma cells treated with 25 μ M of cyclopropene derivatives **20** or **21** and BDP-FL-tetrazine for bioorthogonal labelling (green), or with MitoTracker[®] Red CM-H2XRos (violet), or DAPI (blue). Images are representative of at least two independent experiments. Scale bars correspond to 50 μ m, magnification 640 \times . Pearson correlation coefficient (PCC) was calculated for colocalised nuclei and mitochondria using colocal2 function (imageJ). Bottom scheme shows the general cycloaddition reaction of cyclopropenes **20** and **21** with BDP-FL-tetrazine to give fluorescent diazines.

Surprisingly, the adamantyl group of complex **21** affected the distribution within the cell, resulting in a selective accumulation within mitochondria. In contrast, complex **20** was detected in mitochondria, nuclei, and cytoplasm, indicating a rather unspecific distribution. Pearson's correlation coefficient (PCC) was used to quantify the accumulation within the cell organelles, with values near 1 standing for a complete overlay of both images. Mitochondria

which play a major role in crucial metabolic functions of the cell and the regulation of apoptosis, but also in cancer-specific phenomena such as the overproduction of ROS, are an important target for cancer treatment.^{35, 36} When we assume similar mitochondrial mechanisms of action for **20/21** and **9b/10b** the latter are likely to operate by induction of ROS-induced cancer cell death.³⁷ To further substantiate the comparability of complexes **9**, **10**, and **17** their uptake into 518A2 cells was quantified by ICP-MS analysis, yielding values between 8 and 19 ng of gold per 1×10^6 cells for compounds **9a-e**, **10b** and **17** (Fig. S4, Supporting Information). In comparison, the uptake of auranofin was 13-fold higher with 255 ng, which constitutes a significantly poorer uptake of the test substances.

Influence on endothelial tube formation

Another consequence of elevated oxidative stress in cancer cells is the upregulation of proliferation-enhancing transcription factors such as NF- κ B, VEGF or HIF-1 α which are responsible for tumour growth, migration, invasion or the induction of angiogenesis.³⁸⁻⁴⁰

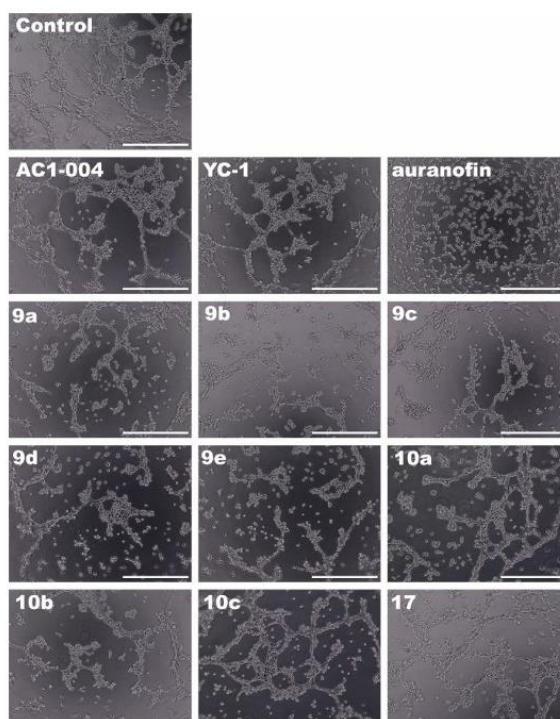


Figure 7: The ability of EA.hy926 endothelial hybrid cells to form tubular structures on Matrigel[®] when treated with substances **9a-e**, **10a-c**, **17**, **AC1-004**, YC-1, and auranofin (20 μ M) as well as negative control DMSO, documented by light microscopy. Images represent one of two independent experiments. Vitality was checked via MTT assays (vitality of control: > 80%, **10b** > 60%, auranofin < 60%). Scale bars correspond to 500 μ m, magnification 100 \times .

The development of new blood vessels promotes the growth of tumors and increases the risk of metastasis.⁴¹ The investigation of agents that inhibit angiogenesis in tumor tissue constituted a key

point in the development of new cancer therapies.⁴² The anti-angiogenic potential of the test compounds **9a-e**, **10a-c**, **17**, **AC1-004**, YC-1, and auranofin (20 μM) was examined by their inhibitory effects on the *in vitro* formation of vessel-like tubes by EA.hy926 endothelial hybrid cells (Fig. 7).⁴³ Growing these cells on a solubilised basement membrane matrix for 10 h led to the formation of polygonal tubes mimicking 2D vessel-like structures in the solvent-treated wells. Upon addition of the test compounds, different changes in the extent of tube formation were observed. Auranofin had by far the strongest inhibitory effect, apparent from its suppression of tubular structure formation and a strong reduction of cell vitality as determined by concomitant MTT assays. Complexes **9** and **10b** also showed distinct inhibitory effects on the migration of cells and the formation of cell-cell junctions, leaving merely small contiguous cell clusters and isolated tubes aside of individual cells. **10a**, **10b**, **17**, **AC1-004** and YC-1 led to the formation of polygonal structures similar to solvent-treated cells, not indicating any noteworthy anti-angiogenic effect.

Anti-angiogenic effect on zebrafish larvae

To confirm the anti-angiogenic properties *in vivo* and to investigate possible toxic effects in a vertebrate model, the angiogenesis of zebrafish larvae (24 hpf, hours post fertilisation) was investigated under compound exposure. Initially, the larvae showed a concentration-dependent tolerance for the test substances, which is why the concentrations shown vary between 1 and 10 μM (Fig. 8).

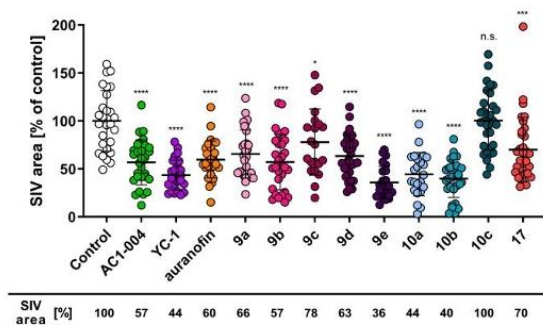


Figure 8: At least 21 zebrafish larvae were treated with test compounds **9c**, **10a-c**, **17**, YC-1 (10 μM), **9d** (5 μM), **9a**, **9b**, **9e**, **AC1-004** and auranofin (1 μM) for 48 h. To estimate the antiangiogenic effect the SIV (subintestinal vessel) area was quantified via ImageJ and quoted as the mean \pm SD with solvent treated fish set to 100%. Significance is given as n.s.: > 0.05; *: < 0.05; **: < 0.001; ***: < 0.0001, One-way ANOVA with Dunnett's multiple comparison test (GraphPad prism 9).

While compounds **9a**, **9b**, **9e**, **AC1-004** and auranofin were tolerated up to a maximum concentration of only 1 μM , complex **9d** was tolerated with a maximum concentration of 5 μM , and compounds **9c**, **10a-c**, **17**, and YC-1 even at 10 μM . The 4-(adamantan-2-yl)benzenethiolato complexes, as well as YC-1, and **9c** showed significantly fewer toxic effects compared to **AC1-004**, auranofin, and three of the thiophenolato complexes, with **9d** lying in between. Considering the effect on the formation of the subintestinal vein (SIV) in zebrafish larvae, an impairment of angiogenesis was observed for

all test compounds except **10c**. The activity was reduced by a benzyl group on the NHC ligand (**9c** and **10c**) and for the chlorido complex **17**. The strongest anti-angiogenic effect was exhibited by **9e**, **10a**, **10b** and YC-1 which is known to inhibit HIF-1 α and VEGF.⁴⁴ As applied only at a concentration of 1 μM , **9e** was the most intrinsically active inhibitor of angiogenesis.

Materials and methods

Chemical synthesis

General

Starting compounds were purchased from Sigma-Aldrich (St. Louis, United States), TCI (Tokio, Japan), Merck (Darmstadt, Germany), abcr (Karlsruhe, Germany), Acros Organics (Fair Lawn, United States), VWR (Radnor, United States) and used without further purification. All reactions with moisture-sensitive reagents were carried out under an argon atmosphere in water-free solvents. Unless stated otherwise, the solvents were purified and dried using standard methods.

Nuclear magnetic resonance (NMR) spectra were run on a Bruker (Bellerica, USA) DRX spectrometer at ambient temperature. Chemical shifts are given in ppm (δ) downfield from tetramethylsilane as internal standard. As internal standard for ¹H-NMR spectra the resonance signal of the residual proton of CDCl₃ (δ = 7.26 ppm), DMSO-d₆ (δ = 2.50 ppm) or MeOD-d₄ (δ = 3.31 ppm) was used; for ¹³C-NMR spectra the resonance signal of carbon atom of CDCl₃ (δ = 77.1 ppm), DMSO-d₆ (δ = 39.5 ppm) or MeOD-d₄ (δ = 49.0 ppm) was used. The ¹H-NMR spectra were measured at 500 MHz and ¹³C-NMR spectra at 125 MHz. For signal multiplicities the following abbreviations were used: s = singlet, d = doublet, t = triplet, sept = septet, m = multiplet, dd = doublet of doublets, dt = doublet of triplets, dq = doublet of quartets with the prefix v meaning virtual. Melting points were taken with an Electrothermal 9100 apparatus and are uncorrected. Mass spectra were recorded on a ThermoFisher Scientific (Waltham, United States) UPLC/Orbitrap MS system (HRMS-ESI).

Synthetic route to 4-(adamant-2-yl)benzenethiol (**4**)

2-Phenyladamantane (**2**)

2-Bromoadamantane **1** (1.36 g, 6.32 mmol, 1.00 eq.) was dissolved in dry benzene (30 mL) at 0 $^{\circ}\text{C}$ and FeBr₃ (187 mg, 632 μmol , 0.10 eq.) was added portionwise. The mixture was left stirring for 1 h at rt after which it was heated to 80 $^{\circ}\text{C}$ for 24 h. The suspension was filtered and the filtrate was evaporated. The product was isolated as a brownish oil (1.12 g, 5.27 mmol, 84%). ¹H NMR (500 MHz, CDCl₃) δ_{H} 7.47 (d, J = 6.8 Hz, 2H, H^{ar}), 7.44 (d, J = 6.8 Hz, 2H, H^{ar}), 7.29 (d, J = 7.4 Hz, 1H, H^{ar}), 3.14 (s, 1H, H^{ada}), 2.60 (s, 2H, H^{ada}), 2.16 - 1.97 (m, 7H, H^{ada}), 1.90 (s, 3H, H^{ada}), 1.71 - 1.65 (m, 2H, H^{ada}) ppm; ¹³C NMR (126 MHz, CDCl₃) δ_{C} 143.0 (s, C^{ar}), 126.8 (s, C^{ar}), 125.5 (s, C^{ar}), 123.8 (s, C^{ar}), 45.5 (s, C^{ada}), 37.9 (s, C^{ada}), 36.6 (s, C^{ada}), 30.6 (s, C^{ada}), 29.7 (s, C^{ada}), 26.7 (s, C^{ada}), 26.5 (s, C^{ada}) ppm.

The NMR data matched previously reported spectra.⁴⁵

4-(Adamant-2-yl)benzenesulfonyl chloride (**3**)

Compound **2** (300 mg, 1.41 mmol, 1.00 eq.) was dissolved in dry CH₂Cl₂ (5 mL) at 0 $^{\circ}\text{C}$ and NaCl (82.6 mg, 1.41 mmol, 1.00 eq.) was

added. Chlorosulfonic acid (470 μL , 7.06 mmol, 5.00 eq.) was added dropwise and the solution was left stirring at rt for 4.5 h. The mixture was poured on ice and the resulting emulsion was diluted with CH_2Cl_2 (50 mL). The organic phase was separated, the aqueous phase was extracted with CH_2Cl_2 (3 x 50 mL), and the combined organic phases were washed with $\text{NaHCO}_3(\text{aq.})$ (100 mL), dried over Na_2SO_4 , filtered and concentrated in vacuo. The product was isolated as a white solid (430 mg, 1.38 mmol, 98%) of m.p. 125 $^\circ\text{C}$; ^1H NMR (500 MHz, CDCl_3) δ_{H} 7.98 (d, $J = 8.7$ Hz, 2H, H^{ar}), 7.59 (d, $J = 8.7$ Hz, 2H, H^{ar}), 3.07 (s, 1H, H^{ada}), 2.51 (d, $J = 3.5$ Hz, 2H, H^{ada}), 2.09 - 1.90 (m, 6H, H^{ada}), 1.85 - 1.69 (m, 5H, H^{ada}), 1.65 - 1.60 (m, 1H, H^{ada}) ppm; ^{13}C NMR (126 MHz, CDCl_3) δ_{C} 153.4 (s, C^{ar}), 141.1 (s, C^{ar}), 128.1 (s, C^{ar}), 126.8 (s, C^{ar}), 47.2 (s, C^{ada}), 38.7 (s, C^{ada}), 37.3 (s, C^{ada}), 31.8 (s, C^{ada}), 30.9 (s, C^{ada}), 27.6 (s, C^{ada}), 27.3 (s, C^{ada}) ppm; HRMS (ESI): m/z calculated for $\text{C}_{16}\text{H}_{19}\text{O}_2\text{S}$ [$\text{M} - \text{Cl}$] $^+$: 275.11058. Found: 275.10955 [$\text{M} - \text{Cl}$] $^+$.

4-(Adamant-2-yl)benzenethiol (**4**)

Compound **3** (900 mg, 2.90 mmol, 1.00 eq.) and DMAc (805 mL, 8.69 mmol, 3.00 eq.) were dissolved in DCE (18 mL) and the resulting solution was treated with a suspension of Me_2SiCl_2 (1.23 mL, 10.1 mmol, 3.50 eq.) and with zinc (663 mg, 10.1 mmol, 3.50 eq.). After stirring at 75 $^\circ\text{C}$ for 2.5 h, the suspension was filtered and the solvent was evaporated. The residue was purified via column chromatography (cyclohexane) to give a white solid (329 mg, 1.35 mmol, 46%) with R_f 0.46 (cyclohexane) and m.p. 145 $^\circ\text{C}$; ^1H NMR (500 MHz, CDCl_3) δ_{H} 7.47 (d, $J = 8.4$ Hz, 2H, H^{ar}), 7.30 (d, $J = 8.4$ Hz, 2H, H^{ar}), 2.97 (s, 1H, H^{ada}), 2.43 (d, $J = 3.7$ Hz, 2H, H^{ada}), 2.05 - 1.97 (m, 3H, H^{ada}), 1.96 - 1.91 (m, 2H, H^{ada}), 1.84 - 1.69 (m, 5H, H^{ada}), 1.55 (d, $J = 3.7$ Hz, 2H, H^{ada}) ppm; ^{13}C NMR (126 MHz, CDCl_3) δ_{C} 144.0 (s, C^{ar}), 133.7 (s, C^{ar}), 128.1 (s, C^{ar}), 127.7 (s, C^{ar}), 46.6 (s, C^{ada}), 39.1 (s, C^{ada}), 37.8 (s, C^{ada}), 32.0 (s, C^{ada}), 31.1 (s, C^{ada}), 27.6 (s, C^{ada}), 28.0 (s, C^{ada}), 27.7 (s, C^{ada}) ppm.

General procedure for the synthesis of chlorido gold complexes **8**

5-(Methoxycarbonyl)-1,3-dialkyl-1H-benzimidazolium halide (**7**) (1.00 eq.) was dissolved in dry CH_2Cl_2 (15 mL/mmol). The solution was shielded from light before Ag_2O (0.70 eq.) was added. The mixture was stirred at rt for 6 h, treated with $\text{AuCl}(\text{SMe}_2)$ (1.10 eq.), and the resulting suspension was left stirring at rt for another 18 h. The mixture was filtered over Celite and the solvent was evaporated. Redissolving the residue in CH_2Cl_2 and precipitating the complex in pentane afforded the chlorido gold complexes as white to yellowish powders.

(5-Methoxycarbonyl)-1,3-dimethylbenzimidazol-2-ylidene gold(I) chloride (**8a**)

84.0 mg (192 μmol , 64%) from **7a** (100 mg, 301 μmol , 1.00 eq.), Ag_2O (48.8 mg, 211 μmol , 0.70 eq.) and $\text{AuCl}(\text{SMe}_2)$ (97.6 mg, 331 μmol , 1.10 eq.) in dry CH_2Cl_2 (5.00 mL). ^1H NMR (500 MHz, CDCl_3) δ_{H} 8.20 (d, $J = 1.4$ Hz, 1H, H^{ar}), 8.17 (dd, $J = 8.5$ Hz, 1.4 Hz, 1H, H^{ar}), 7.51 (d, $J = 8.5$ Hz, 1H, H^{ar}), 4.09 (s, 3H, NMe), 4.08 (s, 3H, NMe), 3.98 (s, 3H, OMe) ppm; ^{13}C NMR (125 MHz, CDCl_3) δ_{C} 182.0 (s, NCN), 166.2 (s, COOMe), 136.6 (s, C^{ar}), 133.7 (s, C^{ar}), 127.0 (s, C^{ar}), 126.3 (s, C^{ar}), 113.3 (s, C^{ar}), 111.2 (s, C^{ar}), 52.8 (s, OMe), 35.5 (NMe) ppm.

(5-Methoxycarbonyl)-1,3-diethylbenzimidazol-2-ylidene gold(I) chloride (**8b**)

75.0 mg (191 μmol , 63%) from **7b** (110 mg, 305 μmol , 1.00 eq.), Ag_2O (49.5 mg, 214 μmol , 0.70 eq.) and $\text{AuCl}(\text{SMe}_2)$ (99.0 mg, 336 μmol , 1.10 eq.) in dry CH_2Cl_2 (5.00 mL). ^1H NMR (500 MHz, CDCl_3) δ_{H} 8.19 (d, $J = 1.4$ Hz, 1H, H^{ar}), 8.14 (dd, $J = 8.5$ Hz, 1.4 Hz, 1H, H^{ar}), 7.52 (d, $J = 8.5$ Hz, 1H, H^{ar}), 4.68 - 4.41 (m, 4H, NCH_2), 3.98 (s, 3H, OMe), 1.56 (q, $J = 7.0$ Hz, 6H, CH_3) ppm; ^{13}C NMR (125 MHz, CDCl_3) δ_{C} 180.3 (s, NCN), 166.3 (s, COOMe), 135.7 (s, C^{ar}), 132.8 (s, C^{ar}), 126.8 (s, C^{ar}), 126.2 (s, C^{ar}), 113.4 (s, C^{ar}), 111.3 (s, C^{ar}), 52.8 (s, OMe), 44.3 (NCH_2), 15.9 (CH_3) ppm.

(5-Methoxycarbonyl)-1,3-dibenzylbenzimidazol-2-ylidene gold(I) chloride (**8c**)

80.0 mg (161 μmol , 53%) from **7c** (100 mg, 228 μmol , 1.00 eq.), Ag_2O (37.1 mg, 160 μmol , 0.70 eq.) and $\text{AuCl}(\text{SMe}_2)$ (74.1 mg, 252 μmol , 1.10 eq.) in dry CH_2Cl_2 (5.00 mL). ^1H NMR (500 MHz, CDCl_3) δ_{H} 8.08 (d, $J = 1.4$ Hz, 1H, H^{ar}), 8.00 (dd, $J = 8.7$ Hz, 1.4 Hz, 1H, H^{ar}), 7.45 - 7.40 (m, 1H, H^{ar}), 7.38 - 7.33 (m, 10H, H^{ar}), 5.78 (d, $J = 2.9$ Hz, 4H, NCH_2), 3.90 (s, 3H, OMe) ppm; ^{13}C NMR (125 MHz, CDCl_3) δ_{C} 182.1 (s, NCN), 166.0 (s, COOMe), 136.2 (s, C^{ar}), 134.2 (s, C^{ar}), 134.1 (s, C^{ar}), 133.3 (s, C^{ar}), 129.3 (s, C^{ar}), 129.0 (s, C^{ar}), 127.6 (s, C^{ar}), 127.5 (s, C^{ar}), 127.2 (s, C^{ar}), 126.4 (s, C^{ar}), 114.1 (s, C^{ar}), 112.2 (s, C^{ar}), 53.3 (s, NCH_2), 53.1 (NCH_2), 52.8 (OMe) ppm.

(5-Methoxycarbonyl)-1,3-dipentylbenzimidazol-2-ylidene gold(I) chloride (**8d**)

37.0 mg (67.5 μmol , 50%) from **7d** (60.0 mg, 135 μmol , 1.00 eq.), Ag_2O (21.9 mg, 94.5 μmol , 0.70 eq.) and $\text{AuCl}(\text{SMe}_2)$ (43.8 mg, 149 μmol , 1.10 eq.) in dry CH_2Cl_2 (5.00 mL). ^1H NMR (500 MHz, CDCl_3) δ_{H} 8.18 (d, $J = 1.3$ Hz, 1H, H^{ar}), 8.13 (dd, $J = 8.6$ Hz, 1.4 Hz, 1H, H^{ar}), 7.50 (d, $J = 8.7$ Hz, 1H, H^{ar}), 4.50 (dt, $J = 9.9$ Hz, 7.4 Hz, 4H, NCH_2), 3.99 (s, 3H, OMe), 1.99 - 1.91 (m, 4H, CH_2), 1.42 - 1.33 (m, 8H, CH_2), 0.90 (dt, $J = 6.9$ Hz, 4.1 Hz, 6H, CH_3) ppm; ^{13}C NMR (125 MHz, CDCl_3) δ_{C} 180.9 (s, NCN), 166.2 (s, COOMe), 136.0 (s, NCN), 133.0 (s, C^{ar}), 126.7 (s, C^{ar}), 125.9 (s, C^{ar}), 113.4 (s, C^{ar}), 111.3 (s, C^{ar}), 52.7 (s, OMe), 49.2 (NCH_2), 29.8 (s, CH_2), 29.7 (s, CH_2), 28.8 (s, CH_2), 28.7 (s, CH_2), 22.3 (s, CH_2), 13.9 (s, CH_3) ppm.

(5-Methoxycarbonyl)-1,3-diisopropylbenzimidazol-2-ylidene gold(I) chloride (**8e**)

100 mg (203 μmol , 77%) from **7e** (90.0 mg, 263 μmol , 1.00 eq.), Ag_2O (42.8 mg, 185 μmol , 0.70 eq.) and $\text{AuCl}(\text{SMe}_2)$ (85.5 mg, 290 μmol , 1.10 eq.) in dry CH_2Cl_2 (5.00 mL). ^1H NMR (500 MHz, CDCl_3) δ_{H} 8.34 (d, $J = 1.4$ Hz, 1H, H^{ar}), 8.07 (dd, $J = 8.7$ Hz, 1.5 Hz, 1H, H^{ar}), 7.68 (d, $J = 8.7$ Hz, 1H, H^{ar}), 5.52 (dsept, $J = 7.1$ Hz, 3.6 Hz, 2H, NCH), 3.98 (s, 3H, OMe), 1.76 (dd, $J = 13.4$ Hz, 7.0 Hz, 12H, CH_3) ppm; ^{13}C NMR (125 MHz, CDCl_3) δ_{C} 177.8 (s, NCN), 165.1 (s, COOMe), 134.2 (s, C^{ar}), 131.1 (s, C^{ar}), 125.0 (s, C^{ar}), 124.2 (s, C^{ar}), 113.7 (s, C^{ar}), 111.6 (s, C^{ar}), 53.7 (s, NCH), 53.6 (s, NCH), 51.6 (s, OMe), 20.8 (s, CH_3), 20.6 (CH_3) ppm.

General procedure for the synthesis of thiophenolato complexes **9**

Sodium (2.00 eq.) was dissolved in dry MeOH (200 mL/mmol). The resulting solution of sodium methoxide was treated with thiophenol

(1.00 eq.) and stirred for 1 h at rt. The respective gold chlorido complex **8** (1.00 eq.) was added portionwise to the now yellow solution of sodium thiophenolate. After stirring at rt for 24 h the solvent was evaporated and the remainder was suspended in CH_2Cl_2 and filtered. The filtrate was concentrated in vacuo and the residue was precipitated in pentane. The thiophenolato complexes **9** could be isolated as yellowish powders after filtration and drying in vacuo.

[Thiophenolato(5-methoxycarbonyl-1,3-dimethylbenzimidazol-2-ylidene)] gold(I) (9a)

17.5 mg (34.3 μmol , 68%) from sodium (2.32 mg, 100 μmol , 2.00 eq.), thiophenol (5.45 μL , 50.4 μmol , 1.00 eq.) and **8a** (22.0 mg, 50.4 μmol , 1.00 eq.) in dry MeOH (10 mL). m.p. 195 °C (decomp.); ^1H NMR (500 MHz, CDCl_3) δ_{H} 8.18 (s, 1H, H^{ar}), 8.16 (s, 1H, H^{ar}), 7.61 (d, $J = 7.5$ Hz, 2H, H^{ar}), 7.50 (d, $J = 8.5$ Hz, 1H, H^{ar}), 7.09 (t, $J = 7.5$ Hz, 2H, H^{ar}), 6.96 (t, $J = 7.5$ Hz, 1H, H^{ar}), 4.09 (s, 3H, NMe), 4.08 (s, 3H, NMe), 3.99 (s, 3H, OMe) ppm; ^{13}C NMR (125 MHz, CDCl_3) δ_{C} 192.5 (s, NCN), 166.3 (s, COOMe), 142.3 (s, C^{ar}), 136.7 (s, C^{ar}), 133.8 (s, C^{ar}), 132.6 (s, C^{ar}), 128.0 (s, C^{ar}), 126.7 (s, C^{ar}), 126.1 (s, C^{ar}), 123.2 (s, C^{ar}), 113.1 (s, C^{ar}), 110.1 (s, C^{ar}), 52.7 (s, OMe), 35.1 (s, NMe) ppm; HRMS (ESI): m/z calculated for $\text{C}_{17}\text{H}_{17}\text{AuN}_2\text{O}_2\text{S} + \text{H}^+$ [M + H] $^+$: 511.07545. Found: 442.08198 [(NHC)Au(MeCN)] $^+$; 605.14561 [(NHC) $_2$ Au] $^+$; 911.12265 [2M-SPh] $^+$.

[Thiophenolato(5-methoxycarbonyl-1,3-diethylbenzimidazol-2-ylidene)] gold(I) (9b)

11.0 mg (20.4 μmol , 63%) from sodium (1.48 mg, 64.6 μmol , 2.00 eq.), thiophenol (3.35 μL , 32.3 μmol , 1.00 eq.) and **8b** (15.0 mg, 32.3 μmol , 1.00 eq.) in dry MeOH (5 mL). m.p. 165 °C (decomp.); ^1H NMR (500 MHz, CDCl_3) δ_{H} 8.20 (d, $J = 1.3$ Hz, 1H, H^{ar}), 8.15 (dd, $J = 8.5$ Hz, 1.3 Hz, 1H, H^{ar}), 7.67 - 7.60 (m, 2H, H^{ar}), 7.52 (d, $^3J = 8.5$ Hz, 1H, H^{ar}), 7.10 (t, $J = 7.7$ Hz, 2H, H^{ar}), 7.01 - 6.92 (m, 1H, H^{ar}), 4.59 (dq, $J = 9.9$ Hz, 7.3 Hz, 4H, NCH_2), 3.99 (s, 3H, OMe), 1.59 (vq, $J = 7.3$ Hz, 6H, CH_3) ppm; ^{13}C NMR (125 MHz, CDCl_3) δ_{C} 190.9 (s, NCN), 166.4 (s, COOMe), 142.3 (s, C^{ar}), 136.0 (s, C^{ar}), 133.0 (s, C^{ar}), 132.7 (s, C^{ar}), 128.0 (s, C^{ar}), 126.6 (s, C^{ar}), 125.9 (s, C^{ar}), 123.2 (s, C^{ar}), 113.2 (s, C^{ar}), 110.1 (s, C^{ar}), 52.7 (s, OMe), 44.0 (s, NCH_2), 15.7 (s, CH_3) ppm; HRMS (ESI): m/z calculated for $\text{C}_{19}\text{H}_{21}\text{AuN}_2\text{O}_2\text{S} + \text{H}^+$ [M + H] $^+$: 539.10675. Found: 470.11337 [(NHC)Au(MeCN)] $^+$; 661.20776 [(NHC) $_2$ Au] $^+$; 967.18469 [2M-SPh] $^+$. Crystal data: $\text{C}_{19}\text{H}_{21}\text{AuN}_2\text{O}_2\text{S}$, $M = 538.41$, monoclinic, space group P21/c; $a = 13.180(3)$ Å, $b = 13.170(3)$ Å, $c = 10.710(2)$ Å, $\alpha = 90^\circ$, $\beta = 101.60(3)^\circ$, $\gamma = 90^\circ$, $V = 1821.1(7)$ Å 3 , $Z = 4$, $\lambda = 0.71073$ Å, $\mu = 8.208$ mm $^{-1}$, $T = 133$ K; 28 885 reflections measured, 4398 unique; $R [I > 2s(I)] = 0.0367$, $\text{GOF} = 1.071$. CCDC 2214175.

[Thiophenolato(5-methoxycarbonyl-1,3-dibenzylbenzimidazol-2-ylidene)] gold(I) (9c)

19.0 mg (28.7 μmol , 56%) from sodium (2.34 mg, 102 μmol , 2.00 eq.), thiophenol (5.20 μL , 51.0 μmol , 1.00 eq.) and **8c** (30.0 mg, 51.0 μmol , 1.00 eq.) in dry MeOH (10 mL). m.p. 165 °C (decomp.); ^1H NMR (500 MHz, CDCl_3) δ_{H} 8.10 (d, $J = 1.3$ Hz, 1H, H^{ar}), 8.01 (dd, $J = 8.6$ Hz, 1.4 Hz, 1H, H^{ar}), 7.54 (d, $J = 7.6$ Hz, 2H, H^{ar}), 7.46 - 7.42 (m, 2H, H^{ar}), 7.41 - 7.37 (m, 3H, H^{ar}), 7.36 - 7.32 (m, 5H, H^{ar}), 7.00 (d, $J = 7.5$ Hz, 2H, H^{ar}), 6.93 (t, $J = 7.3$ Hz, 1H, H^{ar}), 5.79 (d, $J = 3.6$ Hz, 4H, NCH_2), 3.91 (s, 3H, OMe) ppm; ^{13}C NMR (125 MHz, CDCl_3) δ_{C} 192.6 (s, NCN),

166.1 (s, COOMe), 142.0 (s, C^{ar}), 136.3 (s, C^{ar}), 134.4 (s, C^{ar}), 134.3 (s, C^{ar}), 133.4 (s, C^{ar}), 132.6 (s, C^{ar}), 129.2 (s, C^{ar}), 128.8 (s, C^{ar}), 127.9 (s, C^{ar}), 127.5 (s, C^{ar}), 127.4 (s, C^{ar}), 126.9 (s, C^{ar}), 126.1 (s, C^{ar}), 123.2 (s, C^{ar}), 113.9 (s, C^{ar}), 111.9 (s, C^{ar}), 52.9 (s, OMe), 52.6 (s, NCH_2) ppm; HRMS (ESI): m/z calculated for $\text{C}_{29}\text{H}_{25}\text{AuN}_2\text{O}_2\text{S} + \text{H}^+$ [M + H] $^+$: 663.13805. Found: 594.14455 [(NHC)Au(MeCN)] $^+$; 1215.24784 [2M-SPh] $^+$.

[Thiophenolato(5-methoxycarbonyl-1,3-dipentylbenzimidazol-2-ylidene)] gold(I) (9d)

27.0 mg (43.4 μmol , 92%) from sodium (2.18 mg, 94.7 μmol , 2.00 eq.), thiophenol (4.92 μL , 47.4 μmol , 1.00 eq.) and **8d** (26.0 mg, 47.4 μmol , 1.00 eq.) in dry MeOH (5 mL); m.p. 100 °C; ^1H NMR (500 MHz, CDCl_3) δ_{H} 8.18 (d, $J = 1.3$ Hz, 1H, H^{ar}), 8.13 (dd, $J = 8.6$ Hz, 1.4 Hz, 1H, H^{ar}), 7.66 - 7.61 (m, 2H, H^{ar}), 7.50 (d, $J = 8.5$ Hz, 1H, H^{ar}), 7.09 (t, $J = 7.7$ Hz, 2H, H^{ar}), 7.01 - 6.94 (m, 1H, H^{ar}), 4.51 (dt, $J = 10.3$ Hz, 7.5 Hz, 4H, NCH_2), 3.99 (s, 3H, OMe), 1.97 (sext., 4H, CH_2), 1.39 (dp, $J = 10.1$ Hz, 3.4 Hz, 8H, CH_2), 0.89 (dt, $J = 7.0$ Hz, 3.8 Hz, 6H, CH_3) ppm; ^{13}C NMR (125 MHz, CDCl_3) δ_{C} 191.5 (s, NCN), 166.3 (s, COOMe), 142.4 (s, C^{ar}), 136.2 (s, C^{ar}), 133.1 (s, C^{ar}), 132.6 (s, C^{ar}), 127.9 (s, C^{ar}), 126.5 (s, C^{ar}), 125.8 (s, C^{ar}), 123.1 (s, C^{ar}), 113.4 (s, C^{ar}), 111.2 (s, C^{ar}), 52.7 (s, OMe), 49.0 (NCH_2), 30.0 (s, CH_2), 29.9 (s, CH_2), 28.9 (s, CH_2), 28.8 (s, CH_2), 22.4 (s, CH_2), 13.9 (s, CH_3) ppm; HRMS (ESI): m/z calculated for $\text{C}_{25}\text{H}_{33}\text{AuN}_2\text{O}_2\text{S} + \text{H}^+$ [M + H] $^+$: 623.20065. Found: 554.20621 [(NHC)Au(MeCN)] $^+$; 1135.37090 [2M-SPh] $^+$.

[Thiophenolato(5-methoxycarbonyl-1,3-diisopropylbenzimidazol-2-ylidene)] gold(I) (9e)

30.0 mg (53.0 μmol , 65%) from sodium (3.73 mg, 162 μmol , 2.00 eq.), thiophenol (8.44 μL , 81.2 μmol , 1.00 eq.) and **8e** (40.0 mg, 81.2 μmol , 1.00 eq.) in dry MeOH (7 mL). m.p. 165 °C (decomp.); ^1H NMR (500 MHz, CDCl_3) δ_{H} 8.33 (d, $J = 1.5$ Hz, 1H, H^{ar}), 8.08 (dd, $J = 8.7$ Hz, 1.5 Hz, 1H, H^{ar}), 7.67 (d, $J = 8.7$ Hz, 1H, H^{ar}), 7.64 - 7.61 (m, 2H, H^{ar}), 7.10 (t, $J = 7.8$ Hz, 2H, H^{ar}), 7.01 - 6.94 (m, 1H, H^{ar}), 5.52 (dsept, $J = 7.0$ Hz, 5.2 Hz, 2H, NCH), 3.99 (s, 3H, OMe), 1.78 (dd, $J = 13.9$ Hz, 7.0 Hz, 12H, CH_3) ppm; ^{13}C NMR (125 MHz, CDCl_3) δ_{C} 189.7 (s, NCN), 166.3 (s, COOMe), 142.3 (s, C^{ar}), 135.5 (s, C^{ar}), 132.6 (s, C^{ar}), 128.0 (s, C^{ar}), 125.9 (s, C^{ar}), 125.3 (s, C^{ar}), 123.2 (s, C^{ar}), 114.7 (s, C^{ar}), 112.6 (s, C^{ar}), 54.2 (s, NCH), 54.1 (s, NCH), 52.7 (s, OMe), 22.0 (s, CH_3), 21.9 (CH_3) ppm; HRMS (ESI): m/z calculated for $\text{C}_{21}\text{H}_{25}\text{AuN}_2\text{O}_2\text{S} + \text{H}^+$ [M + H] $^+$: 567.13805. Found: 498.14430 [(NHC)Au(MeCN)] $^+$.

General procedure for the synthesis of thiolato complexes 10

The respective gold chlorido complex **8** (1.00 eq.) was dissolved in dry CH_2Cl_2 (100 mL/mmol) and KO^tBu (2.00 eq.) was added. The solution was left stirring for 1 h at rt and then treated in portions with 4-(adamantan-2-yl)benzenethiol (**4**) (1.00 eq.). After stirring at rt for 24 h the suspension was filtered over Celite and the filtrate was evaporated to dryness. The remainder was precipitated in pentane to afford the target complexes **10** as yellowish powders after filtration and drying in vacuo.

[[4-(Adamant-2-yl)benzenethiolato](5-methoxycarbonyl-1,3-dimethylbenzimidazol-2-ylidene)] gold(I) (**10a**)

15.0 mg (23.3 μ mol, 20%) from KO^tBu (32.1 mg, 286 μ mol, 2.00 eq.), **4** (28.0 mg, 114 μ mol, 1.00 eq.) and **8a** (50.0 mg, 114 μ mol, 1.00 eq.) in dry CH₂Cl₂ (10 mL). m.p. 150 °C (decomp.); ¹H NMR (500 MHz, CDCl₃) δ _H 8.18 - 8.14 (m, 2H, H^{ar}), 7.55 - 7.51 (m, 2H, H^{ar}), 7.49 (dd, *J* = 8.4 Hz, 0.7 Hz, 1H, H^{ar}), 7.07 - 7.02 (m, 2H, H^{ar}), 4.08 (d, *J* = 5.3 Hz, 6H, NMe), 3.98 (s, 3H, OMe), 2.90 (s, 1H, CH), 2.37 (d, *J* = 3.2 Hz, 2H, H^{ada}), 1.98 - 1.78 (m, 8H, H^{ada}), 1.73 (s, 4H, H^{ada}) ppm; ¹³C NMR (125 MHz, CDCl₃) δ _C 192.3 (s, NCN), 166.4 (s, COOMe), 139.5 (s, C^{ar}), 137.7 (s, C^{ar}), 136.8 (s, C^{ar}), 133.8 (s, C^{ar}), 132.4 (s, C^{ar}), 126.8 (s, C^{ar}), 126.7 (s, C^{ar}), 126.1 (s, C^{ar}), 113.2 (s, C^{ar}), 111.1 (s, C^{ar}), 110.1 (s, C^{ar}), 52.8 (s, OMe), 46.4 (s, C^{ada}), 39.2 (s, C^{ada}), 38.1 (s, C^{ada}), 35.3 (s, NMe), 35.2 (s, NMe), 32.0 (s, C^{ada}), 31.1 (s, C^{ada}), 28.2 (s, C^{ada}), 27.9 (s, C^{ada}) ppm; HRMS (ESI): *m/z* calculated for C₂₇H₃₁AuN₂O₂S + H⁺ [M + H]⁺: 645.18500. Found: 442.08118 [(NHC)Au(MeCN)]⁺; 605.14348 [(NHC)₂Au]⁺; 1045.23011 [2M-SPhAda]⁺.

[[4-(Adamant-2-yl)benzenethiolato](5-methoxycarbonyl-1,3-diethylbenzimidazol-2-ylidene)] gold(I) (**10b**)

45.0 mg (67.0 μ mol, 77%) from KO^tBu (19.1 mg, 172 μ mol, 2.00 eq.), **4** (21.1 mg, 86.2 μ mol, 1.00 eq.) and **8b** (40.0 mg, 86.1 μ mol, 1.00 eq.) in dry CH₂Cl₂ (7 mL). m.p. 150 °C (decomp.); ¹H NMR (500 MHz, CDCl₃) δ _H 8.24 (d, *J* = 1.3 Hz, 1H, H^{ar}), 8.19 (dd, *J* = 8.6 Hz, 1.3 Hz, 1H, H^{ar}), 7.62 (d, *J* = 8.6 Hz, 2H, H^{ar}), 7.56 (d, ³*J* = 8.6 Hz, 1H, H^{ar}), 7.17 - 7.10 (m, 2H, H^{ar}), 4.64 (dq, *J* = 9.3 Hz, 7.3 Hz, 4H, NCH₂), 4.04 (s, 3H, OMe), 2.98 (s, 1H, CH), 2.44 (t, *J* = 3.2 Hz, 2H, H^{ada}), 2.06 - 1.86 (m, 4H, H^{ada}), 1.62 (q, 8H, CH₃, H^{ada}) ppm; ¹³C NMR (125 MHz, CDCl₃) δ _C 191.3 (s, NCN), 166.4 (s, COOMe), 139.5 (s, C^{ar}), 138.0 (s, C^{ar}), 136.0 (s, C^{ar}), 133.0 (s, C^{ar}), 132.5 (s, C^{ar}), 126.7 (s, C^{ar}), 126.6 (s, C^{ar}), 126.0 (s, C^{ar}), 113.4 (s, C^{ar}), 111.2 (s, C^{ar}), 52.8 (s, OMe), 46.4 (s, C^{ada}), 44.1 (d, *J* = 3.4 Hz, NCH₂), 39.3 (s, C^{ada}), 38.1 (s, NMe), 32.1 (s, NMe), 28.2 (s, C^{ada}), 28.0 (s, C^{ada}), 15.8 (s, CH₃), 27.9 (s, CH₃) ppm; HRMS (ESI): *m/z* calculated for C₂₉H₃₅AuN₂O₂S + H⁺ [M + H]⁺: 673.21630. Found: 470.11294 [(NHC)Au(MeCN)]⁺; 661.20724 [(NHC)₂Au]⁺; 1101.29313 [2M-SPhAda]⁺.

[[4-(Adamant-2-yl)benzenethiolato](5-methoxycarbonyl-1,3-dibenzylbenzimidazol-2-ylidene)] gold(I) (**10c**)

27.0 mg (33.4 μ mol, 40%) from KO^tBu (23.8 mg, 212 μ mol, 2.00 eq.), **4** (20.8 mg, 84.9 μ mol, 1.00 eq.) and **8c** (50.0 mg, 84.9 μ mol, 1.00 eq.) in dry CH₂Cl₂ (7 mL). m.p. 175 °C (decomp.); ¹H NMR (500 MHz, CDCl₃) δ _H 8.09 (d, *J* = 1.4 Hz, 1H, H^{ar}), 8.01 (dd, *J* = 8.6 Hz, 1.4 Hz, 1H, H^{ar}), 7.48 (d, *J* = 8.1 Hz, 2H, H^{ar}), 7.44 (dd, *J* = 7.6 Hz, 1.7 Hz, 2H, H^{ar}), 7.40 (d, *J* = 6.6 Hz, 3H, H^{ar}), 7.36 - 7.30 (m, 6H, H^{ar}), 6.99 (d, *J* = 8.0 Hz, 2H, H^{ar}), 5.79 (d, *J* = 3.2 Hz, 4H, NCH₂), 3.91 (s, 3H, OMe), 2.90 (s, 1H, CH), 2.36 (d, *J* = 3.9 Hz, 2H, H^{ada}), 1.99 - 1.86 (m, 6H, H^{ada}), 1.82 - 1.77 (m, 3H, H^{ada}), 1.74 (s, 3H, H^{ada}) ppm; ¹³C NMR (125 MHz, CDCl₃) δ _C 192.7 (s, NCN), 166.1 (s, COOMe), 139.3 (s, C^{ar}), 137.5 (s, C^{ar}), 136.3 (s, C^{ar}), 134.4 (s, C^{ar}), 134.3 (s, C^{ar}), 133.4 (s, C^{ar}), 132.5 (s, C^{ar}), 129.2 (s, C^{ar}), 128.7 (s, C^{ar}), 127.5 (s, C^{ar}), 126.8 (s, C^{ar}), 126.6 (s, C^{ar}), 126.1 (s, C^{ar}), 113.82 (s, C^{ar}), 111.9 (s, C^{ar}), 52.9 (s, NCH₂), 52.7 (s, NCH₂), 52.6 (s, OMe), 46.3 (s, C^{ada}), 39.2 (s, NCH₂), 38.0 (s, C^{ada}), 31.9 (s, NMe), 31.0 (s, NMe), 28.1 (s, C^{ada}), 27.8 (s, C^{ada}) ppm; HRMS (ESI):

m/z calculated for C₃₉H₃₉AuN₂O₂S + H⁺ [M + H]⁺: 797.24760. Found: 594.14365 [(NHC)Au(MeCN)]⁺; 909.26784 [(NHC)₂Au]⁺; 1349.35422 [2M-SPhAda]⁺.

Synthetic route to [chlorido(5-(4-(adamant-1-yl)phenoxy)carbonyl)-1,3-diethylbenzimidazol-2-ylidene]gold(I) (**17**)

1-(tert-Butyl) 1H-benzimidazole-1,5-dicarboxylate (**12**)

Benzimidazole carboxylic acid (**11**) (1.50 g, 9.25 mmol, 1.00 eq.) was dissolved in 10% Na₂CO_{3(aq)} (22.5 mL) and 1,4-dioxane (13.5 mL) and cooled to 0 °C. Boc₂O (2.38 mL, 11.1 mmol, 1.20 eq.) was added dropwise and the mixture was left stirring at rt for 16 h. The solution was washed with Et₂O (3 x 50 mL) and the aqueous phase was acidified with 2N HCl. After extraction with EtOAc (3 x 60 mL), the combined organic phases were dried over MgSO₄, filtered and concentrated. The residue was dried in vacuo affording **12** (1.95 g, 7.44 mmol, 80%) as a beige powder. ¹H NMR (500 MHz, CDCl₃) δ _H 8.81 (d, *J* = 1.6 Hz, 1H, H^{ar}), 8.62 (s, 1H, H^{ar}), 8.60 (d, *J* = 1.6 Hz, 1H, H^{ar}), 8.55 (s, 1H, H^{ar}), 8.20 (dd, *J* = 8.6 Hz, 1.6 Hz, 1H, H^{ar}), 8.16 (dd, *J* = 8.4 Hz, 1.6 Hz, 1H, H^{ar}), 8.09 (d, *J* = 8.7 Hz, 1H, H^{ar}), 7.88 (d, *J* = 8.5 Hz, 1H, H^{ar}), 1.74 (s, 9H, CH₃), 1.72 (s, 9H, CH₃) ppm; ¹³C NMR (125 MHz, DMSO-d₆) δ _C 167.7 (s, COOH), 147.8 (d, *J* = 3.1 Hz, NCOOR), 147.3 (s, C^{ar}), 144.0 (s, C^{ar}), 134.6 (s, C^{ar}), 131.4 (s, C^{ar}), 127.8 (s, C^{ar}), 127.3 (s, C^{ar}), 126.7 (s, C^{ar}), 125.7 (s, C^{ar}), 122.0 (s, C^{ar}), 120.5 (s, C^{ar}), 116.3 (s, C^{ar}), 114.6 (s, C^{ar}), 86.4 (d, *J* = 10.0 Hz, OC(CH₃)₃), 28.0 (s, CH₃) ppm. Even though distinguishable, the regioisomers were not separated. The NMR data matched previously reported spectra.⁴⁶

5-(4-(Adamant-1-yl)phenyl) 1-(tert-butyl) benzimidazole-1,5-dicarboxylate (**13**)

A suspension of carboxylic acid **12** (1.05 g, 4.00 mmol, 1.30 eq.) in dry CH₂Cl₂ (40 mL) was cooled to 0 °C and treated in portions with DMAP (467 mg, 4.00 mmol, 1.30 eq.) and EDC-HCl (764 mg, 4.00 mmol, 1.30 eq.). The resulting solution was left stirring at 0 °C for 1 h and then treated dropwise with a solution of 4-(adamantan-1-yl)phenol (700 mg, 3.07 mmol, 1.00 eq.) in dry CH₂Cl₂ (20 mL) over a period of 30 min. The solution was stirred for a further 24 h at rt, diluted with EtOAc and washed with 0.5M H₂SO₄. The aqueous phase was extracted with EtOAc (3 x 70 mL) and the combined organic phases were dried over Na₂SO₄. The solvent was evaporated after filtration and the residue was purified via column chromatography (cyclohexane/EtOAc 3:1) affording ester **13** as a yellowish oily mixture of regioisomers (1.25 g, 2.64 mmol, 86%) with *R*_f 0.36/0.28 (cyclohexane/EtOAc 3:1); ¹H NMR (500 MHz, CDCl₃) δ _H 8.87 (d, *J* = 1.7 Hz, 1H, H^{ar}), 8.66 (d, *J* = 1.5 Hz, 1H, H^{ar}), 8.60 (s, 1H, H^{ar}), 8.53 (s, 1H, H^{ar}), 8.24 (ddd, *J* = 15.4 Hz, 8.5 Hz, 1.7 Hz, 2H, H^{ar}), 8.10 (d, *J* = 8.6 Hz, 1H, H^{ar}), 7.88 (d, *J* = 8.4 Hz, 1H, H^{ar}), 7.46 - 7.39 (m, 4H, H^{ar}), 7.23 - 7.16 (m, 4H, H^{ar}), 2.11 (s, 6H, H^{ada}), 1.93 (d, *J* = 2.9 Hz, 12H, H^{ada}), 1.82 - 1.74 (m, 12H, H^{ada}), 1.73 (s, 18H, CH₃) ppm; ¹³C NMR (125 MHz, CDCl₃) δ _C 165.4 (d, *J* = 13.5 Hz, COOR), 149.0 (d, *J* = 4.0 Hz, C^{ar}), 148.7 (s, C^{ar}), 147.9 (s, NCOOR), 147.7 (s, NCOOR), 144.7 (s, C^{ar}), 144.0 (s, C^{ar}), 143.5 (s, C^{ar}), 135.0 (s, C^{ar}), 131.2 (s, C^{ar}), 127.2 (s, C^{ar}), 126.6 (s, C^{ar}), 126.3 (s, C^{ar}), 126.0 (d, *J* = 1.8 Hz, C^{ar}), 123.3 (s, C^{ar}), 121.1 (s, C^{ar}), 121.0 (s, C^{ar}), 120.6 (s, C^{ar}), 117.2 (s, C^{ar}), 114.4 (s, C^{ar}),

86.5 (d, $J = 9.0$ Hz, $\text{OC}(\text{CH}_3)_3$), 43.3 (s, C^{ada}), 36.8 (s, C^{ada}), 36.0 (s, C^{ada}), 28.9 (s, C^{ada}), 28.1 (d, $J = 4.6$ Hz, CH_3) ppm.

5-(4-(Adamant-1-yl)phenoxy)carbonylbenzimidazole (**14**)

A solution of compound **13** (300 mg, 635 μmol , 1.00 eq.) in CH_2Cl_2 (20 mL) was treated dropwise with TFA (1.02 mL, 13.3 mmol, 21.0 eq.) was added dropwise and then stirred for a further 4 h at rt. The solvent was evaporated and the residue was dissolved in toluene and evaporated three times to remove any residual TFA. The free amine **14** was obtained as a colourless powder (237 mg, 635 μmol , quant.) of m.p. xx °C. ^1H NMR (500 MHz, MeOD-d_4) δ_{H} 9.52 (s, 1H, NCHN), 8.67 (d, $J = 1.5$ Hz, 1H, H^{ar}), 8.42 (dd, $J = 8.7$ Hz, 1.6 Hz, 1H, H^{ar}), 8.01 (d, $J = 8.7$ Hz, 1H, H^{ar}), 7.47 (d, $J = 8.8$ Hz, 2H, H^{ar}), 7.20 (d, $J = 8.8$ Hz, 2H, H^{ar}), 2.11 (s, 3H, H^{ada}), 1.98 (d, $J = 2.9$ Hz, 6H, H^{ada}), 1.84 (dq, $J = 12.1$ Hz, 5.8 Hz, 6H, H^{ada}) ppm; ^{13}C NMR (125 MHz, MeOD-d_4) δ_{C} 164.3 (s, COOR), 149.3 (s, C^{ar}), 148.6 (s, C^{ar}), 142.5 (s, C^{ar}), 134.3 (s, C^{ar}), 128.0 (s, C^{ar}), 125.7 (s, C^{ar}), 120.7 (s, C^{ar}), 116.7 (s, C^{ar}), 114.5 (s, C^{ar}), 43.1 (s, C^{ada}), 36.4 (s, C^{ada}), 35.8 (s, C^{ada}), 29.1 (s, C^{ada}) ppm.

5-(4-(Adamant-1-yl)phenoxy)carbonyl-1-ethylbenzimidazole (**15**)

A solution of **14** (237 mg, 635 μmol , 1.00 eq.) in DMF (10 mL) was treated with K_2CO_3 (176 mg, 1.28 mmol, 2.00 eq.) and EtI (103 μl , 1.28 mmol, 2.00 eq.) and stirred at 50 °C for 24 h. The solvent was evaporated, the residue was dissolved in CH_2Cl_2 , and the resulting suspension was filtered to remove excess K_2CO_3 . The solvent was evaporated and the remainder was purified by column chromatography ($\text{CH}_2\text{Cl}_2/\text{MeOH}$; 95:5) to afford **15** as yellowish oily mixture of regioisomers (205 mg, 512 μmol , 80%) with R_f 0.36/0.28; ^1H NMR (500 MHz, CDCl_3) δ_{H} 8.71 (d, $J = 1.5$ Hz, 1H, H^{ar}), 8.32 (d, $J = 1.5$ Hz, 1H, H^{ar}), 8.17 (td, $J = 8.6$, 1.6 Hz, 2H, H^{ar}), 8.08 (s, 1H, H^{ar}), 8.04 (s, 1H, H^{ar}), 7.88 (d, $J = 8.5$ Hz, 1H, H^{ar}), 7.48 (d, $J = 8.5$ Hz, 1H, H^{ar}), 7.45 – 7.40 (m, 4H, H^{ar}), 7.19 (dd, $J = 8.7$ Hz, 3.5 Hz, 4H, H^{ar}), 4.30 (dq, $J = 17.0$ Hz, 7.3 Hz, 4H, CH_2), 2.11 (s, 6H, H^{ada}), 1.94 (s, 12H, H^{ada}), 1.78 (q, $J = 10.9$ Hz, 12H, H^{ada}), 1.59 (vq, $J = 7.4$ Hz, 6H, CH_3) ppm; ^{13}C NMR (125 MHz, CDCl_3) δ_{C} 165.8 (d, $J = 10.8$ Hz, COOR), 149.0 (s, C^{ar}), 148.8 (d, $J = 10.9$ Hz, C^{ar}), 147.9 (s, C^{ar}), 145.2 (s, C^{ar}), 144.3 (s, C^{ar}), 143.7 (s, C^{ar}), 137.3 (s, C^{ar}), 133.5 (s, C^{ar}), 126.0 (d, $J = 8.6$ Hz, C^{ar}), 124.9 (s, C^{ar}), 124.2 (s, C^{ar}), 124.1 (s, C^{ar}), 123.8 (s, C^{ar}), 123.6 (s, C^{ar}), 121.1 (d, $J = 6.4$ Hz, C^{ar}), 120.3 (s, C^{ar}), 112.7 (s, C^{ar}), 109.5 (s, C^{ar}), 43.3 (s, C^{ada}), 40.2 (d, $J = 3.6$ Hz, NCH_2), 36.8 (s, C^{ada}), 36.0 (d, $J = 2.6$ Hz, C^{ada}), 29.0 (s, C^{ada}), 15.4 (d, $J = 16.7$ Hz, CH_3) ppm.

5-(4-(adamant-1-yl)phenoxy)carbonyl-1,3-diethylbenzimidazolium iodide (**16**)

Benzimidazole **15** (205 mg, 512 μmol , 1.00 eq.) was dissolved in 1,4-dioxane (10 mL) and treated with EtI (82.3 μl , 1.02 mmol, 2.00 eq.). The solution was stirred at 130 °C for 24 h, the solvent was evaporated, and the residue dried in vacuo to afford **17** as a yellow powder (285 mg, 512 μmol , quant.) of m.p. xx °C. ^1H NMR (500 MHz, CDCl_3) δ_{H} 11.4 (s, 1H, NCHN), 8.57 (d, $J = 1.4$ Hz, 1H, H^{ar}), 8.49 (dd, $J = 8.7$ Hz, 1.4 Hz, 1H, H^{ar}), 7.88 (d, $J = 8.8$ Hz, 1H, H^{ar}), 7.44 (d, $J = 8.8$ Hz, 2H, H^{ar}), 7.18 (d, $J = 8.8$ Hz, 2H, H^{ar}), 4.77 (dq, $J = 7.3$ Hz, 5.2 Hz, 4H, NCH_2), 2.11 (s, 3H, H^{ada}), 1.93 (s, 6H, H^{ada}), 1.83 (q, $J = 7.5$ Hz, 6H, H^{ada}), 1.80 – 1.73 (m, 6H, CH_3) ppm; ^{13}C NMR (125 MHz, CDCl_3) δ_{C} 163.6 (s, COOR), 149.7 (s, C^{ar}), 148.1 (s, C^{ar}), 134.3 (s, C^{ar}), 131.2 (s,

C^{ar}), 129.0 (s, C^{ar}), 128.7 (s, C^{ar}), 126.3 (s, C^{ar}), 120.8 (s, C^{ar}), 115.6 (s, C^{ar}), 113.4 (s, C^{ar}), 43.6 (d, $J = 11.8$ Hz, NCH_2), 43.2 (s, C^{ada}), 36.7 (s, C^{ada}), 28.9 (s, C^{ada}), 14.9 (d, $J = 8.2$ Hz, CH_3) ppm.

[Chlorido(5-(4-(adamant-1-yl)phenoxy)carbonyl)-1,3-diethylbenzimidazol-2-ylidene]gold(I) (**17**)

A solution of **16** (100 mg, 180 μmol , 1.00 eq.) in dry CH_2Cl_2 (10 mL) was treated with Ag_2O (25.0 mg, 108 μmol , 0.60 eq.), stirred at rt for 6 h while being shielded from light, and finally treated with $\text{AuCl}(\text{SMe}_2)$ (58.2 mg, 198 μmol , 1.10 eq.) and LiCl (76.2 mg, 1.80 mmol, 10.0 eq.). The mixture was left stirring for another 24 h, filtered over Celite, and concentrated in vacuo. The residue was purified by column chromatography (cyclohexane/EtOAc; 1:1) to afford **17** as a colourless powder (78.0 mg, 118 μmol , 66%) with R_f 0.67 and m.p. 310 °C (decomp.); ^1H NMR (500 MHz, CDCl_3) δ_{H} 8.35 (s, 1H, H^{ar}), 8.31 (d, $J = 8.6$, 1H, H^{ar}), 7.59 (d, $J = 8.5$ Hz, 1H, H^{ar}), 7.44 (d, $J = 8.4$ Hz, 2H, H^{ar}), 7.18 (d, $J = 8.8$ Hz, 2H, H^{ar}), 4.60 (dq, $J = 7.3$ Hz, 7.2 Hz, 4H, NCH_2), 2.12 (s, 3H, H^{ada}), 1.93 (s, 6H, H^{ada}), 1.78 (q, $J = 12.5$ Hz, 6H, H^{ada}), 1.58 (dt, $J = 11.6$ Hz, 5.7 Hz, 6H) ppm; ^{13}C NMR (125 MHz, CDCl_3) δ_{C} 180.7 (NCN), 164.5 (s, COOR), 149.5 (s, C^{ar}), 148.3 (s, C^{ar}), 136.0 (s, C^{ar}), 132.8 (s, C^{ar}), 126.5 (s, C^{ar}), 126.3 (s, C^{ar}), 126.2 (s, C^{ar}), 120.9 (s, C^{ar}), 113.9 (s, C^{ar}), 111.3 (s, C^{ar}), 44.3 (d, $J = 2.7$ Hz, NCH_2), 43.3 (s, C^{ada}), 36.7 (s, C^{ada}), 36.1 (s, C^{ada}), 28.9 (s, C^{ada}), 15.6 (d, $J = 22.6$ Hz, CH_3) ppm; HRMS (ESI): m/z calculated for $\text{C}_{28}\text{H}_{32}\text{AuClN}_2\text{O}_2 + \text{H}^+$ [$\text{M} + \text{H}$] $^+$: 661.18961. Found: 666.23766 [(NHC)Au(MeCN)] $^+$.

Synthetic route to clickable cyclopropenes **20** and **21**

[Chlorido(5-(2,3-dimethylcycloprop-2-en-1-yl)methoxy)carbonyl]-1,3-diethylbenzimidazol-2-ylidene] gold(I) (**19**)

A solution of benzimidazolium iodide **18** (150 mg, 352 μmol , 1.00 eq.) in dry CH_2Cl_2 (15 mL) was shielded from light and treated with Ag_2O (49.0 mg, 211 μmol , 0.60 eq.). The mixture was stirred at rt for 6 h, then treated with $\text{AuCl}(\text{SMe}_2)$ (114 mg, 387 μmol , 1.10 eq.) and left stirring at rt for another 18 h. The mixture was filtered over Celite and the solvent was evaporated. Redissolving the residue in CH_2Cl_2 and precipitating the complex from *n*-pentane afforded complex **19** as a white powder (139 mg, 262 μmol , 74%) of m.p. 140 °C; ^1H NMR (500 MHz, CDCl_3) δ_{H} 8.21 (d, $J = 1.4$ Hz, 1H, H^{ar}), 8.16 (dd, $J = 8.5$ Hz, 1.4 Hz, 1H, H^{ar}), 7.52 (d, $J = 8.5$ Hz, H^{ar}), 4.61 – 4.54 (m, 4H, NCH_2), 4.27 (d, $J = 5.2$ Hz, 2H, CH_2), 2.03 (s, 6H, CH_3), 1.68 (t, $J = 5.2$ Hz, 1H, CH), 1.60 – 1.53 (m, 6H, CH_3) ppm; ^{13}C NMR (125 MHz, CDCl_3) δ_{C} 180.0 (s, NCN), 165.8 (s, COOCH_2), 135.5 (s, C^{ar}), 132.7 (s, C^{ar}), 127.6 (s, C^{ar}), 125.9 (s, C^{ar}), 113.2 (s, C^{ar}), 111.0 (s, C^{ar}), 109.7 (s, C=C), 73.3 (s, OCH_2), 44.3 (d, $J = 2.8$ Hz, CH_3), 19.3 (s, CH), 15.6 (d, $J = 15.4$ Hz, CH_3), 10.5 (s, CH_3) ppm; m/z (EI, pos): 530 [M] $^+$, 500 [M-Et] $^+$, 433 [$\text{M-C}_6\text{H}_9\text{O}$] $^+$, 369 [$\text{M-Cl-C}_7\text{H}_9\text{O}_2$] $^+$.

5-(((2,3-dimethylcycloprop-2-en-1-yl)methoxy)carbonyl)-1,3-diethylbenzimidazol-2-ylidene gold(I) thiophenolato (**20**)

A solution of complex **19** (60.0 mg, 113 μmol , 1.00 eq.) in dry CH_2Cl_2 (10 mL) was treated with KO^tBu (15.2 mg, 136 μmol , 1.20 eq.), left stirring for 1 h at rt, and then treated with thiophenol (12.2 μl , 120 μmol , 1.06 eq.). After stirring at rt for 24 h the suspension was

filtered and the solvent was evaporated. The residue was precipitated from *n*-pentane to leave the product complex as a yellowish powder (56.0 mg, 92.6 μ mol, 82%) after filtration and drying in vacuo; m.p. 110 °C; ^1H NMR (500 MHz, CDCl_3) δ_{H} 8.21 (d, $J = 1.4$ Hz, 1H, H^{ar}), 8.16 (dd, $J = 8.5$ Hz, 1.4 Hz, 1H, H^{ar}), 7.64 (dd, $J = 8.3$ Hz, 1.2 Hz, 2H, H^{ar}), 7.51 (d, $J = 8.5$ Hz, 1H, H^{ar}), 7.10 (t, $J = 7.7$ Hz, 2H, H^{ar}), 6.97 (d, $J = 7.3$ Hz, 1H, H^{ar}), 4.59 (dq, $J = 11.2$ Hz, 7.3 Hz, 4H, NCH_2), 4.28 (d, $J = 5.2$ Hz, 2H, CH_2), 2.04 (s, 6H, CH_3), 1.69 (t, $J = 5.2$ Hz, 1H, CH), 1.58 (dt, $J = 9.3$ Hz, 7.3 Hz 6H, CH_3) ppm; ^{13}C NMR (125 MHz, CDCl_3) δ_{C} 190.8 (s, NCN), 166.0 (s, COOCH_2), 142.3 (s, C^{ar}), 135.7 (s, C^{ar}), 132.9 (s, C^{ar}), 132.6 (s, C^{ar}), 128.0 (s, C^{ar}), 127.5 (s, C^{ar}), 125.8 (s, C^{ar}), 123.2 (s, C^{ar}), 113.2 (s, C^{ar}), 110.9 (s, C^{ar}), 109.7 (s, C=C), 73.2 (s, OCH_2), 44.0 (d, $J = 2.7$ Hz, CH_3), 19.3 (s, CH), 15.7 (d, $J = 15.4$ Hz, CH_3), 10.5 (s, CH_3) ppm; m/z (EI, pos): 604 $[\text{M}]^+$, 524 $[\text{M}-\text{C}_6\text{H}_5]^+$, 479 $[\text{M}-\text{C}_6\text{H}_5\text{O}_2]^+$, 415 $[\text{M}-\text{SPh}-\text{C}_6\text{H}_5]^+$, 298 $[\text{M}-\text{AuSPh}]^+$.

[[4-(Adamant-2-yl)benzenethiolato[5-((2,3-dimethylcycloprop-2-en-1-yl)methoxycarbonyl)-1,3-diethylbenzimidazol-2-ylidene]] gold(I) (21)

A solution of complex **19** (40.0 mg, 75.4 μ mol, 1.00 eq.) in dry CH_2Cl_2 (7 mL) was treated with KO^tBu (16.9 mg, 151 μ mol, 2.00 eq.), left stirring for 1 h at rt, nd then treated with thiol **4** (18.4 mg, 75.4 μ mol, 1.00 eq.). After stirring at rt for 48 h the suspension was filtered over Celite and the solvent was evaporated. The residue was precipitated from *n*-pentane to afford the product complex as a brown powder (40.0 mg, 54.1 μ mol, 72%) after filtration and drying in vacuo; m.p. 160 °C; ^1H NMR (500 MHz, CDCl_3) δ_{H} 8.20 (d, $J = 1.4$ Hz, 1H, H^{ar}), 8.16 (dd, $J = 8.5$ Hz, 1.4 Hz, 1H, H^{ar}), 7.56 (d, $J = 8.2$ Hz, 2H, H^{ar}), 7.51 (d, $J = 8.6$ Hz, 1H, H^{ar}), 7.07 (d, $J = 8.0$ Hz, 2H, H^{ar}), 4.58 (dq, $J = 9.1$ Hz, 7.3 Hz, 4H, NCH_2), 4.20 (d, $J = 5.2$ Hz, 2H, CH_2), 2.91 (s, 1H, H^{ada}), 2.38 (s, 2H, H^{ada}), 2.03 (s, 6H, CH_3), 1.97 – 1.64 (m, 4H, H^{ada}), 1.92 – 1.87 (m, 2H, H^{ada}), 1.85 – 1.78 (m, 2H, CH^{ada}), 1.73 (s, 3H, H^{ada}), 1.68 (t, $J = 5.2$ Hz, 1H, CH), 1.57 (dt, $J = 9.3$ Hz, 7.3 Hz 6H, CH_3), 1.51 (s, 1H, H^{ada}) ppm; ^{13}C NMR (125 MHz, CDCl_3) δ_{C} 192.1 (s, NCN), 166.0 (s, COOCH_2), 139.5 (s, C^{ar}), 135.8 (s, C^{ar}), 135.6 (s, C^{ar}), 132.8 (s, C^{ar}), 132.3 (s, C^{ar}), 127.5 (s, C^{ar}), 126.6 (s, C^{ar}), 125.8 (s, C^{ar}), 113.2 (s, C^{ar}), 111.0 (s, C^{ar}), 109.7 (s, C=C), 73.3 (s, OCH_2), 46.3 (s, CH), 44.0 (d, $J = 3.6$ Hz, CH_3), 39.1 (s, C^{ada}), 38.0 (s, C^{ada}), 31.9 (s, C^{ada}), 31.0 (s, C^{ada}), 28.1 (s, C^{ada}), 27.8 (s, C^{ada}), 19.3 (s, CH), 15.7 (d, $J = 14.5$ Hz, CH_3), 10.5 (s, CH_3) ppm; m/z (EI, pos): 738 $[\text{M}]^+$, 415 $[\text{M}-\text{SPhAda}-\text{C}_6\text{H}_5]^+$, 370 $[\text{M}-\text{SPhAda}-\text{C}_6\text{H}_5\text{O}_2]^+$, 298 $[\text{M}-\text{AuSPhAda}]^+$.

Biological evaluation

Cell culture conditions

Cell lines were cultivated in Dulbecco's Modified Eagle Medium (DMEM, Capricorn scientific) supplemented with 10% fetal bovine serum (Sigma life science) and 1% ZellShield® (Minerva Biolabs) under standard cell culture conditions (37 °C, 5% CO_2 , 95% humidity). 518A2 melanoma (Department of Radiotherapy, Medical University of Vienna, Austria)¹, KB-V1^{vb1} (ACC-149) multi drug resistant (MDR) cervix carcinoma, U-87 glioblastoma, HT-29 (ACC-299), HCT-116 (ACC-581) and HCT-116p53^{-/-} (p53 knockout mutant) colon carcinoma, MCF-7 (ACC-115) breast carcinoma, EA.hy926 (ATCC® CRL-2922™) endothelial hybrid cells were cultivated under cell

culture conditions and passaged every three to five days. Resistant KB-V1^{vb1} cells had been treated with 340 nm vinblastine 24 h after every passage. Cells were tested for mycoplasma using MycoSPY® PCR test kit (Biontexas).

MTT-assay

The MTT (3-(4,5-dimethylthiazol-2-yl)-2,5-diphenyltetrazolium bromide) assay was performed to determine the anti-proliferative properties of compounds **9a-e**, **10a-c**, **17**, **20** and **21**, as well as the positive controls **AC1-004**, YC-1, and auranofin against 518A2 melanoma, KB-V1^{vb1} cervix carcinoma, U-87 glioblastoma, HT-29, HCT-116, HCT-116p53^{-/-} colon carcinoma, MCF-7 breast carcinoma and EA.hy926 endothelial hybrid cells as described previously.⁴⁷

ROS level determination via DCFH-DA fluorescence

518A2 melanoma cells were seeded (1×10^5 cells/mL, 0.1 mL/well) in black 96-well cell culture plates for 24 h under cell culture conditions. The cells were treated with 20 μM DCFH-DA (2',7'-dichlorodihydrofluorescein diacetate) solution in serum free DMEM (Dulbecco's modified eagle medium) for 30 min and gently washed twice with PBS. Substance treatment (5, 10, 20 μM) was carried out in serum free DMEM for 1 h followed by another washing step. The fluorescence of DCF (2',7'-dichlorodihydrofluorescein) was measured at λ_{ex} : 485 nm λ_{em} : 535 nm with a TECAN infinite F200 microplate reader. Untreated cells were taken as blank values and negative controls set to 100%.

Cell cycle analysis

The analysis of the numbers of treated cells in the different phases of the cell cycle was performed as described previously.⁴⁷ Briefly, 518A2 melanoma cells were cultivated in 6-well cell culture plates for 24 h, treated with test compounds and harvested after another 24 h. After ethanol fixation and propidium iodide (PI) staining 10,000 cells were analysed with a Beckman Coulter Cytomics FC500 flow cytometer (λ_{ex} : 488 nm λ_{em} : 570 nm). Cell cycle phases were determined by CXP software (Beckman Coulter).

Immunofluorescence staining of the actin cytoskeleton

518A2 melanoma cells were grown (1×10^5 cells/mL, 0.5 mL/well) on coverslips in 24-well cell culture plates for 24 h under cell culture conditions. The cells were treated for another 24 h with 1, 5 or 10 μM of test compounds under cell culture conditions. After a washing step with cytoskeletal buffer (CB: 10 mM MES, 3 mM MgCl_2 , 138 mM KCl, 2 mM EGTA, pH 6.8), the cells were fixed and permeabilised in 3.7% formaldehyde solution (0.2% Triton X-100 in CB) for 5 min, incubated with ice-cold ethanol for 10 s and rehydrated in PBS (phosphate buffered saline). Immunofluorescence staining was done using 100 nM Actistain 488 phalloidin and 1 $\mu\text{g}/\text{mL}$ DAPI (4',6-diamidin-2-phenylindol) in PBS for 30 min in the dark. The coverslips were washed again with PBS and embedded in ProLong™ Glass Antifade Mountant. The results were documented using a Leica TCS SP5 confocal microscope and the images were processed with imageJ.

Intracellular localisation of the cyclopropene derivatives

518A2 melanoma cells were prepared as previously described for immunofluorescence staining. After 24 h of incubation under cell

culture conditions, the cells were incubated with 1 μM MitoTrack[®] Red CM-H2XRos for 30 min and with 25 μM of the cyclopropenes **20** and **21** for 20 min. The cells were washed with PBS, fixed with 3.7% formaldehyde for 10 min and incubated with a BDP-FL-tetrazine solution for 1 h. The nuclei were counterstained with 1 μM /mL DAPI for another 30 min. The embedding and the documentation were performed like the immunofluorescence probes.

EA.hy926 tube formation assay

EA.hy926 endothelial hybrid cells were cultivated for 24 h in EndoPrime low serum medium (Capricorn), trypsinised and counted. The surfaces of the angiogenesis μ -slides (Ibidi) were coated with Matrigel[®] (Corning), a basement membrane matrix, and seeded with EA.hy926 endothelial hybrid cells (4×10^5 cells/mL, 50 μL /well). Cells were treated with test compounds (20 μM) or solvent and incubated till tubes had formed in the control wells. The anti-angiogenic effects were documented via light microscopy (Zeiss Axiovert 135 with AxioVert MRC5) and images were processed using imageJ. Viability was ascertained concomitantly via MTT assays.

Zebrafish angiogenesis assay

The assay was performed as previously described.⁴⁸ Briefly, the zebrafish larvae were manually dechorionated 24 h past fertilisation (hpf), treated with test compounds for 48 h and the results documented by fluorescence microscopy (Leica MZ10F with Zeiss AxioCam Mrc). The images were analysed with imageJ and the area of subintestinal vessels (SIVs) was determined for each compound.

Thioredoxin reductase inhibition assay

The thioredoxin reductase (TrxR) colorimetric assay kit (Cayman chemical) was performed according to the manufacturer's instructions. A cell extract of 518A2 melanoma cells was used to determine the inhibitory effect of the test compounds. The absorbance was measured at 405 nm with a TECAN infinite F200 plate reader.

Caspase 3/7 activity assay

518A2 melanoma cells were seeded (2×10^5 cells/mL, 67.5 μL /well) in black 96-well cell culture plates and incubated for 24 h under cell culture conditions. The cells were incubated with solvent or test compounds for 6 h. The activity of caspases 3 and 7 was determined using the Cell Meter[™] caspase 3/7 activity apoptosis assay kit (AAT Bioquest). 7.5 μL of caspase substrate solution was added to each well and incubated for 1 h. Fluorescence was measured (λ_{ex} : 485 nm and λ_{em} : 535 nm) with a TECAN infinite F200 microplate reader with blank probes subtracted from the values and negative controls set to 100%.

Electrophoretic mobility shift assay (EMSA)

Test compounds or cisplatin (0, 25, 50, 75, 100 μM) were diluted in TE-buffer (50 mM Tris-HCl, 1 mM EDTA, pH 7.5) and incubated with 0.5 μg /mL circular pBR322 plasmid DNA (Thermo scientific) for 24 h at 37 $^{\circ}\text{C}$. The samples were heat shocked at 95 $^{\circ}\text{C}$ for 10 min with electrophoresis sample buffer and applied to a 1% agarose gel with $0.5 \times \text{TBE}$ -buffer (89 mM Tris, 89 mM boric acid, 2 mM EDTA, pH 8.3).

Electrophoresis was carried out at 66 V and 15 mA/h for 4 h. The DNA was stained with 10 μg /mL ethidium bromide in $0.5 \times \text{TBE}$ -buffer for 30 min and visualised using UV excitation.

Cellular gold uptake quantified via ICP-MS

518A2 melanoma cells were seeded (0.25×10^6 cells/mL, 8 mL) in Sarstedt tissue culture dishes for 24 h, then treated with compounds **9a-e**, **10b**, **17**, and auranofin (5 μM) for 6 h. After washing with PBS, the cells were trypsinated and counted. The cell pellets were solubilised in nitrohydrochloric acid (37 % HCl, 65 % HNO₃, 1:3) at 100 $^{\circ}\text{C}$ for 20 min and diluted with ddH₂O (1:7). The content of gold within the cells was quantified by ICP-MS analytic (Agilent 7500ce, Cetac ASX-510). Values from two independent experiments were quoted as means \pm SD in ng/ 10^6 cells.

Conclusions

The aim of this study was the synthesis and biological evaluation of NHC gold complexes that are structurally similar to the HIF-1 α inhibitor **AC1-004** and potentially combine the anticancer effects of the latter with the known antioxidant properties of gold complexes.⁴⁹ Twelve new (N,N'-dialkylbenzimidazol-2-ylidene)(thiolato) gold(I) complexes with variance in N-substituents and thiolato ligands were investigated. The benzimidazolium ligands could be attached to an AuCl fragment in one step via intermediate silver complexes, affording the NHC chlorido gold complexes with yields averaging 60%. While the subsequent substitution of the chlorido for a thiophenol ligand to give complexes **9** also proceeded well with yields of ca. 60%, the novel 4-(adamant-2-yl)benzenethiol ligand was less easy to attach. Only the complexes **10a-c**, carrying relatively small N-residues, could be obtained in about 40% yield, whereas the isopropyl and pentyl bearing NHC chlorido gold complexes **8d** and **8e** did not undergo ligand substitution. The crystal structure of **9b** confirmed the linear geometry of the gold(I) coordination and the *trans* effect of the NHC ligand through noticeably shortened Au-S bond length. The stability of the complexes in aqueous milieu over the course of three days was confirmed for one representative of each series, i. e. **9b**, **10b** and **17**. The efficacy of the new test complexes against human cancer cell lines in terms of *IC*₅₀ values in MTT assays spanned a wide range from 2.1 to >50 μM , depending on the substituents of the NHC ligand, as well as on the nature of the thiolato ligand. Longer and branched alkyl substituents (**9d-e**) improved the efficacy, whereas benzyl groups led to a loss of efficacy (**12c**, **13c**). The 4-(adamant-2-yl)phenyl moiety (**10a-c**, **17**, **21**), which is reportedly responsible for the destabilization of HIF-1 α by **AC1-004**, led to a lower efficacy. For the influence on the cellular ROS levels there is a clear SAR. Thiophenolato complexes **9** induced higher ROS levels than their respective 4-(adamant-2-yl)-thiophenolato analogues **10** with identical N-residues. Likewise, in both series **9** and **10**, ROS induction was increasingly pronounced when going from bulkier to smaller N-residues. No such ROS level influencing effects were observed for the controls **AC1-004** and YC-1, nor for the chlorido complex **17**. We found an inhibition of tumoral TrxRs by the complexes **9** and **10** to be causative for the increased ROS levels in tumour cells. In line with this finding, the cyclopropene

derivatives **20** and **21** accumulated in the mitochondria of melanoma cells, which are mainly responsible for the redox metabolism and proliferation signalling in the cell.⁵⁰ The adamantyl residue (**21**) ensures a more selective subcellular accumulation in the mitochondria, but has no influence on uptake into the cell. Some of the test compounds had an influence on the distribution of cells in the different phases of the cell cycle. A clear SAR could not be identified, but **9d** stood out with a distinct S-phase arrest and caspase 3/7 induction. However, any direct interaction with DNA, which is a major cause of S-phase arrest, could be ruled out by EMSA.⁵¹ The observed alteration of actin filaments in treated cells might be linked to the overproduction of mitochondrial ROS and to TrxR inhibition, leading to an aberrant motility, shape, and membrane integrity of the cells and eventual cell death.³¹ The already advanced degradation of the actin cytoskeleton caused by **9d**, **9e** and auranofin could also indicate an ongoing apoptosis, associated with a degradation by caspases.⁵² It is not clear whether the strong anti-angiogenic effects observed by gold complexes **9a-e** and **10b**, compared to controls YC-1 and **AC1-004**, in the tube-formation assay are due to degradation of the actin cytoskeleton or to an inhibition of the Akt signalling pathway as is the case for **AC1-004** and a resulting HIF-1 α -destabilisation.⁸ The strong anti-angiogenic potential of the test compounds was confirmed by the reduction of blood vessel development in zebrafish.⁵³ In summary, some of the new complexes exhibited, unlike **AC1-004** on which they were modelled, distinct pleiotropic effects on cancer cells such as ROS increase, alteration of the cell cycle, actin reorganisation, and restricted angiogenesis. Whether the latter is possibly associated with HIF-1 α inhibition needs to be ascertained in follow-up studies. We found that thiophenolato complexes with large N-substituents were more efficacious, whereas the 4-(adamant-2-yl)benzenethiolato derivatives with small alkyl substituents accumulated more selectively in the mitochondria and were better tolerated in the zebrafish model. This tentative SAR should now enable a more rational optimisation of this compound class, e.g. by starting with **9e**, the most promising complex of the current study.

Conflicts of interest

There are no conflicts to declare.

Acknowledgements

R. S. thanks the Deutsche Forschungsgemeinschaft (DFG) for a grant (Scho 402/12-2). We thank Dr. Ulrike Lacher for measuring and analysing mass spectra, Anthony Putratama for the synthesis of precursors, Prof. Dr. Obst for the ICP-MS measurements, and Alexander Goller (all at the University of Bayreuth) for solving the crystal structure.

Notes and references

1. D. Hanahan, *Cancer Discov.*, 2022, **12**, 31-46.
2. D.-W. Shen, L. M. Pouliot, M. D. Hall and M. M. Gottesman, *Pharmacol. Rev.*, 2012, **64**, 706-721.
3. J. Zhou, Y. Kang, L. Chen, H. Wang, J. Liu, S. Zeng and L. Yu, *Front. Pharmacol.*, 2020, **11**.
4. M. Höckel and P. Vaupel, *J. Natl. Cancer Inst.*, 2001, **93**, 266-276.
5. S. J. Yeung, J. Pan and M. H. Lee, *Cell. Mol. Life Sci.*, 2008, **65**, 3981-3999.
6. S. H. Li, D. H. Shin, Y.-S. Chun, M. K. Lee, M.-S. Kim and J.-W. Park, *Mol. Cancer Ther.*, 2008, **7**, 3729-3738.
7. D. Bhattarai, X. Xu and K. Lee, *Med. Res. Rev.*, 2018, **38**, 1404-1442.
8. M.-S. Won, N. Im, S. Park, S. K. Boovanahalli, Y. Jin, X. Jin, K.-S. Chung, M. Kang, K. Lee, S.-K. Park, H. M. Kim, B. M. Kwon, J. J. Lee and K. Lee, *Biochem. Biophys. Res. Commun.*, 2009, **385**, 16-21.
9. S. I. Bär, M. Gold, S. W. Schleser, T. Rehm, A. Bär, L. Köhler, L. R. Carnell, B. Biersack and R. Schobert, *Chem. Eur. J.*, 2021, **27**, 5003-5010.
10. A. Nguyen, A. Vessières, E. Hillard, S. Top, P. Pigeon and G. Jaouen, *CHIMIA* 2007, **61**, 716-724.
11. S. Knauer, B. Biersack, M. Zoldakova, K. Effenberger, W. Milius and R. Schobert, *Anticancer Drugs*, 2009, **20**, 676-681.
12. R. A. Sánchez-Delgado, A. Anzellotti and L. Suárez, *Met Ions Biol Syst*, 2004, **41**, 379-419.
13. L. Kober, S. W. Schleser, S. I. Bär and R. Schobert, *J. Biol. Inorg. Chem.*, 2022, **27**, 10.1007/s00775-022-01968-x
14. W. Fiskus, N. Saba, M. Shen, M. Ghias, J. Liu, S. D. Gupta, L. Chauhan, R. Rao, S. Gunewardena, K. Schorno, C. P. Austin, K. Maddocks, J. Byrd, A. Melnick, P. Huang, A. Wiestner and K. N. Bhalla, *Cancer Res.*, 2014, **74**, 2520-2532.
15. P. V. Raninga, A. C. Lee, D. Sinha, Y.-Y. Shih, D. Mittal, A. Makhale, A. L. Bain, D. Nanayakarra, K. F. Tonissen, M. Kalimutho and K. K. Khanna, *Int. J. Cancer*, 2020, **146**, 123-136.
16. C. Marzano, V. Gandin, A. Folda, G. Scutari, A. Bindoli and M. P. Rigobello, *Free Radic. Biol. Med.*, 2007, **42**, 872-881.
17. X. Zhang, K. Selvaraju, A. A. Saei, P. D'Arcy, R. A. Zubarev, E. S. J. Arnér and S. Linder, *Biochimie*, 2019, **162**, 46-54.
18. P. Zou, M. Chen, J. Ji, W. Chen, X. Chen, S. Ying, J. Zhang, Z. Zhang, Z. Liu, S. Yang and G. Liang, *Oncotarget*, 2015, **6**.
19. H. Uchiro and S. Kobayashi, *Tetrahedron Lett.*, 1999, **40**, 3179-3182.
20. S. I. Bär, S. W. Schleser, N. Oberhuber, A. Herrmann, L. Schlotte, S. E. Weber and R. Schobert, *J. Inorg. Biochem.*, 2022, **238**, 112028.
21. D. L. Kokkin, R. Zhang, T. C. Steimle, I. A. Wyse, B. W. Pearlman and T. D. Varberg, *J. Phys. Chem. A*, 2015, **119**, 11659-11667.
22. T. Onodera, I. Momose and M. Kawada, *Chem. Pharm. Bull.*, 2019, **67**, 186-191.
23. D. W. Shen, C. Cardarelli, J. Hwang, M. Cornwell, N. Richert, S. Ishii, I. Pastan and M. M. Gottesman, *J. Biol. Chem.*, 1986, **261**, 7762-7770.
24. H. Yang, R. M. Villani, H. Wang, M. J. Simpson, M. S. Roberts, M. Tang and X. Liang, *J. Exp. Clin. Cancer Res.*, 2018, **37**, 266.
25. G.-Y. Liou and P. Storz, *Free Radic. Res.*, 2010, **44**, 479-496.
26. R. P. Rastogi, S. P. Singh, D. P. Häder and R. P. Sinha, *Biochem. Biophys. Res. Commun.*, 2010, **397**, 603-607.

27. M. C. C. Sachweh, W. C. Stafford, C. J. Drummond, A. R. McCarthy, M. Higgins, J. Campbell, B. Brodin, E. S. J. Arnér and S. Laín, *Oncotarget*, 2015, **6**.
28. H. Hwang-Bo, J. W. Jeong, M. H. Han, C. Park, S. H. Hong, G. Y. Kim, S. K. Moon, J. Cheong, W. J. Kim, Y. H. Yoo and Y. H. Choi, *Gen. Physiol. Biophys.*, 2017, **36**, 117-128.
29. J. Bartek, C. Lukas and J. Lukas, *Nat. Rev. Mol. Cell Biol.*, 2004, **5**, 792-804.
30. J. E. Leadsham, V. N. Kotiadis, D. J. Tarrant and C. W. Gourlay, *Cell Death Differ.*, 2010, **17**, 754-762.
31. V. E. Franklin-Tong and C. W. Gourlay, *Biochem. J.*, 2008, **413**, 389-404.
32. J. C. Mills, N. L. Stone and R. N. Pittman, *J. Cell Biol.*, 1999, **146**, 703-708.
33. B. Huppertz, H.-G. Frank and P. Kaufmann, *Anat. Embryol.*, 1999, **200**, 1-18.
34. K. Bertheussen, M. van de Plassche, T. Bakkum, B. Gagestein, I. Ttofi, A. J. C. Sarris, H. S. Overkleeft, M. van der Stelt and S. I. van Kasteren, *Angew. Chem. Int. Ed.*, 2022, **61**, e202207640.
35. S. Fulda, L. Galluzzi and G. Kroemer, *Nat. Rev. Drug Discov.*, 2010, **9**, 447-464.
36. P. E. Porporato, N. Filigheddu, J. M. B.-S. Pedro, G. Kroemer and L. Galluzzi, *Cell Res.*, 2018, **28**, 265-280.
37. Y. Yang, S. Karakhanova, W. Hartwig, J. G. D'Haese, P. P. Philippov, J. Werner and A. V. Bazhin, *J. Cell. Physiol.*, 2016, **231**, 2570-2581.
38. F. Hecht, C. F. Pessoa, L. B. Gentile, D. Rosenthal, D. P. Carvalho and R. S. Fortunato, *Tumor Biol.*, 2016, **37**, 4281-4291.
39. M. Ushio-Fukai and Y. Nakamura, *Cancer Lett.*, 2008, **266**, 37-52.
40. P. Wigner, R. Grębowski, M. Bijak, J. Saluk-Bijak and J. Szemraj, *Int. J. Mol. Sci.*, 2021, **22**.
41. J. Folkman, *Semin. Oncol.*, 2002, **29**, 15-18.
42. G. U. Dachs and G. M. Tozer, *Eur. J. Cancer*, 2000, **36**, 1649-1660.
43. E. Aranda and G. Owen, *Biol. Res.*, 2009, **42**, 377-389.
44. E. J. Yeo, Y. S. Chun and J. W. Park, *Biochem. Pharmacol.*, 2004, **68**, 1061-1069.
45. J. J. Dunsford, E. R. Clark and M. J. Ingleson, *Angew. Chem. Int. Ed.*, 2015, **54**, 5688-5692.
46. Z. Zhang, P. Chaltin, A. Van Aerschot, J. Lacey, J. Rozenski, R. Busson and P. Herdewijn, *Bioorg. Med. Chem.*, 2002, **10**, 3401-3413.
47. L. H. F. Köhler, S. Reich, G. Begemann, R. Schobert and B. Biersack, *Chem. Med. Chem.*, 2022, **17**, e202200064.
48. B. Linder, L. H. F. Köhler, L. Reisbeck, D. Menger, D. Subramaniam, C. Herold-Mende, S. Anant, R. Schobert, B. Biersack and D. Kögel, *Biomolecules*, 2021, **11**.
49. M. Mora, M. C. Gimeno and R. Visbal, *Chem. Soc. Rev.*, 2019, **48**, 447-462.
50. M. Idelchik, U. Begley, T. J. Begley and J. A. Melendez, *Semin. Cancer Biol.*, 2017, **47**, 57-66.
51. D. K. Orren, L. N. Petersen and V. A. Bohr, *Mol. Biol. Cell*, 1997, **8**, 1129-1142.
52. J. Rao and N. Li, *Curr. Cancer Drug Targets*, 2004, **4**, 345-354.
53. H. Draut, T. Rehm, G. Begemann and R. Schobert, *Chem. Biodivers.*, 2017, **14**, e1600302.

Supporting Information

Anti-tumoural NHC Au(I) thiolato complexes derived from HIF-1 α inhibitor AC1-004 target the mitochondrial redox system and show antiangiogenic effects in vivo

Sebastian W. Schleser^{†a}, Leonhard H. F. Köhler^{†a}, Florian Riethmüller^a, Sebastian Reich^a, Robin Fertig^b, Gerrit Begemann^c, Rhett Kempe^b and Rainer Schobert^a

¹Chair of Organic Chemistry I, University of Bayreuth, Bayreuth, 95440, Germany.

²Chair of Inorganic Chemistry II, University of Bayreuth, Bayreuth, 95440, Germany.

³Developmental Biology, University of Bayreuth, Bayreuth, 95440, Germany.

Table of content

NMR spectra of complexes 9a-e , 10a-c , 17 , 20 and 21	- 3 -
Stability Studies via ¹ H NMR	- 14 -
Thioredoxin reductase inhibition assay	- 16 -
Caspase 3/7 activity assay	- 16 -
Electrophoretic mobility shift assay	- 17 -
Quantification of cellular uptake by ICP-MS analysis	- 17 -
Crystallography of 9b	- 18 -
References	- 18 -

NMR spectra of complexes **9a-e**, **10a-c**, **17**, **20** and **21**

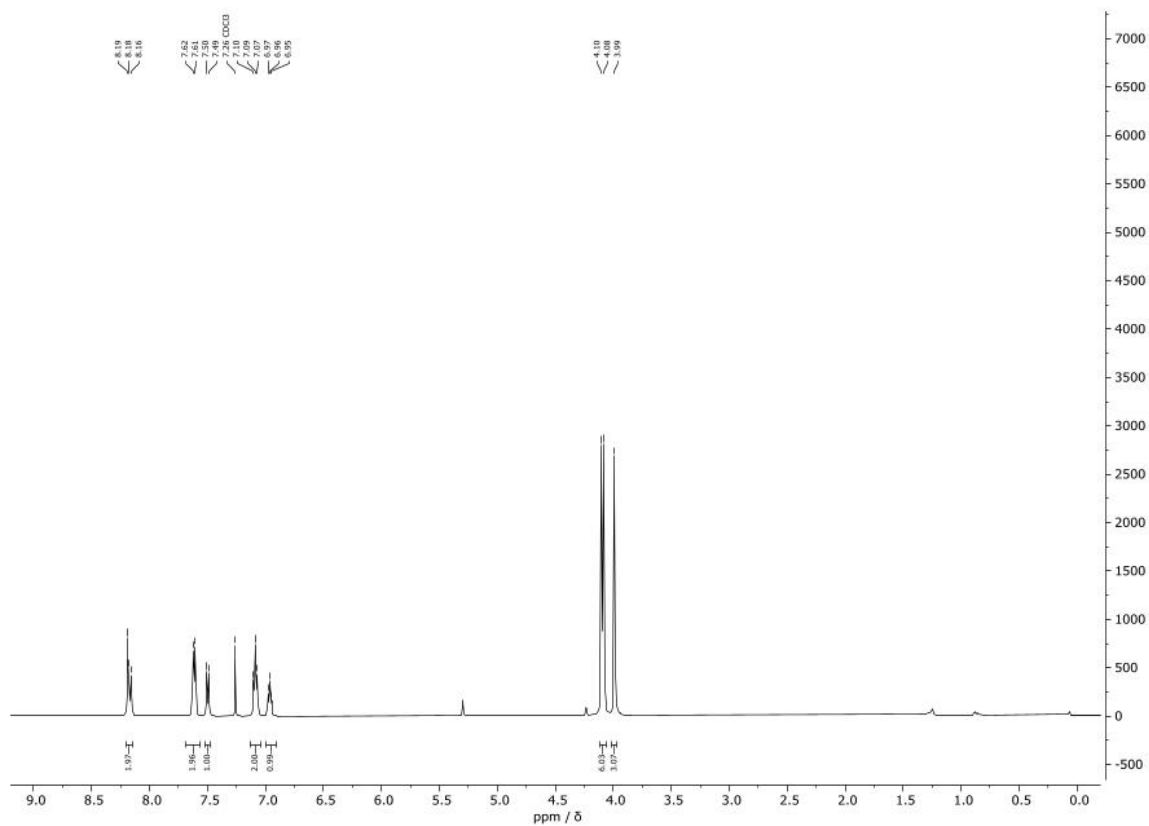


Fig. S1. ¹H spectrum of **9a** in CDCl₃.

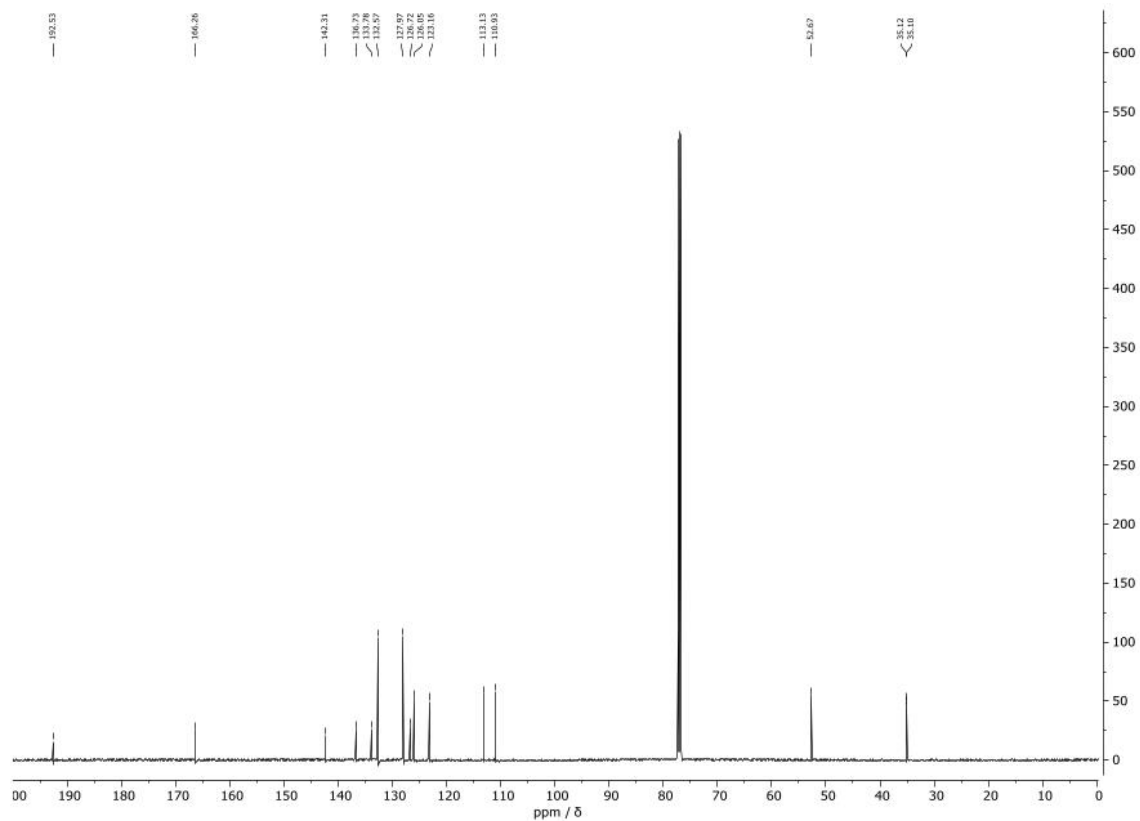


Fig. S2. ^{13}C spectrum of **9a** in CDCl_3 .

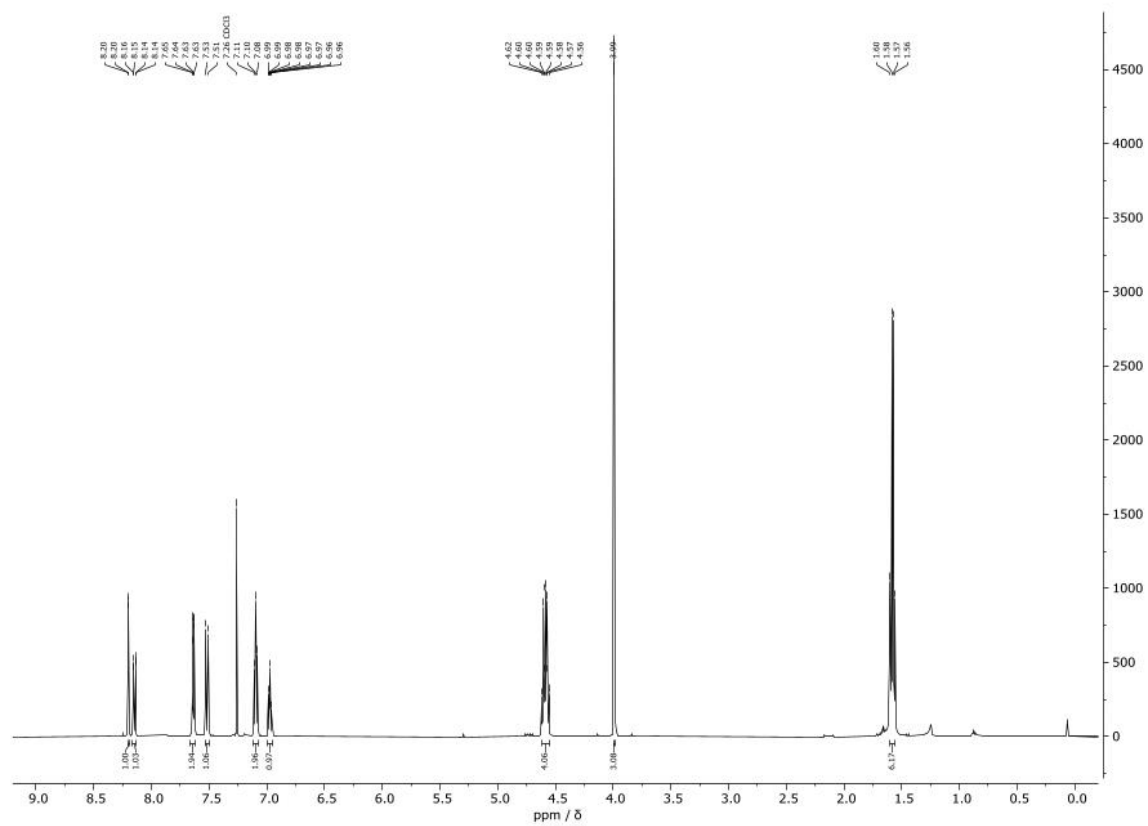


Fig. S3. ^1H spectrum of **9b** in CDCl_3 .

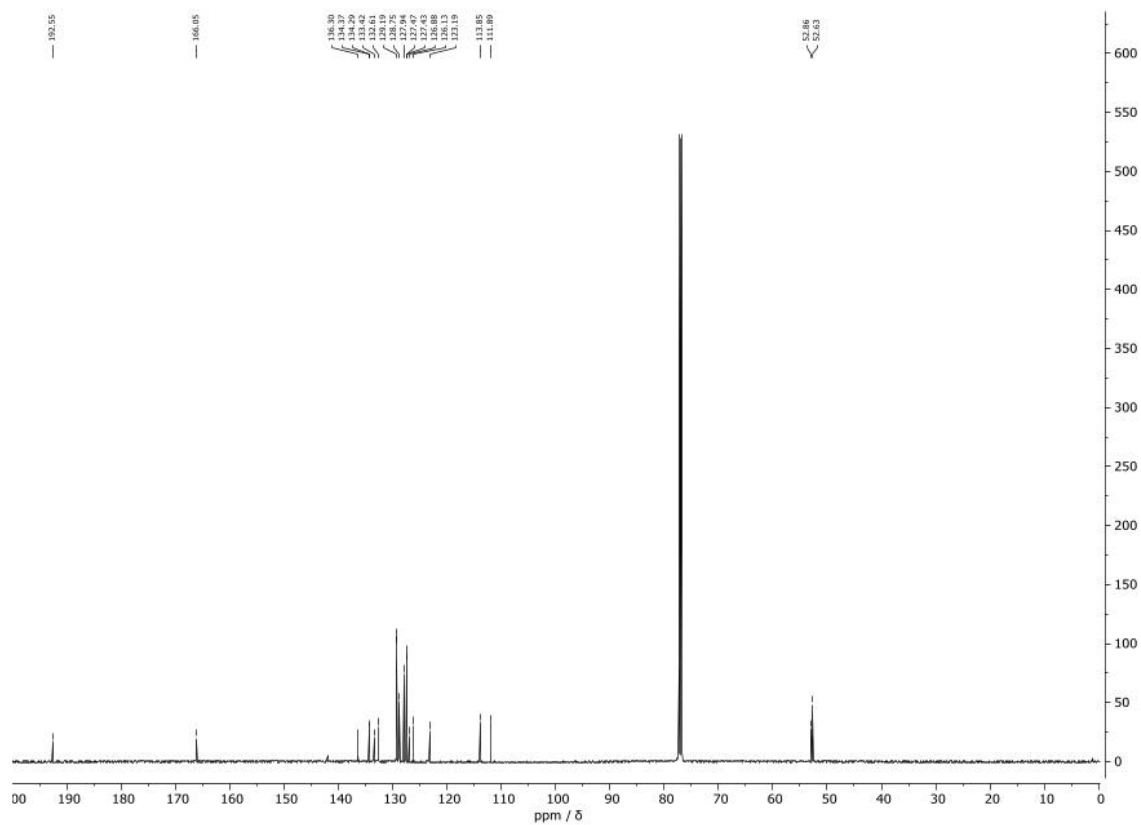


Fig. S6. ^{13}C spectrum of **9c** in CDCl_3 .

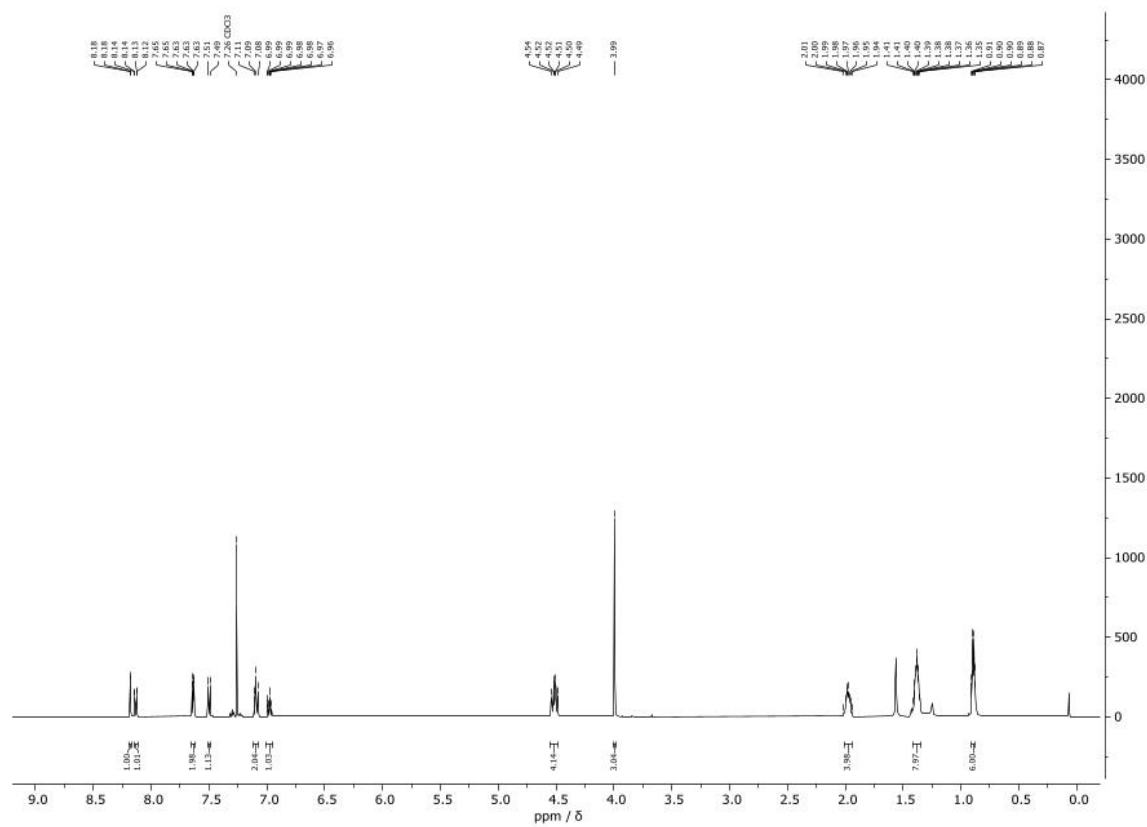


Fig. S7. ^1H spectrum of **9d** in CDCl_3 .

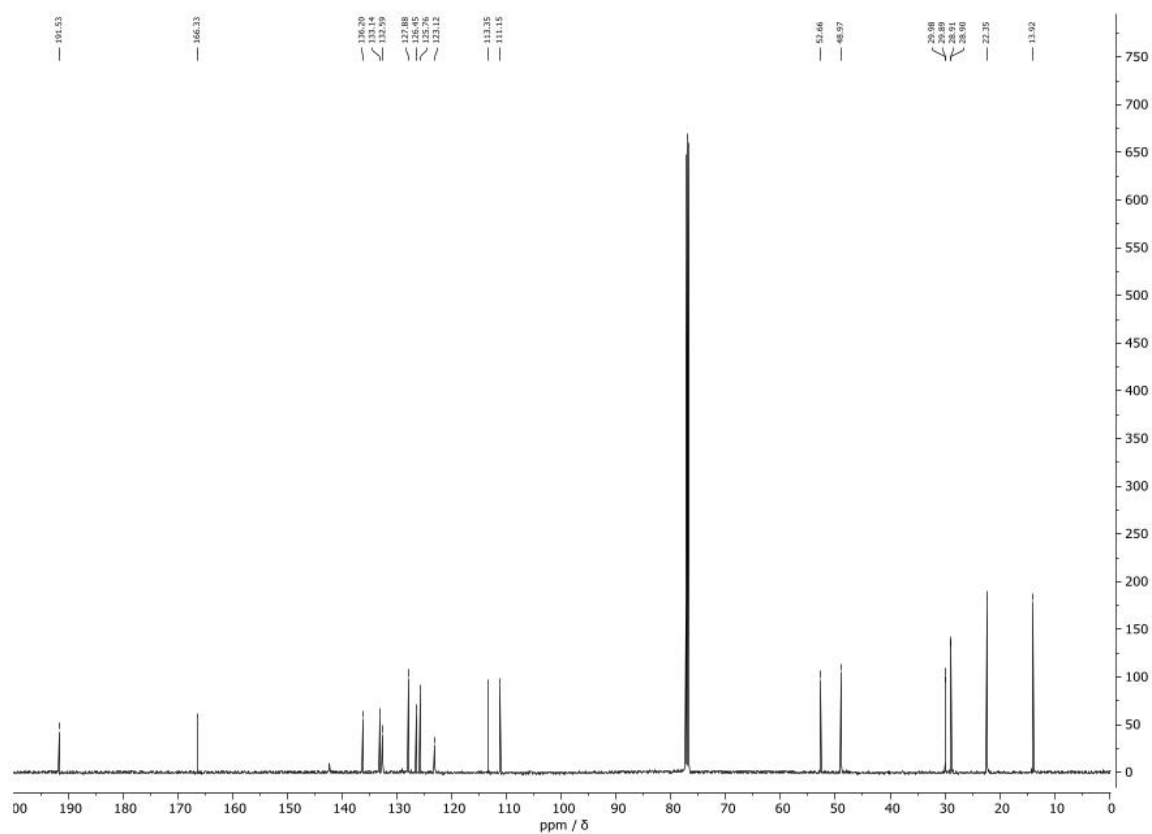


Fig. S8. ^{13}C spectrum of **9d** in CDCl_3 .

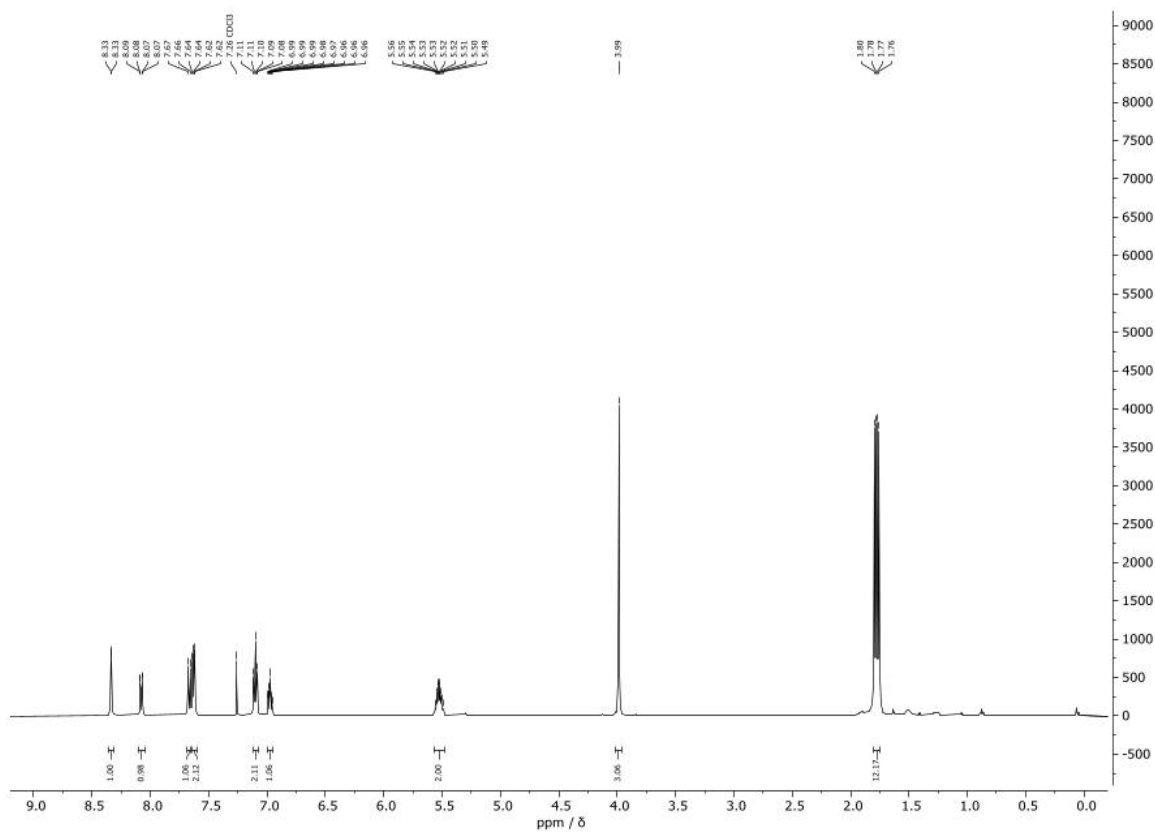


Fig. S9. ^1H spectrum of **9e** in CDCl_3 .

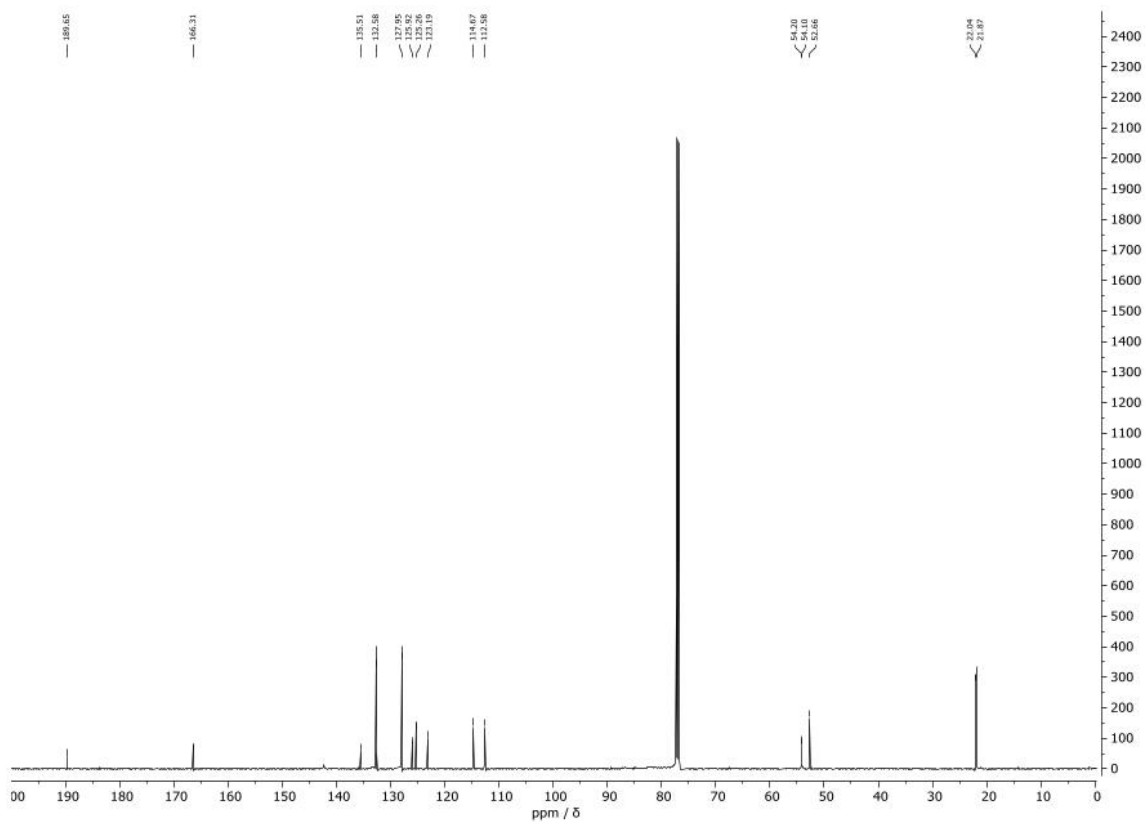


Fig. S10. ^{13}C spectrum of **9e** in CDCl_3 .

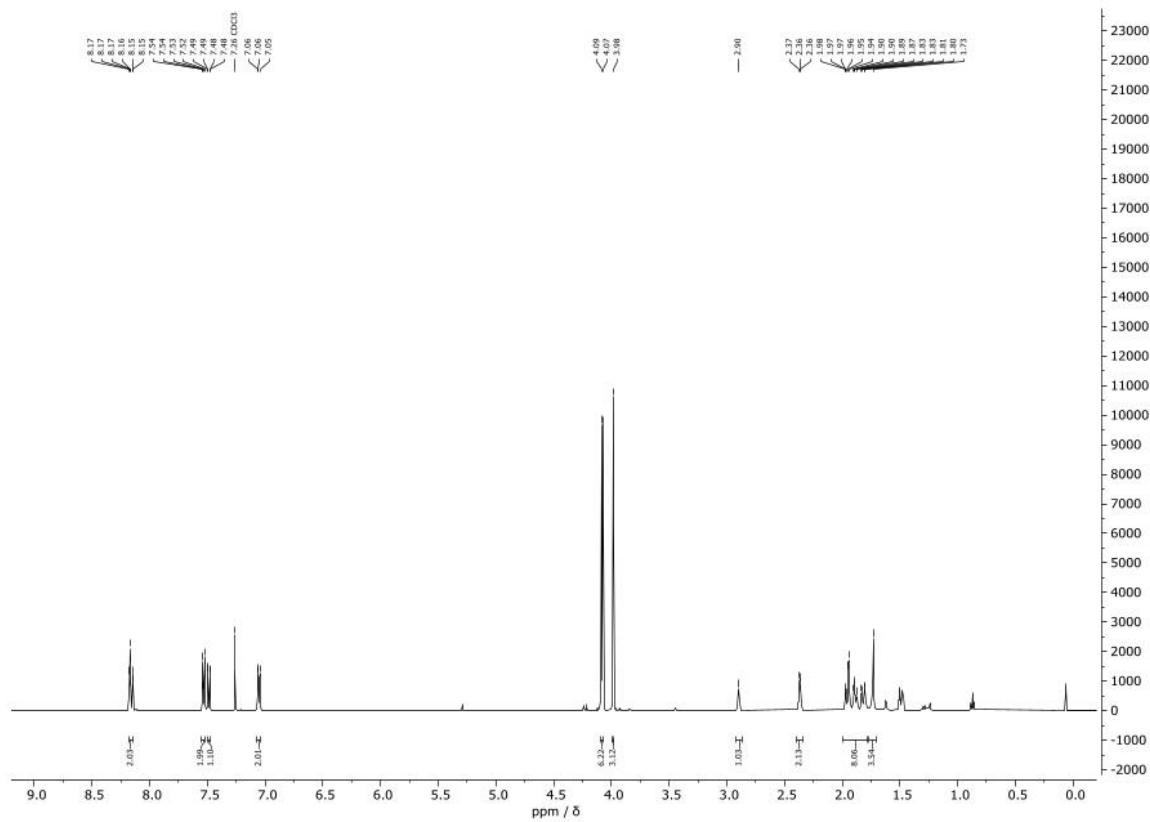


Fig. S11. ^1H spectrum of **13a** in CDCl_3 .

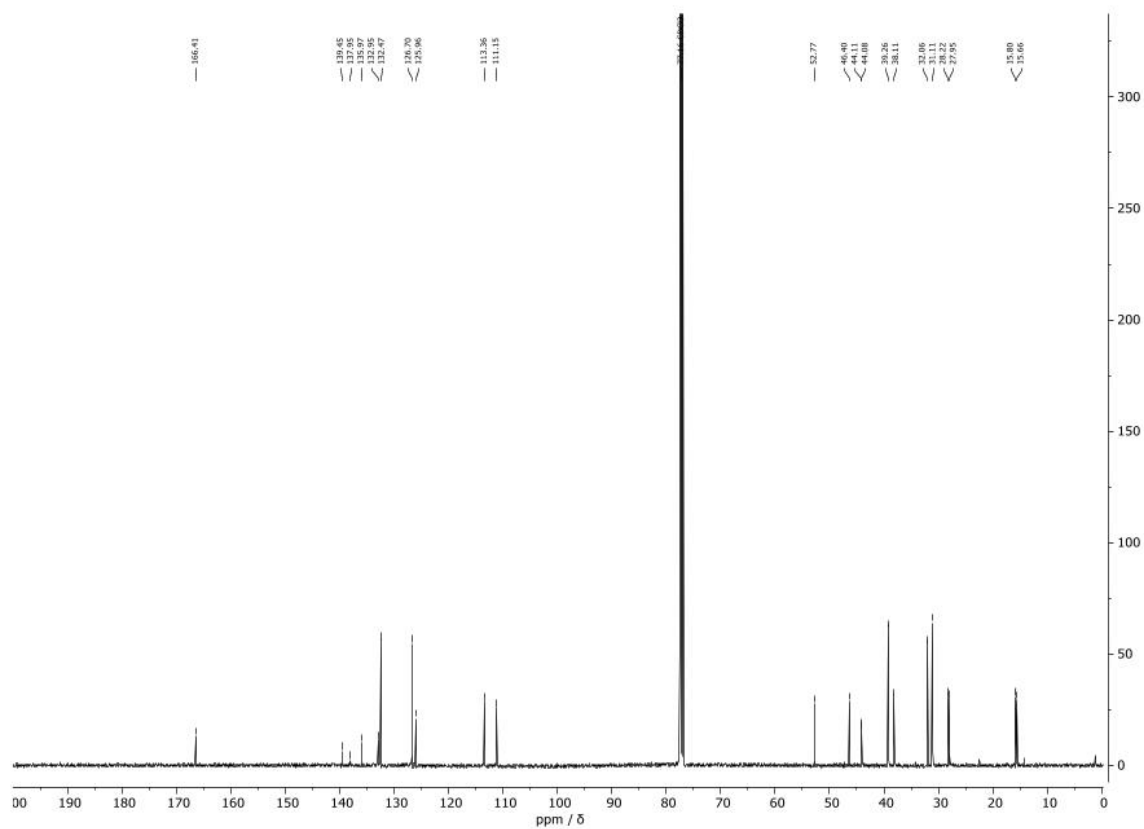


Fig. S14. ^{13}C spectrum of **10b** in CDCl_3 .

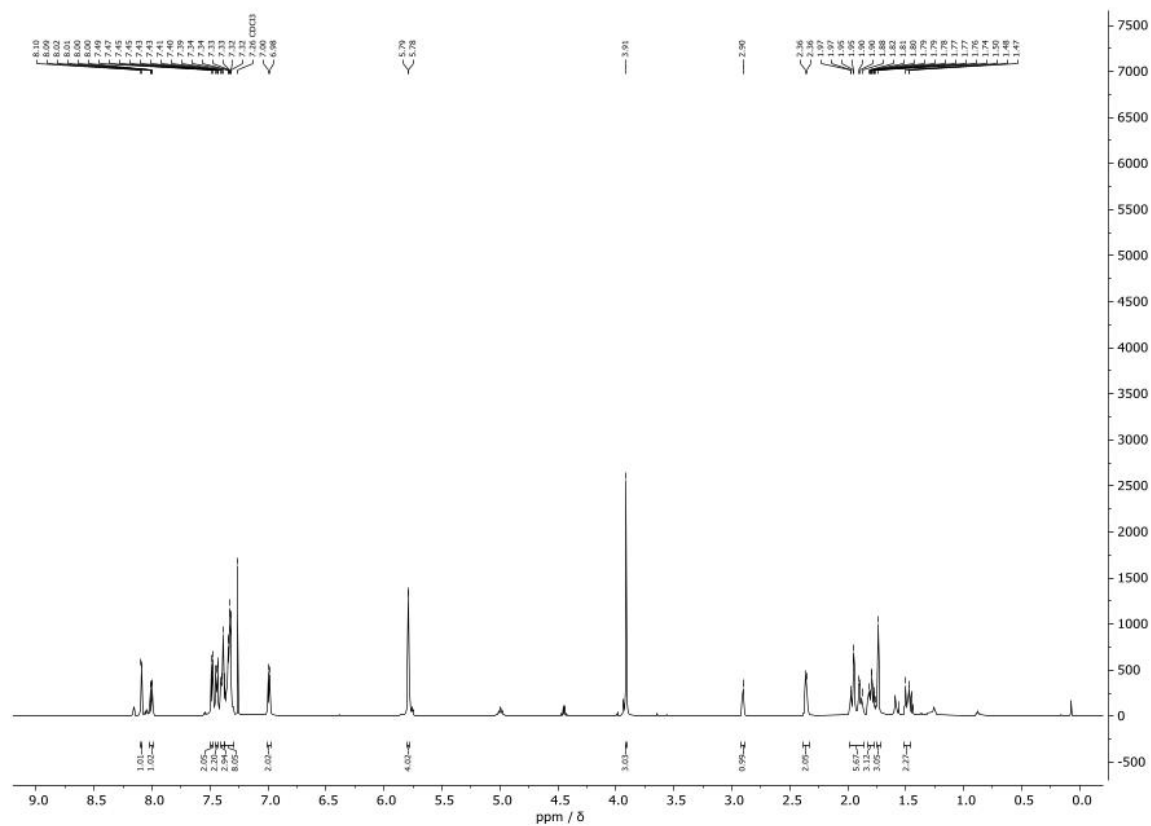


Fig. S15. ^1H spectrum of **10c** in CDCl_3 .

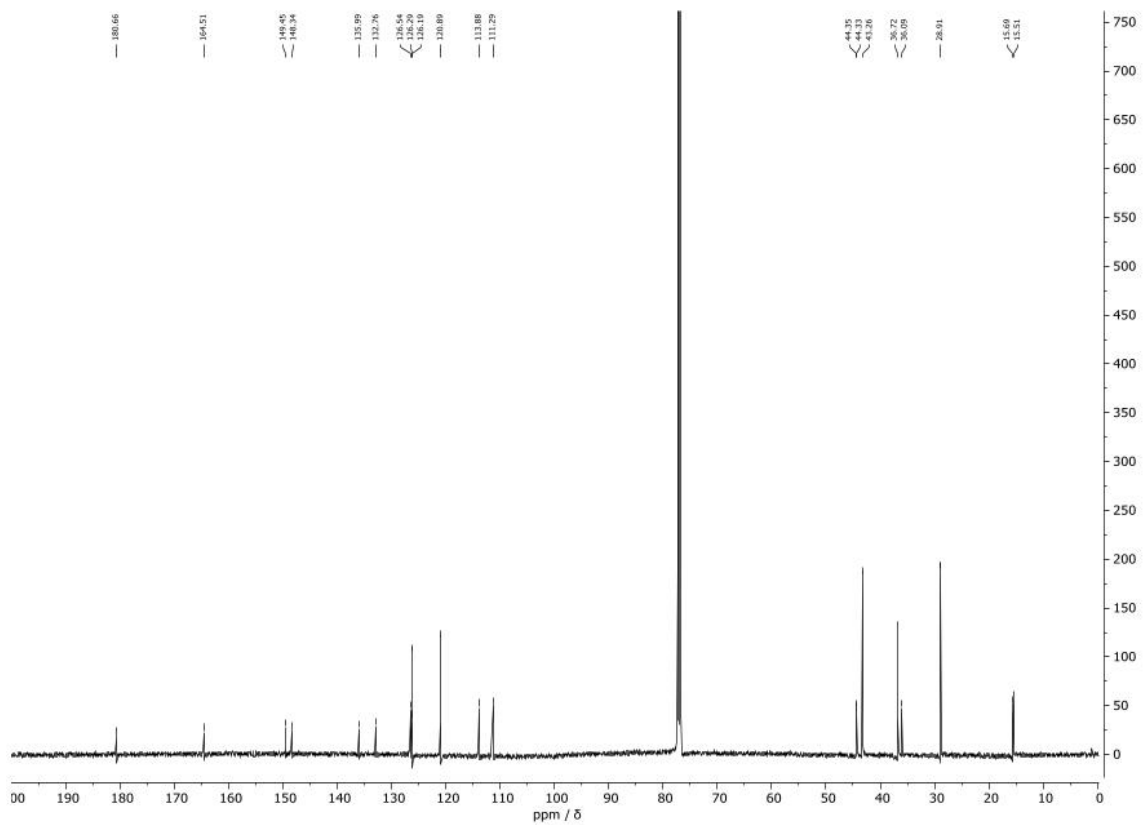


Fig. S18. ^{13}C spectrum of **17** in CDCl_3 .

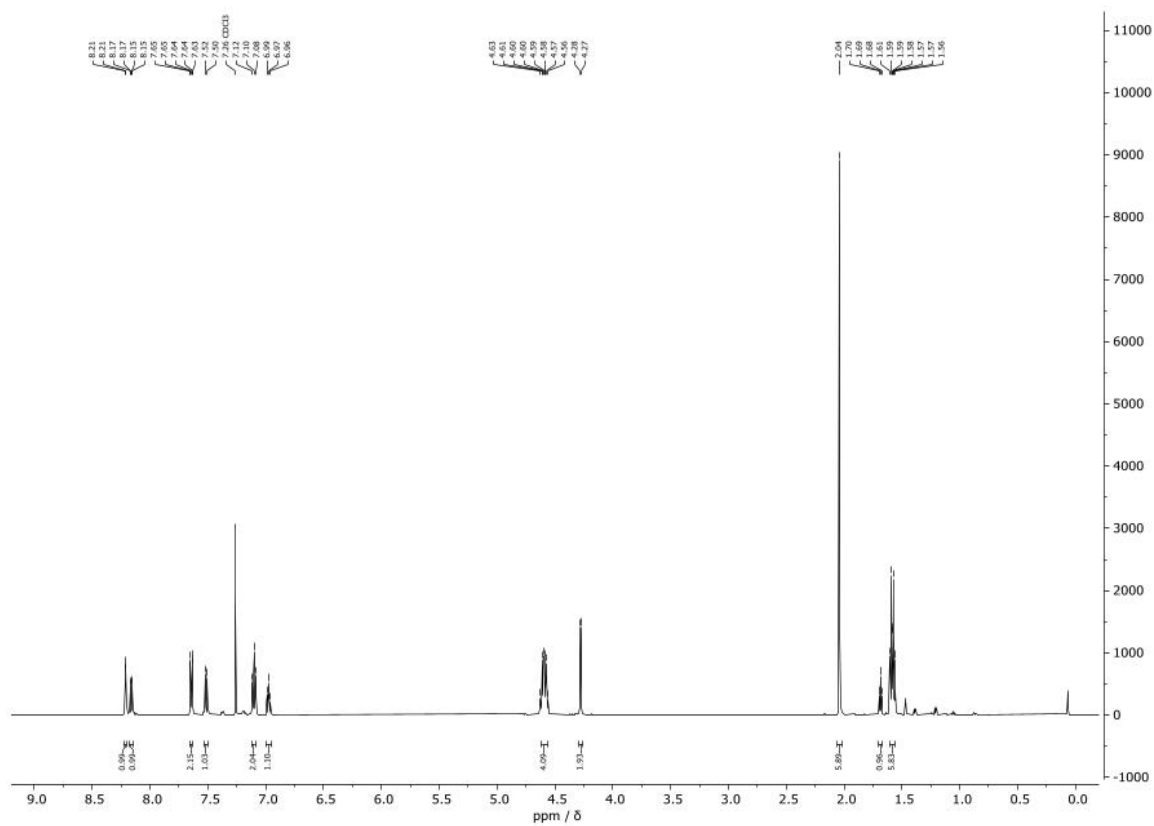


Fig. S19. ^1H spectrum of **20** in CDCl_3 .

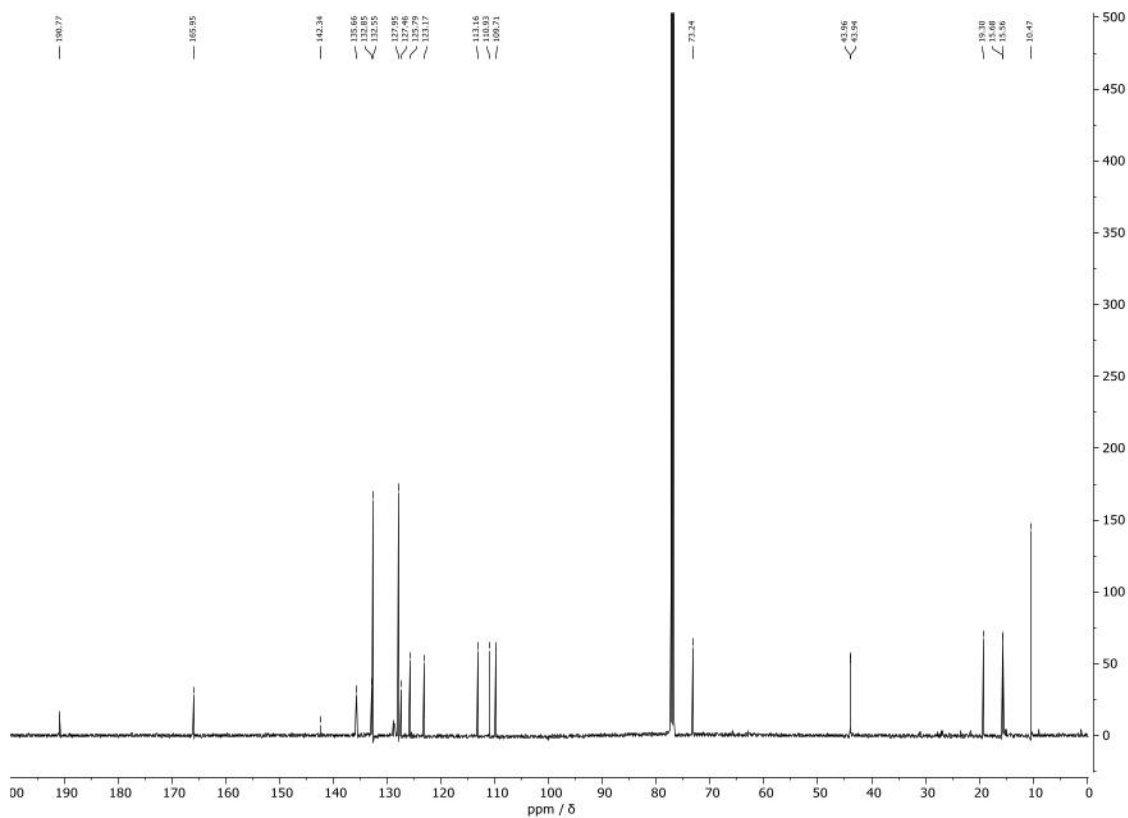


Fig. S20. ^{13}C spectrum of **20** in CDCl_3 .

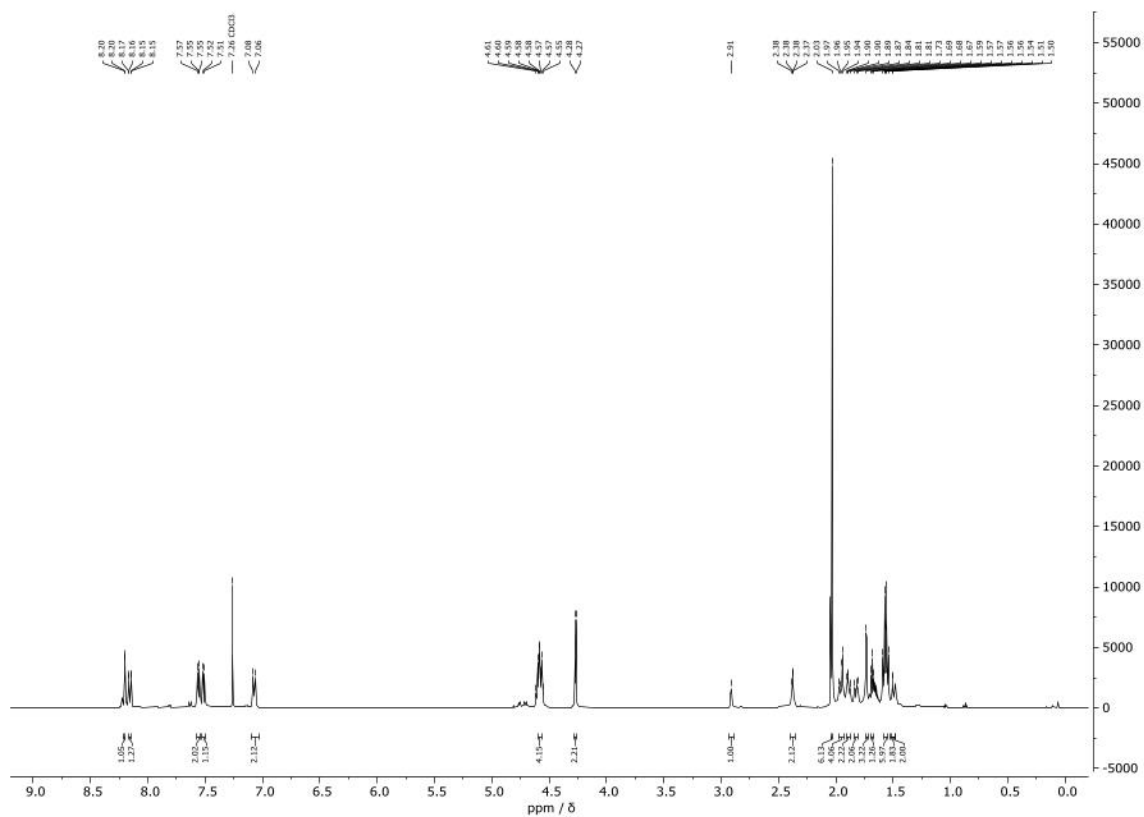


Fig. S21. ^1H spectrum of **21** in CDCl_3 .

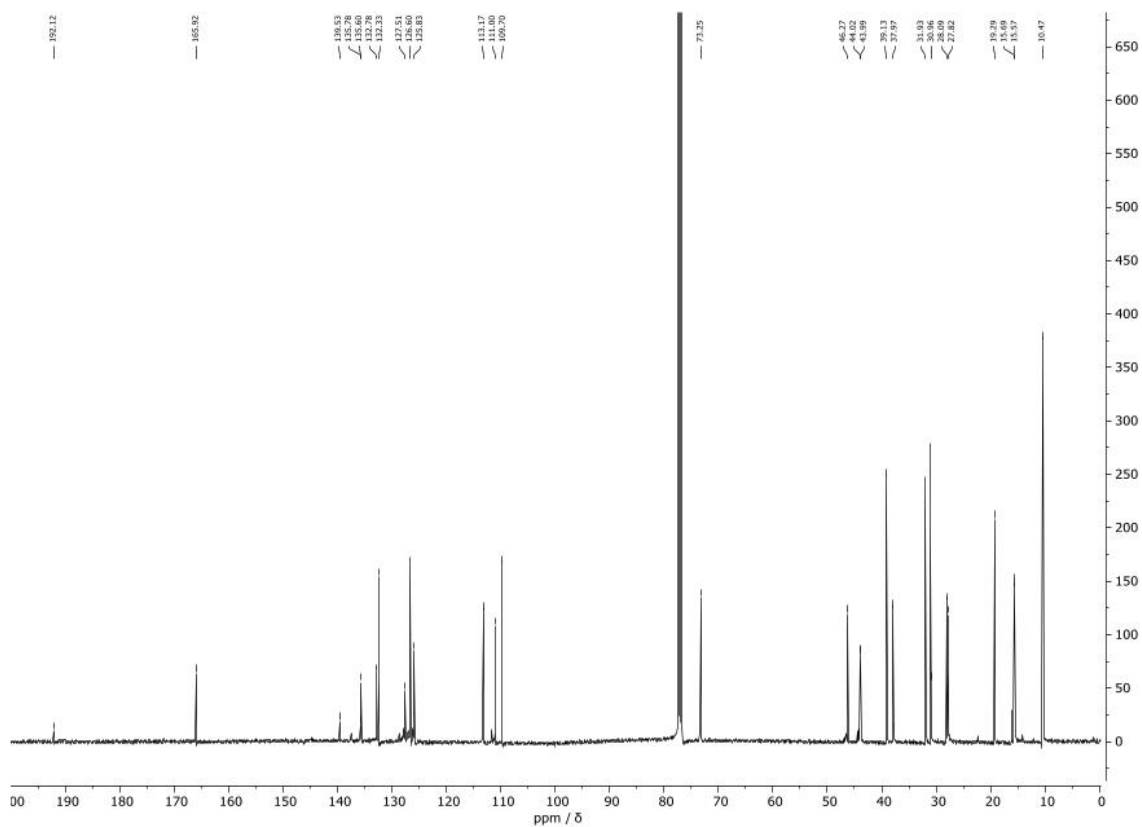


Fig. S22. ^{13}C spectrum of **21** in CDCl_3 .

Stability Studies via ^1H NMR

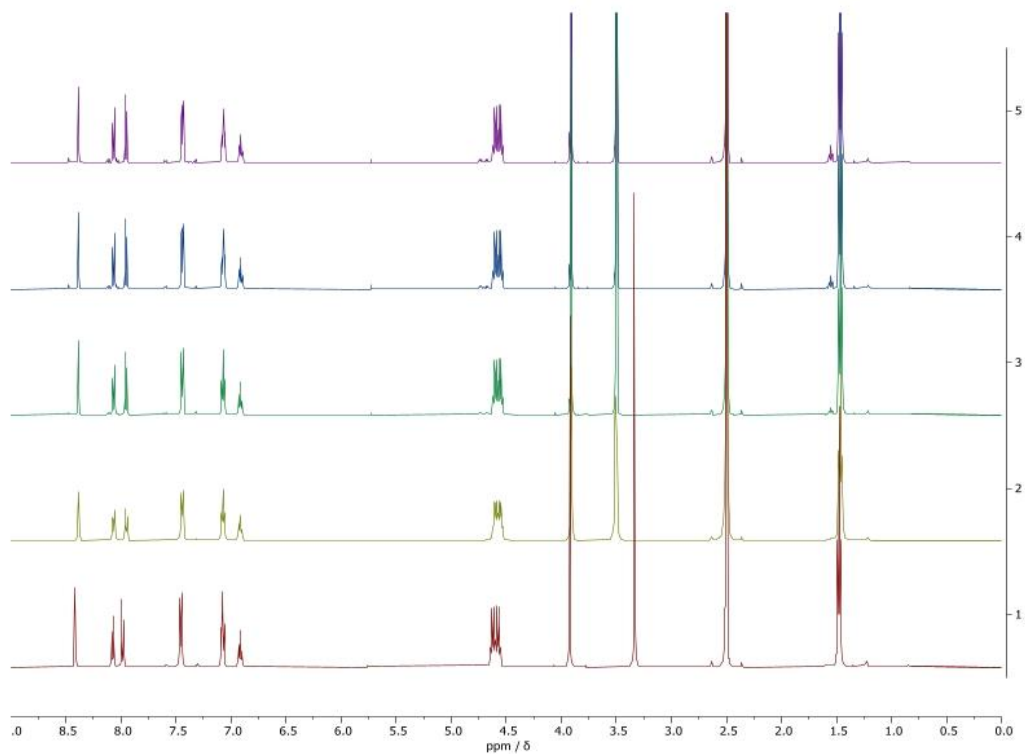


Fig. S23. ^1H -NMR spectrum of **9b** in DMSO-d_6 after 0h (red), + 5% D_2O 0h (yellow), 24h (green), 48h (cyan) and 72h (purple),

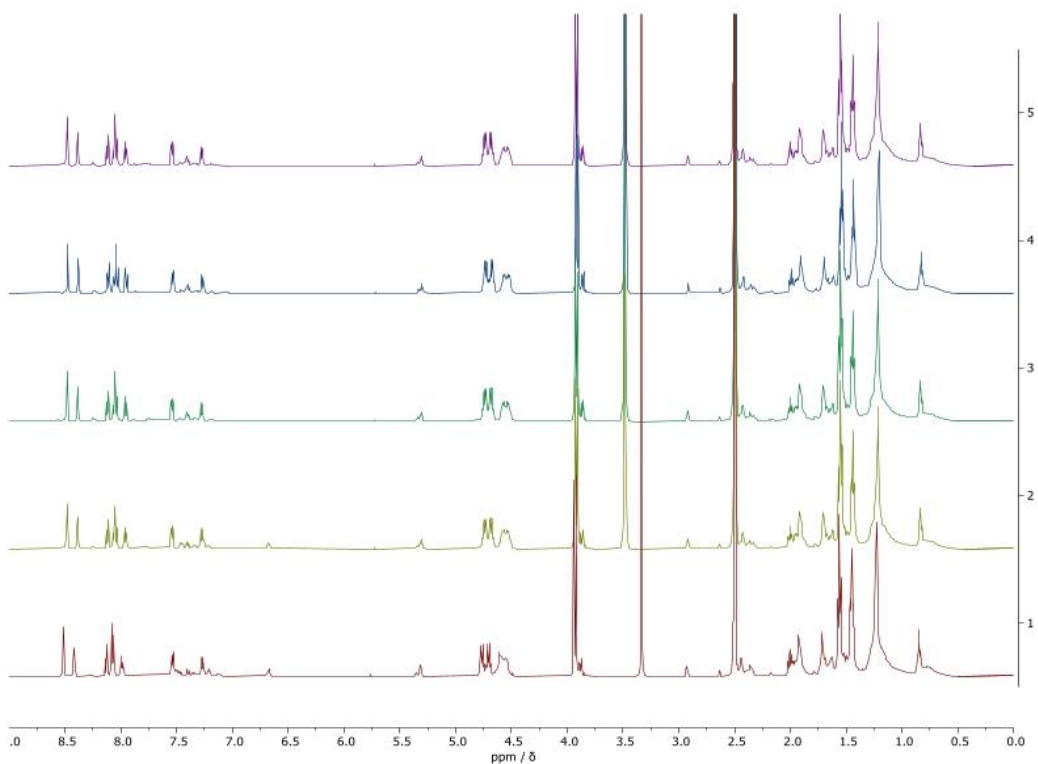


Fig. S24. $^1\text{H-NMR}$ spectrum of **10b** in DMSO-d_6 after 0h (red), + 5% D_2O 0h (yellow), 24h (green), 48h (cyan) and 72h (purple).

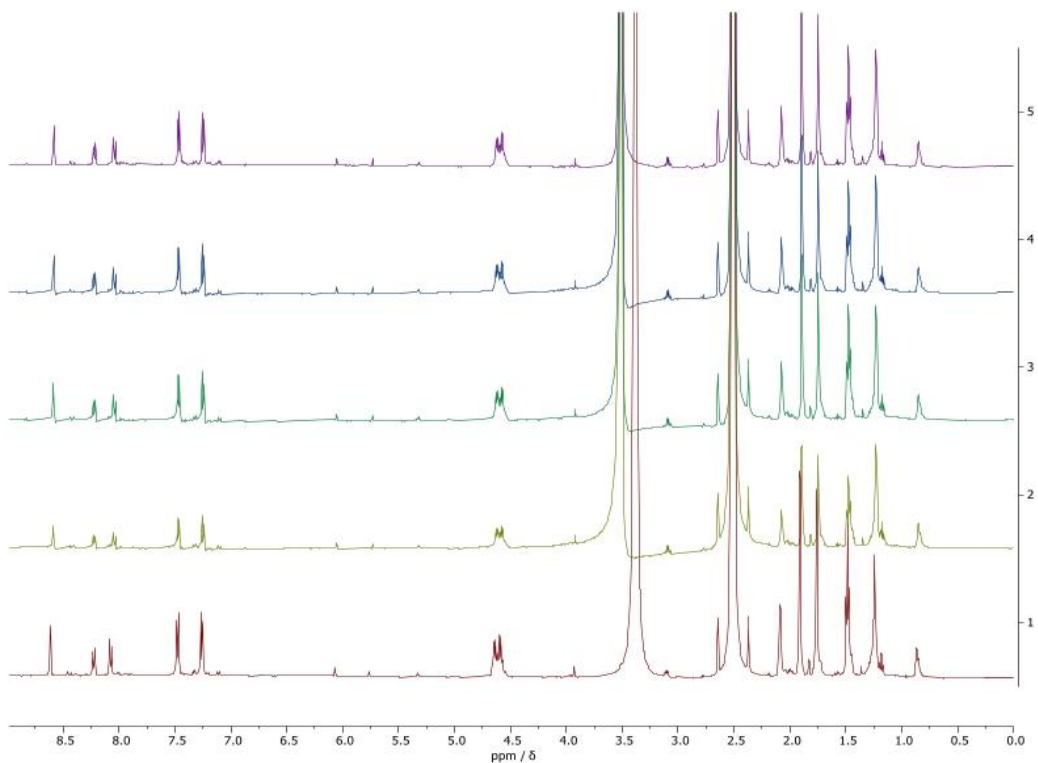


Fig. S25. $^1\text{H-NMR}$ spectrum of **17** in DMSO-d_6 after 0h (red), + 5% D_2O 0h (yellow), 24h (green), 48h (cyan) and 72h (purple).

Thioredoxin reductase inhibition assay

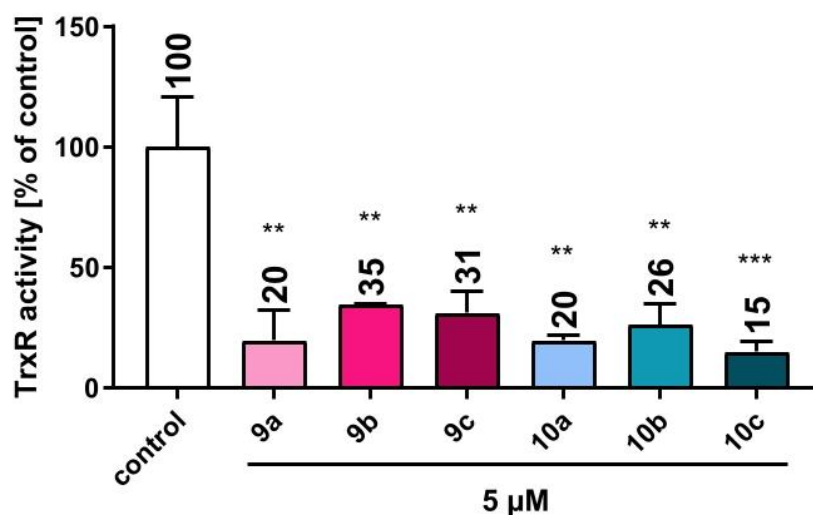


Fig. S26. Substance-dependent inhibition of thioredoxin reductase (TrxR) activity in 518A2 melanoma cell extract was determined using the Thioredoxin Reductase Colorimetric Assay Kit (Cayman). The TrxR activity was measured as mean \pm SEM (absorbance at 405 nm) after treatment with test compounds **9a-c** and **10a-c** (5 μ M). Significance is given as **: < 0.01; ***: < 0.001, One-way ANOVA with Dunnett's multiple comparison test (GraphPad prism 9).

Caspase 3/7 activity assay

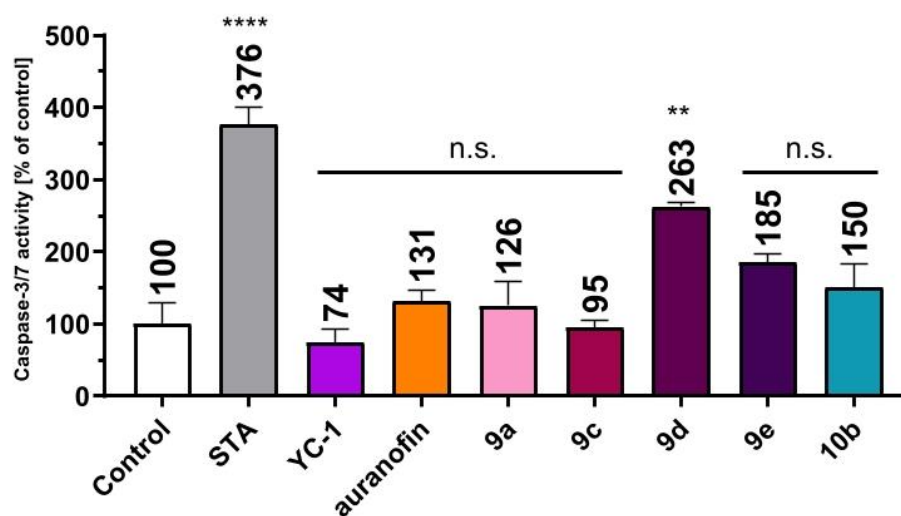


Fig. S27. Caspase-3/7 activation of **9a**, **9c-e**, **10b**, YC-1, auranofin (10 μ M) or staurosporine (1 μ M) in 518A2 melanoma cells after 6 h treatment under cell culture conditions, measured with Cell Meter™ Caspase 3/7 activity apoptosis assay kit by means of fluorescence \pm SD (λ_{ex} = 500 nm, λ_{em} = 522 nm). Significance was stated as n.s.: > 0.05; **: < 0.01; ****: < 0.001, One-way ANOVA with Dunnett's multiple comparison test (GraphPad prism 9).

Electrophoretic mobility shift assay

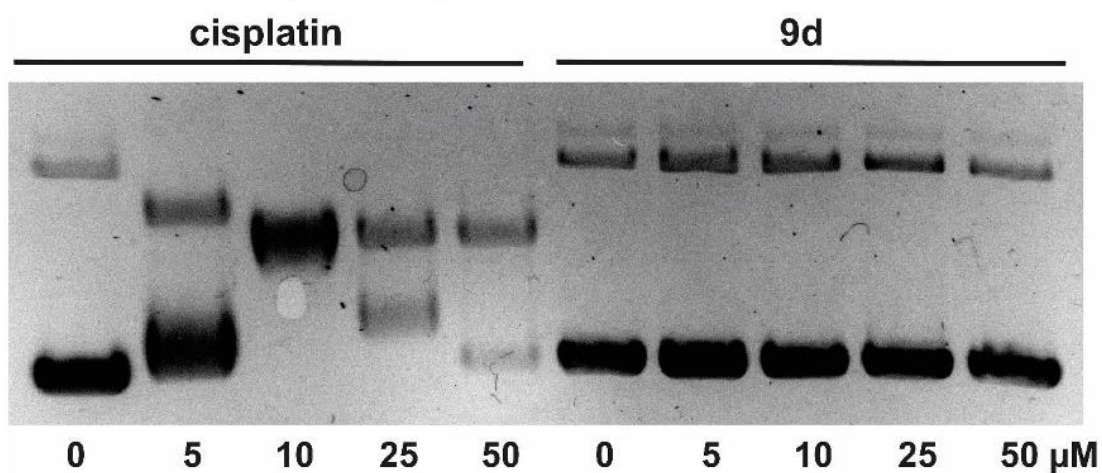


Fig. S28. Electrophoretic mobility shift assay of **9d** and control cisplatin (0, 5, 10, 25, 50 μM) with 0.5 μg/mL pBR322 plasmid DNA visualized by UV excitation. Upper band (open circular) lower band (supercoiled).

Quantification of cellular uptake by ICP-MS analysis

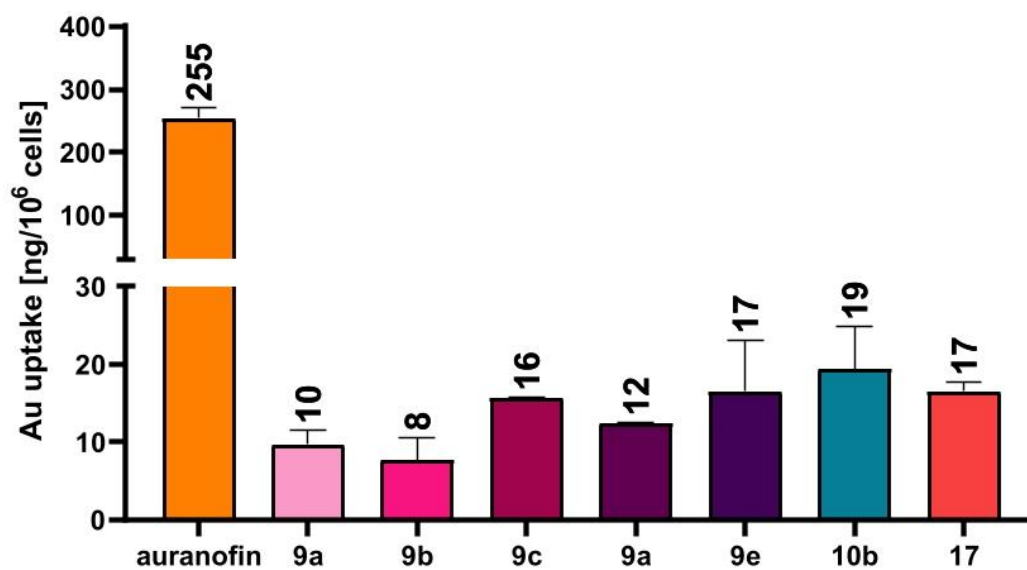


Fig. S29. Accumulation of gold in 518A2 melanoma cells treated with the test compounds **9a-e**, **10b**, **17**, and auranofin (5 μM) for 6 h measured by ICP-MS analysis.

Crystallography of **9b**

Formula	C ₁₉ H ₂₁ AuN ₂ O ₂ S
Formula weight	538.41
Crystal system	Monoclinic
Space group	<i>P21/c</i>
<i>a</i> [Å]	13.180(3)
<i>b</i> [Å]	13.170(3)
<i>c</i> [Å]	10.710(2)
α [°]	90
β [°]	101.60(3)
γ [°]	90
Cell volume [Å ³]	1821.1(7)
<i>Z</i>	4
Crystal size [mm ³]	0.086 x 0.06 x 0.049
Habit	Plate
Color	Clear colorless
Density [gcm ⁻³]	1.964
<i>T</i> [K]	170
Theta range	3.095 – 29.165
Unique reflections	4398
Observed reflections [<i>I</i> > 2s(<i>I</i>)]	10580
Parameters	229
<i>wR</i> ₂ (all data)	0.088
<i>R</i> [<i>I</i> > 2s(<i>I</i>)]	0.0367
X-ray source	$\lambda(\text{Mo-K}\alpha) = 0.71073 \text{ \AA}$

References

- Dolomanov, O.V., Bourhis, L.J., Gildea, R.J, Howard, J.A.K. & Puschmann, H. (2009), *J. Appl. Cryst.* 42, 339-341.
Sheldrick, G.M. (2015). *Acta Cryst.* A71, 3-8.
Sheldrick, G.M. (2015). *Acta Cryst.* C71, 3-8.

4.3 Publication II

Journal of Inorganic Biochemistry 238 (2023) 112028



Contents lists available at ScienceDirect

Journal of Inorganic Biochemistry

journal homepage: www.elsevier.com/locate/jinorgbio



Trans-[bis(benzimidazol-2-ylidene)dichlorido]platinum(II) complexes with peculiar modes of action and activity against cisplatin-resistant cancer cells

Sofia I. Bär¹, Sebastian W. Schleser¹, Natalie Oberhuber, Alexander Herrmann, Luca Schlotte, Stefanie E. Weber, Rainer Schobert*

Organic Chemistry Laboratory, University of Bayreuth, Universitaetsstrasse 30, 95447 Bayreuth, Germany

ARTICLE INFO

Keywords:

Trans-NHC platinum complexes
Anticancer drugs
DNA binding
Cisplatin resistance
Click chemistry
Subcellular localisation

ABSTRACT

Three series of *cis*- and *trans*-[bis(benzimidazol-2-ylidene)dichlorido]platinum(II) and *cis*-[(benzimidazol-2-ylidene)(DMSO)dichlorido]platinum(II) complexes were synthesised and screened for cytotoxicity against six human cancer cell lines. Depending on their N-alkyl and 5-alkoxycarbonyl substituents, two-digit nanomolar to single-digit micromolar IC_{50} values against cancer cell lines intrinsically resistant to or ill-responding to cisplatin were reached by both *cis*- and *trans*-configured complexes. The stability of the complexes under aqueous biotest conditions was shown via ¹H and ¹⁹⁵Pt NMR monitoring to be dependent on their configuration and their N-substituents. Localisation studies employing click reactions with 1-alkyne- or cyclopropene-tagged derivatives revealed that the *cis*-complexes accumulated in the cell nuclei and the *trans*-complexes in the mitochondria. While the most active *cis*-complexes showed modes of action akin to those of cisplatin, the most active *trans*-complexes differed from cisplatin by much lower rates of cellular uptake and ROS production, and by their non-interaction with the cell cycle and the DNA of cancer cells. Thus, we identified structural key elements for the synthesis of optimised *trans*-configured NHC platinum(II) complexes with high activity also against cisplatin-refractory cancer cells.

1. Introduction

N-heterocyclic carbene (NHC) complexes of platinum are of interest both as potential catalysts and anticancer agents, depending on their particular structures and ligands [1–3]. Bioactive NHC complexes of platinum have received increasing attention in recent years, due to their advantages over the clinical mainstay anticancer drug cisplatin (CDDP) [4], whose applicability is limited by side effects and by triggering tumour resistance. They are an ideal playground for drug developers because of their structural simplicity and variability, and their ease of synthesis and purification when compared e.g. with monoclonal antibodies. Readily adjustable structural parameters such as the bulkiness and electronic effects of the N-substituents, as well as the choice, positioning and substitutability of further ligands allow a finetuning of their lipophilicity, membrane pervasiveness and interference with DNA and proteins. Libraries of structural derivatives are easily accessible for rational structure-activity studies [5]. Accordingly, a large number of new platinum complexes have been synthesised and screened in recent

years, with only a few being active against CDDP-resistant cancers. Concluding from the inactivity of the *trans*-isomer of cisplatin (*trans*-[diammine-dichlorido]platinum(II); a.k.a. transplatin), it was assumed that *trans*-configured complexes of platinum(II) are generally unsuitable as chemotherapeutics [6,7]. Over the years, however, numerous exceptions to this rule have accumulated, necessitating a reevaluation of *trans* platinum complexes [8]. Early on, it was observed that substitution of ammine ligands with bulkier ligands in transplatin may result in a high anticancer activity [8,9]. By now, there are a large number of *trans* platinum complexes with a broad spectrum of properties and modes of action [10]. A comparatively new development of the last decade are platinum NHC complexes, which combine the strong cytotoxic effect of DNA-binding complex fragments with the chemical stability and structural variability of NHC ligands [5]. Some of them, and *trans*-configured complexes in particular, are active even against CDDP resistant cancer cells and tumours [5].

* Corresponding author.

E-mail address: rainer.schobert@uni-bayreuth.de (R. Schobert).

¹ These authors contributed equally to this work.

<https://doi.org/10.1016/j.jinorgbio.2022.112028>

Received 15 August 2022; Received in revised form 27 September 2022; Accepted 11 October 2022

Available online 14 October 2022

0162-0134/© 2022 Elsevier Inc. All rights reserved.

2. Experimental

2.1. General

Starting compounds were purchased from *Sigma-Aldrich* (St. Louis, United States), *TCI* (Tokio, Japan), *Merck* (Darmstadt, Germany), *abc* (Karlsruhe, Germany), *Acros Organics* (Fair Lawn, United States), *VWR* (Radnor, United States) and used without further purification. All reactions with moisture-sensitive reagents were carried out under an argon atmosphere in water-free solvents. Unless stated otherwise, the solvents were purified and dried using standard methods. Synthetic protocols for precursors **2–7**, **14–15** and **17–21** can be found in the supporting information.

Elemental analyses were carried out with a *Perkin-Elmer* (Waltham, United States) 2400 CHN elemental analyzer. Nuclear magnetic resonance (NMR) spectra were measured using a *Bruker* (Billerica, USA) DRX spectrometer at ambient temperature. Chemical shifts are given in parts per million (δ) downfield from tetramethylsilane as internal standard. As internal standard for ^1H NMR spectra the resonance signal of the residual proton of CDCl_3 ($\delta = 7.26$ ppm), $\text{DMSO}-d_6$ ($\delta = 2.50$ ppm) or $\text{MeOD}-d_4$ ($\delta = 3.31$ ppm) was used. For ^{13}C NMR spectra the resonance signal of the carbon atom of CDCl_3 ($\delta = 77.1$ ppm), $\text{DMSO}-d_6$ ($\delta = 39.5$ ppm) or $\text{MeOD}-d_4$ ($\delta = 49.0$ ppm) was used. The ^1H NMR spectra were measured at 500 MHz, ^{13}C NMR spectra at 125 MHz and ^{195}Pt NMR spectra at 107 MHz. For signal multiplicities the following abbreviations were used: s = singlet, d = doublet, t = triplet, m = multiplet, dd = doublet of doublets, dt = doublet of triplets, dq = doublet of quartets with the prefix v meaning virtual. Coupling constants are given in Hz. Melting points were taken with an Electrothermal 9100 apparatus and are uncorrected. Mass spectra were recorded either on a Varian (Palo Alto, USA) MAT 311A (EI) or a ThermoFisher Scientific (Waltham, United States) UPLC/Orbitrap MS system (HRMS-ESI).

2.2. Chemistry

2.2.1. General synthesis of *trans*-[Pt^{II}Cl₂(NHC)₂] complexes **8** and **9**

The silver complexes **6a-c** or **7a-c** (1.00 eq.) and K_2PtCl_4 (0.50 eq.) were dissolved in CH_2Cl_2 (1 mL/10 μmol) and stirred at rt. for 4 d. The solution was filtered over celite and the solvent was evaporated. The crude products were purified by column chromatography (silica gel 60, EtOAc/MeOH 98:2) and subsequently precipitated from *n*-pentane at 4 °C affording the products as white powders after drying in vacuo.

2.2.1.1. trans-[Dichlorido-bis(5-(methoxycarbonyl)-1,3-dimethylbenzimidazol-2-ylidene)]platinum(II) (8a). 51.0 mg (75.6 μmol , 67%) from **6a** (78.0 mg, 224 μmol , 1.00 eq.), K_2PtCl_4 (46.6 mg, 112 μmol , 0.50 eq.), CH_2Cl_2 (20.0 mL); $R_f = 0.78$ (EtOAc/MeOH 98:2); m.p. 320 °C; ^1H NMR (500 MHz, CDCl_3) $\delta = 8.15$ (s, 2H, H^{ar}), 8.08 (d, $J = 8.4$ Hz, 2H, H^{ar}), 7.45 (vdd, $J = 8.5$ Hz, 2H, H^{ar}), 4.42 (vdd, $J = 9.9$ Hz, 2.1 Hz, 4H, NCH₂), 3.98 (s, 6H, OCH₃); ^{13}C NMR (125 MHz, CDCl_3) $\delta = 181.0$ (s, NCN), 166.7 (s, COOMe), 137.8 (s, C^{ar}), 134.8 (s, C^{ar}), 125.5 (s, C^{ar}), 125.1 (s, C^{ar}), 112.3 (s, C^{ar}), 110.1 (s, C^{ar}), 52.6 (s, OCH₃), 34.3 (s, NCH₃), 34.2 (s, NCH₃); ^{195}Pt NMR (107 MHz, CDCl_3) $\delta = -3247.8$; m/z (EI, pos): 674 [M]⁺, 638 [M-Cl]⁺, 601 [M-2Cl]⁺; Anal. Calcd. for $\text{C}_{22}\text{H}_{24}\text{Cl}_2\text{N}_4\text{O}_4\text{Pt}$ (674.4): C, 39.18; H, 3.59; N, 8.31. Found: C, 38.10; H, 3.69; N, 7.67.

2.2.1.2. trans-[Dichlorido-bis(5-(methoxycarbonyl)-1,3-diethylbenzimidazol-2-ylidene)]platinum(II) (8b). 93.0 mg (127 μmol , 93%) from **6b** (103 mg, 274 μmol , 1.00 eq.), K_2PtCl_4 (56.9 mg, 137 μmol , 0.50 eq.) in CH_2Cl_2 (30.0 mL). $R_f = 0.78$ (EtOAc/MeOH 98:2); m.p. 250 °C; ^1H NMR (500 MHz, CDCl_3) $\delta_{\text{H}} = 8.15$ (s, 2H, H^{ar}), 8.04 (vdd, $J = 8.5$ Hz, 1.4 Hz, 2H, H^{ar}), 7.46 (vdd, $J = 8.5$ Hz, 1.4 Hz, 2H, H^{ar}), 5.05–4.92 (m, 8H, NCH₂), 3.98 (s, 6H, OCH₃), 1.78 (t, $J = 7.3$ Hz, 12H, CH₃); ^{13}C NMR (125 MHz, CDCl_3) $\delta_{\text{C}} = 181.4$ (s, NCN), 166.8 (s, COOMe), 137.0 (s,

Car), 133.9 (s, C^{ar}), 125.3 (s, C^{ar}), 124.9 (s, C^{ar}), 112.4 (s, C^{ar}), 110.1 (s, C^{ar}), 52.5 (s, OCH₃), 42.9 (s, NCH₂), 15.3 (s, CH₃); ^{195}Pt NMR (107 MHz, CDCl_3) $\delta_{\text{Pt}} = -3267.0$; m/z (EI, pos): 730 [M]⁺, 693 [M-Cl]⁺, 657 [M-2Cl]⁺; Anal. Calcd. for $\text{C}_{26}\text{H}_{32}\text{Cl}_2\text{N}_4\text{O}_4\text{Pt}$ (730.6): C, 42.75; H, 4.42; N, 7.67. Found: C, 43.52; H, 4.55; N, 7.42.

2.2.1.3. trans-[Dichlorido-bis(5-(methoxycarbonyl)-1,3-dibenzylbenzimidazol-2-ylidene)]platinum(II) (8c). 106 mg (108 μmol , 90%) from **6c** (120 mg, 240 μmol , 1.00 eq.), K_2PtCl_4 (49.8 mg, 120 μmol , 0.50 eq.) in CH_2Cl_2 (20.0 mL). $R_f = 0.88$ (EtOAc/MeOH 98:2); m.p. 290 °C; ^1H NMR (500 MHz, CDCl_3) $\delta_{\text{H}} = 7.92$ (s, 2H, H^{ar}), 7.83 (vdd, $J = 8.6$ Hz, 1.5 Hz, 2H, H^{ar}), 7.55–7.43 (m, 8H, H^{ar}), 7.28–7.12 (m, 14H, H^{ar}), 6.10 (vdd, $J = 4.3$ Hz, 8H, NCH₂), 3.86 (s, 6H, OCH₃); ^{13}C NMR (125 MHz, CDCl_3) $\delta_{\text{C}} = 182.0$ (s, NCN), 166.5 (s, COOMe), 137.8 (s, C^{ar}), 135.4 (s, C^{ar}), 134.4 (s, C^{ar}), 128.9 (s, C^{ar}), 128.1 (s, C^{ar}), 127.7 (s, C^{ar}), 127.6 (s, C^{ar}), 125.6 (s, C^{ar}), 125.1 (s, C^{ar}), 113.2 (s, C^{ar}), 111.2 (s, C^{ar}), 52.5 (s, OCH₃), 52.0 (s, NCH₂), 51.7 (s, NCH₂); ^{195}Pt NMR (107 MHz, CDCl_3) $\delta_{\text{Pt}} = -3285.7$; m/z (EI, pos): 978 [M]⁺, 942 [M-Cl]⁺, 905 [M-2Cl]⁺; Anal. Calcd. for $\text{C}_{46}\text{H}_{40}\text{Cl}_2\text{N}_4\text{O}_4\text{Pt}$ (978.8): C, 56.45; H, 4.12; N, 5.72. Found: C, 55.61; H, 4.06; N, 5.61.

2.2.1.4. trans-[Dichlorido-bis(5-(ethoxycarbonyl)-1,3-dimethylbenzimidazol-2-ylidene)]platinum(II) (9a). 115 mg (164 μmol , 79%) from **7a** (150 mg, 415 μmol , 1.00 eq.), K_2PtCl_4 (86.1 mg, 207 μmol , 0.50 eq.) in CH_2Cl_2 (40.0 mL). $R_f = 0.76$ (EtOAc/MeOH 98:2); m.p. 340 °C; ^1H NMR (500 MHz, CDCl_3) $\delta_{\text{H}} = 8.14$ (s, 2H, H^{ar}), 8.07 (vdd, $J = 8.4$ Hz, 1.4 Hz, 2H, H^{ar}), 7.44 (vdd, $J = 8.5$ Hz, 1.3 Hz, 2H, H^{ar}), 4.51–4.37 (m, 16H, OCH₂, NCH₃), 1.45 (t, $J = 7.1$ Hz, CH₃); ^{13}C NMR (125 MHz, CDCl_3) $\delta_{\text{C}} = 180.9$ (s, NCN), 166.3 (s, COOCH₂), 137.8 (s, C^{ar}), 134.8 (s, C^{ar}), 125.9 (s, C^{ar}), 125.1 (s, C^{ar}), 112.2 (s, C^{ar}), 110.0 (s, C^{ar}), 61.6 (s, OCH₂), 34.3 (s, NCH₃), 14.5 (s, CH₃); ^{195}Pt NMR (107 MHz, CDCl_3) $\delta_{\text{Pt}} = -3246.9$. m/z (EI, pos): 702 [M]⁺, 666 [M-Cl]⁺, 630 [M-2Cl]⁺. Anal. Calcd. for $\text{C}_{24}\text{H}_{28}\text{Cl}_2\text{N}_4\text{O}_4\text{Pt}$ (702.5): C, 41.03; H, 4.02; N, 7.98. Found: C, 40.26; H, 4.42; N, 7.75.

2.2.1.5. trans-[Dichlorido-bis(5-(ethoxycarbonyl)-1,3-diethylbenzimidazol-2-ylidene)]platinum(II) (9b). 24.0 mg (31.6 μmol , 20%) from **7b** (156 mg, 324 μmol , 1.00 eq.), K_2PtCl_4 (67.3 mg, 162 μmol , 0.50 eq.) in CH_2Cl_2 (30.0 mL). $R_f = 0.84$ (EtOAc/MeOH 98:2); m.p. 260 °C; ^1H NMR (500 MHz, CDCl_3) $\delta_{\text{H}} = 8.08$ (s, 2H, H^{ar}), 7.98 (vdd, $J = 8.5$ Hz, 1.4 Hz, 2H, H^{ar}), 7.39 (vdd, $J = 8.5$ Hz, 1.3 Hz, 2H, H^{ar}), 4.98–4.80 (m, 8H, NCH₂), 4.37 (q, $J = 7.1$ Hz, 4H, OCH₂), 1.38 (t, $J = 7.1$ Hz, 6H, CH₃); ^{13}C NMR (125 MHz, CDCl_3) $\delta_{\text{C}} = 181.1$ (s, NCN), 166.2 (s, COOCH₂), 136.7 (s, C^{ar}), 133.8 (s, C^{ar}), 125.5 (s, C^{ar}), 124.7 (s, C^{ar}), 112.2 (s, C^{ar}), 110.0 (s, C^{ar}), 61.4 (s, OCH₂), 42.8 (d, $J = 6.5$ Hz, NCH₂), 15.2 (s, CH₃), 15.0 (s, CH₃), 14.4 (s, CH₃); ^{195}Pt NMR (107 MHz, CDCl_3) $\delta_{\text{Pt}} = -3271.4$; m/z (EI, pos): 758 [M]⁺, 685 [M-Cl]⁺, 657 [M-2Cl]⁺; Anal. Calcd. for $\text{C}_{28}\text{H}_{36}\text{Cl}_2\text{N}_4\text{O}_4\text{Pt}$ (758.6): C, 44.33; H, 4.78; N, 7.39. Found: C, 43.96; H, 4.67; N, 7.40.

2.2.1.6. trans-[Dichlorido-bis(5-(ethoxycarbonyl)-1,3-dibenzylbenzimidazol-2-ylidene)]platinum(II) (9c). 82.0 mg (81.4 μmol , 42%) from **7c** (200 mg, 389 μmol , 1.00 eq.), K_2PtCl_4 (80.8 mg, 195 μmol , 0.50 eq.) in CH_2Cl_2 (39.0 mL). $R_f = 0.87$ (EtOAc/MeOH 98:2); m.p. 190 °C; ^1H NMR (500 MHz, CDCl_3) $\delta_{\text{H}} = 7.91$ (s, 2H, H^{ar}), 7.83 (d, $J = 8.5$ Hz, 2H, H^{ar}), 7.54–7.42 (m, 8H, H^{ar}), 7.25–7.21 (m, 12H, H^{ar}), 7.18 (d, $J = 8.7$ Hz, 2H, H^{ar}), 6.12–6.06 (m, 8H, NCH₂), 4.31 (q, $J = 7.1$ Hz, 4H, OCH₂), 1.33 (t, $J = 7.1$ Hz, 6H, CH₃); ^{13}C NMR (125 MHz, CDCl_3) $\delta_{\text{C}} = 181.7$ (s, NCN), 165.9 (s, COOCH₂), 137.1 (s, C^{ar}), 135.4 (s, C^{ar}), 134.3 (s, C^{ar}), 128.8 (s, C^{ar}), 128.0 (s, C^{ar}), 127.6 (s, C^{ar}), 125.8 (s, C^{ar}), 124.9 (s, C^{ar}), 113.1 (s, C^{ar}), 111.1 (s, C^{ar}), 61.3 (s, OCH₂), 51.5 (d, $J = 6.5$ Hz, NCH₂), 14.3 (s, CH₃); ^{195}Pt NMR (107 MHz, CDCl_3) $\delta_{\text{Pt}} = -3284.8$; m/z (EI, pos): 1006 [M]⁺, 969 [M-Cl]⁺, 933 [M-2Cl]⁺. Anal. Calcd. for $\text{C}_{46}\text{H}_{40}\text{Cl}_2\text{N}_4\text{O}_4\text{Pt}$ (1006.9): C, 57.26; H, 4.40; N, 5.56. Found: C, 57.05; H, 4.24; N, 5.50.

2.2.2. General synthesis of *cis*-[Pt^{II}Cl₂(DMSO)(NHC)] complexes 10 and 11

The silver complexes **6a–c** or **7a–c** (1.00 eq.) and K₂PtCl₄ (1.00 eq.) were dissolved in DMSO (1 mL/10 μmol). The mixture was stirred at 60 °C for 24 h. The silver halides were precipitated by adding CH₂Cl₂ and the resulting solution was filtered over celite. DMSO was removed via extraction with water followed by drying of the organic layer over Na₂SO₄ and removal of the solvent. The crude product was purified by column chromatography (silica gel 60, EtOAc/MeOH 98:2) and precipitated from *n*-pentane at 4 °C affording the product as white powder after drying in vacuo.

2.2.2.1. cis-[Dichlorido-(5-methoxycarbonyl-1,3-dimethylbenzimidazol-2-ylidene)(dimethylsulfoxide)] platinum(II) (10a). 47.0 mg (85.7 μmol, 80%) from **6a** (37.0 mg, 107 μmol, 1.00 eq.), K₂PtCl₄ (44.2 mg, 106 μmol, 1.00 eq.) in DMSO (10.0 mL). R_f = 0.50 (EtOAc/MeOH 98:2); m.p. 195 °C; ¹H NMR (500 MHz, CDCl₃) δ_H = 8.17 (s, 1H, H^{ar}), 8.10 (vdd, *J* = 8.5 Hz, 1.4 Hz, 1H, H^{ar}), 7.48 (d, *J* = 8.6 Hz, 1H, H^{ar}), 4.27 (vd, *J* = 8.7 Hz, 6H, NCH₃), 3.98 (s, 3H, OCH₃), 3.58 (d, *J* = 2.0 Hz, 6H, SCH₃); ¹³C NMR (125 MHz, CDCl₃) δ_C = 166.1 (s, COOMe), 158.4 (s, NCN), 136.9 (s, C^{ar}), 133.9 (s, C^{ar}), 126.4 (s, C^{ar}), 125.8 (s, C^{ar}), 112.8 (s, C^{ar}), 110.6 (s, C^{ar}), 52.8 (s, OCH₃), 46.2 (s, SCH₃), 34.9 (s, NCH₃); ¹⁹⁵Pt NMR (107 MHz, CDCl₃) δ_{Pt} = -3560.7; *m/z* (EI, pos): 548 [M]⁺, 469 [M-DMSO]⁺, 433 [M-DMSO-Cl]⁺. Anal. Calcd. for C₁₃H₁₈Cl₂N₂O₃PtS (548.3): C, 28.48; H, 3.31; N, 5.11; S, 5.85. Found: C, 28.19; H, 3.25; N, 4.97; S, 5.69.

2.2.2.2. cis-[Dichlorido-(5-methoxycarbonyl-1,3-diethylbenzimidazol-2-ylidene)(dimethylsulfoxide)] platinum(II) (10b). 190 mg (330 μmol, 84%) from **6b** (150 mg, 399 μmol, 1.00 eq.), K₂PtCl₄ (165 mg, 399 μmol, 1.00 eq.) in DMSO (40.0 mL). m.p. 180 °C; ¹H NMR (500 MHz, CDCl₃) δ_H = 8.18 (s, 1H, H^{ar}), 8.08 (vdd, *J* = 8.6 Hz, 1.4 Hz, 1H, H^{ar}), 7.50 (d, *J* = 8.6 Hz, 1H, H^{ar}), 4.87 (q, *J* = 7.4 Hz, 4H, NCH₂), 3.98 (s, 3H, OCH₃), 3.57 (s, 6H, SCH₃), 1.66 (t, *J* = 7.3 Hz, 6H, CH₃); ¹³C NMR (125 MHz, CDCl₃) δ_C = 166.3 (s, COOMe), 157.2 (s, NCN), 136.2 (s, C^{ar}), 133.2 (s, C^{ar}), 126.3 (s, C^{ar}), 125.6 (s, C^{ar}), 113.2 (s, C^{ar}), 111.1 (s, C^{ar}), 52.7 (s, OCH₃), 44.1 (s, SCH₃), 41.2 (s, NCH₂), 14.7 (s, CH₃); ¹⁹⁵Pt NMR (107 MHz, CDCl₃) δ_{Pt} = -3556.2; *m/z* (EI, pos): 576 [M]⁺, 498 [M-DMSO]⁺, 426 [M-DMSO-Cl]⁺. Anal. Calcd. for C₁₅H₂₂Cl₂N₂O₃PtS (576.4): C, 31.26; H, 3.85; N, 4.86; S, 5.56. Found: C, 30.51; H, 3.81; N, 5.00; S, 5.79.

2.2.2.3. cis-[Dichlorido-(5-methoxycarbonyl-1,3-dibenzylbenzimidazol-2-ylidene)(dimethylsulfoxide)] platinum(II) (10c). 145 mg (207 μmol, 86%) from **6c** (120 mg, 240 μmol, 1.00 eq.), K₂PtCl₄ (99.7 mg, 240 μmol, 1.00 eq.) in DMSO (25.0 mL). m.p. 250 °C; ¹H NMR (500 MHz, CDCl₃) δ_H = 7.99 (s, 1H, H^{ar}), 7.94 (d, *J* = 8.6 Hz, 1H, H^{ar}), 7.45–7.39 (m, 11H, H^{ar}), 6.18 (vdd, *J* = 30.8 Hz, 16.0 Hz, 2H, NCH₂), 6.00 (vdd, *J* = 31.8 Hz, 16.0 Hz, 2H, NCH₂), 3.89 (s, 3H, OCH₃), 3.11 (s, 3H, SCH₃), 3.02 (s, 3H, SCH₃); ¹³C NMR (125 MHz, CDCl₃) δ_C = 165.6 (s, COOMe), 160.1 (s, NCN), 136.4 (s, C^{ar}), 134.1 (s, C^{ar}), 133.9 (s, C^{ar}), 133.7 (s, C^{ar}), 128.9 (s, C^{ar}), 128.3 (s, C^{ar}), 127.2 (s, C^{ar}), 126.3 (s, C^{ar}), 125.5 (s, C^{ar}), 113.3 (s, C^{ar}), 111.5 (s, C^{ar}), 52.4 (s, CH₃), 52.2 (s, CH₃), 52.1 (s, CH₃), 45.2 (s, NCH₂), 45.0 (s, NCH₂); ¹⁹⁵Pt NMR (107 MHz, CDCl₃) δ_{Pt} = -3545.6; *m/z* (EI, pos): 550 [M-DMSO-2Cl]⁺. Anal. Calcd. for C₂₅H₂₆Cl₂N₂O₃PtS (700.5): C, 42.86; H, 3.74; N, 4.00; S, 4.58. Found: C, 42.91; H, 3.79; N, 4.32; S, 4.40.

2.2.2.4. cis-[Dichlorido-(5-ethoxycarbonyl-1,3-dimethylbenzimidazol-2-ylidene)(dimethylsulfoxide)] platinum(II) (11a). 221 mg (393 μmol, 75%) from **7a** (190 mg, 526 μmol, 1.00 eq.), K₂PtCl₄ (218 mg, 526 μmol, 1.00 eq.) in DMSO (50.0 mL). m.p. 260 °C; ¹H NMR (500 MHz, CDCl₃) δ_H = 8.15 (s, 1H, H^{ar}), 8.09 (d, *J* = 8.5 Hz, 1H, H^{ar}), 7.47 (d, *J* = 8.5 Hz, 1H, H^{ar}), 4.43 (q, *J* = 6.8 Hz, 2H, OCH₂), 4.28 (s, 3H, NCH₃), 4.26 (s, 3H, NCH₃), 3.57 (s, 6H, SCH₃), 1.43 (t, 3H, *J* = 7.1 Hz, CH₃); ¹³C NMR (125

MHz, CDCl₃) δ_C = 165.6 (s, COOCH₂), 158.2 (s, NCN), 136.8 (s, C^{ar}), 133.9 (s, C^{ar}), 126.7 (s, C^{ar}), 125.7 (s, C^{ar}), 112.7 (s, C^{ar}), 110.6 (s, C^{ar}), 61.6 (s, OCH₂), 46.3 (s, SCH₃), 41.1 (s, SCH₃) 34.9 (d, *J* = 5.0 Hz, NCH₃), 14.4 (s, CH₃); ¹⁹⁵Pt NMR (107 MHz, CDCl₃) δ_{Pt} = -3560.0; *m/z* (EI, pos): 562 [M]⁺, 484 [M-DMSO]⁺, 447 [M-DMSO-Cl]⁺, 412 [M-DMSO-2Cl]⁺. Anal. Calcd. for C₁₄H₂₀Cl₂N₂O₃PtS (562.4): C, 29.90; H, 3.58; N, 4.98; S, 5.70. Found: C, 30.22; H, 3.68; N, 4.80; S, 5.72.

2.2.2.5. cis-[Dichlorido-(5-ethoxycarbonyl-1,3-diethylbenzimidazol-2-ylidene)(dimethylsulfoxide)] platinum(II) (11b). 120 mg (251 μmol, 88%) from **7b** (111 mg, 285 μmol, 1.00 eq.), K₂PtCl₄ (118 mg, 285 μmol, 1.00 eq.) in DMSO (29.0 mL); m.p. 190 °C; ¹H NMR (500 MHz, CDCl₃) δ_H = 8.17 (s, 1H, H^{ar}), 8.08 (vdd, *J* = 8.5 Hz, 1.6 Hz, 1H, H^{ar}), 7.49 (d, *J* = 8.5 Hz, 1H, H^{ar}), 4.91–4.83 (m, 4H, NCH₂), 4.44 (q, *J* = 7.1 Hz, 2H, OCH₂), 3.57 (s, 6H, SCH₃), 1.66 (vdt, *J* = 11.3 Hz, 7.3 Hz, 6H, CH₃), 1.44 (t, *J* = 7.1 Hz, 3H, CH₃); ¹³C NMR (125 MHz, CDCl₃) δ_C = 165.5 (s, COOCH₂), 157.0 (s, NCN), 135.9 (s, C^{ar}), 133.0 (s, C^{ar}), 126.4 (s, C^{ar}), 125.3 (s, C^{ar}), 112.9 (s, C^{ar}), 110.7 (s, C^{ar}), 61.5 (s, OCH₂), 46.1 (s, SCH₃), 43.8 (d, *J* = 5.0 Hz, NCH₂) 14.5 (s, CH₃), 14.3 (s, CH₃); ¹⁹⁵Pt NMR (107 MHz, CDCl₃) δ_{Pt} = -3557.1; *m/z* (EI, pos): 590 [M]⁺, 512 [M-DMSO]⁺, 476 [M-DMSO-Cl]⁺, 439 [M-DMSO-2Cl]⁺. Anal. Calcd. for C₁₆H₂₄Cl₂N₂O₃PtS (590.4): C, 32.55; H, 4.10; N, 4.74; S, 5.43. Found: C, 33.34; H, 3.78; N, 4.81; S, 5.27.

2.2.2.6. cis-[Dichlorido-(5-ethoxycarbonyl-1,3-dibenzylbenzimidazol-2-ylidene)(dimethylsulfoxide)] platinum(II) (11c). 52.0 mg (79.8 μmol, 83%) from **7c** (49.0 mg, 95.4 μmol, 1.00 eq.), K₂PtCl₄ (39.6 mg, 95.4 μmol, 1.00 eq.) in DMSO (10.0 mL). m.p. 210 °C; ¹H NMR (500 MHz, CDCl₃) δ_H = 7.98 (s, 1H, H^{ar}), 7.93 (d, *J* = 8.6 Hz, 1H, H^{ar}), 7.46–7.31 (m, 11H, H^{ar}), 6.16 (vdd, *J* = 20.2 Hz, 15.9 Hz, 2H, NCH₂), 6.01 (vdd, *J* = 23.2 Hz, 16.9 Hz, 2H, NCH₂), 4.33 (q, *J* = 7.1 Hz, 2H, OCH₂), 3.11 (s, 3H, SCH₃), 3.03 (s, 3H, SCH₃), 1.43 (t, *J* = 7.1 Hz, 3H, CH₃); ¹³C NMR (125 MHz, CDCl₃) δ_C = 165.5 (s, COOCH₂), 160.2 (s, NCN), 136.7 (s, C^{ar}), 134.5 (s, C^{ar}), 134.3 (s, C^{ar}), 134.1 (s, C^{ar}), 129.3 (s, C^{ar}), 128.7 (s, C^{ar}), 127.6 (s, C^{ar}), 127.0 (s, C^{ar}), 125.9 (s, C^{ar}), 113.7 (s, C^{ar}), 111.8 (s, C^{ar}), 61.4 (s, OCH₂), 52.8 (s, SCH₃), 52.5 (s, SCH₃) 45.5 (s, NCH₂), 45.4 (s, NCH₂), 14.4 (s, CH₃); ¹⁹⁵Pt NMR (107 MHz, CDCl₃) δ_{Pt} = -3545.5; *m/z* (EI, pos): 561 [M-DMSO-2Cl]⁺. Anal. Calcd. for C₂₆H₂₈Cl₂N₂O₃PtS (714.6): C, 43.70; H, 3.95; N, 3.92; S, 4.49. Found: C, 43.24; H, 3.48; N, 3.87; S, 4.84.

2.2.3. General synthesis of *cis*-[Pt^{II}Cl₂(NHC)₂] complexes 12 and 13

The *cis*-[Pt^{II}Cl₂(DMSO)(NHC)] complexes **10a–b** or **11a–b** (1.00 eq.), KO^tBu (1.50 eq.) and the respective benzimidazolium chloride **4** or **5** (1.20 eq.) were dissolved in dry CH₂Cl₂ (1 mL/10 μmol). The mixture was stirred at rt. for 3 d under inert gas atmosphere. The solution was filtered over Celite and the solvent was evaporated. The crude product was purified by column chromatography (silica gel 60, EtOAc/MeOH 98:2) and precipitated from *n*-pentane at 4 °C affording the product as white powder after drying in vacuo.

2.2.3.1. cis-[Dichlorido-bis(5-methoxycarbonyl-1,3-dimethylbenzimidazol-2-ylidene)platinum(II) (12a). 28.0 mg (41.5 μmol, 46%) from **10a** (50.0 mg, 91.2 μmol, 1.00 eq.), KO^tBu (15.5 mg, 137 μmol, 1.50 eq.) and benzimidazolium chloride **4a** (26.0 mg, 109 μmol, 1.20 eq.) in dry CH₂Cl₂ (10.0 mL); R_f = 0.50 (EtOAc/MeOH 98:2); m.p. 240 °C; ¹H NMR (500 MHz, CDCl₃) δ_H = 8.06 (s, 2H, H^{ar}), 8.02 (d, *J* = 8.6 Hz, 2H, H^{ar}), 7.40 (vdd, *J* = 8.5 Hz, 3.5 Hz, 2H, H^{ar}), 4.23 (vt, *J* = 6.4 Hz, 12H, NCH₃), 3.94 (s, 6H, OCH₃); ¹³C NMR (125 MHz, CDCl₃) δ_C = 166.2 (s, COOMe), 162.7 (s, NCN), 137.2 (s, C^{ar}), 134.2 (s, C^{ar}), 126.2 (s, C^{ar}), 125.7 (s, C^{ar}), 112.4 (s, C^{ar}), 110.4 (s, C^{ar}), 52.7 (s, OMe), 35.3 (NCH₃), 35.2 (NCH₃); ¹⁹⁵Pt NMR (107 MHz, CDCl₃) δ_{Pt} = -3656.8; HRMS (ESI): *m/z* calculated for C₂₂H₂₄Cl₂N₄O₄Pt [M]: 673.08223. Found: 679.13933 [M-Cl + MeCN]⁺. Anal. Calcd.: C, 39.18; H, 3.59; N, 8.31. Found: C, 38.08; H, 3.68; N, 7.88.

2.2.3.2. cis-[Dichlorido-bis(5-methoxycarbonyl-1,3-diethylbenzimidazol-2-ylidene)]platinum(II) (12b). 25.0 mg (34.2 μmol, 26%) from **10b** (75.0 mg, 130 μmol, 1.00 eq.), KO^tBu (21.9 mg, 195 μmol, 1.50 eq.) and benzimidazolium chloride **4b** (42.0 mg, 156 μmol, 1.20 eq.) in dry CH₂Cl₂ (15.0 mL); R_f = 0.51 (EtOAc/MeOH 98:2); m.p. 250 °C; ¹H NMR (500 MHz, CDCl₃) δ_H = 8.09 (s, 2H, H^{ar}), 8.01 (d, *J* = 8.5 Hz, 2H, H^{ar}), 7.43 (vdd, *J* = 8.5 Hz, 3.5 Hz, 2H, H^{ar}), 5.09 (vdq, *J* = 9.7 Hz, 7.1 Hz, 4H, NCH₂), 4.68 (vdq, *J* = 9.7 Hz, 7.1 Hz, 4H, NCH₂), 3.95 (s, 6H, OCH₃), 1.50–1.46 (m, 12H, CH₃); ¹³C NMR (125 MHz, CDCl₃) δ_C = 166.2 (s, COOMe), 162.0 (s, NCN), 136.4 (s, C^{ar}), 133.3 (s, C^{ar}), 125.8 (s, C^{ar}), 125.3 (s, C^{ar}), 112.7 (s, C^{ar}), 110.7 (s, C^{ar}), 52.6 (s, OMe), 44.0 (s, NCH₂), 43.9 (s, NCH₂), 14.1 (s, CH₃); ¹⁹⁵Pt NMR (107 MHz, CDCl₃) δ_{Pt} = -3627.6; HRMS (ESI): *m/z* calculated for C₂₆H₃₂Cl₂N₄O₄Pt [M]: 729.14483. Found: 735.20132 [M-Cl + MeCN]⁺, 695.17263 [M-Cl]⁺, 658.19338 [M-2Cl]⁺; Anal. Calcd.: C, 42.75; H, 4.42; N, 7.67. Found: C, 42.66; H, 4.37; N, 7.50.

2.2.3.3. cis-[Dichlorido-bis(5-ethoxycarbonyl-1,3-dimethylbenzimidazol-2-ylidene)]platinum(II) (13a). 30.0 mg (42.7 μmol, 26%) from **11a** (93.0 mg, 165 μmol, 1.00 eq.), KO^tBu (27.8 mg, 248 μmol, 1.50 eq.) and benzimidazolium chloride **5a** (50.6 mg, 198 μmol, 1.20 eq.) in dry CH₂Cl₂ (15.0 mL). R_f = 0.20 (EtOAc/MeOH 98:2); m.p. 320 °C; ¹H NMR (500 MHz, CDCl₃) δ_H = 8.09–8.00 (m, 4H, H^{ar}), 7.39 (vdd, *J* = 8.5 Hz, 4.3 Hz, 2H, H^{ar}), 4.41 (vdq, *J* = 8.7 Hz, 7.2 Hz, 6H, OCH₂), 4.23 (vdd, *J* = 10.3 Hz, 5.8 Hz, 12H, NCH₃), 1.44 (t, *J* = 7.1 Hz, 6H, CH₃); ¹³C NMR (125 MHz, CDCl₃) δ_C = 166.7 (s, COOEt), 162.6 (s, NCN), 137.0 (s, C^{ar}), 134.1 (s, C^{ar}), 126.5 (s, C^{ar}), 125.6 (s, C^{ar}), 112.2 (s, C^{ar}), 110.1 (s, C^{ar}), 61.6 (s, OCH₂), 35.2 (NCH₃), 35.1 (NCH₃), 14.4 (s, CH₃); ¹⁹⁵Pt NMR (107 MHz, CDCl₃) δ_{Pt} = -3654.3; *m/z* (EI, pos): 702 [M], 666 [M-Cl], 630 [M-2Cl]; Anal. Calcd. for C₂₄H₂₈Cl₂N₄O₄Pt (702.5): C, 41.03; H, 4.02; N, 7.98. Found: C, 41.88; H, 3.03; N, 7.75.

2.2.3.4. cis-[Dichlorido-bis(5-ethoxycarbonyl-1,3-diethylbenzimidazol-2-ylidene)]platinum(II) (13b). 80.0 mg (105 μmol, 57%) from **11b** (110 mg, 186 μmol, 1.00 eq.), KO^tBu (31.4 mg, 280 μmol, 1.50 eq.) and the respective benzimidazole chloride (**5b**) (63.2 mg, 224 μmol, 1.20 eq.) in dry CH₂Cl₂ (20.0 mL); R_f = 0.50 (EtOAc/MeOH 98:2); m.p. 290 °C; ¹H NMR (500 MHz, CDCl₃) δ_H = 8.08 (s, 2H, H^{ar}), 8.01 (d, *J* = 8.6 Hz, 2H, H^{ar}), 7.42 (vdd, *J* = 8.6 Hz, 4.3 Hz, 2H, H^{ar}), 5.14–5.03 (m, 4H, NCH₂), 4.72–4.63 (m, 4H, NCH₂), 4.41 (q, *J* = 7.0 Hz, 4H, OCH₂), 1.48 (vdd, *J* = 7.2 Hz, 3.0 Hz, 12H, CH₃), 1.41 (t, *J* = 7.1 Hz, 6H, CH₃); ¹³C NMR (125 MHz, CDCl₃) δ_C = 166.7 (s, COOEt), 161.7 (s, NCN), 136.3 (s, C^{ar}), 133.3 (s, C^{ar}), 126.2 (s, C^{ar}), 125.3 (s, C^{ar}), 112.7 (s, C^{ar}), 110.7 (s, C^{ar}), 61.6 (s, OCH₂), 44.0 (s, NCH₂), 43.9 (s, NCH₂), 14.5 (s, CH₃), 14.4 (s, CH₃), 14.3 (s, CH₃); ¹⁹⁵Pt NMR (107 MHz, CDCl₃) δ_{Pt} = -3627.9; *m/z* (EI, pos): 758 [M]⁺, 722 [M-Cl]⁺, 657 [M-2Cl]⁺; Anal. Calcd. for C₂₈H₃₆Cl₂N₄O₄Pt (758.6): C, 44.33; H, 4.78; N, 7.39. Found: C, 43.40; H, 4.56; N, 7.05.

2.2.4. Synthesis of clickable complexes 16 and 22

cis-[Dichlorido-(5-methoxycarbonyl-1,3-dipropargylbenzimidazol-2-ylidene)(dimethylsulfoxid)]platinum(II) (16).

Cis-[Cl₂(DMSO)₂]Pt(II) (60.0 mg, 142 μmol, 1.00 eq.) and benzimidazolium chloride **15** (94.4 mg, 327 μmol, 2.30 eq.) were dissolved in dry CH₂Cl₂ (15 mL) and treated with KO^tBu (47.8 mg, 426 μmol, 3.00 eq.). The mixture was stirred at rt. for 18 h and filtered over Celite®. The solvent was evaporated and the crude product was purified by column chromatography (silica gel 60, EtOAc/MeOH 98:2) affording **16** as a yellow powder (60.7 mg, 112 μmol, 79%) after drying in vacuo; m.p. 310 °C; R_f = 0.50 (EtOAc/MeOH 98:2); ¹H NMR (500 MHz, CDCl₃) δ_H = 8.36 (d, *J* = 1.4 Hz, 2H, H^{ar}), 8.15 (dd, *J* = 8.6 Hz, 1.4 Hz, 2H, H^{ar}), 7.70 (d, *J* = 8.6 Hz, 2H, H^{ar}), 6.00 (dt, *J* = 18.0 Hz, 2.7 Hz, 4H, NCH₂), 5.30 (dt, *J* = 18.0 Hz, 2.1 Hz, 4H, NCH₂), 3.60 (s, 6H, SCH₃), 3.99 (s, 6H, OMe), 2.56 (dt, *J* = 5.3 Hz, 2.6 Hz, 4H, CH); ¹³C NMR (125 MHz, CDCl₃) δ_C = 165.9 (s, COOMe), 159.5 (s, NCN), 135.8 (s, C^{ar}), 132.9 (s, C^{ar}), 127.1 (s, C^{ar}), 126.4 (s, C^{ar}), 113.5 (s, C^{ar}), 111.6 (s, C^{ar}), 76.2 (s), 76.1

(s), 75.5 (s), 75.4 (s), 52.7 (s, OCH₂), 46.0 (s, SCH₃), 38.6 (s, NCH₂), 38.5 (s, NCH₂); ¹⁹⁵Pt NMR (107 MHz, CDCl₃) δ_{Pt} = -3550.2; HRMS (ESI): *m/z* calculated for C₁₇H₁₈Cl₂N₂O₃PtS [M]: 595.00629. Found: 638.04989 [M-Cl + DMSO]⁺, 601.06189 [M-Cl + MeCN]⁺, 560.03634 [M-Cl]⁺, 482.02161 [M-Cl-DMSO]⁺; Anal. Calcd.: C, 34.24; H, 3.04; N, 4.70; S, 5.38. Found: C, 31.04; H, 3.94; N, 4.49; S, 5.97.

2.2.4.1. trans-[Dichlorido-bis(5-(dimethylcyclopropenyl)methyl-carbonyl-1,3-diethylbenzimidazol-2-ylidene)]platinum(II) (22). Silver complex **21** (46.0 mg, 86.3 μmol, 1.00 eq.) and K₂PtCl₄ (18.0 mg, 43.0 μmol, 0.50 eq.) were dissolved in CH₂Cl₂ (5 mL) and stirred at rt. for 4 d. The solution was filtered over celite® and the solvent was evaporated. The crude products were purified by column chromatography (silica gel 60, EtOAc/MeOH 98:2) and subsequently precipitated from *n*-pentane at 4 °C affording the product as white solid (12.0 mg, 13.9 μmol, 32%) after drying in vacuo; m.p. 230 °C; R_f = 0.90 (EtOAc/MeOH 98:2) ¹H NMR (500 MHz, CDCl₃) δ_H = 8.17 (s, 2H, H^{ar}), 8.06 (dd, *J* = 8.4, 1.4 Hz, 2H, H^{ar}), 7.46 (dd, *J* = 8.6, 1.3 Hz, 2H, H^{ar}), 5.00 (dq, *J* = 14.1 Hz, 7.0 Hz, 8H, NCH₂), 4.28 (d, *J* = 5.1 Hz, 2H, OCH₂), 2.04 (s, 12H, CH₃), 1.78 (dt, *J* = 8.9, 5.4, 12H, CH₃), 1.70 (t, *J* = 5.1 Hz, 2H, CH); ¹³C NMR (125 MHz, CDCl₃) δ_C = 179.9 (s, NCN), 165.3 (s, COOCH₂), 135.6 (s, C^{ar}), 132.7 (s, C^{ar}), 124.9 (s, C^{ar}), 123.6 (s, C^{ar}), 111.1 (s, C^{ar}), 108.9 (s), 108.7 (s), 71.8 (OCH₂), 41.7 (d, *J* = 5.0 Hz, CH₂), 18.3 (CH), 14.1 (d, *J* = 15.4 Hz, CH₃), 9.4 (s, CH₃); ¹⁹⁵Pt NMR (107 MHz, CDCl₃) δ_{Pt} = -3265.5; HRMS (ESI): *m/z* calculated for C₃₆H₄₄Cl₂N₄O₄Pt [M]: 861.23874. Found: 861.23819; Anal. Calcd.: C, 50.12; H, 5.14; N, 6.49. Found: C, 49.39; H, 3.82; N, 5.77.

2.3. Biochemical evaluation

2.3.1. Stock solutions and dilution series

Stock solutions of test compounds were dissolved in DMSO (10 mM) if not noted otherwise and stored at -23 °C. When applying them to biotests, the desired predilution series was freshly diluted with water or PBS and then added to the cell culture media.

2.3.2. MTT cell viability assay [11]

All complexes stable in solution were investigated for their anti-proliferative effect on nine human cell lines, using the 3-(4,5-dimethylthiazol-2-yl)-2,5-diphenyltetrazolium bromide (MTT) based cell viability assay. Cells were seeded in 96 well microtiter plates (Sarstedt) with a cell density of 0.05 × 10⁶ cells per mL and 100 μL per well and incubated for 24 h. A dilution series of test compounds was added to the wells, ranging in twelve steps from 100 μM – 5 nM, equal amounts of DMSO were added as controls. Treated cells were incubated for a further 72 h. Then, 12.5 μL per well of MTT solution (0.05% in PBS) were added, followed by another 2 h of incubation. The plates were centrifuged, the medium was discarded and 25 μL per well of SDS solution in DMSO (10% SDS, 0.6% AcOH in DMSO) were added to dissolve formazan and the plates were incubated for a further hour. Absorbances at 570 nm and 630 nm were measured using a plate reader (Tecan). The background absorbance (630 nm) was subtracted from the formazan signal (570 nm). The resulting absorbance is directly proportional to the amount of viable cells, the control was normalised to 100% viable cells and, accordingly, the viability of cells treated with the test compounds was calculated. IC₅₀ values were calculated based on a sigmoidal fit model using GraphPad Prism. Means and SD were calculated from at least four independent experiments. To calculate the selectivity index (SI), the mean value of all IC₅₀ values across the cancer cell lines was first calculated for each test substance. The IC₅₀ value for the non-malignant cells (HDFa) was then divided by the mean value over all cancer cell lines. The higher the resulting ratio, the more selective the compound is for cancer over HDFa cells.

2.3.3. Cellular uptake measurement via ICP-MS

Cells were seeded at a density of 2×10^6 cells per dish in cell culture dishes (Sarstedt) and grown overnight, then treated with test compounds at a final concentration of $5 \mu\text{M}$ for 5 h. The cell monolayer was washed twice with PBS, the cells were harvested by trypsination, counted and pelleted (4°C , 150 g , 5 min). The cell pellets were solubilised with aqua regia (reflux, 20 min), the platinum content was determined by ICP-MS. Means and SD were calculated from at least two independent experiments.

2.3.4. LDH cytotoxicity assay^[12]

Cells were seeded in 96 well flat bottom microtiter plates (Sarstedt) with $100 \mu\text{L}$ per well and a cell density of 0.05×10^6 cells per mL. Wells containing medium alone were additionally set for background measurement. The cells were allowed to grow overnight, then treated with $11.1 \mu\text{L}$ of 10-fold concentrated test compound dilutions and further incubated for 24 h. As positive control $10 \mu\text{L}$ per well of lysis solution (9% Triton-X100 in Millipore H_2O) were added and incubated for 45 min to maintain maximum LDH release. The same amount was added to maximum release background correction wells, containing medium only. After centrifugation (4°C , 150 g , 5 min) $50 \mu\text{L}$ of the supernatant of each well were transferred on a fresh microtiter plate followed by addition of $50 \mu\text{L}$ LDH assay buffer (223 mg 2-*p*-iodophenyl-3-*p*-nitrophenyl-5-phenyltetrazolium chloride, 57 mg *N*-methylphenazonium methyl sulfate, 575 mg *N*-adenine dinucleotide, 3.2 g lactic acid in 480 mL 200 mM Tris-Cl, pH 8.0) per well. The plate was incubated in the dark for 10–30 min at rt. $50 \mu\text{L}$ stop solution (1 M acetic acid) were added per well and the absorbance was measured at 490 nm. The mean value of the background wells was subtracted from the negative control and the test wells as well as the mean value of the maximum release wells was subtracted from the value of the maximum LDH release wells. The percentage of LDH release was calculated, the maximum LDH release was set to 100% and the negative control at 0% release. Means and SD were calculated from at least three independent experiments.

2.3.5. Apoptotic events

2.3.5.1. Caspase 3/7 activation. The assay was conducted, following the manufacturer's instructions, using the Cell Meter Caspase 3/7 activity apoptosis assay kit (AAT Bioquest). Briefly, the cells were seeded in 96 well flat black microtiter plates at a density of 0.22×10^6 cells per mL and $90 \mu\text{L}$ per well. After 24 h of incubation, $10 \mu\text{L}$ per well of prediluted test compounds were added to obtain a final concentration of $10 \mu\text{M}$, and the cells were incubated for a further 6 h. $100 \mu\text{L}$ per well of Caspase 3/7 substrate working solution were added and the plates were incubated for another hour in the dark at rt. The fluorescence was measured using a microplate reader (Tecan) at ex/em = 490/525 nm.

2.3.5.2. Mitochondrial membrane potential assay. To assess the effect of the test compounds on the mitochondrial membrane potential (MMP) the cationic dye tetramethylrhodamine methyl ester (TMRM) was used. Due to its delocalised lipophilic cation (DLC) character, TMRM accumulates in mitochondria quantitatively, proportional to the MMP. The cells were seeded in 96 well flat black microtiter plates (Brand) with a cell density of 0.2×10^6 cells per mL and $100 \mu\text{L}$ per well. A corresponding MTT was conducted identically in transparent 96 well microtiter plates (Sarstedt). The plates were incubated for 24 h under standard cell culture conditions. The medium was replaced by $90 \mu\text{L}$ per well standard assay buffer (80 mM NaCl, 75 mM KCl, 25 mM D-Glucose, 25 mM HEPES, pH 7.4 in H_2O) and $10 \mu\text{L}$ per well of tenfold dilutions of test compounds were added. Carbonyl cyanide *m*-chlorophenylhydrazine (CCCP), a known decoupling agent, served as a positive control [13] and a corresponding dilution of DMSO served as a negative control. Substance-treated cells were further incubated for 1 h. $10 \mu\text{L}$ per well of a TMRM solution ($2 \mu\text{M}$ in standard assay buffer) were added and the

cells were incubated for a further 10 min at rt. Each well was rinsed three times with PBS, $100 \mu\text{L}$ per well of PBS were added and the fluorescence of remaining TMRM was measured (ex/em 535/590 nm). The results were standardised by correlation with those of the corresponding MTT assays and normalised with respect to the negative control.

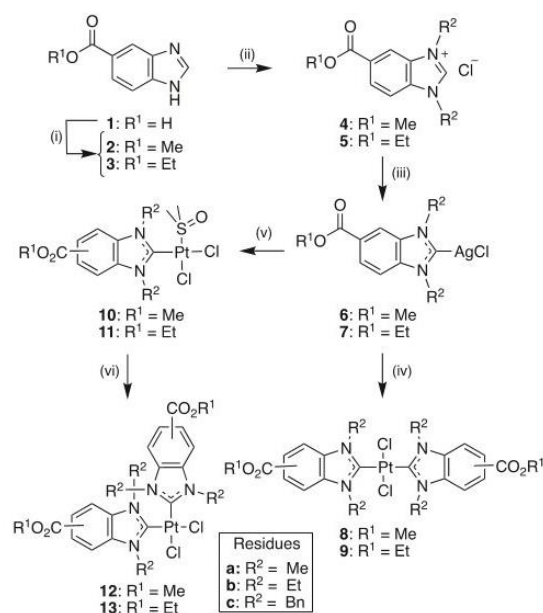
2.3.5.3. Reactive oxygen species (ROS) assay [14]. The cellular levels of ROS were determined by means of 2,7-dichlorofluorescein diacetate (DCFH-DA). The assay is based on the oxidation of DCFH-DA by intracellular ROS to give strongly fluorescent 2,7-dichlorodihydrofluorescein. The cells were seeded in 96 flat black well plates (Brand) with $100 \mu\text{L}$ per well and a density of 0.2×10^6 cells per mL. A corresponding MTT was conducted identically in transparent 96 well microtiter plate (Sarstedt). The cells were allowed to grow for 24 h. The medium was replaced by serum-free medium containing DCFH-DA ($20 \mu\text{M}$) followed by 30 min of incubation to enable cells to take up the dye. To eliminate remaining dye, the cells were rinsed twice with PBS, and fresh medium was added. $11.1 \mu\text{L}$ of tenfold predilutions of the test compounds were added per well. Corresponding dilutions of DMSO served as negative and of CDDP served as positive control. The treated cells were incubated for 1 h, before being rinsed twice again with PBS. After addition of $100 \mu\text{L}$ of fresh PBS per well the fluorescence was measured (ex/em 485/535 nm). The results were standardised by correlation with those of the corresponding MTT assays and normalised with respect to the negative control.

2.3.6. Influence on the cell cycle

HCT116^{wt} cells were seeded in 6 well plates (Sarstedt) with 3 mL per well and a cell density of 0.05×10^6 cells per mL, incubated for 24 h, treated with concentrations of the test compounds corresponding to their IC_{50} values, and incubated for a further 24 h. The supernatant of each sample was transferred into a separate tube on ice, the cell monolayer was rinsed once with PBS, and the cells were harvested using trypsin and also transferred into the tube. The cells were pelleted (4°C , 150 g , 5 min), resuspended in 1 mL of ice-cold EtOH (70%) and stored for at least 1 h at 4°C . prior to propidium iodide (PI) staining, the cells were centrifuged (150 g , 5 min), the supernatant was discarded, and the cells were layered with 1 mL PBS for 5 min. The cells were centrifuged again and the resulting pellet was resuspended in $200 \mu\text{L}$ of PI staining solution ($50 \mu\text{g/mL}$ PI, 1% sodium citrate in PBS) containing $1 \mu\text{L}$ RNase (10 mg/mL stock solution) and incubated in the dark for 30 min at 37°C . The cell cycle phase distribution was assessed by flow cytometry (Beckmann Coulter). Means and SD were calculated from at least three independent experiments.

2.3.7. DNA interaction

2.3.7.1. Ethidium bromide saturation assay (EtdBr assay). The interaction of the test complexes with linear DNA was assessed using the EtdBr assay, which is based on the fact that ethidium bromide intercalates into DNA enhancing its fluorescence while intercalation is hindered by alterations of the DNA structure, e.g. by small molecules interfering with DNA [15]. In wells of a 96 well black flat bottom microtiter plates a solution of $1 \mu\text{g}$ of linear salmon sperm DNA (ThermoFisher) in TE buffer (10 mM Tris-Cl, 1 mM EDTA, pH 8.0) was treated with concentration series (final concentrations: $25 \mu\text{M}$, $50 \mu\text{M}$, $75 \mu\text{M}$ and $100 \mu\text{M}$) of compounds. A corresponding amount of DMSO was used as a control ($0 \mu\text{M}$). After an incubation period of 2 h at 37°C , $100 \mu\text{L}$ per well of ethidium bromide solution ($10 \mu\text{g/mL}$ in TE buffer) was added and the plate was incubated for 5 min in the dark. Background samples were prepared analogously but without DNA addition. The fluorescence of any EtdBr-DNA adducts was monitored at an excitation wavelength of 535 nm and an emission wavelength of 595 nm. After background subtraction, changes in fluorescence intensity were calculated in relation to the control (set to 100%). Means and SD were calculated from at



Scheme 1. General synthetic route to *trans*-bis(NHC)-, *cis*-NHC(DMSO)- and *cis*-bis(NHC)platinum(II) complexes. Reagents and conditions: (i) MeOH or EtOH, H₂SO₄, reflux, 24 h; (ii) 1. MeI or EtI or BnBr, K₂CO₃, MeCN, reflux, 24 h; 2. Ag₂CO₃, HNO₃, then HCl, EtOH, r.t., light exclusion, 3.5 h; (iii) Ag₂O, CH₂Cl₂, light exclusion, r.t., 24 h; (iv) 0.5 eq. K₂PtCl₄, CH₂Cl₂, r.t., 4 d; (v) 1.0 eq. K₂PtCl₄, DMSO, 60 °C, 24 h; (vi) benzimidazolium salt 4 or 5, KOtBu, CH₂Cl₂, r.t., 3d.

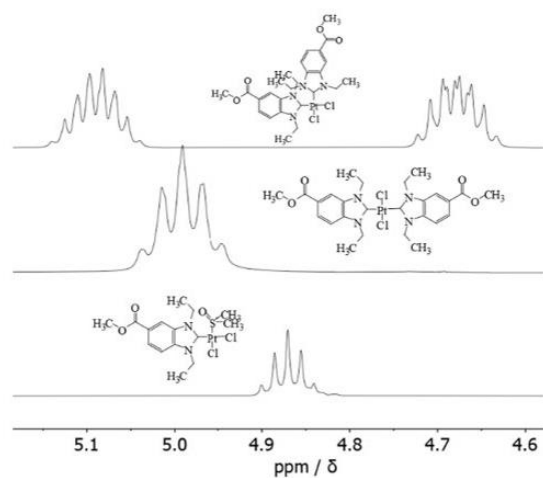
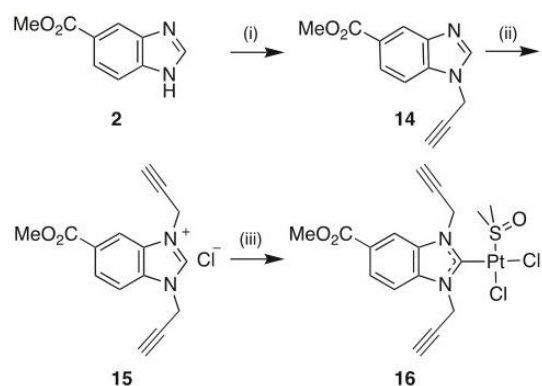


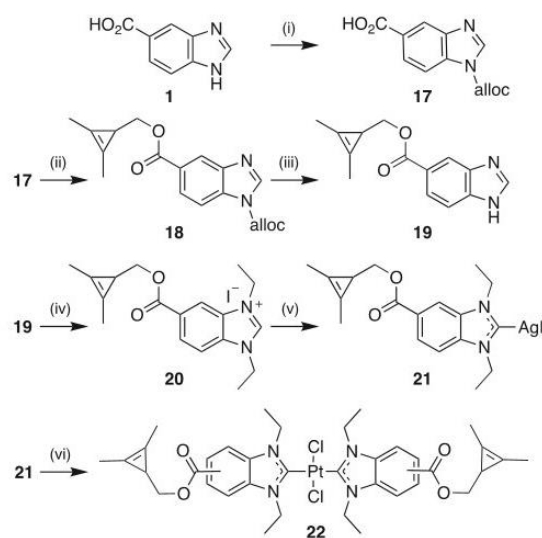
Fig. 1. NCH₂ signals in ¹H NMR spectra of *cis*-DMSO(NHC) complex **10b** (bottom), *trans*-bis(NHC) complex **8b** (middle), and *cis*-bis(NHC) complex **12b** (top), recorded in CDCl₃.

least three independent experiments.

2.3.7.2. Electrophoretic mobility shift assay (EMSA). To distinguish whether the DNA interaction is of an electrostatic or covalent nature, a



Scheme 2. Synthesis of propargyl-bearing *cis*-(DMSO)(NHC) platinum(II) complex **16**. Reagents and conditions: (i) Propargyl bromide, K₂CO₃, MeCN, 60 °C, 24 h, 81%; (ii) 1. Propargyl bromide, 1,4-dioxane, 130 °C, 24 h; 2. Ag₂CO₃, HNO₃, then HCl, EtOH, r.t., light exclusion, 3.5 h, 52% over two steps; (iii) *cis*-(DMSO)₂PtCl₂, CH₂Cl₂, r.t., 24 h, 79%.



Scheme 3. Synthesis of cyclopropene-bearing *trans*-bis(NHC) platinum(II) complex **22**. Reagents and conditions: (i) Alloc-Cl, 10% Na₂CO_{3(aq.)}, 1,4-dioxane, r.t., 16 h, 97%; (ii) EDC-HCl, DMAP, CH₂Cl₂, r.t., 24 h, 58%; (iii) Pd(dppa)₂, dppb, Et₂NH, r.t., THF, 4 h, 75%; (iv) EtI, K₂CO₃, MeCN, reflux, 48 h, 72%; (v) Ag₂O, CH₂Cl₂, light exclusion, r.t., 24 h, 58%; (vi) 0.5 eq. K₂PtCl₄, CH₂Cl₂, r.t., 4 d, 32%.

second DNA interaction assay was conducted. 1.5 μg of circular plasmid pBR322 DNA were incubated in TE buffer (10 mM Tris-Cl, 1 mM EDTA, pH 8.0) with different concentrations of test compounds (final concentrations: 5 μM, 10 μM, 25 μM and 50 μM). A corresponding volume of DMSO was added to the control (0 μM) with a final volume of 20 μL of each sample. The samples were incubated for 16 h at 37 °C and subjected to 1% agarose gel electrophoresis in 0.5×TBE buffer (45 mM Tris-Cl, 45 mM boric acid, 1.25 mM EDTA, pH 8.0) for 4 h at 66 V. The agarose gel was stained for 20 min with EtBr (10 μg/mL in 0.5 TBE buffer) solution and the results documented using UV excitation.

Table 1

Means \pm SD ($n = 4$) of IC_{50} values [μ M] of complexes **8–13** and CDDP against nine human cell lines and their respective selectivity indices (SI). Determined by MTT assays over 72 h, calculated of four independent measurements. * data from [19], n.d. = not determined.

	IC_{50} 72 h (μ M)									
	518A2	HCT116 ^{wt}	HCT116 ^{p53-}	U87	EaHy926	HeLa	MCF7	HT29	HDFa	SI
8a	13.8 \pm 0.7	22.6 \pm 0.4	25.3 \pm 3.9	1.1 \pm 0.5	>50	>50	25.4 \pm 2.7	31.0 \pm 3.7	n.d.	n.d.
8b	>50	>50	3.8 \pm 0.5	>50	>50	3.3 \pm 0.8	0.56 \pm 0.05	>50	n.d.	n.d.
8c	>50	0.16 \pm 0.02	0.49 \pm 0.04	>50	0.12 \pm 0.03	0.05 \pm 0.02	0.26 \pm 0.06	3.7 \pm 0.4	>50	> 3.8
9a	15.3 \pm 1	3.3 \pm 0.7	0.7 \pm 0.08	14 \pm 1.2	6.1 \pm 0.2	12.6 \pm 1.4	4.0 \pm 0.8	7.9 \pm 0.9	n.d.	n.d.
9b	>50	>50	31.9 \pm 4	>50	>50	>50	4.3 \pm 0.2	34.8 \pm 4.4	n.d.	n.d.
9c	>50	>50	>50	>50	>50	>50	>50	>50	n.d.	n.d.
10a	>50	>50	>50	>50	>50	>50	>50	>50	n.d.	n.d.
10b	>50	45.7 \pm 2.9	17.7 \pm 0.4	16.3 \pm 2.9	>50	33.9 \pm 4.0	>50	>50	n.d.	n.d.
10c	19.2 \pm 1.5	16.3 \pm 1.6	1.6 \pm 0.1	1.07 \pm 0.04	9.4 \pm 0.3	1.3 \pm 0.3	24.0 \pm 3.5	>50	n.d.	n.d.
11a	>50	>50	>50	>50	>50	>50	>50	>50	n.d.	n.d.
11b	>50	>50	>50	>50	>50	>50	>50	>50	n.d.	n.d.
11c	14.6 \pm 1.3	16.4 \pm 1.3	9.5 \pm 1.5	>50	45.6 \pm 5.9	>50	48.2 \pm 1.9	>50	n.d.	n.d.
12a	>50	35.6 \pm 3.4	>50	>50	48.7 \pm 1.4	>50	>50	>50	n.d.	n.d.
12b	31.2 \pm 2.2	2.3 \pm 0.2	1.7 \pm 0.2	1.3 \pm 0.1	4.8 \pm 0.5	2.9 \pm 2	>50	>50	>50	> 2.8
13a	>50	>50	>50	>50	>50	>50	>50	>50	n.d.	n.d.
13b	14.2 \pm 2.3	6.9 \pm 0.5	16.2 \pm 2.6	32.5 \pm 1.0	3.5 \pm 2	18.4 \pm 2.2	>50	>50	n.d.	n.d.
CDDP	2.6 \pm 0.7*	0.14 \pm 0.03*	2.0 \pm 0.3*	3.8 \pm 0.3	0.63 \pm 0.1*	8.6 \pm 0.6	5.4 \pm 0.7	>50	>50*	> 5.5

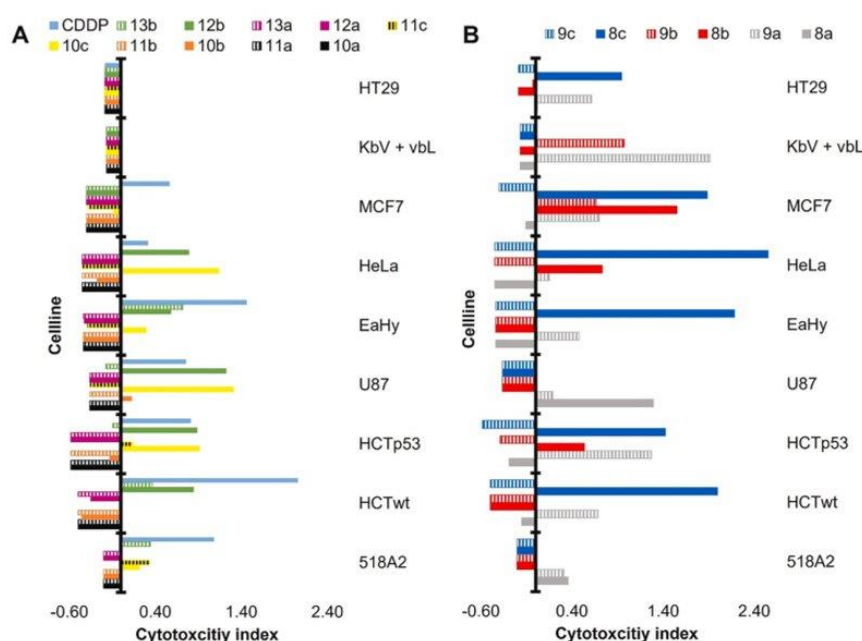


Fig. 2. Cytotoxicity indices (CI) of the complexes **8a–13b** across all tested cancer cell lines. To determine the CI, the IC_{50} values were logarithmised with log base of 10 and then the mean value of the logarithmised IC_{50} values over all tested compounds were determined for each cell line. The difference between the individual values and this mean value gave the individual CI for each substance and cell line. The different colours indicate the methyl and ethyl esters that belong together structurally. **A)** CIs of all *cis*-configured complexes. **B)** CIs of all *trans*-configured complexes.

2.3.8. Intracellular localisation using click chemistry

To assess the localisation of active complexes of the *cis* (e.g. **10**) and *trans* (e.g. **8**) series in HCT116 colon carcinoma cells, we used the 'clickable' congeners **16** and **22**. HCT116 cells (0.1×10^6 cells per mL, 0.5 mL per well) were seeded onto cover slips (borosilicate glass, Carl Roth) inside the wells of 24-well microtiter plates and were allowed to grow overnight. The medium was removed and the cells were washed with 1 mL PBS and treated with complexes **16** or **22** at a final concentration of 25 μ M for 30 min at 37 °C. Fixation, blocking and permeabilisation was done analogously to the fluorescence staining of the

cytoskeleton. 200 μ L of click working solution [for **16**: 2 mM $CuSO_4$, 5 mM sodium ascorbate, 0.1 mM 3-azido-7-hydroxycoumarin, in PBS. For **22**: BDP-FL-tetrazin (Lumiprobe Catalog Number: 114E0) in PBS 1:1000] were added to each well. The cells were incubated for 30 min at rt. in the dark before the click solution was discarded and the cells were washed three times with PBS for 5 min. For co-staining, the cells were either treated with propidium iodide (50 μ g/mL, after fixation and permeabilisation) or Mitotracker™ Red CM-H2Xros (before substance addition, ThermoFisher Scientific, 250 nM in FBS-free DMEM). Cover-slips were mounted (VECTASHIELD® PLUS Antifade Mounting

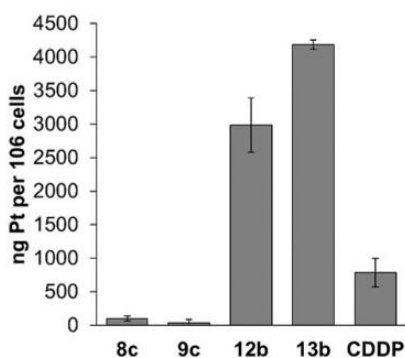


Fig. 3. Cellular uptake of *trans*-bis(NHC)Cl₂Pt complexes **8c** and **9c** as well as *cis*-bis(NHC)Cl₂Pt complexes **12b** and **13b**, and of CDDP into HCT116^{wt} cells after 5 h treatment with 5 μM. Measured via ICP-MS.

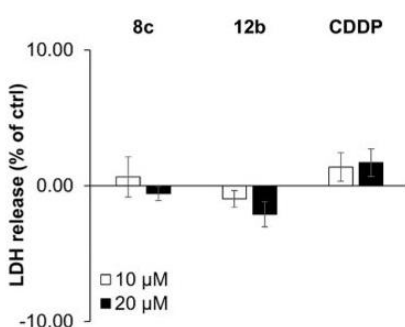


Fig. 4. LDH release, measured as formazan absorbance of HCT116^{wt} cells after 24 h treatment with complexes **8c**, **12b** or CDDP in different concentrations, relative to a negative control which was set as 0%. Mean ± SD; n = 3.

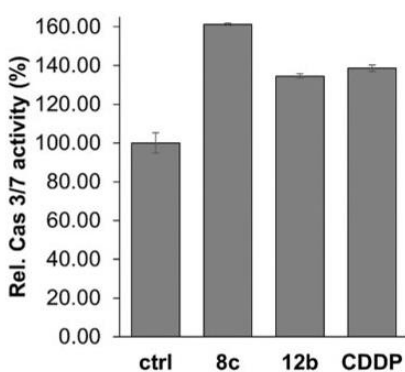


Fig. 5. Relative levels of caspase-3/7 activity in HCT116^{wt} cells after 6 h incubation with 10 μM of complexes **8c** and **12b**. An equal concentration of CDDP served as a positive control and corresponding amounts of DMSO as a negative control (ctrl). Fluorescence values were corrected for the cell viability obtained from corresponding MTT assays and normalised relative to the negative control set at 100%. Means ± SD, n = 3.

Medium) and fluorescence images were acquired using fluorescence microscopy. Images were processed using Image J.

3. Results and discussion

3.1. Complex syntheses

The synthetic route (Scheme 1) leading to *cis*- and *trans*-[bis(5-alkoxycarbonyl-1,3-dialkyl-benzimidazol-2-ylidene)dichlorido]platinum(II), and *cis*-[(DMSO)(5-alkoxycarbonyl-1,3-dialkyl-benzimidazol-2-ylidene)dichlorido]platinum(II) complexes, respectively, follows protocols previously published by Rehm et al. [16] All in vitro evaluated complexes were characterised by ¹H, ¹³C and ¹⁹⁵Pt NMR spectra, EI or ESI mass spectrometry and elemental analysis.

Benzimidazole-5-carboxylic acid (**1**) was converted to either methyl ester **2** or ethyl ester **3** via Fischer esterification [17]. These esters were N,N'-dialkylated with MeI, EtI or BnBr in one step following a protocol by Schmidt et al., leading to the benzimidazolium halides in nearly quantitative yields with high purity [18]. As the required excess of benzyl bromide could not be removed by rotary evaporation, the 1,3-dibenzylbenzimidazolium bromides needed several precipitation cycles for sufficient purity. Anion metathesis was necessary for the iodides in order to prevent a halide exchange in the final *cis*-bis(NHC) complexes [19]. Treatment of the iodides and bromides with AgNO₃ and then HCl afforded the corresponding benzimidazolium chlorides **4** and **5**. However, a similar procedure was not necessary for the synthesis of the *trans*-bis(NHC) complexes **8** and **9** since there is no excess of free anions, and because the silver halides precipitate from CH₂Cl₂ as easy to remove by-products.

The NHC-silver(I) complexes **6a–c** and **7a–c** were obtained by treating the benzimidazolium halides with half an equivalent of Ag₂O in the dark for 24 h. Consumption of the starting material was monitored by the vanishing of the 2-H signal in the ¹H NMR spectra. Filtration over Celite® and precipitation from pentane led to white or beige powders, which were used without further purification. Transmetalation with 0.5 equivalents of K₂PtCl₄ for four days in CH₂Cl₂ led to the *trans*-[bis(NHC)dichlorido]platinum(II) complexes **8a–c** and **9a–c**. The *cis*-[(DMSO)(NHC)Cl₂]Pt^{II} complexes **10** and **11**, which were used as precursors for the *cis*-[bis(NHC)dichlorido]platinum(II) complexes **12** and **13**, were obtained by stirring the respective silver complex with an equimolar amount of K₂PtCl₄ in excess DMSO as described previously [20]. This route is also applicable to the synthesis of complexes bearing two different *cis*-positioned NHC ligands which are not accessible from the more common (DMSO)₂PtCl₂ [21] or (COD)PtCl₂ [22] precursors. The monocarbene complexes **10** and **11** were treated with an excess of the respective benzimidazolium chloride **4** or **5** and KOtBu in CH₂Cl₂ to liberate the corresponding NHC ligand. While **10a**, **10b** as well as **11a** and **11b** were readily converted into their respective *cis*-bis(NHC) complexes, the N,N'-dibenzyl substituted complexes **10c** and **11c** did not react under identical or modified conditions, possibly due to the steric demand of the benzyl residues.

The configuration of the complexes was confirmed by ¹H NMR spectra. While the *trans*-bis(NHC) complexes **8** and **9** displayed a single signal group for all identical NCH_n protons, the corresponding protons of the *cis*-bis(NHC) complexes **12** and **13** resonated as two separate signal groups. The perpendicular orientation of the NHC ligands relative to the plane spanned by PtCl₂ leads to one proton facing a chlorido ligand while the other is facing the second carbene ligand. Due to the square planar nature of such complexes [16,20,23,24] the *cis*-configuration leads to higher steric hinderance and thus to an upfield shift. This effect increases with the size of the N-substituent. Fig. 1 depicts the NCH₂ range of the ¹H NMR spectra of complexes **12b** and **8b**. It shows a virtual doublet of quartets (vdq) for the *trans*-bis(NHC) complex **8b** at 4.99 ppm and two dq at 5.09 ppm and 4.68 ppm for the *cis*-bis(NHC) complex **12b**. A smaller DMSO ligand, *cis*-positioned to the NHC ligand as in complex **10b**, obviously does not lead to a split of the NCH₂ proton signals

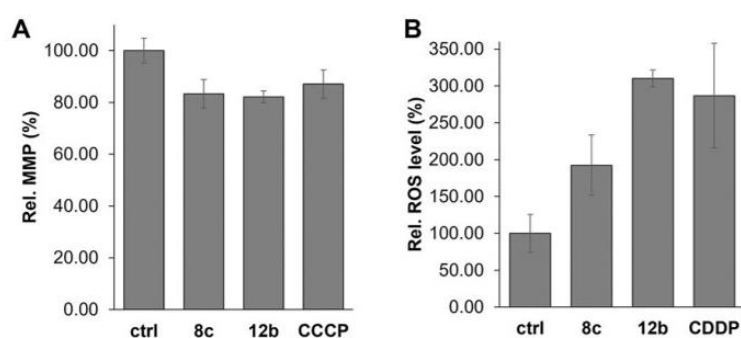


Fig. 6. A) Relative mitochondrial membrane potential/integrity (MMP) of HCT116^{wt} cells treated with complexes **8c** and **12b** (10 μ M) for 1 h. Carboxyanide-*m*-chlorophenylhydrazine (CCCP) served as a positive control, corresponding amounts of DMSO as a negative control (ctrl). B) Relative intracellular reactive oxygen species levels of HCT116^{wt} cells treated with complexes **8c** and **12b** (10 μ M) for 1 h. CDDP served as a positive control, corresponding amounts of DMSO as a negative control (ctrl). Mean \pm SD, $n = 3$.

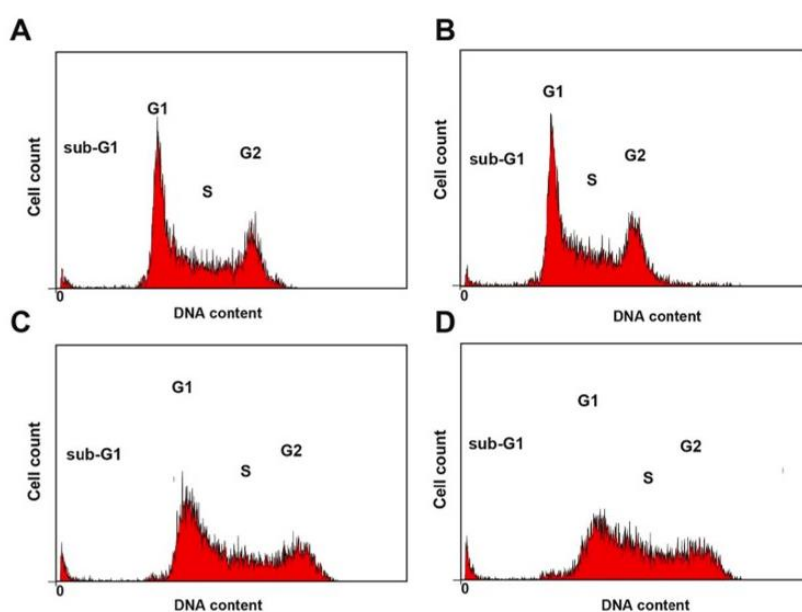


Fig. 7. Cell cycle profiles of HCT116^{wt} cells treated for 24 h with IC₅₀ concentrations of **8c** (B), **12b** (C) and CDDP (D), the corresponding amount of DMSO was used as a control (A). Images are representative of at least three experiments.

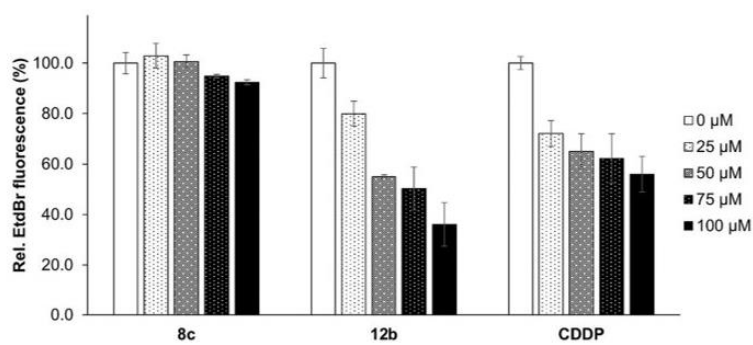


Fig. 8. Relative EtBr fluorescence intensities of intercalated EtBr in linear salmon sperm DNA after 2 h incubation with CDDP, **12b** or **8c**. Mean \pm SD, $n = 3$.

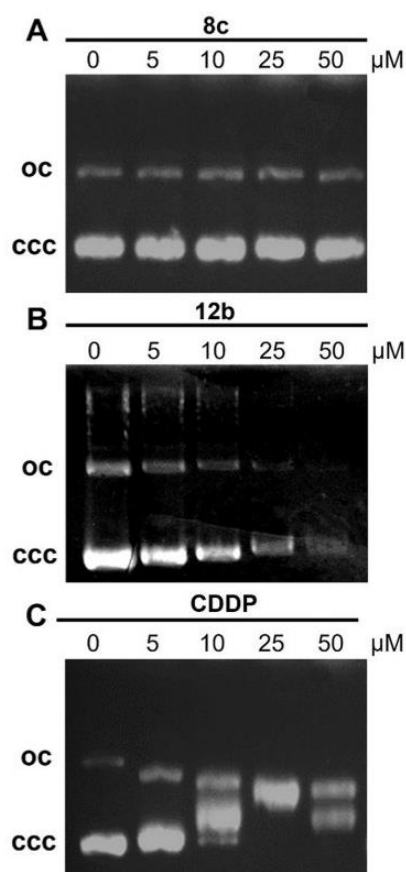


Fig. 9. EMSAs with circular plasmid DNA after 16 h treatment with complexes **8c** (A) and **12b** (B). CDDP was used as a positive control (C). Images were documented under UV excitation and they are representative of at least two independent experiments.

(Fig. 1).

In line with this reasoning, the *N*-benzyl substituted *cis*-(DMSO)(NHC) complex **10c** showed a similar if smaller split of its NCH₂ signal with two virtual doublets of doublets (vdd) at 6.18 ppm and 6.00 ppm. These vdd are 45 Hz apart, consistent with the doublet caused by the methyl groups of DMSO, thereby confirming the *cis* and perpendicular orientation relative to the PtCl₂ square. The first splitting to give a doublet consequently originates from the spatial arrangement of protons. The further doublet overlapping on this apparently comes from the ester group, which is either above or below the plane spanned by the ligands. This holds for all complexes and, due to the restricted rotatability of the NHC ligands [25], leads to two constitutional isomers and consequently to two possible arrangements of the *cis*-(DMSO)(NHC) complexes and four of the bis(NHC) complexes.

Differences can also be seen in the ppm range of the chemical shift of the CN carbon in ¹³C NMR spectra and of the shift of platinum in ¹⁹⁵Pt spectra (cf. Supporting Information). The chemical shifts of the C-2 in ¹³C NMR spectra of *trans*-bis(NHC) complexes lie around 181 ppm, those of *cis*-bis(NHC) complexes around 162 ppm and those of *cis*-(DMSO)(NHC) complexes around 158 ppm. The same holds for the shifts of Pt in ¹⁹⁵Pt spectra. *Trans*-Bis(NHC) complexes lie around -3270 ppm, *cis*-bis(NHC) complexes at -3640 ppm and *cis*-(DMSO)(NHC) complexes at

-3550 ppm.

Neither the *cis*-(DMSO)(NHC) complexes **10** and **11** nor the *cis*-bis(NHC)-complexes **12** and **13** showed a change of their signals in ¹H NMR spectra over a period of at least three days when dissolved in DMSO +5% D₂O, i.e. under test conditions. They can thus be considered stable. Exemplary ¹⁹⁵Pt NMR stability studies in DMSO-*d*₆ without the addition of D₂O were conducted with one complex of each series, i. e. **10c** and **13b**. They revealed that neither a change of the shift of the platinum signal nor any new peak appeared over the course of three days (cf. Supporting Information).

Some *trans*-bis(NHC) complexes, and **9a** in particular, however, showed intriguing stability pattern. Its ¹H NMR spectrum in DMSO-*d*₆ right after the addition of water showed twice as many signals in the aromatic region compared to its spectrum recorded in CDCl₃ (cf. Supporting Information). In addition, the clear splits visible in the latter blur into undefined multiplets for the NMe and the OCH₂ group, respectively, and into a virtual doublet of triplets of the aliphatic CH₃. These in turn converge over the time period of three days to form a new species whose shifts are slightly elevated but match the expected range and multiplicity of such complexes. Additionally, a ¹⁹⁵Pt NMR stability study with **9a** in DMSO-*d*₆ was carried out. The results are consistent with the findings of the ¹H measurements. In the spectra measured after 0 h a shift of -600 ppm was observed, probably due to an exchange of a chlorido for a DMSO ligand leading to a cationic complex. This is in keeping with reports that *trans*-platinum complexes are more reactive than their *cis*-analogues [26–28]. However, the spectrum did not keep changing over time. Addition of AgBF₄ after 72 h then caused the residual platinum signal of the starting material at -3255 ppm to completely disappear. A mass spectrum of this solution taken after 96 h showed only the mass of Pt(NHC)₂(DMSO)Cl. The same complex dissolved in CDCl₃ + 5% D₂O with intense and hourlong vortexing before each measurement showed no change in its ¹⁹⁵Pt or ¹H NMR spectra. Consequently, it can be assumed that no ligand exchange with water took place. A comparison of the *trans*-bis(NHC) complexes **8a–c** and **9a–c** with each other revealed that the ¹H NMR spectra of the benzyl substituted complexes did not change much over time. The number of signals of the *N*-ethyl substituted complexes **8b** and **9b** increased with time, indicating a slow ligand exchange. In contrast, the number of peaks of the *N*-methyl substituted complexes **8a** and **9a** decreased with time, converging to the spectrum obtained in CDCl₃, and so indicating a faster ligand exchange. The rate of the ligand exchange seems to depend on the size of the *N*-substituent.

Another point worth mentioning is that the ester functionality does not undergo saponification neither under mildly basic and aqueous conditions caused by the intermediate AgOH and the leaving group H₂O during the formation of (NHC)Ag(I) salts [29], nor under strongly basic conditions which prevail during the synthesis of the *cis*-bis(NHC) complexes. Furthermore, the respective *trans*-bis(NHC) complexes are way less polar than their *cis*-(DMSO)(NHC) or *cis*-bis(NHC) analogues as indicated by TLC and their solubilities.

Our group has recently shown that *cis*-bis(NHC) complexes behave akin to cisplatin and accumulate in the cell nuclei [19]. The aim of this work was therefore to investigate the subcellular accumulation of *cis*-(DMSO)(NHC) complexes **10** and **11** and especially that of the promising *trans*-bis(NHC) complexes **8** and **9**. Hence, clickable analogues were synthesised. The propargyl group was chosen as *N*-substituent with the smallest possible structural alteration (Scheme 2). The *N,N'*-dipropargyl benzimidazolium salt **15** could not be prepared like the salts **4** and **5** via one-pot *N,N'*-dialkylation. As a workaround, salt **15** was prepared in three steps with a purification via column chromatography of the *mono*-propargylated intermediate **14**. The former could neither be converted to the *cis*-(NHC)(DMSO) platinum complex **16** in several steps via an intermediate silver complex, in analogy to the conversion of the salts **4**, **5** to the complexes **10**, **11** in scheme 1. We assume that the formation of silver alkyne π -complexes is favoured over that of the desired carbene complex. Complex **16** was eventually obtained by deprotonating salt **15** and reacting the resulting carbene right away with *cis*-(DMSO)₂PtCl₂.

10

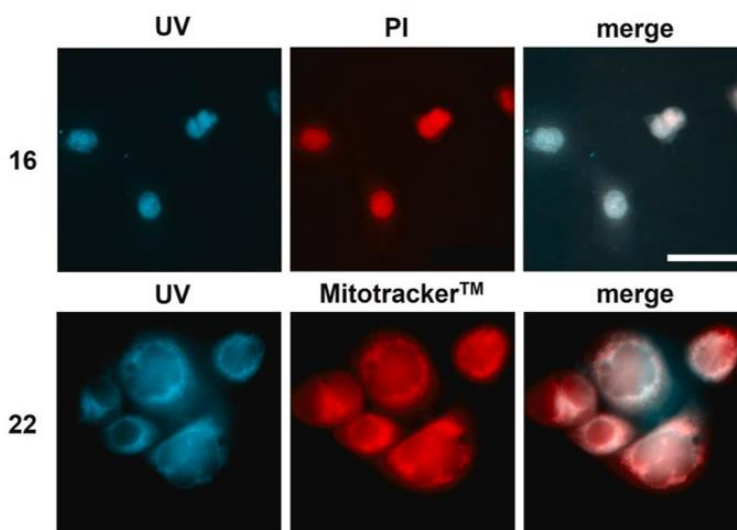


Fig. 10. Fluorescence microscopy images of HCT116 colon cancer cells treated 30 min with 25 μM of complexes **16** or **22** followed by click chemistry with fluorophore bearing reagents (ex/em 350/420–480 nm). Nuclei were counterstained with PI (ex/em 490/640), mitochondria were counterstained using Mitotracker™ (ex/em 580/610). The images shown are representative of at least four independent experiments. Scale bar corresponds to 30 μM .

The circumstance that complexation with silver led to decomposition also made transmetalation with K_2PtCl_4 to give the corresponding *trans* complexes impossible. Neither are there any platinum dichlorido precursors with good leaving groups in *trans* position. Treating the carbene obtained in situ by deprotonation of salt **15** with K_2PtCl_4 also failed to afford the corresponding *trans* complex. This is consistent with literature describing problems of Cu-catalysed click chemistry of azides with alkynes, especially in the presence of d^{10} metals [5]. Accordingly, a different click chemistry methodology was chosen for the visualisation of *trans* complexes differing structurewise only marginally from the complexes **8** and **9**. The methyl or ethyl ester groups of the latter were replaced by (2,3-dimethylcycloprop-2-en-1-yl)methoxycarbonyl residues, capable of undergoing metal-free, ring-strain promoted *Diels-Alder*-type click reactions with tetrazines (Scheme 3). This is the first time this methodology was applied to the visualisation of an organometallic compound. The required (2,3-dimethylcycloprop-2-en-1-yl)methanol was synthesised as described in literature [30]. The amine of benzimidazole **1** had to be protected with an alloc group prior to a *Steglich-Hassner* esterification which afforded ester **18**. Its deprotection gave ester **19** which was N,N-diethylated furnishing benzimidazolium iodide **20**. The latter was converted with Ag_2O to silver NHC complex **21** which was transmetalated with K_2PtCl_4 to give the desired *trans*-bis(NHC) platinum complex **22**.

3.2. Anticancer activity

3.2.1. Cytotoxicity and cellular uptake

The complexes were investigated for their cytotoxicity over 72 h against various human cancer cell lines including 518A2 melanoma, HCT116^{wt} and its HCT116^{p53-/-} knockout mutant colon carcinoma, U87 glioblastoma, EaHy926 somatic cell hybrid, HeLa cervix carcinoma, MCF7 breast cancer, and HT-29 colon cancer cells, as well as human non-malignant dermal fibroblasts HDFa using the MTT cell viability assay. Their IC_{50} values are shown in Table 1.

To better identify the most active compounds across all cell lines, the cytotoxicity indices of the substances were determined with respect to the cell lines used (Fig. 2)

The complexes **9c**, **10a**, **11a**, **11b**, **12a** and **13a** showed no

significant cytotoxic effect on the cancer cell lines studied. The complexes **8a**, **8b**, **9b**, **10b**, **11c** and **13b** were moderately active with IC_{50} values in the one- to two-digit micromolar range. Conspicuous cytotoxicities were observed for the complexes **8c**, **9a**, **10c** and **12b**, with *trans*-bis(NHC) complex **8c** and *cis*-bis(NHC) complex **12b** in particular standing out with two-digit nanomolar IC_{50} values.

Complexes of the methyl ester series tend to be more cytotoxic than their ethyl analogues, and the *cis*-bis(NHC) complexes were more cytotoxic than the corresponding *cis*-(DMSO)(NHC) complexes. Furthermore, the *trans*-bis(NHC) complexes tended to be more cytotoxic than the *cis* complexes, and cytotoxicity generally increased with the size of the substituents at the N-atoms of the benzimidazole. The finding that platinum(II) complexes with *trans*-positioned leaving groups may also be cytotoxic against cancer cells, like the more common *cis*-configured platinum(II) complexes, is not new. It has even been reported that *trans* complexes of platinum(II) may show activity against CDDP resistant tumour cell lines [9]. This fits with our findings for *trans*-bis(NHC) complexes **8c** and **9a** which showed antiproliferative activity against CDDP-resistant HT-29 colon carcinoma cells.

3.2.2. Uptake in cancer cells measured with ICP-MS

In order to clarify whether the high cytotoxicity of complexes **8c** and **12b** is intrinsic and structure-dependent, or a consequence of a particularly high cellular concentration, we assessed their cellular uptake by HCT116^{wt} colon carcinoma cells via ICP-MS in comparison to CDDP and ethyl esters **9c** and **13b**, which are structurewise closely related to **8c** and **12b** (Fig. 3).

The uptake of the *trans*-bis(NHC) complexes **8c** and **9c** is apparently more limited than that of the *cis*-complexes **12b**, **13b** and CDDP. The divergence in cellular uptake is not related to the respective IC_{50} values. The impressive cytotoxicity of complex **8c** against HCT116^{wt} cells exceeded that of **12b**, **13b** and CDDP by far, despite its comparatively low uptake, whereas **9c** is completely inactive. Therefore, the strong cytotoxicity of **8c** is intrinsic, structure-dependent and based on mechanistic reasons. As recently shown by Rehm et al., the uptake of platinum compounds may also be directly linked to structural features [23]. A generally weak uptake of *trans*-platinum complexes is assumed.

3.2.3. Unselective toxicity

In order to assess the degree of toxicity leading to necrosis caused by complexes **8c** and **12b**, a lactate dehydrogenase (LDH) release assay was conducted. LDH release is considered as a benchmark for necrotic cells, as it is a consequence of plasma membrane permeabilisation [12]. LDH release assays were conducted with HCT116^{wt} cells. LDH release is measured as absorbance by a coloured formazan which is the product of an LDH-associated NADH reduction of a colourless tetrazolium salt [12]. No significant increase in LDH levels was detected after an incubation period of 24 h (Fig. 4). This indicates that the complexes have no unselective cytotoxic effects and that the membrane integrity of HCT116^{wt} cells was maintained over 24 h of exposure to concentrations clearly exceeding the IC₅₀ of the complexes. Thus, a key precondition for suitability as potential drugs was fulfilled, and their mode of action was further investigated.

3.2.4. Induction of apoptosis, mediated by caspase-3/-7 activation

The absence of an LDH increase upon cell treatment with compounds **8c** and **12b** hints at a medicinally favourable apoptotic rather than necrotic type of cancer cell death. Mechanistically, this would imply that the complexes trigger an apoptosis cascade via activation of caspases [31]. To confirm this for the complexes **8c** and **12b**, a caspase-3/7 activation assay was performed [32]. Both complexes activated caspases-3/7 in HCT116^{wt} colon carcinoma cells at least as strongly as CDDP did (Fig. 5).

3.2.5. Mitochondrial membrane potential and ROS levels

Closely linked to apoptotic events is the loss of the mitochondrial membrane potential (MMP) and the resulting increase in intracellular ROS levels [32,33]. The MMP can be assessed by means of the fluorescent, cationic dye tetramethylrhodamin methyl ester (TMRM⁺) which accumulates in the negatively charged intact mitochondrial membranes [5]. The integrity of MMP in HCT116^{wt} cells was distinctly diminished upon treatment with complexes **8c** and **12b** (Fig. 6A). The disturbance of the MMP often leads to a rise in intracellular ROS levels, due to the permeability of the mitochondrial membranes allowing intramitochondrial ROS to enter the cytosol [6]. The ROS levels in HCT116^{wt} cells treated with complexes **8c** and **12b** were assessed with dichlorodihydrofluorescein diacetate (DCFH-DA), a fluorogenic dye which measures hydroxyl, peroxy and other reactive oxygen species in live cells (Fig. 6B). Treatment of the cells with complexes **8c** or **12b** led to an increase of ROS levels, most distinctly so for the *cis*-complex **12b**, probably because of the lower uptake of *trans*-complex **8c** into these cells. Together with the results of the caspase-3/7 activation assays, these studies suggest a mitochondria-associated induction of apoptosis by both complexes **8c** and **12b**.

3.2.6. Influence on the cell cycle

The clinically established *cis*-configured platinum(II) complexes structurally modify cellular DNA and so interfere with its normal function. As a consequence, alterations of the cell cycle occur due to an inhibition of the cellular replication and transcription machinery, eventually leading to cell apoptosis [34]. Cisplatin typically induces an S-Phase or a dual S-/G₂M-Phase arrest in cancer cells [20,23]. We now monitored the interference of the platinum(II) complexes **8c** and **12b** at their respective IC₅₀ concentrations with the cell cycle of HCT116^{wt} cells using propidium iodide staining and flow cytometry. No significant changes in the typical cell cycle progression of these colon cancer cells, compared to the control (Fig. 7A), was observed upon treatment with *trans*-complex **8c** (Fig. 7B). In contrast, treatment with *cis*-complex **12b** (Fig. 7C) led to a distinct change in cell cycle phase distribution similar to CDDP (Fig. 7D). Therefore, a mode of action similar to that of cisplatin may be assumed for *cis*-complex **12b**, whereas *trans*-complex **8c** seems to act in a different way.

3.2.7. DNA interaction

The mechanism of action of CDDP and most other effective *cis*-configured Pt(II) complexes is based on the formation of strong coordinative bonds between the metal centre and DNA bases [35]. Due to the *cis* configuration of complex **12b** and the CDDP-like type of cell cycle arrest it elicits in treated cancer cells, a DNA-associated mechanism of action is standing to reason. To verify this and to further elucidate the mechanism of action of the *trans*-complexes, DNA-based ethidium bromide (EtdBr) saturation assays and electrophoretic mobility shift assays (EMSA) were performed. Incubation of linear salmon sperm DNA with complex **12b** led to a strong concentration-dependent reduction of the fluorescence of intercalated EtdBr as the metalated DNA offers fewer accessible sites for intercalation. This effect was even more pronounced for complex **12b** when compared to that by CDDP (Fig. 8). The *trans*-bis (NHC) complex **8c** did not give rise to such an effect, indicating a mode of action not associated with DNA metalation.

In order to identify the nature of the DNA interaction of complex **12b** an EMSA was conducted. The comparison of EtdBr and EMSA results allows to distinguish between strong covalent/coordinative and merely electrostatic interactions of metalating agents and DNA. Treatment of circular plasmid DNA with *cis*-complex **12b** (Fig. 9B) revealed a concentration-dependent relaxation of the ccc (covalently closed circular) form to the oc (open circular) form akin to, yet less pronounced than, that caused by CDDP (Fig. 9C). In line with its lack of interaction with linear DNA in the EtdBr assay, the *trans*-complex **8c** had no effect on circular plasmid DNA either (Fig. 9A), also indicating a DNA-independent mode of action.

These findings support a DNA-associated mode of action for *cis*-complex **12b**. Together with its CDDP-like cell cycle arrest, the results of our study suggest a mode of action of **12b** quite reminiscent of that of CDDP. The mechanisms of action leading to the extraordinary cytotoxic effect of the *trans* platinum(II) complex **8c** remains to be elucidated in more detail.

3.2.8. Intracellular localisation

Complexes **16** and **22** were synthesised as representatives of the groups of *cis*- and *trans*-complexes that can be converted to fluorescent products using click chemistry after they have reached their respective cellular targets. Using this method, the distribution of the complexes inside the treated cells can be traced. An enrichment of *cis*-complex **16** in the area of the nuclei of treated colon cancer cells was observed, matching the DNA-binding properties of *cis*-Pt complexes in general and those of the *cis*-complexes studied here. In contrast, *trans*-complex **22** accumulated in regions outside the nuclei, mainly in the area of the cytoplasm including mitochondria (Fig. 10). This suggests that the *trans*-complexes **8** and **9** very likely do not interfere with DNA, as already suspected. In the past, we had already reported on NHC-platinum complexes which accumulate in mitochondria and interfere with mitochondrial function [19]. The current findings underline the suitability of *trans*-complexes of platinum(II) as anti-cancer compounds targeting structures other than DNA.

4. Conclusion

The current work studied the influence of the N-alkyl and 5-alkoxy-carbonyl substituents of *cis*- and *trans*-[bis(benzimidazol-2-ylidene)dichlorido]platinum(II) complexes **12/13** and **8/9** on their stability in aqueous media, their cytotoxicity against cancer cells, and their underlying properties and modes of action.

The intrinsic cytotoxicity and the cell line specificity of both series of complexes depended to a large extent on their ester and their N-alkyl residues whereas their uptake into cancer cells did not. However, the most active *trans*-complexes and the most active *cis*-complexes carried different such residues. Far less was taken up of *trans*-complexes **8/9** by HCT116 colon carcinoma cells when compared to *cis*-complexes **12/13**.

While the *cis*-complexes appeared to operate by mechanisms of

action akin to those of cisplatin, the *trans*-complexes addressed different targets, e.g. such associated with mitochondria rather than DNA, although having a lesser effect on the mitochondrial membrane potential and the release of ROS. The subcellular localisation of *trans* complex 22 in mitochondrial organelles by the first-time bioorthogonal clicking of a cyclopropene-bearing complex with a fluorogenic tetrazine supports this finding. The *trans*-complexes had also no effect on the cell cycle of cancer cells. Most intriguing, however, is their high activity against cisplatin-refractory cancer cells.

Combination therapies of inactive transplatin with drugs affecting the DNA and its function such as the antimetabolite 5-fluorouracil had been reported to enhance the anticancer effect of the latter [36]. It would be interesting to test whether combinations of our active *trans*-complexes with 5-FU lead to an even greater overall anticancer effect.

Further work is necessary to fully elucidate the mode of action of *trans*-[bis(benzimidazol-2-ylidene)dichlorido]platinum(II) complexes and to pinpoint the optimum set of N- and aryl-substituents.

Source of funding

Deutsche Forschungsgemeinschaft grant Scho 402/12-2

Declaration of Competing Interest

The authors declare that they have no known competing financial interests or personal relationships that could have appeared to influence the work reported in this paper.

Data availability

Data will be made available on request.

Acknowledgements

R.S. thanks the Deutsche Forschungsgemeinschaft for financial support (grant Scho 402/12-2). We thank Dr. Ulrike Lacher (University of Bayreuth) for mass spectra. We thank Kim Wagner for supporting work on MTTs and buffer preparation, as well as Manuel Wayand and Moritz Röder for precursor synthesis.

Appendix A. Supplementary data

Supplementary data to this article can be found online at <https://doi.org/10.1016/j.jinorgbio.2022.112028>.

References

- S. Zhao, Z. Yang, G. Jiang, S. Huang, M. Bian, Y. Lu, W. Liu, An overview of anticancer platinum N-heterocyclic carbene complexes, *Coord. Chem. Rev.* 449 (2021) 214217, <https://doi.org/10.1016/j.ccr.2021.214217>.
- S.B. Aher, P.N. Muskawar, K. Thenmozhi, P.R. Bhagat, Recent developments of metal N-heterocyclic carbenes as anticancer agents, *Eur. J. Med. Chem.* 81 (2014) 408–419, <https://doi.org/10.1016/j.ejmech.2014.05.036>.
- A.V. Astakhov, S.B. Soliev, E.G. Gordeev, V.M. Chernyshev, V.P. Ananikov, Relative stabilities of M/NHC complexes (M = Ni, Pd, Pt) against R-NHC, X-NHC and X-X couplings in M(0)/M(ii) and M(ii)/M(iv) catalytic cycles: a theoretical study, *Dalton Trans.* 4845 (2019) 17052–17062, <https://doi.org/10.1039/C9DT03266E>.
- B. Rosenberg, L. VanCamp, The successful regression of large solid sarcoma 180 tumors by platinum compounds, *Cancer Res.* 306 (1970) 1799–1802.
- S. Bellemin-Lapomnaz, N-heterocyclic carbene platinum complexes: a big step forward for effective antitumor compounds, *Chem. Eur. J.* 20201 (2020) 10–20, <https://doi.org/10.1002/cejc.201900960>.
- M.J. Cleare, J.D. Hoeschele, Studies on the antitumor activity of group VIII transition metal complexes. Part I. Platinum (II) complexes, *Bioinorg.* 23 (1973) 187–210, [https://doi.org/10.1016/S0006-3061\(00\)80249-5](https://doi.org/10.1016/S0006-3061(00)80249-5).
- S.E. Sherman, S.J. Lippard, Structural aspects of platinum anticancer drug interactions with DNA, *Chem. Rev.* 875 (1987) 1153–1181, <https://doi.org/10.1021/cr00081a013>.
- M. Coluccia, G. Natile, Trans-platinum complexes in cancer therapy, *Anti Cancer Agents Med. Chem.* 71 (2007) 111–123, <https://doi.org/10.2174/187152007779314080>.
- G. Natile, M. Coluccia, Current status of trans-platinum compounds in cancer therapy, *Coord. Chem. Rev.* 216 (2001) 383–410, [https://doi.org/10.1016/S0010-8545\(01\)00315-0](https://doi.org/10.1016/S0010-8545(01)00315-0).
- U. Kalinowska-Lis, J. Ochocki, K. Matlowska-Wasowska, Trans geometry in platinum antitumor complexes, *Coord. Chem. Rev.* 252 (2008) 1328–1345, <https://doi.org/10.1016/j.ccr.2007.07.015>.
- D.M.L. Morgan, Tetrazolium (MTT) assay for cellular viability and activity, in: D. M.L. Morgan (Ed.), *Polyamine Protocols*, Humana Press, Totowa, NJ, 1998, pp. 179–184.
- F.K. Chan, K. Moriwaki, M.J. De Rosa, Detection of necrosis by release of lactate dehydrogenase activity, *Methods Mol. Biol.* 979 (2013) 65–70, https://doi.org/10.1007/978-1-62703-290-2_7.
- C.E. Ganote, S.C. Armstrong, Effects of CCCP-induced mitochondrial uncoupling and cyclosporin A on cell volume, cell injury and preconditioning protection of isolated rabbit cardiomyocytes, *J. Mol. Cell. Cardiol.* 357 (2003) 749–759, [https://doi.org/10.1016/S0022-2828\(03\)00114-7](https://doi.org/10.1016/S0022-2828(03)00114-7).
- E. Eruslanov, S. Kusmartsev, Identification of ROS using oxidized DCFDA and flow-cytometry, in: D. Armstrong (Ed.), *Advanced Protocols in Oxidative Stress II*, Humana Press, Totowa, NJ, 2010, pp. 57–72.
- C. Qiao, S. Bi, Y. Sun, D. Song, H. Zhang, W. Zhou, Study of interactions of anthraquinones with DNA using ethidium bromide as a fluorescence probe, *Spectrochim. Acta A Mol. Biomol. Spectrosc.* 701 (2008) 136–143, <https://doi.org/10.1016/j.saa.2007.07.038>.
- T. Rehm, M. Rothemund, T. Dietel, R. Kempe, R. Schobert, Synthesis, structures and cytotoxic effects in vitro of cis- and trans-[PtIVCl4(NHC)2] complexes and their PtII precursors, *Dalton Trans.* 4843 (2019) 16358–16365, <https://doi.org/10.1039/C9DT02438G>.
- K. Salorinne, R.W.Y. Man, C.-H. Li, M. Taki, M. Nambo, C.M. Crudden, Water-soluble N-heterocyclic carbene-protected gold nanoparticles: size-controlled synthesis, stability, and optical properties, *Angew. Chem. Int. Ed.* 5622 (2017) 6198–6202, <https://doi.org/10.1002/anie.201701605>.
- C. Schmidt, B. Karge, R. Misgeld, A. Prokop, R. Franke, M. Brönstrup, I. Ott, Gold(II) NHC complexes: antiproliferative activity, cellular uptake, inhibition of mammalian and bacterial thioredoxin reductases, and gram-positive directed antibacterial effects, *Chem. Eur. J.* 238 (2017) 1869–1880, <https://doi.org/10.1002/chem.201604512>.
- M. Rothemund, S.I. Bär, T. Rehm, H. Kostrhunova, V. Brabec, R. Schobert, Antitumor effects of mitochondria-targeting neutral and cationic cis-bis(1,3-dibenzylimidazol-2-ylidene)Cl(L)Pt(ii) complexes, *Dalton Trans.* 4926 (2020) 8901–8910, <https://doi.org/10.1039/D0DT01664K>.
- J.K. Muenzner, T. Rehm, B. Biersack, A. Casini, I.A. de Graaf, P. Worawutputtpong, A. Noor, R. Kempe, V. Brabec, J. Kasparkova, R. Schobert, Adjusting the DNA interaction and anticancer activity of Pt(II) N-heterocyclic carbene complexes by steric shielding of the trans leaving group, *J. Med. Chem.* 5815 (2015) 6283–6292, <https://doi.org/10.1021/acs.jmedchem.5b00896>.
- S. Fantasia, A. Pasini, S.P. Nolan, Platinum(II) mediated C(sp3)-H activation of tetramethylthiourea, *Dalton Trans.* 38 (2009) 8107–8110, <https://doi.org/10.1039/b911164f>.
- L.C. Lewis-Alleyne, B.S. Bassil, T. Böttcher, G.-V. Röschenhaler, Selective synthesis of cis- and trans-[(NHCMe)2PtCl2] and [(NHCMePt(cod)Cl]/[(NHCMePtCl3)] using NHCMeSiCl4, *Dalton Trans.* 4342 (2014) 15700–15703, <https://doi.org/10.1039/C4DT02214A>.
- T. Rehm, M. Rothemund, A. Bär, T. Dietel, R. Kempe, H. Kostrhunova, V. Brabec, J. Kasparkova, R. Schobert, N,N-Dialkylbenzimidazol-2-ylidene platinum complexes – effects of alkyl residues and ancillary cis-ligands on anticancer activity, *Dalton Trans.* 4748 (2018) 17367–17381, <https://doi.org/10.1039/C8DT03360A>.
- T. Rehm, M. Rothemund, J.K. Muenzner, A. Noor, R. Kempe, R. Schobert, Novel cis-[(NHC)1(NHC)2(L)Cl]platinum(ii) complexes – synthesis, structures, and anticancer activities, *Dalton Trans.* 4539 (2016) 15390–15398, <https://doi.org/10.1039/C6DT02350A>.
- C.P. Newman, R.J. Deeth, G.J. Clarkson, J.P. Rourke, Synthesis of mixed NHC/L platinum(II) complexes: restricted rotation of the NHC Group, *Organometallics* 2625 (2007) 6225–6233, <https://doi.org/10.1021/om700671y>.
- T. Peleg-Shulman, Y. Najajreh, D. Gibson, Interactions of cisplatin and transplatin with proteins. Comparison of binding kinetics, binding sites and reactivity of the Pt-protein adducts of cisplatin and transplatin towards biological nucleophiles, *J. Inorg. Biochem.* 91 (2002) 306–311, [https://doi.org/10.1016/S0162-0134\(02\)00362-8](https://doi.org/10.1016/S0162-0134(02)00362-8).
- T. Kishimoto, Y. Yoshikawa, K. Yoshikawa, S. Kameda, Different effects of cisplatin and Transplatin on the higher-order structure of DNA and gene expression, *Int. J. Mol. Sci.* 211 (2019), <https://doi.org/10.3390/ijms21010034>.
- V. Marchán, E. Pedroso, A. Grandas, Insights into the reaction of transplatin with DNA and proteins: methionine-mediated formation of histidine-guanine trans-Pt (NH3)2 cross-links, *Chemistry* 10 (2004) 5369–5375, <https://doi.org/10.1002/chem.200400470>.
- J.M. Hayes, M. Viciano, E. Peris, G. Ujaque, A. Lledós, Mechanism of formation of silver N-heterocyclic carbenes using silver oxide: a theoretical study, *Organometallics* 2625 (2007) 6170–6183, <https://doi.org/10.1021/om700898d>.
- J.M.J.M. Ravasco, C.M. Monteiro, A.F. Trindade, Cyclopropenes: a new tool for the study of biological systems, *Org. Chem. Front.* 46 (2017) 1167–1198, <https://doi.org/10.1039/C7QO00054E>.
- S. Fulda, K.M. Debatin, Caspase activation in cancer therapy, in: *Madame Curie Bioscience Database [Internet]*, Landes Bioscience, Austin (TX), 2022.
- M.P. Murphy, How mitochondria produce reactive oxygen species, *Biochem. J.* 4171 (2009) 1–13, <https://doi.org/10.1042/bj20081386>.

- [33] J.D. Ly, D.R. Grubb, A. Lawen, The mitochondrial membrane potential ($\Delta\psi$) in apoptosis; an update, *Apoptosis* 82 (2003) 115–128, <https://doi.org/10.1023/a:1022945107762>.
- [34] S. Ahmad, Platinum-DNA interactions and subsequent cellular processes controlling sensitivity to anticancer platinum complexes, *Chem. Biodivers.* 73 (2010) 543–566, <https://doi.org/10.1002/cbdv.200800340>.
- [35] J. Reedijk, P.H. Lohman, Cisplatin: synthesis, antitumour activity and mechanism of action, *Pharm. Weekbl. Sci.* 75 (1985) 173–180, <https://doi.org/10.1007/bf02307573>.
- [36] B. Nakata, S. Yamagata, I. Kanehara, T. Shirasaka, K. Hirakawa, Transplatin, a cisplatin trans-isomer, may enhance the anticancer effect of 5-fluorouracil, *J. Exp. Clin. Cancer Res.* 252 (2006) 195–200.

SUPPORTING INFORMATION

***Trans*-[bis(benzimidazol-2-ylidene)dichlorido]platinum(II) complexes with peculiar modes of action and activity against cisplatin-resistant cancer cells**

Sofia I. Bär⁺, Sebastian W. Schleser⁺, Natalie Oberhuber, Alexander Herrmann, Luca Schlotte, Stefanie E. Weber and Rainer Schobert*

Organic Chemistry Laboratory, University of Bayreuth, Universitaetsstrasse 30, 95447 Bayreuth, Germany

⁺These authors contributed equally to this work

*Corresponding author

E-mail address: rainer.schobert@uni-bayreuth.de

Fax: 0049-921-552671

Phone: 0049-921-552679

Conflicts of interest: There are no conflicts of interest

Source of funding: Deutsche Forschungsgemeinschaft grant Scho 402/12-2

Table of content

1 Synthesis and characterization of used precursors	III
1.1 General procedure for the esterification of 1H-Benzimidazole-5-carboxylic acid.....	III
1.2 General procedure for N-alkylation and halide exchange	IV
1.3 General procedure for silver complexation	IX
1.4 Procedures for the synthesis of the precursors of clickable complexes 16 and 22	XI
2. Biological evaluation	XVI
2.1 Stock solutions	XVI
2.2 Cell culture conditions	XVI
Appendix.....	XVI
NMR spectra of Pt(II) complexes	XVI
Stability studies of Pt(II) complexes	XLIV

1 Synthesis and characterization of used precursors

1.1 General procedure for the esterification of 1H-Benzimidazole-5-carboxylic acid

1H-benzimidazol-5-carboxylic acid (1.00 eq.) was suspended in ROH (3 mL/mmol) and concentrated H₂SO₄ (2.40 eq.) was added to the solution. Subsequently the mixture was stirred at 100 °C for 24 h. Afterwards, the solvent was removed under reduced pressure and the residue was dissolved in EtOAc (50 mL/mmol). The organic phase was then washed with saturated Na₂CO_{3(aq.)} (50 mL/mmol). The aqueous phase was extracted with EtOAc (3 · 50 mL/mmol) and the combined organic phases were washed with brine (50 mL/mmol), dried over Na₂SO₄ and filtrated. The solvent was evaporated and the product could be afforded as brown powder after drying in vacuum.

Methyl 1H-benzimidazol-5-carboxylate (2)

872 mg (4.96 mmol, 80%) from **1** (1.00 g, 6.70 mmol, 1.00 eq.), H₂SO₄ (783 µL, 14.8 mmol, 2.40 eq.) in MeOH (15.0 mL). ¹H NMR (500 MHz, CDCl₃) δ_H = 11.2 (s, 1H, NH), 8.43 (s, 1H, H^{ar}), 8.25 (s, 1H, H^{ar}), 8.03 (vdd, *J* = 8.5 Hz, 1.5 Hz, 1H, H^{ar}), 7.69 (d, *J* = 8.5 Hz 1H, H^{ar}), 3.95 (s, 3H, OCH₃); ¹³C NMR (125 MHz, CDCl₃) δ_C = 167.7 (s, COOCH₃), 142.8 (s, C^{ar}), 125.1 (s, C^{ar}), 124.5 (s, C^{ar}), 52.3 (s, OCH₃).

The NMR spectra match previously reported data.^[1]

Ethyl 1H-benzimidazol-5-carboxylate (3)

2.01 g (10.6 mmol, 86%) from **1** (2.00 g, 12.3 mmol, 1.00 eq.), H₂SO₄ (1.59 mL, 29.6 mmol, 2.40 eq.) in EtOH (30.0 mL). ¹H NMR (500 MHz, DMSO-d₆) δ_H = 13.0 (s, 1H, NH), 8.45 (s, 1H, H^{ar}), 8.34 (s, 1H, H^{ar}), 8.02 (vdd, *J* = 8.5 Hz, 1.6 Hz, 1H, H^{ar}), 7.69 (d, *J* = 8.7 Hz, 1H, H^{ar}), 4.39 (q, *J* = 7.1 Hz 2H, OCH₂), 1.38 (t, *J* = 7.1 Hz, 3H, CH₃); ¹³C NMR (125 MHz, CDCl₃) δ_C

= 167.4 (s, COOCH₂), 143.3 (s, C^{ar}), 140.9 (s, C^{ar}), 137.9 (s, C^{ar}), 125.2 (s, C^{ar}), 124.4 (s, C^{ar}), 118.3 (s, C^{ar}), 114.9 (s, C^{ar}), 61.2 (s, OCH₂), 14.4 (s, CH₃).

The NMR spectra match previously reported data.^[2]

1.2 General procedure for N-alkylation and halide exchange

1H-benzimidazol-5-carboxylate (1.00 eq.) and K₂CO₃ (1.70 eq.) were suspended in MeCN (20 mL/mmol). The mixture was treated with RX (6.00 eq.) and stirred at reflux for 24 h. Subsequently the solvent was removed under reduced pressure and the residue was dissolved in CH₂Cl₂. After filtration, the solvent was concentrated in vacuum and the residue was precipitated in ether. Drying the precipitate *in vacuo* afforded the product as pale yellow to brown powder. The respective halide (1.00 eq.) and Ag₂CO₃ (1.14 eq.) were suspended in EtOH (20 mL/mmol). Concentrated HNO₃ (10 drops/mmol) was added and the suspension was stirred for 3.5 h while being shielded from light. After the silver halides were filtered off, concentrated HCl (2.30 eq.) was added dropwise and the solution stirred for 10 min. Afterwards the solution was neutralized by adding saturated NaHCO_{3(aq)} and filtered once more. Subsequently the solvent was evaporated and the residue was dissolved in CH₂Cl₂. After another filtration step, the solution was concentrated and precipitated in *n*-pentane. After drying *in vacuo*, the product could be isolated as white to yellow powder.

1,3-dimethyl-5-(methoxycarbonyl)-1H-benzimidazol-3-ium chloride (4a)

850 mg (2.56 mmol, 90%) from **2** (500 mg, 2.84 mmol, 1.00 eq.), K₂CO₃ (667 mg, 4.82 mmol, 1.70 eq.) and MeI (1.06 mL, 17.0 mmol, 6.00 eq.) in MeCN (50.0 mL). ¹H NMR (500 MHz, CDCl₃) δ_H = 11.3 (s, 1H, CH), 8.42 (s, 1H, H^{ar}), 8.37 (d, *J* = 1.5 Hz, 1H, H^{ar}), 7.78 (d, *J* = 1.5 Hz, 1H, H^{ar}), 4.31 (s, 6H, CH₃), 4.02 (s, 3H, OCH₃); ¹³C NMR (125 MHz, CDCl₃) δ_C = 165.2

(s, COOCH₃), 134.5 (s, C^{ar}), 131.8 (s, C^{ar}), 129.6 (s, C^{ar}), 128.5 (s, C^{ar}), 114.8 (s, C^{ar}), 112.9 (s, C^{ar}), 52.9 (s, OCH₃), 34.4 (NCH₃), 33.8 (s, NCH₃).

170 mg (706 μmol, 59%) from 1,3-dimethyl-5-(methoxycarbonyl)-1H-benzimidazol-3-ium iodide (400 mg, 1.20 mmol, 1.00 eq.), Ag₂CO₃ (379 mg, 1.37 mmol, 1.14 eq.), HNO₃ (12 drops) and HCl (229 μL, 2.77 mmol, 2.30 eq.) in EtOH (25.0 mL). ¹H NMR (500 MHz, CDCl₃) δ_H = 11.0 (s, 1H, CH), 8.41 (s, 1H, H^{ar}), 8.34 (vdd, *J* = 8.7 Hz, 1.5 Hz, 1H, H^{ar}), 7.78 (d, *J* = 8.7 Hz, 1H, H^{ar}), 4.26 (d, *J* = 4.3 Hz, 6H, CH₃), 4.01 (s, 3H, OCH₃); ¹³C NMR (125 MHz, CDCl₃) δ_C = 165.3 (s, COOCH₃), 147.0 (s, NCN), 134.7 (s, C^{ar}), 131.8 (s, C^{ar}), 129.3 (s, C^{ar}), 128.2 (s, C^{ar}), 114.7 (s, C^{ar}), 112.9 (s, C^{ar}), 53.0 (s, OCH₃), 33.9 (NCH₃), 33.8 (s, NCH₃).

1,3-dimethyl-5-(methoxycarbonyl)-1H-benzimidazol-3-ium chloride (4b)

1.20 g (3.33 mmol, 98%) from Methyl 1H-benzimidazol-5-carboxylate (**2**) (600 mg, 3.41 mmol, 1.00 eq.), K₂CO₃ (800 mg, 5.79 mmol, 1.70 eq.) and EtI (1.64 mL, 20.4 mmol, 6.00 eq.) in MeCN (50.0 mL). ¹H NMR (500 MHz, CDCl₃) δ_H = 11.5 (s, 1H, CH), 8.44 (s, 1H, H^{ar}), 8.36 (d, *J* = 1.5 Hz, 1H, H^{ar}), 7.79 (d, *J* = 1.5 Hz, 1H, H^{ar}), 4.73 (vdq, *J* = 7.4 Hz, 4.0 Hz, 4H, CH₂), 4.03 (s, 3H, OCH₃), 1.83 (vdt, *J* = 10.0 Hz, 7.5 Hz, 6H, CH₃); ¹³C NMR (125 MHz, CDCl₃) δ_C = 165.3 (s, COOCH₂), 143.6 (NCN), 131.1 (s, C^{ar}), 129.3 (s, C^{ar}), 128.2 (s, C^{ar}), 115.0 (s, C^{ar}), 113.5 (s, C^{ar}), 53.0 (s, OCH₃), 43.7 (NCH₂), 43.5 (NCH₂), 14.9 (s, CH₃).

330 mg (1.23 mmol, 88%) from 1,3-diethyl-5-(methoxycarbonyl)-1H-benzimidazol-3-ium iodide (500 mg, 1.39 mmol, 1.00 eq.), Ag₂CO₃ (436 mg, 1.58 mmol, 1.14 eq.), HNO₃ (14 drops) and HCl (264 μL, 3.19 mmol, 2.30 eq.) in EtOH (25.0 mL). ¹H NMR (500 MHz, CDCl₃) δ_H = 11.0 (s, 1H, CH), 8.42 (s, 1H, H^{ar}), 8.32 (d, *J* = 8.7 Hz, 1H, H^{ar}), 7.82 (vdd, *J* = 8.8 Hz, 2.9 Hz, 1H, H^{ar}), 4.69 (vdq, *J* = 7.4 Hz, 2.0 Hz, 4H, CH₂), 4.00 (s, 3H, OCH₃), 1.77 – 1.65 (m, 6H, CH₃). ¹³C NMR (125 MHz, CDCl₃) δ_C = 165.3 (s, COOCH₃), 134.1 (s, C^{ar}), 131.7 (s, C^{ar}), 129.2

(s, C^{ar}), 128.1 (s, C^{ar}), 115.0 (s, C^{ar}), 113.2 (s, C^{ar}), 53.0 (s, OCH₃), 43.3 (NCH₂), 14.8 (s, CH₃), 14.7 (s, CH₃).

1,3-dimethyl-5-(methoxycarbonyl)-1H-benzimidazol-3-ium chloride (4c)

937 mg (2.14 mmol, 76%) from **2** (500 mg, 2.84 mmol, 1.00 eq.), K₂CO₃ (667 mg, 4.82 mmol, 1.70 eq.) and BnBr (2.02 mL, 17.0 mmol, 6.00 eq.) in MeCN (50.0 mL). ¹H NMR (500 MHz, CDCl₃) δ_H = 12.0 (s, 1H, CH), 8.28 (s, 1H, H^{ar}), 8.18 (vdd, *J* = 8.8 Hz, 1.5 Hz, 1H, H^{ar}), 7.62 (m, 3H, H^{ar}), 7.53 (m, 2H, H^{ar}), 7.46 (m, 6H, H^{ar}), 5.89 (s, 4H, CH₂), 3.95 (s, 3H, OCH₃). ¹³C NMR (125 MHz, CDCl₃) δ_C = 165.1 (s, COOMe), 145.3 (NCN), 134.1 (s, C^{ar}), 132.4 (s, C^{ar}), 132.2 (s, C^{ar}), 131.3 (s, C^{ar}), 129.5 (s, C^{ar}), 129.4 (s, C^{ar}), 129.3 (s, C^{ar}), 128.5 (s, C^{ar}), 128.1 (s, C^{ar}), 115.6 (s, C^{ar}), 114.2 (s, C^{ar}), 53.0 (s, OCH₃), 52.2 (s, NCH₂), 52.0 (s, NCH₂).

208 mg (513 μmol, 58%) from 1,3-dibenzyl-5-(methoxycarbonyl)-1H-benzimidazol-3-ium bromide (400 mg, 914 μmol, 1.00 eq.), Ag₂CO₃ (288 mg, 1.04 mmol, 1.14 eq.), HNO₃ (11 drops) and HCl (174 μL, 2.10 mmol, 2.30 eq.) in EtOH (25.0 mL). ¹H NMR (500 MHz, CDCl₃) δ_H = 11.4 (s, 1H, CH), 8.24 (vd, 1H, *J* = 1.4 Hz, H^{ar}), 8.12 (vdd, *J* = 8.7 Hz, 1.4 Hz, 1H, H^{ar}), 7.69 (d, *J* = 8.8 Hz, 1H, H^{ar}), 7.48 – 7.43 (m, 4H, H^{ar}), 7.37 – 7.27 (m, 6H, H^{ar}), 5.78 (vd, *J* = 8.8 Hz, 4H, CH₂), 3.90 (s, 3H, OCH₃); ¹³C NMR (125 MHz, CDCl₃) δ_C = 165.2 (s, COOCH₃), 146.5 (s, NCN), 134.2 (s, C^{ar}), 132.5 (s, C^{ar}), 132.4 (s, C^{ar}), 131.4 (s, C^{ar}), 129.5 (s, C^{ar}), 129.4 (s, C^{ar}), 129.3 (s, C^{ar}), 129.2 (s, C^{ar}), 129.1 (s, C^{ar}), 128.4 (s, C^{ar}), 128.2 (s, C^{ar}), 128.0 (s, C^{ar}), 115.5 (s, C^{ar}), 114.0 (s, C^{ar}), 52.9 (s, OCH₃), 51.8 (NCH₂), 51.7 (s, NCH₂).

1,3-dimethyl-5-(ethoxycarbonyl)-1H-benzimidazol-3-ium chloride (5a)

400 mg (1.07 mmol, 68%) from **3** (300 mg, 1.58 mmol, 1.00 eq.), K₂CO₃ (371 mg, 2.68 mmol, 1.70 eq.) and MeI (761 μL, 9.46 mmol, 6.00 eq.) in MeCN (30.0 mL). ¹H NMR (500 MHz, CDCl₃) δ_H = 11.3 (s, 1H, CH), 8.34 (s, 1H, H^{ar}), 8.31 (dd, *J* = 8.7 Hz, 1.3 Hz, 1H, H^{ar}), 7.76 (dd, *J* = 8.7 Hz, 1.5 Hz, 1H, H^{ar}), 4.46 (q, *J* = 7.1 Hz, 2H, OCH₂), 4.16 (s, 6H, NCH₃), 1.45 (t, *J* =

7.1 Hz, 3H, CH₃); ¹³C NMR (125 MHz, CDCl₃) δ_C = 164.8 (s, COOCH₂), 144.9 (s, NCN), 134.5 (s, C^{ar}), 131.7 (s, C^{ar}), 129.7 (s, C^{ar}), 128.2 (s, C^{ar}), 114.7 (s, C^{ar}), 113.3 (s, C^{ar}), 62.1 (s, OCH₃), 34.8 (NCH₃), 34.5 (s, NCH₃), 14.3 (s, CH₃).

530 mg (2.08 mmol, 80%) from 1,3-dimethyl-5-(ethoxycarbonyl)-1H-benzimidazol-3-ium iodide (900 mg, 2.60 mmol, 1.00 eq.), Ag₂CO₃ (817 mg, 2.96 mmol, 1.14 eq.), HNO₃ (25 drops) and HCl (495 μL, 5.98 mmol, 2.30 eq.) in EtOH (50.0 mL). ¹H NMR (500 MHz, CDCl₃) δ_H = 10.9 (s, 1H, CH), 8.35 (s, 1H, H^{ar}), 8.30 (d, *J* = 8.7 Hz, 1H, H^{ar}), 7.71 (d, *J* = 8.7 Hz, 1H, H^{ar}), 4.41 (q, *J* = 7.1 Hz, 2H, OCH₂), 4.19 (d, *J* = 6.8 Hz, 6H, NCH₃), 1.40 (t, *J* = 7.1 Hz, 3H, CH₃); ¹³C NMR (125 MHz, CDCl₃) δ_C = 164.9 (s, COOCH₂), 146.1 (s, NCN), 134.5 (s, C^{ar}), 131.8 (s, C^{ar}), 129.6 (s, C^{ar}), 128.1 (s, C^{ar}), 114.6 (s, C^{ar}), 113.0 (s, C^{ar}), 62.1 (s, OCH₂), 33.8 (NCH₃), 33.7 (s, NCH₃), 14.3 (s, CH₃).

1,3-diethyl-5-(ethoxycarbonyl)-1H-benzimidazol-3-ium chloride (5b)

883 mg (2.55 mmol, 97%) from **3** (500 mg, 2.63 mmol, 1.00 eq.), K₂CO₃ (618 mg, 4.47 mmol, 1.70 eq.) and EtI (982 μL, 15.8 mmol, 6.00 eq.) in MeCN (50.0 mL). ¹H NMR (500 MHz, CDCl₃) δ_H = 11.1 (s, 1H, CH), 8.44 (s, 1H, H^{ar}), 8.36 (vdd, *J* = 8.8 Hz, 1.4 Hz, 1H, H^{ar}), 7.83 (vdd, *J* = 8.7 Hz, 1.54 Hz, 1H, H^{ar}), 4.68 (vdq, *J* = 7.4 Hz, 3.6 Hz, 4H, CH₂), 4.50 (q, *J* = 7.1 Hz, 2H, OCH₂), 1.74 (vdt, *J* = 9.7 Hz, 7.3 Hz, 6H, CH₃), 1.48 (t, *J* = 7.1 Hz, 3H, CH₃); ¹³C NMR (125 MHz, CDCl₃) δ_C = 164.8 (s, COOCH₂), 146.7 (s, NCN), 134.0 (s, C^{ar}), 131.2 (s, C^{ar}), 129.7 (s, C^{ar}), 128.1 (s, C^{ar}), 114.9 (s, C^{ar}), 112.9 (s, C^{ar}), 62.2 (s, OCH₂), 43.3 (vd, *J* = 3.2 Hz, NCH₂), 14.9 (s, CH₃), 14.7 (s, CH₃), 14.3 (s, CH₃).

422 mg (1.66 mmol, 80%) from 1,3-diethyl-5-(ethoxycarbonyl)-1H-benzimidazol-3-ium iodide (717 mg, 1.92 mmol, 1.00 eq.), Ag₂CO₃ (602 mg, 2.18 mmol, 1.14 eq.), HNO₃ (20 drops) and HCl (365 μL, 4.41 mmol, 2.30 eq.) in EtOH (50.0 mL). ¹H NMR (500 MHz, CDCl₃)

$\delta_{\text{H}} = 11.4$ (s, 1H, CH), 8.42 (s, 1H, H^{ar}), 8.36 (dd, $J = 8.7$ Hz, 1.4 Hz, 1H, H^{ar}), 7.79 (dd, $J = 8.7$ Hz, 1.54 Hz, 1H, H^{ar}), 4.73 (dq, $J = 7.4$ Hz, 1.3 Hz, 4H, CH₂), 4.48 (q, $J = 7.2$ Hz, 2H, OCH₂), 1.81 (dt, $J = 10.0$ Hz, 7.4 Hz, 6H, CH₃), 1.46 (t, $J = 7.2$ Hz, 3H, CH₃); ¹³C NMR (125 MHz, CDCl₃) $\delta_{\text{C}} = 164.8$ (s, COOCH₂), 143.3 (NCN), 133.9 (s, C^{ar}), 131.1 (s, C^{ar}), 129.6 (s, C^{ar}), 128.2 (s, C^{ar}), 114.9 (s, C^{ar}), 113.6 (s, C^{ar}), 62.1 (s, OCH₃), 43.7 (NCH₂), 43.5 (NCH₂), 14.9 (s, CH₃), 14.8 (s, CH₃), 14.3 (s, CH₃) .

1,3-dibenzyl-5-(ethoxycarbonyl)-1H-benzimidazol-3-ium chloride (5c)

933 mg (2.07 mmol, 98%) from **3** (400 mg, 2.10 mmol, 1.00 eq.), K₂CO₃ (494 mg, 3.58 mmol, 1.70 eq.) and BnBr (1.50 mL, 12.6 mmol, 6.00 eq.) in MeCN (40.0 mL). ¹H NMR (500 MHz, CDCl₃) $\delta_{\text{H}} = 12.1$ (s, 1H, CH), 8.30 (s, 1H, H^{ar}), 8.21 (d, $J = 8.5$ Hz, 1H, H^{ar}), 7.72-7.36 (m, 11H, H^{ar}), 5.93 (s, 4H, CH₂), 4.43 (q, $J = 7.1$ Hz, 2H, OCH₂), 1.42 (t, $J = 7.1$ Hz, 3H, CH₃); ¹³C NMR (125 MHz, CDCl₃) $\delta_{\text{C}} = 164.6$ (s, COOCH₂), 134.0 (s, C^{ar}), 132.5 (s, C^{ar}), 132.3 (s, C^{ar}), 131.2 (s, C^{ar}), 129.5 (s, C^{ar}), 129.4 (s, C^{ar}), 129.3 (s, C^{ar}), 129.2 (s, C^{ar}), 128.5 (s, C^{ar}), 128.4 (s, C^{ar}), 128.0 (s, C^{ar}), 115.5 (s, C^{ar}), 114.3 (s, C^{ar}), 61.9 (s, OCH₂), 52.0 (NCH₂), 51.9 (s, NCH₂), 14.2 (s, CH₃).

72.0 mg (177 μ mol, 67%) from 1,3-diethyl-5-(ethoxycarbonyl)-1H-benzimidazol-3-ium bromide (120 mg, 266 μ mol, 1.00 eq.), Ag₂CO₃ (83.6 mg, 303 μ mol, 1.14 eq.), HNO₃ (3 drops) and HCl (50.6 μ L, 612 μ mol, 2.30 eq.) in EtOH (5.00 mL). ¹H NMR (500 MHz, CDCl₃) $\delta_{\text{H}} = 11.3$ (s, 1H, CH), 8.21 (s, 1H, H^{ar}), 8.12 (dd, $J = 8.7$ Hz, 1.4 Hz, 1H, H^{ar}), 7.64 (d, $J = 8.7$ Hz, 1H, H^{ar}), 7.46-7.42 (m, 4H, H^{ar}), 7.35-7.25 (m, 6H, H^{ar}), 5.77 (s, 2H, NCH₂), 5.76 (s, 2H, NCH₂), 4.34 (q, $J = 7.1$ Hz, 2H, OCH₂), 1.35 (t, $J = 7.1$ Hz, 3H, CH₃); ¹³C NMR (125 MHz, CDCl₃) $\delta_{\text{C}} = 164.7$ (s, COOCH₂), 146.5 (NCN), 134.1 (s, C^{ar}), 132.5 (s, C^{ar}), 132.4 (s, C^{ar}), 131.4 (s, C^{ar}), 129.5 (s, C^{ar}), 129.4 (s, C^{ar}), 129.3 (s, C^{ar}), 128.4 (s, C^{ar}), 128.0 (s, C^{ar}), 115.5 (s, C^{ar}), 114.0 (s, C^{ar}), 62.0 (s, OCH₂), 51.9 (NCH₂), 51.8 (s, NCH₂), 14.2 (s, CH₃).

1.3 General procedure for silver complexation

Benzimidazoleium-5-carboxylate chloride (1.00 eq.) and Ag₂O (0.50 eq.) were dissolved in CH₂Cl₂ (25 mL/mmol) and stirred for 24 h while being shielded from light. Subsequently the solution was filtered over Celite, concentrated and the residue precipitated in *n*-pentane. After drying *in vacuo*, the product could be isolated as white powder.

[5-methoxycarbonyl-1,3-dimethylbenzimidazol-2-ylidene] silver(I) chlorido (6a)

385 mg (1.11 mmol, 89%) from **04a** (300 mg, 1.25 mmol, 1.00 eq.), Ag₂O (144 mg, 623 μmol, 0.50 eq.) in CH₂Cl₂ (30.0 mL). ¹H NMR (500 MHz, DMSO-d₆) δ_H = 8.19 (s, 1H, H^{ar}), 8.14 (vdd, *J* = 8.5 Hz, 1.5 Hz, 1H, H^{ar}), 7.50 (vdd, *J* = 8.6 Hz, 0.6 Hz, 1H, H^{ar}), 4.11 (d, *J* = 6.7 Hz, 6H, NCH₃), 3.99 (s, 3H, OCH₃); ¹³C NMR (125 MHz, CDCl₃) δ_C = 166.3 (s, COOCH₃), 137.1 (s, C^{ar}), 134.2 (s, C^{ar}), 126.5 (s, C^{ar}), 125.8 (s, C^{ar}), 113.2 (s, C^{ar}), 111.0 (s, C^{ar}), 52.7 (s, OCH₃), 36.0 (s, NCH₃).

[5-methoxycarbonyl-1,3-diethylbenzimidazol-2-ylidene] silver(I) chlorido (6b)

34.0 mg (90.5 μmol, 35%) from **04b** (70.0 mg, 261 μmol, 1.00 eq.), Ag₂O (36.2 mg, 133 μmol, 0.50 eq.) in CH₂Cl₂ (50.0 mL). ¹H NMR (500 MHz, DMSO-d₆) δ_H = 8.43 (s, 1H, H^{ar}), 8.07 (d, *J* = 8.5 Hz, 1H, H^{ar}), 7.99 (d, *J* = 8.6 Hz, 1H, H^{ar}), 4.63 (q, *J* = 7.3 Hz, 4H, CH₂), 3.93 (s, 3H, OCH₃), 1.49 (t, *J* = 7.5 Hz, 6H, CH₃); ¹³C NMR (125 MHz, CDCl₃) δ_C = 198.1 (s, NCN), 166.7 (s, COOCH₃), 136.6 (s, C^{ar}), 133.6 (s, C^{ar}), 125.4 (s, C^{ar}), 124.9 (s, C^{ar}), 112.9 (s, C^{ar}), 110.6 (s, C^{ar}), 52.5 (s, OCH₃), 44.3 (d, *J* = 4.1 Hz, NCH₂), 16.1 (s, CH₃), 16.0 (s, CH₃).

[5-methoxycarbonyl-1,3-dibenzylbenzimidazol-2-ylidene] silver(I) chlorido (6c)

Yield: 452 mg (904 μmol, 89%) from **04c** (400 mg, 1.02 mmol, 1.00 eq.), Ag₂O (142 mg, 611 μmol, 0.50 eq.) in CH₂Cl₂ (25.0 mL). ¹H NMR (500 MHz, CDCl₃) δ_H = 8.29 (s, 1H, H^{ar}), 7.99 (vdd, *J* = 8.7 Hz, 1.5 Hz, 1H, H^{ar}), 7.87 (d, *J* = 8.7 Hz, 1H, H^{ar}), 7.38-7.27 (m, 10H, H^{ar}),

5.86 (s, 2H, CH₂), 5.80 (s, 2H, CH₂) 3.86 (s, 3H, OCH₃); ¹³C NMR (125 MHz, CDCl₃) δ_C = 196.2 (s, NCN), 166.2 (s, COOCH₃), 136.9 (s, C^{ar}), 135.2 (s, C^{ar}), 135.1 (s, C^{ar}), 134.0 (s, C^{ar}), 129.1 (s, C^{ar}), 129.0 (s, C^{ar}), 128.4 (s, C^{ar}), 127.3 (s, C^{ar}), 126.2 (s, C^{ar}), 125.6 (s, C^{ar}), 113.6 (s, C^{ar}), 111.8 (s, C^{ar}), 53.5 (s, OCH₃), 53.2 (NCH₂), 52.5 (s, NCH₂).

[5-ethoxycarbonyl-1,3-dimethylbenzimidazol-2-ylidene] silver(I) chlorido (7a)

434 mg (1.20 mmol, 92%) from **05a** (380 mg, 1.49 mmol, 1.00 eq.), Ag₂O (173 mg, 746 μmol, 0.50 eq.) in CH₂Cl₂ (40.0 mL). ¹H NMR (500 MHz, CDCl₃) δ_H = 8.21 (s, 1H, H^{ar}), 8.17 (vdd, *J* = 8.5 Hz, 1.5 Hz, 1H, H^{ar}), 7.53 (d, *J* = 8.5 Hz 1H, H^{ar}), 4.45 (q, *J* = 7.0 Hz, 2H, OCH₂), 4.12 (s, 6H, NCH₃), 1.45 (t, *J* = 7.0 Hz, 3H, CH₃); ¹³C NMR (125 MHz, CDCl₃) δ_C = 191.8 (s, NCN), 165.8 (s, COOCH₂), 137.1 (s, C^{ar}), 134.2 (s, C^{ar}), 126.9 (s, C^{ar}), 125.9 (s, C^{ar}), 113.2 (s, C^{ar}), 111.0 (s, C^{ar}), 61.7 (s, OCH₂), 36.1 (d, *J* = 3.6 Hz, NCH₃), 14.4 (s, CH₃).

[5-ethoxycarbonyl-1,3-diethylbenzimidazol-2-ylidene] silver(I) chlorido (7b)

507 mg (1.30 mmol, 74%) from **(5b)** (450 mg, 1.59 mmol, 1.00 eq.), Ag₂O (205 mg, 883 μmol, 0.50 eq.) in CH₂Cl₂ (45.0 mL). ¹H NMR (500 MHz, CDCl₃) δ_H = 8.22 (s, 1H, H^{ar}), 8.14 (vdd, *J* = 8.6 Hz, 1.4 Hz, 1H, H^{ar}), 7.55 (d, *J* = 8.6 Hz 1H, H^{ar}), 4.52 (vdq, *J* = 9.0 Hz, 7.3 Hz, 4H, NCH₂), 4.45 (q, *J* = 7.1 Hz, 2H, OCH₂), 1.57 (vdt, *J* = 9.0 Hz, 7.3 Hz, 6H, CH₃), 1.44 (t, *J* = 7.1 Hz, 3H, CH₃); ¹³C NMR (125 MHz, CDCl₃) δ_C = 189.3 (s, NCN), 165.8 (s, COOCH₂), 136.2 (s, C^{ar}), 133.3 (s, C^{ar}), 126.8 (s, C^{ar}), 125.7 (s, C^{ar}), 113.3 (s, C^{ar}), 111.2 (s, C^{ar}), 61.7 (s, OCH₂), 45.0 (d, *J* = 2.7 Hz, NCH₂), 16.1 (s, CH₃), 16.0 (s, CH₃), 14.4 (s, CH₃).

Chlorido [5-ethoxycarbonyl-1,3-dibenzylbenzimidazol-2-ylidene] silver(I) chlorido (7c)

313 mg (609 μmol, 83%) from **5c** (300 mg, 737 μmol, 1.00 eq.), Ag₂O (85.4 mg, 369 μmol, 0.50 eq.) in CH₂Cl₂ (15.0 mL). ¹H NMR (500 MHz, CDCl₃) δ_H = 8.10 (s, 1H, H^{ar}), 8.01 (d, *J* = 8.6 Hz, 1H, H^{ar}), 7.40 – 7.30 (m, 11H, H^{ar}), 5.68 (s, 4H, NCH₂), 4.37 (q, *J* = 7.1 Hz, 2H, OCH₂), 1.37 (t, *J* = 7.1 Hz, 3H, CH₃); ¹³C NMR (125 MHz, CDCl₃) δ_C = 196.0 (s, NCN), 165.7 (s,

COOCH₂), 136.8 (s, C^{ar}), 135.0 (s, C^{ar}), 134.0 (s, C^{ar}), 129.1 (s, C^{ar}), 128.5 (s, C^{ar}), 127.4 (s, C^{ar}), 127.3 (s, C^{ar}), 126.7 (s, C^{ar}), 113.7 (s, C^{ar}), 111.7 (s, C^{ar}), 61.5 (s, OCH₂), 53.5 (NCH₂), 53.3 (s, NCH₂), 14.3 (s, CH₃).

1.4 Procedures for the synthesis of the precursors of clickable complexes **16** and **22**

Methyl 1-(prop-2-yn-1-yl)-1H-benzimidazol-5-carboxylate (14)

2 (600 mg, 3.41 mmol, 1.00 eq.) and K₂CO₃ (471 mg, 3.41 mmol, 1.00 eq.) were suspended in DMF (50 mL). The mixture was treated with bromopropyne (760 μL, 6.82 mmol, 80% in toluene, 2.00 eq.) and stirred at 60 °C for 24 h. Subsequently the solvent was removed under reduced pressure and the residue was dissolved in chloroform (150 mL). Water (2 · 150 mL) was added to remove K₂CO₃ and the combined aqueous phases were extracted with chloroform (150 mL). The combined organic phases were dried over Na₂SO₄, filtered and the solvent was concentrated in vacuum. The crude product was purified by column chromatography (Silica gel 60, EtOAc/MeOH 95:5) affording it as brown powder (594 mg, 2.76 mmol, 81%) after drying *in vacuo*. R_f = 0.52 (EtOAc/MeOH 95:5); ¹H NMR (500 MHz, CDCl₃) δ_H = 8.54 (dd, *J* = 1.5 Hz, 0.7 Hz, 1H, H^{ar}), 8.24 (dd, *J* = 1.5 Hz, 0.7 Hz, 1H, H^{ar}), 8.16 (s, 1H, H^{ar}), 8.11 (s, 1H, H^{ar}), 8.08 (dd, *J* = 8.5 Hz, 1.5 Hz, 1H, H^{ar}), 8.03 (dd, *J* = 8.5 Hz, 1.6 Hz, 1H, H^{ar}), 7.83 (dd, *J* = 8.5 Hz, 0.7 Hz, 1H, H^{ar}), 7.51 (dd, *J* = 8.6 Hz, 0.6 Hz, 1H, H^{ar}), 4.99 (d, *J* = 2.6 Hz, 4H, NCH₂), 3.97 (s, 6H, OMe), 2.54 (dt, *J* = 6.1 Hz, 2.6 Hz, 2H, CH). ¹³C NMR (125 MHz, CDCl₃) δ_C = 167.4 (s, COOMe), 167.3 (s, COOMe), 147.4 (s, C^{ar}), 144.8 (s, C^{ar}), 143.9 (s, C^{ar}), 143.6 (s, C^{ar}), 136.5 (s, C^{ar}), 133.1 (s, C^{ar}), 125.3 (s, C^{ar}), 125.0 (s, C^{ar}), 124.9 (s, C^{ar}), 124.0 (s, C^{ar}), 123.0 (s, C^{ar}), 120.3 (s, C^{ar}), 112.0 (s, C^{ar}), 109.5 (s, C^{ar}), 75.6 (s, CH), 75.4 (s, CH), 52.3 (OMe), 52.2 (OMe), 34.9 (NCH₂).

5-(methoxycarbonyl)-1,3-di(prop-2-yn-1-yl)-1H-benzimidazol-3-ium chloride (15)

14 (561 mg, 2.62 mmol, 1.00 eq.) and bromopropyne (1.16 mL, 10.5 mmol, 80% in toluene, 4.00 eq.) were dissolved in 1,4-dioxane (20 mL). The mixture was stirred at 130 °C for 24 h. Subsequently the solution was cooled to rt and filtered. The filter cake was rinsed with cold 1,4-dioxane and dried in vacuum affording the product as brown powder (784 mg, 2.35 mmol, 90%) after drying *in vacuo*. ¹H NMR (500 MHz, CDCl₃) δ_H = 11.8 (s, 1H, NCHN), 8.61 (s, 1H, H^{ar}), 8.39 (dd, *J* = 8.8 Hz, 1.4 Hz, 1H, H^{ar}), 8.00 (d, *J* = 8.8 Hz, 1H, H^{ar}), 5.68 (d, *J* = 2.6 Hz, 4H, NCH₂), 4.03 (s, 3H, OMe), 2.71 (dt, *J* = 10.9 Hz, 2.6 Hz, 2H, CH). ¹³C NMR (125 MHz, CDCl₃) δ_C = 166.1 (s, COOMe), 144.9 (s, C^{ar}), 133.6 (s, C^{ar}), 130.9 (s, C^{ar}), 129.9 (s, C^{ar}), 128.7 (s, C^{ar}), 115.7 (s, C^{ar}), 114.0 (s, C^{ar}), 78.4 (s, CH), 78.2 (s, CH), 53.1 (OMe), 38.4 (NCH₂).

5-(methoxycarbonyl)-1,3-di(prop-2-yn-1-yl)-1H-benzimidazol-3-ium bromide (400 mg, 1.20 mmol, 1.00 eq.) and Ag₂CO₃ (377 mg, 1.37 mmol, 1.14 eq.) were suspended in EtOH (25 mL). Concentrated HNO₃ (12 drops) was added and the suspension was stirred for 3.5 h while being shielded from light. After the silver halides were filtered off, concentrated HCl (300 μL, 2.76 mmol, 2.30 eq.) was added dropwise and the solution stirred for 10 min. Afterwards the solution was neutralized by adding saturated NaHCO_{3(aq)} and filtered once more. Subsequently the solvent was evaporated and the residue was dissolved in CH₂Cl₂. After another filtration step, the solution was concentrated and precipitated in *n*-pentane. After drying *in vacuo*, the product could be isolated as yellow powder (202 mg, 700 μmol, 58%). ¹H NMR (500 MHz, CDCl₃) δ_H = 11.2 (s, 1H, NCHN), 8.55 (s, 1H, H^{ar}), 8.33 (dd, *J* = 8.7 Hz, 1.5 Hz, 1H, H^{ar}), 8.00 (d, *J* = 8.8 Hz, 1H, H^{ar}), 5.52 (t, *J* = 3.2 Hz, 4H, NCH₂), 4.03 (s, 3H, OMe), 2.69 (dt, *J* = 10.2 Hz, 2.6 Hz, 2H, CH).

1-((allyloxy)carbonyl)-1H-benzimidazol-5-carboxylic acid (17)

1 (1.30 g, 8.02 mmol, 1.00 eq.) was dissolved in 10% Na₂CO_{3(aq.)} (22.5 mL) and 1,4-dioxane (13.5 mL) and cooled to 0 °C. Allyl chloroformate (1.71 mL, 16.0 mmol, 2.00 eq.) was added dropwise and the mixture was left stirring at rt for 16 h. Afterwards the solution was washed with Et₂O (3 · 50 mL) and the aqueous phase was acidified with 2 n HCl. After extraction with EtOAc (5 · 60 mL), the combined organic phases were dried over MgSO₄, filtrated and the solvent was evaporated. The residue was dried in vacuo affording **17** (1.91 g, 7.78 mmol, 97%) as beige powder. ¹H NMR (500 MHz, MeOD) δ_H = 8.56 (s, 1H, H^{ar}), 8.46 (s, 1H, H^{ar}), 7.90 – 7.85 (m, 1H, H^{ar}), 7.56 (d, *J* = 8.4 Hz, 1H, H^{ar}), 6.04 – 5.96 (m, 1H, H^{alloc}), 5.41 – 5.36 (m, 1H, H^{alloc}), 5.25 (d, *J* = 10.5 Hz, 1H, H^{alloc}), 4.86 (d, *J* = 6.9 Hz, 2H, H^{alloc}); ¹³C NMR (125 MHz, MeOD) δ_C = 168.3 (s, COOH), 148.7 (s), 146.2 (s), 130.9 (s), 126.7 (s), 125.8 (s), 124.0 (s), 121.5 (s), 119.3 (s), 119.2 (s), 116.1 (s), 113.8 (s), 68.6 (s).

Only one regioisomer shown.

1-allyl 5-((2,3-dimethylcycloprop-2-en-1-yl)methyl) 1H-benzimidazol-1,5-dicarboxylate (18)

17 (1.86 g, 7.55 mmol, 1.30 eq.) was suspended in dry CH₂Cl₂ (100 mL) and cooled to 0 °C. DMAP (922 mg, 7.55 mmol, 1.30 eq.) and EDC·HCl (1.45 g, 7.55 mmol, 1.30 eq.) were added portionwise and the solution was left stirring at 0 °C for 1h after which 2,3-Dimethyl-2-cyclopropene-1-methanol (570 mg, 5.81 mmol, 1.00 eq.) in dry CH₂Cl₂ (30 mL) was added dropwise over a period of 30 min. After complete addition, stirring was continued for 24 h at rt. Consequently the solution was diluted with EtOAc and washed with 0.5 m H₂SO₄. The aqueous phase was extracted with EtOAc (3 · 100 mL) and the combined organic phases were dried over Na₂SO₄. The solvent was evaporated after filtration and the residue was purified via column chromatography (Cyclohexane/EtOAc 3:1) affording the ester as yellowish oil (1.10 g, 3.37 mmol, 58%). R_f (Cyclohexane/EtOAc 3:1): 0.20; 0.16; ¹H NMR (500 MHz, CDCl₃) δ_H = 8.48 (s, 1H, H^{ar}), 8.45 (d, *J* = 1.5 Hz, 1H, H^{ar}), 8.09 (dd, *J* = 8.5 Hz, 1.5 Hz, H^{ar}), 8.00 (d, *J* =

8.6 Hz, 1H, H^{ar}), 6.08 – 6.00 (m, 1H, H^{Alloc}), 5.47 (dd, $J = 17.2$ Hz, 1.4 Hz, 1H, H^{Alloc}), 5.38 (dd, $J = 10.4$ Hz, 1.2 Hz, 1H, H^{Alloc}), 4.94 (d, $J = 8.6$ Hz, 2H, CH₂^{Alloc}), 4.20 (d, $J = 5.2$ Hz, OCH₂), 2.00 (s, 6H, CH₃), 1.63 (t, $J = 5.2$ Hz, 1H, CH); ¹³C NMR (125 MHz, CDCl₃) $\delta_C = 166.5$ (s, COOCH₂), 148.9 (s, NCOOCH₂), 143.8 (s, NCN), 134.2 (s, C^{ar}), 130.4 (s, C^{ar}), 127.7 (s, C^{ar}), 126.9 (s, C^{ar}), 122.5 (s, C^{ar}), 120.8 (s, C^{ar}), 114.0 (s, C^{ar}), 109.7 (s, C=C), 72.7 (s, OCH₂), 68.7 (s, OCH₂), 26.9 (s), 19.2 (s), 10.4 (s, CH₃).

Only one regioisomer shown.

(2,3-dimethylcycloprop-2-en-1-yl)methyl 1H-benzimidazol-5-carboxylate (19)

18 (450 mg, 1.38 mmol, 1.00 eq.) was dissolved in dry THF (10 mL) and Et₂NH (428 μ L, 4.14 mmol, 3.00 eq.), dppb (29.4 mg, 68.9 μ mol, 0.05 eq.) and Pd(dba)₂ (39.6 mg, 68.9 μ mol, 0.05 eq.) were added. The solution was left stirring at rt for 1h after which it was filtrated over a bed of Celite® and silica. The solvent was evaporated and the residue was purified via column chromatography (EtOAc/MeOH 98:2) affording the ester as yellow oil (250 mg, 1.03 mmol, 75%). Rf (Cyclohexane/EtOAc 3:1): 0.24; ¹H NMR (500 MHz, MeOD) $\delta_H = 8.33$ (s, 2H, H^{ar}), 7.98 (dd, $J = 8.5$ Hz, 1.5 Hz, 1H, H^{ar}), 7.67 (d, $J = 8.6$ Hz, H^{ar}), 4.24 (d, $J = 5.0$ Hz, 1H, H^{ar}), 2.04 (s, 6H, CH₃), 1.67 (t, $J = 5.0$ Hz, 1H, CH); ¹³C NMR (125 MHz, MeOD) $\delta_C = 167.3$ (s, COOCH₂), 143.7 (s, NCN), 123.6 (s, C^{ar}), 109.7 (s, C=C), 71.9 (s, OCH₂), 38.6 (s, OCH₂), 19.2 (s, CH), 8.8 (s, CH₃).

5-(((2,3-dimethylcycloprop-2-en-1-yl)methoxy)carbonyl)-1,3-diethyl-1H-benzimidazol-3-ium iodide (20)

19 (275 mg, 1.14 mmol, 1.00 eq.) and K₂CO₃ (314 mg, 2.27 mmol, 2.00 eq.) were suspended in MeCN (20 mL). The mixture was treated with EtI (1.64 mL, 20.5 mmol, 18.0 eq.) and stirred

at 70 °C for 24 h. Subsequently the solvent was removed under reduced pressure and the residue was dissolved in CH₂Cl₂. After filtration, the solvent was evaporated affording the ylidine iodide as yellow powder (246 mg, 825 μmol, 72%). ¹H NMR (500 MHz, CDCl₃) δ_H = 11.25 (s, NCHN), 8.41 (d, *J* = 1.4 Hz, 1H, H^{ar}), 8.34 (dd, *J* = 8.7 Hz, 1.5 Hz, 1H, H^{ar}), 7.81 (d, *J* = 8.8 Hz, H^{ar}), 4.74 (vp, *J* = 7.3 Hz, 4H, NCH₂), 4.29 (d, *J* = 5.2 Hz, 2H, CH₂), 2.02 (s, 6H, CH₃), 1.80 (dt, *J* = 9.2 Hz, 7.3 Hz, 6H, CH₃), 1.67 (t, *J* = 5.2 Hz, 1H, CH); ¹³C NMR (125 MHz, CDCl₃) δ_C = 164.9 (s, COOCH₂), 143.5 (s, NCN), 133.8 (s, C^{ar}), 131.1 (s, C^{ar}), 130.3 (s, C^{ar}), 128.2 (s, C^{ar}), 114.9 (s, C^{ar}), 113.1 (s, C^{ar}), 109.6 (s, C=C), 73.9 (s, OCH₂), 43.5 (d, *J* = 18.2 Hz, CH₃), 19.3 (s, CH), 14.9 (d, *J* = 3.5 Hz, CH₃), 10.5 (s, CH₃).

(5-(((2,3-dimethylcycloprop-2-en-1-yl)methoxy)carbonyl)-1,3-diethylbenzimidazol-2-ylidene silver(I) iodide (21)

20 (88.0 mg, 206 μmol, 1.00 eq.) was dissolved in dry DCM (10 mL). The solution was shielded from light before Ag₂O (28.7 mg, 124 μmol, 0.60 eq.) was added. The mixture was stirred at rt for 18 hours after which the mixture was filtered over Celite® and the solvent was evaporated. Redissolving the residue in DCM and precipitating the complex in *n*-pentane afforded **21** as white powder (64.0 mg, 63.8 μmol, 58%). ¹H NMR (500 MHz, CDCl₃) δ_H = 8.16 (d, *J* = 1.4 Hz, 1H, H^{ar}), 8.07 (dd, *J* = 8.5 Hz, 1.4 Hz, 1H, H^{ar}), 7.45 (d, *J* = 8.5 Hz, H^{ar}), 4.61 (vp, *J* = 7.1 Hz, 4H, NCH₂), 4.26 (d, *J* = 5.1 Hz, 2H, CH₂), 2.03 (s, 6H, CH₃), 1.68 (t, *J* = 5.1 Hz, 1H, CH), 1.54 (dt, *J* = 7.2 Hz, 5.7 Hz, 6H, CH₃); ¹³C NMR (125 MHz, CDCl₃) δ_C = 197.0 (s, NCN), 166.3 (s, COOCH₂), 136.4 (s, C^{ar}), 133.5 (s, C^{ar}), 126.3 (s, C^{ar}), 124.8 (s, C^{ar}), 112.8 (s, C^{ar}), 110.5 (s, C^{ar}), 109.7 (s, C=C), 72.9 (s, OCH₂), 44.2 (s, CH₃), 19.3 (s, CH), 16.0 (d, *J* = 9.0 Hz, CH₃), 10.4 (s, CH₃).

2. Biological evaluation

2.1 Stock solutions

The test compounds were dissolved in DMSO with a concentration of 10 mM and stored at -23 °C. Prior to biological experiments they were diluted to desired concentration with sterile Millipore water.

2.2 Cell culture conditions

518A2 human melanoma cells (Department of Radiotherapy & Radiobiology, University Hospital Vienna, Austria), HCT116^{wt} (DSMZ ACC-581) and its HCT116^{p53^{-/-}} knockout mutant colon carcinoma cells, U87 glioblastoma cells (ATCC HTB-14), EA.hy926 somatic cell hybrid cells (ATCC CRL-2922), HeLa cervix carcinoma cells (DSMZ ACC-57), MCF-7 breast cancer cells (DSMZ ACC-115), HT-29 cisplatin resistant colon cancer cells (DSMZ ACC-299) and non-malignant human dermal fibroblasts HDFa (ATCC PCS-201-012) were cultured in Dulbeccos Modified Eagle medium (PAN biotech), supplemented with 10% (v/v) fetale bovine serum (Sigma Aldrich) and 1% (v/v) ZellShield (Minerva Biolabs) at 37 °C under 95% humidity and 5% CO₂. If not noted otherwise, all bioassay steps including cells were conducted under these standard cell culture conditions.

Appendix

NMR spectra of Pt(II) complexes

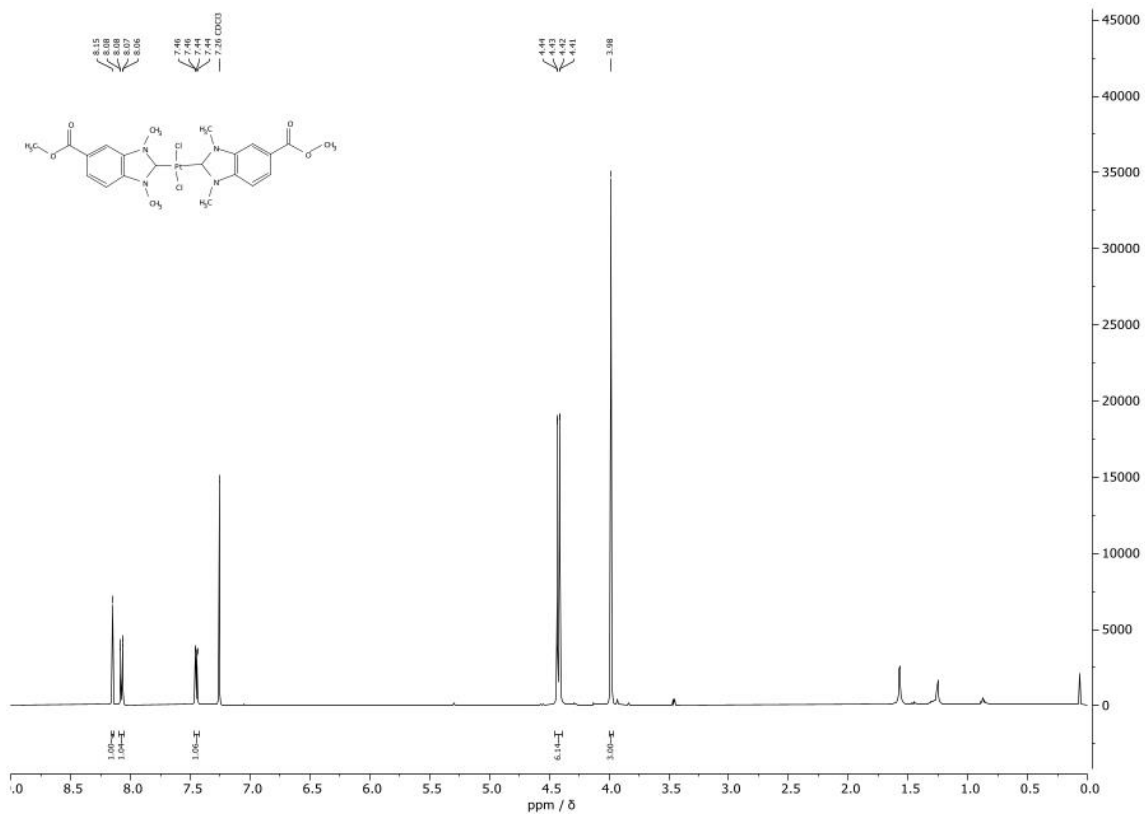


Fig. 1. $^1\text{H-NMR}$ spectrum of **8a** in CDCl_3 .

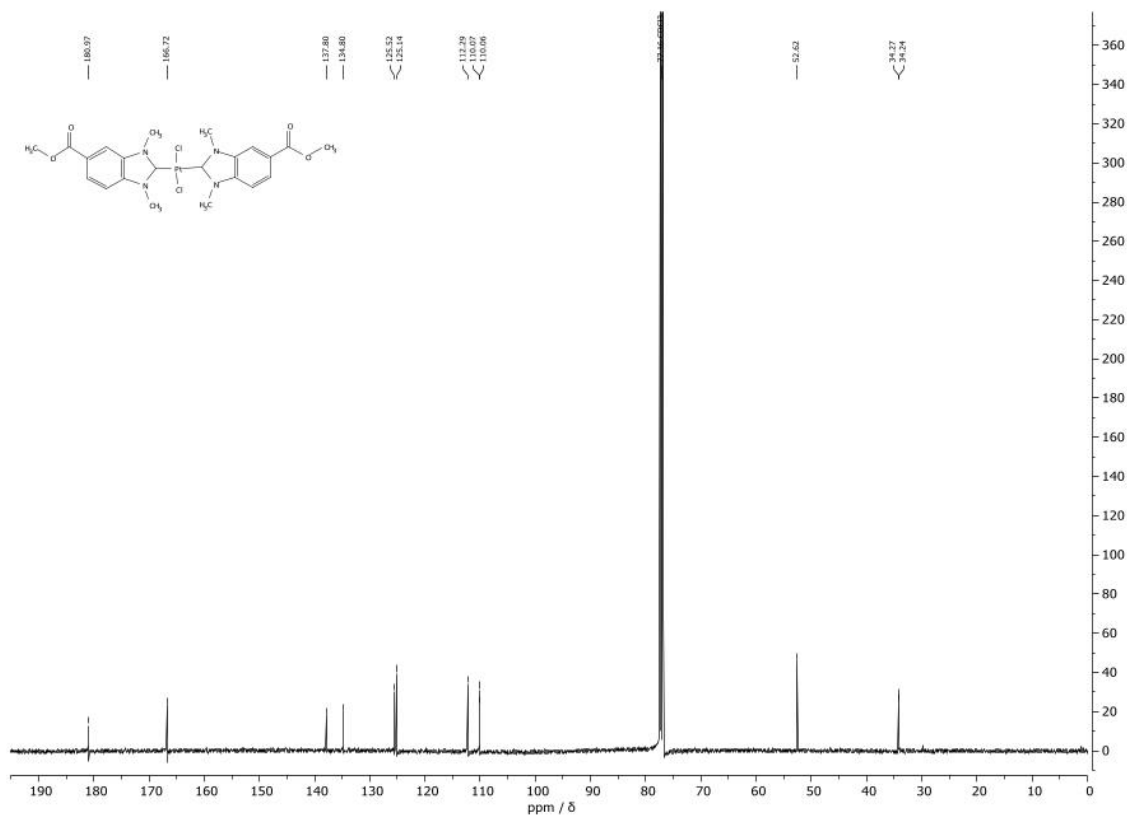


Fig. 2. $^{13}\text{C-NMR}$ spectrum of **8a** in CDCl_3 .

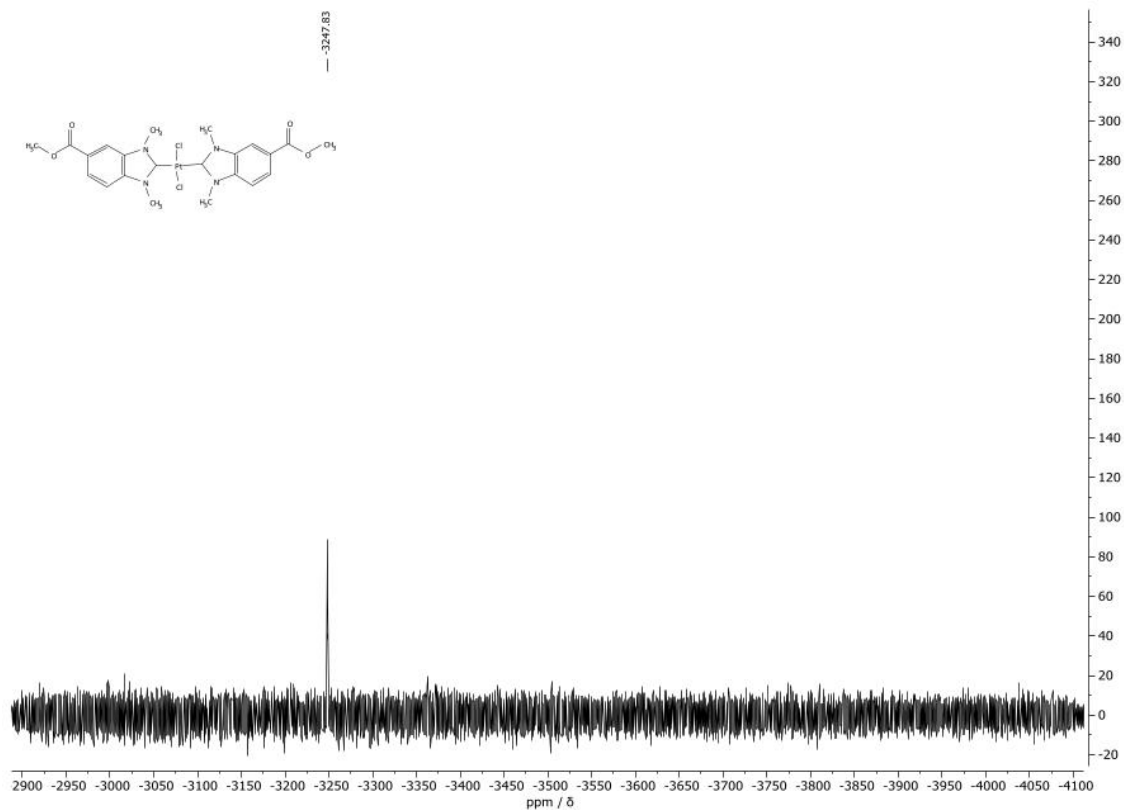


Fig. 3. ^{195}Pt -NMR spectrum of **8a** in CDCl_3 .

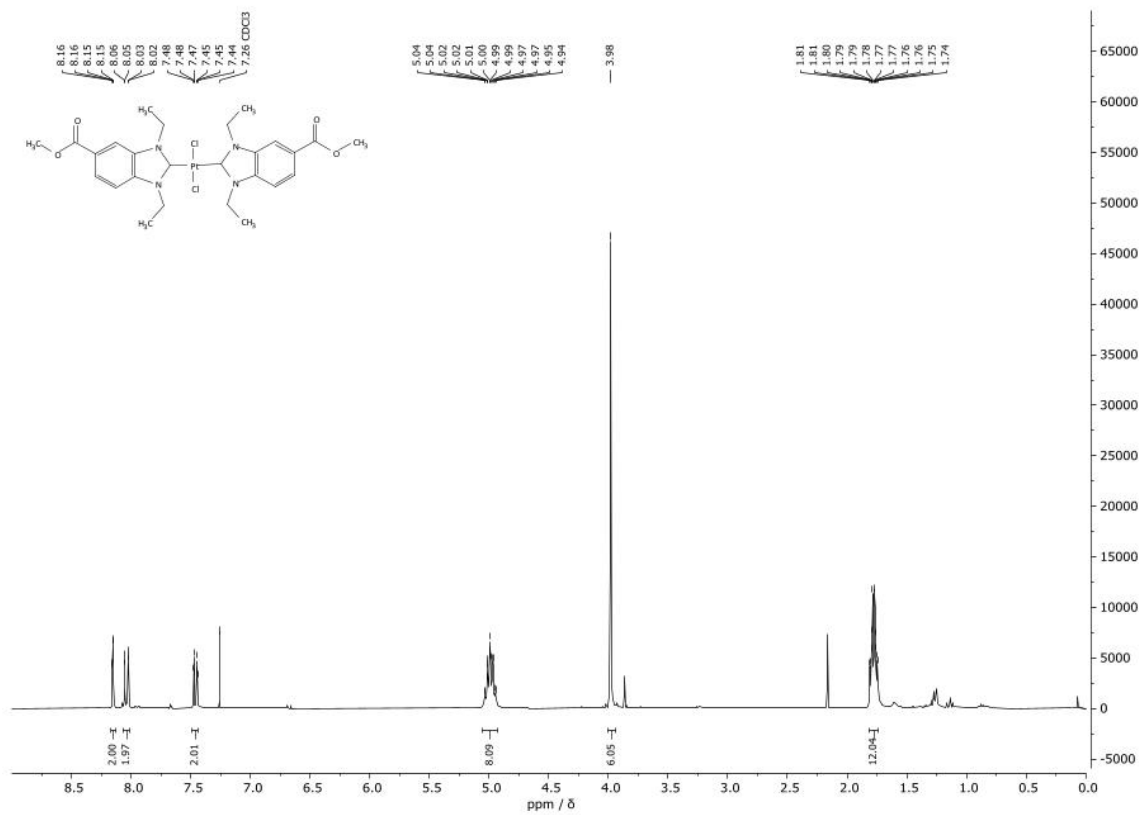


Fig. 4. ^1H -NMR spectrum of **8b** in CDCl_3 .

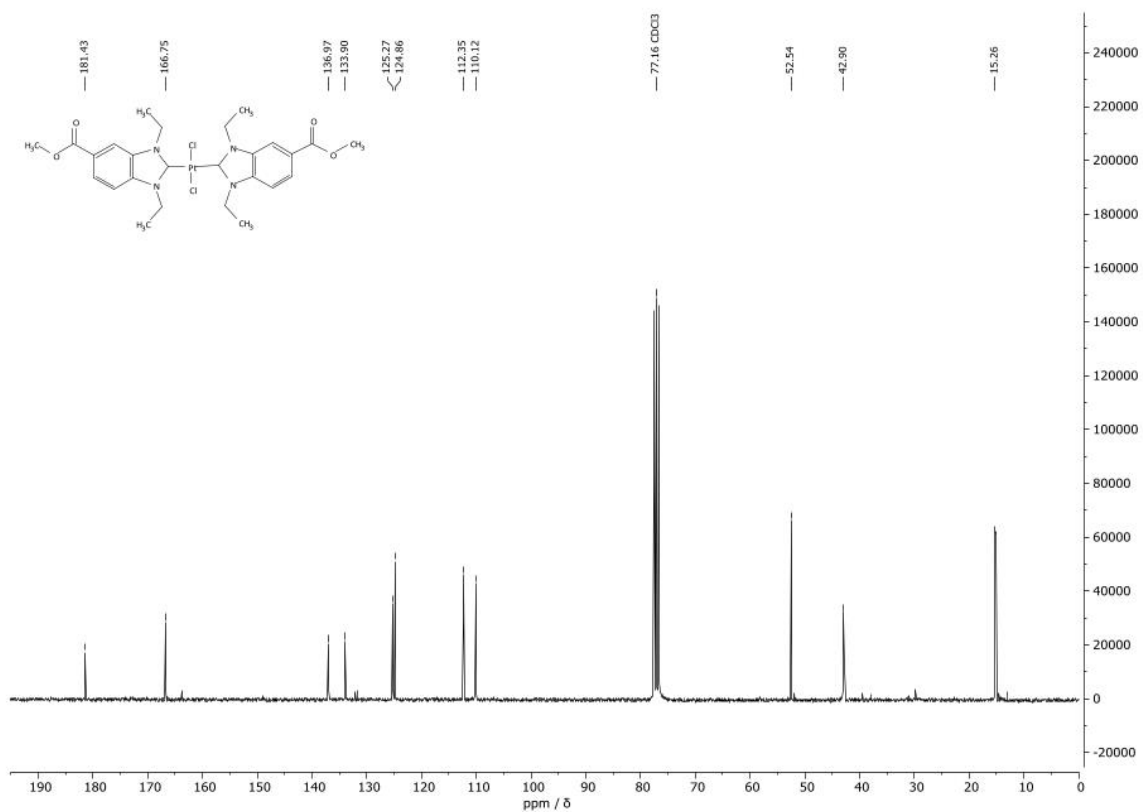


Fig. 5. ^{13}C -NMR spectrum of **8b** in CDCl_3 .

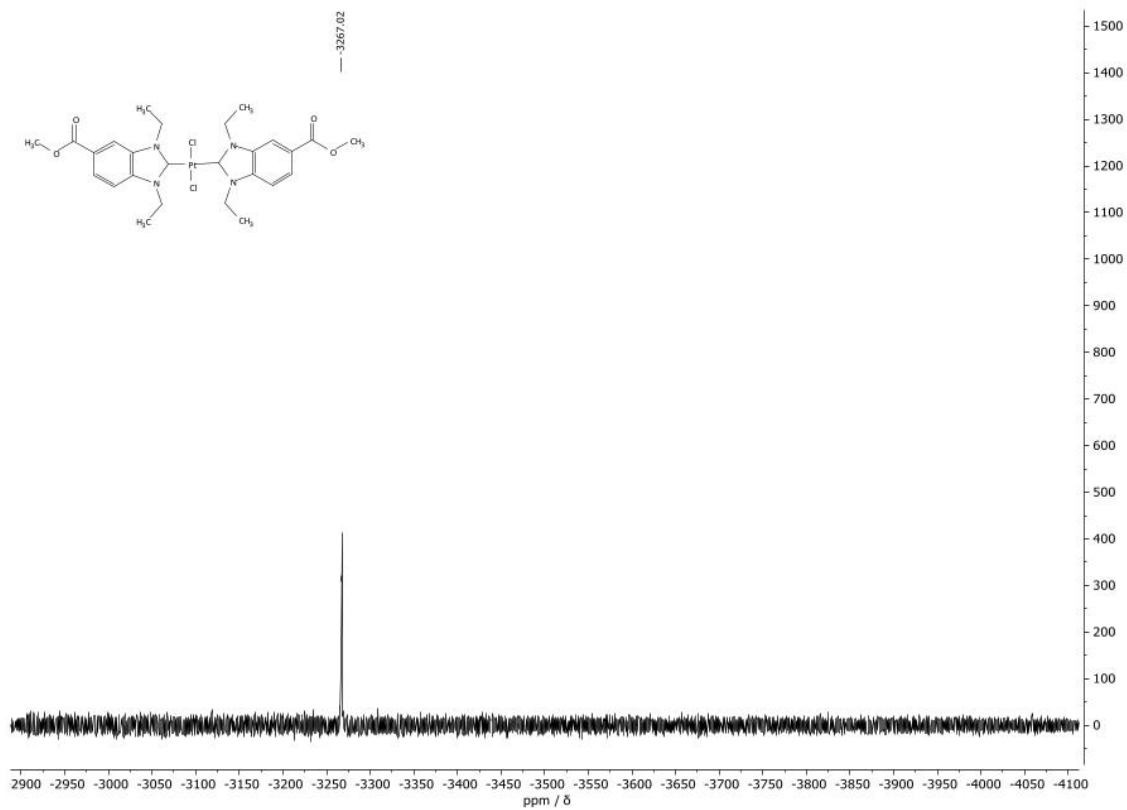


Fig. 6. ^{195}Pt -NMR spectrum of **8b** in CDCl_3 .

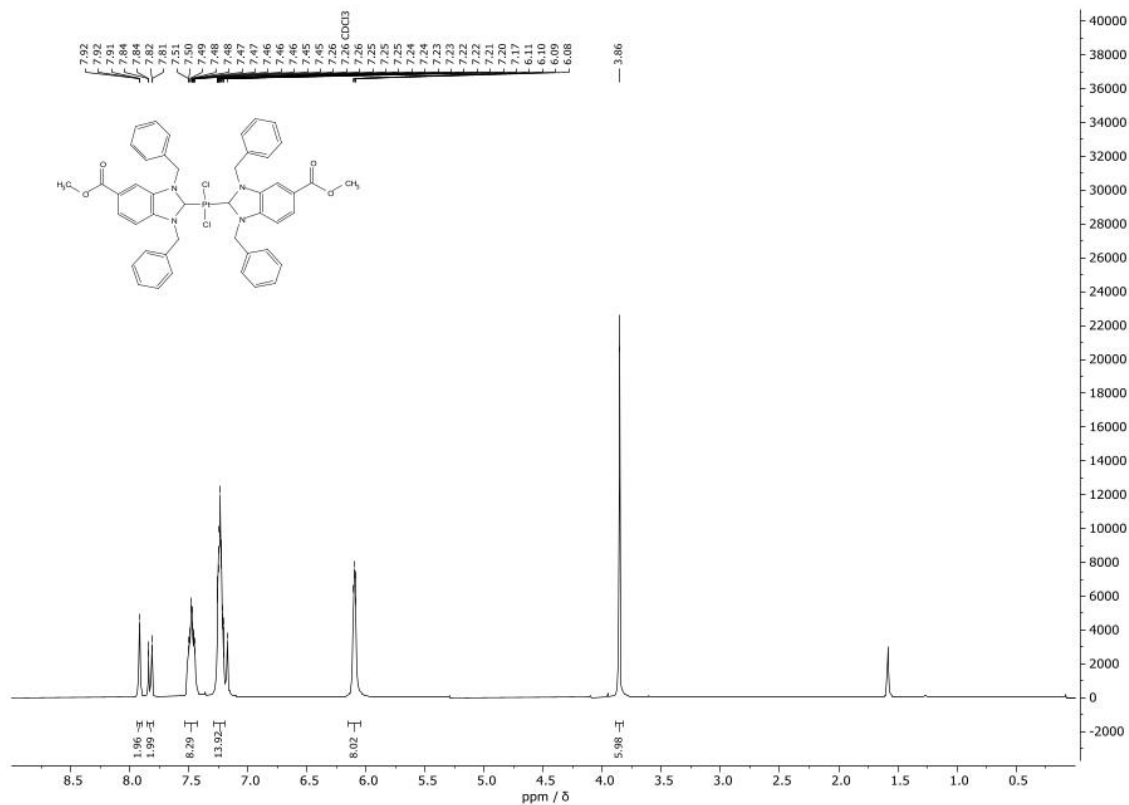


Fig. 7. $^1\text{H-NMR}$ spectrum of **8c** in CDCl_3 .

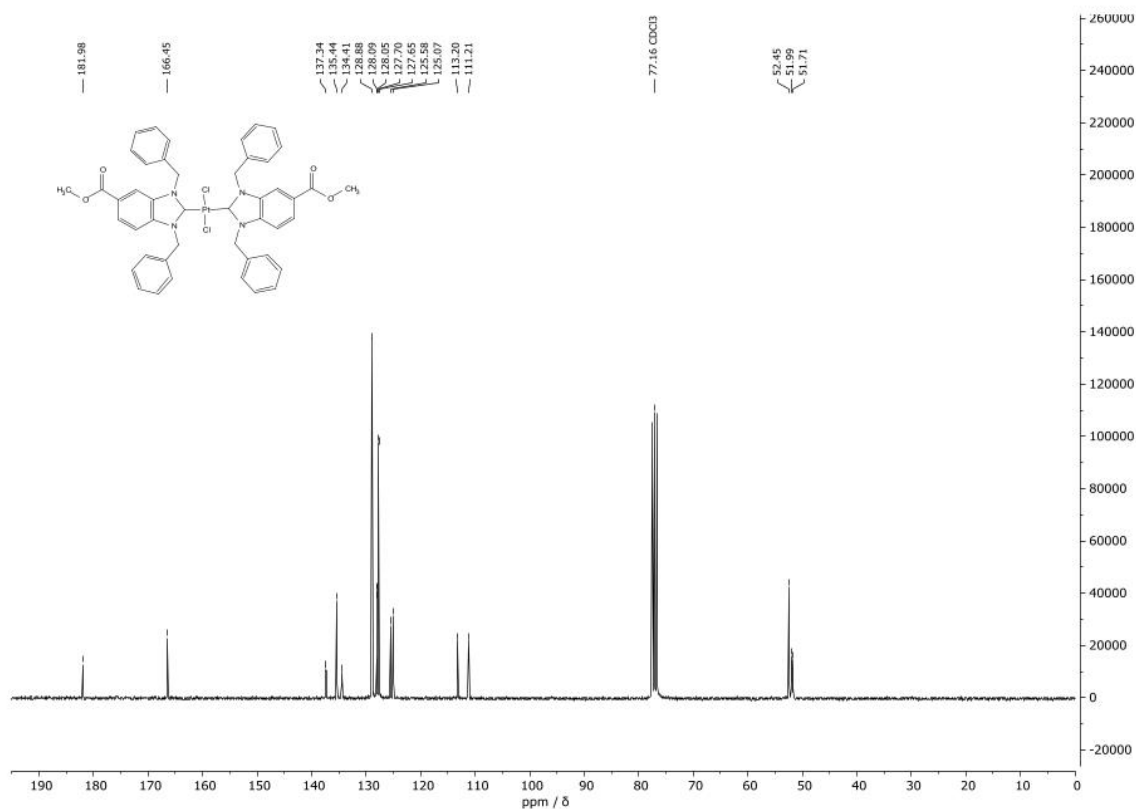
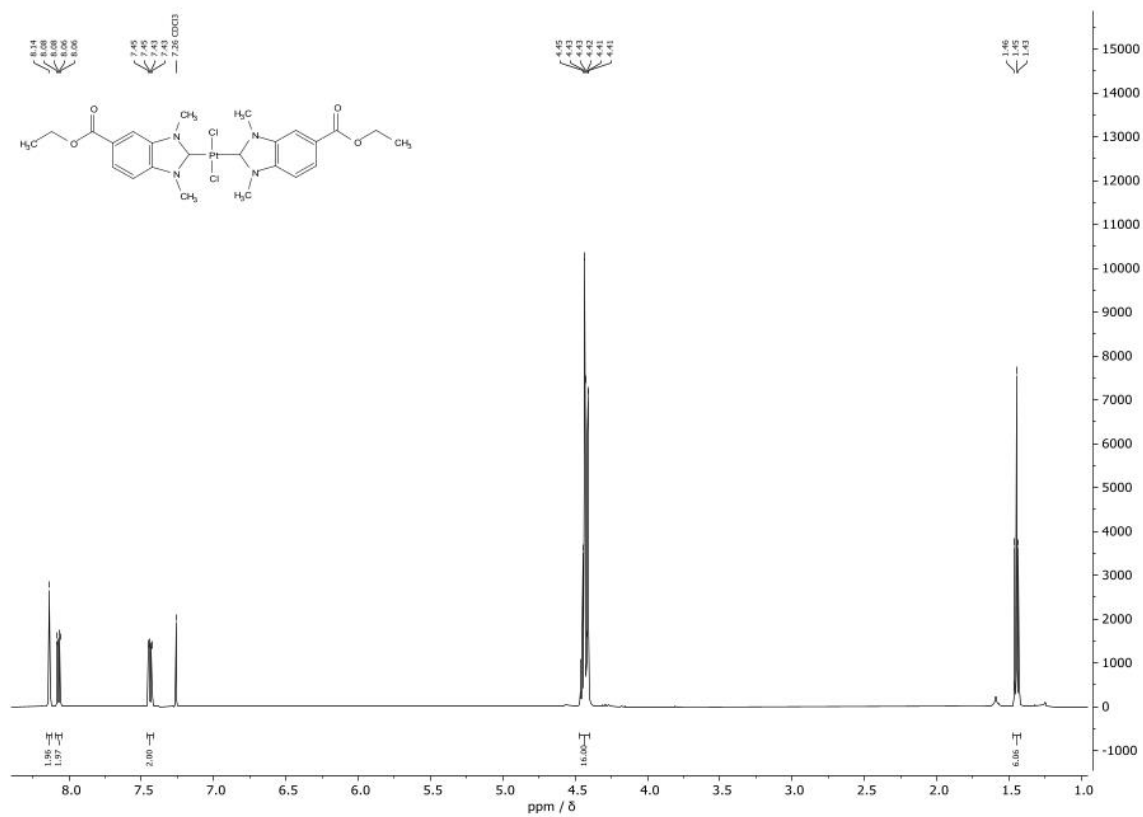
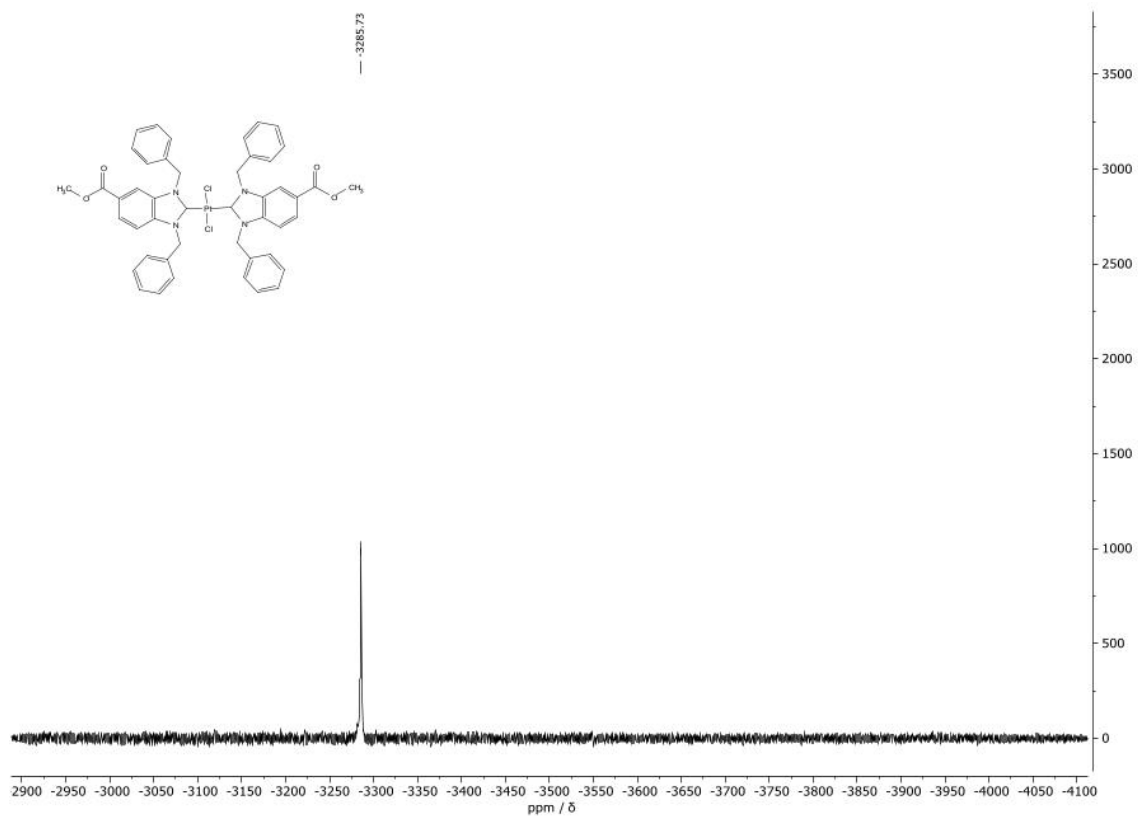


Fig. 8. $^{13}\text{C-NMR}$ spectrum of **8c** in CDCl_3 .

XX



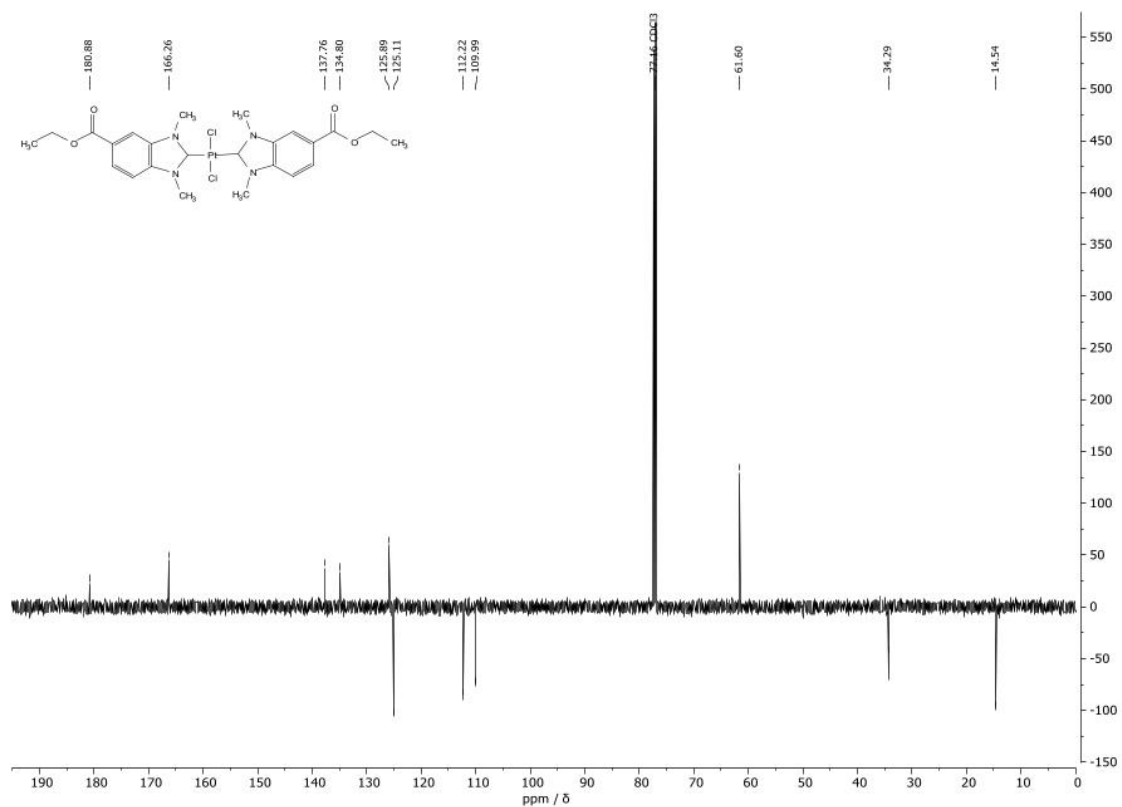


Fig. 11. ^{13}C -NMR spectrum of **9a** in CDCl₃.

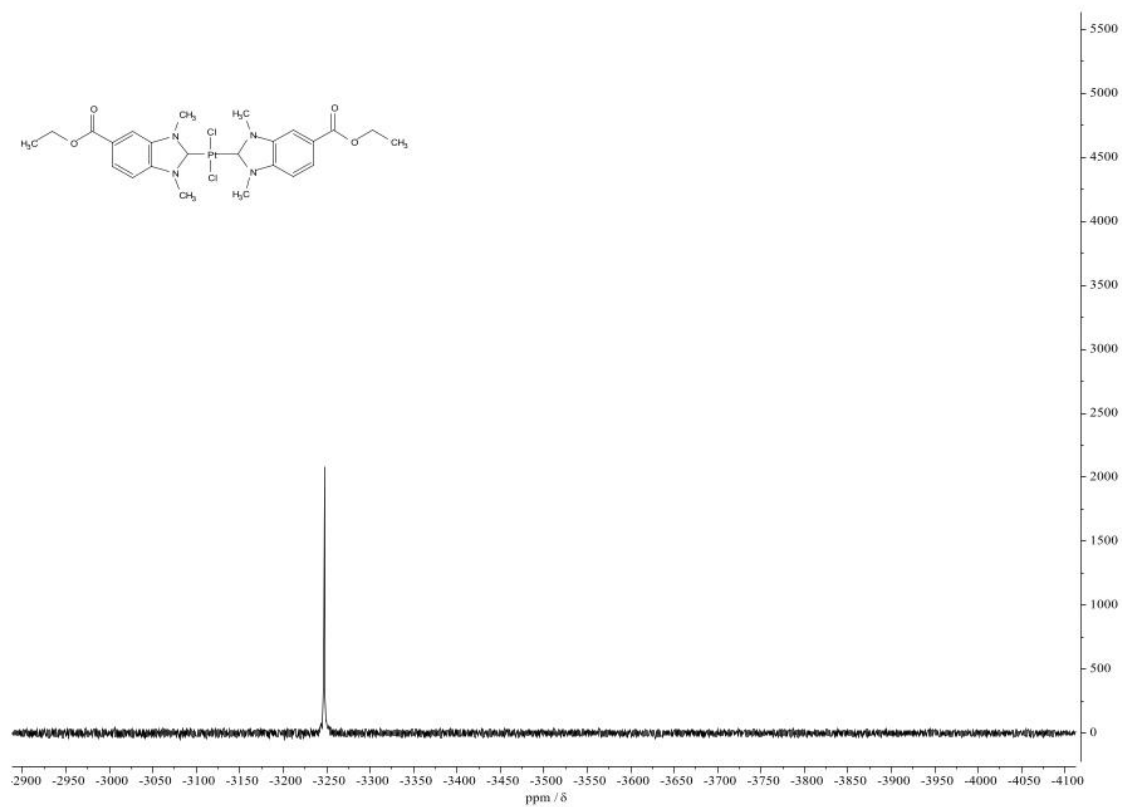


Fig. 12. ^{195}Pt -NMR spectrum of **9a** in CDCl₃.

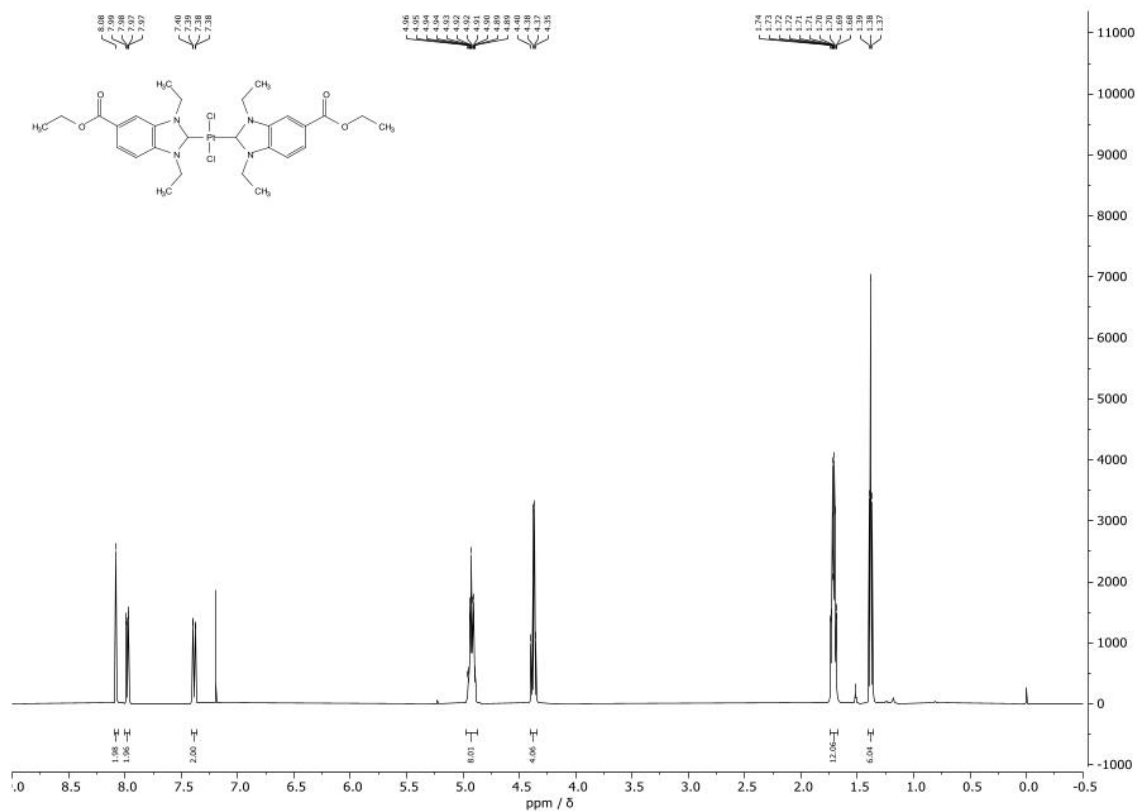


Fig. 13. $^1\text{H-NMR}$ spectrum of **9b** in CDCl_3 .

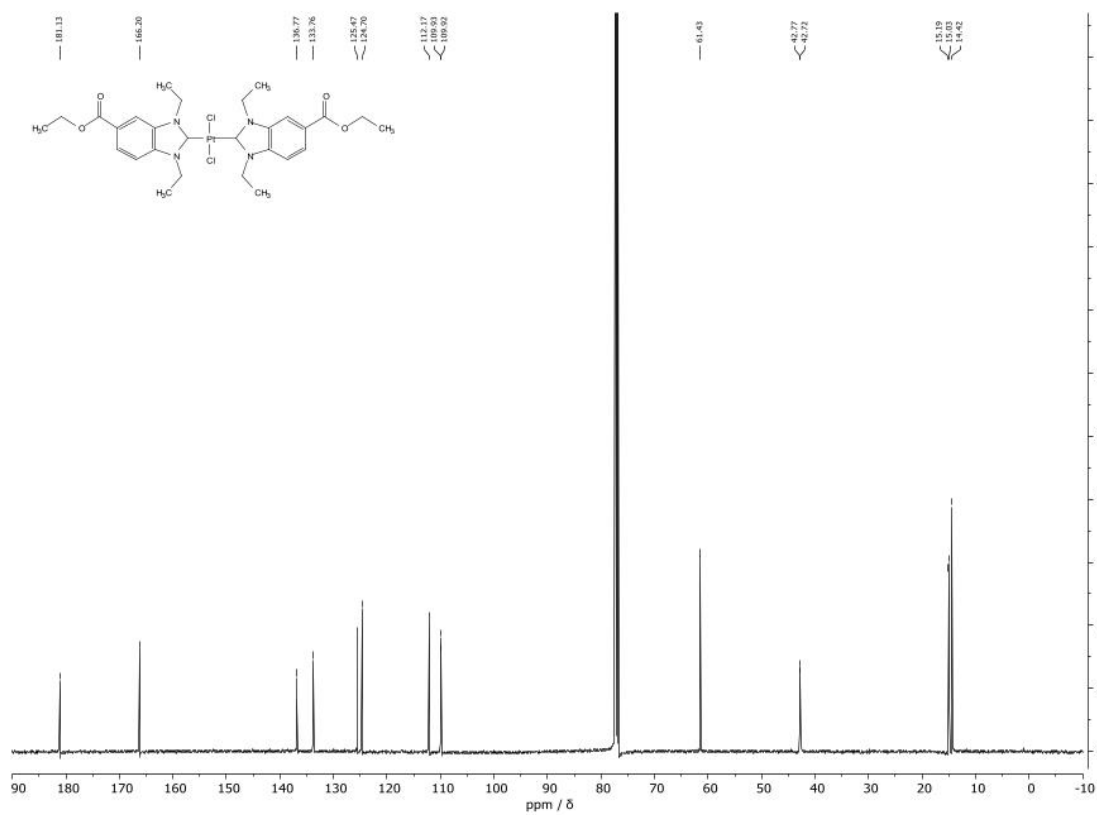


Fig. 14. $^{13}\text{C-NMR}$ spectrum of **9b** in CDCl_3 .

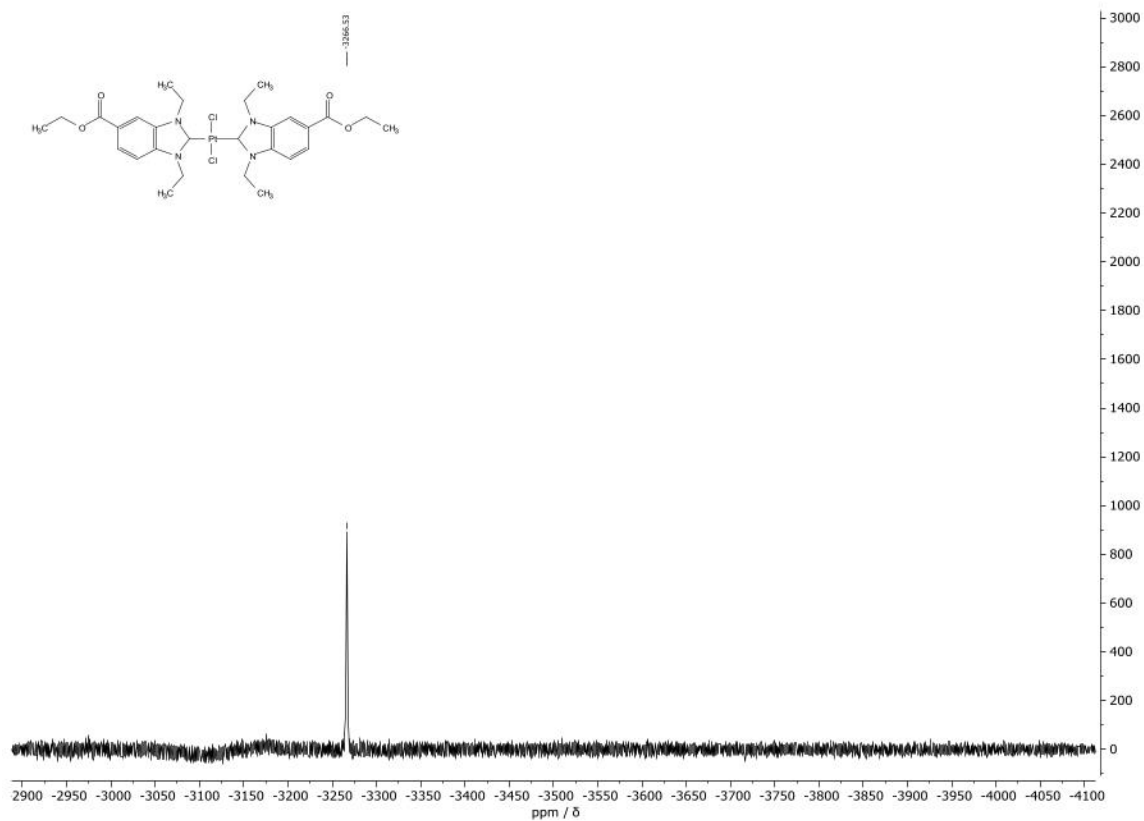


Fig. 15. ^{195}Pt -NMR spectrum of **9b** in CDCl_3 .

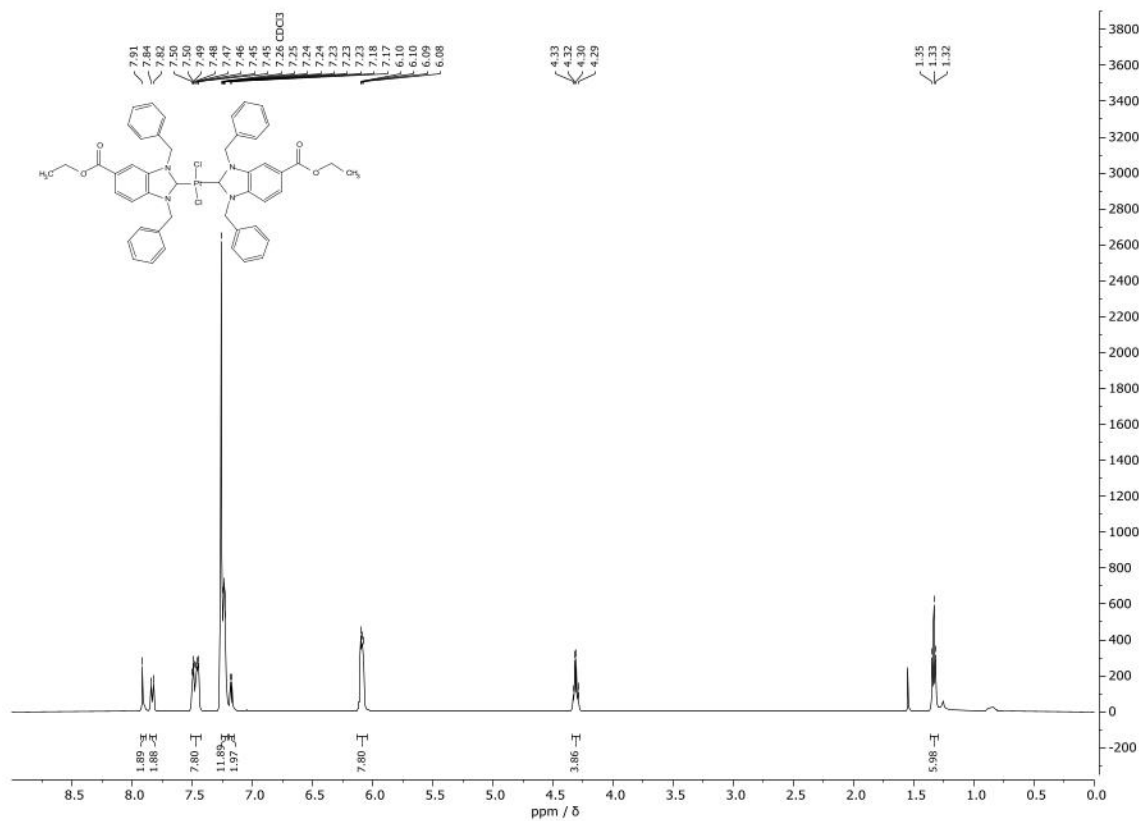


Fig. 16. ^1H -NMR spectrum of **9c** in CDCl_3 .

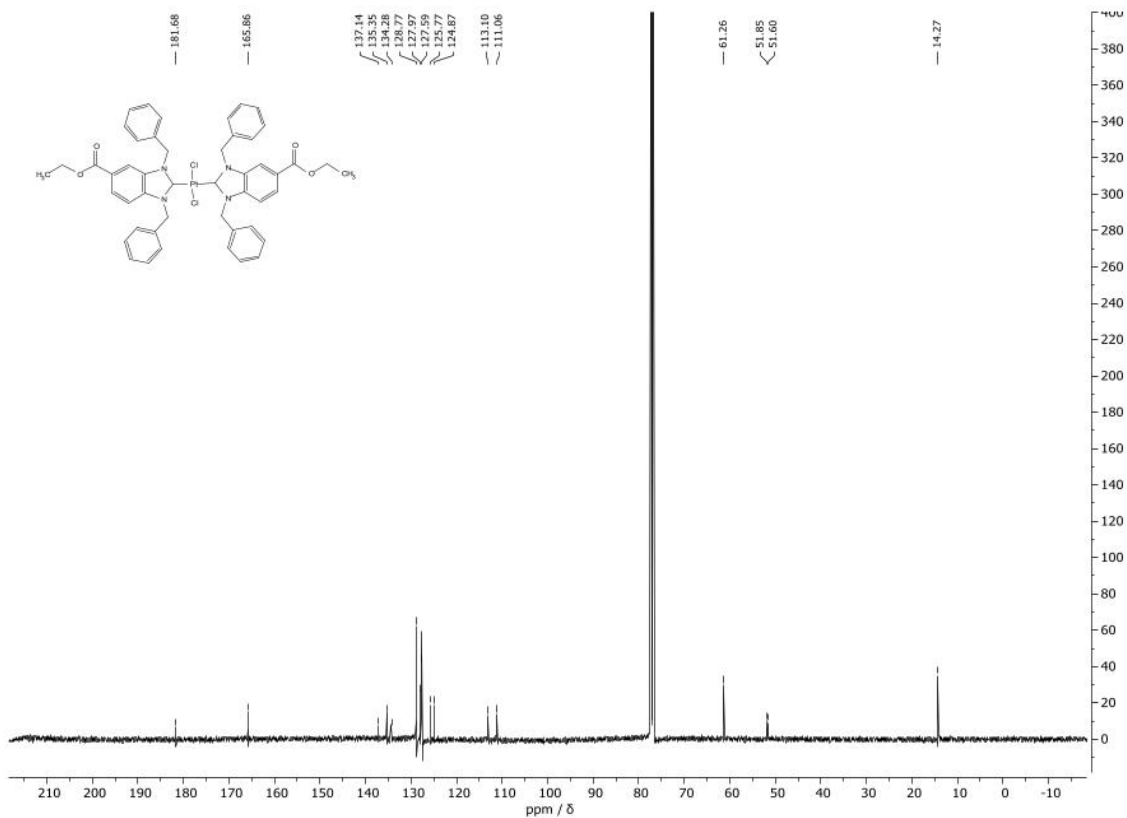


Fig. 17. ^{13}C -NMR spectrum of **9c** in CDCl_3 .

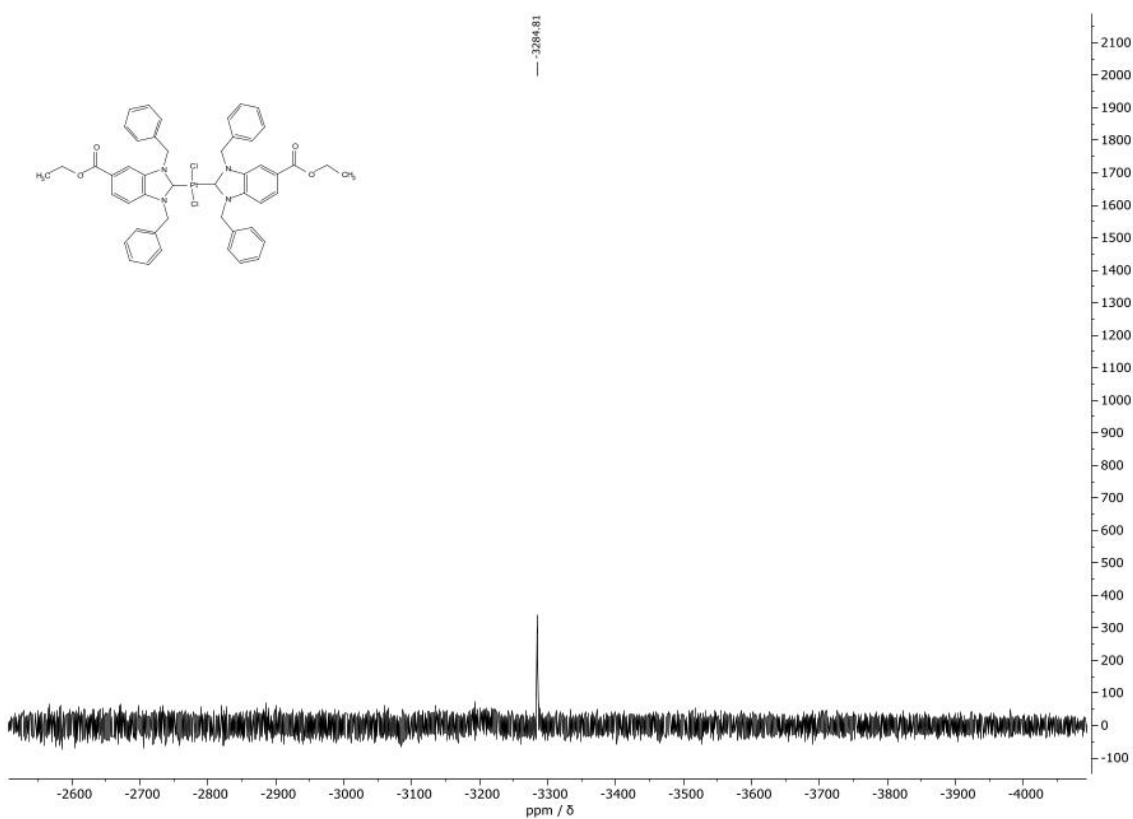
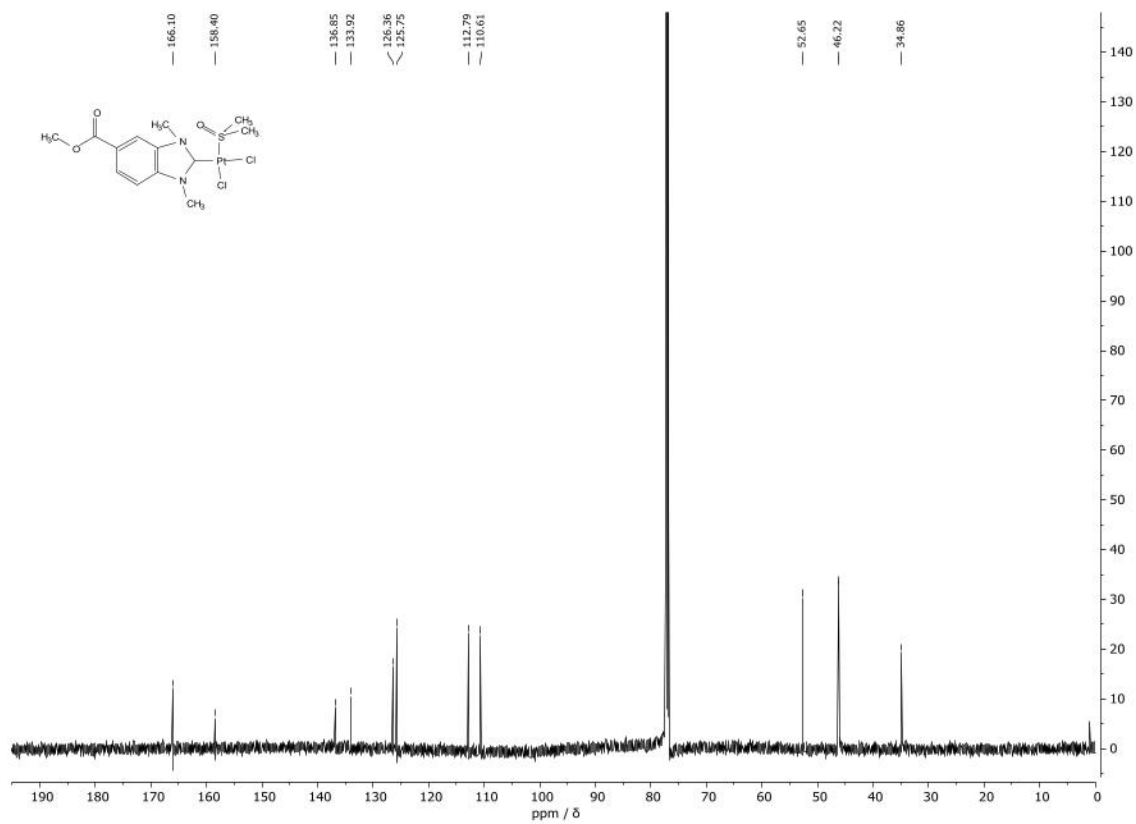
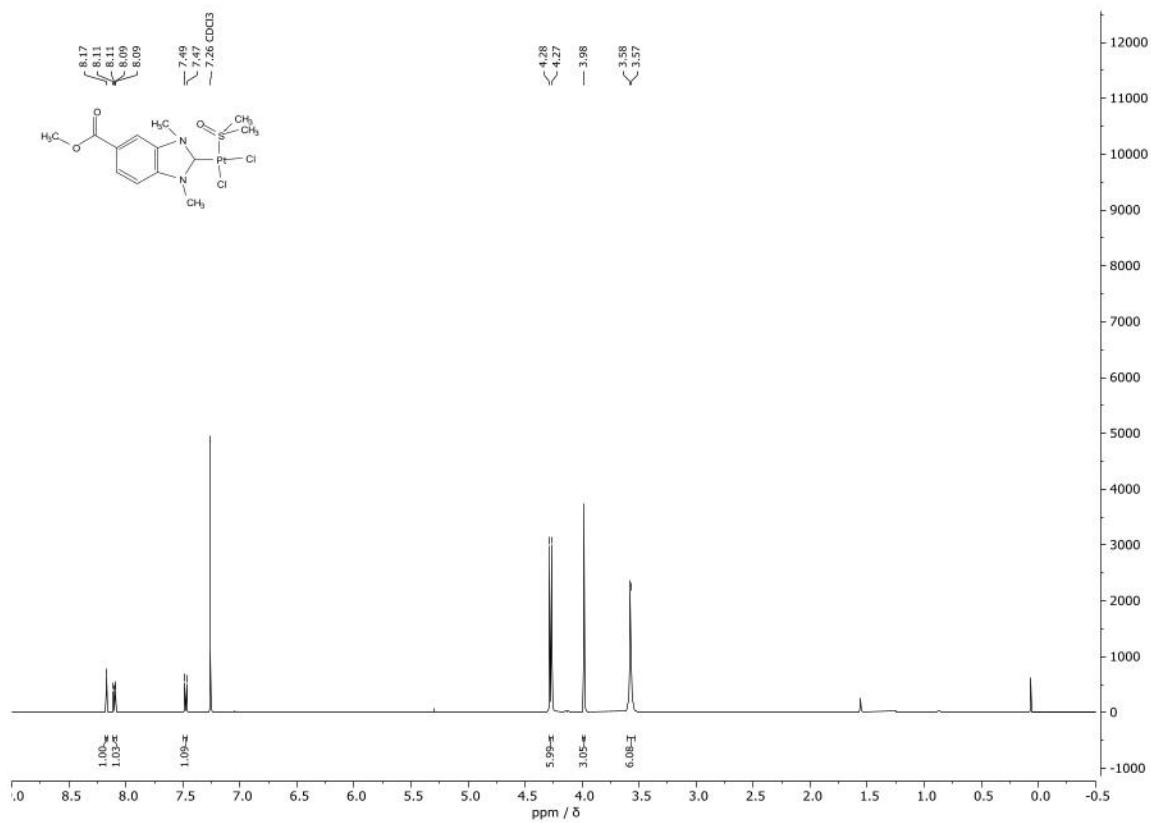


Fig. 18. ^{195}Pt -NMR spectrum of **9c** in CDCl_3 .



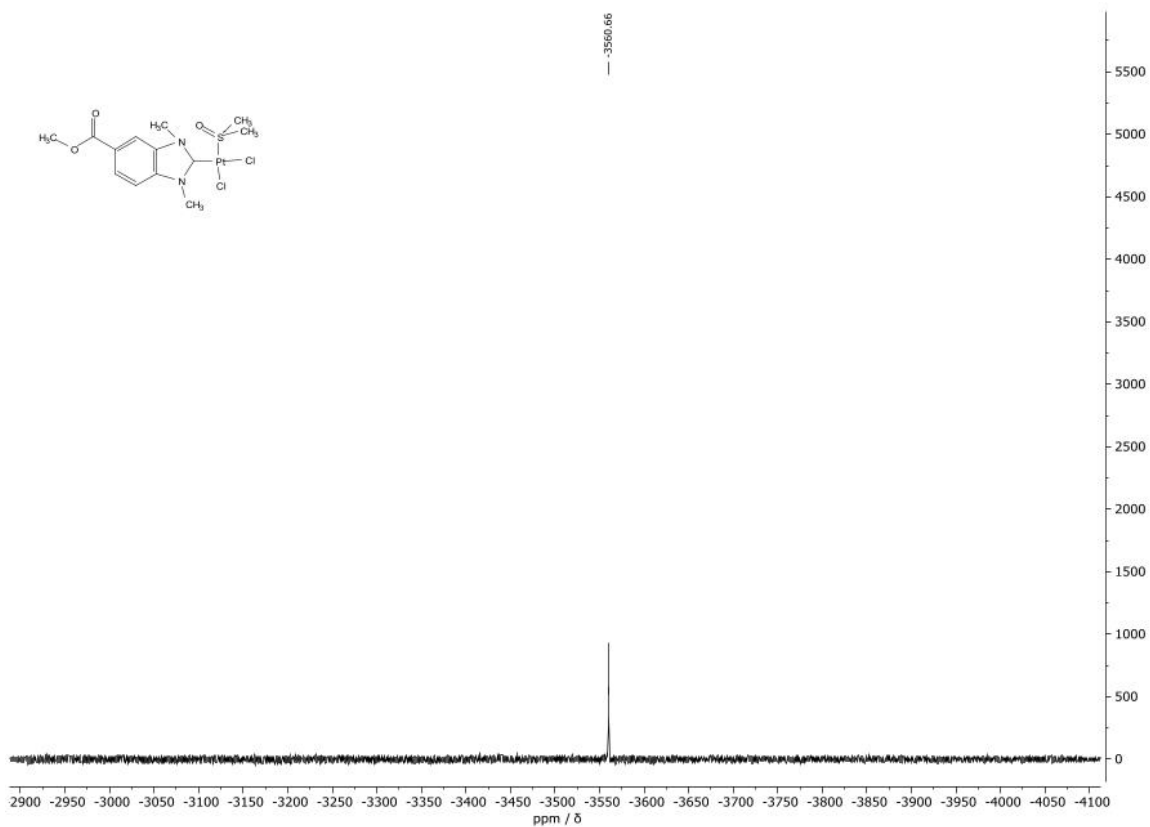


Fig. 21. ^{195}Pt -NMR spectrum of **10a** in CDCl_3 .

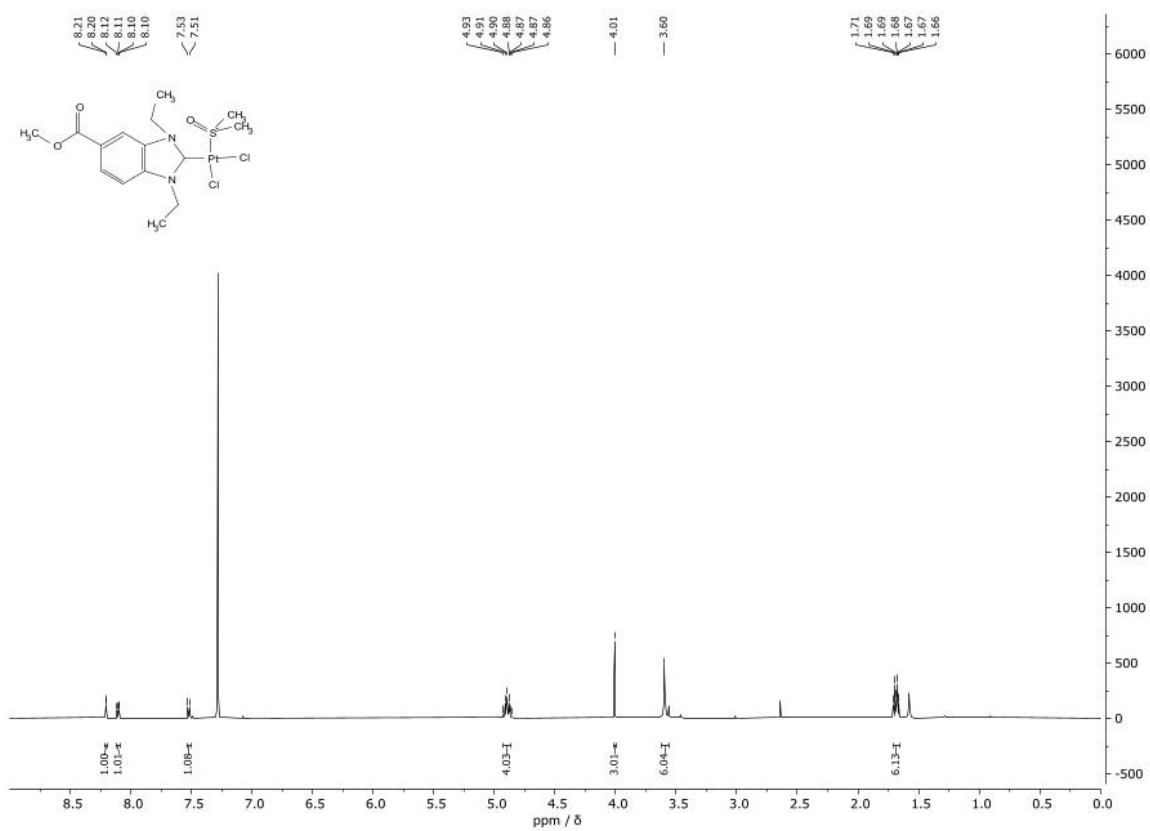


Fig. 22. ^1H -NMR spectrum of **10b** in CDCl_3 .

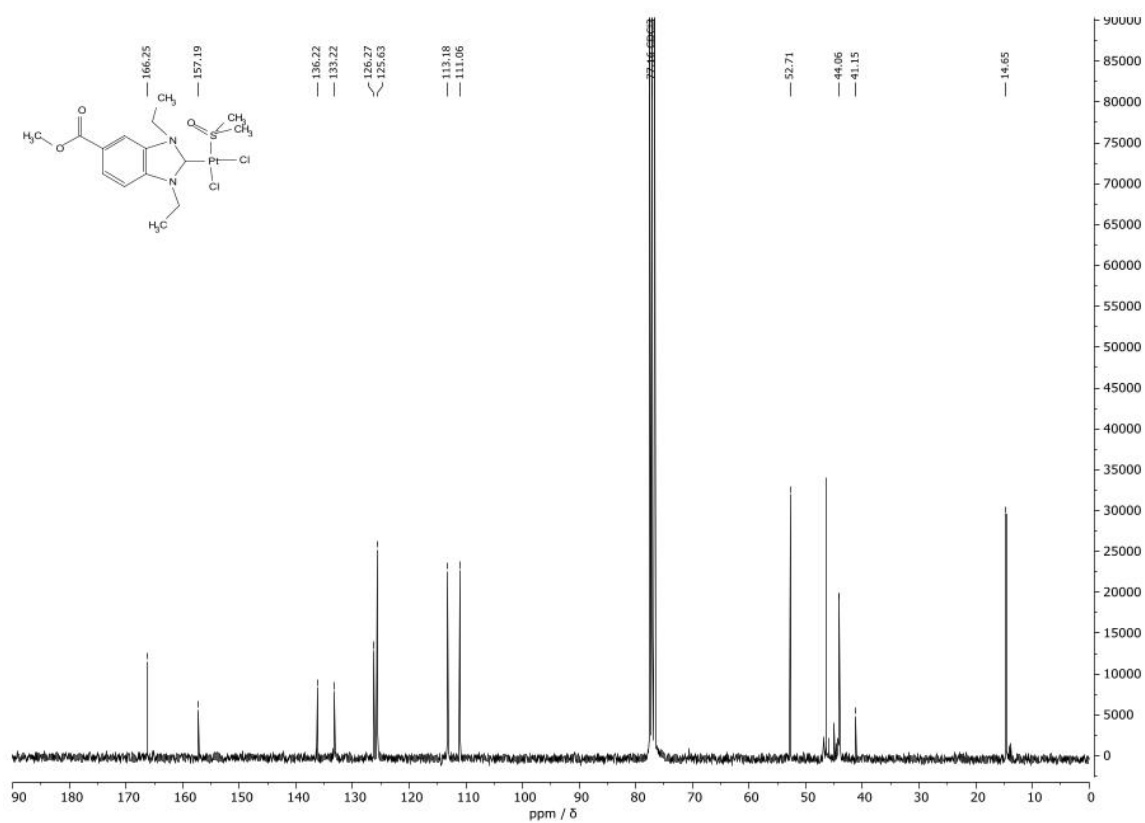


Fig. 23. ^{13}C -NMR spectrum of **10b** in CDCl_3 .

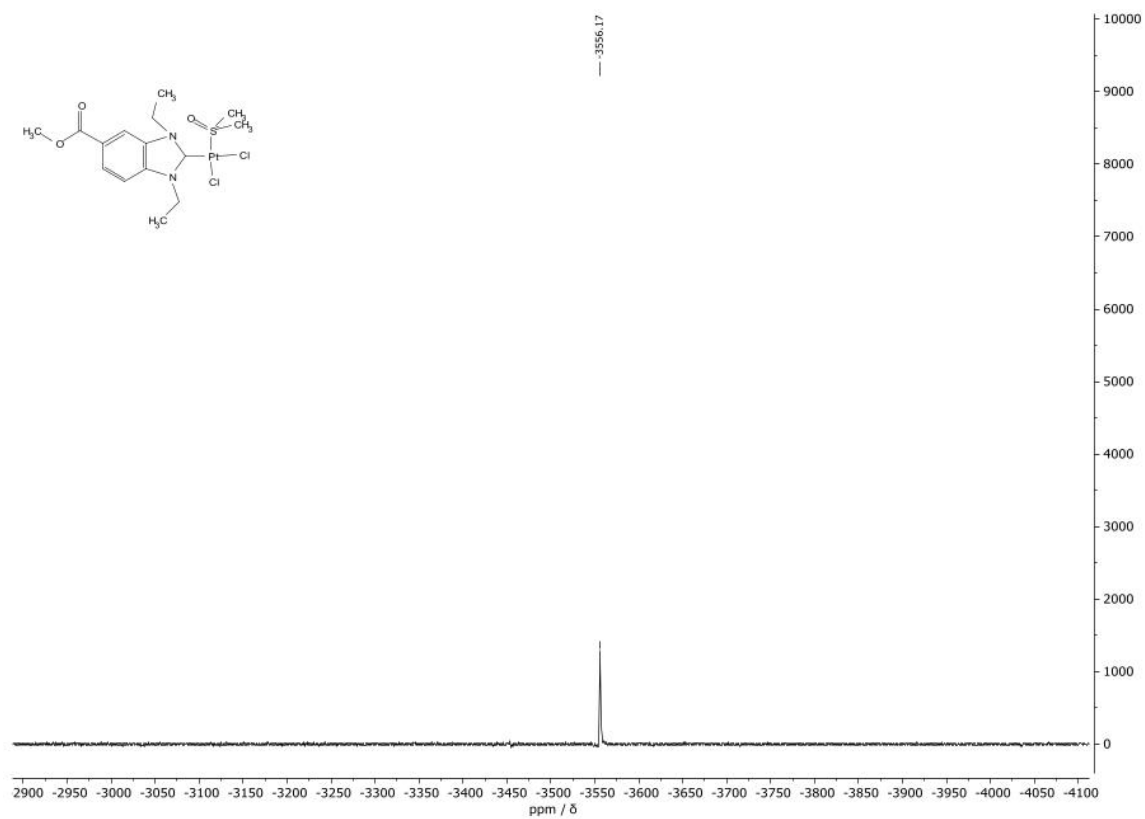


Fig. 24. ^{195}Pt -NMR spectrum of **10b** in CDCl_3 .

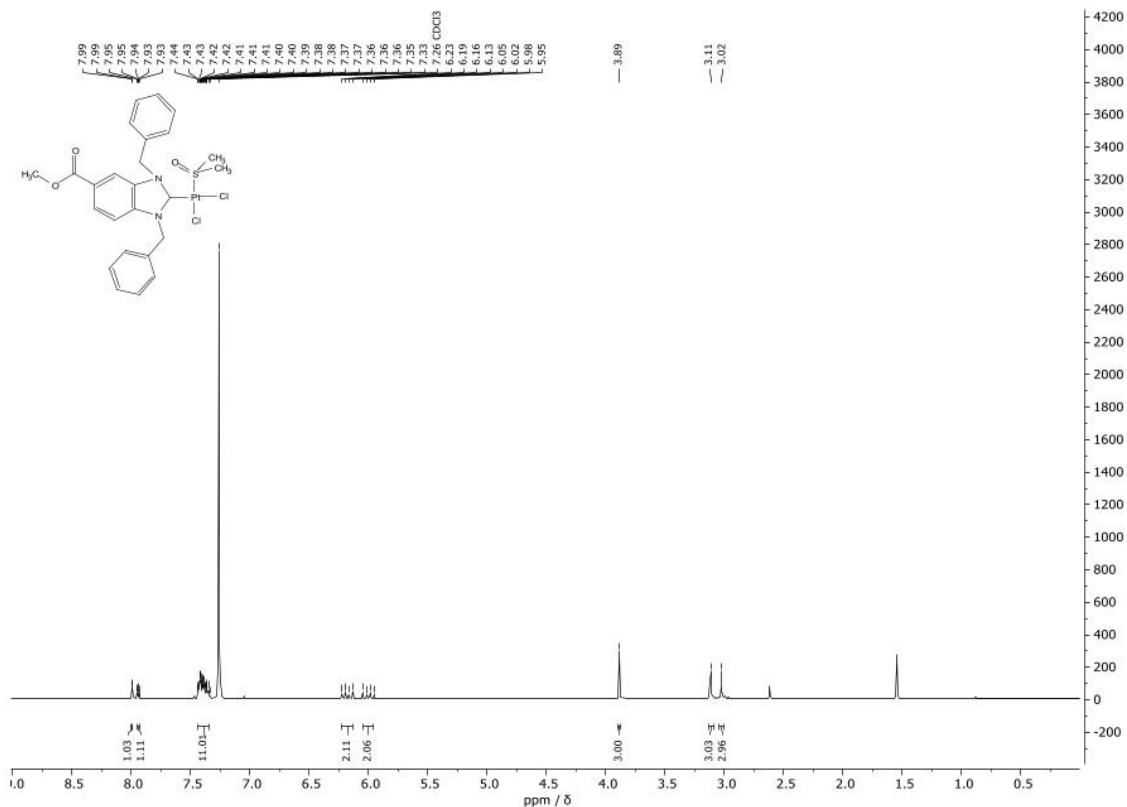


Fig. 25. ¹H-NMR spectrum of 10c in CDCl₃.

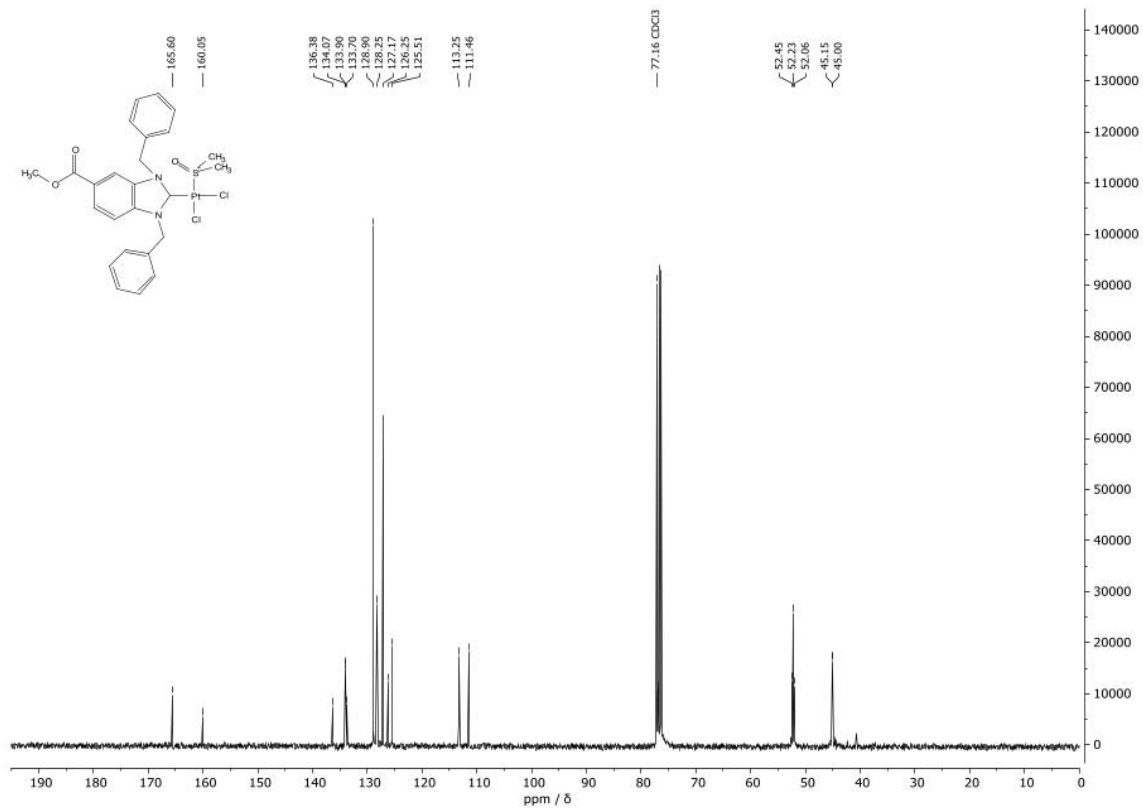


Fig. 26. ¹³C-NMR spectrum of 10c in CDCl₃.

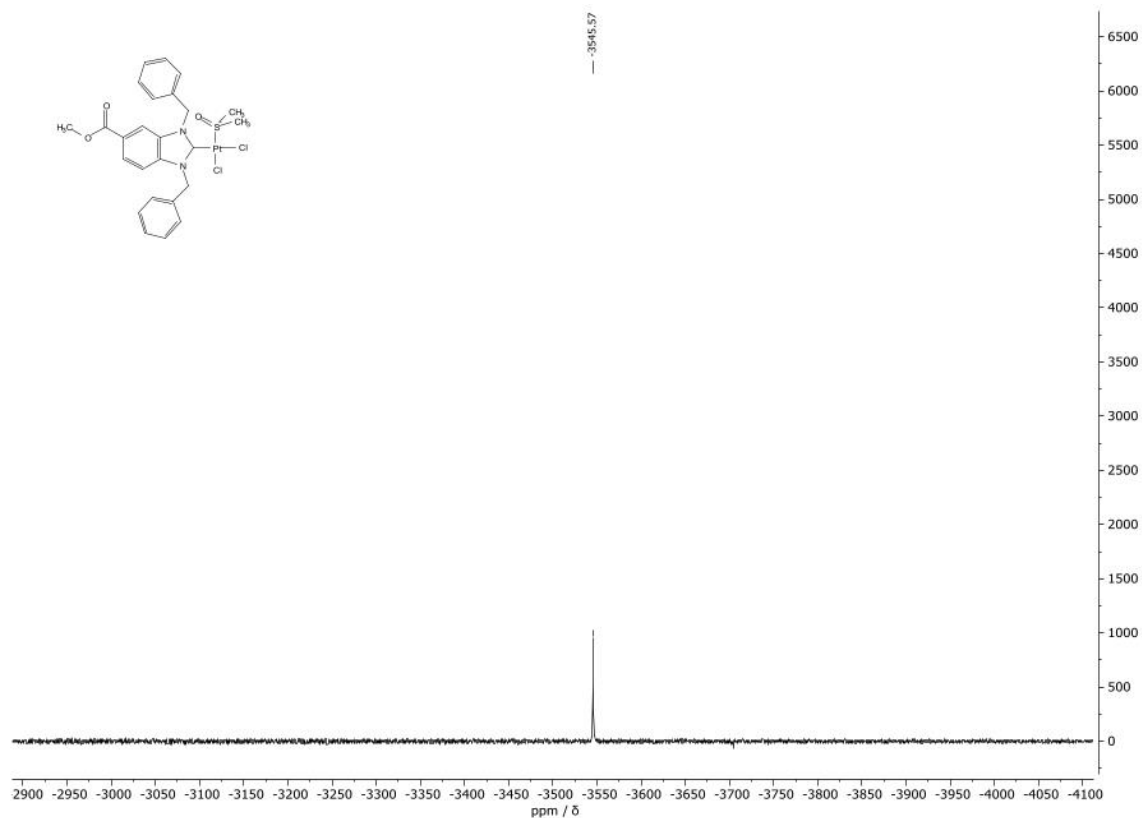


Fig. 27. ^{195}Pt -NMR spectrum of **10c** in CDCl_3 .

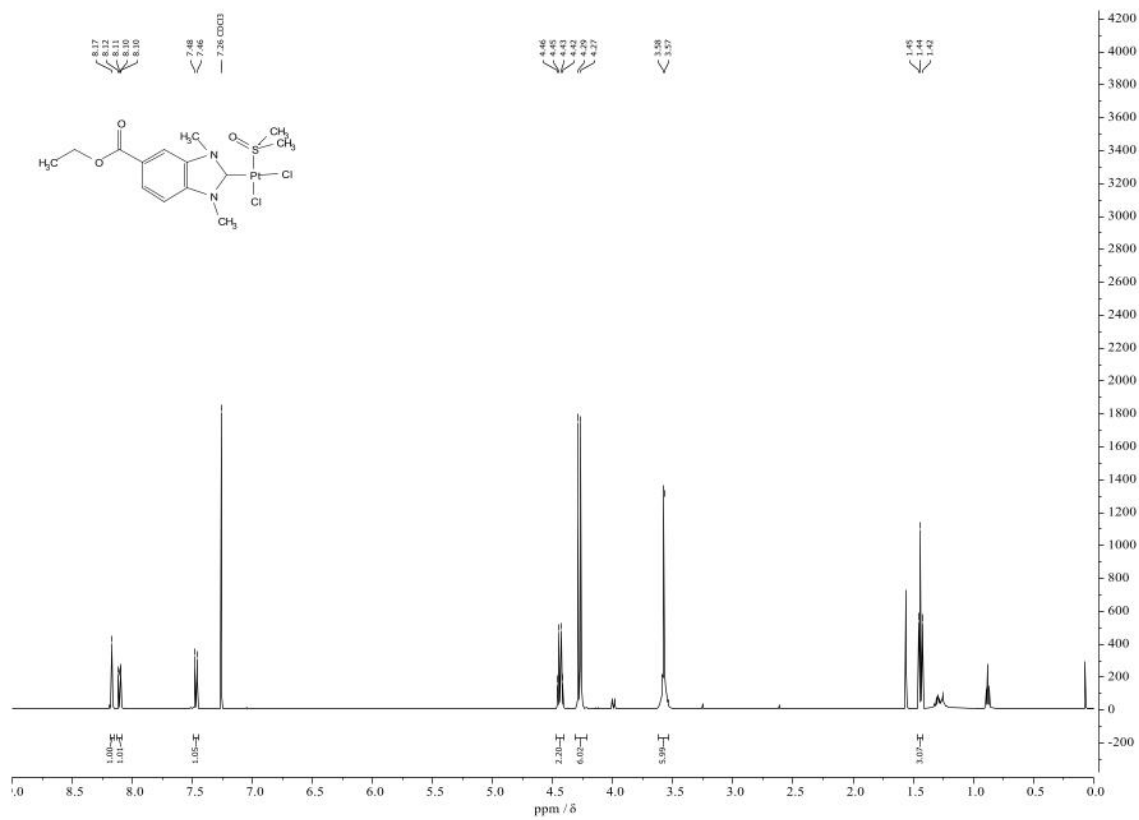


Fig. 28. ^1H -NMR spectrum of **11a** in CDCl_3 .

XXX

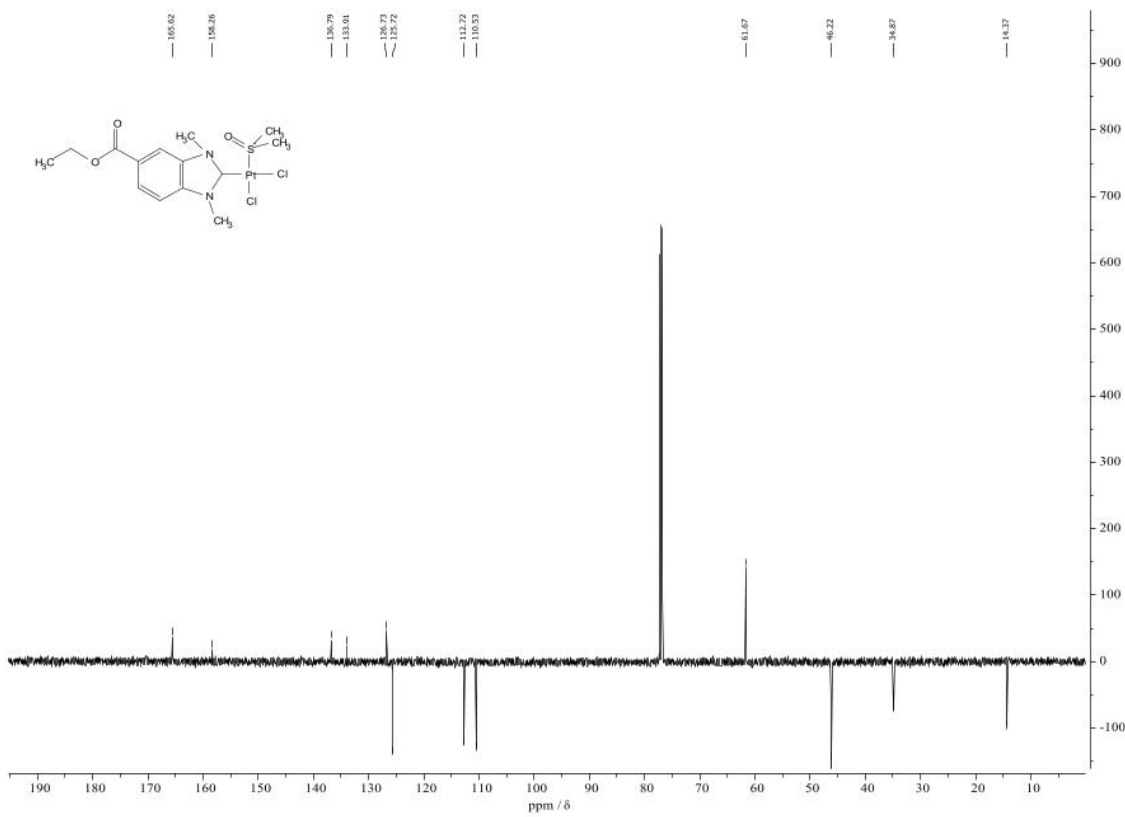


Fig. 29. ¹³C-NMR spectrum of **11a** in CDCl₃.

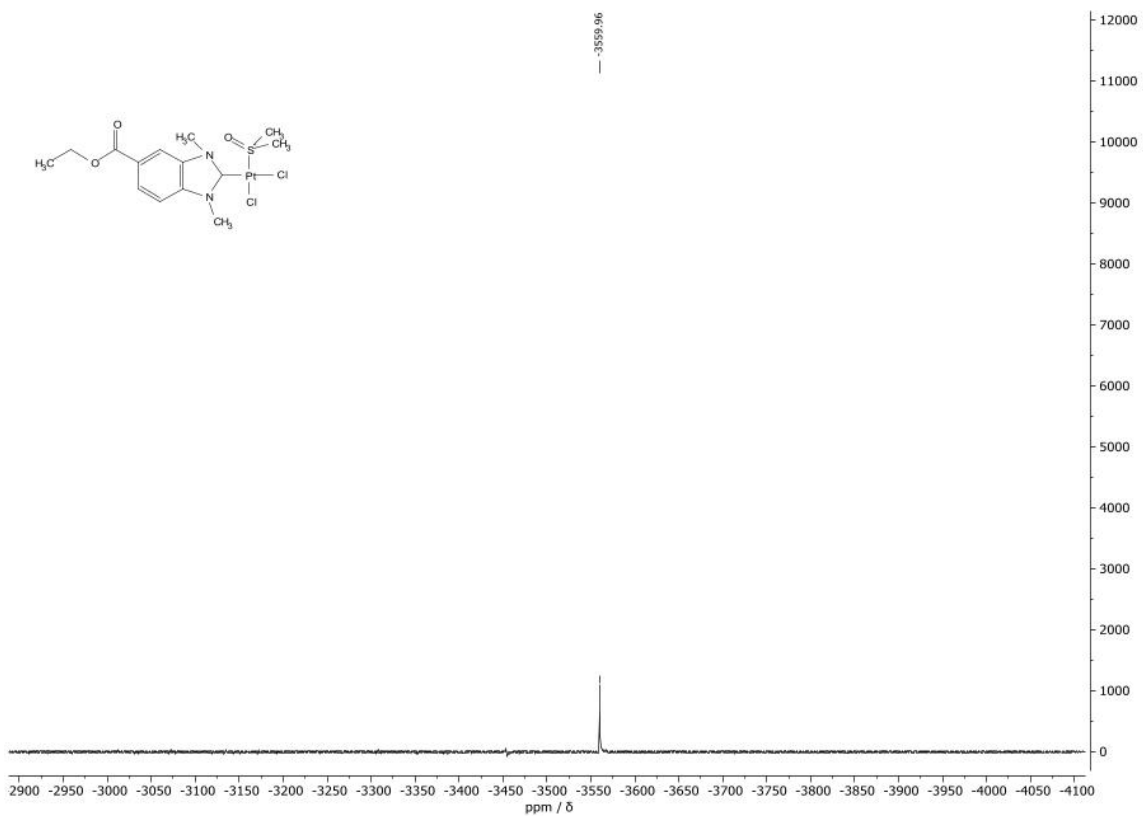


Fig. 30. ¹⁹⁵Pt-NMR spectrum of **11a** in CDCl₃.

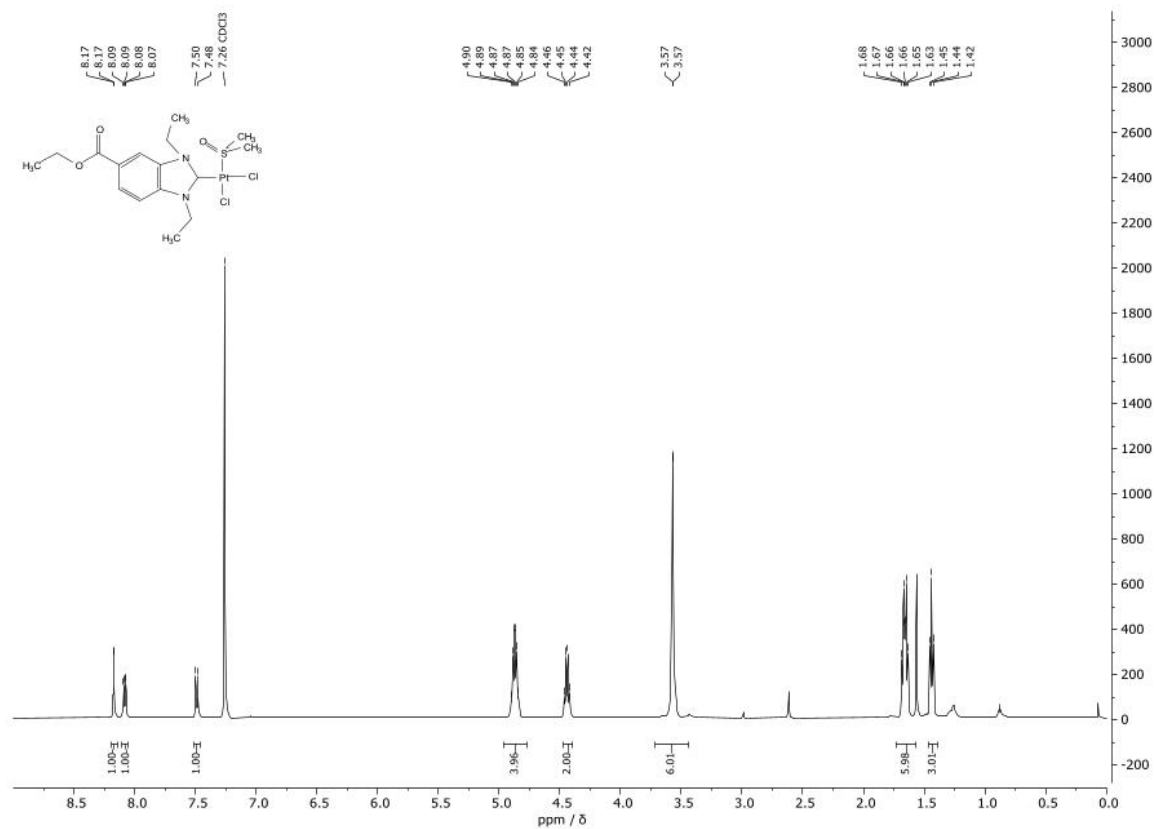


Fig. 31. ¹H-NMR spectrum of **11b** in CDCl₃.

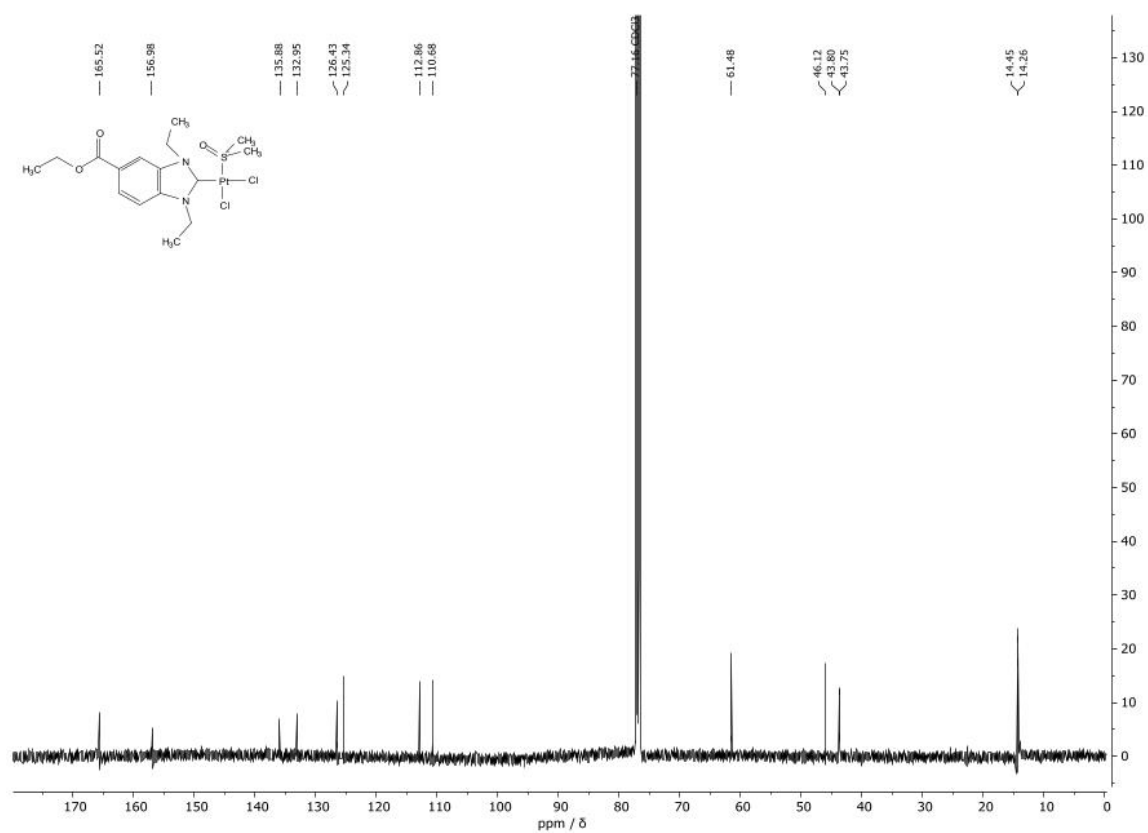


Fig. 32. ¹³C-NMR spectrum of **11b** in CDCl₃.

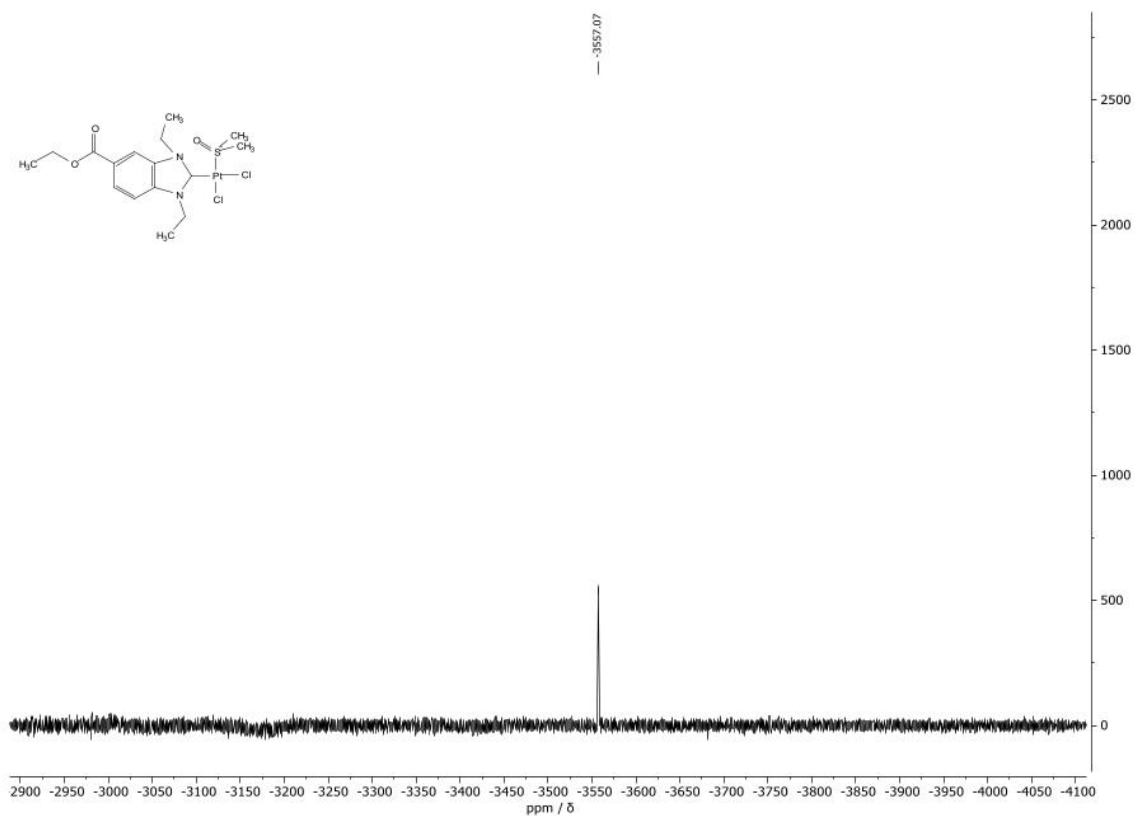


Fig. 33. ^{195}Pt -NMR spectrum of **11b** in CDCl_3 .

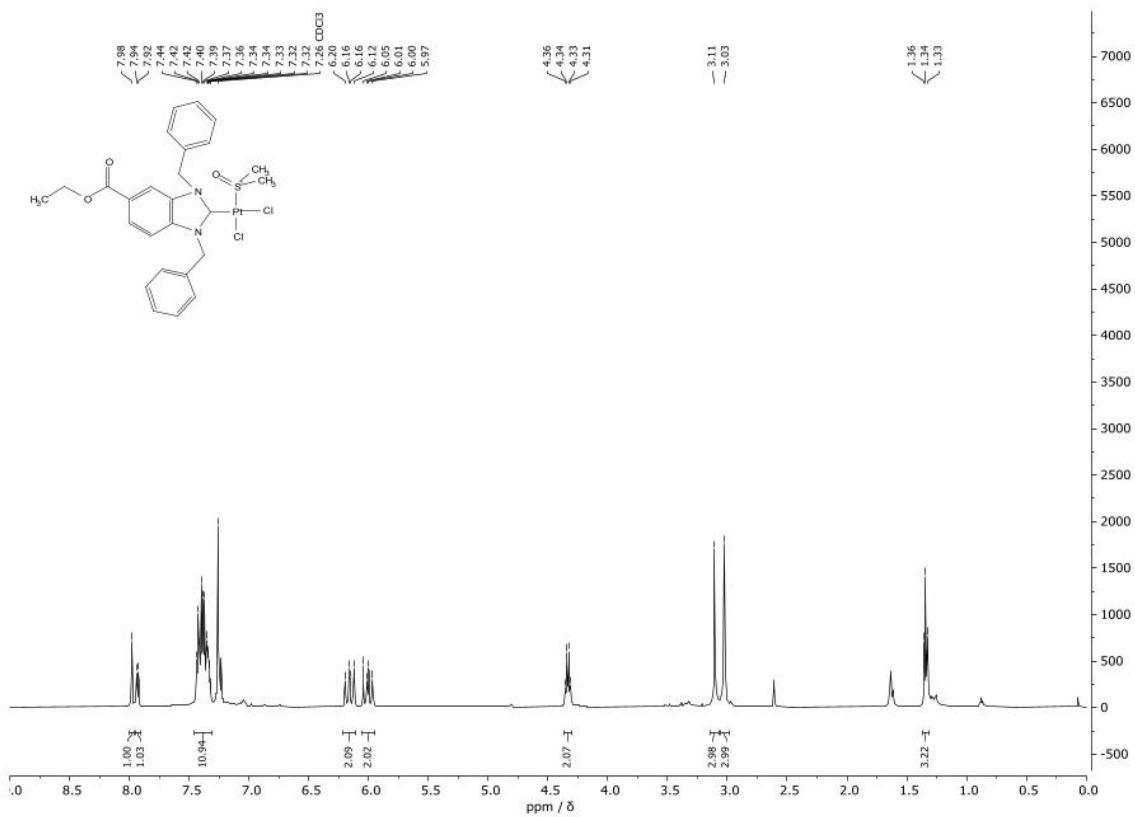


Fig. 34. ^1H -NMR spectrum of **11c** in CDCl_3 .

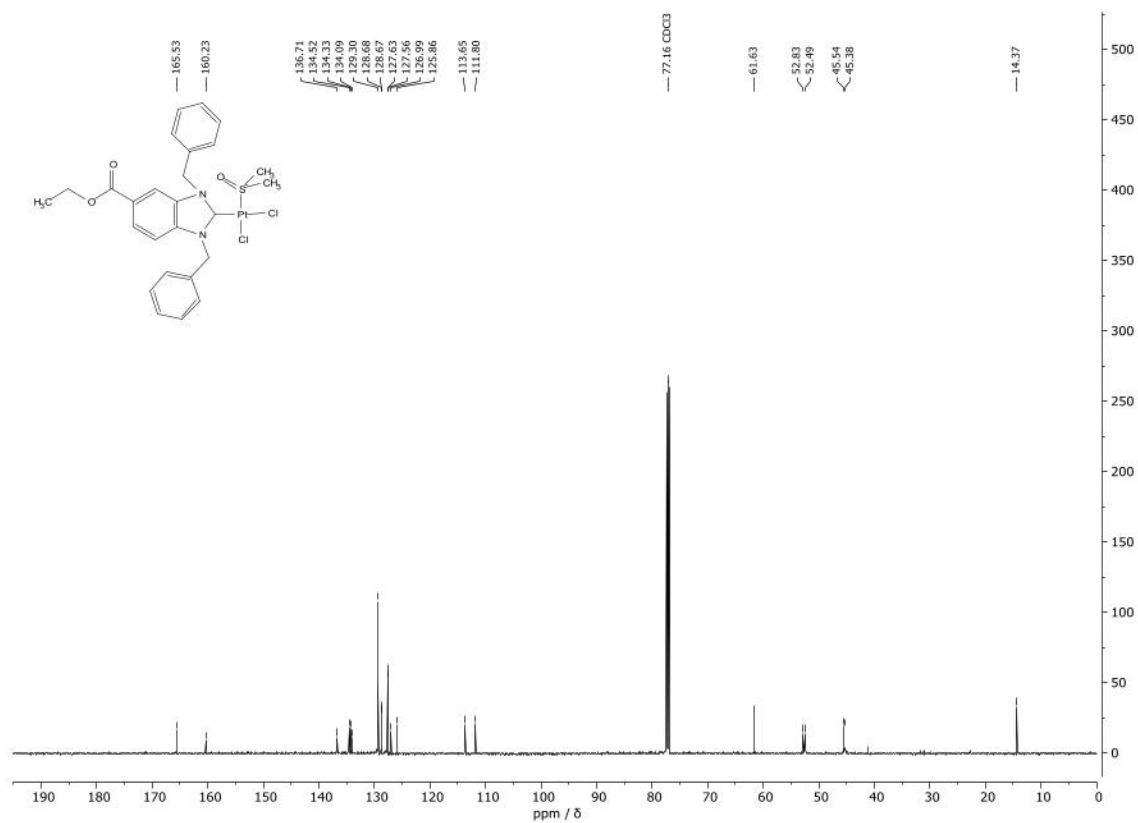


Fig. 35. ^{13}C -NMR spectrum of **11c** in CDCl_3 .

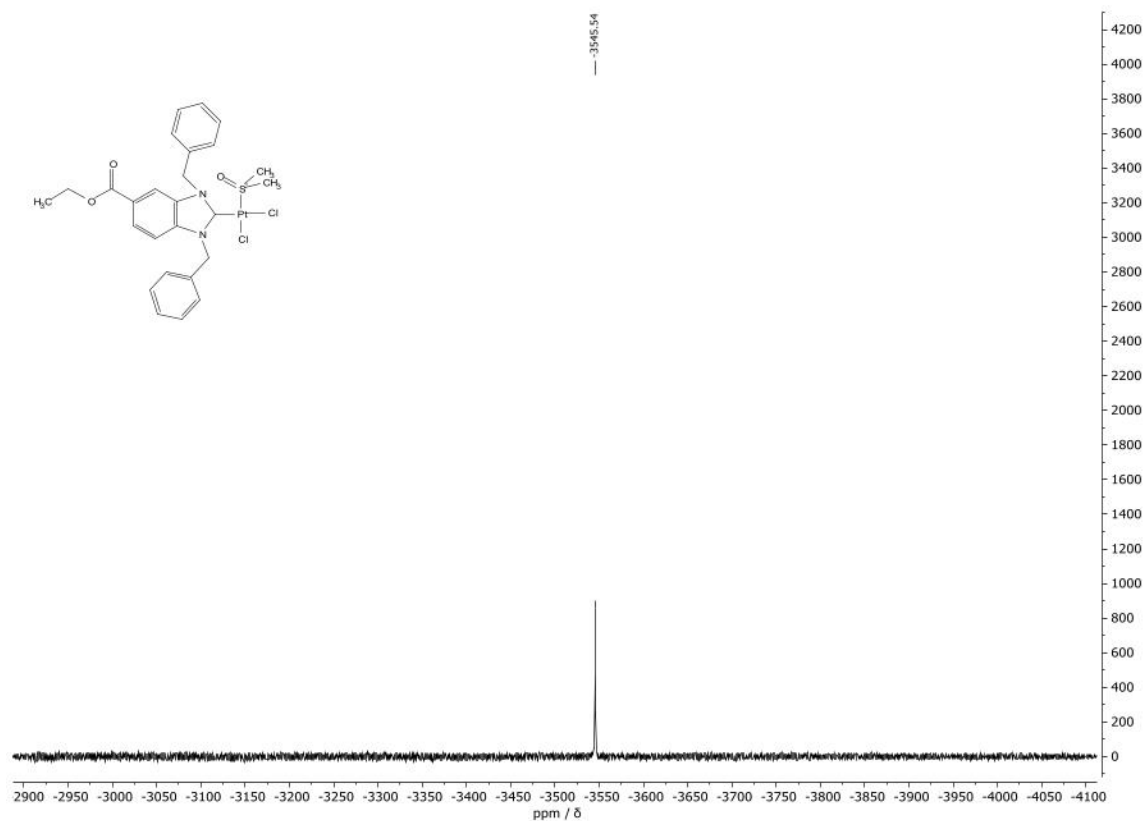


Fig. 36. ^{195}Pt -NMR spectrum of **11c** in CDCl_3 .

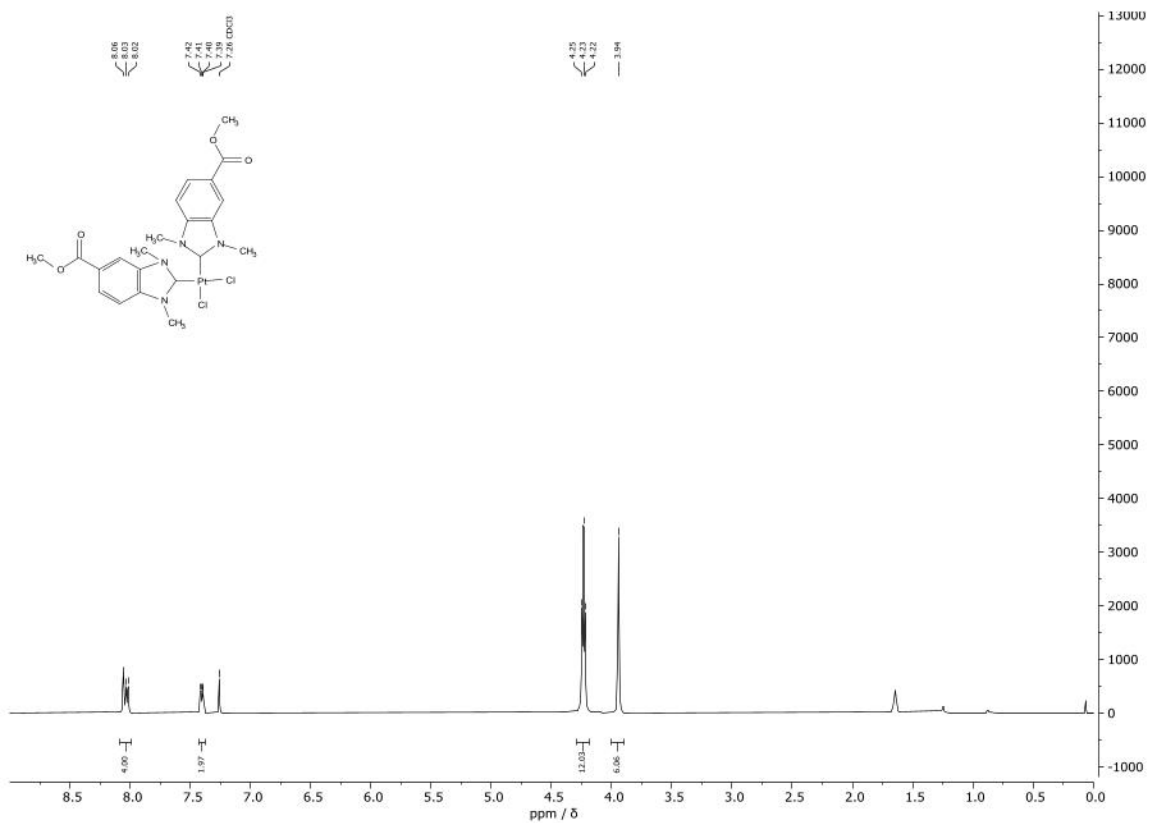


Fig. 37. $^1\text{H-NMR}$ spectrum of **12a** in CDCl_3 .

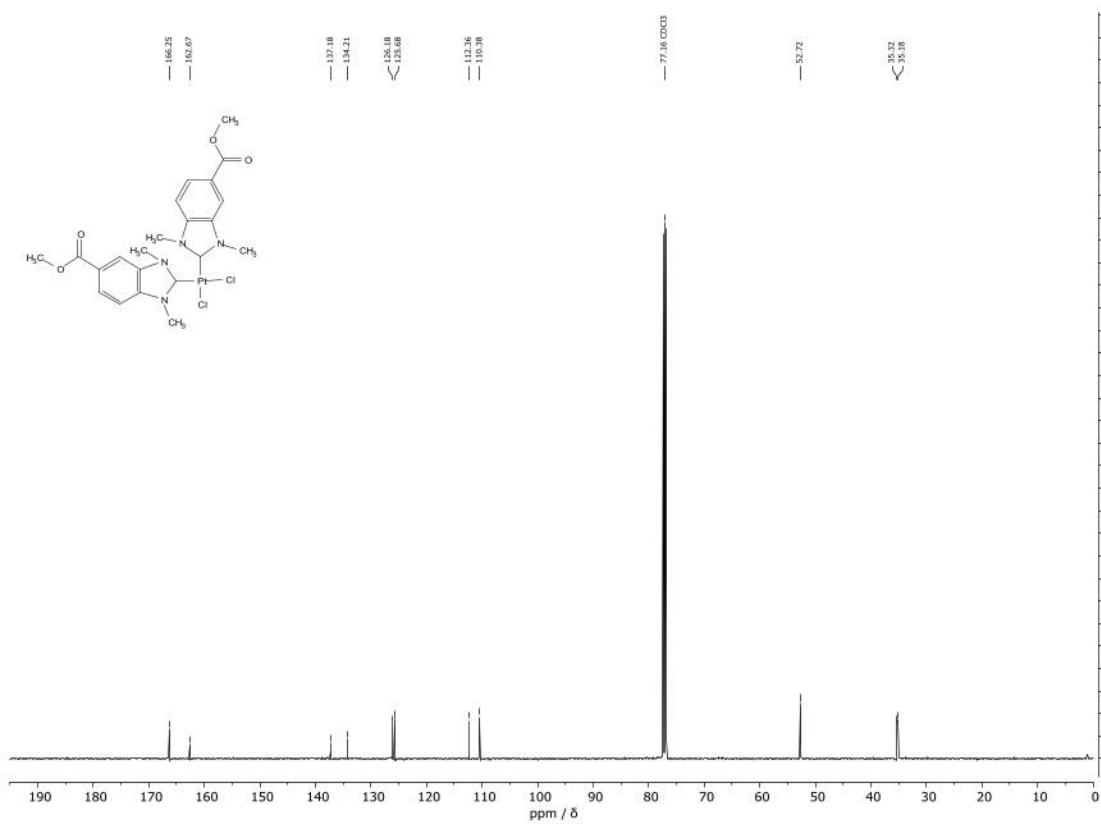


Fig. 38. $^{13}\text{C-NMR}$ spectrum of **12a** in CDCl_3 .

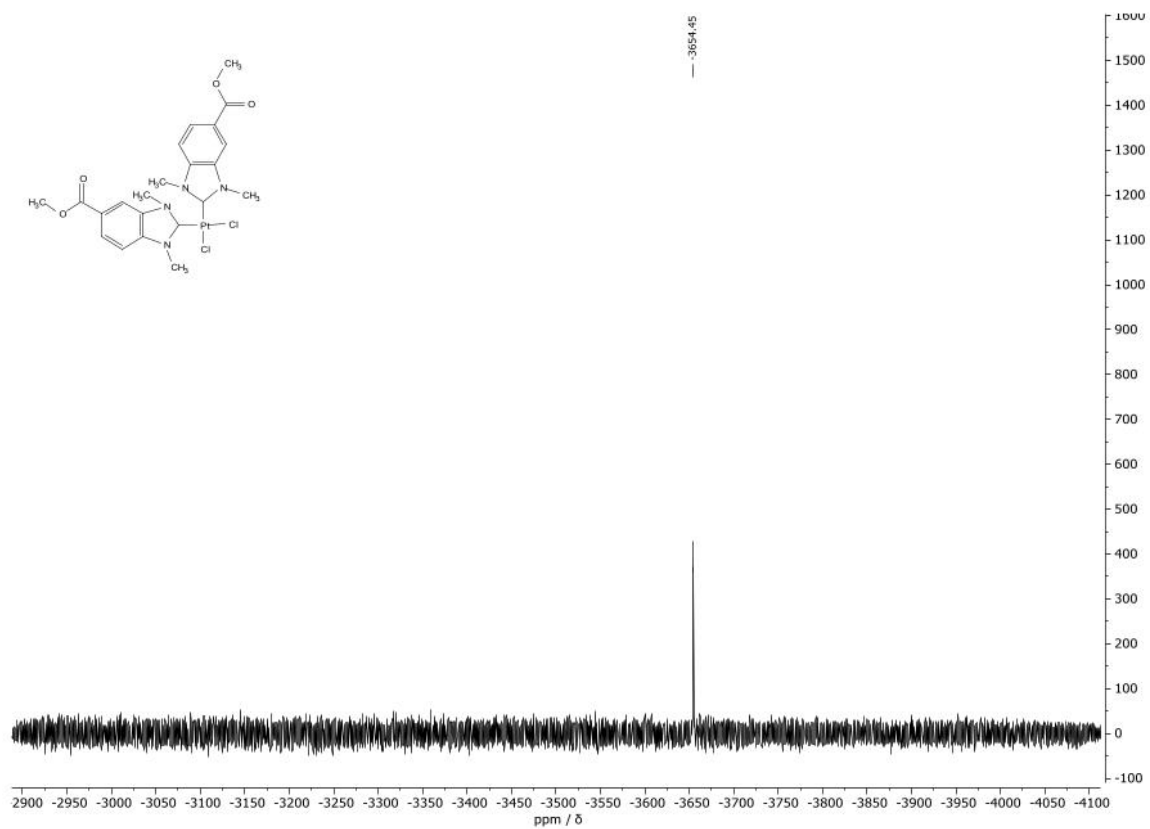


Fig. 39. ^{195}Pt -NMR spectrum of **12a** in CDCl_3 .

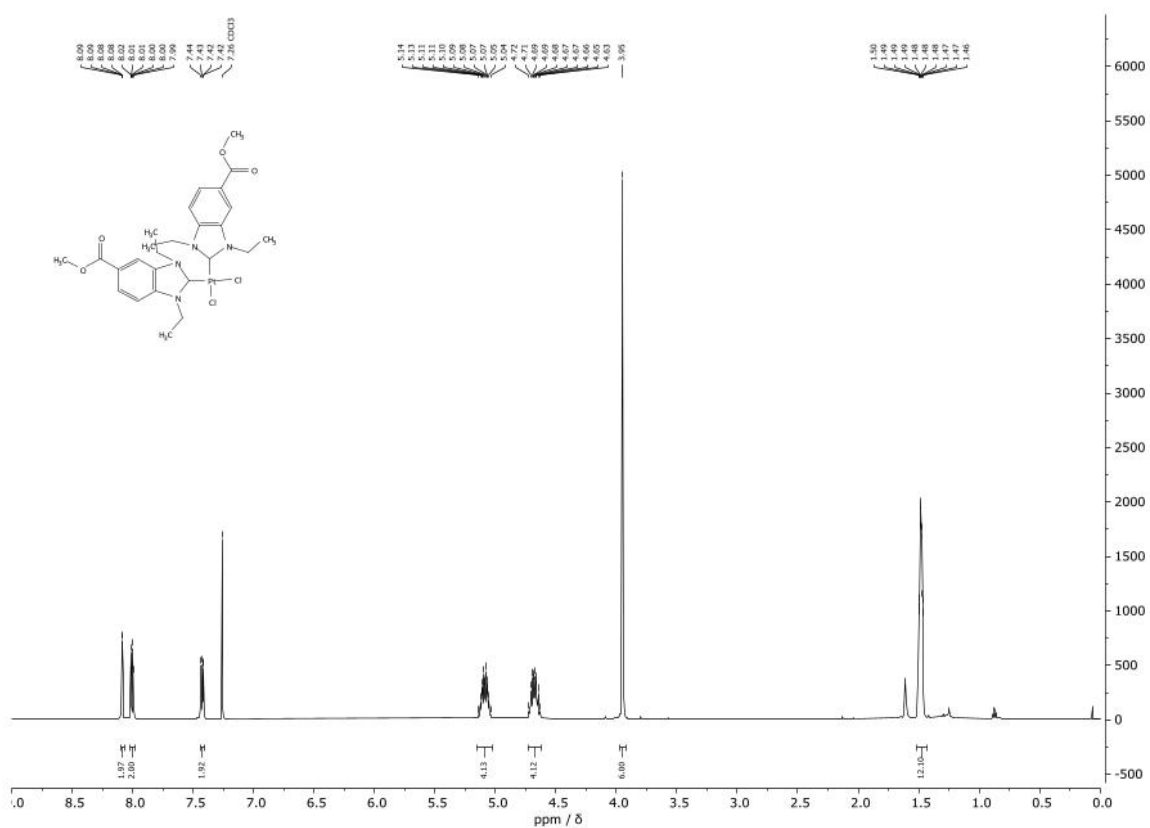


Fig. 40. ^1H -NMR spectrum of **12b** in CDCl_3 .

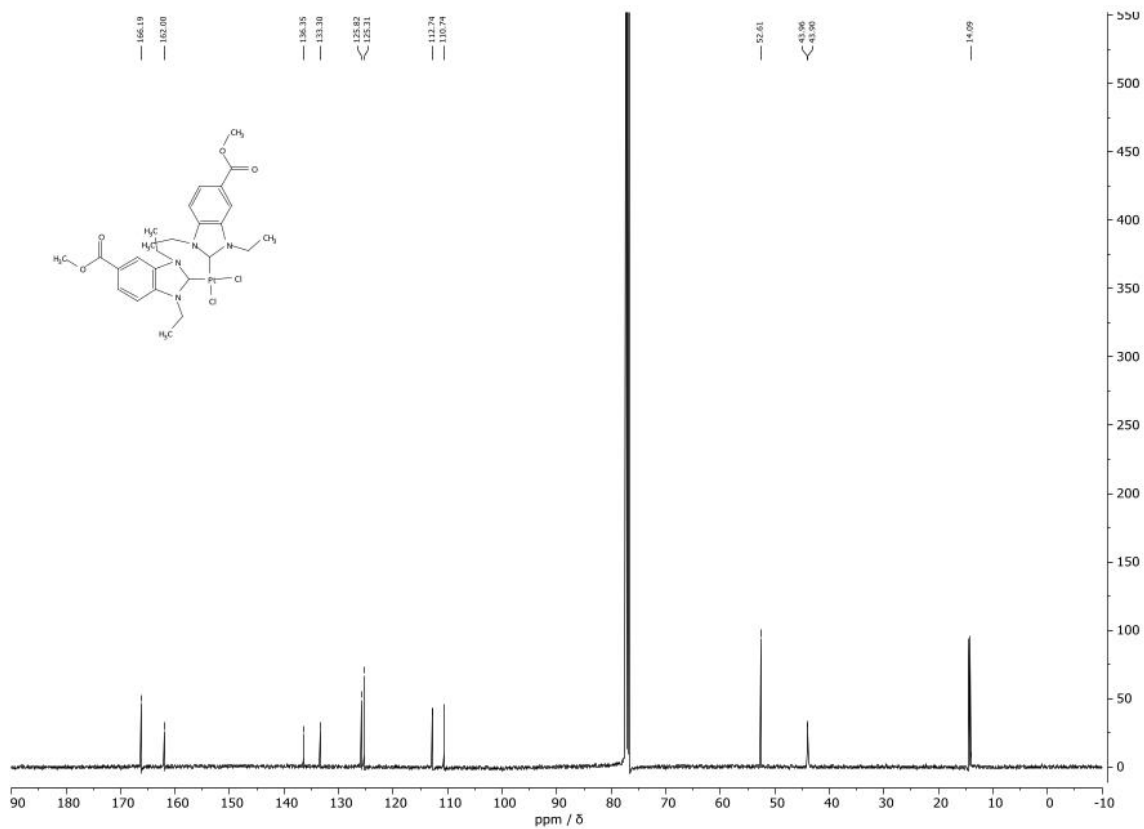


Fig. 41. ^{13}C -NMR spectrum of **12b** in CDCl_3 .

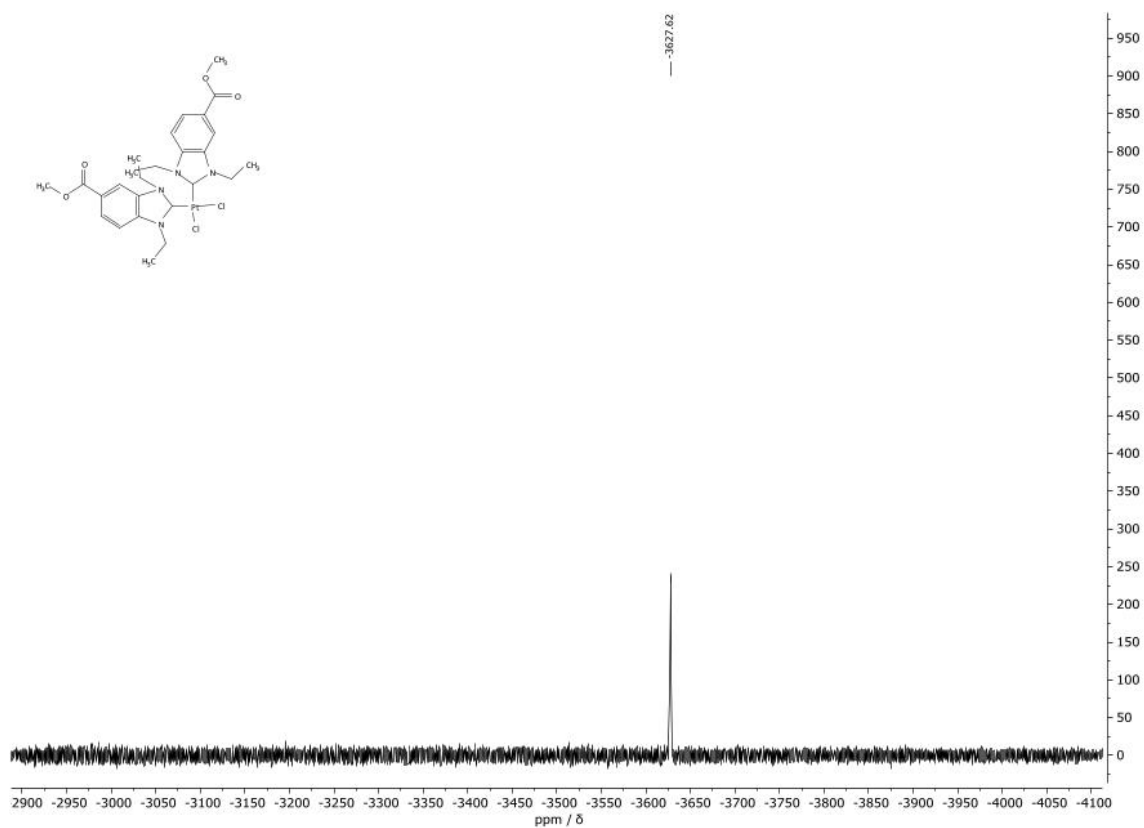


Fig. 42. ^{195}Pt -NMR spectrum of **12b** in CDCl_3 .

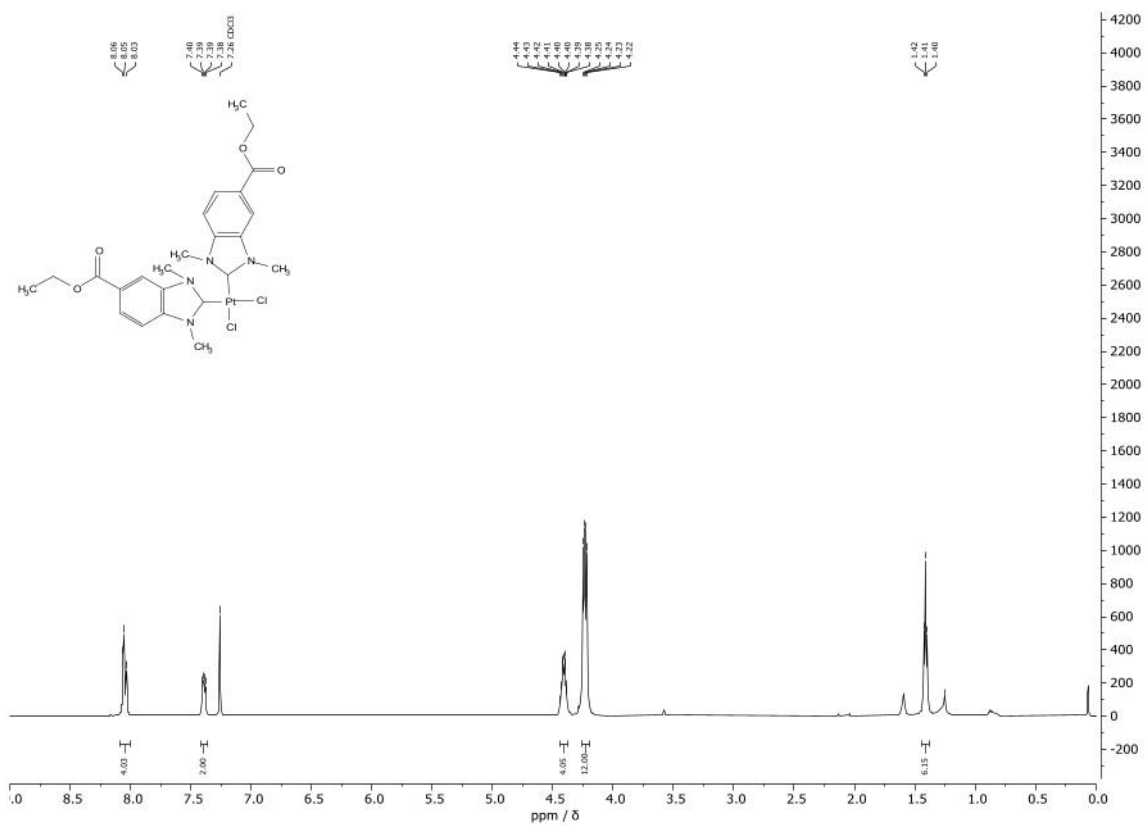


Fig. 43. $^1\text{H-NMR}$ spectrum of **13a** in CDCl_3 .

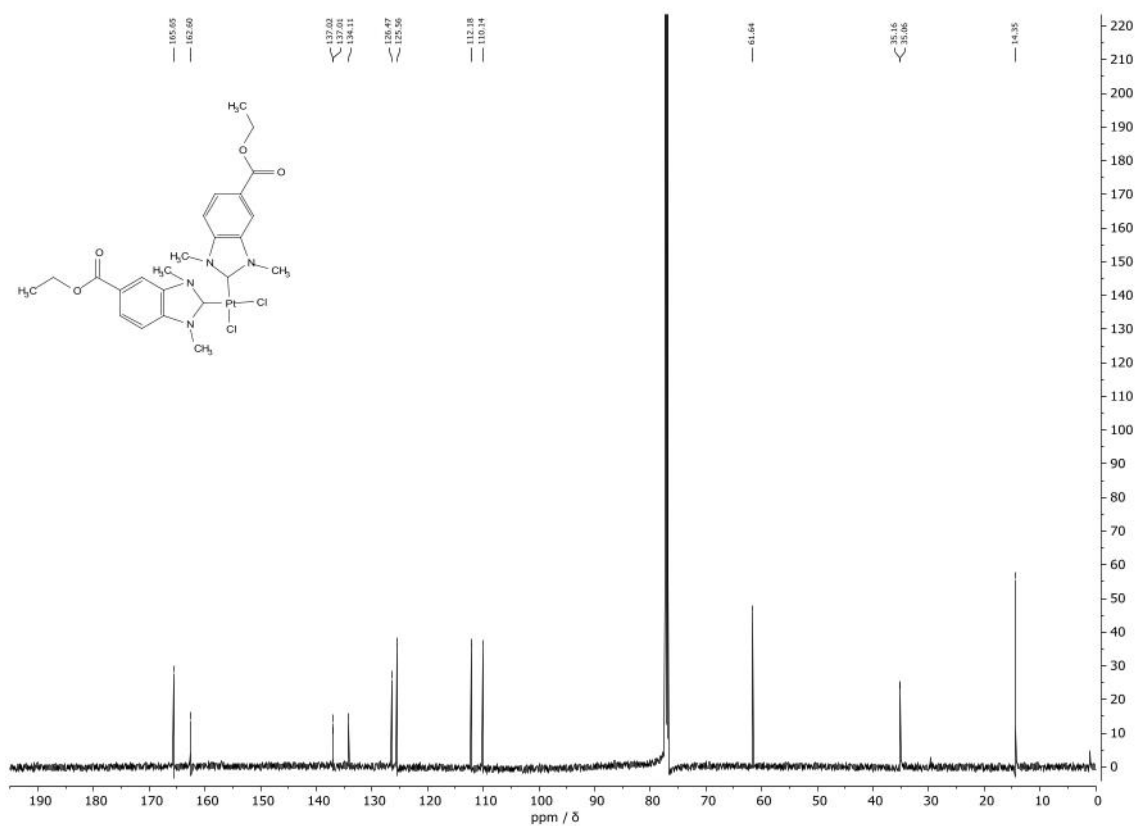


Fig. 44. $^{13}\text{C-NMR}$ spectrum of **13a** in CDCl_3 .

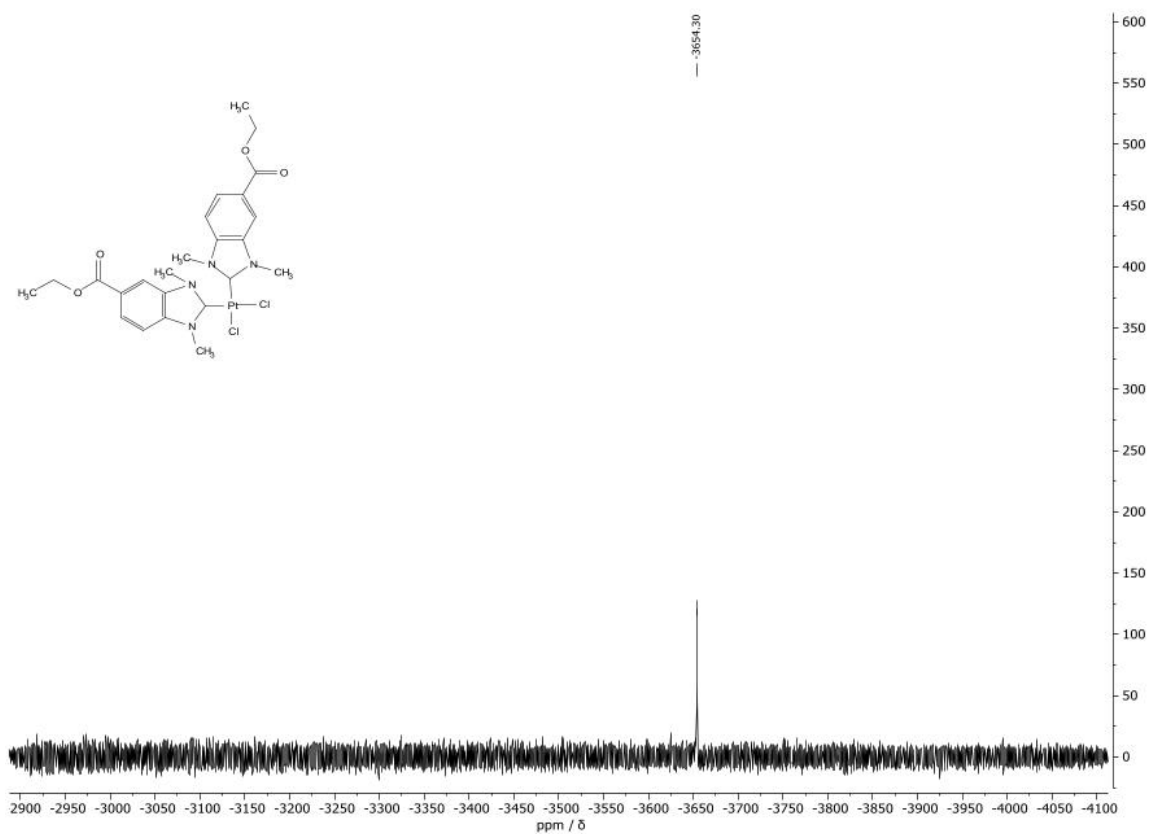


Fig. 45. ^{195}Pt -NMR spectrum of **13a** in CDCl_3 .

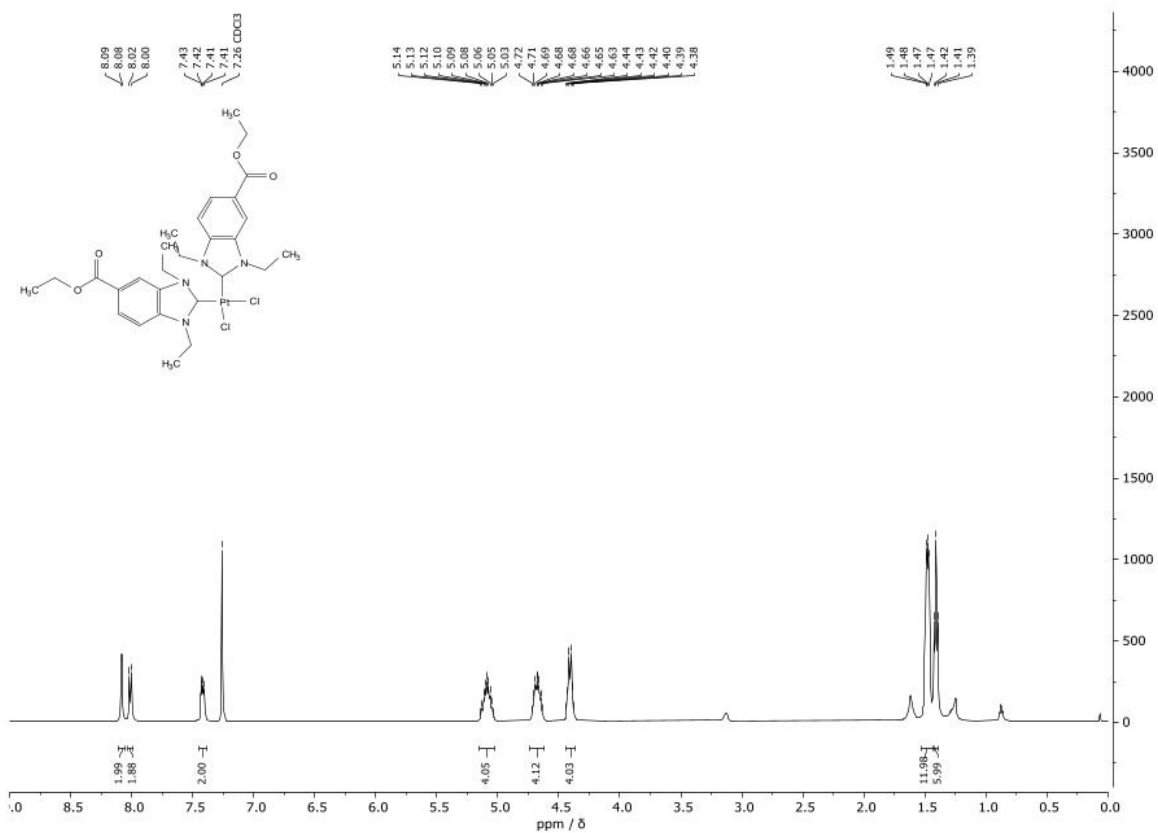


Fig. 46. ^1H -NMR spectrum of **13b** in CDCl_3 .

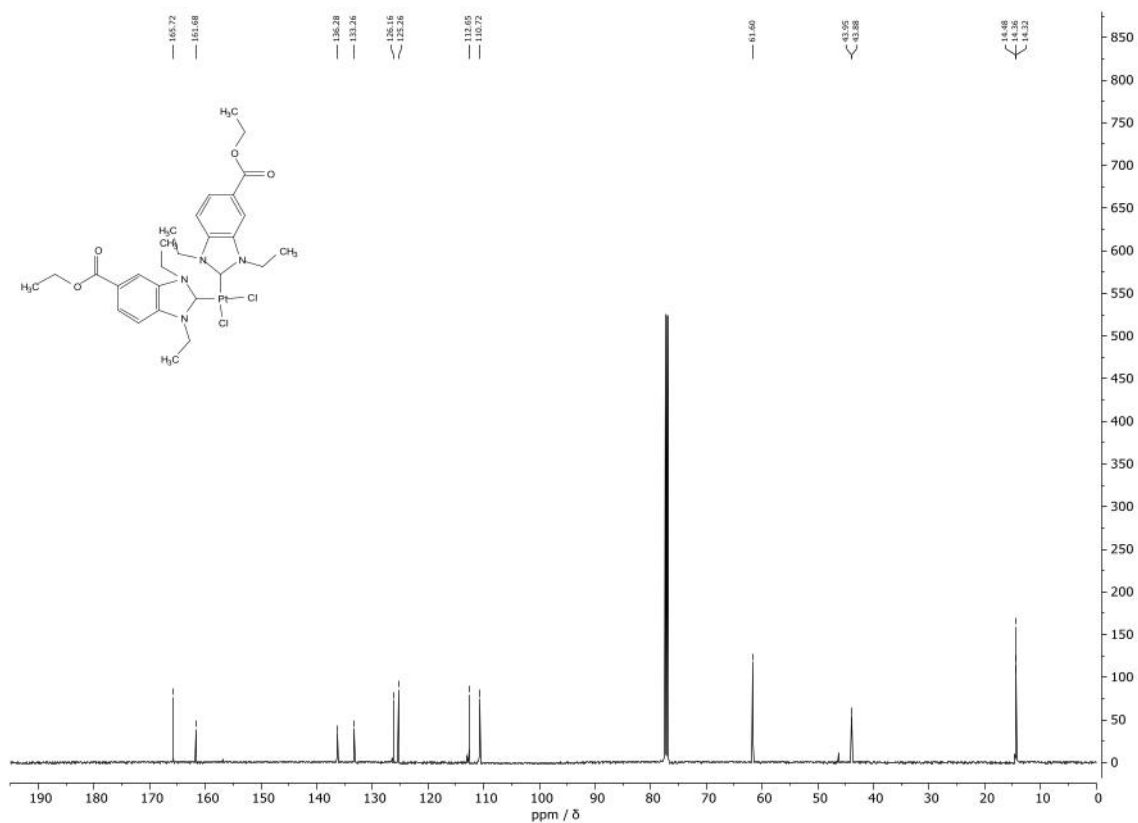


Fig. 47. ^{13}C -NMR spectrum of **13b** in CDCl_3 .

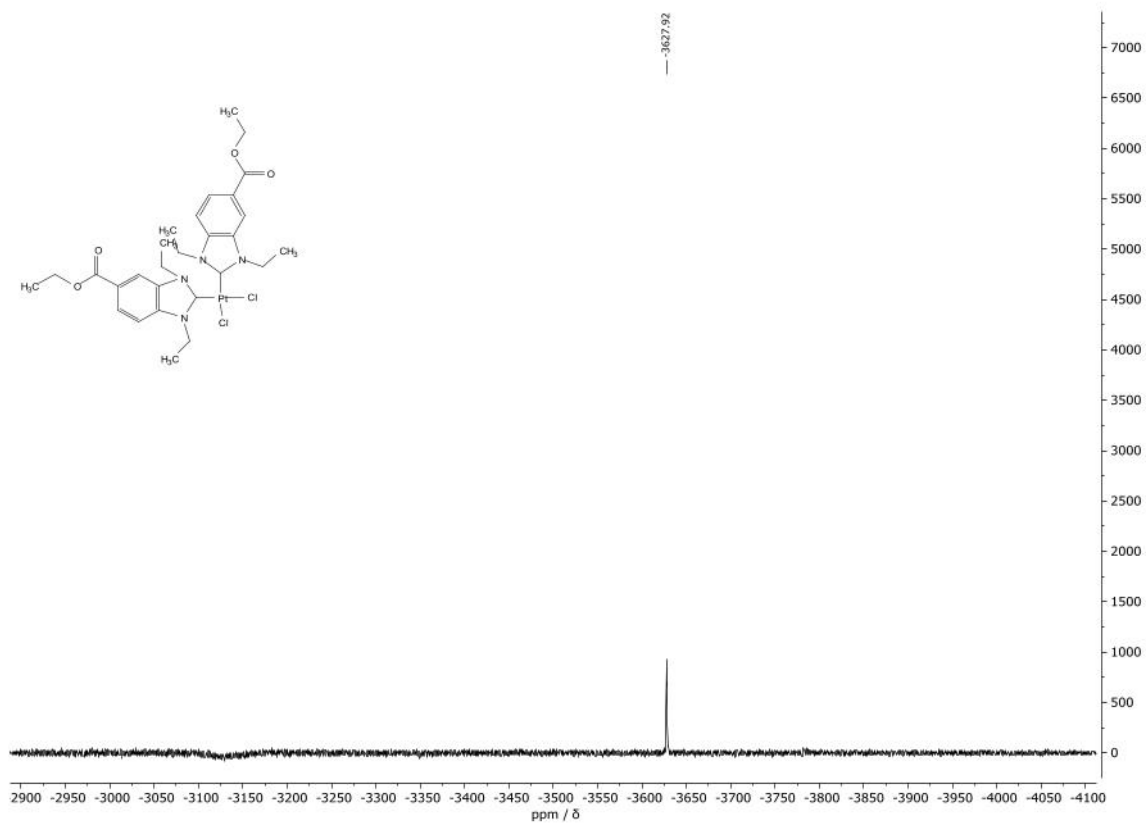


Fig. 48. ^{195}Pt -NMR spectrum of **13b** in CDCl_3 .

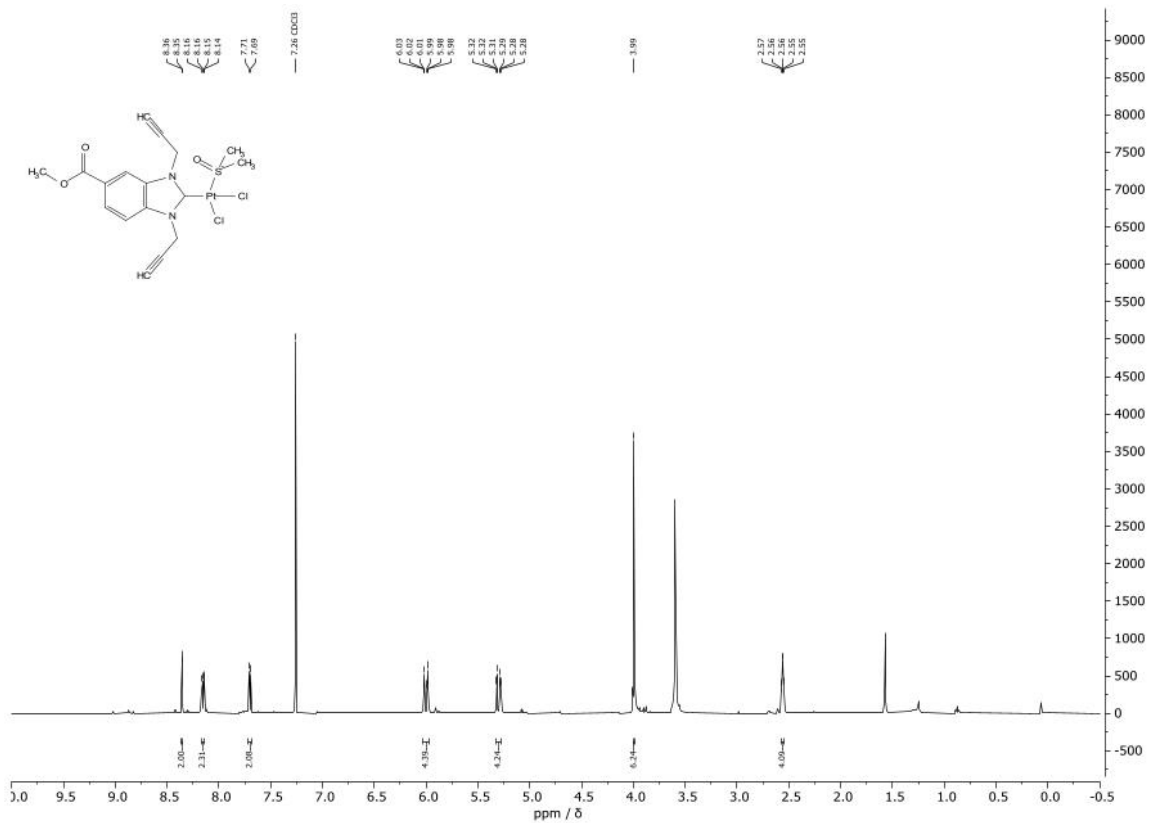


Fig. 49. ¹H-NMR spectrum of **16** in CDCl₃.

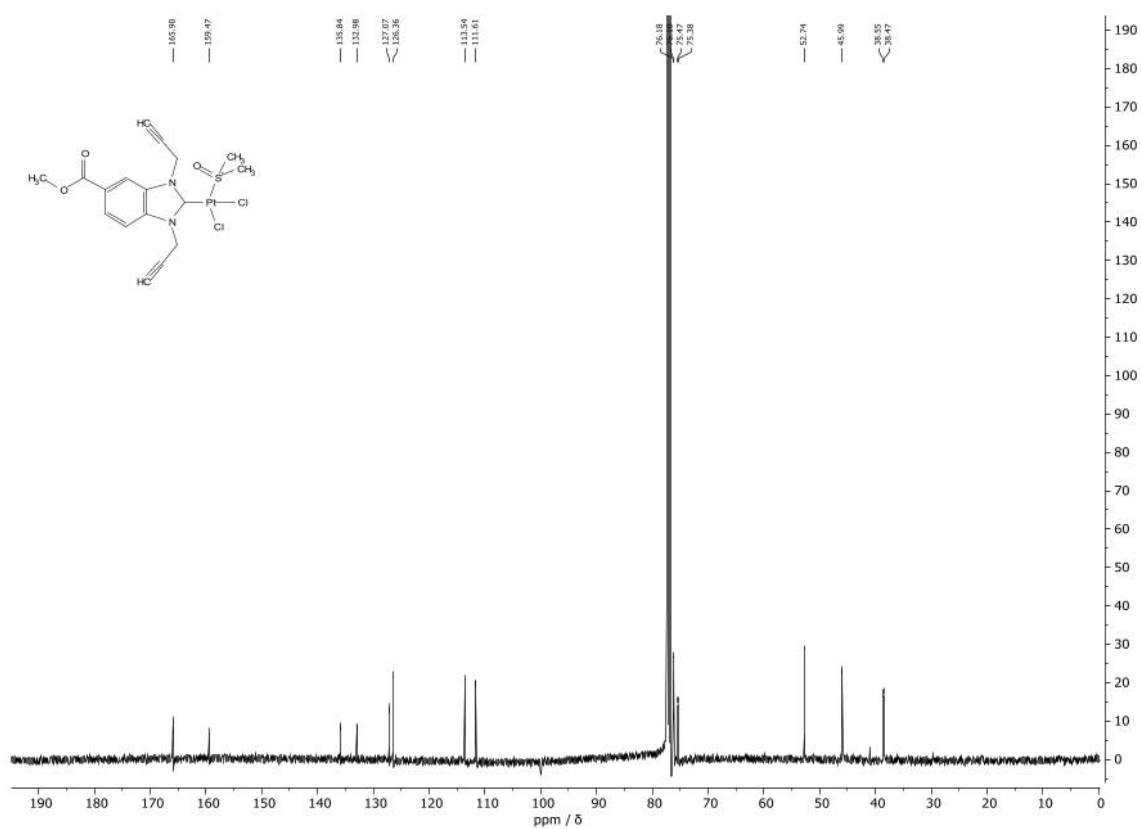


Fig. 50. ¹³C-NMR spectrum of **16** in CDCl₃.

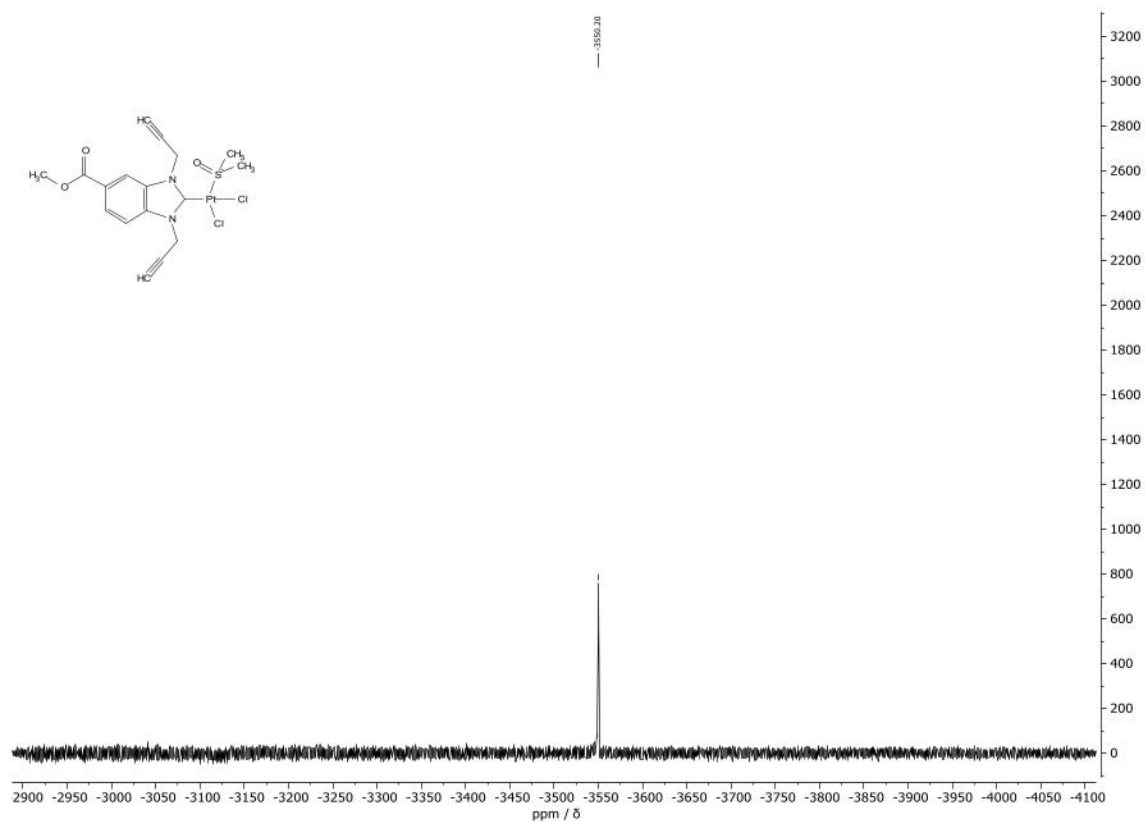


Fig. 51. ^{195}Pt -NMR spectrum of 16 in CDCl_3 .

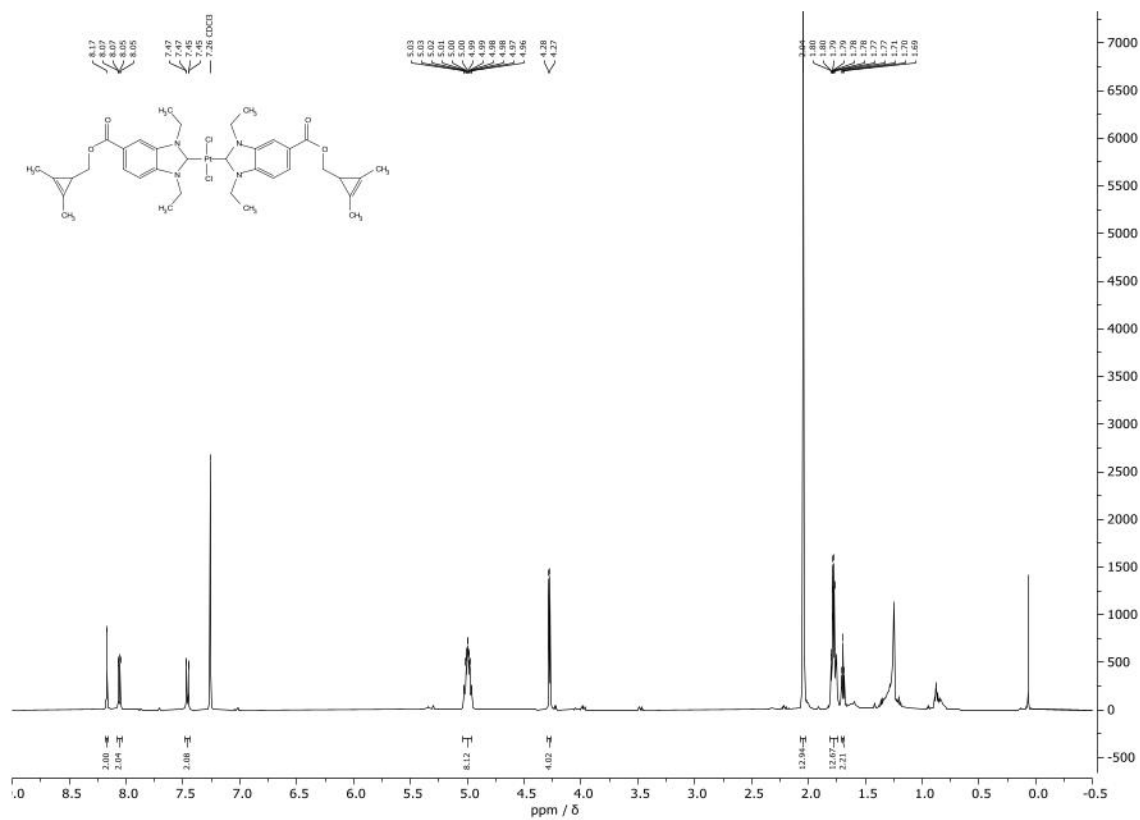


Fig. 52. ^1H -NMR spectrum of 22 in CDCl_3 .

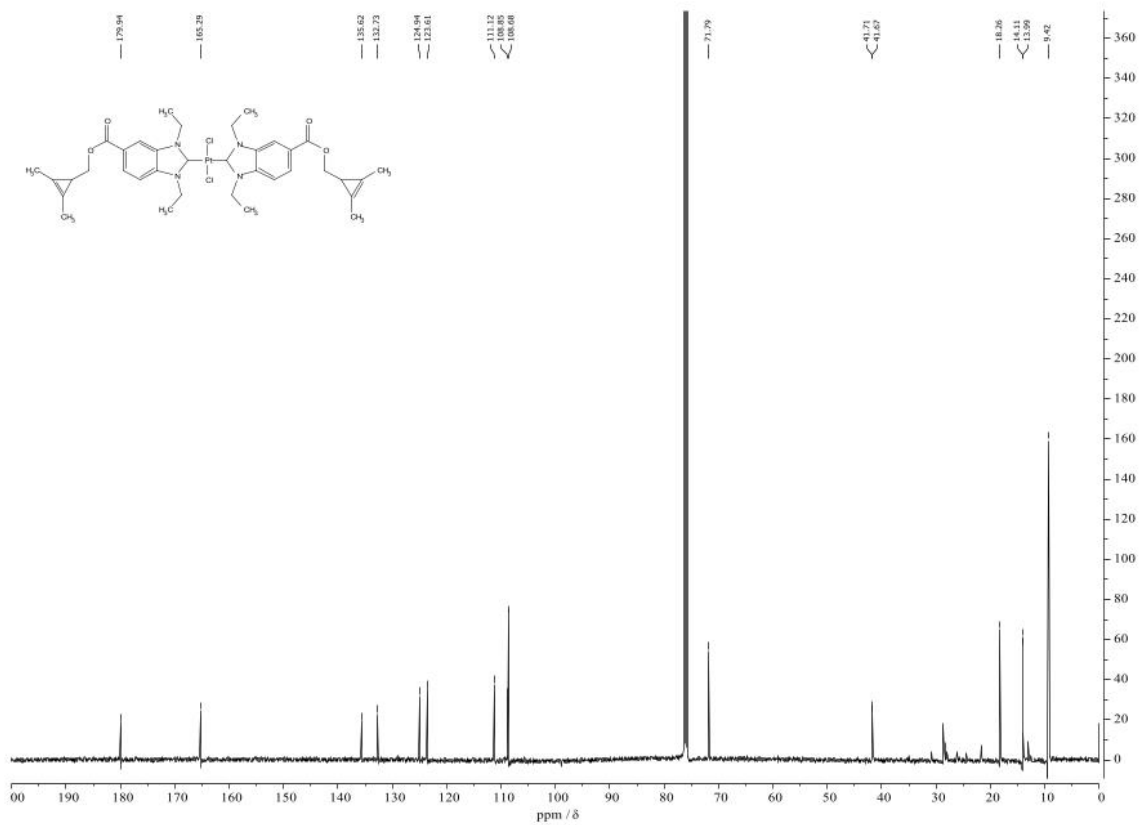


Fig. 53. ^{13}C -NMR spectrum of **22** in CDCl_3 .

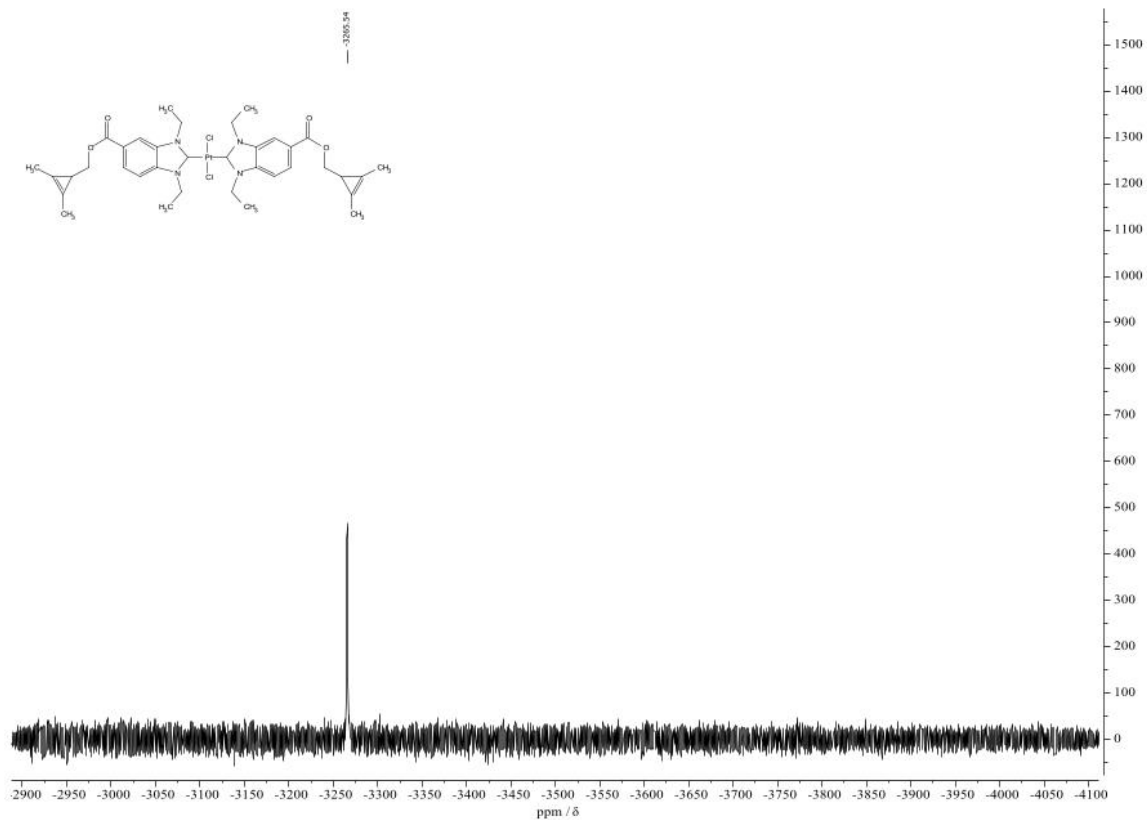


Fig. 54. ^{195}Pt -NMR spectrum of **22** in CDCl_3 .

Stability studies of Pt(II) complexes

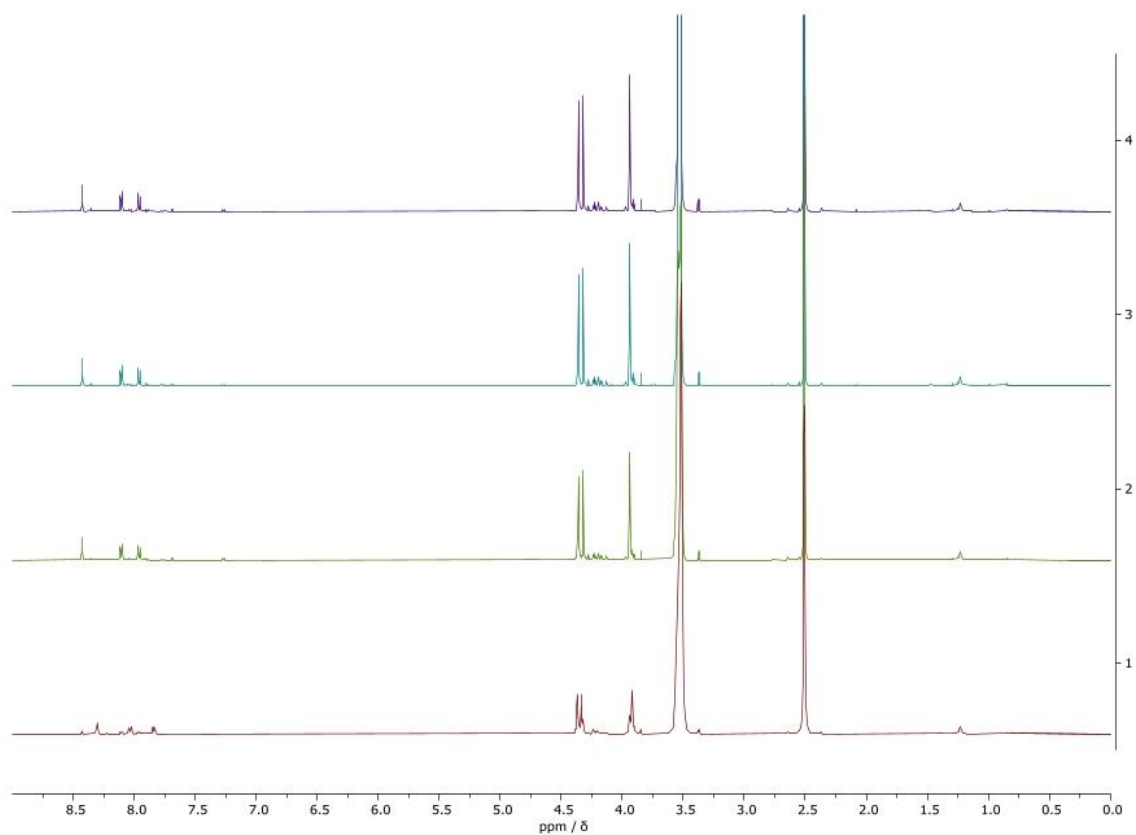


Fig. 55. ¹H-NMR spectrum of **8a** in DMSO-d₆ + 5% D₂O after 0h (red), 24h (green), 48h (cyan) and 72h (purple).

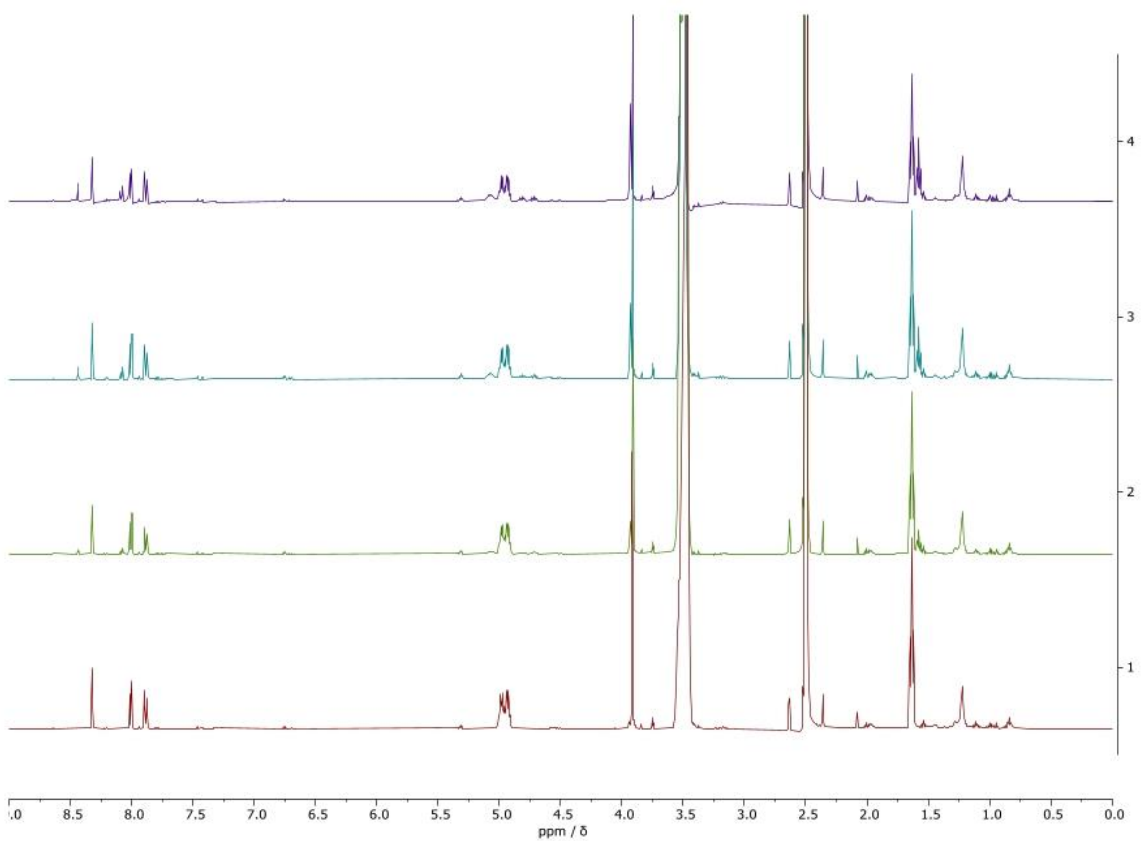


Fig. 56. ¹H-NMR spectrum of **8b** in DMSO-d₆ + 5% D₂O after 0h (red), 24h (green), 48h (cyan) and 72h (purple).

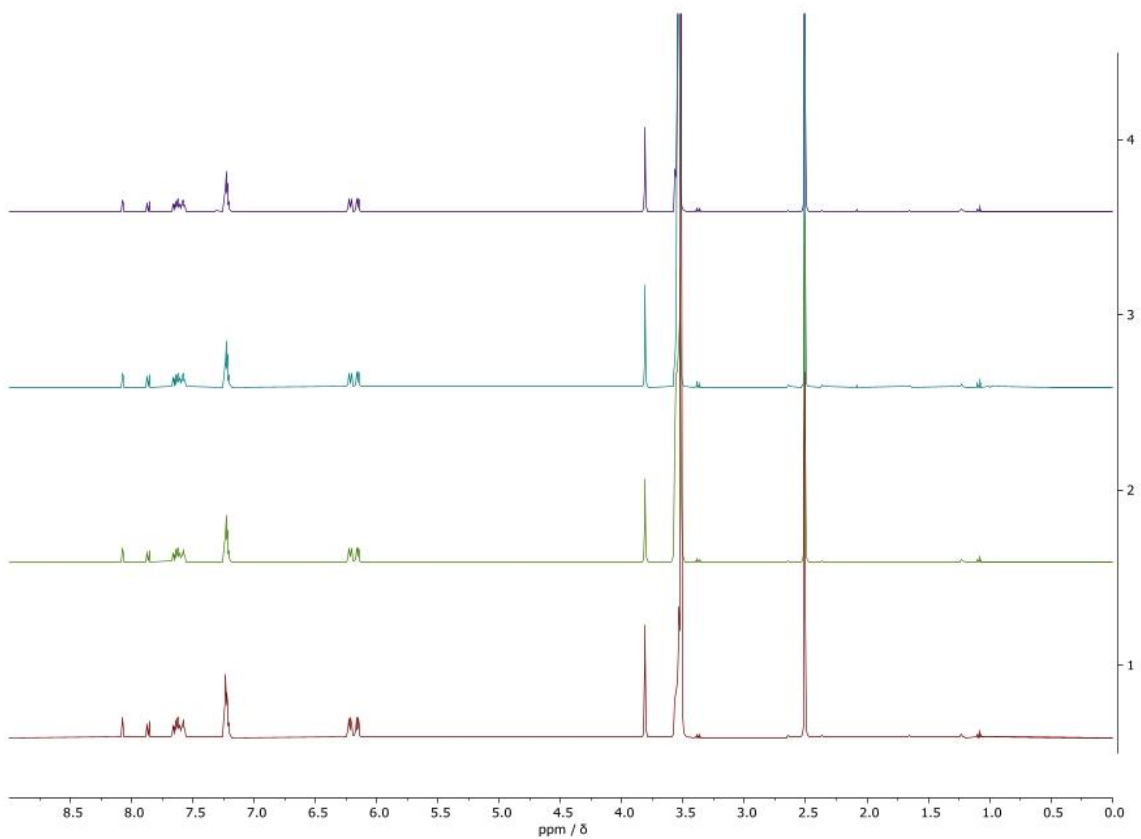


Fig. 57. ¹H-NMR spectrum of **8c** in DMSO-d₆ + 5% D₂O after 0h (red), 24h (green), 48h (cyan) and 72h (purple).

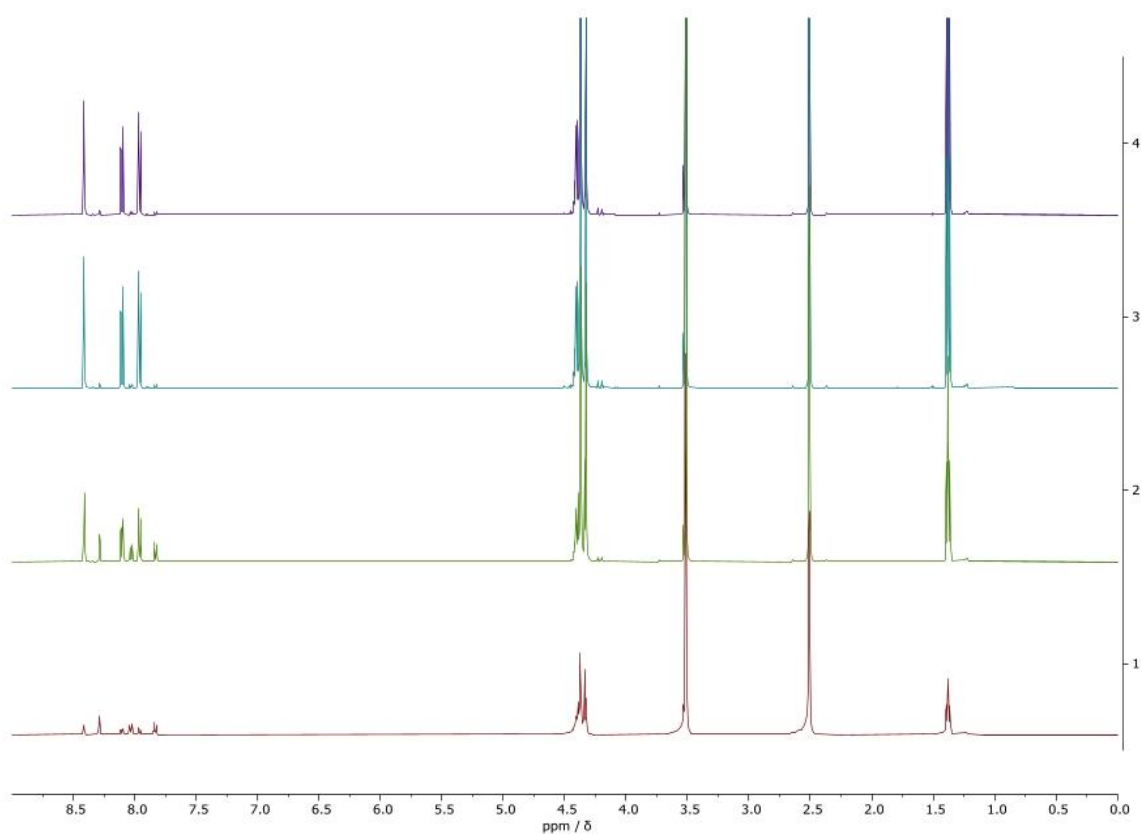


Fig. 58. ¹H-NMR spectrum of **9a** in DMSO-d₆ + 5% D₂O after 0h (red), 24h (green), 48h (cyan) and 72h (purple).

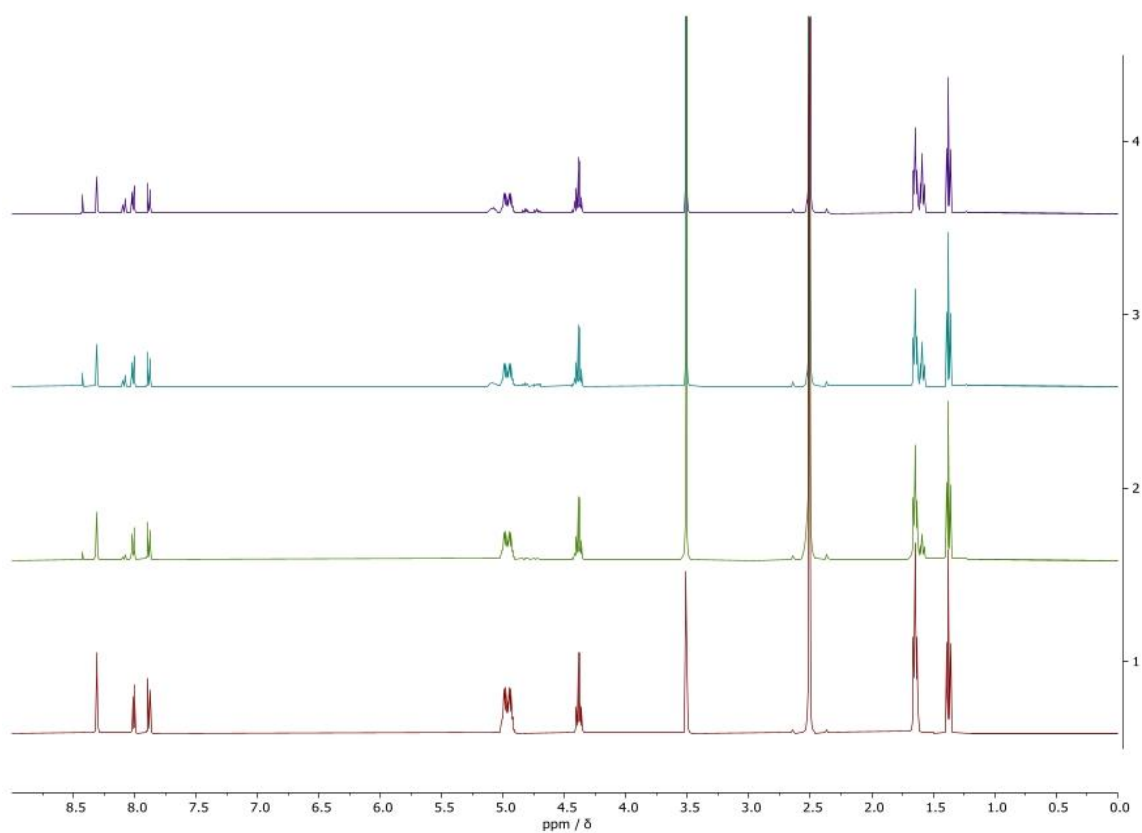


Fig. 59. ¹H-NMR spectrum of **9b** in DMSO-d₆ + 5% D₂O after 0h (red), 24h (green), 48h (cyan) and 72h (purple).

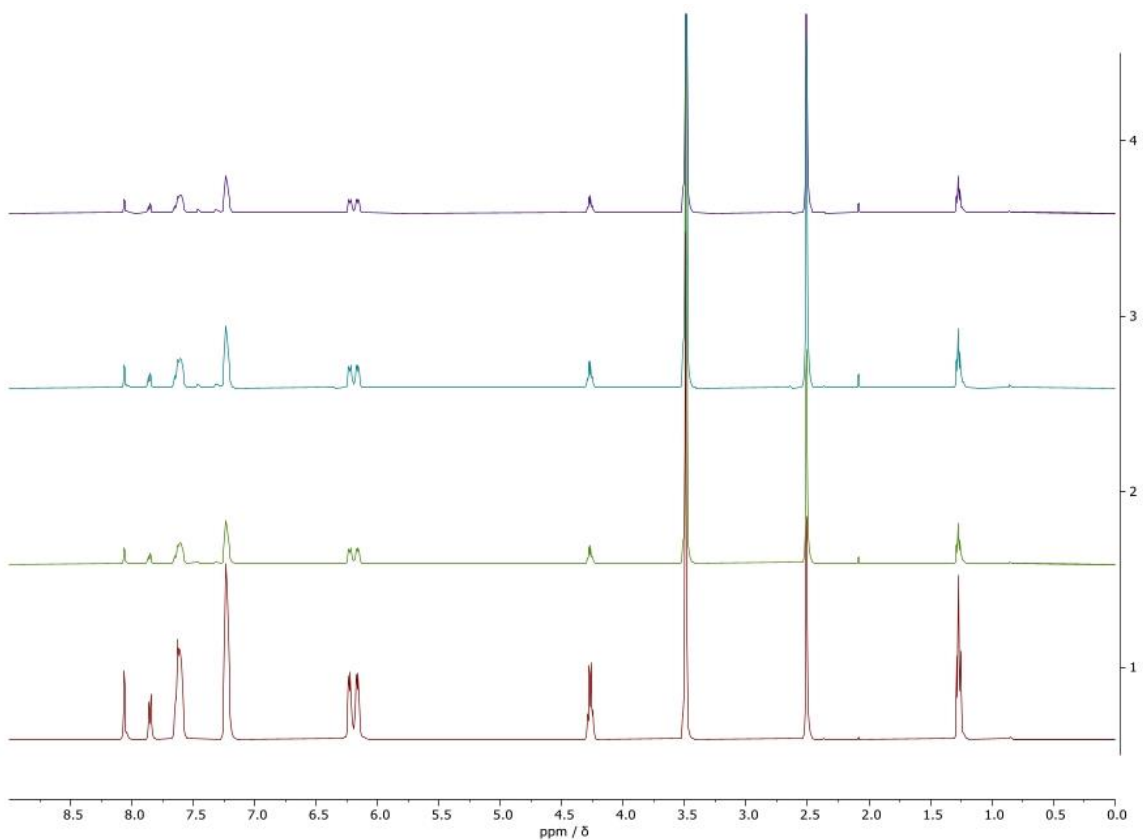


Fig. 60. ¹H-NMR spectrum of **9c** in DMSO-d₆ + 5% D₂O after 0h (red), 24h (green), 48h (cyan) and 72h (purple).

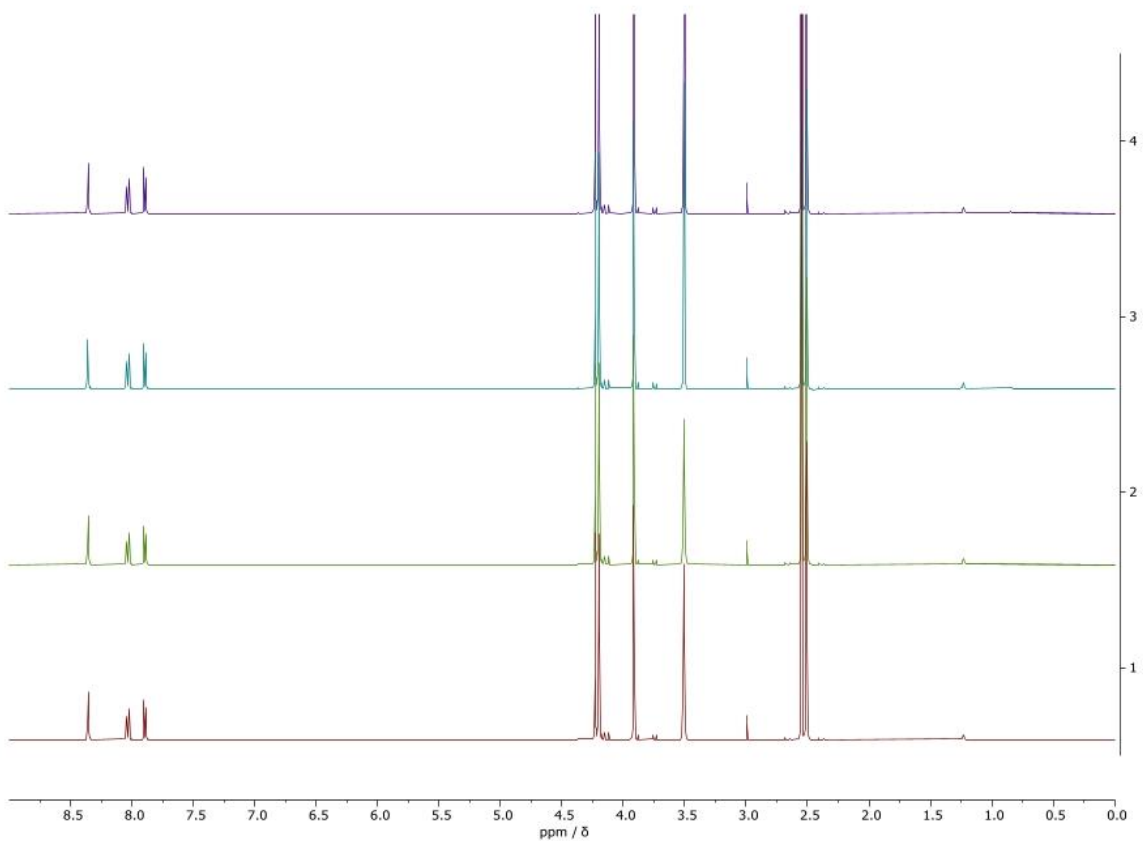


Fig. 61. ¹H-NMR spectrum of **10a** in DMSO-d₆ + 5% D₂O after 0h (red), 24h (green), 48h (cyan) and 72h (purple).

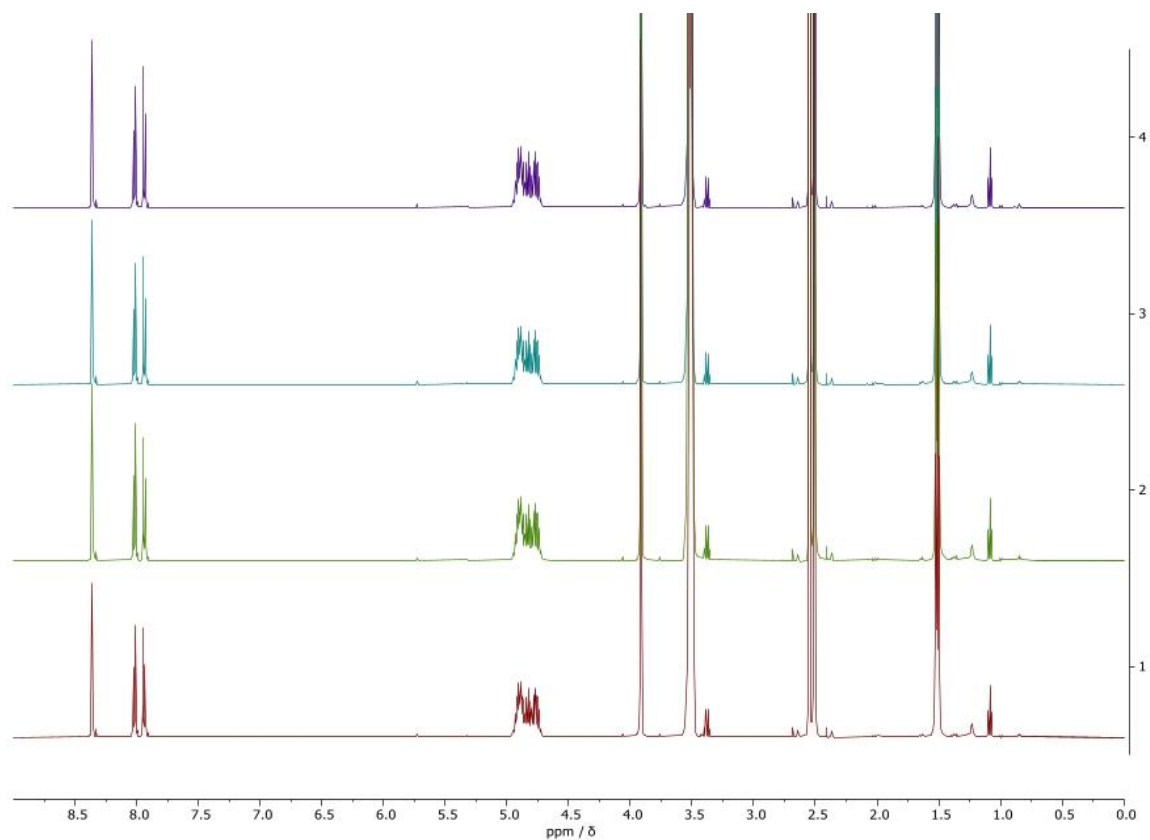


Fig. 62. ¹H-NMR spectrum of **10b** in DMSO-d₆ + 5% D₂O after 0h (red), 24h (green), 48h (cyan) and 72h (purple).

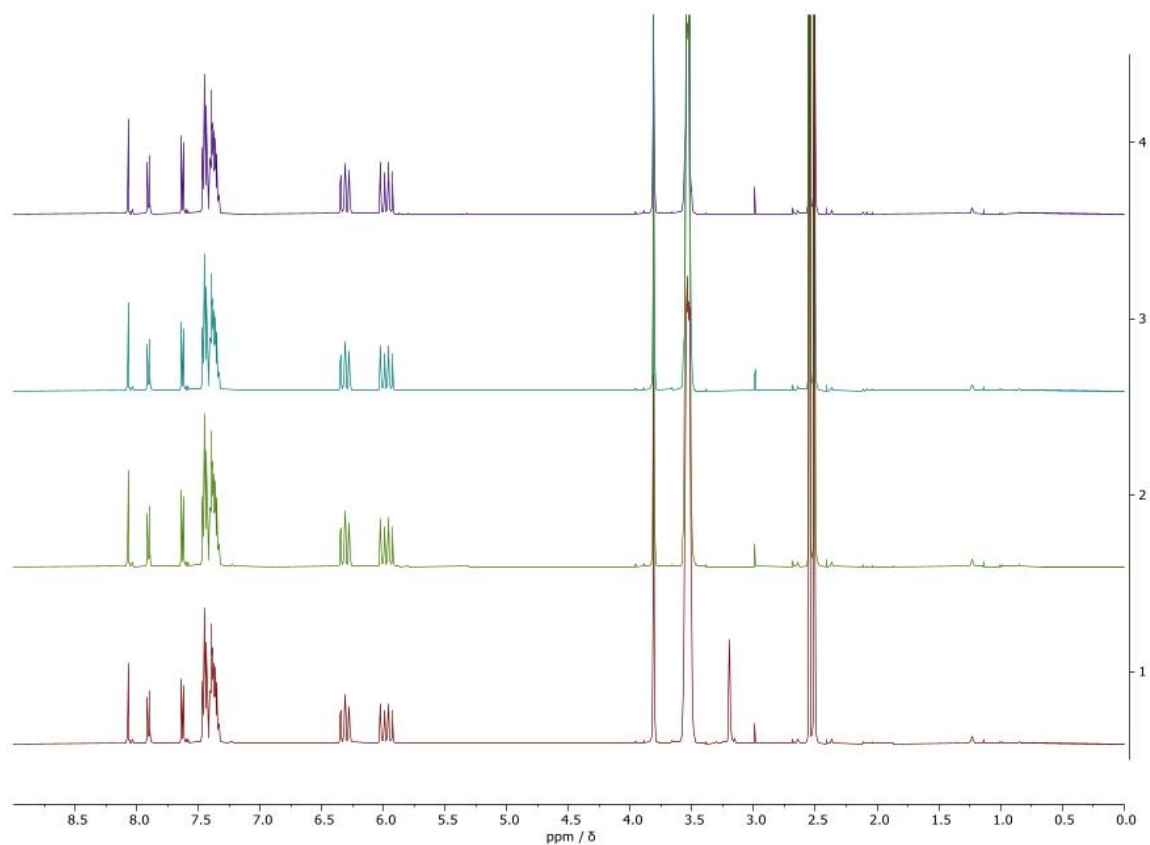


Fig. 63. ¹H-NMR spectrum of **10c** in DMSO-d₆ + 5% D₂O after 0h (red), 24h (green), 48h (cyan) and 72h (purple).

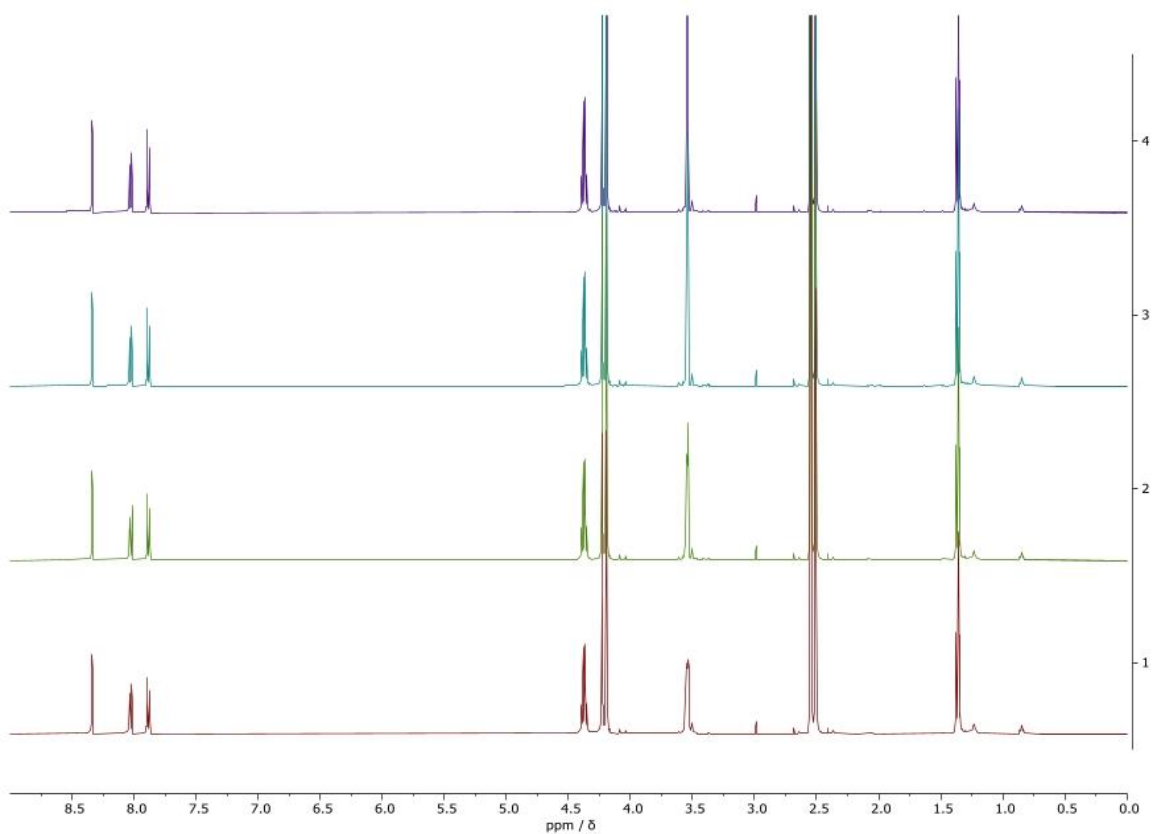


Fig. 64. ¹H-NMR spectrum of **11a** in DMSO-d₆ + 5% D₂O after 0h (red), 24h (green), 48h (cyan) and 72h (purple).

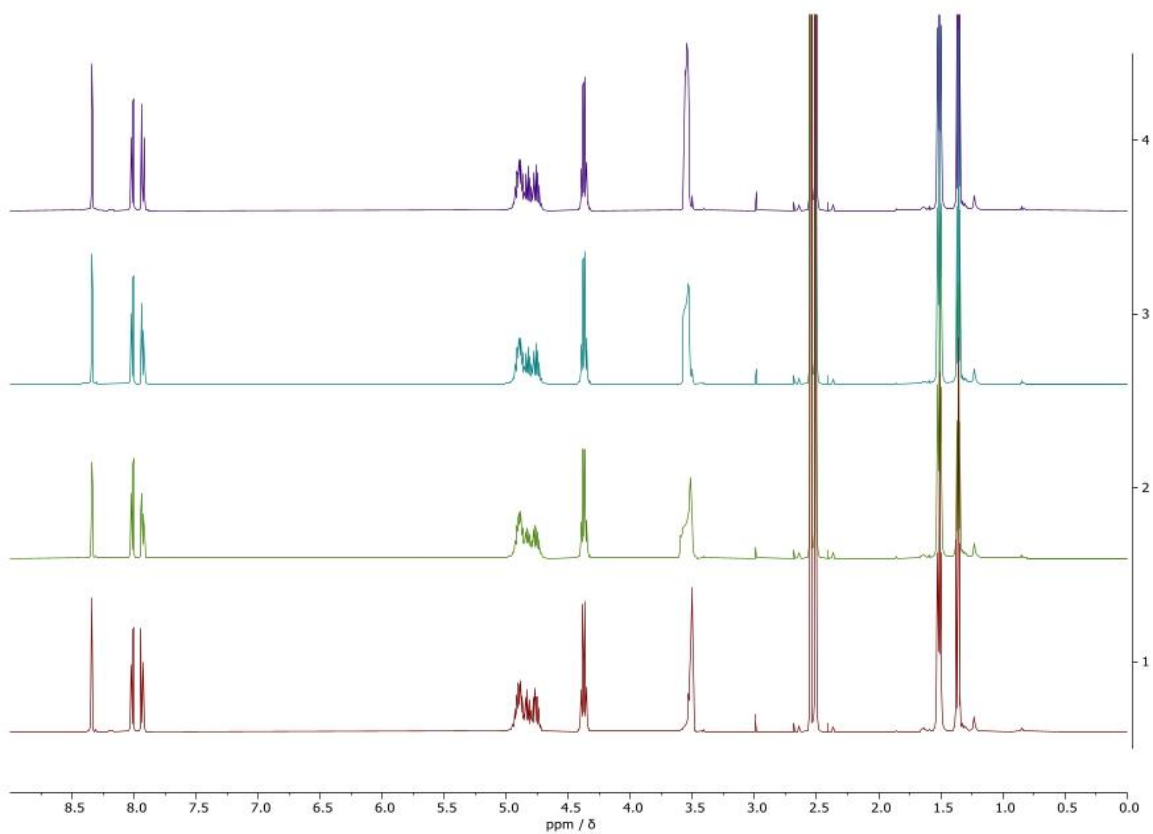


Fig. 65. ¹H-NMR spectrum of **11b** in DMSO-d₆ + 5% D₂O after 0h (red), 24h (green), 48h (cyan) and 72h (purple).

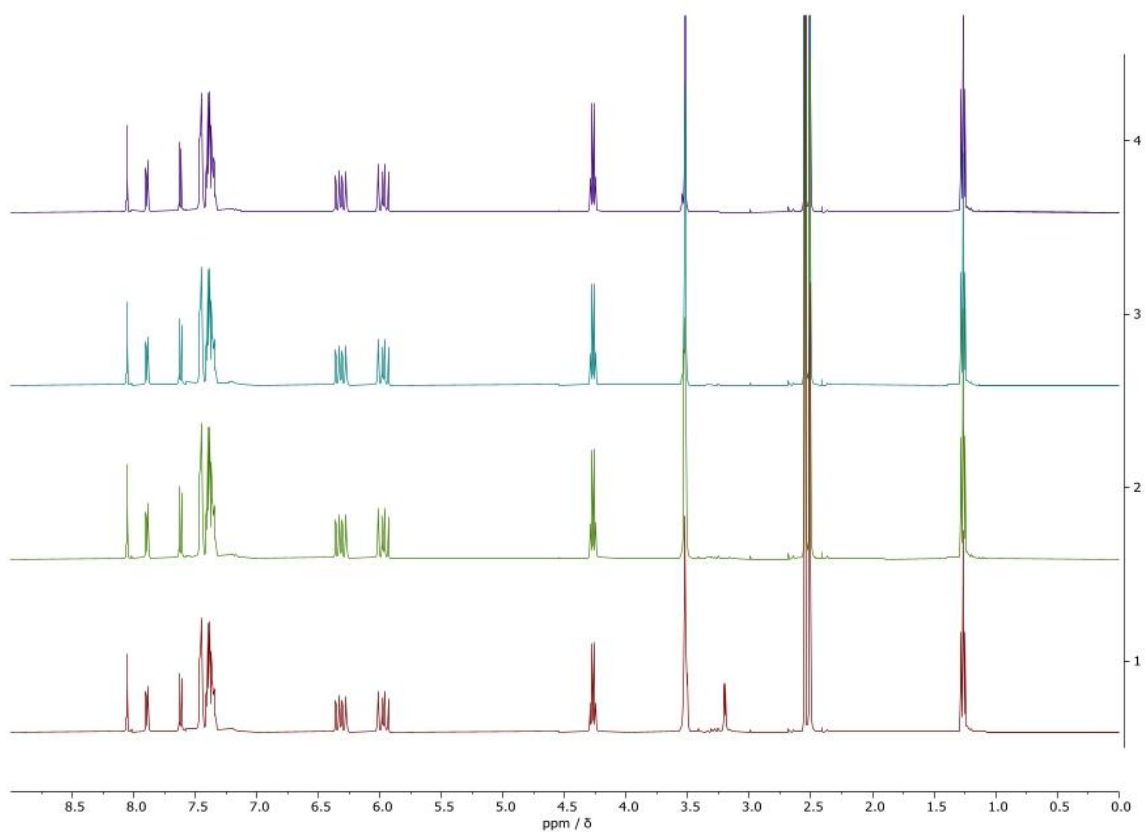


Fig. 66. ¹H-NMR spectrum of **11c** in DMSO-d₆ + 5% D₂O after 0h (red), 24h (green), 48h (cyan) and 72h (purple).

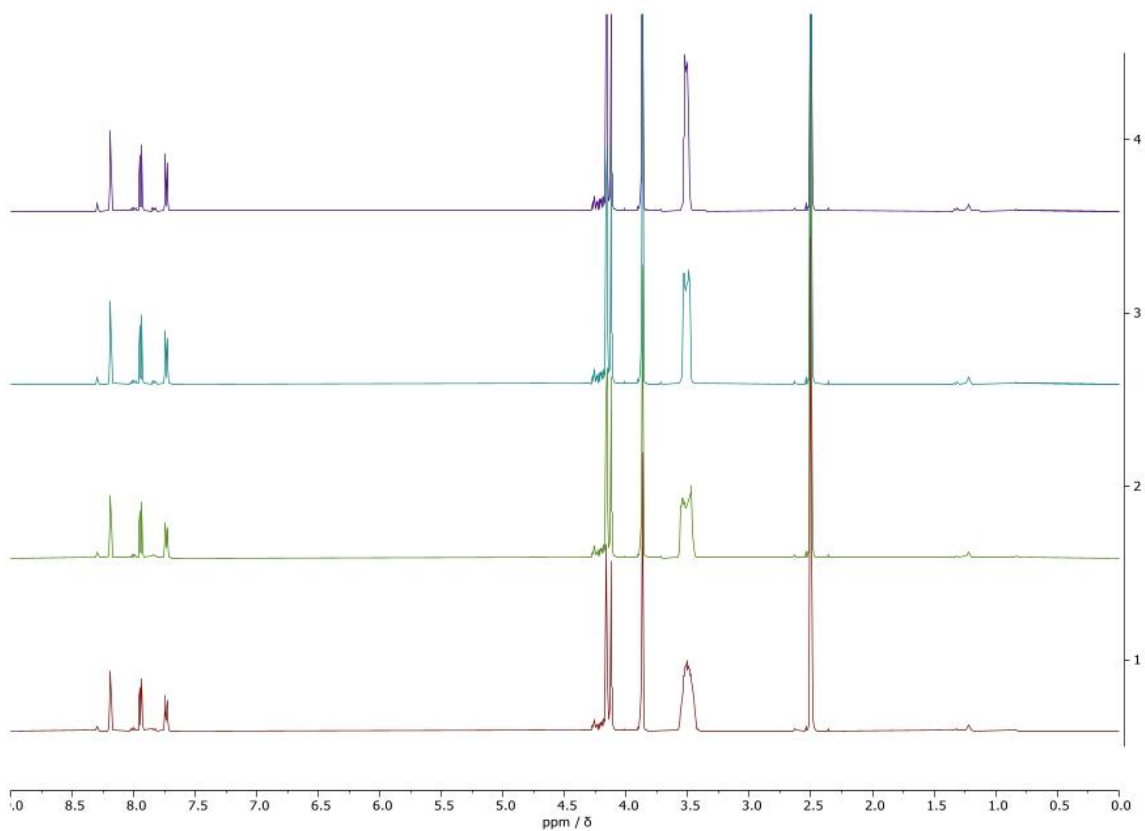


Fig. 67. ¹H-NMR spectrum of **12a** in DMSO-d₆ + 5% D₂O after 0h (red), 24h (green), 48h (cyan) and 72h (purple).

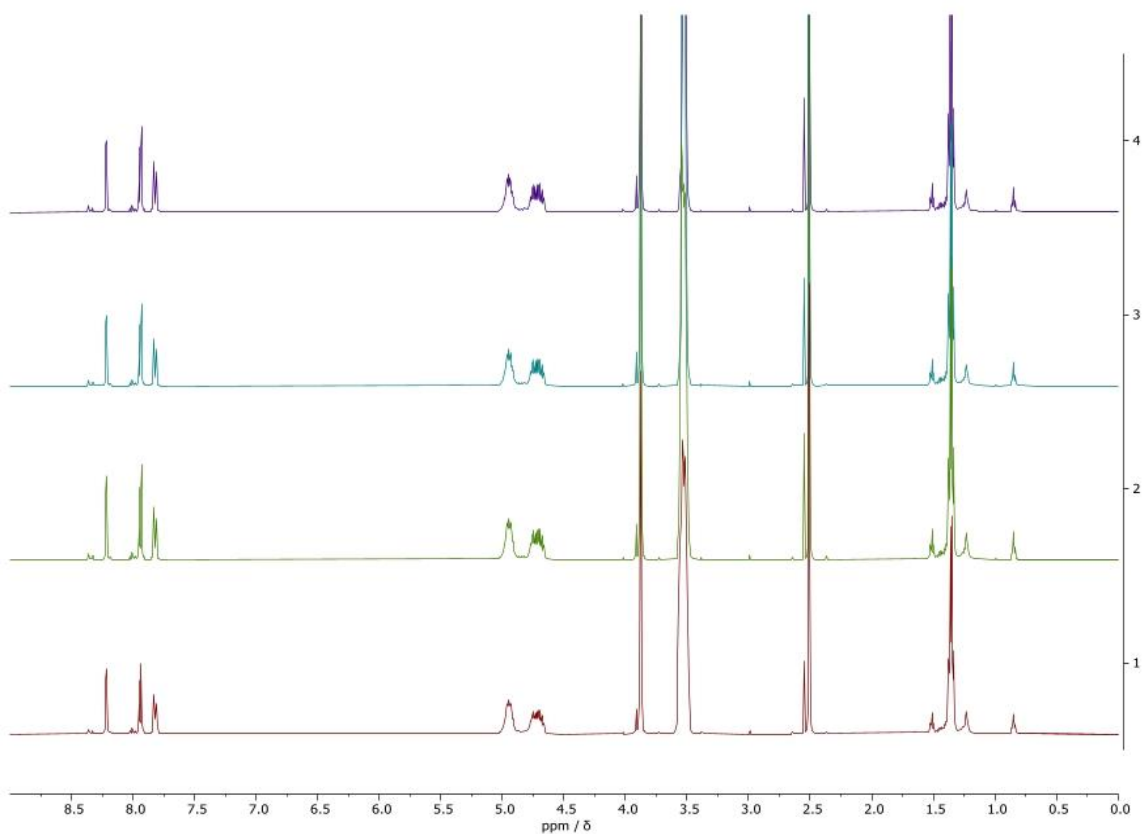


Fig. 68. ¹H-NMR spectrum of **12b** in DMSO-d₆ + 5% D₂O after 0h (red), 24h (green), 48h (cyan) and 72h (purple).

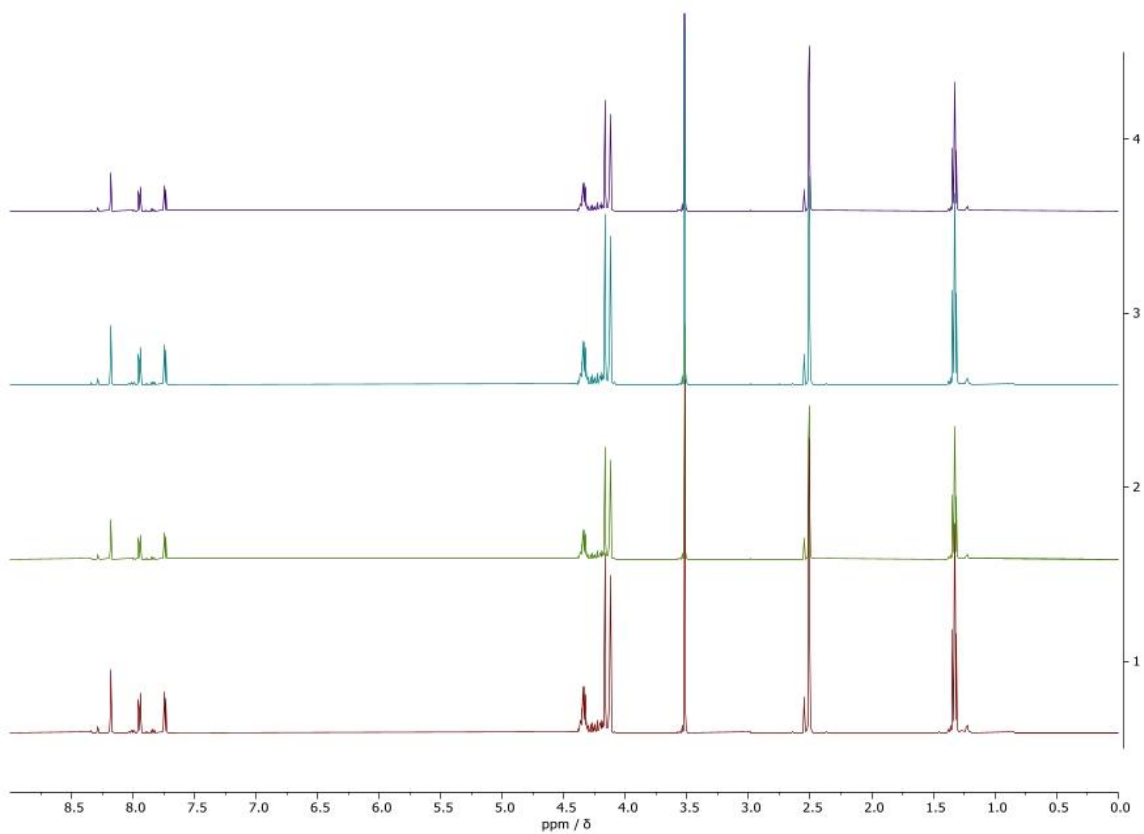


Fig. 69. ¹H-NMR spectrum of **13a** in DMSO-d₆ + 5% D₂O after 0h (red), 24h (green), 48h (cyan) and 72h (purple).

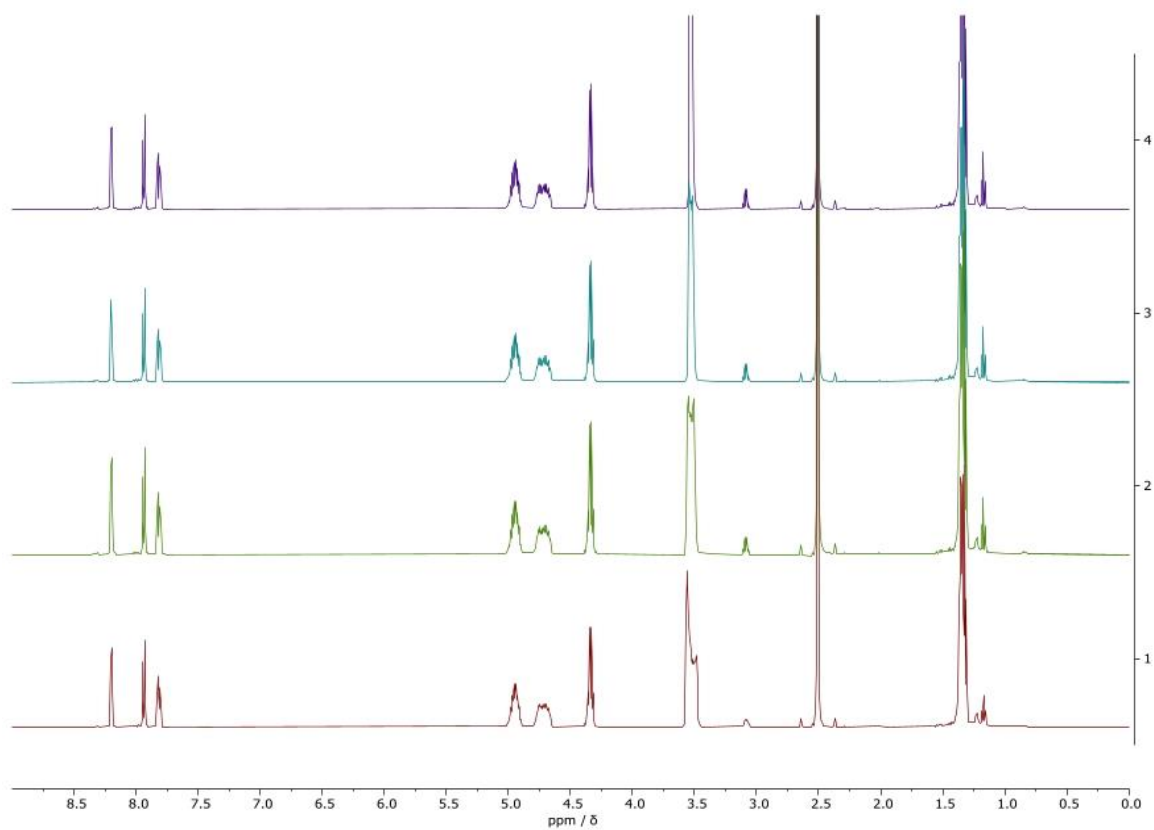


Fig. 70. $^1\text{H-NMR}$ spectrum of **13b** in $\text{DMSO-d}_6 + 5\% \text{D}_2\text{O}$ after 0h (red), 24h (green), 48h (cyan) and 72h (purple).

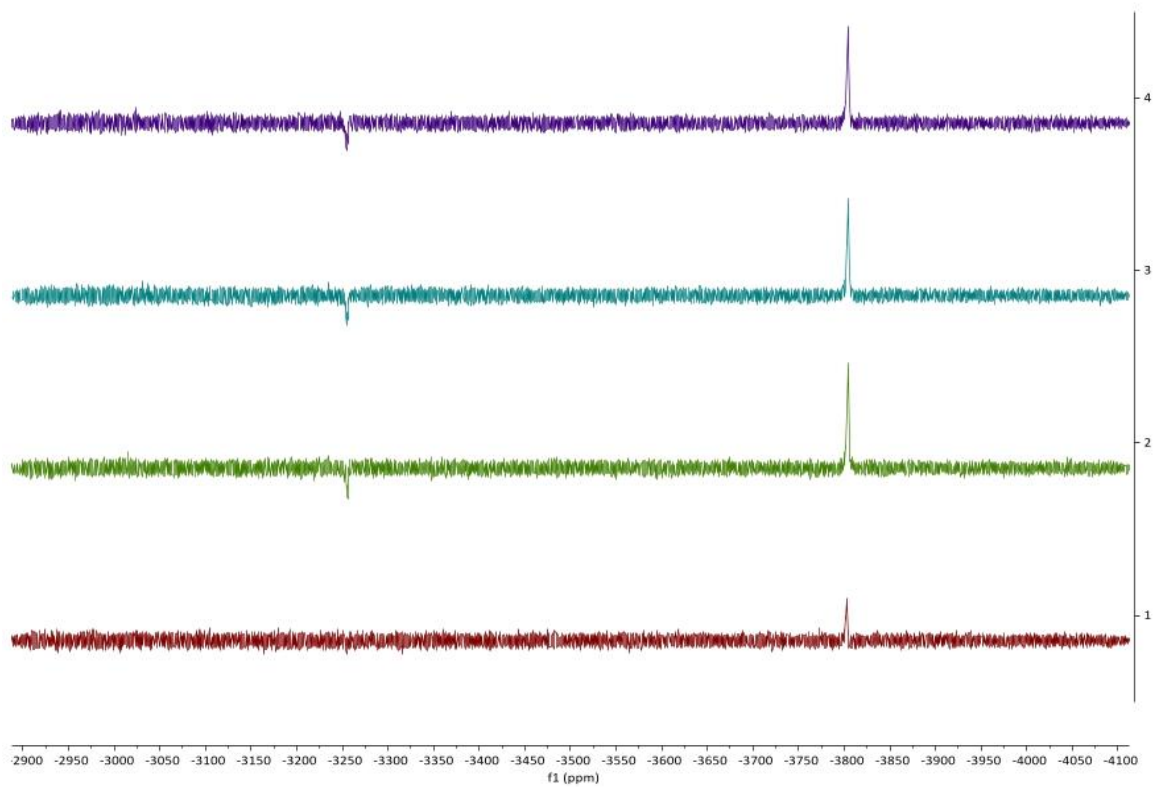


Fig. 71. $^{195}\text{Pt-NMR}$ spectrum of **9a** in DMSO-d_6 after 0h (red), 24h (green), 48h (cyan) and 72h (purple).

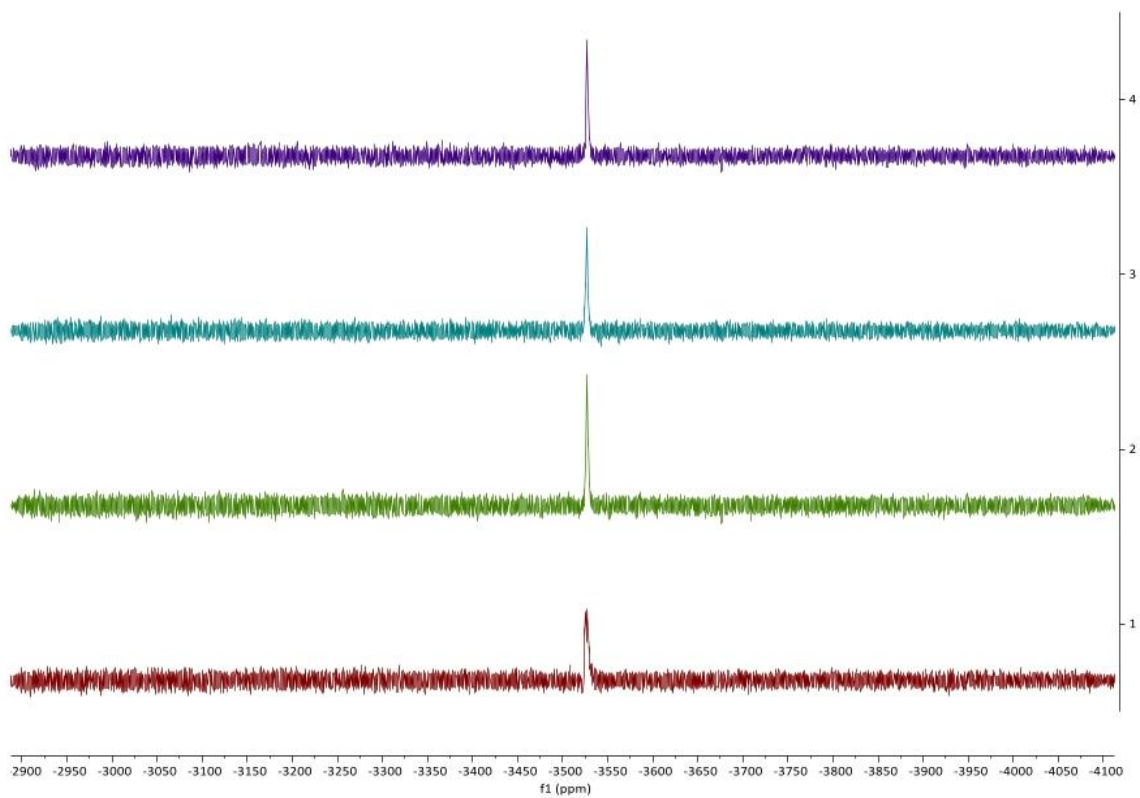


Fig. 72. ^{195}Pt -NMR spectrum of **10c** in DMSO-d_6 after 0h (red), 24h (green), 48h (cyan) and 72h (purple).

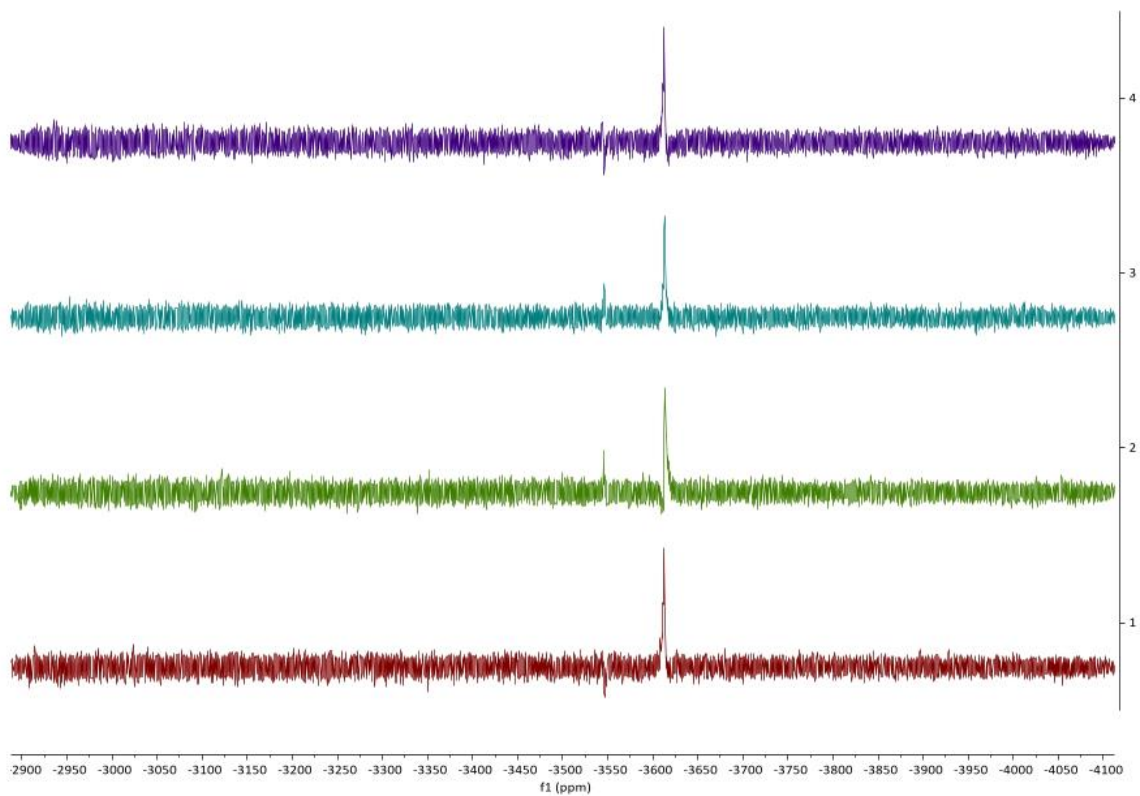


Fig. 73. ^{195}Pt -NMR spectrum of **13b** in DMSO-d_6 after 0h (red), 24h (green), 48h (cyan) and 72h (purple).

References

1. Senadi, G.C., Kudale, V.S., and Wang, J.-J., *Sustainable methine sources for the synthesis of heterocycles under metal- and peroxide-free conditions*, *Green Chem.*, 21 (2019), 979-985, <https://doi.org/10.1039/C8GC03839B>
2. Gao, X., et al., *Atmospheric CO₂ promoted synthesis of N-containing heterocycles over B(C₆F₅)₃ catalyst*, *New Journal of Chemistry*, 40 (2016), 8282-8287, <https://doi.org/10.1039/C6NJ01721E>

Ligand Effects

Guided Antitumoural Drugs: (Imidazol-2-ylidene)(L)gold(I) Complexes Seeking Cellular Targets Controlled by the Nature of Ligand L

Sofia I. Bär⁺, Madeleine Gold⁺, Sebastian W. Schleser, Tobias Rehm, Alexander Bär, Leonhard Köhler, Lucas R. Carnell, Bernhard Biersack, and Rainer Schobert^{*[a]}

Abstract: Three [1,3-diethyl-4-(*p*-methoxyphenyl)-5-(3,4,5-trimethoxyphenyl)imidazol-2-ylidene](L)gold(I) complexes, **4a** (L = Cl), **5a** (L = PPh₃), and **6a** (L = same N-heterocyclic carbene (NHC)), and their fluorescent [4-(anthracen-9-yl)-1,3-diethyl-5-phenylimidazol-2-ylidene](L)gold(I) analogues, **4b**, **5b**, and **6b**, respectively, were studied for their localisation and effects in cancer cells. Despite their identical NHC ligands, the last three accumulated in different compartments of melanoma cells, namely, the nucleus (**4b**), mitochondria (**5b**), or lysosomes (**6b**). Ligand L was also more decisive for

the site of accumulation than the NHC ligand because the couples **4a/4b**, **5a/5b**, and **6a/6b**, carrying different NHC ligands, afforded similar results in cytotoxicity tests, and tests on targets typically found at their sites of accumulation, such as DNA in nuclei, reactive oxygen species and thioredoxin reductase in mitochondria, and lysosomal membranes. Regardless of the site of accumulation, cancer cell apoptosis was eventually induced. The concept of guiding a bioactive complex fragment to a particular subcellular target by secondary ligand L could reduce unwanted side effects.

Introduction

Although N-heterocyclic carbene (NHC) complexes have been much used as catalysts, their medicinal relevance was recognised surprisingly late, given their chemical stability under physiological conditions and their structural flexibility.^[1,2] Unlike cisplatin (CDDP) and related platinum coordination complexes, which all lead to DNA adducts, resulting in an inhibition of the cancer cell cycle and eventually in apoptotic cancer cell death,^[3] NHC complexes of various metals may address a broader array of molecular targets. Complexes with the character of delocalised lipophilic cations (DLCs) were found to selectively accumulate in mitochondria, which can be explained by their negative inner transmembrane potential.^[4,5] Because cancer cells have a more hyperpolarised mitochondrial membrane potential (MMP) than normal cells, the selective accumulation of metal–carbene complexes with DLC character in cancer cells can be expected.^[5,6] With the detection of antitu-

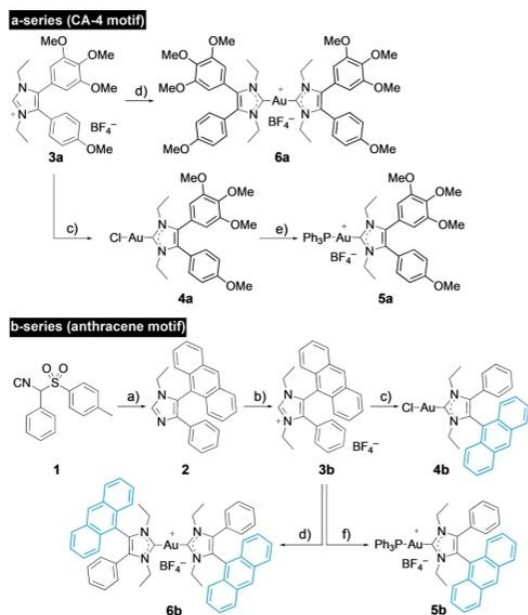
mour activity of the antirheumatic gold(I) compound auranofin, (2,3,4,6-tetra-*O*-acetyl-1-thio-β-D-glucopyranosato)(triethylphosphane)gold, gold complexes came to the fore as potential anticancer drug candidates.^[7] Auranofin mainly acts through the inhibition of mitochondrial thioredoxin reductase (TrxR) and by enhancing the mitochondrial permeability.^[8,9] Through the inhibition of TrxR activity, the intracellular levels of reactive oxygen species (ROS) rise, which damages predominantly cancer cells because of their elevated ROS levels compared with healthy cells.^[10] As a result, cytochrome c is released into the cytosol, triggering apoptotic cell death.^[11] Due to their stability, NHC ligands can also be annulated and substituted in multifarious ways, allowing the mimicking or combinatorial attachment of pharmacophores to afford pleiotropic drugs.^[12] Herein, we report on NHC gold(I) complexes **4a–6a**, carrying a 1,3-diethyl-4-(4-methoxyphenyl)-5-(3,4,5-trimethoxyphenyl)imidazol-2-ylidene ligand, akin to the natural antimetabolic combretastatin A4 (CA-4), and differing only in the second ligand on the gold atom (Scheme 1). Preliminary studies had shown strong cytotoxicity against cancer cells with IC₅₀ values in the low triple- to double-digit nanomolar range for complex **6a**, but its actual mechanism of action remained unclear.^[13] A second series of complexes **4b–6b**, bearing the same “second ligands L”, yet a better detectable fluorescent 1,3-diethyl-4-(anthracen-9-yl)-5-phenylimidazol-2-ylidene ligand, were synthesised and studied for their intracellular accumulation and their modes of anticancer action. The aim of this study was to find out whether ligand L could be used to set the site of accumulation, and thus, the targets and nature of antitumour effects of gold complexes with identical or closely related NHC li-

[a] S. I. Bär,⁺ M. Gold,⁺ S. W. Schleser, Dr. T. Rehm, A. Bär, L. Köhler, L. R. Carnell, Dr. B. Biersack, Prof. Dr. R. Schobert
Organic Chemistry Laboratory, University Bayreuth
Universitätsstr. 30, 95447 Bayreuth (Germany)
E-mail: Rainer.Schobert@uni-bayreuth.de

[†] These authors contributed equally to this work.

Supporting information and the ORCID identification numbers for the authors of this article can be found under:
<https://doi.org/10.1002/chem.202005451>.

© 2020 The Authors. Chemistry - A European Journal published by Wiley-VCH GmbH. This is an open access article under the terms of the Creative Commons Attribution License, which permits use, distribution and reproduction in any medium, provided the original work is properly cited.



Scheme 1. Syntheses of complexes **4–6**: a) 9-formylanthracene, EtNH₂/THF, AcOH, EtOH, reflux, 2 h, then **1**, K₂CO₃, reflux 6 h, 61%; b) **1**, MeCN, reflux, 48 h; 2) NaBF₄, acetone, RT, 1 h, 95%; c) Ag₂O (0.5 equiv), CH₂Cl₂, RT, 5 h, then [AuCl(SMe₂)] (1 equiv), LiCl, RT, 24 h, 92%; d) Ag₂O (0.5 equiv), CH₂Cl₂, RT, 5 h, then [AuCl(SMe₂)] (0.5 equiv), RT, 24 h, 88%; e) PPh₃, NaBF₄, CH₂Cl₂, RT, 24 h, 79%; f) [AuCl(PPh₃)], KOTBu, CH₂Cl₂, RT, 24 h, 70%.

gands. This was particularly tempting because similar *cis*-[bis(1,3-dibenzylimidazol-2-ylidene)Cl(L)]Pt^{II} complexes were previously shown by us to always accumulate in mitochondria, regardless of the charge of the complex and nature of ligands L.^[14] Likewise, Ott et al. reported a triad of (1,3-diethylbenzimidazol-2-ylidene)(L)gold(I) complexes with the same ligands (L = Cl, PPh₃, NHC), which all localised in the mitochondria, albeit to different degrees.^[15]

Results and Discussion

Synthesis

The new gold(I) NHC complexes were prepared from imidazolium salts **3a** and **3b** (Scheme 1). Compound **3b** was synthesised analogously to known compound **3a** by the van Leusen reaction of toluenesulfonylmethyl isocyanide (TosMIC) reagent **1** with 9-formylanthracene, followed by N-alkylation and anion exchange of the resulting imidazole **2**. Reactions of **3a** and **3b** with Ag₂O and transmetalation of the corresponding silver carbene complexes with different amounts of [AuCl(SMe₂)] afforded mono- and bis-carbene gold(I) complexes **4a/b** and **6a/b** analogously to literature procedures.^[12,13] New cationic complex **5a** was prepared by the reaction of complex **4a** with triphenylphosphane. Complex **5b** was obtained by diprotonation of **3b** and reaction of the free carbene with [AuCl(PPh₃)]. The stability of all complexes **4–6** in aqueous solution was ascertained by ¹H NMR spectroscopic monitoring over a period of 72 h (see the Supporting Information).

Cytotoxicity against cancer cells

All complexes **4–6** had an antiproliferative effect, with IC₅₀ values in the three-digit nanomolar to low double-digit micromolar range, on cells of the human cancer cell lines HCT-116^{wt}, its p53 knockout mutant HCT-116^{p53-/-} (both colon cancer), 518A2 (melanoma), HeLa, and multi-drug-resistant KB-V1^{Vbl} (both cervical carcinoma; Table 1). For complexes **4a**, **5a** and **6a** bearing a CA-4 analogous NHC ligand, we found that the cytotoxicity increased with their DLC character, that is, in the order **4a** < **5a** < **6a**, except for the KB-V1^{Vbl} cells. A similar trend was observed for the anthracenyl complexes (**4b** < **5b** < **6b**), with the exception of bis-NHC complex **6b**, which is less active than phosphane complex **5b** in 518A2 melanoma and HeLa cervical carcinoma cells. This conformity of cytotoxicities of the **a** and **b** series of complexes suggests similar mechanisms of action. Interestingly, all tested gold complexes, including auranofin, were more active against the p53-knockout mutant HCT-116^{p53-/-}, if compared with its wild-type analogue HCT-116^{wt} expressing functional p53 protein. We assume that complexes **4–6** induce cancer cell death in a way that is inde-

Table 1. Inhibitory concentrations, IC₅₀^[a] [μM], of complexes **4–6** upon application to cells of HCT-116^{wt} and HCT-116^{p53-/-} knockout mutant colon carcinomas, 518A2 melanoma, HeLa and mdr KB-V1^{Vbl} cervical carcinomas, and human adult dermal fibroblast cells HDFa.

	IC ₅₀ [μM] ^[a]					
	HCT-116 ^{wt}	HCT-116 ^{p53-/-}	518A2	HeLa	KB-V1 ^{Vbl}	HDFa
4a	6.6 ± 0.8	2.2 ± 0.4	19.8 ± 2.0	12.4 ± 0.5	> 50	24.6 ± 3.4
4b	16.4 ± 0.2	8.4 ± 0.3	7.9 ± 0.8	23.7 ± 1.1	5.9 ± 1.3	9.0 ± 1.3
5a	1.1 ± 0.3	0.6 ± 0.1	5.0 ± 0.3	3.6 ± 0.7	0.6 ± 0.2	5.8 ± 0.9
5b	1.3 ± 0.6	0.4 ± 0.1	2.9 ± 0.5	1.8 ± 0.4	2.2 ± 0.2	5.9 ± 0.2
6a	0.2 ± 0.02	0.05 ± 0.001	0.4 ± 0.1	0.3 ± 0.02	4.6 ± 0.2	1.4 ± 0.2
6b	0.3 ± 0.03	0.2 ± 0.05	5.5 ± 0.4	3.6 ± 0.4	0.7 ± 0.2	3.2 ± 0.4
auranofin	11.9 ± 0.4	5.0 ± 0.2	1.8 ± 0.03	2.6 ± 0.4	n.d. ^[b]	13.7 ± 1.0

[a] Values are the means ± standard deviation (SD) determined in four independent experiments and derived from dose-response curves after 72 h incubation by using the 3-(4,5-dimethylthiazol-2-yl)-2,5-diphenyltetrazolium bromide (MTT) assay. [b] Not determined.

pendent of p53, as already shown for auranofin^[16,17] and for related (1,3-diethylbenzimidazol-2-ylidene)gold(I) complexes.^[18] Complexes **4b**, **5** and **6** were also quite active against the multi-drug-resistant cell line KB-V1^{vb}, which expresses high levels of Pg-p, an ATP-dependent efflux pump, capable of expelling a variety of xenobiotics. Complexes **5a** and **6b** appear to have a particularly low affinity for Pg-p. Cationic complexes **5b** and **6a** showed some selectivity for cancer over non-malignant cells and are particularly interesting candidates for further studies.

Intracellular localisation

The fluorescent complexes **4b**, **5b** and **6b** were synthesised as easy-to-track analogues of complexes **4a**, **5a** and **6a**, respectively. Well-observable, flat 518A2 melanoma cells were treated with the **b** complexes, then counterstained with dyes specifically accumulating in particular cancer-relevant cellular organelles, and eventually fixed and examined through confocal microscopy (Figure 1). By counterstaining with Nuclear Green, neutral chloride complex **4b** could be localised in the area of

the nucleus and to a minor degree in the cytoplasm. This is in line with reports on the nuclear accumulation of neutral gold(I) complexes bearing an aryl-substituted NHC ligand.^[19,20] Many established first-line anticancer drugs target cancer cell nuclei,^[21] yet suffer from therapeutic shortcomings, including off-target side effects and an early onset of resistance, owing to insufficient nuclear accumulation.^[22] Against this background, the enrichment of new (NHC)AuCl complex **4b** predominantly in cancer cell nuclei is remarkable. Cationic phosphane complex **5b** accumulated in the mitochondria, as demonstrated by counterstaining of treated 518A2 cells with red mitochondria-selective MitoTracker (Figure 1). Apparently, the DLC character of this complex favours accumulation in the negatively charged mitochondrial compartments over any potential DNA intercalation of the planar anthracene residue. Mitochondria are considered to be promising targets for cancer therapy. A distinct disruption of the MMP typically results in the induction of apoptosis. One of the pro-apoptotic stimuli is an increased mitochondrial ROS production, which, in turn, causes disruption of the MMP.^[23] Cationic bis-NHC complex **6b** accumulated mainly in lysosomes within the cytoplasm. It

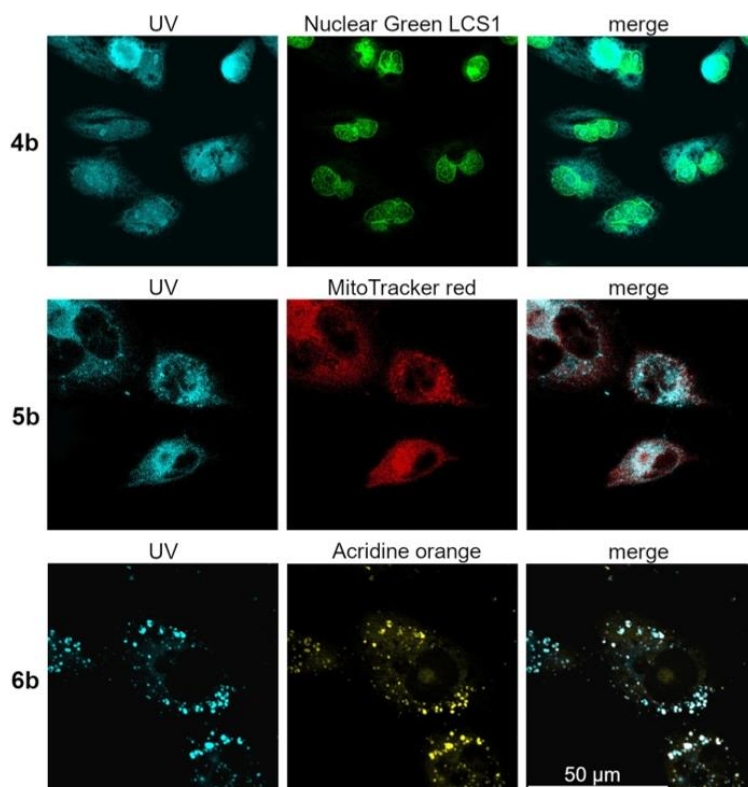


Figure 1. Confocal fluorescence microscopy images of 518A2 melanoma cells incubated for 30 min with 30 μM of complexes **4b–6b** ($\lambda_{\text{exc}} = 350$ nm and $\lambda_{\text{em}} = 420\text{--}480$ nm). The nuclei were counterstained with Nuclear Green LCS1 (abcam; $\lambda_{\text{exc}} = 514$ nm and $\lambda_{\text{em}} = 520\text{--}535$ nm), the mitochondria with MitoTrackerTM (Thermo Fisher; $\lambda_{\text{exc}} = 580$ nm and $\lambda_{\text{em}} = 595\text{--}610$ nm) and the lysosomes with acridine orange solution (5 $\mu\text{g mL}^{-1}$, ABCR GmbH; $\lambda_{\text{exc}} = 350$ nm and $\lambda_{\text{em}} = 600\text{--}660$ nm). Images are representative of at least four independent experiments; 2000-fold magnification.

should be noted that Gust et al. found an accumulation of all three [1,3-diethyl-4,5-di(*p*-fluorophenyl)imidazol-2-ylidene](L)-gold(I) analogues of complexes **4a**, **5a** and **6a** in the nuclei of MCF-7 and HT-29 cells upon a 24 h long exposure.^[24] So, the organelle-selective accumulation of our **a** complexes after only 30 min might be a kinetic effect. The bottom row of Figure 1 shows confocal fluorescence microscopy images of 518A2 melanoma cells treated with complex **6b** and lysotropic acridine orange, as well as the good match of the blue fluorescence of **6b** (UV) with the orange fluorescence of the counterstained lysosomes. Lysosomes are the recycling centres of the cell and are involved in cellular digestion processes, such as autophagy, endocytosis and phagocytosis. Moreover, the release of lysosomal hydrolases, so called cathepsins, is involved in the induction of cell death.^[25,26] Cathepsins mediate caspase- and mitochondrion-independent cell death, especially in cancer cells with mutations in genes involved in the classic apoptotic pathway, for example, the TP53 tumour suppressor gene.^[27]

Induction of cancer cell apoptosis

The majority of p53 mutations are missense mutations, as in the case of 518A2 melanoma cells,^[28] leading to the expression of dysfunctional p53 proteins with oncogenic activities intensifying malignant properties of cancer cells, such as clinical drug resistance.^[29] Because the p53-independent induction of cancer cell apoptosis had been reported for auranofin^[17,30] and for (1,3-diethylbenzimidazol-2-ylidene)gold(I) complexes,^[18] we investigated if complexes **4–6** also lead to an activation of apoptosis (Figure 2). Upon treatment of 518A2 melanoma cells with these complexes, the activation of effector caspases-3 and -7 was observed, which we assumed to be p53 independent, given the results from our cytotoxicity studies. The treated cells showed the typical morphological signs of apoptosis, as well as translocalisation of phosphatidylserines to the outer leaflet of the plasma membrane, which indicated early rather than late apoptosis or necrosis (see the Supporting Informa-

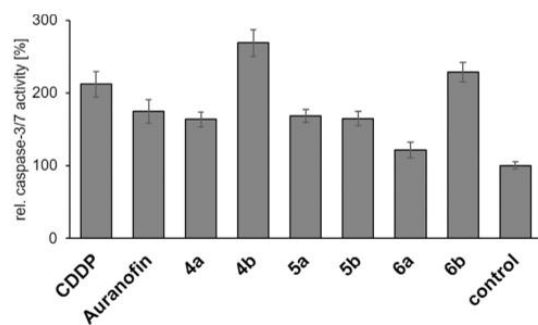


Figure 2. Induction of effector caspase-3/-7 activity in 518A2 melanoma cells after treatment with 5 μ M **4–6** for 6 h, measured by means of the Apo-ONE[®] Homogenous Caspase-3/7 Assay Kit (Promega). CDDP was used as a positive control. The vitality of cells was simultaneously tested by MTT assays and was > 80% for all experiments, except for complex **6a** (70%). All experiments were performed in triplicate and results quoted as means \pm SD. The solvent-treated negative control was set to 100%.

tion). Because about 50% of all human tumours bear p53 mutations, drugs that induce p53-independent programmed cell death are of particular interest.^[31,32]

Mechanism of action of complexes **4a** and **4b** in the nucleus

The antiproliferative effect of CDDP and other platinum complexes is based mainly on their interaction with cellular DNA.^[33,33] Because of the localisation of neutral complex **4b** in the nuclear area, a potential DNA interaction of **4b** and its close structural analogue **4a** was examined by ethidium bromide (EtdBr) saturation assays (Figure 3) and electrophoretic mobility shift assays (EMSAs; Figure 4).

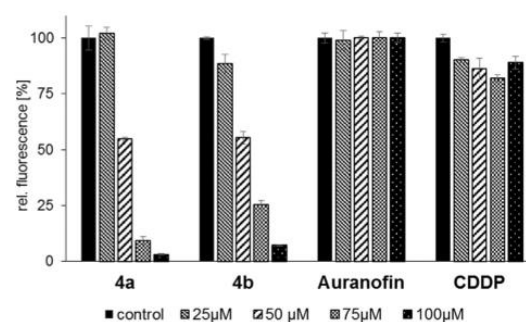


Figure 3. EtdBr saturation assays with 25, 50, 75 and 100 μ M **4a**, **4b** and auranofin. CDDP was used as a positive control. Negative controls were treated with an equivalent amount of solvent (DMF or H₂O). All experiments were carried out in triplicate with negative controls set to 100%.

Addition of complexes **4a** or **4b** to linear, double-stranded salmon sperm DNA led to a distinct concentration-dependent displacement, and thus, to a reduction of the fluorescence of intercalated EtdBr, exceeding that caused by CDDP by far. This suggests a strong interaction of both complexes **4** with this DNA form, possibly associated with an alteration of the DNA morphology. Auranofin showed no such effect (Figure 3). In the EMSA with circular plasmid DNA, a slight relaxation, that is, despiralisation, of the covalently closed circular (ccc) DNA form for the benefit of the open circular (oc) form was observed after incubation with complex **4a**, and a stronger relaxation after treatment with complex **4b** (Figure 4). In contrast to CDDP, gold NHC complexes are known to bind non-covalently to DNA, which may be the reason for their weaker effects in the EMSA.^[34]

Although auranofin had previously been reported to interact neither with linear DNA nor with circular plasmid DNA,^[35] various other gold(I) complexes with readily displaceable ligands (e.g., Cl⁻) had shown affinity to different types of DNA.^[35,36] Irreparable DNA damage induces apoptosis, normally triggered by the tumour suppressor protein p53. However, apoptosis as a consequence of DNA damage caused by metal complexes had also been reported to proceed independently of p53,^[37,38] through the mitogen-activated protein kinase (MAPK) signal-

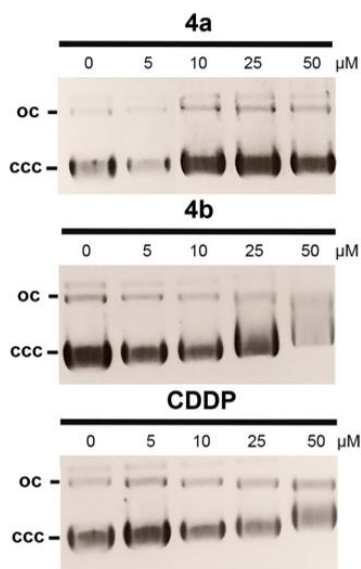


Figure 4. EMSAs with circular pBR322 plasmid DNA after 24 h treatment with complexes **4a** or **4b**, as visualised by UV radiation. CDDP was used as a positive control. Images are representative of at least two independent experiments.

ling pathway involving JNK, p38 and ERK1/2.^[37,18] Whether complexes **4**, which we have found to induce cancer cell apoptosis and to be cytotoxic independently of functional p53, operate by a similar mechanism remains to be shown. At present, we cannot exclude that their reactions with further biologically relevant macromolecules might also play a role.^[39]

Mechanism of action of complexes **5a** and **5b** in mitochondria

Because cationic triphenylphosphane complex **5b** was localised in the mitochondria of 518A2 melanoma cells, we anticipated a mitochondria-associated mode of action for **5b** and closely related complex **5a**. The anticancer effect of auranofin, and several other gold(I) complexes, mainly relies on the inhibition of TrxR.^[40,41] TrxRs, which catalyse the reduced nicotinamide adenine dinucleotide phosphate (NADPH)-dependent reduction of the redox protein thioredoxin (Trx) and other compounds, are key enzymes for cellular protection against oxidative stress.^[42] To date, three different isoforms of TrxR are known: cytosolic TrxR1, mitochondrial TrxR2 and testis-specific TrxR3.^[43] Gold complexes, such as auranofin, are thought to inhibit TrxRs by releasing monovalent Au^I species, which bind to selenocysteine residues in the active site of the enzyme.^[44] This is in line with reports that mono-NHC gold(I) complexes with good leaving groups, such as halides or phosphanes, are better TrxR inhibitors than bis-NHC complexes.^[45] For instance, sub-micromolar IC₅₀ values were reported by Gust et al. for donor-substituted (1,3-diethyl-4,5-diarylimidazol-2-ylide-

ne)(PPh₃)gold(I) complexes,^[24] and by Ott et al. for benzimidazol-2-ylidene analogues,^[15,46] whereas few inhibitory bis(1,3-diarylimidazol-2-ylidene) complexes have been reported, to date.^[45,47]

If applied in low sub-micromolar concentrations, complexes **5a** and **5b** strongly inhibited the panTrxR activity in colorimetric TrxR microplate assays with 5,5'-dithiobis(2-dinitrobenzoic acid (DTNB; Ellman's reagent) as a substrate (Figure 5). Because many tumours have elevated TrxR levels,^[43] and tumour cells are more sensitive to oxidative stress, due to their a priori high intracellular ROS levels relative to non-malignant cells, TrxR are interesting targets for selective antitumour therapy.

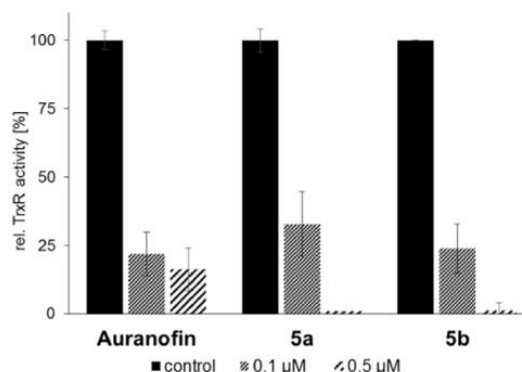


Figure 5. Concentration-dependent inhibition of TrxR activity in cell lysates of 518A2 melanoma cells by gold(I) complexes **5a** and **5b**, and auranofin as a positive control. TrxR-independent substrate reduction was accounted for by experiments in the presence and absence of the specific TrxR inhibitor aurothiomalate. All values are means \pm SD of at least three independent experiments with negative controls set to 100%.

TrxR inhibition generally leads to an accumulation of oxidised Trx and ROS in mitochondria, resulting in an increase of mitochondrial permeability.^[40] Upon treatment of 518A2 melanoma cells with complexes **5a** and **5b**, we observed a distinct reduction of the MMP through a fluorescence-based microplate assay (Figure 6), exceeding that induced by auranofin, which is in keeping with their stronger TrxR inhibition.

We confirmed these results by an assessment of the intracellular ROS concentrations after treatment of 518A2 melanoma cells with auranofin, CCCP and complexes **5a** and **5b** using the cell permeant, fluorogenic dye 2',7'-dichlorofluorescein diacetate (DCFH-DA). After diffusion into the cells, DCFH-DA is deacetylated by cellular esterases to a non-fluorescent compound, which is later oxidised by hydroxyl, peroxy or other ROS to the intensely fluorescent 2',7'-dichlorofluorescein (DCF), detectable by fluorescence spectroscopy (Figure 7).

We conclude that the cytotoxicity of complexes **5** originates mainly from their inhibition of TrxR in the mitochondria of cancer cells and the subsequent alteration of the intracellular ROS equilibrium.^[40] Elevated concentrations of hydrogen peroxide and oxidised Trx2 affect further intra-mitochondrial targets, leading to the opening of the mitochondrial permeability

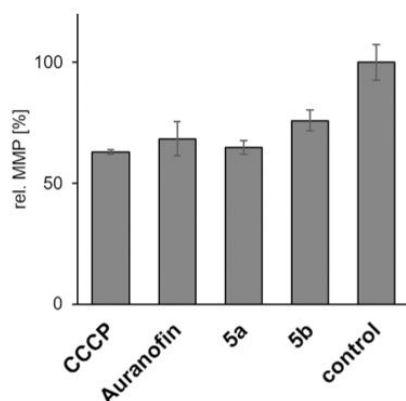


Figure 6. Relative MMP in 518A2 melanoma cells after treatment (45 min) with complexes **5a** and **5b** (10 μM each). Carbonyl cyanide-*m*-chlorophenylhydrazone (CCCP) and auranofin (10 μM , each) were used as positive controls and solvent-treated negative controls were set to 100%. Assays were carried out in triplicate.

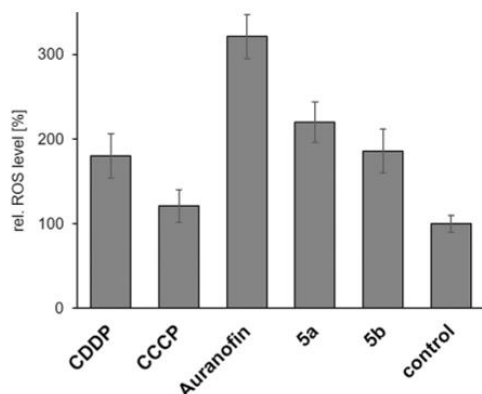


Figure 7. Influence of gold(I) complexes **5a** and **5b**, and auranofin (10 μM each), as well as CCCP (10 μM) as a positive control, on the levels of ROS in 518A2 melanoma cells, as determined by fluorescence-based DCFH-DA assays after an incubation time of 1 h. Negative controls were treated identically with solvent. All values are mean values \pm 5D from at least four independent experiments with negative controls set to 100%.

transition pore and/or to an increase of the permeability of the outer membrane.^[9,48] As a result, hydrogen peroxide is released into the cytosol where it oxidises cytosolic Trx1 irreversibly, due to the inhibition of TrxRs. The elevated levels of hydrogen peroxide and oxidised Trx in the cytosol then activate various signalling pathways, eventually leading to apoptosis, which is likely to be dependent on p38/ERK1/2, rather than p53, as shown for auranofin.^[40,49] Because cancer cells, unlike non-malignant cells, are not normally susceptible to mitochondrial membrane permeability transition, the induction of this condition by mitochondria-targeting complexes, such as **5**, could be exploited in a therapeutic context.^[50]

Mechanism of action of complexes **6a** and **6b** in lysosomes

The cationic bis-NHC complex **6b** was localised in the lysosomes of 518A2 melanoma cells. Lysosomes mediate the degradation of macromolecules of intracellular origin or those that are internalised by endocytosis or phagocytosis.^[51] These single-membrane acidic organelles (pH 4.5–4.8) are involved in various cellular pathways and different types of cell death, and their functionality is thus inevitable for cellular homeostasis.^[51] Various forms of cellular stress lead to lysosomal swelling and lysosomal membrane permeabilisation (LMP), resulting in the release of intralysosomal cargo into the cytoplasm.^[51] Amongst others, cathepsins B and D are released into the cytoplasm under stress, where they induce different forms of cell death, including the p53-independent, lysosome-dependent apoptotic cell death.^[26,31,51,52] To detect a potential induction of LMP by complexes **6**, we performed a time-dependent staining of lysosomes in solvent- and complex-treated 518A2 melanoma cells (Figure 8). Because the cytotoxicity of both complexes against 518A2 cells in MTT assays was quite different ($\text{IC}_{50}(\mathbf{6a}) = 0.4 \mu\text{M}$, $\text{IC}_{50}(\mathbf{6b}) = 5.5 \mu\text{M}$), we adjusted their concentrations accordingly to ensure a sufficient cell viability. The incubation with either complex **6a** or **6b** led to an induction of LMP. The lysotropic orange dye used in this assay selectively accumulates in intact acidic lysosomes. If LMP occurs, the dye is released into the cytosol and the fluorescence of defined lysosomal compartments disappears. As expected, complex **6a**, which had proved to be more active in MTT assays, also led to faster lysosomal disruption after only 2 h of incubation. Cells treated with **6b** showed first signs of LMP only after 4 h of treatment.

Conclusion

The [4-(anthracen-9-yl)-1,3-diethyl-5-phenylimidazol-2-ylidene] (L)gold(I) complexes **4b**, **5b**, and **6b** accumulated quickly in different compartments of 518A2 melanoma cells, that is, neutral chlorido complex **4b** in the nuclei, cationic phosphane complex **5b** in mitochondria and large delocalised cationic bis-NHC complex **6b** in the lysosomes. The analogous **a** series of complexes carried a slightly different 4,5-diarylimidazol-2-ylidene ligand. The fact that all couples **4a/4b**, **5a/5b** and **6a/6b** afforded similar results in cytotoxicity tests with cancer cells, and in tests on targets typically found at the identified sites of accumulation, supports the assumption that **a** complexes localise similarly to the **b** complexes, and that the nature of ligand L, which is responsible for the charge, size and lipophilicity of the complex, is decisive for the site of accumulation. However, this phenomenon might be limited to divalent gold(I)-NHC or even to (imidazol-2-ylidene)gold(I) complexes because a comparable series of *cis*-[bis(1,3-dibenzylimidazol-2-ylidene)]Cl(L)Pt^{II}^[14] and (1,3-diethylbenzimidazol-2-ylidene)(L)gold(I) complexes,^[15] carrying the same ligands L (Cl, PPh₃ or the same NHC ligand), were previously shown to accumulate in mitochondria, regardless of the charge of the complex and the nature of ligand L. The different distributions of DLC complexes **5** (in mitochondria) and **6** (in lysosomes) is explicable by the higher molecular weight and steric demand of

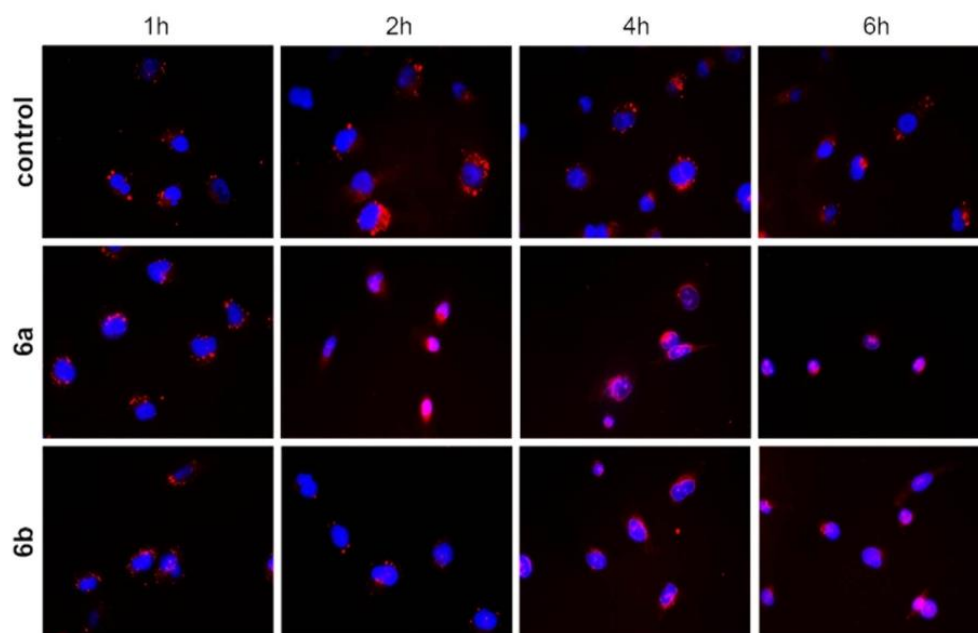


Figure 8. Fluorescence microscopy images of 518A2 melanoma cells treated with solvent (DMF), or complexes **6a** (0.4 μM) or **6b** (5.5 μM) for 1, 2, 4 or 6 h under standard cell-culture conditions; 30 min before each time interval ended, cells were stained with Lysosomal Staining Reagent Orange (Abcam). Nuclear counterstaining was performed by using blue 4',6-diamidino-2-phenylindole (DAPI). Images are representative of at least ten independent measurements at 400-fold magnification.

the latter, which are too large for embedding in the mitochondrial membrane, and thus, are dealt with by the cellular "waste-to-energy plants", the lysosomes. Once fully understood, the concept of controlling the intracellular distribution of metallodrugs by the choice of secondary ligands and charge of the complex could be exploited in rational drug design.

For the mode of action of new complexes **4–6**, we found an eventual induction of p53-independent apoptotic cell death, which was initiated by different effects of the three complex types at their respective sites of accumulation.

Acknowledgements

We thank the Deutsche Forschungsgemeinschaft (DFG) for a grant (Scho 402/12-2). Furthermore, we would like to thank Luisa Kober for her support in identifying the target structures of the compounds, and Dr. Julienne K. Münzner and Dr. Matthias Rothemund for preliminary tests. Open access funding enabled and organized by Projekt DEAL.

Conflict of interest

The authors declare no conflict of interest.

Keywords: cancer · drug discovery · gold · metallodrugs · subcellular localisation

- [1] L.-A. Schaper, S. J. Hock, W. A. Herrmann, F. E. Kühn, *Angew. Chem. Int. Ed.* **2013**, *52*, 270–289; *Angew. Chem.* **2013**, *125*, 284–304.
- [2] M.-L. Teyssot, A.-S. Jarrousse, M. Manin, A. Chevry, S. Roche, F. Norre, C. Beaudoin, L. Morel, D. Boyer, R. Mahiou, A. Gautier, *Dalton Trans.* **2009**, 6894–6902.
- [3] a) B. Rosenberg, L. VanCamp, *Cancer Res.* **1970**, *30*, 1799–1802; b) J. Reedijk, P. H. Lohman, *Pharm. Weekbl. Sci.* **1985**, *7*, 173–180; c) M. H. Hanigan, P. Devarajan, *Cancer Ther.* **2003**, *1*, 47–61; d) C. M. Sorenson, M. A. Barry, A. Eastman, *J. Natl. Cancer Inst.* **1990**, *82*, 749–755.
- [4] a) J. S. Modica-Napolitano, J. R. Aprille, *Adv. Drug Delivery Rev.* **2001**, *49*, 63–70; b) C. I. Yeo, K. K. Ooi, E. R. T. Tiekink, *Molecules* **2018**, *23*, 1410.
- [5] S. B. Aher, P. N. Muskawar, K. Thenmozhi, P. R. Bhagat, *Eur. J. Med. Chem.* **2014**, *81*, 408–419.
- [6] a) L. Oehninger, R. Rubbiani, I. Ott, *Dalton Trans.* **2013**, *42*, 3269–3284; b) C. Hu, X. Li, W. Wang, R. Zhang, L. Deng, *Curr. Med. Chem.* **2014**, *21*, 1220–1230; c) A. Gautier, F. Cisnetti, *Metallomics* **2012**, *4*, 23–32.
- [7] a) M. Chaffman, R. N. Brogden, R. C. Heel, T. M. Speight, G. S. Avery, *Drugs* **1984**, *27*, 378–424; b) V. Gandin, A. P. Fernandes, M. P. Rigobello, B. Dani, F. Sorrentino, F. Tisato, M. Björnstedt, A. Bindoli, A. Sturaro, R. Rella, C. Marzano, *Biochem. Pharmacol.* **2010**, *79*, 90–101.
- [8] S. Gromer, L. D. Arscott, C. H. Williams, R. H. Schirmer, K. Becker, *J. Biol. Chem.* **1998**, *273*, 20096–20101.
- [9] M. P. Rigobello, G. Scutari, R. Boscolo, A. Bindoli, *Br. J. Pharmacol.* **2002**, *136*, 1162–1168.
- [10] G.-Y. Liou, P. Storz, *Free Radical Res.* **2010**, *44*, 479–496.
- [11] X. Jiang, X. Wang, *Annu. Rev. Biochem.* **2004**, *73*, 87–106.
- [12] L. Kaps, B. Biersack, H. Müller-Bunz, K. Mahal, J. Münzner, M. Tacke, T. Mueller, R. Schobert, *J. Inorg. Biochem.* **2012**, *106*, 52–58.

- [13] J. K. Muenzner, B. Biersack, H. Kalie, I. C. Andronache, L. Kaps, D. Schuppan, F. Sasse, R. Schobert, *ChemMedChem* **2014**, *9*, 1195–1204.
- [14] M. Rothmund, S. I. Bär, T. Rehm, H. Kostrhunova, V. Brabec, R. Schobert, *Dalton Trans.* **2020**, *49*, 8901–8910.
- [15] R. Rubbiani, S. Can, I. Kitanovic, H. Alborzina, M. Stefanopoulou, M. Koschka, S. Mönchgesang, W. S. Sheldrick, S. Wölfl, I. Ott, *J. Med. Chem.* **2011**, *54*, 8646–8657.
- [16] E. Hedström, S. Eriksson, J. Zawacka-Pankau, E. S. J. Arnér, G. Selivanova, *Cell Cycle* **2009**, *8*, 3584–3591.
- [17] S.-H. Park, J. H. Lee, J. S. Berek, M. C.-T. Hu, *Int. J. Oncol.* **2014**, *45*, 1691–1698.
- [18] X. Cheng, P. Holenya, S. Can, H. Alborzina, R. Rubbiani, I. Ott, S. Wölfl, *Molecular Cancer* **2014**, *13*, 221.
- [19] B. Bertrand, A. de Almeida, E. P. M. van der Burgt, M. Picquet, A. Citta, A. Folda, M. P. Rigobello, P. Le Gendre, E. Bodio, A. Casini, *Eur. J. Inorg. Chem.* **2014**, 4532–4536.
- [20] A. Citta, E. Schuh, F. Mohr, A. Folda, M. L. Massimo, A. Casini, M. P. Rigobello, *Metallomics* **2013**, *5*, 1006–1015.
- [21] a) D. Ingato, J. A. Edson, M. Zakharian, Y. J. Kwon, *ACS Nano* **2018**, *12*, 9568–9577; b) L. H. Hurley, *Nat. Rev. Cancer* **2002**, *2*, 188–200.
- [22] a) A. L. B. Seynhaeve, B. M. Dicheva, S. Hoving, G. A. Koning, T. L. M. ten Hagen, *J. Controlled Release* **2013**, *172*, 330–340; b) M. A. Fuertes, C. Alonso, J. M. Pérez, *Chem. Rev.* **2003**, *103*, 645–662.
- [23] S. Fulda, L. Galluzzi, G. Kroemer, *Nat. Rev. Drug Discovery* **2010**, *9*, 447–464.
- [24] W. Liu, K. Bendorf, M. Proetto, A. Hagenbach, U. Abram, R. Gust, *J. Med. Chem.* **2012**, *55*, 3713–3724.
- [25] a) U. T. Brunk, J. Neuzil, J. W. Eaton, *Redox Rep.* **2001**, *6*, 91–97; b) T. Cirman, K. Oresić, G. D. Mazovec, V. Turk, J. C. Reed, R. M. Myers, G. S. Salvesen, B. Turk, *J. Biol. Chem.* **2004**, *279*, 3578–3587.
- [26] P. Boya, K. Andreau, D. Poncet, N. Zamzami, J.-L. Perfettini, D. Metivier, D. M. Ojcius, M. Jäättelä, G. Kroemer, *J. Exp. Med.* **2003**, *197*, 1323–1334.
- [27] M. Jäättelä, *Oncogene* **2004**, *23*, 2746–2756.
- [28] S. F. Zerp, A. van Elsas, L. T. Peltenburg, P. I. Schrier, *Br. J. Cancer* **1999**, *79*, 921–926.
- [29] A. Parrales, T. Iwakuma, *Front. Oncol.* **2015**, *5*, 288.
- [30] B. Tessoulin, G. Descamps, C. Dousset, M. Amiot, C. Pellat-Deceunynck, *Front. Oncol.* **2019**, *9*, 128.
- [31] H. Erdal, M. Berndtsson, J. Castro, U. Brunk, M. C. Shoshan, S. Linder, *Proc. Natl. Acad. Sci. USA* **2005**, *102*, 192–197.
- [32] a) C. Bérout, T. Soussi, *Nucleic Acids Res.* **1998**, *26*, 200–204; b) L. Bouaoun, D. Sonkin, M. Ardin, M. Hollstein, G. Byrnes, J. Zavadil, M. Olivier, *Hum. Mutat.* **2016**, *37*, 865–876.
- [33] D. P. Bancroft, C. A. Lepre, S. J. Lippard, *J. Am. Chem. Soc.* **1990**, *112*, 6860–6871.
- [34] Ö. Karaca, S. M. Meier-Menches, A. Casini, F. E. Kühn, *Chem. Commun.* **2017**, *53*, 8249–8260.
- [35] C. K. Mirabelli, C.-M. Sung, J. P. Zimmerman, D. T. Hill, S. Mong, S. T. Crooke, *Biochem. Pharmacol.* **1986**, *35*, 1427–1433.
- [36] a) C. E. Blank, J. C. Dabrowiak, *J. Inorg. Biochem.* **1984**, *21*, 21–29; b) S. Urig, K. Fritz-Wolf, R. Réau, C. Herold-Mende, K. Tóth, E. Davioud-Charvet, K. Becker, *Angew. Chem. Int. Ed.* **2006**, *45*, 1881–1886; *Angew. Chem.* **2006**, *118*, 1915–1920.
- [37] S. L. R. Silva, I. R. S. Baliza, R. B. Dias, C. B. S. Sales, C. A. G. Rocha, M. B. P. Soares, R. S. Correa, A. A. Batista, D. P. Bezerra, *Sci. Rep.* **2019**, *9*, 11094.
- [38] a) N. C. de Carvalho, S. P. Neves, R. B. Dias, L. de F. Valverde, C. B. S. Sales, C. A. G. Rocha, M. B. P. Soares, E. R. dos Santos, R. M. M. Oliveira, R. M. Carlos, P. C. L. Nogueira, D. P. Bezerra, *Cell Death Dis.* **2018**, *9*, 79; b) M. Altaf, M. Monim-Ul-Mehboob, A.-N. Kawde, G. Corona, R. Larcher, M. Ogasawara, N. Casagrande, M. Celegato, C. Borghese, Z. H. Siddik, D. Aldinucci, A. A. Isab, *Oncotarget* **2017**, *8*, 490–505.
- [39] L. Ronconi, D. Fregona, *Dalton Trans.* **2009**, 10670–10680.
- [40] A. Bindoli, M. P. Rigobello, G. Scutari, C. Gabbiani, A. Casini, L. Messori, *Coord. Chem. Rev.* **2009**, *253*, 1692–1707.
- [41] a) C. Marzano, V. Gandin, A. Folda, G. Scutari, A. Bindoli, M. P. Rigobello, *Free Radical Biol. Med.* **2007**, *42*, 872–881; b) A. Meyer, C. P. Bagowski, M. Kokoschka, M. Stefanopoulou, H. Alborzina, S. Can, D. H. Vleckner, W. S. Sheldrick, S. Wölfl, I. Ott, *Angew. Chem. Int. Ed.* **2012**, *51*, 8895–8899; *Angew. Chem.* **2012**, *124*, 9025–9030; c) M. G. Fabbri, D. Cirri, A. Pratesi, L. Ciofi, T. Marzo, A. Guerri, S. Nistri, A. Dell'Accio, T. Gamberi, M. Severi, A. Bencini, L. Messori, *ChemMedChem* **2019**, *14*, 182–188.
- [42] D. Mustacich, G. Powis, *Biochem. J.* **2000**, *346*, 1–8.
- [43] S. Urig, K. Becker, *Semin. Cancer Biol.* **2006**, *16*, 452–465.
- [44] D. Parsonage, F. Sheng, K. Hirata, A. Debnath, J. H. McKerrow, S. L. Reed, R. Abagyan, L. B. Poole, L. M. Podust, *J. Struct. Biol.* **2016**, *194*, 180–190.
- [45] C. Zhang, C. Hemmert, H. Gornitzka, O. Cuvillier, M. Zhang, R. W.-Y. Sun, *ChemMedChem* **2018**, *13*, 1218–1229.
- [46] R. Rubbiani, L. Salassa, A. de Almeida, A. Casini, I. Ott, *ChemMedChem* **2014**, *9*, 1205–1210.
- [47] J. F. Arambula, R. McCall, K. J. Sidoran, D. Magda, N. A. Mitchell, C. W. Bielawski, V. M. Lynch, J. L. Sessler, K. Arumugam, *Chem. Sci.* **2016**, *7*, 1245–1256.
- [48] A. G. Cox, K. K. Brown, E. S. J. Arner, M. B. Hampton, *Biochem. Pharmacol.* **2008**, *76*, 1097–1109.
- [49] S.-J. Park, I.-S. Kim, *Br. J. Pharmacol.* **2005**, *146*, 506–513.
- [50] G. Kroemer, L. Galluzzi, C. Brenner, *Physiol. Rev.* **2007**, *87*, 99.
- [51] F. Wang, R. Gómez-Sintes, P. Boya, *Traffic* **2018**, *19*, 918–931.
- [52] a) F. Wang, A. Salvati, P. Boya, *Open Biol.* **2018**, *8*, 170271; b) S. Aits, M. Jäättelä, *J. Cell Sci.* **2013**, *126*, 1905–1912.

Manuscript received: December 23, 2020

Accepted manuscript online: December 28, 2020

Version of record online: February 8, 2021

Chemistry–A European Journal

Supporting Information

Guided Antitumoural Drugs: (Imidazol-2-ylidene)(L)gold(I) Complexes Seeking Cellular Targets Controlled by the Nature of Ligand L

Sofia I. Bär⁺, Madeleine Gold⁺, Sebastian W. Schleser, Tobias Rehm, Alexander Bär,
Leonhard Köhler, Lucas R. Carnell, Bernhard Biersack, and Rainer Schobert^{*[a]}

Author Contributions

S.B. Formal analysis: Lead; Investigation: Lead; Methodology: Lead; Project administration: Lead; Writing – original draft: Lead

M.G. Formal analysis: Equal; Investigation: Equal; Methodology: Equal; Project administration: Equal; Writing – original draft: Equal

S.S. Formal analysis: Supporting; Investigation: Supporting; Methodology: Supporting

T.R. Formal analysis: Supporting; Investigation: Supporting; Methodology: Supporting

A.B. Formal analysis: Supporting; Investigation: Supporting; Methodology: Supporting

L.K. Formal analysis: Supporting; Investigation: Supporting; Methodology: Supporting

L.C. Formal analysis: Supporting; Methodology: Supporting

B.B. Formal analysis: Supporting; Investigation: Supporting; Methodology: Supporting; Project administration: Supporting.

Table of Contents

Experimental Procedures	3
<i>Chemical Synthesis and Analytics</i>	3
General	3
5-(Anthracen-9-yl)-1-ethyl-4-phenylimidazole (2)	3
4-(Anthracen-9-yl)-1,3-diethyl-5-phenylimidazolium tetrafluoroborate (3b)	3
Chlorido-[4-(anthracen-9-yl)-1,3-diethyl-5-phenylimidazol-2-ylidene]gold(I) (4b)	3
[1,3-Diethyl-5-(4-methoxyphenyl)-4-(3,4,5-trimethoxyphenyl)imidazol-2-ylidene](triphenylphosphane)gold(I) tetrafluoroborate (5a).....	3
[4-(Anthracen-9-yl)-1,3-diethyl-5-phenylimidazol-2-ylidene](triphenylphosphane)gold(I) tetrafluoroborate (5b)	4
Bis[4-(anthracen-9-yl)-1,3-diethyl-5-phenylimidazol-2-ylidene]gold(I) tetrafluoroborate (6b).....	4
NMR Spectra.....	4
<i>Biochemical Evaluation</i>	9
Cell lines and culture conditions	9
Intracellular localisation of gold complexes.....	10
Caspase-3/7 activation assay.....	10
Detection of morphological signs of apoptosis.....	10
Annexin-V-FITC/PI staining.....	10
Ethidium bromide saturation assay.....	10
Electrophoretic mobility shift assay (EMSA)	10
Inhibition of thioredoxin reductase (TrxR) activity	11
Mitochondrial membrane potential.....	11
Determination of intracellular concentration of reactive oxygen species (DCFH-DA assay)	11
Lysosomal integrity.....	11
Stability testing via NMR spectroscopy.....	11
Tubulin polymerisation assay	11
Cell cycle analysis.....	12
Results	13
Influence on cellular morphology	13
Apoptosis detection using Annexin V-FITC and PI	14
Stability testing via NMR spectroscopy.....	15
Interaction with tubulin.....	18
Influence on the cell cycle of 518A2 melanoma cells.....	18
References	19
Author Contributions	19

Experimental Procedures

Chemical Synthesis and Analytics

General.

Melting points (uncorrected): GALLENKAMP; IR spectra: PERKIN-ELMER Spectrum One FT-IR spectrophotometer with ATR sampling unit; Nuclear magnetic resonance (NMR) spectra: BRUKER DRX 500 Hz spectrometer, chemical shifts are given in parts per million (δ) downfield from tetramethylsilane as internal standard for ^1H and ^{13}C ; Mass spectra: VARIAN MAT 311A (EI), WATERS UPLC-Q-TOF (ESI), ThermoFisher UPLC/Orbitrap MS system (HRMS-ESI); All starting compounds were purchased from ALDRICH and used without further purification. The known compounds **3a**^[1], **4a**^[1] and **6a**^[1] were prepared according to literature procedures.

5-(Anthracen-9-yl)-1-ethyl-4-phenylimidazole (2). A solution of 9-formylanthracene (700 mg, 3.39 mmol) in ethanol (50 mL) was treated with 2M EtNH₂/THF (8.49 mL, 17.0 mmol). Acetic acid (970 μL) was added and the reaction mixture was refluxed for 2 h. After cooling to room temperature, phenyl-TosMIC **1** (1.39 g, 5.09 mmol) and K₂CO₃ (1.88 g, 13.6 mmol) were added and refluxed again for 6 h. The solvent was evaporated, the residue was dissolved in ethyl acetate (100 mL) and washed with water (100 mL) and brine (100 mL), dried over Na₂SO₄, filtered and the filtrate was concentrated in vacuum. The residue was purified by column chromatography (silica gel 60; EtOAc/MeOH: 97/3). Yield: 726 mg (2.08 mmol, 61%); yellow solid; $R_f = 0.64$; $\nu_{\text{max}}/\text{cm}^{-1}$: 3053, 2977, 2931, 1623, 1599, 1517, 1501, 1458, 1442, 1398, 1373, 1352, 1343, 1314, 1244, 1224, 1175, 1163, 1135, 1117, 1056, 1067, 1011, 983, 951, 917, 899, 852, 813, 799, 771, 744, 715, 728, 692; ^1H NMR (500 MHz, CDCl₃): δ 1.01 (3 H, t, $J = 7.3$ Hz), 3.45 (2 H, q, $J = 7.3$ Hz), 6.96-6.98 (3 H, m), 7.29-7.31 (2 H, m), 7.38-7.41 (2 H, m), 7.48-7.51 (2 H, m) 7.64 (2 H, d, $J = 8.7$ Hz), 7.91 (1 H, s), 8.10 (2 H, d, $J = 8.7$ Hz), 8.64 (1 H, s); ^{13}C NMR (126 MHz, CDCl₃): δ 16.4, 40.1, 123.9, 124.5, 125.4, 125.6, 125.7, 126.1, 126.9, 128.1, 128.8, 128.9, 131.5, 134.0, 134.5, 136.8, 140.0.

4-(Anthracen-9-yl)-1,3-diethyl-5-phenylimidazolium tetrafluoroborate (3b).

Compound **2** (500 mg, 1.43 mmol) was dissolved in acetonitrile (100 mL) and iodoethane (6.34 mL) was added. The reaction mixture was stirred at 85 °C for 48 h. The solvent was evaporated and the remainder was crystallised from CH₂Cl₂/*n*-hexane at 4 °C. Yield: 689 mg (1.37 mmol, 95%); yellow solid; $\nu_{\text{max}}/\text{cm}^{-1}$: 3420, 3118, 3027, 2979, 1622, 1592, 1556, 1520, 1499, 1443, 1386, 1348, 1263, 1193, 1159, 1091, 1074, 1023, 1012, 962, 932, 897, 854, 794, 774, 740, 700; ^1H NMR (500 MHz, CDCl₃): δ 1.28 (3 H, t, $J = 7.3$ Hz), 1.68 (3 H, t, $J = 7.3$ Hz), 3.91 (2 H, q, $J = 7.3$ Hz), 4.52 (2 H, q, $J = 7.3$ Hz), 7.13-7.23 (5 H, m), 7.50-7.55 (2 H, m), 7.59 (2 H, t, $J = 8.1$ Hz), 7.65 (2 H, d, $J = 8.7$ Hz) 8.06 (2 H, d, $J = 8.4$ Hz), 8.62 (1 H, s), 10.83 (1 H, s); ^{13}C NMR (126 MHz, CDCl₃): δ 15.8, 15.9, 43.6, 44.1, 117.0, 124.4, 124.9, 126.0, 128.3, 128.4, 129.1, 129.2, 129.4, 130.4, 131.0, 131.2, 132.0, 133.9. The resulting 4-(anthracen-9-yl)-1,3-diethyl-5-phenylimidazolium iodide (41 mg, 0.081 mmol) was dissolved in acetone (10 mL) and NaBF₄ (13 mg, 0.122 mmol) was added. The reaction mixture was stirred at room temperature for 24 h. After filtration through Mg₂SO₄ the filtrate was concentrated in vacuum and dried. Yield: 38 mg (0.081 mmol, 100%); yellow solid; $\nu_{\text{max}}/\text{cm}^{-1}$: 3464, 3039, 2982, 1622, 1557, 1520, 1499, 1444, 1387, 1349, 1333, 1305, 1263, 1193, 1065, 1023, 963, 932, 897, 854, 774, 740, 727, 700; ^1H NMR (300 MHz, CDCl₃): δ 1.24 (3 H, t, $J = 7.3$ Hz), 1.65 (3 H, t, $J = 7.3$ Hz), 3.88 (2 H, q, $J = 7.3$ Hz), 4.49 (2 H, q, $J = 7.3$ Hz), 7.0-7.2 (5 H, m), 7.4-7.6 (4 H, m), 7.67 (2 H, d, $J = 8.6$ Hz), 8.01 (2 H, d, $J = 8.4$ Hz), 8.58 (1 H, s), 10.66 (1 H, s); ^{13}C NMR (75.5 MHz, CDCl₃): δ 15.7, 15.8, 43.5, 44.0, 117.0, 124.3, 124.9, 125.8, 128.2, 128.3, 129.0, 129.1, 129.4, 130.2, 130.9, 131.0, 131.9, 133.9, 137.2; ^{11}B NMR (96.3 MHz, CDCl₃): δ -0.76.

Chlorido-[4-(anthracen-9-yl)-1,3-diethyl-5-phenylimidazol-2-ylidene]gold(I) (4b).

Compound **3b** (100 mg, 0.198 mmol) was dissolved in CH₂Cl₂ (5 mL) and treated with Ag₂O (27.6 mg, 0.119 mmol). The mixture was stirred in darkness at room temperature for 5 h. Chloro(dimethylsulfide)gold(I) (64.2 mg, 0.218 mmol) and LiCl (84 mg, 1.98 mmol) were added and the reaction mixture was stirred for additional 24 h. The crude product was crystallised from CH₂Cl₂/*n*-hexane at 4 °C. Yield: 111 mg (0.182 mmol, 92%); yellowish solid of mp > 250 °C (dec.); ν_{max} (ATR)/cm⁻¹: 3051, 2976, 2933, 1622, 1500, 1461, 1427, 1443, 1414, 1344, 1294, 1213, 1115, 1088, 1025, 1013, 997, 962, 933, 896, 851, 819, 775, 757, 727, 699, 652, 607, 582; ^1H NMR (500 MHz, CDCl₃): δ 0.98 (3 H, t, $J = 7.2$ Hz), 1.45 (3 H, t, $J = 7.1$ Hz), 3.81 (2 H, q, $J = 7.2$ Hz), 4.37 (2 H, q, $J = 7.2$ Hz), 7.07-7.16 (5 H, m), 7.45-7.55 (4 H, m), 7.60 (2 H, d, $J = 8.4$ Hz), 8.00-8.05 (2 H, m), 8.55 (1 H, s); ^{13}C NMR (125 MHz, CDCl₃): δ 17.0, 17.2, 44.7, 44.8, 120.4, 124.7, 125.7, 127.0, 127.5, 127.6, 128.7, 129.1, 129.2, 129.3, 129.4, 130.2, 131.1, 132.0, 133.0, 170.3; m/z (ESI, %) 614.2 [M⁺+CH₃CN] (100). HRMS (ESI) m/z ((M-Cl+MeCN)⁺) found 614.18508; calcd. 614.18650.

[1,3-Diethyl-5-(4-methoxyphenyl)-4-(3,4,5-trimethoxyphenyl)imidazol-2-ylidene](triphenylphosphane)gold(I) tetrafluoroborate (5a).

Complex **4a** (112 mg, 0.178 mmol) was dissolved in acetone (10 mL) and NaBF₄ (36 mg, 0.33 mmol) and triphenylphosphane (61 mg, 0.23 mmol) were added. The reaction mixture was stirred at room temperature for 24 h. The suspension was filtered, the filtrate concentrated in vacuum, and the residue recrystallized from acetone/*n*-hexane. Yield: 132 mg (0.14 mmol, 79%); colorless solid of mp = 107-110 °C; Elemental analysis (C₄₁H₄₃AuBF₄N₂O₄P, %) found C 52.14 H 4.47 N 2.93; calcd. C 52.25, H 4.60, N 2.97. ν_{max} (ATR)/cm⁻¹: 3056, 2936, 2836, 1607, 1581, 1516, 1504, 1463, 1437, 1415, 1331, 1292, 1248, 1179, 1124, 1099, 1050, 1024, 997, 887, 839, 811, 748, 711, 693 ^1H NMR (500 MHz, CDCl₃): δ 1.42 (3H, t, $J = 7.3$ Hz), 1.49 (3H, $J = 7.2$ Hz), 3.76 (3 H, s), 3.82 (3 H, s), 3.85 (3 H, s), 4.27 (2 H, q, $J = 7.1$ Hz), 4.35 (2 H, q, $J = 7.1$ Hz), 6.44 (3 H, s), 6.92 (6H, vd); 7.21 (3H, vd) 7.46 (15H, m) ^{13}C NMR

(125 MHz, CDCl₃): δ 17.5, 17.8, 44.3, 44.6, 55.3, 56.3, 60.9, 107.7, 114.3, 128.8, 128.9, 130.8, 131.9, 133.9, 134.0; ³¹P NMR (202 MHz, CDCl₃): δ 33.8; *m/z* (ESI, %) 855.0 (100) [M⁺], 721.4 (22). HRMS (ESI) *m/z* (M⁺) found 855.2577; calcd. 855.2620.

[4-(Anthracen-9-yl)-1,3-diethyl-5-phenylimidazol-2-ylidene](triphenylphosphane)gold(I) tetrafluoroborate (5b).

Compound **3b** (100 mg, 0.198 mmol) in dry CH₂Cl₂ (5 mL) was treated with KOtBu (27 mg, 0.238 mmol) and (PPh₃)AuCl (98 mg, 0.198 mmol). The mixture was stirred at room temperature for 24 h. The crude product was filtered and crystallised from CH₂Cl₂/*n*-hexane at 4 °C. Yield: 166 mg (0.191 mmol, 96%); white solid of mp = 165 °C; *v*_{max} (ATR)/cm⁻¹: 3051, 2981, 1977, 1622, 1464, 1432, 1345, 1262, 1095, 1025, 895, 849, 775, 737, 690, 607, 565; ¹H NMR (500 MHz, CDCl₃): δ 1.14 (3 H, t, *J* = 7.2 Hz), 1.59 (3 H, t, *J* = 7.2 Hz), 3.92 (2 H, q, *J* = 7.2 Hz), 4.55 (2 H, q, *J* = 7.2 Hz), 7.10-7.16 (3 H, m), 7.19-7.21 (2 H, m), 7.35-7.39 (6 H, m), 7.42-7.45 (3 H, m), 7.48-7.52 (8 H, m), 7.56-7.59 (2 H, m), 7.73 (2 H, d, *J* = 8.4 Hz), 8.03 (2 H, d, *J* = 8.4 Hz), 8.57 (1H, s); ¹³C NMR (125 MHz, CDCl₃): δ 17.6, 17.8, 44.8, 45.1, 120.2, 125.0, 125.7, 127.4, 127.7, 128.8, 128.9, 129.0, 129.4, 129.6, 130.2, 130.6, 131.1, 132.1, 132.2, 133.4, 133.9, 134.0, 134.1, 183.9; ³¹P NMR (202 MHz, CDCl₃): δ 30.3; *m/z* (ESI, %) 949.4 (100), 835.2 (7) [M⁺], 721.2 (40). HRMS (ESI) *m/z* (M⁺) found 835.2476; calcd. 835.2511.

Bis[4-(anthracen-9-yl)-1,3-diethyl-5-phenylimidazol-2-ylidene]gold(I) tetrafluoroborate (6b).

Compound **3b** (100 mg, 0.198 mmol) was dissolved in CH₂Cl₂/methanol (1:1, 80 mL) and Ag₂O (50.1 mg, 0.216 mmol) was added. The reaction mixture was stirred in the dark at room temperature for 5 h. Chloro(dimethylsulfide)gold(I) (33.9 mg, 0.115 mmol) was added and the reaction mixture was stirred for additional 24 h. The suspension was filtered, the filtrate was concentrated in vacuum and the residue was redissolved in CH₂Cl₂, filtered over MgSO₄/Celite, and the filtrate was concentrated in vacuum and the residue dried in vacuum. Yield: 79 mg (0.080 mmol, 88%); reddish solid of mp > 250 °C (dec.); *v*_{max}/cm⁻¹: 3052, 2965, 2924, 1623, 1595, 1520, 1498, 1460, 1443, 1407, 1378, 1345, 1294, 1260, 1218, 1161, 1088, 1050, 1012, 988, 961, 917, 896, 852, 774, 757, 737, 698; ¹H NMR (500 MHz, CDCl₃): δ 1.13 (6 H, t, *J* = 7.2 Hz), 1.59 (6 H, t, *J* = 7.2 Hz), 3.88 (4 H, q, *J* = 7.2 Hz), 4.49 (4 H, q, *J* = 7.2 Hz), 7.08-7.22 (10 H, m), 7.51 (4 H, t, *J* = 8.7 Hz), 7.58 (4 H, t, *J* = 8.7 Hz), 7.68 (4 H, d, *J* = 8.4 Hz), 8.04 (4 H, d, *J* = 8.4 Hz), 8.58 (2 H, s); ¹³C NMR (126 MHz, CDCl₃): δ 17.6, 17.8, 44.7, 44.8, 119.8, 124.6, 124.7, 125.8, 127.1, 127.8, 127.9, 128.9, 129.1, 129.4, 129.5, 129.6, 130.4, 131.1, 131.2, 132.2, 134.0, 183.6; *m/z* (ESI, %) 949.4 [M⁺] (100). HRMS (ESI) *m/z* (M⁺) found 949.35035; calcd. 949.35390.

NMR Spectra

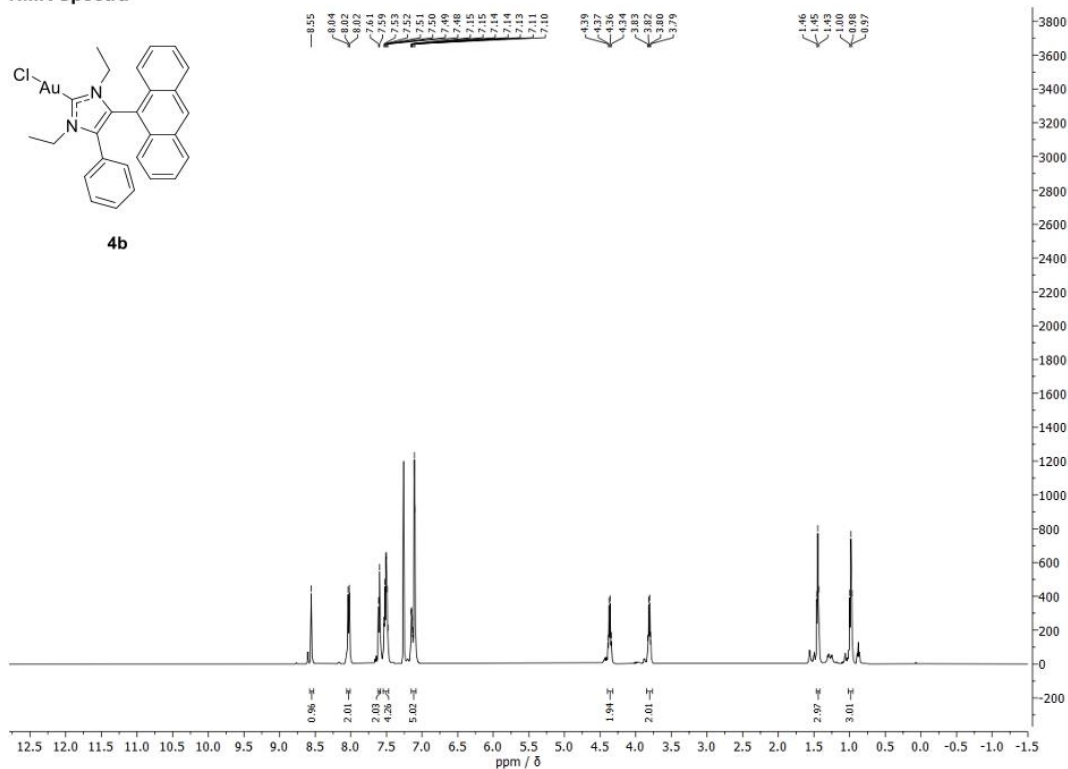
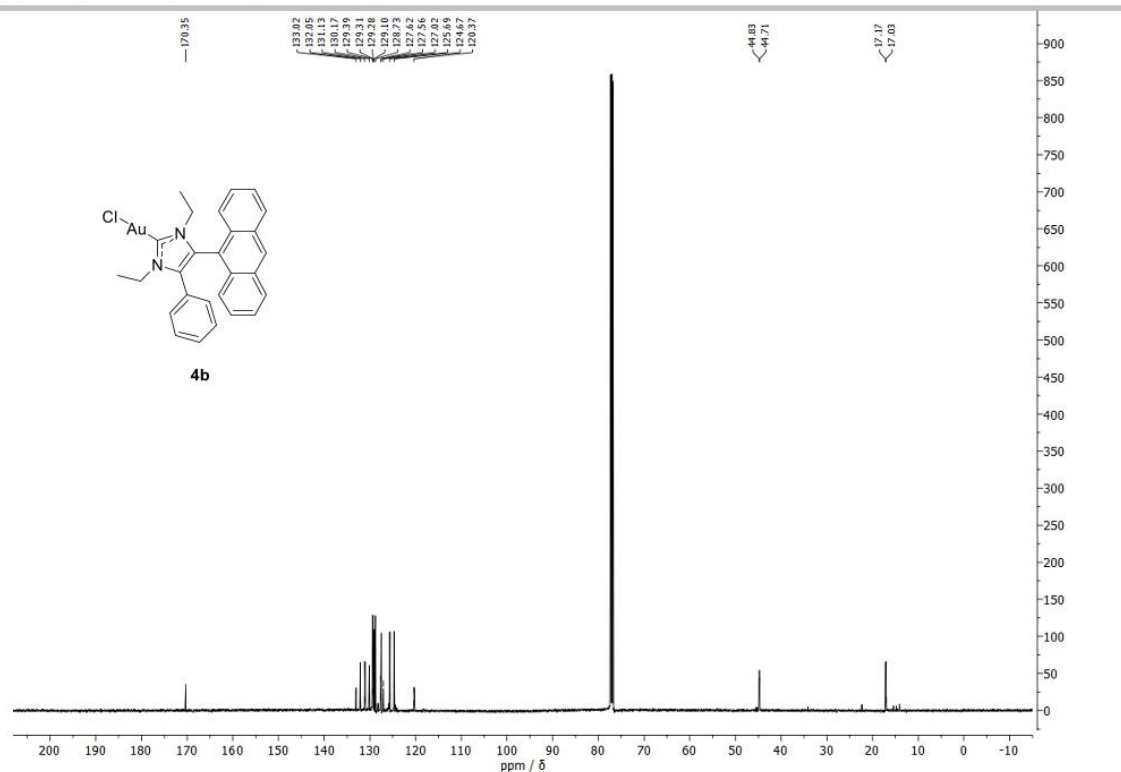
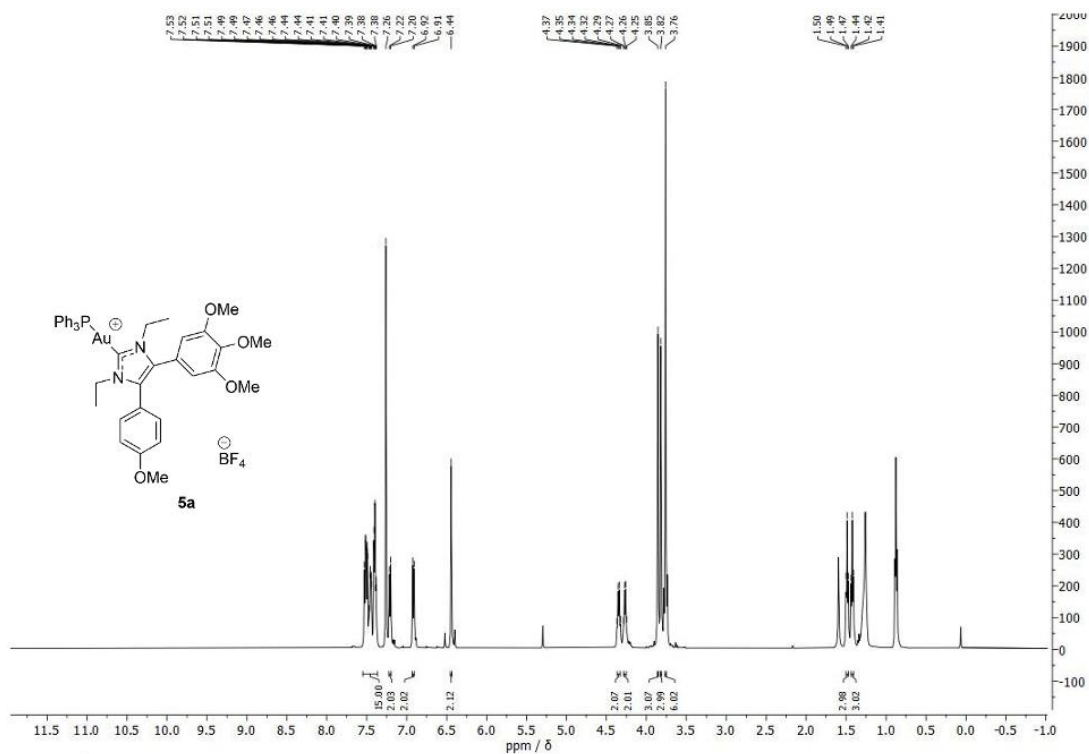


Figure 1: ¹H NMR (500 MHz, CDCl₃) spectrum of **4b**.

Figure 2: ^{13}C NMR (125 MHz, CDCl_3) spectrum of **4b**.Figure 3: ^1H NMR (500 MHz, CDCl_3) spectrum of **5a**.

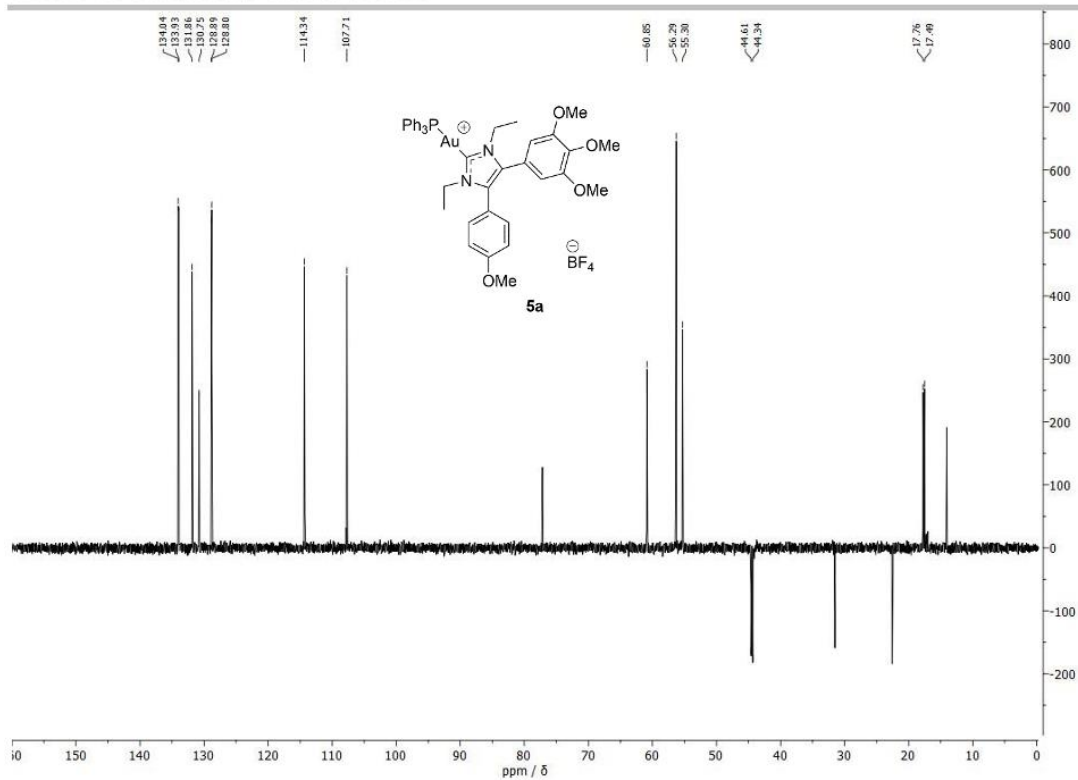


Figure 4: ^{13}C NMR (125 MHz, CDCl_3) spectrum of **5a**.

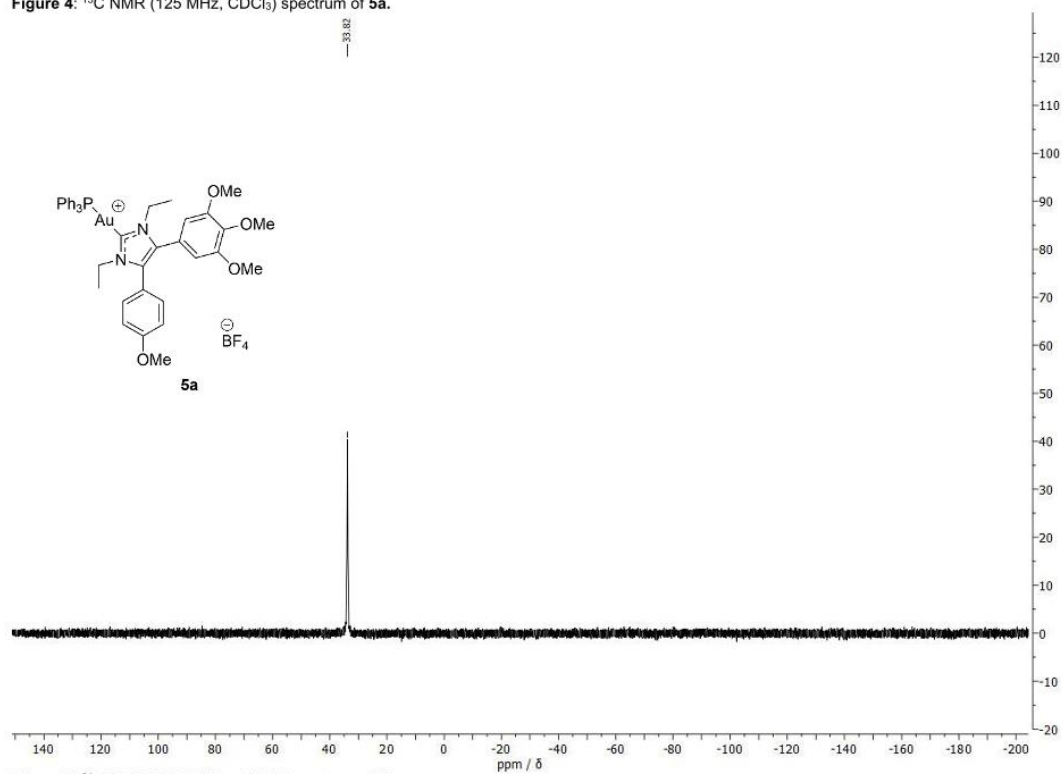
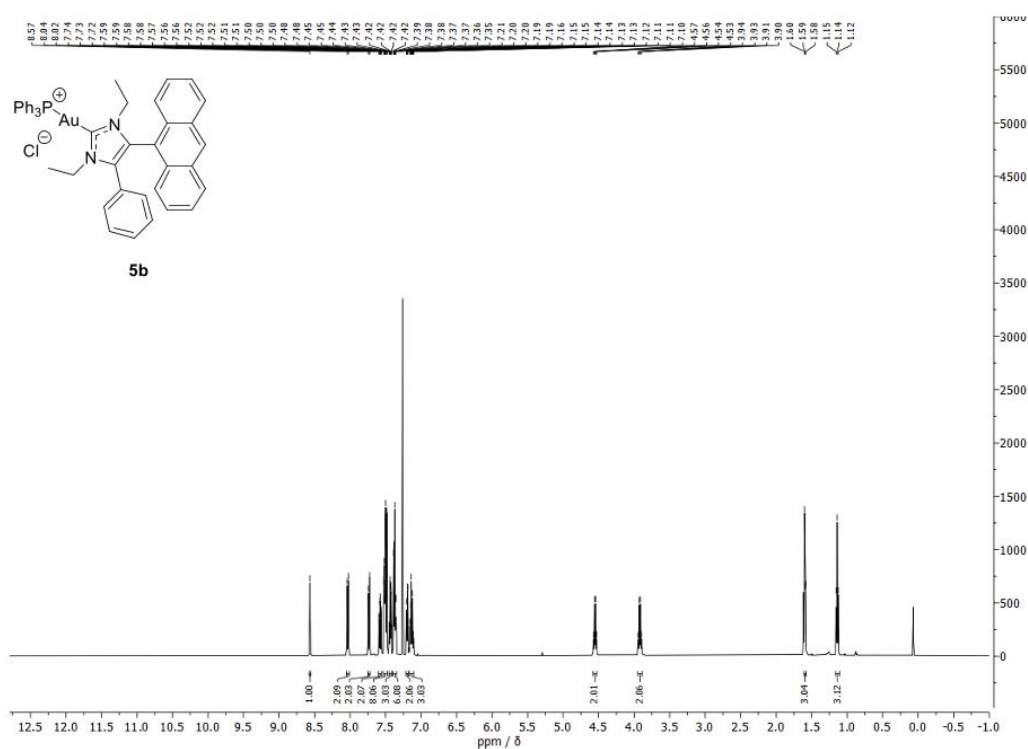
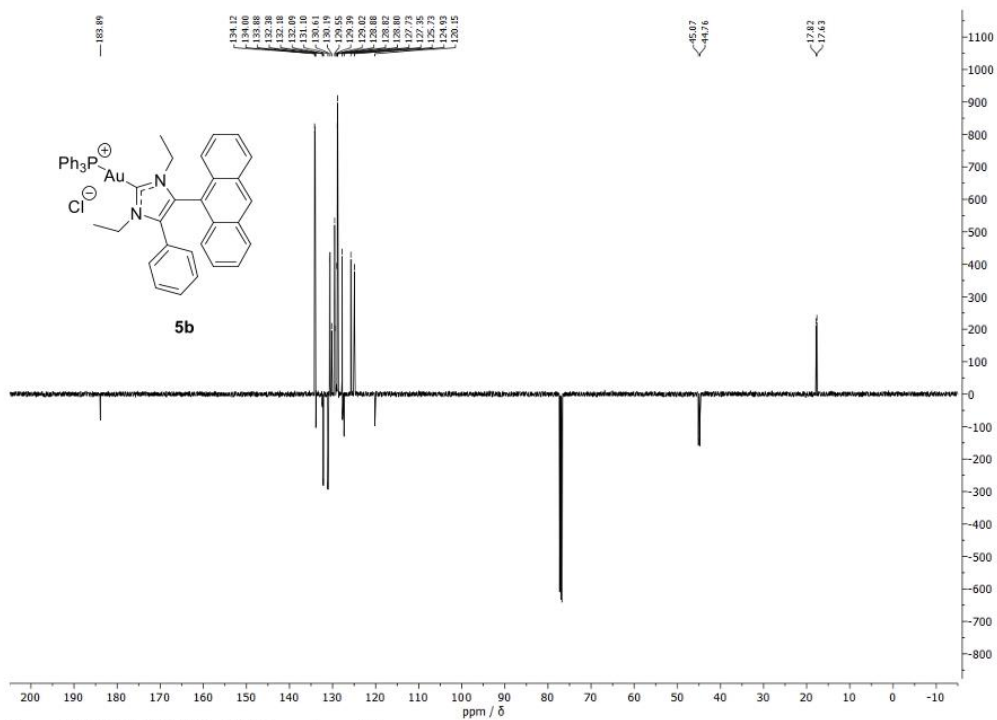


Figure 5: ^{31}P NMR (202.5 MHz, CDCl_3) spectrum of **5a**.

Figure 6: ¹H NMR (500 MHz, CDCl₃) spectrum of **5b**.Figure 7: ¹³C NMR (125 MHz, CDCl₃) spectrum of **5b**.

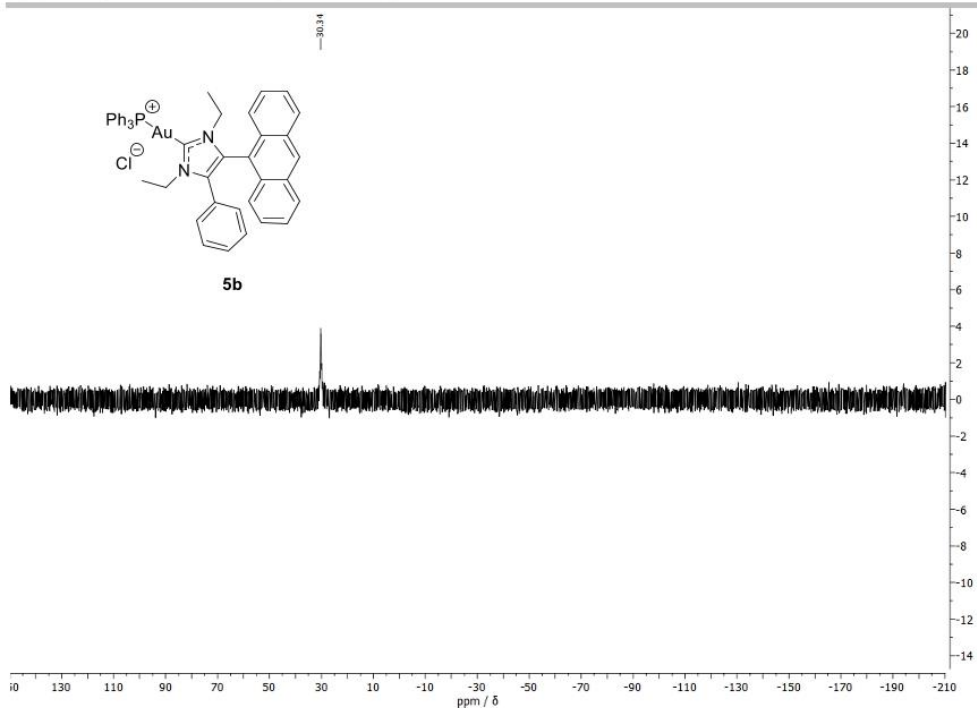


Figure 8: ^{31}P NMR (202.5 MHz, CDCl_3) spectrum of **5b**.

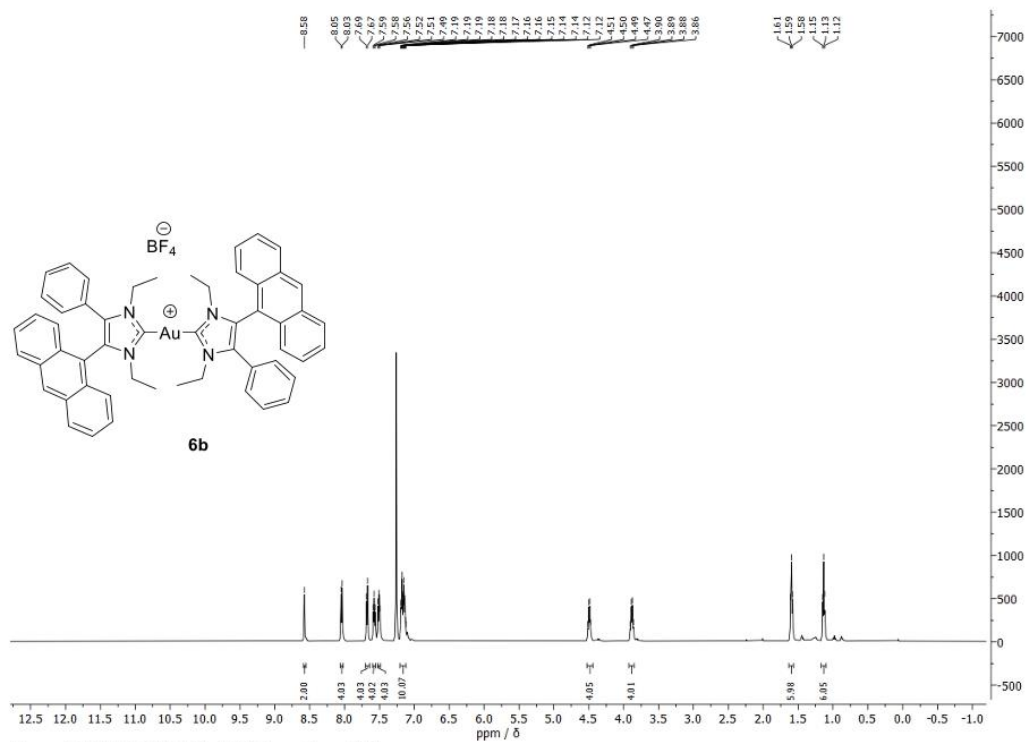


Figure 9: ^1H NMR (500 MHz, CDCl_3) spectrum of **6b**.

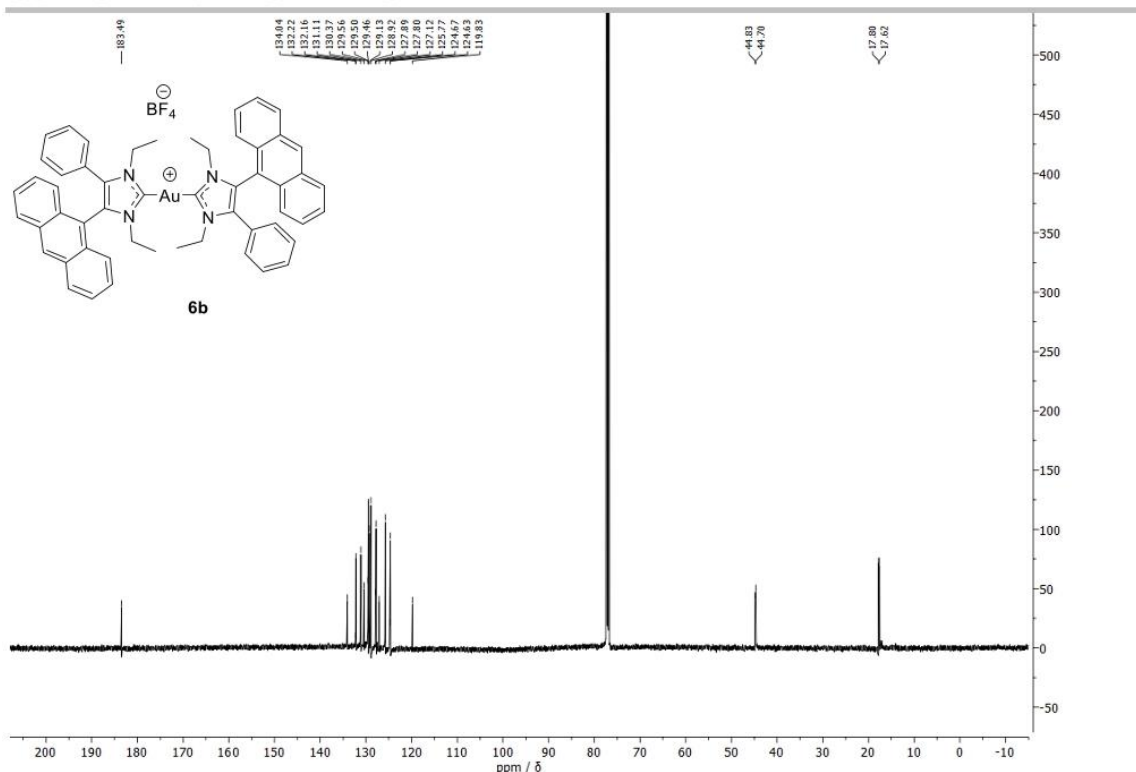


Figure 10: ^{13}C NMR (125 MHz, CDCl_3) spectrum of **6b**.

Biochemical Evaluation

Stock solutions of all test compounds were prepared (10 mM in DMF) and stored for at most one week at $-20\text{ }^\circ\text{C}$. They were diluted, assay-dependent, in ddH_2O , cell culture medium, or buffer.

Cell lines and culture conditions.

518A2 (Department of Radiotherapy and Radiobiology, University Hospital Vienna) human melanoma cells, HCT-116 (ACC-581) human colon carcinoma cells, as well as its p53 knockout mutant cell line HCT-116^{p53-/-}, HeLa cervix carcinoma, KB-V1^{vb1} multi-drug resistant cervix carcinoma cells, and HDFa (ATCC® PCS-201-012™) human dermal fibroblasts were grown in Dulbecco's Modified Eagle Medium (DMEM; Biochrom) supplemented with 10% (v/v) fetal bovine serum (FBS; Biochrom) and 1% (v/v) Antibiotic-Antimycotic solution (Gibco). The cells were incubated at $37\text{ }^\circ\text{C}$, 5% CO_2 , 95% humidified atmosphere and were serially passaged following trypsinisation by using 0.05% trypsin/0.02% EDTA (w/v; Biochrom GmbH, Berlin, Germany). The maximum-tolerated dose of vinblastine was added to the cell culture medium 24 h after every cell passage to keep the KB-V1^{vb1} cells resistant. The 518A2 melanoma cells are not available from cell banks, yet easily identified by their large size and flattened, spread-out morphology. Mycoplasma contamination was frequently monitored, and only mycoplasma-free cultures were used.

Inhibition of cell growth (MTT assay).^[2]

The cytotoxic effect upon treatment with gold complexes **4–6** and auranofin for 72 h was determined by standard MTT assays. The tetrazolium salt 3-(4,5-dimethylthiazol-2-yl)-2,5-diphenyltetrazolium bromide (MTT; ABCR) is reduced by viable cells to a violet, water-soluble formazan. 518A2 melanoma cells, colon carcinoma cells HCT-116 and HCT-116^{p53-/-}, mdr KB-V1^{vb1} and HeLa cervix carcinoma cells (5×10^4 cells mL^{-1} , 100 μL /well), as well as HDFa cells (10×10^4 cells mL^{-1} , 100 μL /well) were seeded in 96-well tissue culture plates and cultured for 24 h at $37\text{ }^\circ\text{C}$, 5% CO_2 and 95% humidity. After treatment with the test compounds incubation of cells was continued for 72 h. Blank and solvent controls were treated identically. After addition of a 5 mg mL^{-1} MTT stock solution in phosphate buffered saline (PBS), microplates were incubated for 2 h at $37\text{ }^\circ\text{C}$, centrifuged at 300 g, $4\text{ }^\circ\text{C}$ for 5 min and the supernatant was discarded. The precipitate of formazan crystals was then redissolved in a 10% (w/v) solution of sodium dodecylsulfate (SDS; Carl Roth) in DMSO containing 0.6% (v/v) acetic acid. To ensure complete dissolution of the formazan, the microplates were incubated for at least 1 h in the dark. Finally the absorbance at $\lambda = 570$ and 630 nm (background) was measured using a microplate reader (Tecan F200). All experiments were carried out in quadruplicate and the percentage of viable cells was calculated as the mean \pm SD with controls set to 100%.

Intracellular localisation of gold complexes.

518A2 melanoma cells (500 $\mu\text{L}/\text{well}$, 0.5×10^5 cells/mL) were seeded on glass coverslips in 24-well plates and incubated under cell culture conditions for 24 h. The medium was aspirated and the cells were washed once with PBS. Nuclear counterstaining was performed with Nuclear Green LCS1 (5 μM ; abcam) with an incubation time of 15 min under standard cell culture conditions. MitoTracker™ (Thermo Fisher) was used for mitochondrial staining, and the cells were incubated with this dye for 30 min. For lysosomal staining, the cells were incubated 20 min in an acridine orange solution (5 $\mu\text{g}/\text{mL}$, 400 $\mu\text{L}/\text{well}$). The cells were then washed twice with PBS and fresh DMEM was added. Then the cells were treated with the test compounds at a concentration of 30 μM and incubated for 30 min at standard cell culture conditions. The cells were fixed for 20 min at rt after a washing step with PBS in 3.7% formaldehyde solution in PBS, then washed three times and the coverslips were mounted in ProLong™ Gold Antifade Mountant (Invitrogen). The localisation of the test compounds was documented using confocal microscopy (Leica Confocal TCS SP5, 1000 \times magnification).

Caspase-3/7 activation assay.

For caspase activity measurements the Apo-ONE® Homogenous Caspase-3/7 Assay Kit (Promega Corp., Wisconsin, USA) was used. 518A2 melanoma cells (67.5 $\mu\text{L}/\text{well}$; 2×10^5 cells mL^{-1}) were grown in black 96-well plates for 24 h (37 °C, 5% CO_2 and 95% humidity). After incubation with different concentrations of the test compounds or solvent for 24 h under cell culture conditions, fluorogenic 1 \times caspase-3/7 substrate solution was added to each well and the substrate transformation by activated caspase-3/7 was performed for 45 min at rt. The fluorescence intensity (λ_{ex} : 485 \pm 20 nm, λ_{em} : 530 \pm 25 nm) was measured using a microplate reader (Tecan F200). Blank values (caspase-3/7 substrate solution plus test compound/solvent) were subtracted to reduce background signals, and a potential loss of cell viability after the incubation with the test compounds was taken into account by performing an MTT-assay as described above. The caspase-3/7 activity of the remaining vital cells was calculated as means \pm SD with solvent controls set to 100%. All experiments were carried out at least in quadruplicate.

Detection of morphological signs of apoptosis.

518A2 melanoma cells (3 mL/well , 5×10^4 cells mL^{-1}) were grown in 6-well plates for 24 h (37 °C, 5% CO_2 and 95% humidity). After incubation with IC_{50} concentrations of the test compounds (staurosporine: 500 nM, **4a**: 19.8 μM , **4b**: 7.9 μM , **5a**: 5.0 μM , **5b**: 2.9 μM , **6a**: 0.4 μM , **6b**: 5.5 μM) or solvent for 2.5 h under cell culture conditions, morphological changes of the cells were documented via brightfield microscopy (ZEISS Axiovert 135 and AxioVert MRc5, 100 \times magnification).

Annexin-V-FITC/PI staining.

For Annexin-V-FITC staining the TACS® Annexin-V-FITC Apoptosis Detection Kit (Trevigen, Maryland, USA) was used. 518A2 melanoma cells were seeded on glass coverslips (500 $\mu\text{L}/\text{well}$, 5×10^4 cells mL^{-1}) in 24-well plates, incubated under cell culture conditions (37 °C, 5% CO_2 and 95% humidity) for 24 h and treated with IC_{50} concentrations of the test compounds (staurosporine: 500 nM, CDDP: 7.8 μM ,^[9] **4a**: 19.8 μM , **4b**: 7.9 μM , **5a**: 5.0 μM , **5b**: 2.9 μM , **6a**: 0.4 μM , **6b**: 5.5 μM) or solvent for a further 45 min under cell culture conditions. Afterwards the medium was aspirated and the cells were stained with 150 μL of Annexin-V-FITC/PI staining solution for 15 min according to the manufacturer's instruction. Apoptosis-induced exposure of phosphatidylserine on the outer leaflet of the cytoplasmic membrane was documented by fluorescence microscopy (ZEISS Imager A1 AX10, 200 \times magnification). For differentiation between early apoptotic and late apoptotic/necrotic cells (which have lost membrane integrity), cells were counterstained with PI (propidium iodide).

Ethidium bromide saturation assay.

A potential DNA interaction of complexes **4–6** was assessed by a fluorescence-based ethidium bromide (EtdBr) staining assay. Salmon sperm DNA (SS-DNA, Sigma-Aldrich) in TE buffer (10 mM Tris-HCl, 1 mM EDTA, pH 8.5) was pipetted into a black 96-well plate to reach a final amount of 1 $\mu\text{g}/100$ μL assay volume and incubated with varying concentrations of test compounds for 2 h at 37 °C. Afterwards, 100 μL of EtdBr solution (10 μg mL^{-1} in TE buffer) was added to each well. The fluorescence (λ_{ex} = 535 nm, λ_{em} = 595 nm) was measured using a microplate reader (Tecan F200) after 5 min of incubation. Each fluorescence value was corrected for intrinsic compound and EtdBr background fluorescence. A decreased fluorescence indicates an interaction between DNA and test compound which prevents the intercalation of EtdBr molecules into the double-stranded SS-DNA. All experiments were carried out in triplicate and the relative EtdBr fluorescence was quoted as means \pm standard deviation with solvent controls set to 100%.

Electrophoretic mobility shift assay (EMSA).

Circular pBR322 plasmid DNA (1.5 μg ; ThermoScientific) was incubated with dilution series (0, 25, 50, 75, 100 μM) of the test compounds or CDDP in TE-buffer (10 mM Tris-HCl, 1 mM EDTA, pH 8.5) for 24 h at 37 °C (20 μL total sample volume). Afterwards the DNA samples were subjected to DNA gel electrophoresis using 1% agarose gel in 0.5 \times TBE-buffer (89 mM Tris, 89 mM boric acid, 25 mM EDTA, pH 8.3). After staining the gels with an EtdBr solution (10 μg mL^{-1} in 0.5 \times TBE-buffer) for 30 min, DNA bands were visualized using UV excitation. All experiments were performed at least in duplicate.

Inhibition of thioredoxin reductase (TrxR) activity.

For the measurement of thioredoxin reductase (TrxR) activity the TrxR Colorimetric Assay Kit (Cayman Chemical) was used according to manufacturer's instructions. 1×10^8 518A2 melanoma cells were harvested using a cell scraper, homogenised in 5 mL cold lysis buffer (50 mM K_3PO_4 , 1 mM EDTA, pH 7.4) on ice and centrifuged for 15 min (4 °C, 10000×g). The protein concentration of the supernatant was determined via Bradford assays. Then, 10 μ L Protease Inhibitor Cocktail Plus (Carl Roth) were added to 1 mL of the cell lysate which was either used for the assay right away or stored at -80 °C. Prior to use, the Assay Buffer was warmed to rt and the cell lysates, NADPH, aurothiomalate (ATM; specific TrxR inhibitor) and rat liver TrxR enzyme were thawed and kept on ice. After determination of the amount of cell lysate to use for optimum TrxR activity, all components were pipetted into the wells of a clear 96 well plate and the enzymatic reactions were initiated by addition of NADPH and 5,5'-dithio-bis(2-dinitrobenzoic acid) (DTNB). Then the absorbance at 405 nm was measured once every minute using a plate reader (Tecan F200) at at least ten time points. The TrxR activity was measured in the presence and absence of ATM. It is established that gold compounds such as ATM are highly specific inhibitors of mitochondrial TrxR.^[4] Therefore, in presence of ATM an inhibition of TrxR can be assumed which allows a correction for TrxR-independent DTNB reduction (e.g. via glutathione). The difference between the two results renders the DTNB reduction due to TrxR activity. By plotting the average absorbance values as a function of time the slope of the linear portion of the curve was obtained, and the change of absorbance (ΔA_{405}) per minute could be determined. The values were corrected for unspecific DTNB reduction and the TrxR activity was calculated using the following formula: TrxR activity [μ mol/min/mL] = [corrected ΔA /min (sample) / 7.92 mM^{-1}] \times [0.2 mL / 0.02 mL] \times sample dilution. The assay was conducted at 22 °C. All experiments were performed in triplicate and the solvent-treated negative controls were set to 100%.

Mitochondrial membrane potential.

518A2 melanoma cells (100 μ L/well, 0.25×10^6 cells/mL) were seeded in transparent (for viability control via MTT) and black 96-well plates, followed by an incubation period of 24 h under cell culture conditions. The medium was replaced by 90 μ L/well standard assay buffer (80 mM NaCl, 75 mM KCl, 25 mM D-Glucose, 25 mM HEPES, pH 7.4 in ddH₂O) and the cells were treated with a volume of 10 μ L of various concentrations of test compounds or solvent (DMF). CCCP (10 μ M) served as a positive control. The cells were incubated for a further 45 min under standard cell culture conditions. Then 10 μ L/well of a TMRM (tetramethylrhodamine methyl ester; Cayman Chemicals) solution were added (2 μ M in standard assay buffer), followed by an incubation period of 10 min under exclusion of light. The cells were washed three times (160 μ L PBS per well) and the fluorescence signal was measured after adding 100 μ L PBS per well (Tecan F200, $\lambda_{\text{ex}}/\lambda_{\text{em}}$: 535/590 nm). The fluorescence signal was correlated to viability, determined by corresponding MTT assays.

Determination of intracellular concentration of reactive oxygen species (DCFH-DA assay).

518A2 melanoma cells were seeded in black 96 well plates (100 μ L/well, 0.1×10^6 cells/mL) and incubated for 24 h under standard cell culture conditions. The medium was replaced by serum-free medium containing 20 μ M DCFH-DA, followed by a further incubation period of 30 min. Cells were washed twice with PBS (100 μ L/well) and fresh medium without FBS was added (100 μ L/well). After treatment with 10 μ M of the test compounds or solvent, the cells were incubated for 1 h under standard cell culture conditions and subsequently washed twice with PBS. The cells were kept in PBS and the fluorescence was measured (Tecan F200, $\lambda_{\text{ex}}/\lambda_{\text{em}}$: 485/535 nm). Solvent-treated cells were taken as negative controls and their fluorescence was set to 100%.

Lysosomal integrity.

518A2 melanoma cells (500 μ L/well, 0.05×10^6 cells/mL) were seeded on glass coverslips in 24 well plates and incubated for 24 h under standard cell culture conditions. Then the cells were treated with the test compounds at IC_{50} concentrations and incubated for 1, 2, 4 or 6 h under standard cell culture conditions. 30 min before each time interval ended, cells were stained with Lysosomal Staining Kit Orange - Cytopainter (Abcam). To this end, medium was aspirated and the cells were washed once with 1 mL HHBS (Hanks Buffer with HEPES; 140 mM NaCl, 5 mM KCl, 1 mM $CaCl_2$, 0.4 mM $MgSO_4 \times 7H_2O$, 0.5 mM $MgCl_2 \times 6H_2O$, 0.3 mM $Na_2HPO_4 \times 2H_2O$, 0.4 mM KH_2PO_4 , 6 mM D-glucose, 20 mM HEPES, pH 7.0). The cells were treated with 300 μ L staining solution, incubated for 30 min under standard cell culture conditions, washed twice with 1 mL HHBS and fixed for 10 min at rt in 1 mL/well 3.7% formaldehyde in PBS. After three further washing steps, the coverslips were washed with 500 μ L ddH₂O and embedded on glass slides with ProLong Gold™ (Invitrogen) containing 1 μ g/mL DAPI. Lysosomal and nuclear staining was documented using a fluorescence microscope (Zeiss Imager A1 AX10, 400-fold magnification).

Stability testing via NMR spectroscopy.

Solutions of the test compounds were freshly prepared corresponding to stock solutions in dimethylformamide-*d*₇, 5 vol-% water-*d*₂ were added. ¹H NMR (500 MHz) spectra (16 scans) were measured at 0 h, 24 h, 48 h and 72 h to demonstrate the stability of the complexes in solution in the presence of water.

Tubulin polymerisation assay.

Purified porcine brain tubulin protein [5 mg/mL in Brinkley's buffer 80 (BRB80)] containing 10% glycerol and 1.5 mM guanosine 5'-triphosphate (GTP)] was pipetted in a black 96-well half-area plate and mixed with the test compounds or solvent (DMSO) to a final concentration of 10 μ M. The microplate was immediately placed in the pre-heated microplate reader (Tecan F200) and polymerisation was measured turbidimetrically at 37 °C by recording the absorption at 340 nm for 2 h in intervals of 20 s. All experiments were at least carried out in duplicate.

Cell cycle analysis.

518A2 melanoma cells (3 mL/well; 5×10^4 cells mL⁻¹) were grown on 6-well tissue culture plates for 24 h (37 °C, 5% CO₂, 95% humidity) and treated with different concentrations of the test compounds or solvent for another 24 h (37 °C, 5% CO₂, 95% humidity). The cells were harvested by trypsinisation and fixed in ice-cold 70% EtOH (1 h, 4 °C). After RNA digestion and propidium iodide (PI; Carl Roth) staining with PI staining solution (50 µg mL⁻¹ PI, 0.1% sodium citrate, 50 µg mL⁻¹ RNase A in PBS) for 30 min at 37 °C to quantitatively stain DNA, the fluorescence intensity of 10 000 single cells was measured at $\lambda_{em} = 570$ nm ($\lambda_{ex} = 488$ nm laser source) with a Beckmann Coulter Cytomics FC500 flow cytometer. The percentage of cells in the different phases of the cell cycle (G1, S and G2/M phase) was determined by CXP software (Beckmann Coulter). The percentage of apoptotic and necrotic cells was derived from sub-G1 peaks.

Results

Influence on cellular morphology

To confirm induction of apoptosis after treatment of 518A2 melanoma cells with complexes **4-6** we additionally documented morphological alterations via brightfield microscopy (Fig. 11).

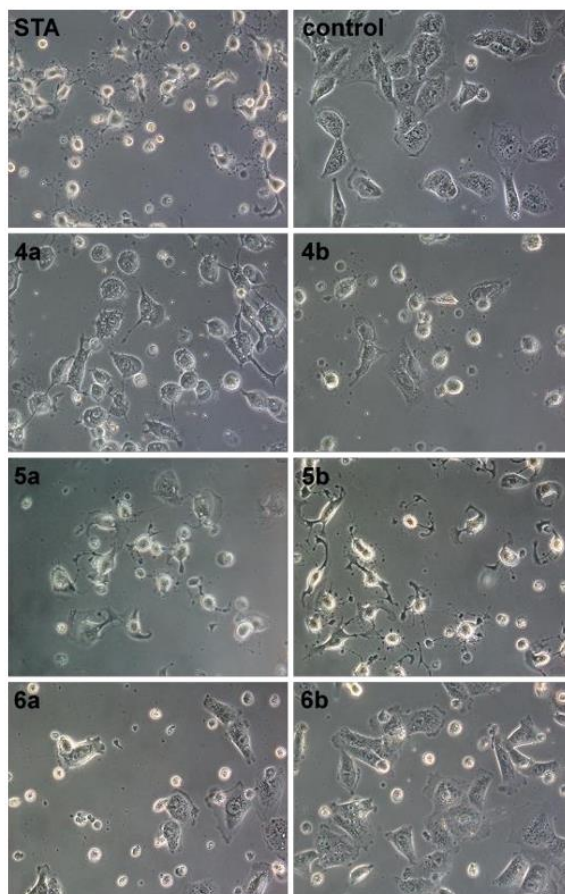


Figure 11: Morphological signs of apoptosis of 518A2 melanoma cells after incubation with staurosporine (STA; 500 nM) as well as IC_{50} concentrations of gold complexes **4-6** for 2.5 h. (**4a**: 19.8 μ M, **4b**: 7.9 μ M, **5a**: 5.0 μ M, **5b**: 2.9 μ M, **6a**: 0.4 μ M, **6b**: 5.5 μ M). Documented using brightfield microscopy, 100 \times magnification. Images are representative of at least three independent experiments.

Apoptosis detection using Annexin V-FITC and PI

Early apoptotic events upon treatment of 518A2 melanoma cells with gold complexes **4-6** were detected by staining of phosphatidylserines on the outer surface of the cytoplasmic membrane with Annexin-V-FITC. Early apoptotic and late apoptotic/necrotic cells could be differentiated by counterstaining with propidium iodide (PI), which can only enter cells lacking membrane integrity. Results were documented via fluorescence microscopy (Fig. 12).

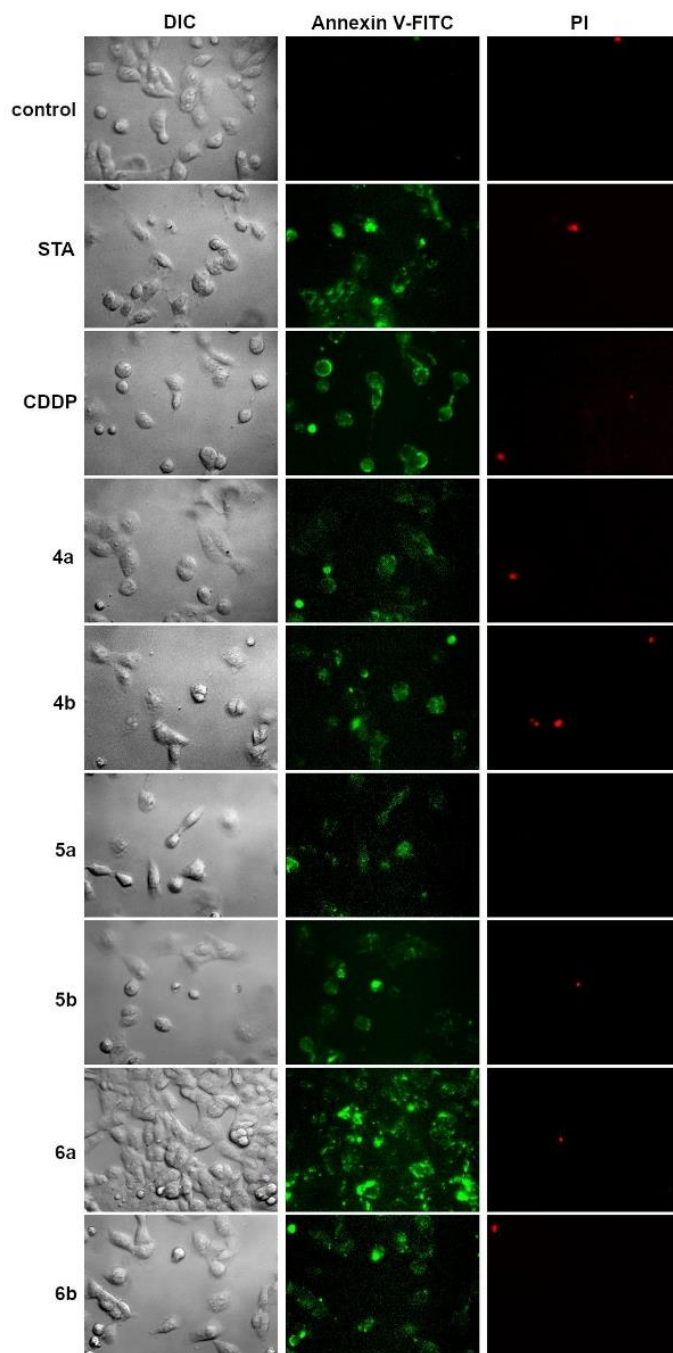


Figure 12: Annexin-V-FITC/PI staining of 518A2 melanoma cells treated with staurosporine (STA; 500 nM), CDDP (7.8 μ M) as well as IC_{50} concentrations of gold complexes **4-6** for 45 min. (**4a**: 19.8 μ M, **4b**: 7.9 μ M, **5a**: 5.0 μ M, **5b**: 2.9 μ M, **6a**: 0.4 μ M, **6b**: 5.5 μ M). Documented using fluorescence microscopy, 200 \times magnification. Images are representative for at least three independent experiments.

Stability testing via NMR spectroscopy

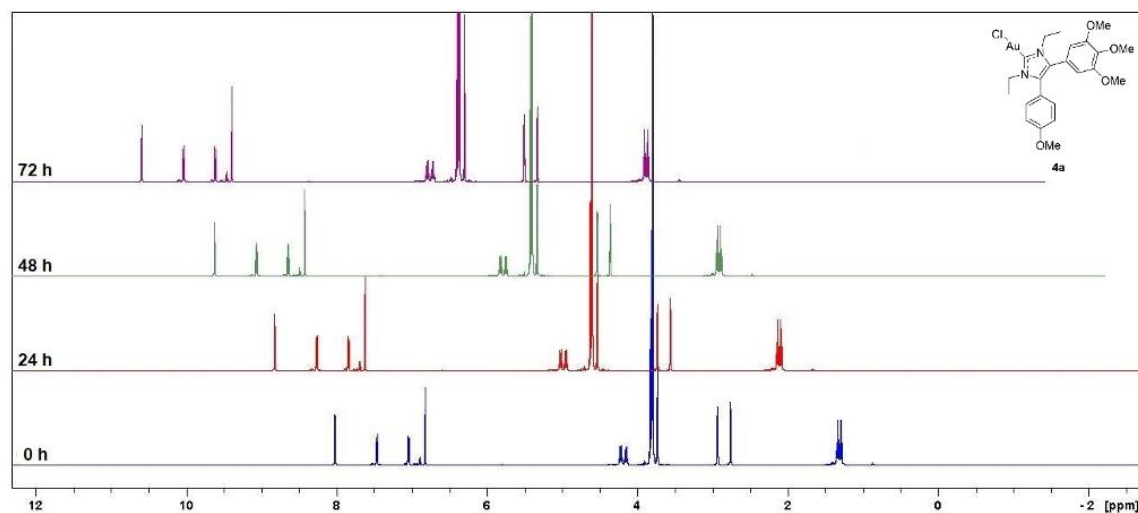


Figure 13: ¹H NMR (500 MHz, dimethylformamide-d₇, 5 vol-% water-d₂) spectra of **4a**; 0 h, 24 h, 48 h and 72 h after preparing of stock solution.

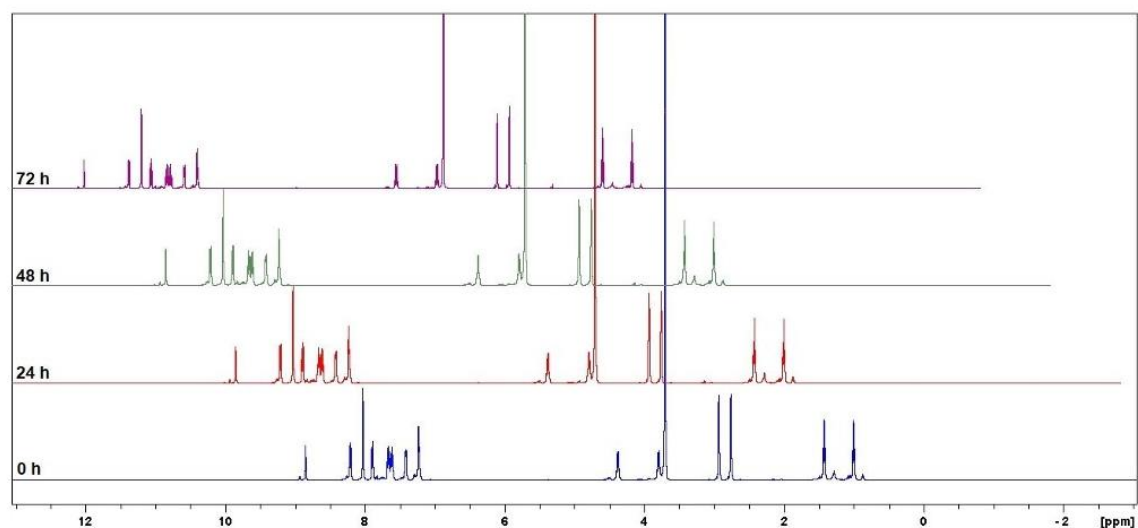


Figure 14: ¹H NMR (500 MHz, dimethylformamide-d₇, 5 vol-% water-d₂) spectra of **4b**; 0 h, 24 h, 48 h and 72 h after preparing of stock solution.

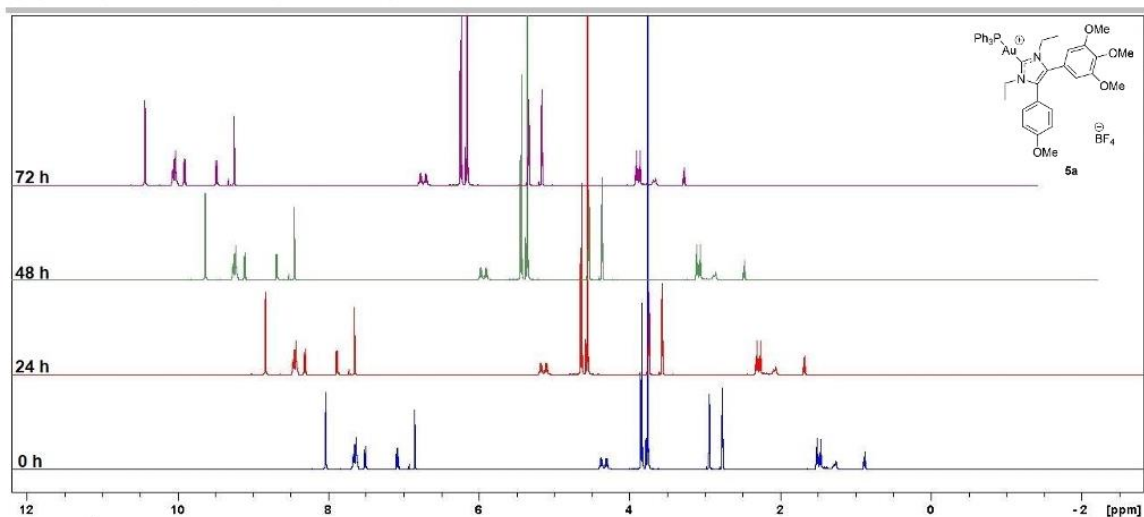


Figure 15: ¹H NMR (500 MHz, dimethylformamide-d₂, 5 vol-% water-d₂) spectra of **5a**; 0 h, 24 h, 48 h and 72 h after preparing of stock solution.

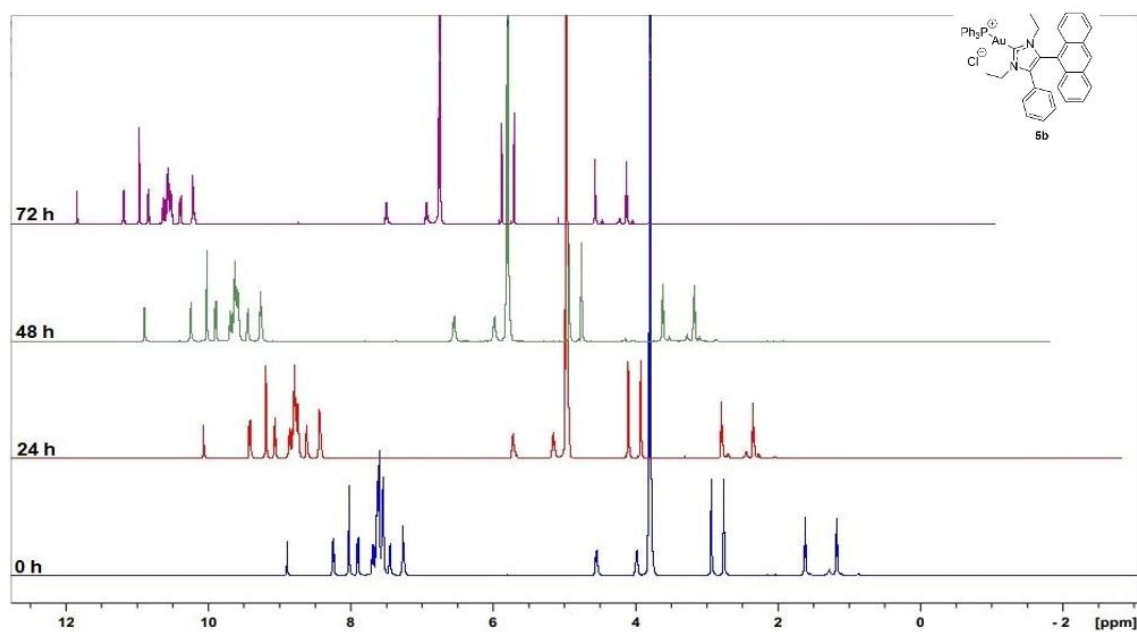


Figure 16: ¹H NMR (500 MHz, dimethylformamide-d₂, 5 vol-% water-d₂) spectra of **5b**; 0 h, 24 h, 48 h and 72 h after preparing of stock solution.

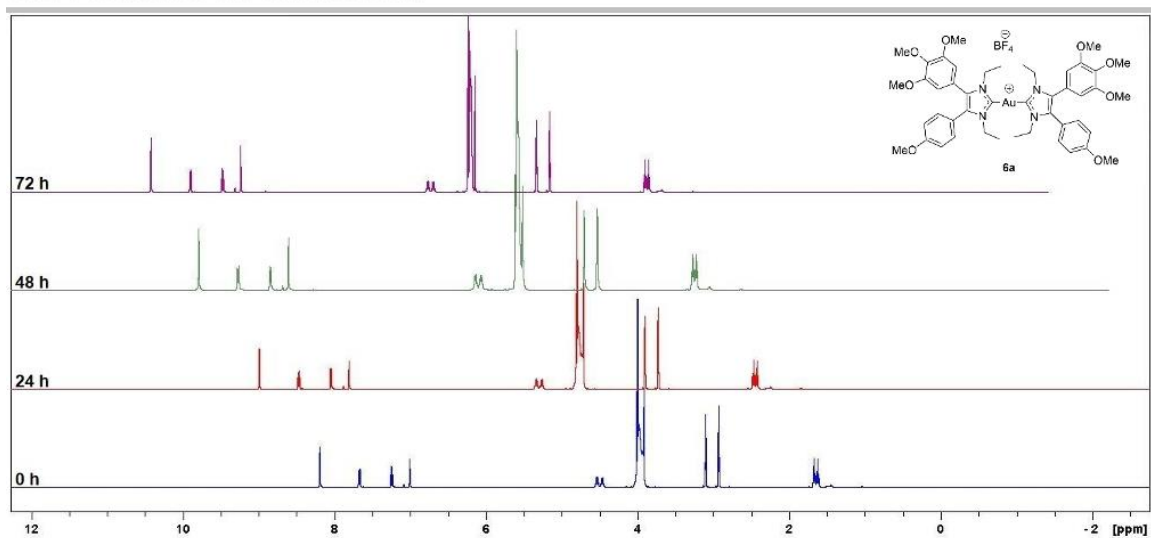


Figure 17: ¹H NMR (500 MHz, dimethylformamide-d₇, 5 vol-% water-d₂) spectra of **6a**; 0 h, 24 h, 48 h and 72 h after preparing of stock solution.

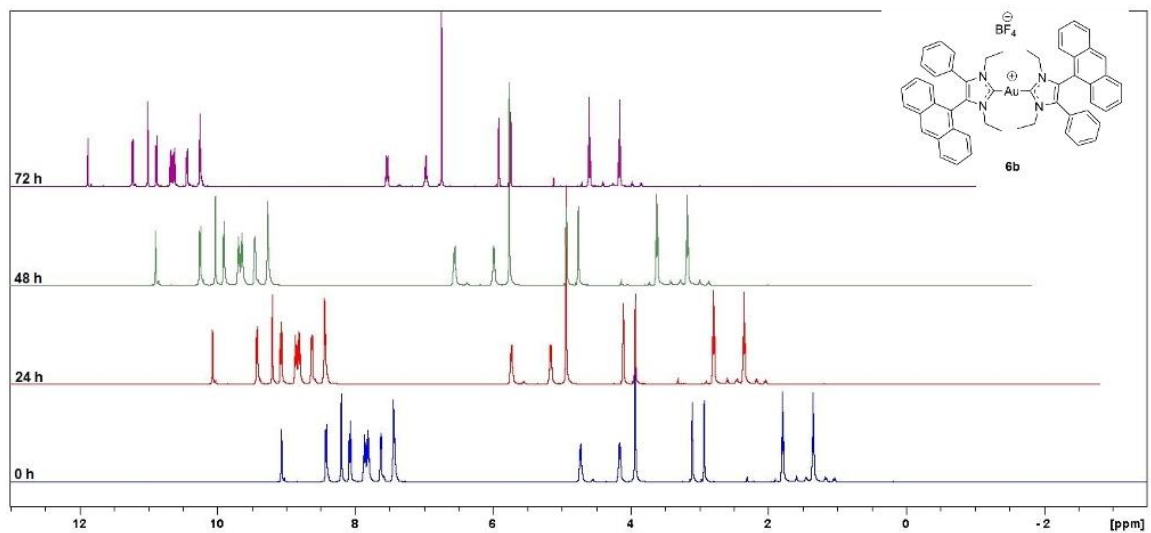


Figure 18: ¹H NMR (500 MHz, dimethylformamide-d₇, 5 vol-% water-d₂) spectra of **6b**; 0 h, 24 h, 48 h and 72 h after preparing of stock solution.

Interaction with tubulin

Figure 19 shows the results from tubulin polymerization assays with complexes **4-6**. The known microtubule-destabilizing compound combretastatin A-4 (CA-4) was used as a positive control. With the exception of complexes **5**, which induce a slight inhibition of tubulin polymerization, no effects could be observed for the other test compounds **4** and **6**.

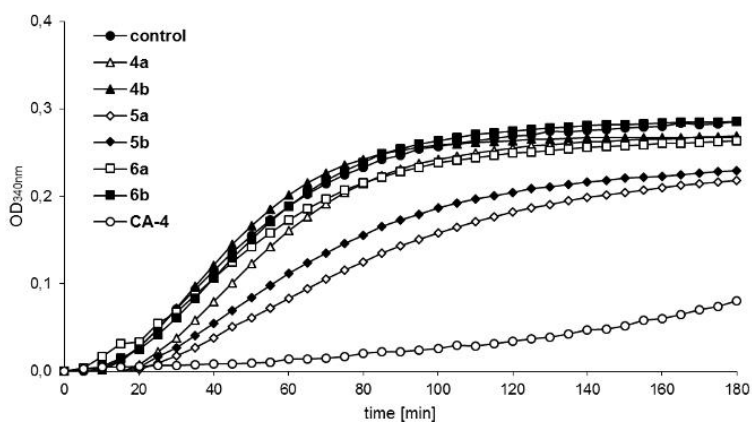


Figure 19: Turbidimetric measurement (OD at 340 ± 20 nm) of the polymerization of monomeric tubulin under the influence of the test compounds **4-6** at a final concentration of $10 \mu\text{M}$. DMF was used as negative control, CA-4 at $10 \mu\text{M}$ was used as positive control. Values are representative of at least two independent measurements.

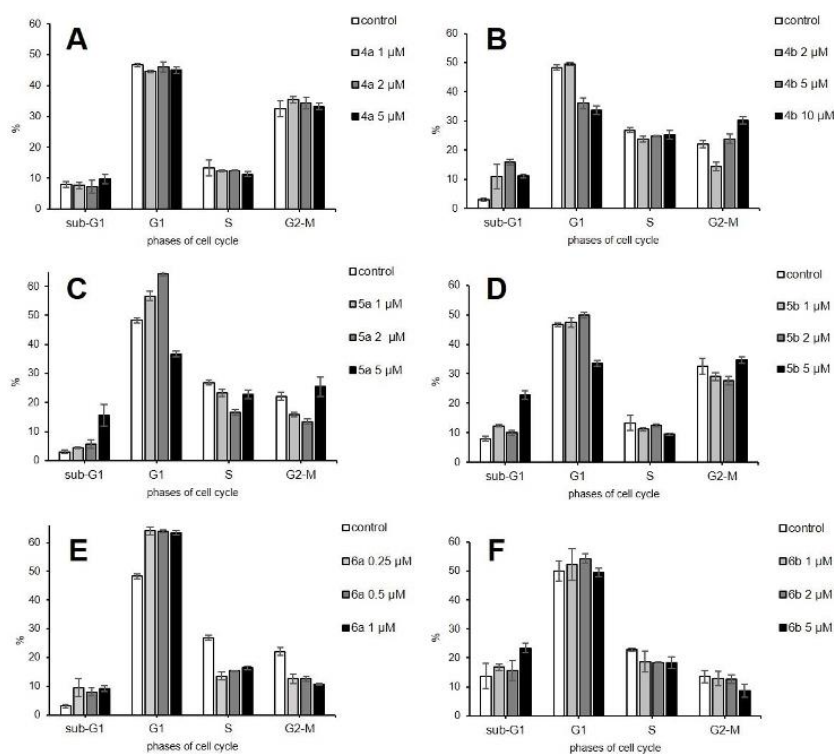
Influence on the cell cycle of 518A2 melanoma cells

Figure 20. Influence of different concentrations of the test compounds **4a** (A), **4b** (B), **5a** (C), **5b** (D), **6a** (E) and **6b** (F) on the cell cycle of 518A2 melanoma cells measured via flow cytometry and PI staining; as a control the respective volume of solvent was used. Concentrations were adjusted to the IC_{50} values of the compounds for 518A2 melanoma cells in MTT assays. Values are means \pm standard deviation derived from three independent assays.

References

- [1] J. K. Muenzner, B. Biersack, H. Kalie, I. C. Andronache, L. Kaps, *et al.*, *Chem. Med. Chem.* **2014**, *9*, 1195-1204.
- [2] T. Mosmann, *J. Immunol. Methods* **1983**, *65*, 55-63.
- [3] M. Gold, Y. Mujahid, K. Ahmed, H. Kostrhunova, J. Kasparkova, *et al.*, *J. Biol. Inorg. Chem.* **2019**, *24*, 647-657.
- [4] M. P. Rigobello, L. Messori, G. Marcon, M. A. Cinellu, M. Bragadin, *et al.*, *J. Inorg. Biochem.* **2004**, *98*, 1634-1641

Author Contributions

S. I. Bär: Experimental studies and data acquisition (biochemical assays and stability tests), formal analysis, chemical analysis, project administration, writing of original draft, creation of graphics and art work; degree: lead, equal to M. Gold;

M. Gold: Experimental studies and data acquisition (biochemical assays and elemental analyses), formal analysis, project administration, writing of original draft, creation of graphics and art work; degree: lead, equal to S. I. Bär;

S. W. Schleser: Synthesis of gold(I) complexes, chemical analysis; degree: supporting;

T. Rehm: Synthesis of gold(I) complexes, chemical analyses; degree: supporting;

A. Bär: Synthesis of gold(I) complexes, writing of original draft; degree: supporting;

B. Biersack: Synthesis of gold(I) complexes, writing of original draft; degree: supporting;

L. Köhler: Experimental studies (EMSA); degree: supporting;

L. R. Carnell: Experimental studies (biochemical assays); degree: supporting;

R. Schobert: Project supervision, writing of original draft, funding acquisition, project coordination; degree: corresponding author;

4.5 List of all publications and poster contributions to conferences

S. W. Schleser, L. H. F. Köhler, F. Riethmüller, S. Reich, R. Fertig, G. Begemann, R. Kempe, R. Schobert, submitted to Dalton Trans.

S. I. Bär, S. W. Schleser, N. Oberhuber, A. Herrmann, L. Schlotte, S. E. Weber and R. Schobert, J. Inorg. Biochem., 238, **2022**, 112028.

S. I. Bär, M. Gold, S. W. Schleser, T. Rehm, A. Bär, L. Köhler, L. R. Carnell, B. Biersack, R. Schobert, Chem. Eur. J. **2021**, 27, 5003.

L. Kober, S. W. Schleser, S. I. Bär, R. Schobert, J. Biol. Inorg. Biochem., 27, **2022**, 731-745.*

S. W. Schleser, L. H. F. Köhler, F. Riethmüller, S. Reich, R. Fertig, R. Kempe, R. Schobert, Bayreuth Natural Products and Drugs Symposium, 2022, Bayreuth, Germany and 22nd Tetrahedron Symposium, Catalysis for a sustainable world, **2022**, Lissabon, Portugal. (Best Poster Award)

*Not part of this cumulative dissertation.

Acknowledgements (German)

Mein größter Dank gilt meinem Doktorvater, Professor Dr. Rainer Schobert, für die bedingungslose Unterstützung während meiner gesamten Zeit am Lehrstuhl. Insbesondere die ausgiebige Freiheit im Rahmen meines Forschungsvorhabens, habe ich ebenso wie die zahlreichen zukunftsweisenden Gespräche, sei es fachlicher oder persönlicher Natur, sehr genossen.

Nicht zu vergessen, gilt mein Dank selbstredend auch Frau Kastner für die unkomplizierte Unterstützung bei jeglichen bürokratischen Aufgaben.

Dr. Thomas Schmalz möchte ich ebenfalls gesondert erwähnen und mich bei ihm für die Mithilfe beim reibungslosen Abwickeln meines Lehrauftrags, der Praktika aber auch für die wissenschaftliche Diskurse bedanken, die ich sehr geschätzt habe.

Auch ein Dankeschön geht an Leonhard H. F. Köhler für die angenehme und ertragreiche Zusammenarbeit. Die große Unterstützung bei der Tetrahedron Konferenz in Lissabon mit anschließendem Posterpreis habe ich sehr geschätzt.

Ein herzliches Merce! gilt auch meiner Laborkollegin Stefanie Weber, welche die viel zu kurze gemeinsame Zeit im Labor sehr angenehm, unterhaltend aber auch unterstützend gestaltet hat. Nicht zuletzt der gemeinsame Musikgeschmack und Humor haben dazu beigetragen, dass ich mich täglich erneut darauf gefreut habe, meinen Arbeitsplatz zu betreten.

Ich möchte mich ebenso bei all meinen Forschungspraktikanten bedanken, die mich auf kurz oder lang im Labor unterstützt haben. Namentlich vor allem Florian Riethmüller, Tim Ziegelmeier, Jonathan Seib und Luca Schlotte. Jeder von ihnen hat einen nennenswerten praktischen Beitrag zu einer der angeführten Publikationen geleistet und mit seiner Art die Promotion bereichert. Ich wünsche ihnen alles Gute für die Zukunft.

Den Axolotl möchte ich ebenfalls Danke sagen, dafür dass sie die Mittagspause immer so erheitert haben. Dafür mussten sie auch gar nicht viel mehr tun als schwimmen. Sie waren schließlich ebenfalls immer das Highlight für meine Besuchenden.

Abseits vom Labor oder dem Hörsaal möchte ich mich allem voran bei Nadine Holzleitner bedanken, die meine Promotion durch alle Hochs und Tiefs begleitet hat, dabei immer ein offenes Ohr hatte und gewiss einen großen Anteil daran hatte, dass die Zeit so angenehm war.

Natürlich bedanke ich mich auch bei meinen Eltern. Zunächst bei meinem Vater, der jeglichen privaten Stress, sei es seitens des Vereins oder etwaige bürokratische Belange, schon seit dem Studium von mir ferngehalten hat. Leider kann er den erfolgreichen Abschluss der Promotion nicht

mehr erleben, ich hoffe aber, ich habe ihn auch währenddessen schon mit Stolz erfüllt. Auch meiner Mama möchte ich dafür Danke sagen, dass sie tatkräftig und seelisch immer einer Stütze war in dieser Zeit.

Ebenso möchten ich den Lektoren Leonhard H. F. Köhler sowie Nadine und Katrin Holzleitner danken, die sich wacker und zügig durch die (themen)fremde Dissertation gekämpft haben.

Last but not least möchte ich der gesamten Mannschaft von Lazio Chrom danken. Allen Widrigkeiten zum Trotz, sei es die Distanz oder die Pandemie, fanden wir immer wieder zusammen und haben wunderschöne Ausflüge und Schafkopfabende miteinander verbracht, deren Termine immer mit einer langen Phase der Vorfreude begleitet wurde. Ich hoffe, wir bleiben auch weiterhin so gut befreundet, wie wir es schon seit dem Studium sind.

Eidesstattliche Versicherung und Erklärung des Verfassers

(§ 8 Satz 2 Nr. 3 PromO Fakultät)

Hiermit versichere ich eidesstattlich, dass ich die Arbeit selbstständig verfasst und keine anderen als die von mir angegebenen Quellen und Hilfsmittel benutzt habe (vgl. Art. 64 Abs. 1 Satz 6 BayHSchG).

(§ 8 Satz 2 Nr. 3 PromO Fakultät)

Hiermit erkläre ich, dass ich die Dissertation nicht bereits zur Erlangung eines akademischen Grades eingereicht habe und dass ich nicht bereits diese oder eine gleichartige Doktorprüfung endgültig nicht bestanden habe.

(§ 8 Satz 2 Nr. 4 PromO Fakultät)

Hiermit erkläre ich, dass ich Hilfe von gewerblichen Promotionsberatern bzw. –vermittlern oder ähnlichen Dienstleistern weder bisher in Anspruch genommen habe noch künftig in Anspruch nehmen werde.

(§ 8 Satz 2 Nr. 7 PromO Fakultät)

Hiermit erkläre ich mein Einverständnis, dass die elektronische Fassung der Dissertation unter Wahrung meiner Urheberrechte und des Datenschutzes einer gesonderten Überprüfung unterzogen werden kann.

(§ 8 Satz 2 Nr. 8 PromO Fakultät)

Hiermit erkläre ich mein Einverständnis, dass bei Verdacht wissenschaftlichen Fehlverhaltens Ermittlungen durch universitätsinterne Organe der wissenschaftlichen Selbstkontrolle stattfinden können.

Ort, Datum

Sebastian Werner Schleser